

VED CREDIT

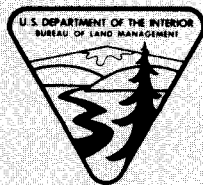
Environmental Assessment of the Alaskan Continental Shelf

**Annual Reports of Principal Investigators
for the year ending March 1977**

Volume XV. Transport



**U.S. DEPARTMENT OF COMMERCE
National Oceanic and Atmospheric Administration**



**U.S. DEPARTMENT OF INTERIOR
Bureau of Land Management**

VOLUME I	RECEPTORS -- MAMMALS
VOLUME II	RECEPTORS -- BIRDS
VOLUME III	RECEPTORS -- BIRDS
VOLUME IV	RECEPTORS -- BIRDS
VOLUME V	RECEPTORS -- BIRDS
VOLUME VI	RECEPTORS -- FISH
VOLUME VII	RECEPTORS -- FISH
VOLUME VIII	RECEPTORS -- FISH
VOLUME IX	RECEPTORS -- FISH
VOLUME X	RECEPTORS -- FISH
VOLUME XI	RECEPTORS -- MICROBIOLOGY
VOLUME XII	EFFECTS
VOLUME XIII	CONTAMINANT BASELINES
VOLUME XIV	TRANSPORT
VOLUME XV	TRANSPORT
VOLUME XVI	HAZARDS
VOLUME XVII	HAZARDS
VOLUME XVIII	HAZARDS DATA MANAGEMENT

Environmental Assessment of the Alaskan Continental Shelf

**Annual Reports of Principal Investigators
for the year ending March 1977**

Volume XV. Transport

Outer Continental Shelf Environmental Assessment Program
Boulder, Colorado

March 1977

U.S. DEPARTMENT OF COMMERCE
National Oceanic and Atmospheric Administration
Environmental Research Laboratory

U.S. DEPARTMENT OF INTERIOR
Bureau of Land Management

DISCLAIMER

The Environmental Research Laboratories do not approve, recommend, or endorse any proprietary product or proprietary material mentioned in this publication. No reference shall be made to the Environmental Research Laboratories or to this publication furnished by the Environmental Research Laboratories in any advertising or sales promotion which would indicate or imply that the Environmental Research Laboratories approve, recommend, or endorse any proprietary product or proprietary material mentioned herein, or which has as its purpose an intent to cause directly or indirectly the advertised product to be used or purchased because of this Environmental Research Laboratories publication.

CONTENTS

<u>RU #</u>	<u>PI - Agency</u>	<u>Title</u>	<u>Page</u>
250	Shapiro, L. - Geophysical Inst. Bates, H. Univ. of Alaska Harrison, W. Fairbanks, AK	Mechanics of Origin of Pressure Ridges, Shear Ridges and Hummock Fields in Landfast Ice	1
257	Stringer, W. - Geophysical Inst. et al. Univ. of Alaska Fairbanks, AK	Morphology of Beaufort, Chukchi and Bering Seas Near Shore Ice Conditions by Means of Satellite and Aerial Remote Sensing	42
259	Sackinger, W. - Geophysical Inst. Nelson, R. Univ. of Alaska Fairbanks, AK	Experimental Measurements of Sea Ice Failure Stresses Near Grounded Structures	151
261	Hunt, W. - Univ. of Alaska Naske, C. Fairbanks, AK	Beaufort Sea, Chukchi Sea, and Bering Strait Baseline Ice Study	180
265	Shapiro, L. - Geophysical Inst. Nelson, R. Univ. of Alaska Fairbanks, AK	Development of Hardware and Procedures for <u>in situ</u> Measurement of Creep in Sea Ice	192
267	Belon, A. - Geophysical Inst. Univ. of Alaska Fairbanks, AK	Operation of an Alaskan Facility for Applications of Remote-sensing Data to OCS Studies	242
289	Royer, T. - Inst. of Marine Science Univ. of Alaska Fairbanks, AK	Circulation and Water Masses in the Gulf of Alaska	270
347	Wise, J. - Arctic Environmental Information & Data Center Anchorage, AK	Marine Climatology of the Gulf of Alaska, the Bering and Beaufort Seas	379

<u>RU #</u>	<u>PI - Agency</u>	<u>Title</u>	<u>Page</u>
347	Wise, J. - AEIDC Univ. of Alaska Anchorage, AK Brower, W. - NOAA/EDS National Climatic Center Asheville, NC	Climatic Atlas of the Outer Continental Shelf Waters and Coastal Regions of Alaska	393
367	Reynolds, R. - Pacific Marine Walter, B. Environmental Lab Seattle, WA	Near-shore Meteorology	406
*407	Lewellen, R. - Arctic Research Littleton, CO	A Study of Beaufort Sea Coastal Erosion Northern Alaska	491
435	Leendertse, J. - The Rand Corp. Santa Monica, CA	The Modeling of Tides and Circulations of the Bering Sea	529
519	Carsey, F. - Polar Research Center Univ. of Washington Seattle, WA	Coastal Meteorology of the Alaskan Arctic Coast	538
541	Coachman, L. - Dept. of Ocean- Aagaard, K. ography Univ. of Washington Seattle, WA Charnell, R. Pacific Marine Schumacher, J. Environmental Lab Muench, R. Seattle, WA	Norton Sound/Chukchi Sea Oceanographic Processes (N-COP)	579

* indicates final report

ANNUAL REPORT

Contract Number: 03-5-022-55

Research Unit Number: 250

Reporting Period: April 1, 1976 to March 31, 1977

Number of Pages: 40

MECHANICS OF ORIGIN OF PRESSURE RIDGES, SHEAR RIDGES
AND HUMMOCK FIELDS IN LANDFAST ICE

Lewis H. Shapiro
Howard F. Bates
William D. Harrison

Geophysical Institute
University of Alaska
Fairbanks, Alaska 99701

March 31, 1977

I. Summary

This report summarizes the results of three studies in progress under this project. The first of these involves the formation of ridges along the shore at Barrow in the late Spring of 1975 and 1976. These events were studied in both years and the following conclusions can be drawn:

1. The initial failure of the ice at the start of the ridging process was predominately by buckling with a subsequent tendency to over-riding.

2. Failure of the ice in compression was observed in both years at a site where the ice was driven on shore against a vertical bank. In 1975 this took the form of extension fracturing with expansion of the ice into an adjacent ice free area. In 1976, no ice free area was present and failure occurred by shear fracturing along planes dipping at about 30° to the surface of the ice sheet.

3. The distribution of the areas of most intense deformation was the same in both years, emphasizing the repeatability of the process.

4. In both years, little or no differential movement occurred between the landfast ice sheet and grounded ridges and blocks of multi-year ice within it. This suggests that the notion of anchoring of the fast ice by such features requires further study.

5. While the compressive strength of sea ice near the melting point (as it was when these events occurred) is lower than that of colder ice, the ice may be capable of transmitting greater forces against a structure when warm than cold. This is because of the increase in ductility associated with increasing temperatures. Cold ice is brittle and failure in bending can be induced at low compressive stress by forcing the ice to bend out-of-plane. In contrast, ice near its melting point bends readily without losing coherence, and continues to transmit horizontal loads until compressive failure occurs.

The second study is based upon observations of vibrations of ice sheets, with amplitudes of a few centimeters and periods of about 10 minutes, in apparent association with increasing stress levels in the ice. Theoretical work is in progress in which the ice-water system is being modeled as an elastic plate on an elastic foundation. The model provides two solutions for which the system is resonant; the higher frequency is of the order of 10 seconds, and the lower of 10 minutes for a particular value of ice-water coupling. However, further work is required to demonstrate the applicability of the model. In addition, the partition of wave energy between ice and water, is also being examined, as is the generation of wave energy during ridging. This is a possible energy sink and thus should be included in models of the ridging process.

Finally, a bathymetry survey of the coast near Barrow was done during the past year, and the results are presented below. The distribution of gouges in the sea floor was studied, and a change in the density of these at a depth of 30 feet was identified. In addition, gouges were found to depths of 120 feet, the limit of the survey.

II. INTRODUCTION

A. General Nature and Scope of Study

The goal of this project is to develop an understanding of the forces and mechanisms involved in the formation of pressure ridges, shear ridges and hummock fields in the near shore zone, and the environmental parameters which cause these features to occur in particular areas. When these results are available, it may prove possible to develop procedures through which average and worst possible occurrences of heavily deformed ice at various localities can be predicted.

The problem of the formation of pressure ridges in drifting pack ice has been treated by Parmerter and Coon (1972, 1973) and this provides a useful starting point for the study of grounded ridges. However, the processes by which ridging occurs in shallow water are different in many respects from those which operate in the open sea. Ridging in pack ice normally occurs at the boundary between the thin ice in refrozen leads and the thicker pack. In the nearshore zone, however, thin ice is usually absent (except for the initial stage of ridging at the edge of the landfast ice, when thin ice may be present over the flaw lead) so that the heavy ice of the pack and landfast ice sheet are directly involved in ridging. Ridging may thus occur at the pack ice-landfast ice boundary, at the shoreline, or at stress concentrations within the landfast ice sheet itself.

The problem of determining the mechanisms and forces involved in the growth of grounded ridges is difficult because of the general lack of field observations upon which to base an analysis of the process. One objective of this project is to contribute towards filling these

data gaps. However, it is important to have as many "working hypotheses" as possible in mind when doing field work, because these serve to indicate the variables which should be measured in the field. Accordingly, simple, semi-quantitative analyses of processes which may operate during ridging are being studied. The input for these is the available data so that there is constant "feedback" between theory and observation as the study progresses.

The final product of this study is partly dependent upon the results of other projects relating to the occurrence of ridges in the landfast ice off the coast of Alaska. When this information becomes available, so that the degree of repeatability of ridging in different areas can be estimated, then the knowledge of mechanisms will be applied to attempt to develop the predictive capability noted above.

B. Specific Objectives

The objectives of this project are:

- (1) To develop an understanding of the environmental parameters which localize pressure ridges, shear ridges (and related shear zones) and hummock fields within the landfast ice zone of the Arctic Coast.
- (2) To gather field data regarding the mechanisms by which these structures form.
- (3) To prepare a semi-quantitative model of the processes involved in the formation of these features, in order to test the validity of the concepts developed in (1) and (2) above.
- (4) To use these results to develop a procedure for estimating average and worst possible occurrences of heavily deformed ice

within the landfast ice zone in terms of environmental parameters (such as water depth, bottom configuration, shoreline geography), ice thickness, and prevailing and unusual meteorological events.

C. Relevance to Problems of Petroleum Development

Within or along the margins of the landfast ice sheet, ridges mark the sites at which stresses in the ice reach their maximum values. It can reasonably be expected that early drilling offshore from the barrier islands along the Arctic coast will occur within the area seasonally covered by landfast ice. Siting of drilling platforms to avoid potential ridging sites where possible, or to compensate for the higher forces through design changes, thus depends upon a capability to predict the severity of the deformation to be expected at any point.

Given a sufficiently long period of observation, it is probable that such predictions could be made on a statistical basis. However, it is unlikely that adequate data will be available to use this procedure prior to the start of offshore development in the Beaufort Sea shelf. Therefore, it is necessary to approach the problem through the development of an understanding of the mechanisms involved in the ridging process and the parameters which cause these to operate. The results of these studies, in combination with a lesser amount of data on occurrences of ridging, may then permit reliable predictions to be made even in the absence of long-term continuous observations.

As lines of intense deformation, ridges and hummock zones act as energy sinks in that they absorb the motion imparted to the ice by the driving forces of wind and currents. Further, once grounded they may tend to anchor the landfast ice sheet thus retarding its motion. Both of these aspects have the potential to be used to protect a properly sited offshore structure, provided again that the location and intensity of ridging is reasonably predictable.

Finally, grounded floes of any size can serve as stress concentrations around which ridges can form. It is reasonable to expect that an offshore structure, whether a drilling platform, pier, gravel island or ice island, will have the same effect. It is therefore important to understand the mechanisms and force levels associated with ridging as an aid in the design of such structures.

III. CURRENT STATE OF KNOWLEDGE

The problem of the origin and growth of pressure ridges in drifting pack ice has been treated in the model of Parmeter and Coon (1972, 1973), but no similar analysis has been done for ridging in the near shore zone. Descriptions of grounded ridges, and some possible mechanisms of origin, have been given by Kovacs (1971), Kovacs and Mellor (1974), Shapiro (1975a,b), Weeks and Kovacs (1970) and Weeks et al. (1971). In addition, Allen (1970), Bruun and Johannesson (1971) and Zubov (1943) have considered the related problem of ice piling in shallow water or against an obstruction.

At present it is possible to identify at least some of the energy sinks in the ridging process and, as shown below, this provides the

basis for preliminary estimates of the required forces. However, in order for these estimates to be refined, there is a need for much more data regarding:

- (1) Cross-sections of grounded ridges and hummock fields.
- (2) Size distribution of the rubble pile.
- (3) Extent of gouging of the sea floor associated with the ridging process.
- (4) Mechanism by which ice is added to the ridge. That is, is the advancing pack ice edge driven directly into the rubble pile, up over it, or at some angle in between?
- (5) Relationship between the relative angle of approach of the ice on opposite sides of a growing ridge to the final form of the ridge.

There is also a need to develop ideas on how the energy lost in frictional work resulting from grinding and rolling between blocks in the growing rubble pile is to be determined.

Finally, there has been no analysis done of the simple kinematics of the ridging process through which the important parameters and additional energy sinks might be identified.

IV. STUDY AREA

The site of most of the field work will be the Naval Arctic Research Laboratory at Barrow, where the University of Alaska sea-ice radar system is located. This system is operated at ranges of three or six miles and provides continuous data on the drift vector of the ice in the near shore area. It is hoped that a sufficient number of ridging events will be observed in these areas over the duration of the program to fill

some of the data gaps noted above. Additional work may also be done at other locations if warranted.

V. SOURCES, METHODS AND RATIONALE OF DATA COLLECTION

Data for this project will come from field work and study of the information from the radar system. This will include mapping, profiling and sampling of typical shear and pressure ridges within the radar field-of-view to determine the geometry and internal structure of these features. The distribution of ridges, their time of formation, and the direction and velocity of the pack ice at those times will be mapped from a combination of air photos and radar data. Finally, field measurements will be made of the thickness of the ice involved in the ridges, and the size and shape of blocks, for information regarding failure mechanisms of the ice which operated during the ridging process.

VI. RESULTS

Little progress has been made on field study of winter ridges to date. This is due to the unusual ice conditions at Barrow in the summer of 1975, during which the landfast ice never went out. Instead, numerous pans of multi-year ice, which formed a significant part of the landfast ice emplaced in the fall of 1974, remained in the area throughout the summer. Shortly after freeze-up in 1975, these moved slightly forming low ridges along their margins. However, because of the presence of these, no new ice was driven into shallow water, so that no new pressure ridges were formed during the winter of 1975-1976.

A similar scarcity of new ridges exists again this year, but one shear ridge was observed to form on the radar data, and field study of this feature is planned.

In June, 1976, the ice was driven onto the beach at Barrow forming a line of ridges similar to those formed in 1975. Field study of these features was conducted, and the results combined, with those from 1975, are summarized below. Study of these features has proved to be valuable because the proximity of the ridges to the beach provides easy access and the absence of snow cover permits details of the structure to be observed. Further, in both years ridges formed within the field-of-view of both the radar system and on 8 mm motion picture camera which produced time-lapse pictures of the process.

During the movement of the ice onto the beach in July, 1975, a bubbler tide gauge recorded apparent vibrations of the ice for several hours prior to the movement. The fact that the ice was actually vibrating was verified by study of the 8 mm time-lapse motion pictures. The implication is that the vibration is related to increasing stress levels in the ice sheet. Since that time other examples of similar vibrations associated with increasing stresses have been observed and measured and a study of this phenomena has been initiated. A report of progress to date is included below. It should be noted also that in considering this problem, a question arose regarding wave motion as an energy sink in the ridging process. This possibility is also under study.

A. Formation of Beach Ridges at Barrow, 1975, 1976

1. Introduction

In the early stages of the break-up of the landfast ice sheet at Barrow in 1975 and 1976, the ice sheet was driven ashore forming a discontinuous line of beach ice piles along the coast. These piles can be regarded as pressure ridges grounded in water depths of 2 m or less and as such, provide a means of studying the formation of these features. A variety of observational systems were available to record the sequence of events in the ridge forming episodes, as well as the movements and deformation of the near shore ice during the same time period. As a result, it has been possible to prepare a rather complete description of the event, and this forms the bulk of this report. Subsequent work will deal with specific aspects of the deformational process.

2. Data Sources

A brief mention of the data sources from which the following discussion is drawn is needed to indicate the scope of observations.

a. Most of the movements of the ice sheet were monitored by the University of Alaska sea ice radar system located at the Naval Arctic Research Laboratory. This is a 3 cm x-band, standard ships radar mounted on a tower about 12 m above sea level with which the position and movement of natural reflectors on the ice are monitored. Data are recorded photographically by a 35 mm camera which photographs the radar screen every 2 1/2 - 3 minutes. The radar was operated at ranges of 5.6 km (3 nautical miles) and 2.8 km (1.5 nautical miles) during the events described here.

b. An 8 mm motion picture camera, equipped with a timer so that a picture was taken every 2 1/2 minutes, was mounted on the radar tower. The field of view of the camera is quite narrow, but in both years ridging occurred directly in front of the radar site, and these episodes were recorded.

c. Imagery from both the LANDSAT and NOAA weather satellite systems which show ice conditions on a regional scale, are available for both years.

d. Vertical air photos were acquired just after the start of the movements in 1975. In addition, observational flights were made in both years during which 35 mm photographs were acquired.

e. One of the authors was present on the site during the event each year, and several man days of field work were devoted to field study.

f. In 1975, measurements of ice thickness and temperature were made daily until a week prior to the movement of the ice sheet. In addition, a bubbler tide gauge was operated under the ice sheet until it was destroyed during the movement.

g. Finally, weather data is available from the National Weather Service and from the NOAA clean air sampling station 2 miles east of NARL.

3. Initial Conditions

In both years, the ice had melted back from the beach forming a shore lead several meters wide before any movement occurred. In 1975, melting had progressed sufficiently that the ice sheet was probably detached from the sea floor, although ice remnants were present along the water line as low, rounded masses. In addition, melting had removed approximately 60 cm from the ice sheet leaving a thickness of about 1 m. Based upon temperature measurements taken about one week before the movement occurred, it can be estimated that the ice sheet was close to melting temperature throughout its thickness.

Much less melting had occurred prior to the movements in 1976. Exact figures are not available, but it can be estimated that no more than 30 cm had been removed, leaving an average thickness of about 1.5 meters. Further, the ice sheet was not completely detached from the sea floor, as evidenced by the presence of about 30 cm of gravel frozen to the base of the ice

In addition, a thin (up to 20-30 cm) foot of ice several meters wide was probably present between the leading edge of the ice sheet and the shore.

No temperature measurements were made in the ice during 1976, so that accurate data are not available. However, freeze-back was observed to occur in a core-hole just prior to the movement indicating that the ice temperature was probably a few degrees below the freezing point.

In both 1975 and 1976, the movement occurred under the influence of winds associated with a low pressure system passing north of Alaska which generated winds from the southwest in the Barrow area. Satellite imagery indicates that the pack ice was tightly compressed with little open water for hundreds of kilometers to the west and northwest of Barrow, while open water was present to the northeast of Point Barrow in both years. The absence of open water to the northwest was confirmed by visual inspection during local flights, and the presence in the pack ice of numerous newly formed pressure ridges was noted in both years. Thus, it appears that the movements resulted from internal stresses in the pack which may have been generated over a distance of up to a few hundred kilometers, as opposed to the local wind field.

4. Timing and Duration of Movements

The movement of the ice sheet in both years, consisted of sporadic bursts of activity with durations of from 5 to 30 minutes, separated by periods of quiet. In 1975, as an example, the initial movement opposite NARL occurred on the evening of July 4, and consisted of a shoreward translation of the ice sheet which lasted about 5 minutes, during which the shore lead closed. Subsequently, the ridges along the beach were built in a 1/2 hour sequence of almost continuous advance of the ice. This was followed by two periods of minor movement, each lasting about 5

minutes, at 2 hour intervals. No further movement of the ice occurred along the beach in this area, although the ice did advance up the beach to the northeast, without the formation of ridges, later on July 5th.

Following this episode, the ice along the beach remained stationary. However, the deformation of the fast ice sheet continued sporadically for the next four days in the form of ridging and rotation of segments of the sheet along fractures.

By the conclusion of the movement episode, the ridge bounding the edge of the fast ice had been segmented and translated up to 250 m shoreward. Assuming an average thickness of 1 m for the ice sheet, this implies that 250 m^3 of ice per meter along the beach was deformed into ridges (less, of course, the initial width of the shore lead).

In contrast to the above, the movements in 1976 were far less extensive. The initial movements occurred on June 22 and 23, when the ice was driven onto the beach all along the shore from almost 1 mile southwest of the radar site, to at least 4 miles to the northeast. Then, on June 25th ridges formed at two locations. The first was just in front of the radar site, and the second was opposite the NARL airport. In addition, some over-riding did occur along the beach in the same areas where ridges were observed to form in 1975. The total movement was probably not greater than 25 meters. Unfortunately, the radar system was not operating when these movements occurred and no observers were present so that accurate measurements could not be obtained.

Finally, on June 28, a series of movements occurred over a time period of about 6 hours. These, too, were not monitored by the radar system, although the 8 mm motion picture camera recorded additional growth of the ridge immediately in front of the radar site. In addition, observations were made during much of this time all along the beach. In one instance it was possible to approximately time the duration and velocity of the ice advance over one

short episode. This lasted about 5 minutes, during which the ice moved at a rate of .3m/min. Other similar examples of short episodes were also observed, but in no case did these exceed a few minutes in duration. This marked the end of the series of events during 1976.

5. Distribution and Form of the Ridges

The distribution of the ridges along the beach was almost identical in both years, with the exception of a single ridge which formed opposite the NARL airport in 1976, where none was present in 1975. In general, the area of most intense deformation extended from just southwest of the NARL airport to almost one mile southwest of the mouth of Salt Lagoon. Outside of this area, the ice was driven onto the beach, but no ridges formed, with the exception noted above.

Within this area, ridging and/or overthrusting of the incoming ice was continuous along the beach, with local topographic highs separated by lower ridges. The features formed during the 1975 event had the appearance of true pressure ridges, with a rubble core over which the incoming ice sheet had been thrust. The core itself was resting on an unbroken sheet of ice which had been thrust onto the beach in the initial stages of the movement. A typical cross-section, representative of the topographic highs is given in schematic form in Figure 1. Note that the dips of the slopes indicated were consistent for most of the ridges.

In 1976, however, the rubble cores were generally absent, and the movements in most cases consisted of simple overthrusting of the incoming ice. Exceptions to this were confined to the ridges at the radar site and opposite the airport.

In summary, the most striking feature of the comparison is the similarity in the distribution of areas of intense deformation in both years. The configuration and orientation of the coast are similar for some distance in both

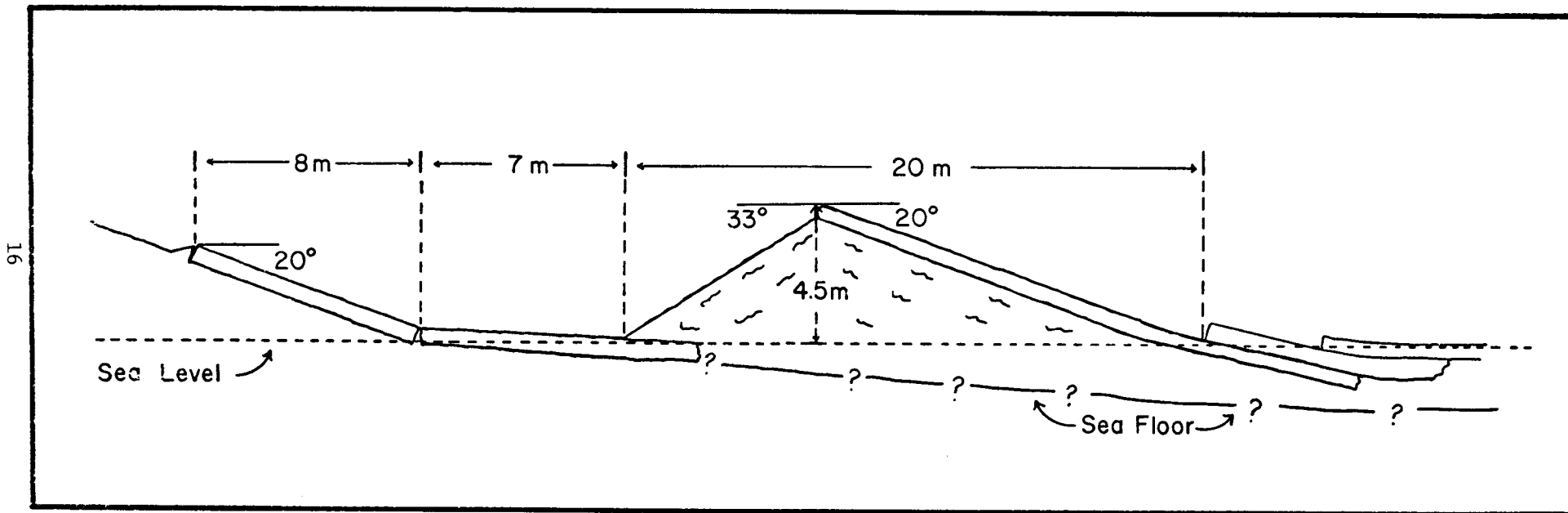


Figure 1. Cross-section of typical beach ice ridge.

directions from the limits of this area, so that these factors can possibly be eliminated from consideration as possible causes for this limitation. Differences in water depth or bottom profiles close to shore may be a factor, but no information is available yet on this possibility.

6. Mechanism of Formation of the Ridges

Information regarding the process of formation of the ridges in 1975 is derived from study of the 8 mm motion picture film acquired by the camera mounted at the radar site and by direct observation. Comparison of the form of this ridge with those at other localities indicates that the observations apply to these as well.

As noted, the initial movement consisted of an advance of the ice sheet several meters up the beach. After this movement stopped, a noticeable bulge appeared in the ice sheet several meters offshore, and a crack appeared at the synclinal bend of the bulge nearest to shore. Note that this crack did not exist prior to the start of the movement. The crack was obvious on the film because the ice on its offshore side was raised and tended to overthrust the onshore side. With continued advance of the ice, thrusting, and overturning occurred along this line forming the start of the rubble core of the ridge. Subsequently, the ice sheet was driven up the offshore side of the ridge, over the top of the rubble. As noted from Figure 1, the dip of this slope was about 20° and subsequent examination showed that few fractures were extended through the ice sheet, although numerous cracks were probably present along the base of the sheet where tensile stresses were greatest.

At the crest of the pile, the dip of the ice sheet flattened, and numerous cracks were present. The first formed of these were parallel to the edge of the ice sheet, and were spaced about 1 m apart, approximately equal to the

thickness of the ice. Subsequently, a second set of fractures with similar spacing formed at right angles to the first set, terminating against these. The result was therefore, the fracture of the ice sheet into roughly cubical blocks which fell forward as the leading edge of the ice was driven over the core. Piling of these thus widened the ridge, so that, in effect, the ice sheet was advancing over a debris pile derived from its leading edge. Clearly, much of the displacement was taken up in this manner.

It is of interest that the ice sheet maintained its integrity while bending through an angle of 20° up the rubble pile, then flattening again. This ability of the ice sheet to flex through relatively large angles without losing coherence was also noted in other areas, and is of importance in evaluating potential hazards to structures as discussed below.

As noted, during 1976 few ridges developed, with most of the deformation along shore taking the form of overthrusting. However, at two localities, processes similar to those above were observed to occur.

The first of these was located adjacent to NARL. At 0800 local time, on June 28, a buckle was observed in the ice parallel to, and 20 m from the shore. Its total length was about 50 meters. At that time, the amplitude was about 1 m, and a crack was present along the crest of the fold. The wavelength was about 15 m, and the buckled area was bounded by cracks normal to the shore. By 0900, the displacement exceeded 1.5 m. At approximately 1000 hours, while a field party was at the site, the ice began to move onshore. The rate .3 m/min given above was measured on the ice just north of the crack normal to shore at this time. South of the crack, however, the ice did not advance on shore, but, instead, the arch continued to rise, until it became unstable and collapsed.

The second example occurred at the radar site. The ridge at that locality moved sporadically throughout the morning of June 28. In one instance, the ice sheet offshore from the ridge was suddenly elevated by about .3 meters in a few moments while one of the field party was coring the ice sheet within a few meters of the ridge. Audible cracking occurred throughout the ridge at that time, and several blocks were dislodged and fell forward.

Later in the day, at the same site, the ice sheet clearly buckled, with three distinct, identifiable crests marked by fractures, and the intervening troughs depressed below sea level. The leading edge of the ice sheet (i.e., the line of contact of the ice sheet and the offshore side of the ridge) was still above sea level, in the approximate position to which it had moved earlier as described above. The first nodal point offshore was a crest so that the buckle was real, and not simple warping associated with bending as might have been the case if the first node were a trough. The amplitude of the crest decreased rapidly, from about 1.5 m at the first crest, .5 at the second, and a few centimeters at the third. The wavelength was approximately 15 m, similar to that of the buckle at the first site described above.

In both of these cases, the preferred failure mode of the ice was by buckling, as was indicated to have occurred in 1975. The difference in style of deformation between the continuous ridges of 1975 and the predominantly overthrust ice sheets of 1976 may have been the result of the greater thickness and strength of the ice in 1976, combined with the generally slower rates of movement during that year.

7. Deformation of the Ice Sheet

Deformation of the fast ice sheet taken as a unit was markedly different between the two years. This undoubtedly reflects the difference in the magni-

tudes of the displacements and the properties of the ice. In 1975, the ice sheet was extensively fractured and new ridges were formed at several localities. The most noticeable fractures formed a set at a spacing of about 1/2 km oriented approximately normal to the shoreline and extending offshore for up to 300-400 meters where they terminated against a line of new pressure ridges. The sense of shear across these fractures was left-lateral, with the south side thrust further up the beach than the north. However, this is exactly the reverse of the sense of rotation of the offshore boundary of the fast ice sheet which would have been expected to produce right-lateral shear across fractures normal to the shoreline. This paradox may be explained by considering deflection of the stress trajectories across internal boundaries within the fast ice, such as pressure ridges or shear zones, many of which did form. However, the analysis of the data is not sufficiently advanced to permit this possibility to be examined.

Between the first line of new ridges and the boundary ridge of the fast ice, fracturing was extensive, although no data are available from which the trends of these could be mapped.

In contrast, fracturing during the 1976 event was restricted to less than 100 meters from the shoreline, and, possibly to the same distance from the bounding ridge. The line of the ridge was apparently unchanged during the movement suggesting that the entire ice sheet moved as a unit.

During both years, numerous blocks of multi-year ice were grounded with the fast ice, and it is of interest to consider the effect of the displacement upon these. In 1975, new pressure ridges were formed around several such blocks grounded in a water depth of about 5 meters, approximately 200 meters offshore opposite the radar site. It could not be determined whether or not these blocks moved prior to the development of the ridges. Further offshore, however, movement of the blocks did occur. In particular, one block 10-15 m in diameter and with 3 meters of freeboard in about 10 meters

of water depth, was observed in the 8 mm film to translate through a distance of at least 200 m before moving out of the field of view of the camera. Unfortunately, ice conditions prevented the field party from visiting the sites of other blocks to examine the degree, (if any) of differential motion between the multi-year blocks and the remainder of the ice sheet.

In 1976, however, one such block was visited after about 15 meters of movement of the ice sheet had occurred. The dimensions of the block and water depth at the site of this block were similar to that described above. The block was examined particularly for evidence of rotation, tilting, or fracturing which would indicate differential motion between the block and the ice sheet during the movement. This would be expected if the block were grounded and the keel and sediments of the sea floor were sufficiently strong to resist the motion. However, no evidence of differential motion was observed. Instead, the block appeared to have displaced smoothly with the remainder of the ice sheet. Further, during a survey flight over the area a search was made for fracturing around other blocks, and none were observed. However, this is clearly not the preferred method of searching for such cracks, and the possibility exists that they were present and not recognized. Still, the available data suggests that, in most cases, the blocks were free to move at the same rate as the ice sheet, though their size and the water depth clearly indicate that they were grounded.

Similarly, the bounding pressure ridge of the fast ice sheet was displaced shoreward in 1976 with no evidence of segmentation or differential motion. In 1975, however, some evidence of differential motion was observed, but most of the deformation involved segments of the ridge displaced as discrete units.

The descriptions above raise questions about the effectiveness of grounded ice masses in anchoring the fast ice and preventing its movement.

The interaction of the ice sheet with the beach proper and with ridges along the beach was studied for information regarding failure mechanisms of the ice sheet. Examples of possible failure in buckling were described above and, in addition, two cases of compressive failure were also observed, one in each year. Both occurred just southwest of the mouth of Salt Lagoon, where the beach is less than 5 m wide, and ends against a vertical, ice-cored bank 2 m high. In 1975, prior to the movement, a small ice-free area was present at the mouth of the lagoon. When the ice moved ashore and was driven against the vertical bank, compressive stresses normal to the shoreline developed. The absence of lateral confining stresses resulting from the presence of the ice-free area, permitted expansion of the ice in that direction. The geometry of the interaction thus placed the ice sheet locally in a state of uniaxial compression. Failure occurred by the formation of extension fractures parallel to the compressive stress direction, with expansion of the ice into the ice free area.

In 1976, no ice-free area had formed at the time the movement occurred. Thus, when the ice was driven against the vertical bank, no lateral expansion was possible, and failure occurred at the bank as shear fractures at about 30° to the ice surface.

8. Discussion and conclusions

a. The observations described above regarding the initial conditions prior to the events of both years, the similarity of weather conditions, and of the distribution of areas of intense deformation all tend to confirm the hypothesis of repeatability, and to a degree predictability, of ridge occurrences. Some randomness due to the character and state of the ice at the time

of the movements must, of necessity, be present, but the major processes and products of the event appear to recur regularly.

b. The ridging process proper is initiated by buckling of the ice, followed by overthrusting. However, it cannot be confirmed as yet that bending stresses are not involved. If these are present, then they would tend to decrease the forces involved.

c. The movements tend to occur in sporadic bursts of a few minutes, separated by periods of no movement. This suggests a process of build-up of stresses sufficient to cause failure of the ice and initiation of motion. The combination of failure and movement then permits the stress to relax, and a period of quiet ensues while the stress rises back to a level sufficient to cause further movement.

d. During the 1975 event, a pressure ridge formed along a line marked by several grounded blocks of multi-year ice about 200 m offshore. This was the only positive example of differential motion between the ice sheet and apparently grounded blocks or ridges within or on its boundaries. This observation introduces uncertainty into the hypothesis that landfast ice is anchored by grounded ridges.

e. Evidence of failure of the ice in compression was observed in both years at a site where the ice was driven against a vertical, ice-cored bank. In one case, failure was by extension, and in the other by shear. Based upon compressive strength test results, the minimum stress required to cause extension failure under these conditions is about 2.8 MPa, and a higher value can be expected for the case of shear fracturing.

f. It is of interest to consider the possibility that ice near the melting point may, under field conditions, be capable of transmitting greater

force to a structure than colder, stronger ice. When cold, the ice is brittle and tends to fail readily in bending at low compressive stresses when under the influence of relatively small, out-of-plane movements. However, with increasing temperature, the ductility of the ice increases, so that even large out-of-plane displacements do not cause loss of coherence. This was illustrated by the extreme bending of the ice sheet over a rubble pile described above. Thus, the cases of compressive failure noted occurred even though the ice sheet was bent sufficiently to conform to the shape of the beach prior to impact with the bank. It can be assumed that if the movement had occurred when the ice was cold, failure in bending would have been initiated before the bank was reached.

B. Vibration of Ice Sheets

This study is based upon a series of observations of vibrations of landfast and drifting ice sheets which appear to be associated with rising stress levels in the ice. This phenomena was first observed in July, 1975, when the landfast ice sheet was driven ashore at Barrow forming the ridges described elsewhere in this report. For several hours prior to the movement of the ice, a bubble tide gauge operating on the sea floor under the ice recorded vibrations of the ice sheet with amplitudes of a few centimeters and an apparent period of about ten minutes. That the ice was indeed vibrating was independently verified by examination of 8 mm time-lapse motion pictures of the ice taken at the time. The tide gauge record indicates an increase in the amplitude of the vibration until the bubbler was destroyed by the movement of the ice.

Direct measurements of rising stress levels in the ice sheet, associated with vibrations with the above period were made at Barrow in April 1976. In that example, sinusoidally varying stresses superimposed on a rising stress curve were recorded by an array of stress transducers embedded in the ice approximately 100 meters from a tide gauge installation. At that time the tide gauge, (also a bubbler gauge, resting on the sea floor) was indicating vibrations in phase with those on the stress transducers emphasizing the correspondence between the two events.

An array of stress transducers installed north of the barrier islands in the Prudhoe Bay area during the spring of 1976 also recorded similar events (R. D. Nelson, Pers. Comm), although these are unsupported by tide gauge records.

Finally, numerous examples of vibration of drifting ice sheets as a precursor to movement have been recorded by the University of Alaska sea ice

radar system at Barrow. Unfortunately, frequency information cannot be extracted from these data in a simple manner.

Based upon the above, it is reasonable to assume that at least some cases of vibration of floating ice sheets with periods of the order of ten minutes are associated with rising stress levels in the ice. If verified and understood, observations of vibrations may prove to be a simple and efficient method of predicting high stress levels in the ice around off-shore structures. The present work is directed toward that end.

Observations

The data shown were taken by a bubbler-type tide gauge placed on the sea bottom at the edge of the fast ice at Point Barrow. Approximately 42 hours of data have been digitized: The amplitude was sampled every 2.3 minutes. These data were Fourier analyzed to obtain the frequency power spectrum for each group of samples. The period of the maximum resolvable frequency is twice the sampling period or 4.6 minutes, so periods below 4.6 minutes will not be detectable in the data.

The data were analyzed in two groups of sets. In one group each set consisted of 64 points, covering 148 minutes. A spectrum was computed for each set of 64 points that overlapped the previous set by 32 points. Thus, each spectrum contains data included in each adjacent spectrum, thereby forming a sort of 'spectral running average'. Figure 2 shows these spectra for the last 12 hours of data that were obtained before the fast ice moved.

The second group consisted of successive sets of 32 points. These spectra therefore did not overlap. Figure 3 shows these spectra for the last 12 hours of data.

Figures 2 and 3 show that, in this instance, the ice did indeed increase in vibration amplitude over a several hour period before it moved onto

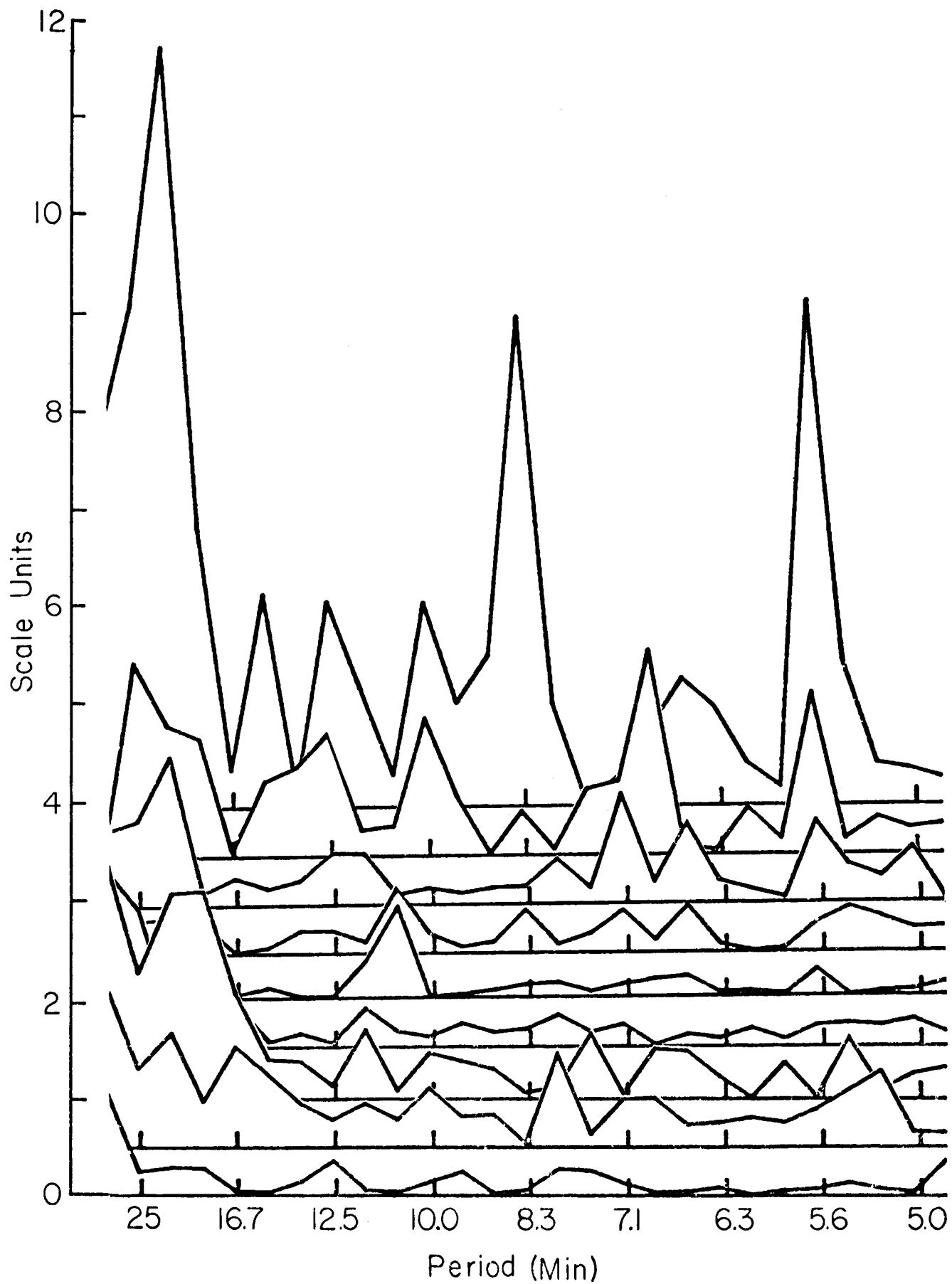


Figure 2. Spectrum of overlapping data sets.
See text for discussion.

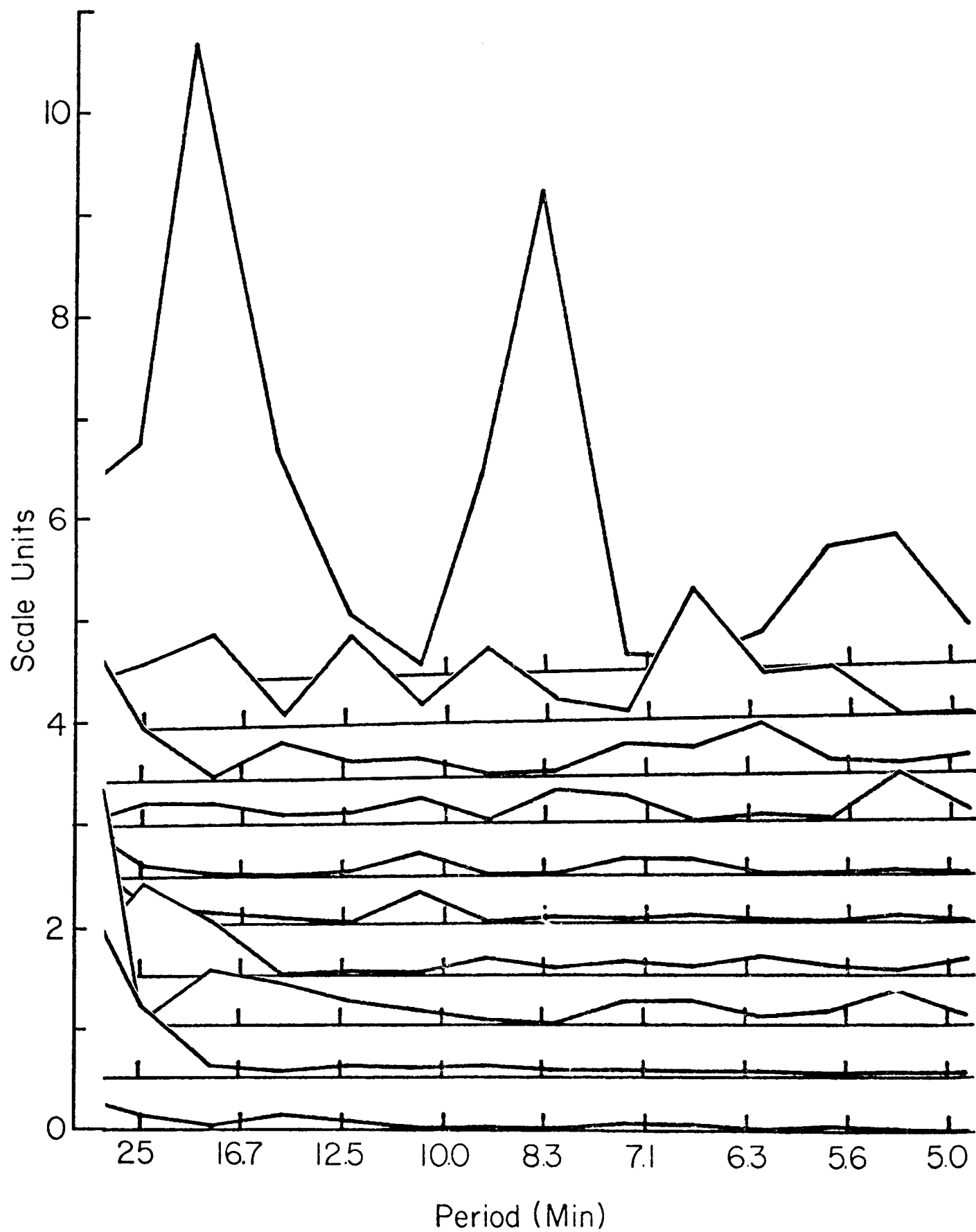


Figure 3. Spectrum of successive data sets.
See text for discussion.

the beach. The vibration had three strong spectral lines with periods ranging from 5 and 20 minutes. One puzzling aspect is that the three strongest spectral lines that appear seem to be harmonically related. That the lines are well defined indicates that only a few relatively high-Q vibration modes were excited, suggesting that resonances in the ice-sea system are involved. The possible existence of such resonances is examined in the remainder of this section of the report.

III. VIBRATION MODEL

The following is a speculative discussion of why we believe the two events to be related. It is emphasized that much of the basic physics involved has yet to be done in the detail needed to prove some of the following statements; however preliminary computations suggest that the notions put forth are reasonable.

An ice sheet can be represented as an elastic plate floating on an incompressible fluid. A plate of finite thickness is capable of both longitudinal and transverse vibrations, in contrast to a membrane which vibrates only transversely. In this report, however, we deal only with transverse vibrations because the observed motion was transverse. For an elastic plate, the equation of motion is (Skudrzyk, 1968):

$$D \Delta^4 w + \rho_i h \frac{\partial^2 w}{\partial t^2} = q. \quad (1)$$

$$D = \frac{E h^3}{12(1 - \nu^2)}.$$

w vertical displacement.

E Young's modulus.

h plate thickness.

ν Poisson's ratio.

q vertical loading force per unit plate area.

ρ_i density of ice.

The vertical loading force strongly affects the motion of the plate. The fluid upon which the plate floats exerts a bouyant force (a force proportional to displacement) upon the vibrating plate. It seems possible that this bouyant force consists of constant and variable components; the constant component is just balanced by the weight of the plate, so only the variable component needs to be included in the loading force term.

A second component of the loading term is the tension of the plate. The wind blowing across a sheet of ice grounded on the downwind edge will couple a compressive force laterally across the sheet that varies as the square of the wind speed. This compressive force acts to load the plate vertically just as does tension in a string or a membrane: As in the use of a string or membrane, the vertical loading due to tension is proportional to the second spatial derivative of the displacement.

Finally, there may be a coupling force due to the momentum of the fluid and the friction in the plate. At present we do not know how to specify these forces. Further study is needed.

One possible way to view the floating ice sheet is as an elastic plate on an elastic foundation. In that case the loading forces would include a Hooke's Law (buoyant) restoring force proportional to the displacement and, if one axis is aligned in the direction of the tension, a one-dimensional tension force:

$$q = -p_0 w - S_x \frac{\partial^2 w}{\partial \mu^2} \quad (2)$$

P_0 pressure per unit displacement.

S_x Tension stress constant.

If the displacement is assumed to be sinusoidal, four real solutions to (1) can be found, two with positive and two with negative arguments.

The development above takes into account only partly the fluid upon which the plate floats. The actual pressure upon the vibrating plate is in general unknown because it depends upon the wave motion in the water as well as in the ice. To actually solve the problem requires that the equations of motion of the ice and of the water be solved simultaneously--a considerable task.

However, insight into the problem can be obtained by examining the problem assuming that the waves in the ice are driven by the waves in the water. It is assumed first that the ice-sea system can be approximated by the elastic plate on an elastic foundation model. Since this is a forced vibration problem, the maximum response of the ice will occur when the natural vibrations in the two media propagate identically; that is, when mechanical resonance occurs for the plate-fluid system. In that event, at the resonant frequencies the waves in the plate and the fluid will have identical phase velocities. Nearly all of the energy in the plate-fluid system flows in the water wave for meter-thick plates floating in water tens of meters deep (see below). Thus, it seems reasonable to assume that the plate does not significantly change the phase velocity of waves from that in water with a free surface. We therefore assume that the solutions to (1) and (2) are of the form

$$w = w_0 \sin \omega \left(t - \frac{x}{v} \right) . \quad (3)$$

where the phase velocity v is that for water waves in water that is shallow compared to the wavelength:

$$v = \sqrt{gd} . \quad (4)$$

g acceleration of gravity.

d depth of water.

ω angular frequency.

Substituting (3) and (4) into (1) and (2) yields the following dispersion relation:

$$\frac{D}{g^2 d^2} \omega^4 - \left\{ \frac{g d \rho_{ih} - S_x}{g d} \right\}^2 + p_o = 0 \quad (5)$$

the two positive engenvalues of (5) are approximately

$$\omega_1 = \sqrt{\frac{p_o}{\rho_{ih} v}}, \quad \omega_u = v^2 \sqrt{\frac{\rho_{ih}}{D}} \quad (6)$$

For values of P_o of the order of ten parts per million of the head represented by the wave height, the lowest resonant frequency is in the neighborhood of ten cycles per hour. While this eigenvalue is in the range of observed vibration frequencies, whether the analysis is correct needs study. The basic question is: Can the ice-sea coupling term be represented by a Hooke's Law force? Alternatively, we can ask: Can the ice-sea system be represented by the elastic plate on an elastic foundation model? Finally does friction in the ice need to be included?

The energy in the ice-sea system is confined almost exclusively to the water. This is shown as follows: The energy in a water wave of amplitude w_o has been shown to be [p370, Lamb (1945)]

$$E_w = 5.0 \times 10^3 w_o^2 \text{ Jm}^{-2} \quad (7)$$

For example a wave 10 cm peak-to-peak has an energy per square meter of surface area of about 13 Joules.

The energy in an ice sheet primarily consists of three components:

(1) Kinetic energy due to vertical speed, (2) Potential energy due to

elastic bending, and (3) Potential energy due to vertical displacement in a gravity field. When the displacement is zero, the vertical speed is greatest, and the potential energy is zero. Thus, the total energy flowing in the ice equals the maximum kinetic energy:

$$E_i = \frac{\rho_i h}{2} \left(\frac{\partial w}{\partial t} \right)^2 \quad w = 0 \quad . \quad (8)$$

Using (3) and evaluation the constants, (8) becomes for 1 m thick ice and wave periods of the order of 10 minutes:

$$E_i = 5.0 \times 10^{-2} w_o^2 J_m^{-2} \quad . \quad (9)$$

The ratio of energy in the water to that in the ice is therefore

$$E_w/E_i = 10^5 \quad . \quad (10)$$

Thus, the only ten parts per million of the total energy in the system flows in the ice.

This result immediately suggests that the effect of the ice on the water waves at system resonance is negligible. Hence the assumption that the phase velocity in the water remains unchanged appears to be a good one. Furthermore the energy that causes the ice to vibrate must travel primarily in the water rather than in the ice. The coupling term can therefore be interpreted as the energy fed from the water into the ice that is needed to overcome viscosity and other losses in the ice.

It must be emphasized that even though so little energy in the wave motion propagates in the ice, the energy is initially couples to the sea from the wind by the ice, probably through the ridging process. One way of viewing the process is to consider that each building ridge acts as an

impulsive source to the ice-sea system, which in turn acts as a band-pass filter. The response of such a system would be a spectral line at each resonant frequency--in this case two lines corresponding to the two position eigenvalues.

IV. CONCLUSION

The ice should vibrate when a strong on-shore wind laterally compresses the sheet. This same compressional force will tend to break loose the fast shore ice and drive the ice ashore when winds are high enough during proper melting conditions. In fact the waves themselves may act to loosen the fast ice from the sea bottom by mechanically lifting the ice and by causing a pumping action on the water under the fast ice.

Whether the movement of the ice can be predicted by monitoring the vibration of the ice is as yet unknown. The data from one of the events studied suggest that such predictions are possible; however more observations are needed before any technique can be proposed.

The two solutions to the lossless case studied above suggest that two entirely different modes are possible: (1) The higher frequency mode depends primarily upon the stiffness of the plate, and (2) the lower frequency mode depends almost entirely upon the membrane characteristics of the plate. The presence of one line or the other may be of importance: That is, the sudden change from the high frequency mode (periods of the order of 10 sec) to the low frequency mode might indicate that a fundamental change in the ice sheet had occurred.

The basic conclusion of this study is that further work--both experimental and theoretical--needs to be done. Experimentally, more wave measurements made during quiet and stormy periods, and during the annual ice movement onto the beach are needed. Theoretically, the equation of motion of the system needs to be determined and solutions obtained.

C. Bathymetric Survey of the Barrow Area

During September, 1976 a bathymetric survey was conducted within the field of view of the University of Alaska sea ice radar system at Barrow, in order to provide data for interpretation of ridging patterns. A continuous recording fathometer was installed for this purpose in the R.V. Natchick, operated by the Naval Arctic Research Laboratory, and the position of the ship during the survey was monitored by the radar system. Track lines are shown in Figure 4, and the resulting bathymetric map in Figure 5.

The records acquired during the survey were examined by E. Riemnitz of the U. S. Geological Survey, who pointed out that numerous gouges in the sea floor were visible on the data (Figure 6). Accordingly, we attempted to determine the distribution of gouges with water depth in the survey area.

The number of gouges which penetrated more than 1 foot into the sea floor were identified and counted by selected intervals of water depth. The length of ship track over each depth interval was identified, and an average number of gouges per nautical mile of track was calculated for each such interval. A plot of the results is given in Figure 7.

A total of 32.7 nautical miles of track was covered during the survey, and most legs were run at a high angle to the coast. Thus, the counts are probably biased toward gouges which are oriented parallel to the coast. Note also that the relatively high number of gouges in the 95-99 foot depth interval largely reflects counts in one small area, and may not be representative of the average. However, gouges were found in depths to 120 feet, the limit to which the survey was extended.

The sea floor was sufficiently rough that it was difficult to establish an accurate datum from which to measure the depth of penetration of the gouges.

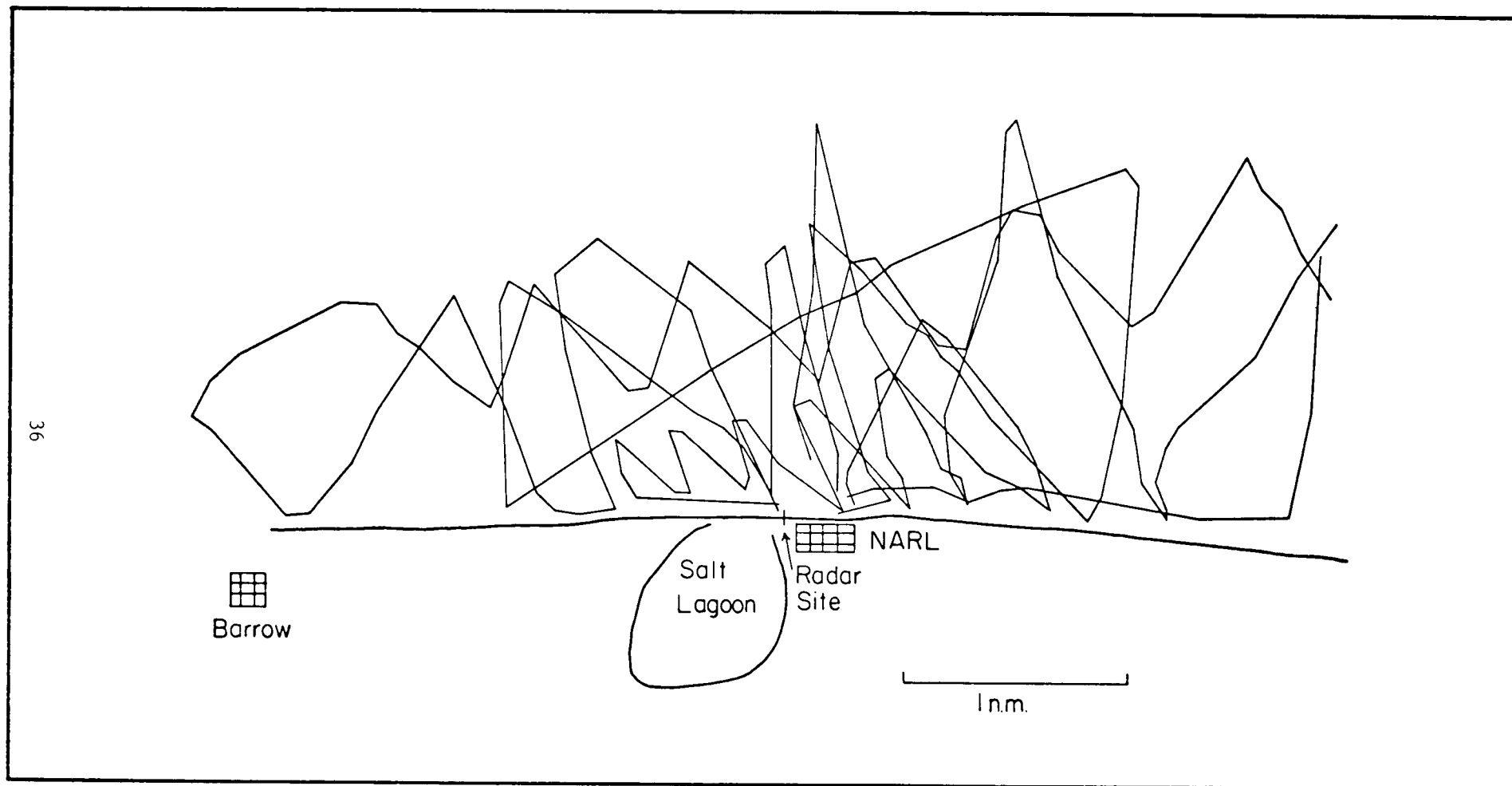


Figure 4. Track lines.

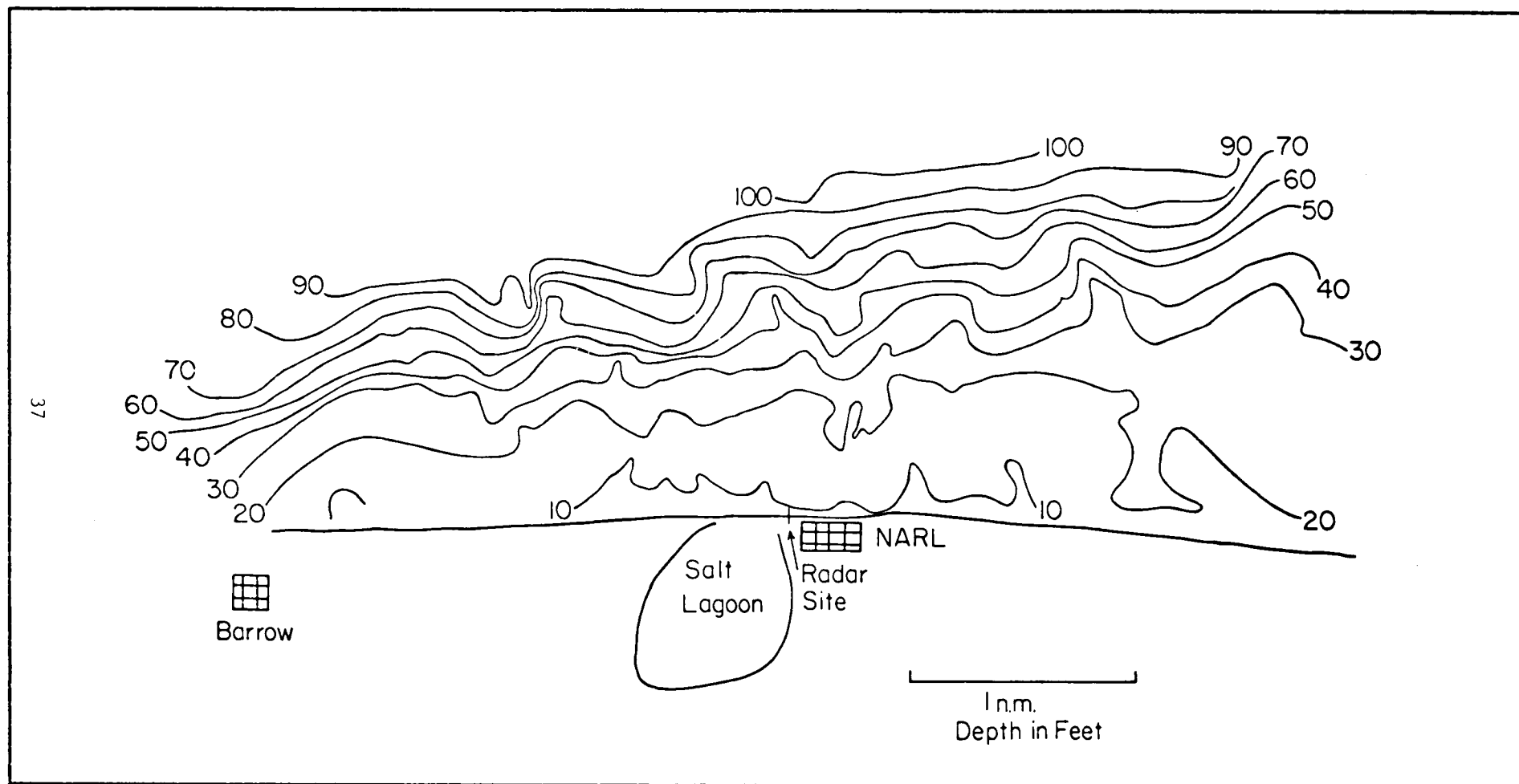
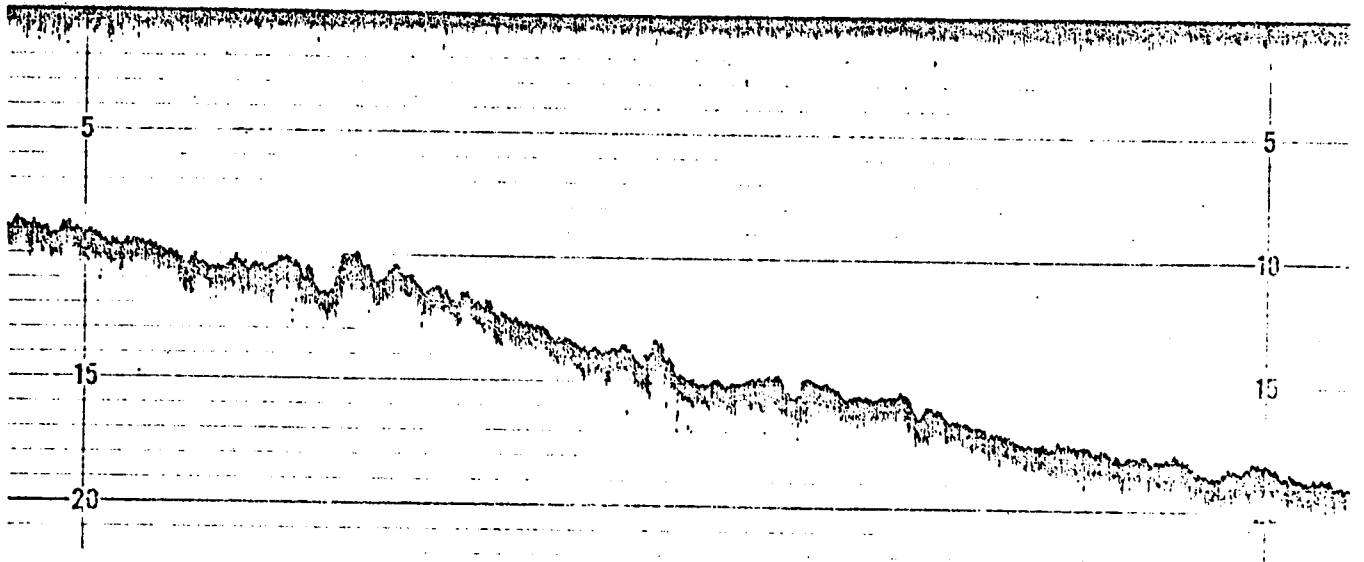
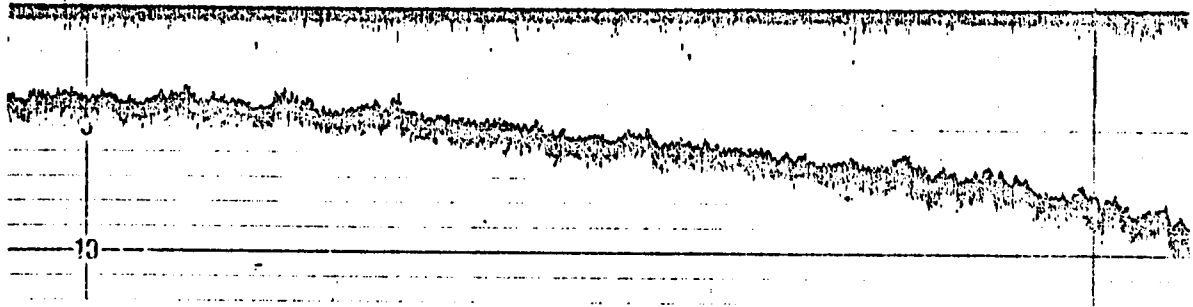
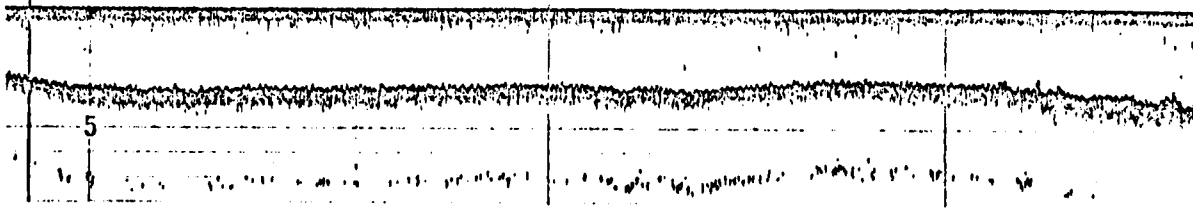


Figure 5. Bathymetry of the Barrow area.



1/4 n.m.
Depths in Fathoms

Figure 6. Sample of data.

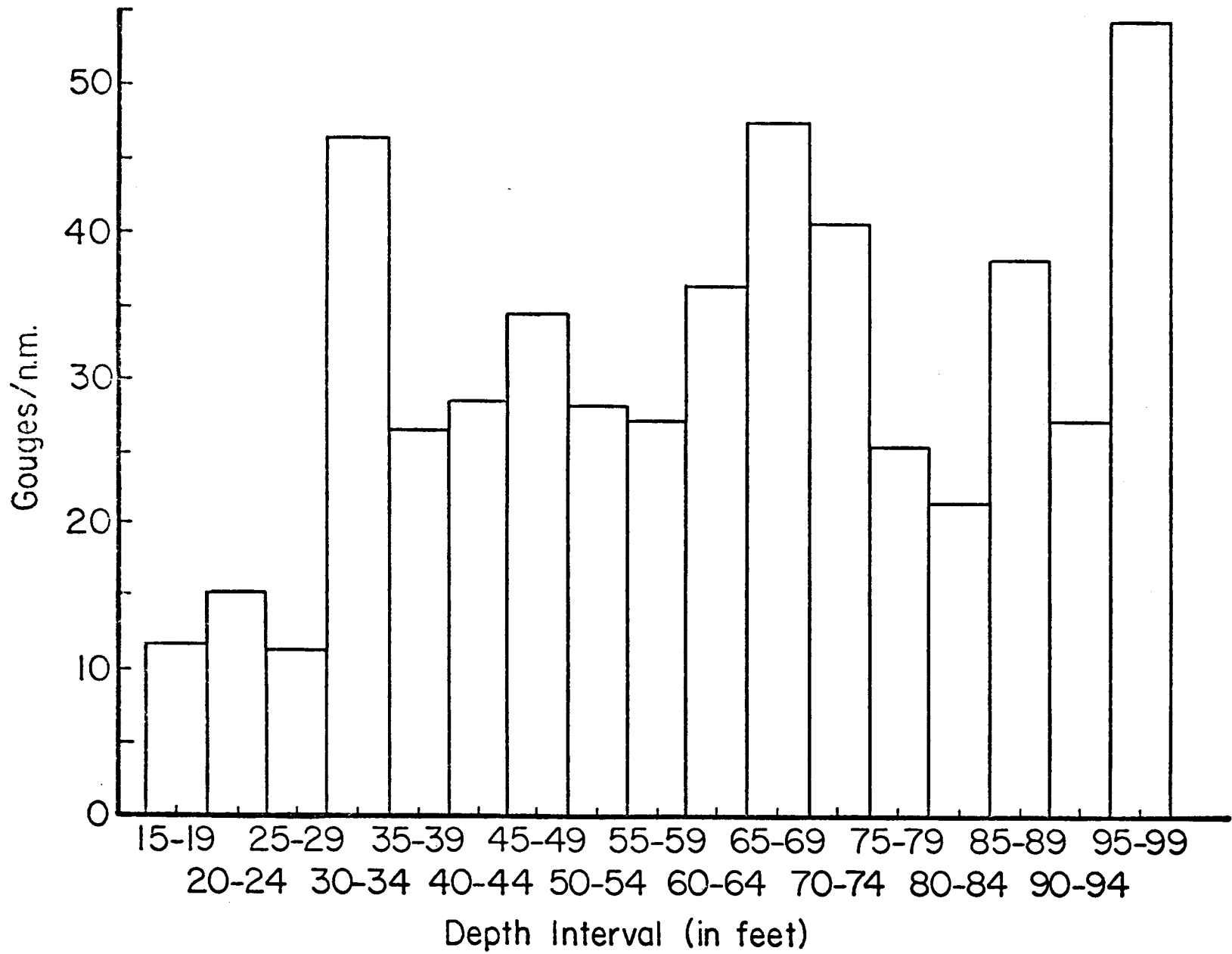


Figure 7. Distribution of gouge density with water depth.

However, it appears that most were in the range of 2-5 feet. The maximum penetration observed was 9 feet.

Based upon the data shown, the change in gouge density across the 30 foot depth contour appears to be real, but the question of the significance of variations in the remainder of the data requires further study.

REFERENCES CITED

- Allen, J. L., 1970, Analysis of forces in a pile-up of ice, in Ice Engineering and Avalanche Forecasting and Control, Proc. Calgary Conf., 1969, Nat'l. Res. Council of Canada, Comm. on Geotech. Res., Tech. Mem. 98, p. 49-56.
- Kovacs, A., 1971, On pressured sea ice, in Sea Ice, Prof. of an Int'l Conf., Reykjavik, Iceland, May 1971, p. 276-298.
- Kovacs, A. and M. Mellor, 1974, Sea ice morphology and ice as a geologic agent in the southern Beaufort Sea, in The Coast and Shelf of the Beaufort Sea, ed. J. C. Reed and J. E. Sater, AINA, p. 113-161.
- Lamb, H., 1945, Hydrodynamics, 6th. ed., Dover Publications, New York, 738 pp.
- Parmeter, R. R. and M.D. Coon, 1972, A model of pressure ridge formation in sea ice, J. Geophys. Res., 77, 6565-6575.
- Parmeter, R. R. and M. D. Coon, 1973, Mechanical models of ridging in the Arctic sea ice cover, AIDJEX Bull. 19, 59-112.
- Shapiro, L. H., 1975a, A preliminary study of the formation of landfast ice at Barrow, Alaska, winter 1973-74, U. of Alaska Geo. Inst. Report UAG R-235.
- Shapiro, L. H., 1975b, A preliminary study of ridging in landfast ice at Barrow, Alaska, using radar data, Proc. 3rd. Int'l. Conf. on Port and Ocean Engineering under Arctic Conditions, Fairbanks, Alaska, August 1975 (in press).
- Skudrzyk, E., 1968, Simple and Complex Vibratory Systems: Penn. State Univ. Press, College Park, Penn, 514 pp.
- Weeks, W. F. and A. Kovacs, 1970, On pressure ridges, USA CRREL draft contract report to the U.S. Coast Guard, 60 pp.
- Weeks, W. F., A. Kovacs and W. D. Hibler III, 1971, Pressure ridge characteristics in the Arctic coastal environment, Proc. 1st Int'l. Conf. on Port and Ocean Eng. under Arctic Conditions, Trondheim, Norway, p. 152-183.
- Zubov, N. N., 1943, Arctic Ice, Izdatel'stro Glavesevmorputi, Moscow (Trans. AD426972, NTIS, Springfield, Va.) 491 p.

ANNUAL REPORT

Contract #03-5-022-55
Research Unit - 257
Reporting Period: 1 April 1976 -
31 March 1977

Number of Pages: 108
Additional Maps: 28

Morphology of Beaufort, Chukchi and Bering Seas Near
Shore Ice Conditions by Means of Satellite and Aerial
Remote Sensing

Principal Investigator

William J. Stringer
Geophysical Institute
University of Alaska

Assisted By

Stephen A. Barrett
Nita Balvin
Diane Thomson

I. Summary of Objectives, Conclusions and Implications with Respect to OCS Oil and Gas Development

The objective of this research unit is to develop a morphology of near shore ice along the Beaufort, Chukchi and Bering coasts of Alaska, and identify those features which may represent hazards imposed by ice conditions on OCS oil and gas development.

The general conclusion is that near shore sea ice behavioral patterns are similar from year to year thereby yielding some predictability in terms of offshore sea ice hazards to oil and gas development.

The implications are that geographical zones of different design and construction criteria can be established in the offshore areas taking into consideration the probability of damage to the structure by adverse ice conditions and the relative risk imposed to the adjacent ecosystems.

II. Introduction

A. General Nature and Scope of Study. The overall objective of this study is to develop a comprehensive morphology of near shore ice conditions along the ice-frequented portions of the Beaufort, Ckukchi and Bering Sea coasts of Alaska.

B. Specific Objectives. Specifically, this comprehensive morphology will include a synoptic picture of the development and extent of fast ice, the construction and location of pressure and shear ridges, the location and persistence of grounded ice features including ice islands, stamuki, ridges and hummock fields and the interrelationships among these phenomena.

C. Relevance to Problems of Petroleum Development. The relevance of this project to petroleum development should be considered in terms of the three main phases of petroleum-related activities: Exploration, development and extraction. Each phase has particular ice-related problems.

1. Exploration. This work, mainly by seismic crews is being carried out currently in the Beaufort Sea --- mainly from fast ice. This reasearch unit has already acted in an advisory role with an oil firm sending seismic crews out on the fast ice. The chief problem here is the relative stability of the ice and the safety of the crews and equipment. Through compilation of persistence values for near shore ice and determination of the relationship of those persistence values to grounded ice features and other factors responsible for ice stability, predictive methods will be developed to determine ice safety in specific areas at specific times.
2. Development. During this phase of petroleum-related activities, permanent structures are constructed for drilling of permanent wells and extraction facilities. Collector pipelines are laid and other permanent facilities are constructed. The considerations involved in the placement of these structures include the probability of ice piling around and upon man-made islands, ridge keel gouging of pipelines and also the effect of the facility

on the morphology of near shore ice and this in turn on the quality and nature of habitats.

The information provided by this research unit will obviously yield information about ice piling and the probability of gouging. Through the development of a morphology of near shore ice including the dynamics of ice behavior near natural obstructions to ice motions, we hope to provide descriptive models of the impact of the creation of man-made islands on the morphology of near shore ice. This can then in turn be related to impact on near shore habitats.

3. Production. This phase of petroleum-related activities would take place over a span of many years. Within this period the greatest environmental problem would be the danger of an oil spill which would become incorporated into the ice. This research unit, through analysis of the fate and trajectories which would be taken by site specific spills will provide information concerning the favorable location of production facilities and anticipate the techniques which may be required to deal with specific spills through prediction of the ice behavior to be anticipated in the location of the spill.

III. Current State of Knowledge

With the exception of site-specific studies performed by other investigators, this report represents the state of knowledge of the coastal-wide morphology of the near shore ice conditions outlined in section II.B. above.

IV. Study Area

The area under study by this research unit is the near-shore coastal zone (to depths of 100-meters) of the Beaufort, Chukchi and Bering Seas.

V. Sources, Methods and Rationale of Data Collection

The chief source of data used by this research unit is Landsat imagery. The reasons for this are that Landsat is highly repetitive and

produces a relatively high resolution map-quality product. Other data used include NOAA satellite imagery, side-looking radar imagery and aerial photography.

Side-looking radar imagery would be utilized a great deal more if it were obtained during the winter period when Landsat imagery is not available and if quality control were performed.

The rationale of the data collection technique is to be able to map near shore ice conditions on a comprehensive basis as often as possible.

VI. Results

In order to reduce the information contained on the individual near shore sea ice condition maps made of each Landsat image to a form which can be utilized by regional planners and other disciplinary studies, the following composite maps have been compiled.

A. Chukchi Sea

1. Contiguous Ice Edge Maps

- a. Yearly Ice Edge Maps: For each year a single map is produced showing the edge of contiguous ice for each useful Landsat cycle. Hence, the map for 1976 shows the edge at four different times during the 1975-76 ice season.
- b. Seasonal Ice Edge Maps: The ice year has been broken into seasonal groupings; late winter, mid-spring and late spring and the ice edges most nearly representing each season for each year drawn. As a result the late winter ice map contains data for each year.
- c. Seasonal Average Ice Edge Maps: Each seasonal map is reduced to a solid line representing seasonal mean ice edge and two dotted lines indicating average observed variations about the mean.

- d. Seasonal Migration of the Average Ice Edge Map: The seasonal means from each of the three Seasonal Average Ice Edge Maps have been drawn together on one map to show the migrations of the edge of contiguous ice from season to season.

2. Ridge System Maps

- a. Yearly Ridge System Maps: All ridge systems identified on each year's maps are collected on one map for each year.
- b. Composite Ridge System Maps: This map shows all ridges observed in the Chukchi Sea to date.

3. Ice Morphology Map

Based on data from the maps described above, and other morphological information obtained from the Landsat-based sea ice maps, an annotated descriptive sea ice map of the Chukchi Sea has been compiled.

- B. Beaufort Sea

1. Contiguous Ice Edge Maps

- a. Yearly Ice Edge Maps: For each year a single map is produced showing the edge of contiguous ice for each Landsat cycle. (Note: The absence of late spring and summer data in these maps is discussed under "VII" Discussion".
- b. Seasonal Ice Edge Maps: The ice year has been broken into seasonal ice groupings; for the Beaufort Sea edge of contiguous ice only one map exists at this time --- that for late winter.

2. Ridge System Map

- a. Yearly Ridge System Maps: All ridge systems identified on each year's maps are collected on one map for each year.
- b. Composite Ridge System Map: This map shows all ridges observed in the Beaufort Sea to date.

3. Ice Morphology Map

Based on data from the maps described above and other morphological information obtained from the Landsat-based sea ice maps, an annotated descriptive sea ice map of the Beaufort Sea has been compiled.

C. Bering Sea

1. Contiguous Ice Edge Maps

- a. Yearly Ice Edge Maps. For each year a single map is produced showing the edge of contiguous ice for each Landsat cycle. (Not reproduced in this report because of lack of preparation time --- see map "C" under this heading for final result.)
- b. Seasonal Ice Edge Maps: The ice year has been broken into seasonal ice groupings; winter, late winter, early spring and mid to late spring. The average contiguous ice edge for each seasonal grouping is shown.

2. Ice Morphology Map

Based on data from the maps described above and other morphological data - including ridges - obtained from the Landsat-based sea ice maps, an annotated descriptive sea ice map of the Chukchi Sea has been compiled.

VII. Discussion

The careful reader of this report will note that analysis of ice conditions in the Chukchi Sea is more advanced than analysis of the Beaufort and Bering Sea ice although the Chukchi Sea work was started later. The reason for this is the several questions were raised about the formation of the near shore ice sheet during the early analysis of Beaufort Sea ice. Chiefly, these questions arose because by February, when the first Landsat imagery becomes available, the near shore ice sheet has already formed in the Beaufort Sea and the active edge of ice is usually well beyond any grounded ice structures. In the Chukchi Sea, although much grounded ice has already formed by February, the active edge of ice advances and retreats during this period. And, because of the highly varied Chukchi shoreline and bathymetric configuration as

well as the much more dynamic ice behavior, a wide range of conditions are exhibited there for analysis. Therefore, the Chukchi Sea ice conditions were analyzed in detail first.

Because of the general rather loose utilization of the term "fast-ice" or "shore fast-ice" we have had a strong inclination to not use the term. For that reason the term "contiguous ice" was invented. Contiguous ice has been used to identify ice which is contiguous or adjacent to the shore and continuous to the first identifiable break. At times in the Beaufort Sea - particularly early spring - contiguous ice can extend well beyond grounded ridges and indeed even beyond the area mapped in this study of near shore ice. For this reason there are few late winter and early spring maps showing the limit of contiguous ice --- it may have been beyond the area mapped.

Contiguous ice limit maps have not been made for late spring and summer in the Beaufort Sea because melting adjacent to the shore breaks continuity of the ice. Still, large expanses of ice - presumably held in place by grounded ridges - remain stationary offshore even until mid-July. During the next quarter we intend to produce maps recording this phenomena.

VIII. Conclusions

The conclusions to date arrived at by this project are summarized by the annotated "Ice Morphology Maps" for the Beaufort, Bering and Chukchi Sea areas. However, some rather general comments can be made which although contained on these maps should be emphasized.

The Beaufort Sea coast is generally ice bound from November until July. Many large grounded features responsible for anchoring near shore ice are formed early in the ice year (November - December). Occasionally large lead systems generally parallel to the coast develop and through freezing and reclosing with shearing motion build large massive shear and pressure ridge systems --- generally offshore from the earlier, well-grounded systems. These latter ridge systems are either not grounded at all or are only poorly grounded. As mentioned earlier, occasionally no motion in ice off the Beaufort coast takes place for long periods of time. During those periods contiguous ice can extend seaward over a hundred kilometers.

During this period, offshore seismic exploration has been performed by oil firms operating from the Prudhoe Bay area. To date they have apparently confined their activities to ice within the barrier of grounded ice. However, this barrier appears to be much stronger in some areas than others. At least once, a shearing event occurred which resulted in fracturing of contiguous ice within this zone just shoreward of a portion of the grounded ice barrier which has consistently given evidence of being poorly grounded. Our conclusion is that some of these exploration activities are being performed in hazardous areas.

The Beaufort Sea Ice Morphology Map shows a broad zone offshore where ridging takes place. Inshore of this zone is an extensive area of well-protected relatively smooth ice located over shallow water. Major sea ice hazards have not occurred within this zone during the period of observation of this study. The ridging zone extends well beyond the 10-fathom isobath and the stable edge of contiguous ice. Inshore from the

edge of contiguous ice conditions are also reasonably stable but the area is obviously the site of ice piling and shearing events. Beyond the average edge of contiguous ice major shearing events can take place at any time during the ice year.

One word of caution should be said about all these conclusions: They are based on observations since the winter of 1973 and it is likely that the conditions observed do not represent a good statistical sampling of Beaufort Sea ice conditions. For instance, during this period of observation the melt season weather conditions have been reasonably mild. Near shore ice has broken up and melted in place. Grounded ridge systems have slowly broken contact with the sea floor and drifted away. We have not had the opportunity to access the potential hazard created if a major storm were to occur during this period when great quantities of highly mobile ice are present in the near shore areas.

The Chukchi Sea Ice Morphology Map has a much different appearance than does the Beaufort Sea Map. One major reason for this is the opportunity for ice to move out of Bering Strait. All during the late winter and spring period, ice moving events take place along the Chukchi coast, often creating shear ridges along shoals jutting seaward from the string of capes and headlands which are so prominent along that coast. Increasingly as one travels to the south, the edge of contiguous ice between headlands is more poorly defined and the ice contained is more prone to seaward motion leaving areas of open water behind. In general, there is often a lead system extending the length of the coast from Barrow to Cape Lisburne.

Just south of Cape Lisburne and north of Point Hope is an area with a constantly reformed polynya. The persistence of this polynya has been documented as part of the summary of fourth quarter operations attached to this report.

South of Point Hope the effect of ice motion out Bering Strait is even more prominent. Another recurring polynya occurs just southeast of Point Hope formed by southward ice motion.

Kotzebue Sound is generally covered by stable ice during much of the ice year, but the presence of a zone of weak and often moving ice just seaward hints that this sheet of ice is probably potentially unstable.

At the southern end of the Chukchi Sea is Bering Strait. Just north of the Strait is a large system of shoals where large extensive shear ridges can be built during ice motion out the Strait.

Ice behavior along the Bering Sea coast is heavily influenced by the continuous presence of open water to the south and the increasingly greater tidal range as one travels from north to south. Off Nome is one of the few places where contiguous ice extends seaward of the 10-fathom isobath. This condition is probably the result of the presence of Sledge Island to the west. To the east, in Norton Sound, ice is almost constantly moving out of the Sound toward the Bering Sea. Within the Sound, contiguous ice is found in areas protected from this movement pattern. At the head of the Sound, Norton Bay is almost always covered with contiguous ice. At the entrance to the Bay there is almost always open water or new ice formed by the outward motion of ice from the Sound.

The broad Yukon Delta lies at the southern side of the mouth of Norton Sound. Shallow waters extend considerable distances in all directions. Occasionally ice motion out of Norton Sound creates shear ridges along the north side of the Delta.

To the south, contiguous ice is generally found on mud flats and shallow areas no deeper than two to three fathoms below mean lower low water.

Even further south, along the north coast of Bristol Bay, contiguous ice is found only in well-protected shallow areas. Presumably the great tides in this area are responsible for this phenomena. Bristol Bay is usually filled with new to late young ice. New ice is constantly being formed along the north side of the Bay and becoming thicker as it moves seaward. On one occasion very extensive shear ridges were observed to be created along the Alaska Peninsula coast of Bristol Bay by motion of the Bristol Bay ice.

IX. Needs For Further Study

The major effort of this project to date has been to map sea ice conditions using Landsat imagery as a main source of information. The resulting maps are to be used by this project as a means of developing a morphology of near shore sea ice conditions and are provided to other investigators as a source of information regarding sea ice conditions which may be of value to their work.

The main thrust of this research unit has been the mapping of sea ice hazards related to offshore petroleum exploration, development and production. Principally, this requirement is being met through statisti-

cal compilation of information regarding the edge of contiguous ice and location of pressure and shear ridges. Map products showing this information for entire coastal areas have been produced from the individual Landsat-derived maps.

Other investigators, on the other hand, seem to require other information which could also be derived from the individual Landsat maps. This other information includes:

1. Mapping of leads and the determination of persistence values for leads used as migration paths.
2. Mapping of polynyas and the determination of persistence values for polynyas used by aquatic animals.
3. Mapping of flooding in near shore areas and determination of statistical data for each flooding area.
4. Mapping of spring and summertime open water in near shore areas and determination of persistence values.

This information can be derived from the Landsat-based maps in a similar fashion to the hazard-related products. However, at this time, these subjects are not included in the work statement for this research unit, and because a significant quantity of time would be required to produce these secondary products we do not propose to prepare them unless instructed to do so.

Also, other hazard-related subjects have been brought to our attention which we do plan to address in the near future. Chief among these is the trajectory taken by an oil spill incorporated into the ice. Because of the quite different near shore ice morphologies in the Beaufort Sea, Chukchi Sea, Northern Bering and Southern Bering Sea area, these trajectory considerations will require site-specific analyses. This work would help fill one the "gaps" identified at the Beaufort Sea Synthesis meeting. (Gap #3 under "physical", page 13, Arctic Project Bulletin #13).

X. Summary of Fourth Quarter Operations

A. Ship or Laboratory Activities

1. Ship or field trip schedule - None
2. Scientific party - None
3. Methods: Sea ice maps prepared from Landsat imagery by overlaying 1:500,000 scale black and white Landsat print with acetate and tracing ice boundaries. The details of this method were described in earlier quarterly reports.
4. Sample localities - None
5. Data collected or analyzed: This quarter the 1975-1976 Beaufort Sea and Bering Sea near shore Landsat data was mapped from hardcopy band 7 imagery at 1:500,000 scale. Particular care, described in earlier reports, has been taken to locate ice features as well as the bathymetric 10-fathom isobath. Half-size (1:1 million scale) reproductions of these maps are reproduced as part of this section of the report as Appendix A.
6. Milestone Chart and data submission schedules (see next page). We have changed the completion date for completion of data products related to the previous year. There are two reasons for this: First, it now takes nearly four months to obtain Landsat data; second, we have found it highly advantageous to analyze an entire year's imagery at one time. Hence, in order to analyze the 1976 ice data for the Beaufort Sea, it was December before the data for July and August could be obtained. The resulting maps are included in this report. The Beaufort Sea summary maps will be featured in our next quarterly report.

B. Problems Encountered/Recommended Changes

We recommend that side-looking radar data of near shore ice conditions be obtained in the Beaufort Sea during November, December and January and that disciplinary scientists from this and other research units be on hand at Barrow to establish quality control, coverage and related parameters.

C. Estimate of Funds Expended

See Geophysical Institute Business Office Financial Report.

MILESTONE CHART

RU #: 257

PI: W. J. Stringer

Major Milestones: Reporting, data management and other significant contractual requirements; periods of field work; workshops; etc.

MAJOR MILESTONES	1976					1977											
	O	N	D	J	F	M	A	M	J	J	A	S	O	N	D		
Satellite data acquisition																	
Aircraft data acquisition																	
"Retroactive" ice maps (previous to funding)																	
"On schedule" ice maps of previous year																	
"Epoch" and "Special event" maps																	
Annual data product (summary of previous year's ice dynamics)																	

56

△ Planned Completion Date

▲ Actual Completion Date

APPENDIX A

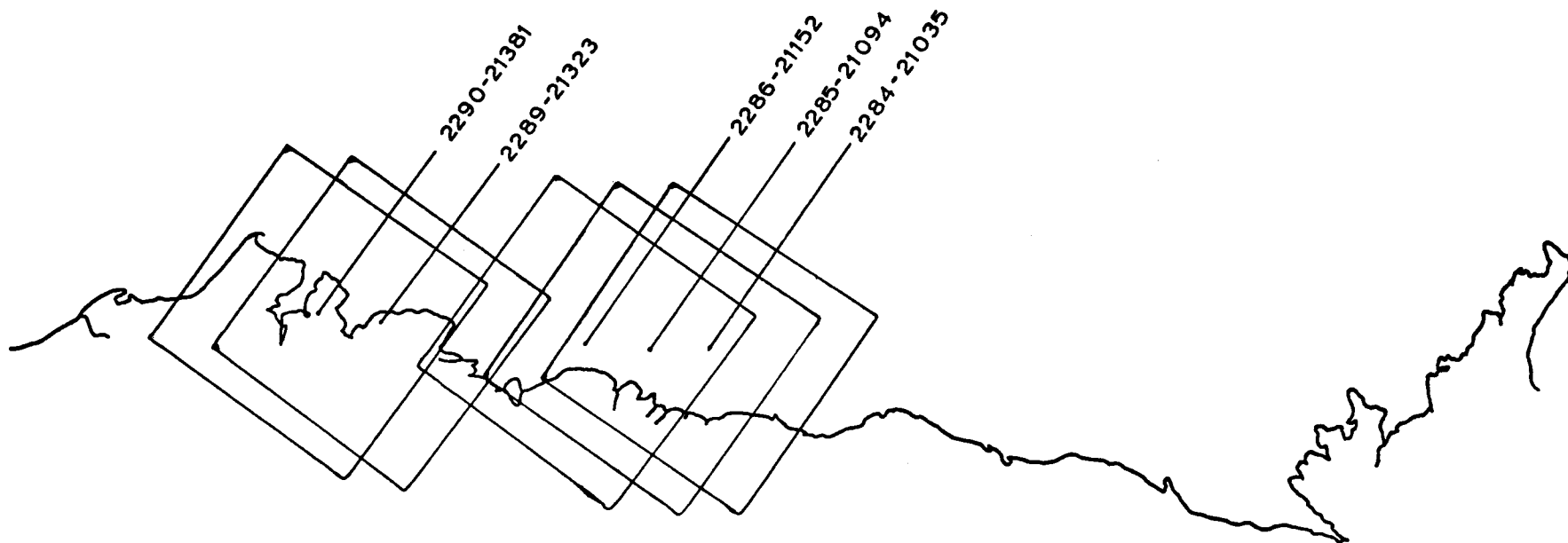
ICE SYMBOLS USED AND THEIR MEANING

Listed below are the symbols used to map near shore ice conditions from LANDSAT imagery. This list of symbols has evolved during the mapping project and reflects ice conditions which can be detected on LANDSAT imagery as well as those ice conditions considered important in the understanding of near shore ice dynamics.

A	River Overflow	Used to denote areas where river water has overflowed onto sea ice.
B	Boundary	Denotes boundary between what appears to be two different ice conditions even though the two ice conditions may not be differentiated by the definitions used.
Bn	Broken New Ice	Sheet of new ice which has been broken - usually into an irregular pattern.
Bpn	Broken Pans and New Ice	A sheet of young or first year ice is broken into pans followed by the freezing of the voids to the new ice stage, followed by the breaking of this entire matrix. Several cycles of this process may be evident, but the most recently-formed ice has developed to the new ice stage.
Bpy	Broken Pans and Young Ice	A sheet of young or first year ice is broken into pans followed by the freezing of the voids to the young ice stage followed by the breaking of this entire matrix. Several cycles of this process may be evident, but the most recently-formed ice has developed to the young ice stage.
By	Broken Young Ice	Sheet of young ice which has been broken - usually into an irregular pattern.
C	Contiguous Ice	Ice stationary and continuous from shore without apparent fractures. This ice is at the time of observation fast with respect to the shore. The symbol is placed within large expanses of such ice and along the landward side of the seaward edge of such ice. Contiguous ice is not necessarily bounded on the seaward edge by grounded ice and can therefore extend seaward considerable distances.
Cf	Fractured Contiguous Ice	Contiguous ice which although not separated from shore by an open lead, is fractured by leads - often perpendicular to the shore.

D	Decayed Ice	Rotting or decaying ice, characterized by a dark mottled effect indicating holes and puddling.
F	Floe	Separately identifiable ice floe. Symbol used to denote floes distinctly visible against background even when completely frozen into surrounding ice.
Fw	Floes in Water	Open water with numerous floes of various sizes (see "Up").
Fy	First Year Ice	Ice cover of age and thickness beyond "young" stage. Used principally to denote large expanses of ice in either contiguous or off-shore category. May be composed of single sheet, many pans frozen together, or many pans compressed and frozen together. Thickness on the order of 30-70 cm.
Fyb	First Year Broken	A broken or fragmented expanse of first year ice.
G	Grounded	Ice which clearly appears to be grounded.
H	Hummock Field	Large expanses of piled ice.
I	Young Ice	Ice appearing light grey on LANDSAT imagery. Can be single sheet or exhibit a variety of conditions (broken, compressed, rafted, etc.). Thickness of the order of 10-30 cm.
L	Lead	A lead, usually open, but may be so narrow that this can not be determined. Large leads denoted by two lines showing boundaries, narrow leads denoted by single line.
M	New Ice	Characterized by dark shade of grey, smooth texture, may exhibit a number of conditions (see I). Thickness on the order of 0-10 cm.
N	Newly Frozen Lead or Polyna	Either new or young ice. Symbol usually written within distinct boundary.
O	Old Frozen Lead	A lead with ice sufficiently old to have either turned light grey or be covered with snow.
P	Partly Frozen Lead	Partly frozen lead. Ice conditions not uniform (as distinct from M) and may vary from new ice to late stages of young ice.

Pn	Pans in Matrix of New Ice	A sheet of ice has broken into pans and the surrounding water has frozen to the new ice stage.
Py	Pans in Matrix of Young Ice	A sheet of ice has broken into pans and the surrounding water has frozen to the young ice stage.
R	Ridge	Denotes shear or pressure ridge or system of ridges.
S	Smooth Ice	Usually used to denote featureless ice of uncertain age in protected areas.
T	Tidal or Tension Cracks	Cracks in near shore ice opened by either tidal action or thermal tension. Identification may be indirect (snow drifts, drainage pattern, etc.).
Up	Unconsolidated Pack	A broken sheet of ice of any age beyond young ice which has been compressed to the point that open water voids are quite small but are not frozen over (see Fw).
W	Water	Open water - symbol often used to denote specific area enclosed by line.
Y	Polynya	More specific than W. Most often used to denote area of open water on lee side of obstruction.
Z	Zone of Shear	Symbol used to denote location of apparent shearing motion on image. The symbol may be specifically located on a lead where shearing motion is taking place, a closed lead where shear piling of ice is apparently occurring or in an ice field where characteristic pattern of leads caused by shearing forces can be seen.



BEAUFORT SEA

22 OCTOBER - 8 NOVEMBER
1975

IMAGES: 2273 - 2290

Figure 1

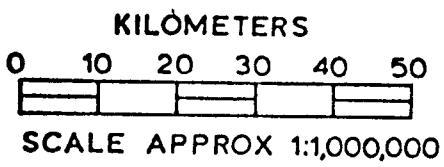
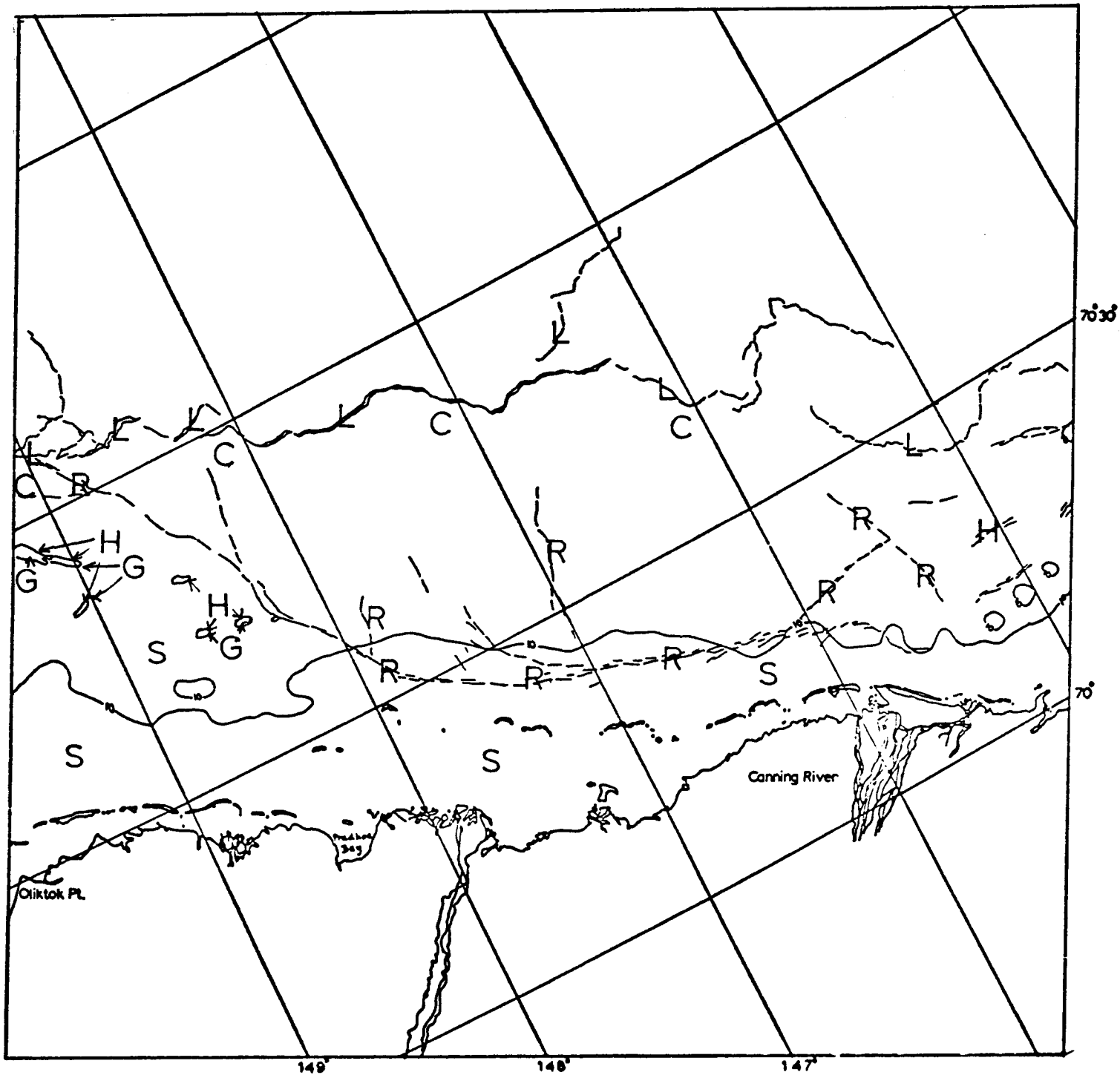
Scenes E2284-21035 through 2290-21381

These scenes from the second through the eighth of November, 1975 show the Beaufort coast of Alaska shortly after freeze-up. Of particular interest are the large grounded hummock fields offshore between Oliktok Point and Prudhoe Bay. These features were created during late winter, 1975 and remained in place during the 1975 melt season. At this time these grounded hummock fields are serving as anchor points for a large sheet of ice between their location and the coast. The grounded hummock fields were created as shear ridges at their present location sometime after March 6, 1975. The ice held in place by these grounded features extends considerably far seaward of the 10-fathom isobath. However, this configuration is not unusual in this vicinity and reoccurs yearly.

To the east, the boundary of contiguous ice is determined by a meandering lead system which is also located quite far seaward of the 10-fathom isobath. However, the apparent boundary of grounded ice is indicated by a large ridge system which angles shoreward - crossing the 10-fathom isobath off Cross Island and finally coinciding with the 10-fathom isobath off the mouth of the Canning River. This occurrence is also not unusual in this vicinity.

North of Oliktok Point it can be seen that the grounded hummock fields in that vicinity are located near shoals above the 10-fathom isobath and seaward extensions of the 10-fathom isobath. Landsat data for other years has also revealed grounded hummock fields in this vicinity.

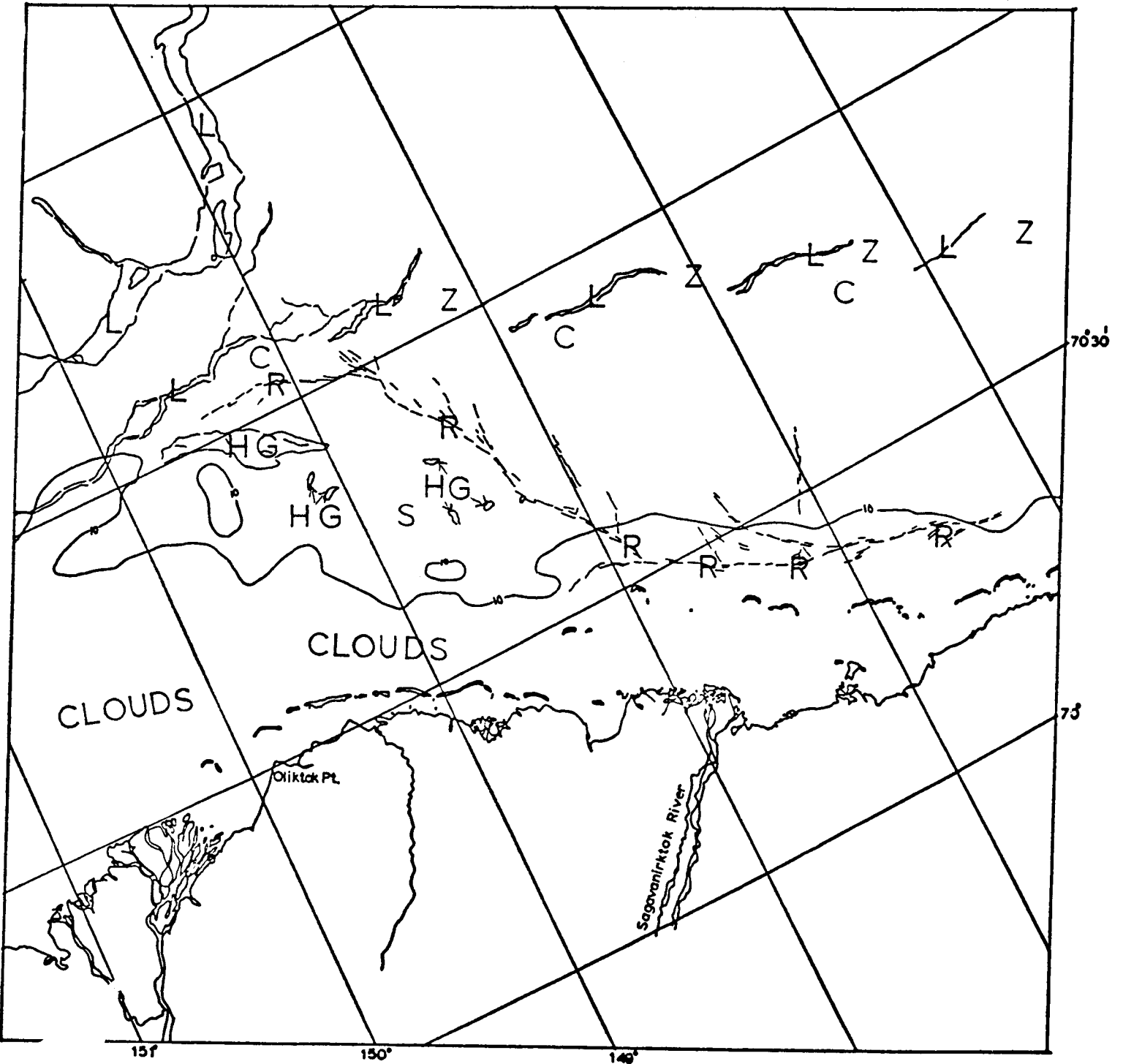
Progressing to the west side of Harrison Bay as seen on Landsat scenes at the end of this sequence, shows the seaward edge of contiguous ice located along an opening lead just seaward of a string of shoals above the 10-fathom isobath. This situation continues to and beyond Point Barrow where the 10-fathom isobath makes an abrupt 90° turn to the southwest.



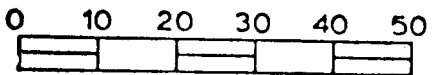
E-2284-21035-7
2 NOV. 1975

BEAUFORT SEA

Figure 1a



KILOMETERS



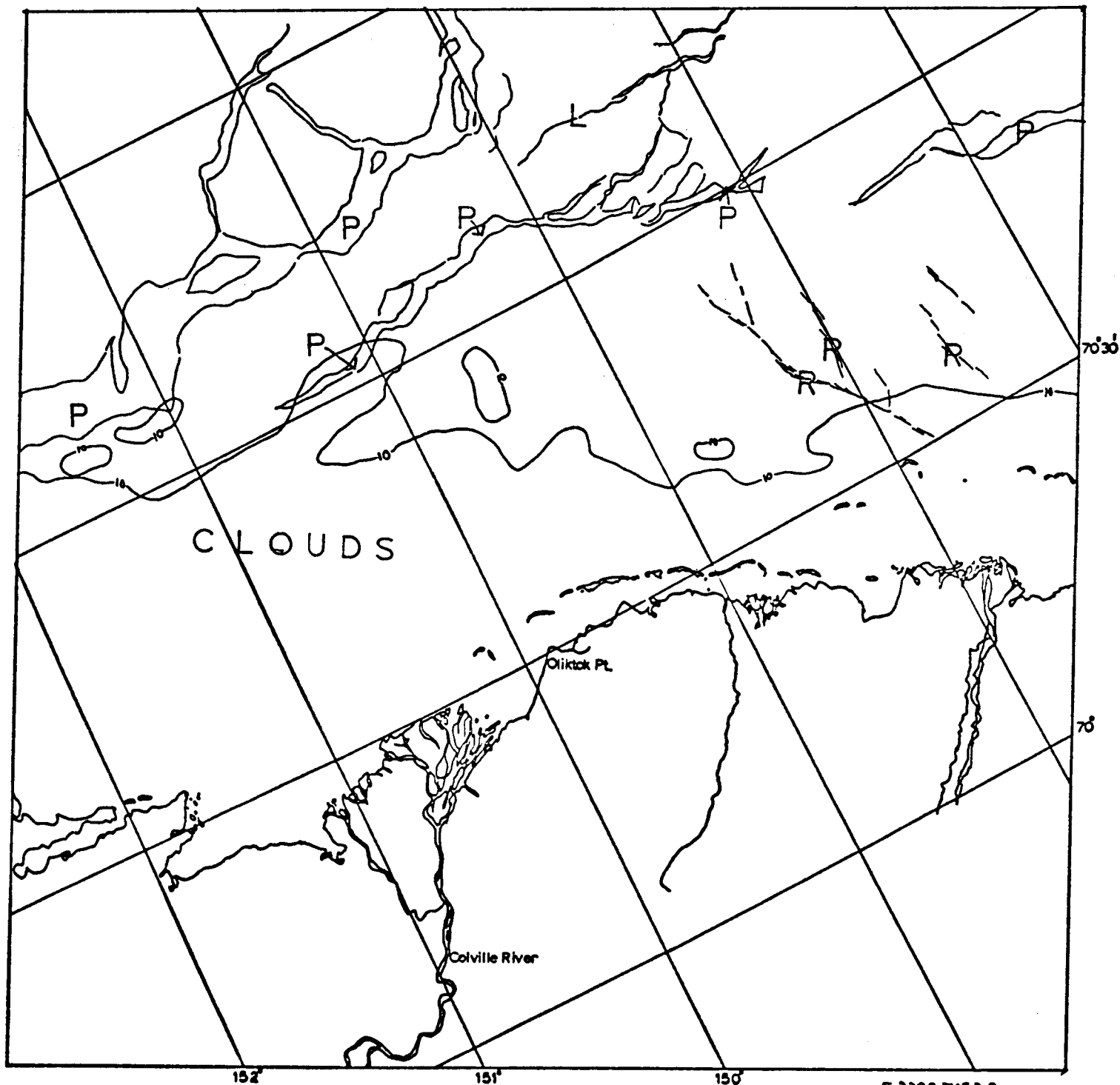
SCALE APPROX 1:1,000,000

E-2265-21094-7

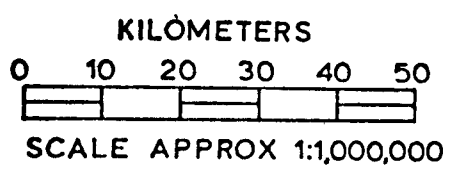
3 NOV. 1975

BEAUFORT SEA

Figure 1b

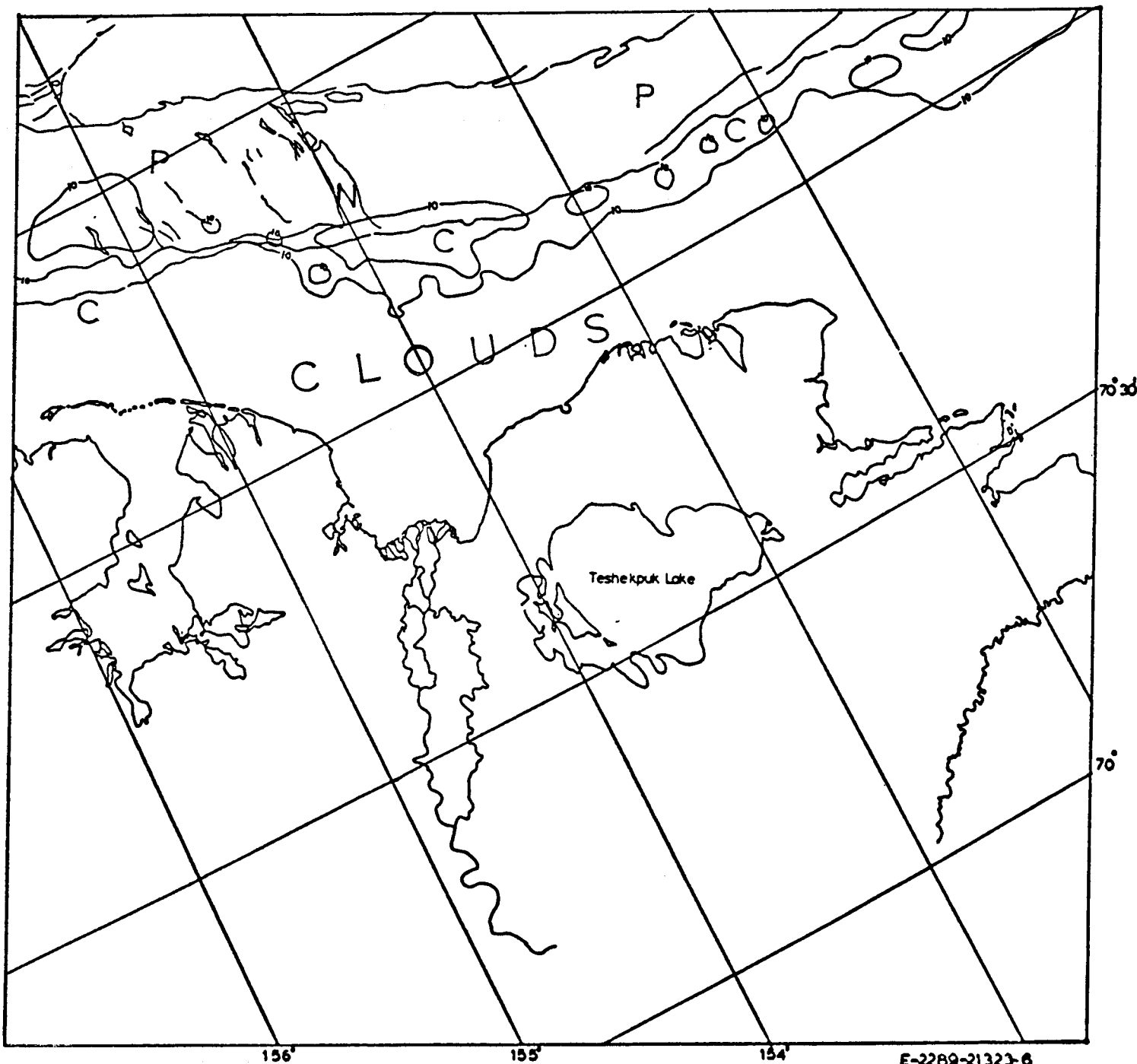


E-2286-21152-6
4 NOV. 1975



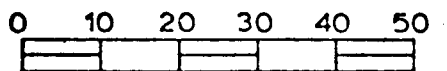
BEAUFORT SEA

Figure 1c



E-2289-21323-6
7 NOV. 1975

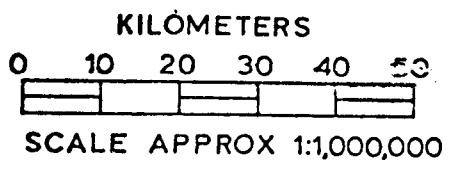
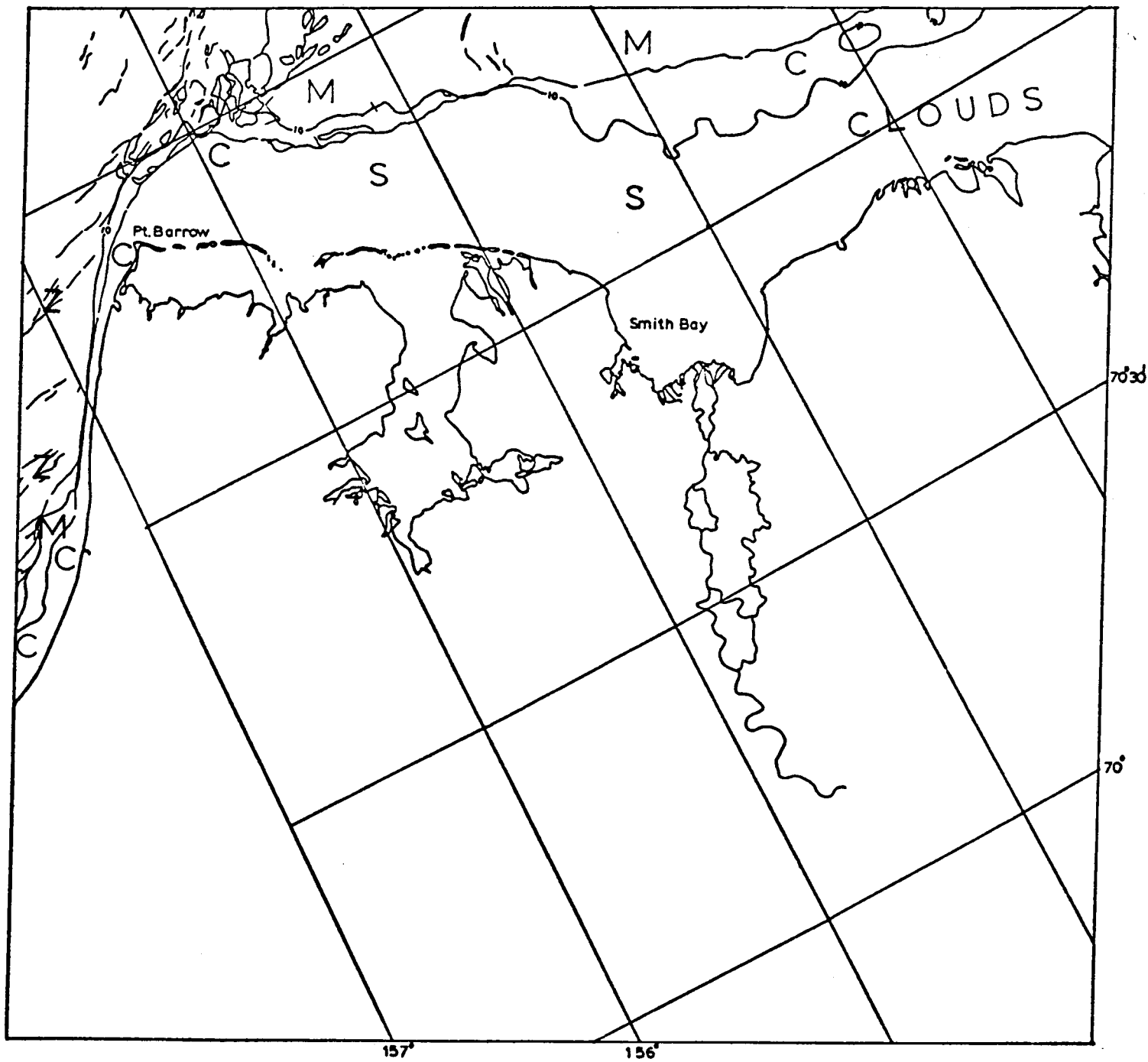
KILÓMETERS



SCALE APPROX 1:1,000,000

BEAUFORT SEA

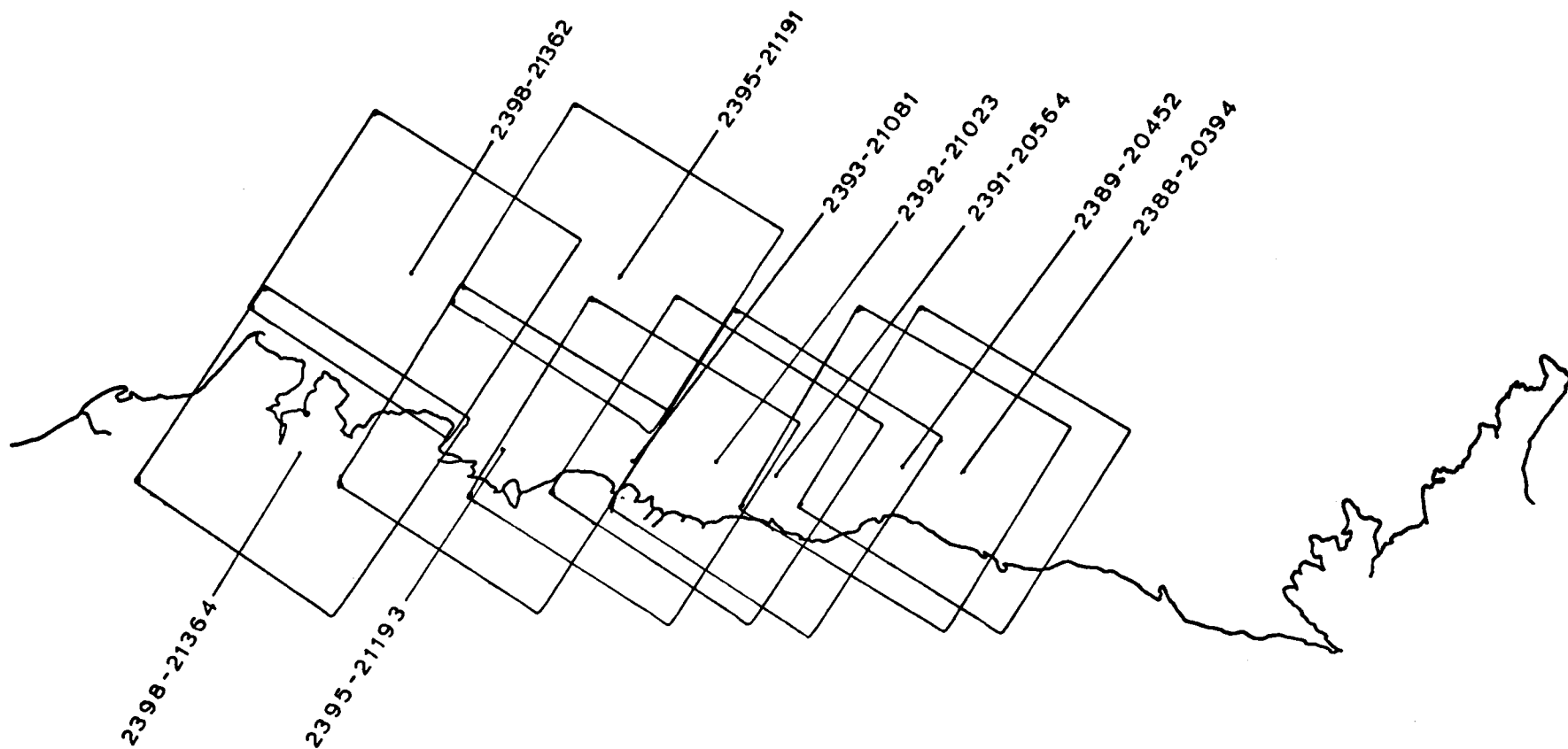
Figure 1d



E-2290-21381-6
8 NOV 1975

BEAUFORT SEA

Figure 1e



BEAUFORT SEA

6 to 23 FEBRUARY 1976

IMAGES: 2381-2398'

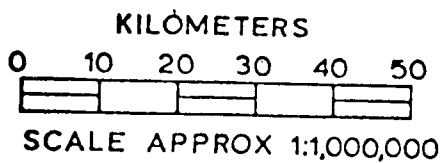
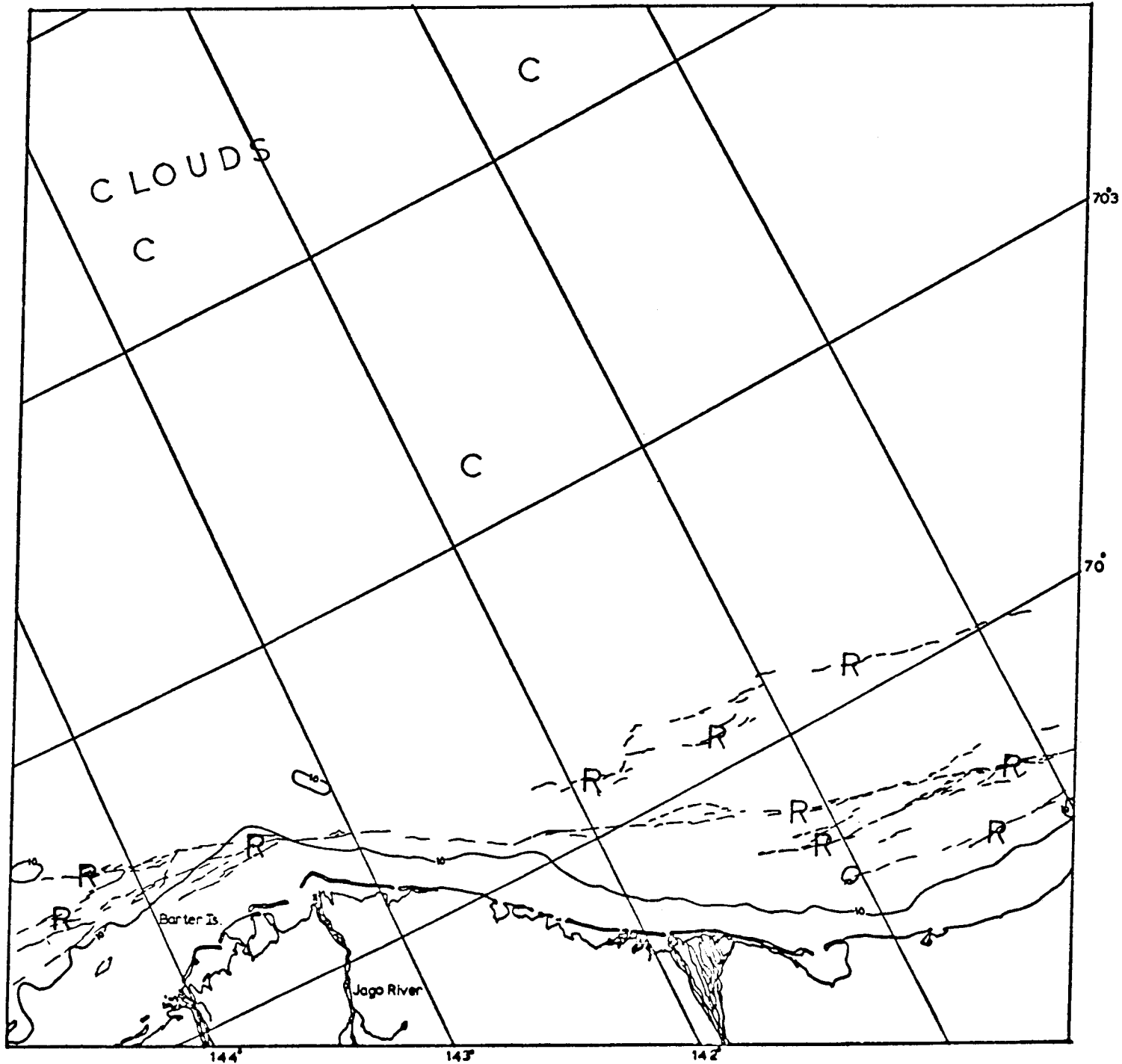
Figure 2

Starting in the extreme east, an extensive system of ridges span the broad embayment west of Barter Island. Off Barter Island this system of ridges becomes tangent to the 10-fathom isobath. There is little doubt that these ridges are grounded at that location.

West of Barter Island the ridge system fans out and fills the space between the 10-fathom isobath and the 10-fathom shoals further offshore. Proceeding to the west, the ridge system separates into two ridge systems separated by several kilometers when opposite the Canning River and returning together in the area off Prudhoe Bay. The more shoreward of the two ridges follows the 10-fathom contour while the more seaward caps the embayment created by the Barter Island headland on the east and the area of shoals and grounded hummock fields off Harrison Bay on the west.

The previous sequence of images described shows that the inner system of ridges was in place the previous November. Apparently the ice within this boundary has been undisturbed during this interval and has merely grown in thickness. West of Harrison Bay the innermost ridge system continues to follow the line of shoals seaward of the 10-fathom isobath.

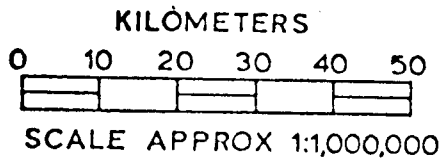
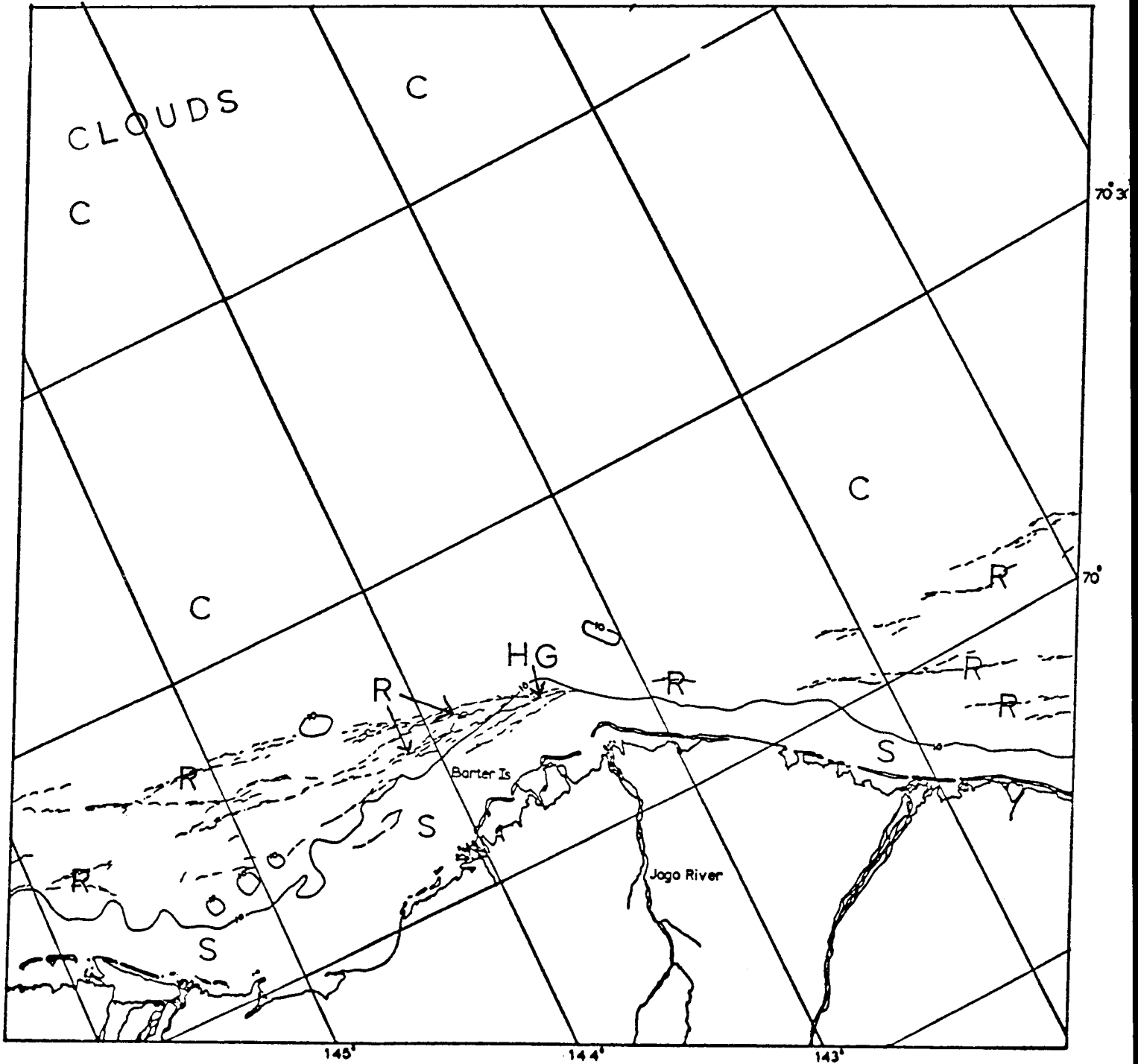
At Point Barrow the edge of contiguous ice is defined by an active lead system along the Chukchi coast and extending on into the Beaufort Sea in a direction nearly parallel to the Chukchi coast. This large lead is the only open water observed on this entire sequence of images. Hence, contiguous ice in the entire Beaufort Sea extended far seaward of grounded ice features during this time.



E-2388-20394-7
 14 FEB. 1978

BEAUFORT SEA

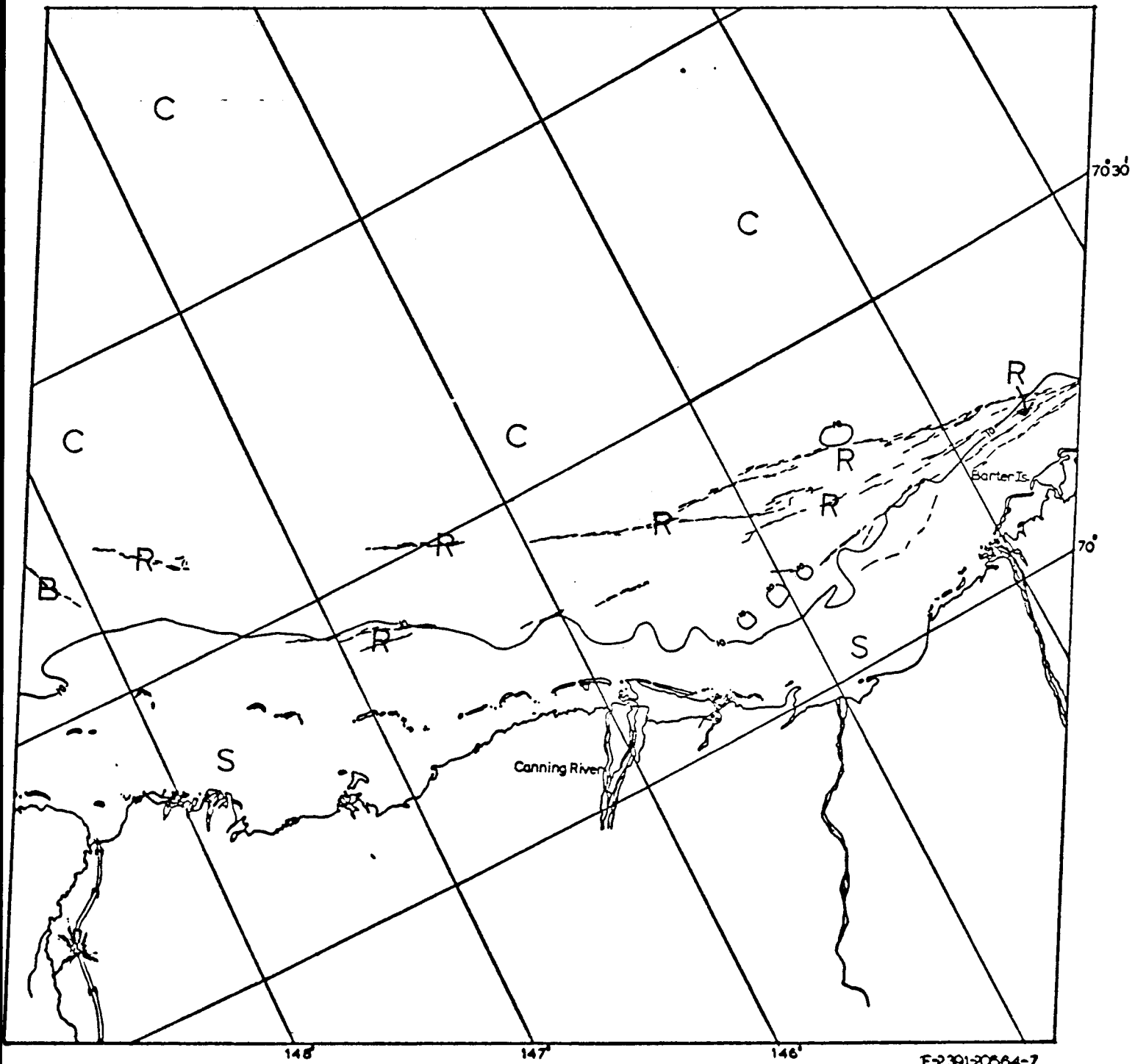
Figure 2a



E-2389-20452-7
 15 FEB. 1976

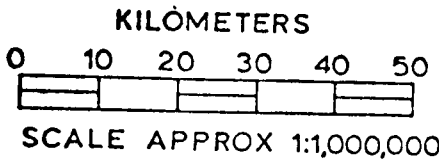
BEAUFORT SEA

Figure 2b



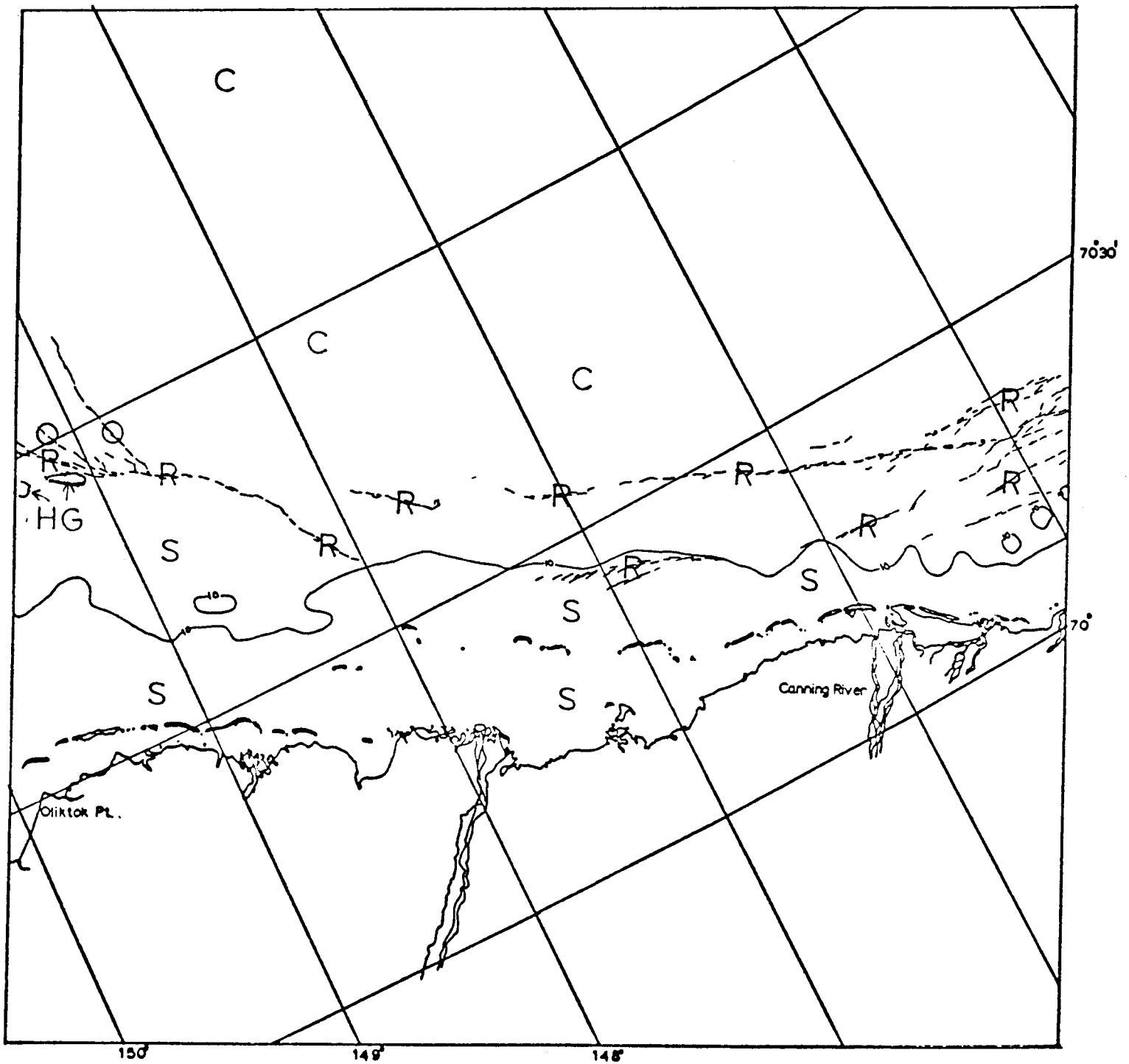
E-2391-20564-7

17 FEB. 1976



BEAUFORT SEA

Figure 2c

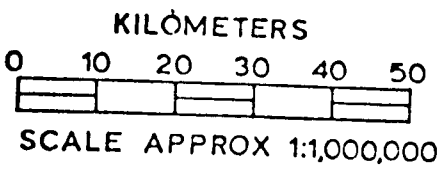
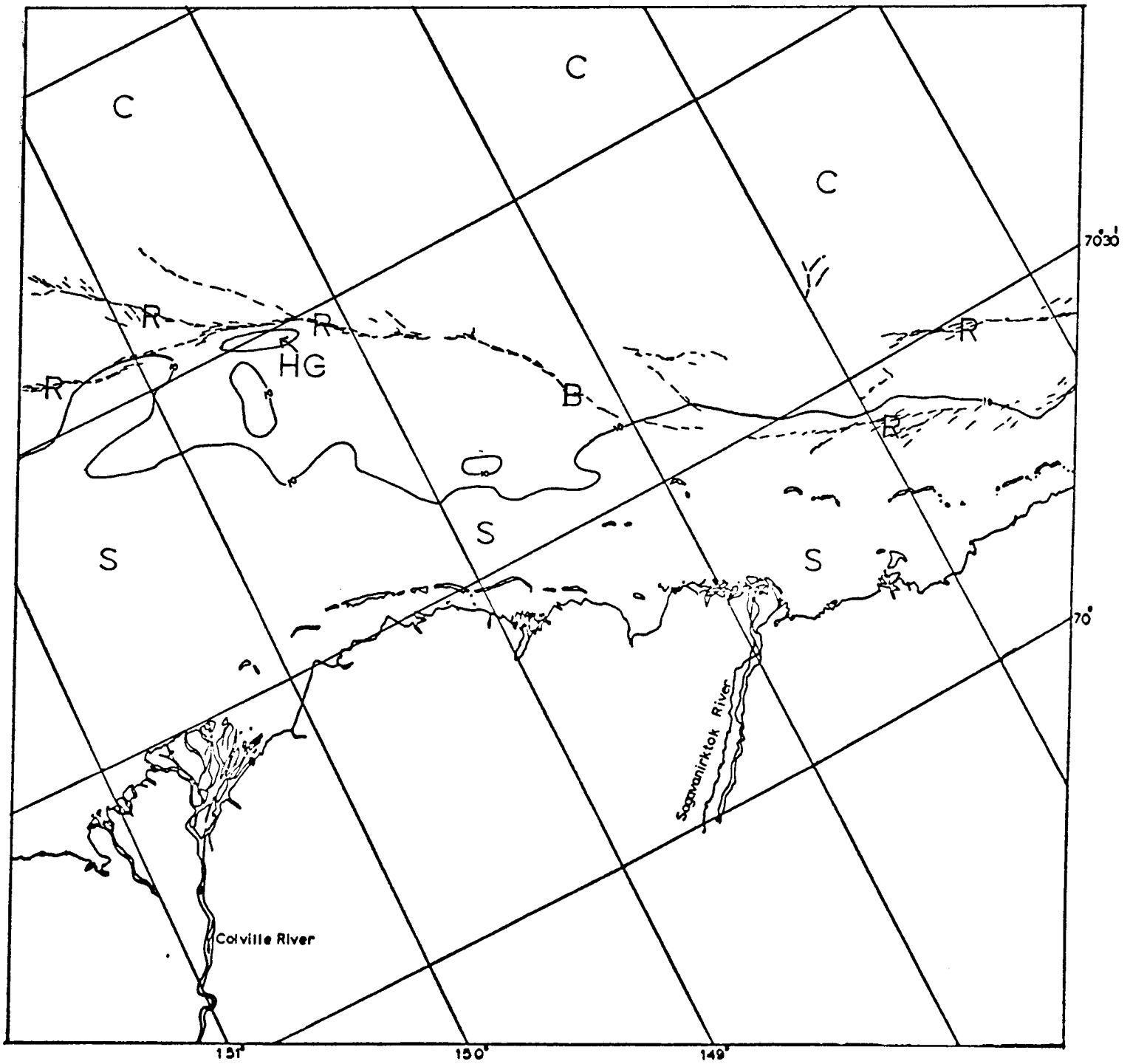


E-2302-21023-9
18 FEB. 1976

KILOMETERS
0 10 20 30 40 50
SCALE APPROX 1:1,000,000

BEAUFORT SEA

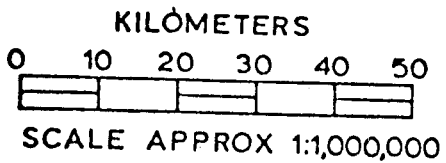
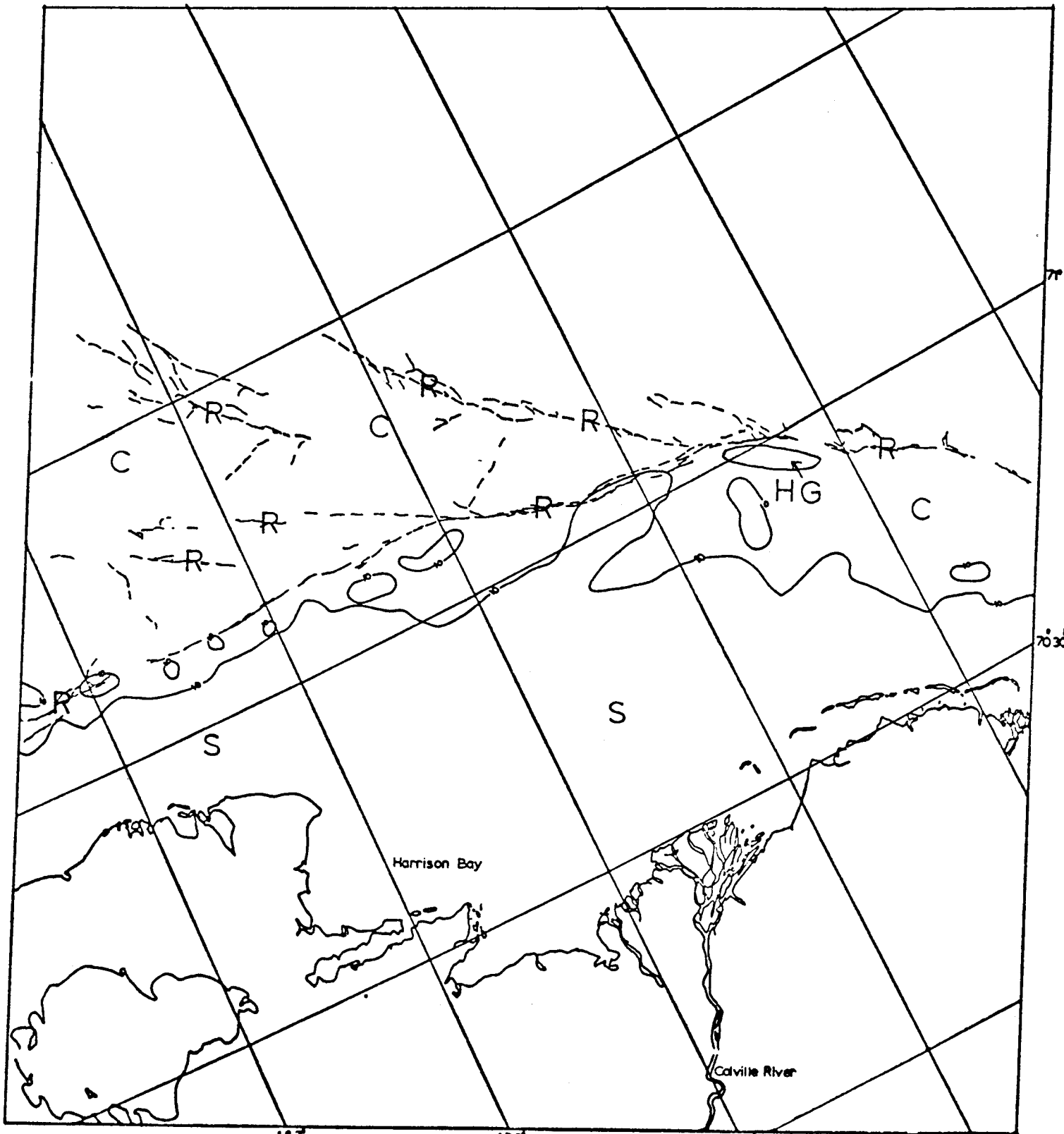
Figure 2d



E-2393-21081-7
19 FEB. 1976

BEAUFORT SEA

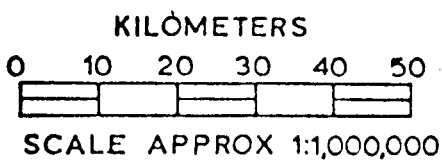
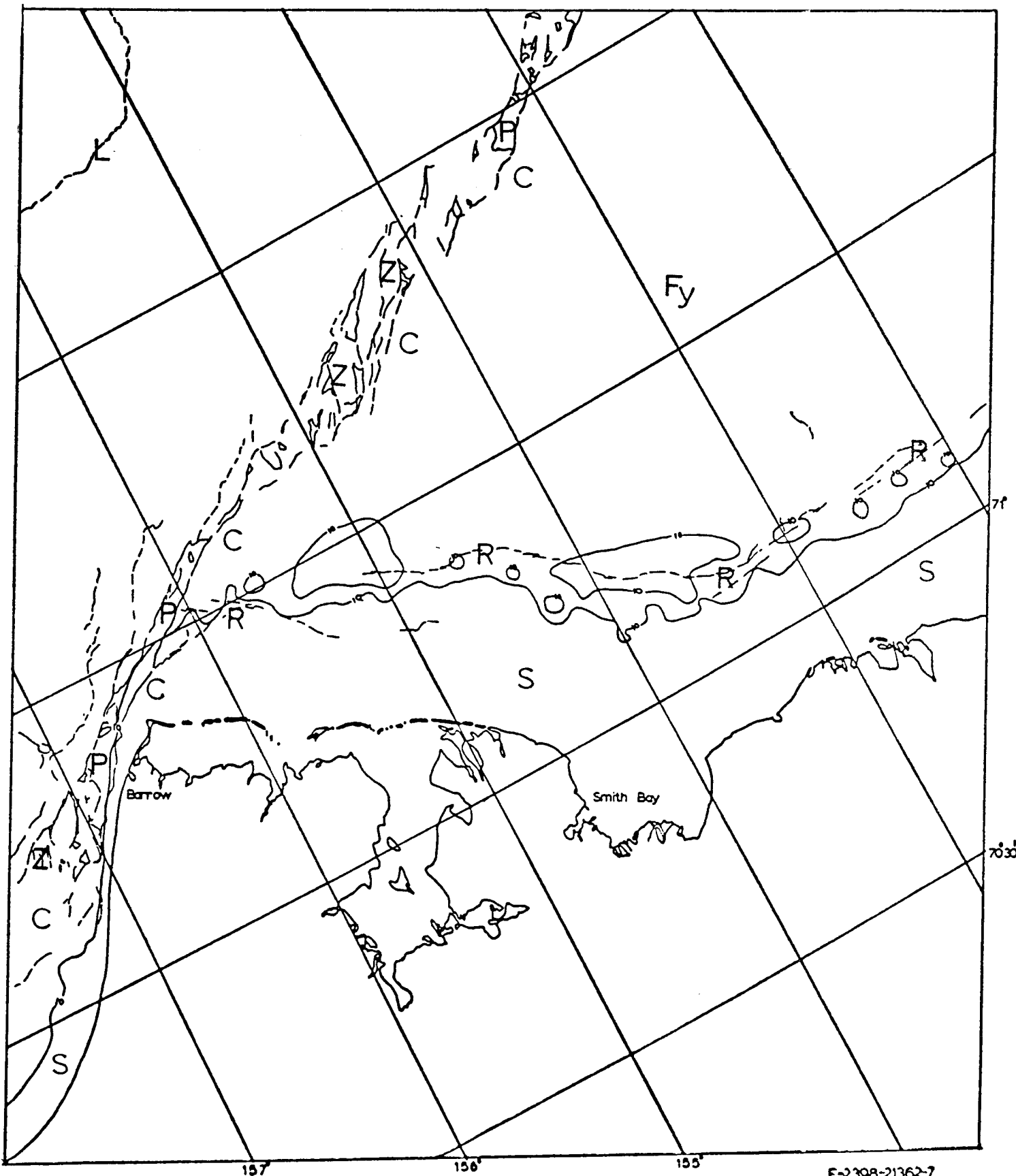
Figure 2e



BEAUFORT SEA

Figure 2f

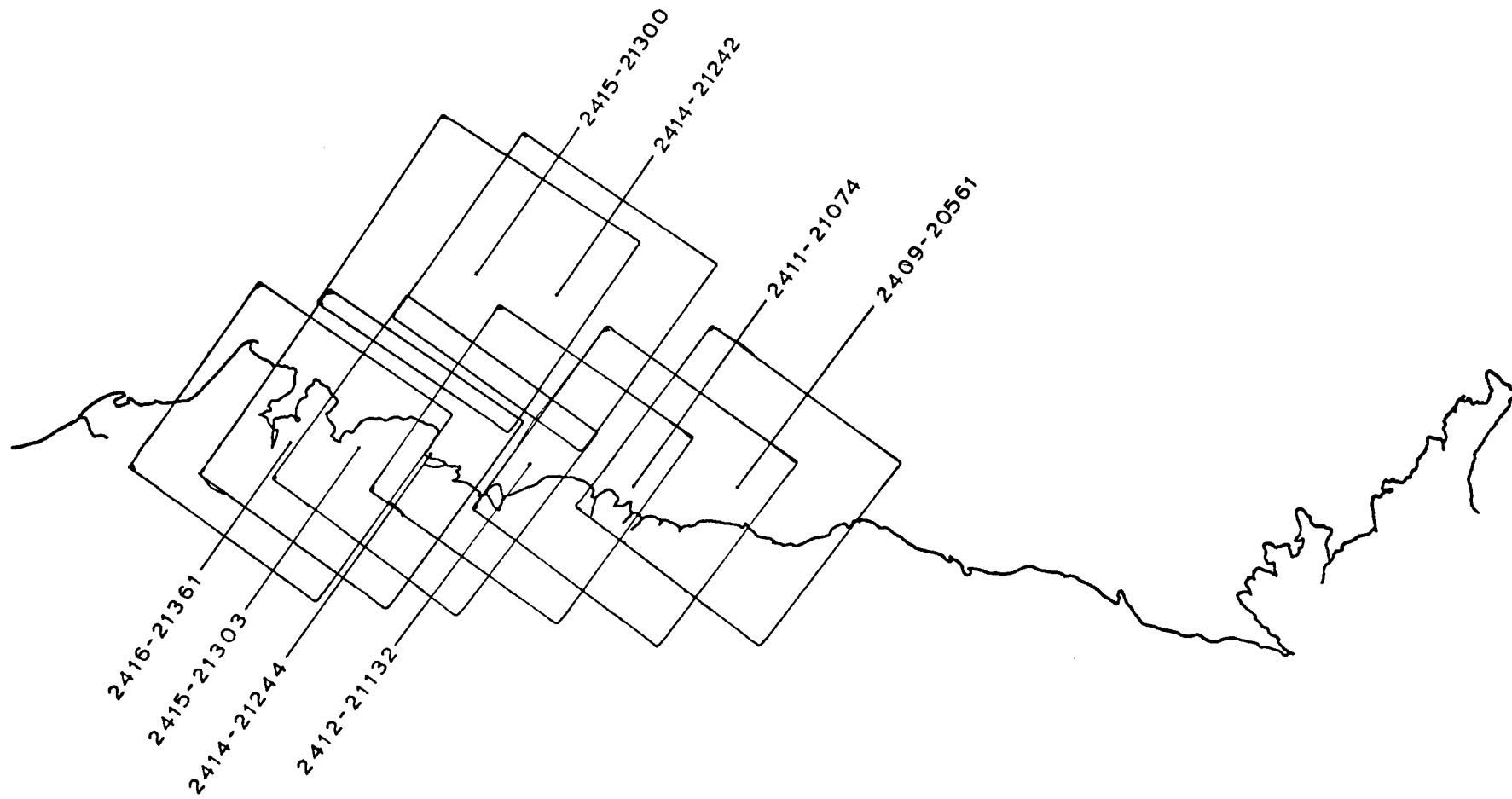
E-2395-21191-7
 -21193-
 21 FEB. 1976



E-2398-21362-7
 -21364-
 24 FEB. 1976

BEAUFORT SEA

Figure 2g



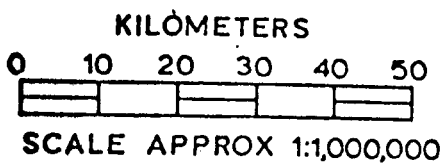
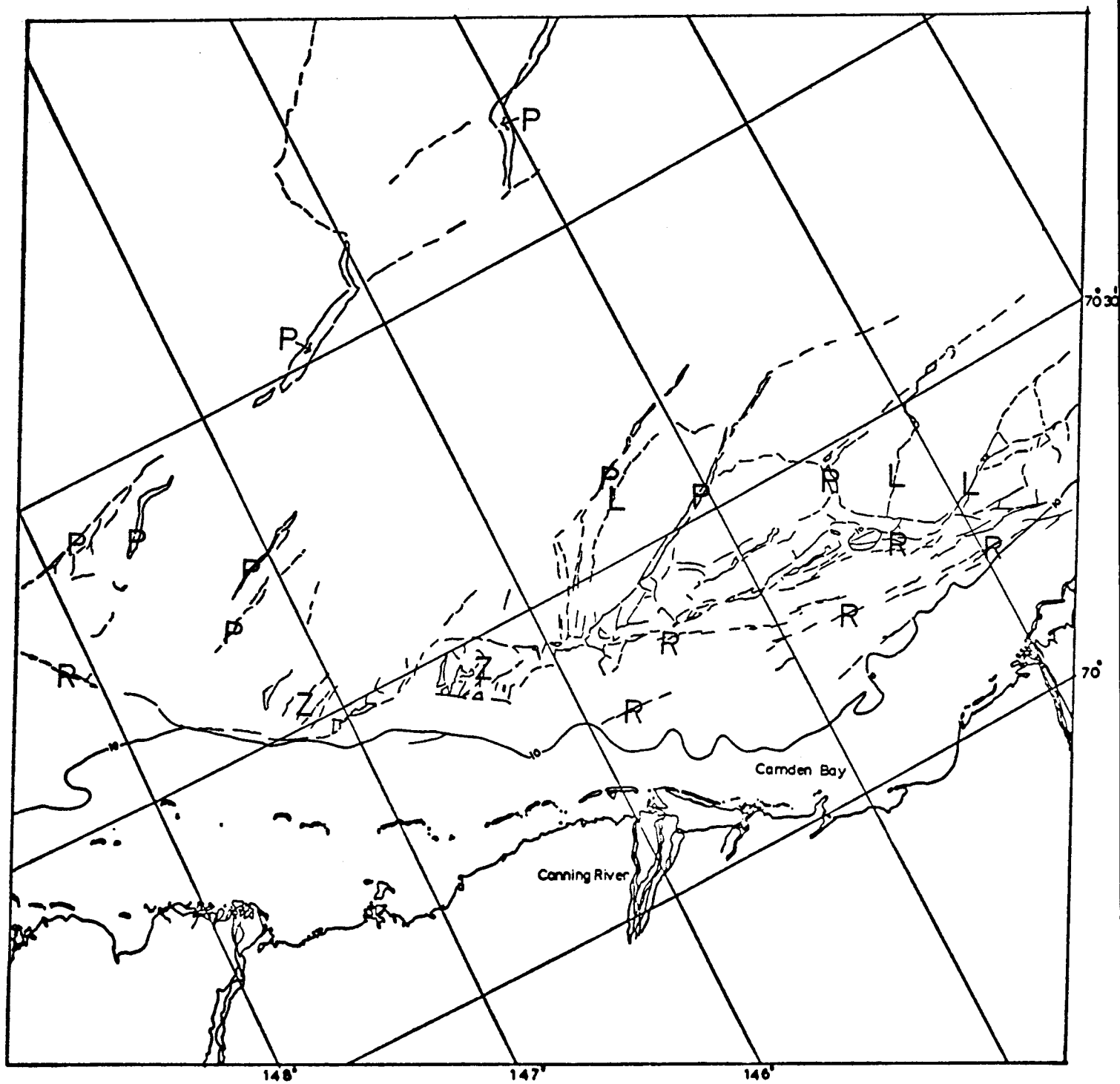
BEAUFORT SEA
24 FEBRUARY to 12 MARCH 1976
IMAGES: 2399 - 2416

Figure 3

Scenes 2409-20561 through 2415-21300

Considerable shear has taken place along the Beaufort coast - in many locations right up to apparently well-grounded ice. In many places shear ridges formed at earlier times have been broken up with the ice. For the most part, the boundary of contiguous ice is now defined by the most shoreward of the large ridge systems identified on the November imagery for this ice year (1975-76).

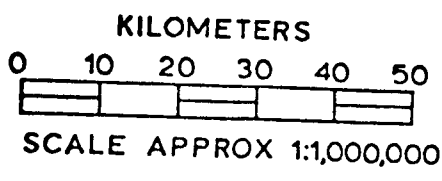
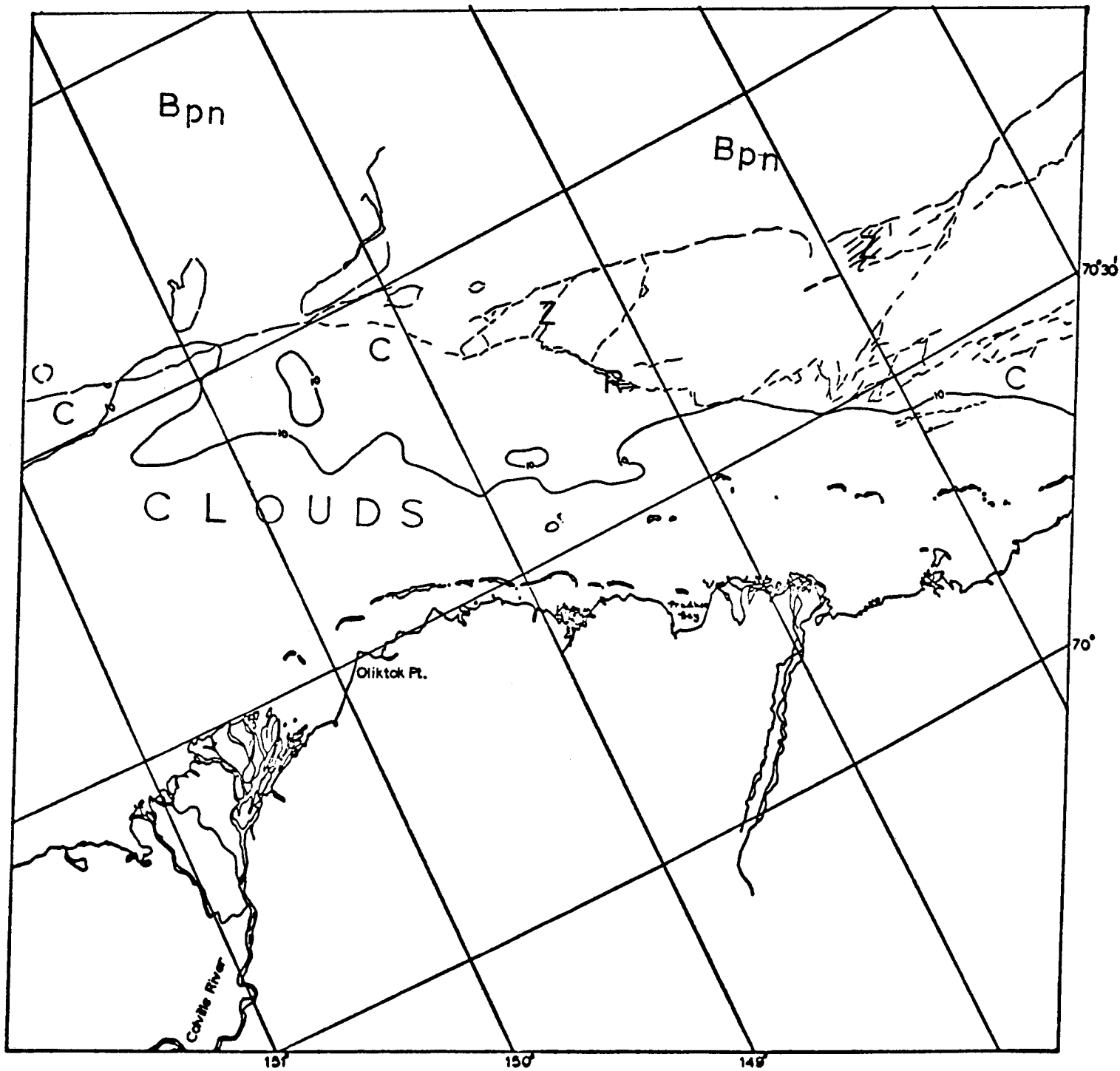
The ice cover on the ocean has been considerably broken by the recent ice-moving event. West of Harrison Bay, on the scale viewed by Landsat, the pans and floes near the stationary ice appear shattered and ground up compared to the floes further seaward. This ground up zone is approximately 10 to 20 km wide.



E-2409-20561-7
6 MARCH 1978

BEAUFORT SEA

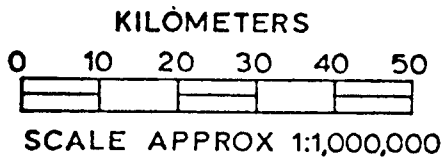
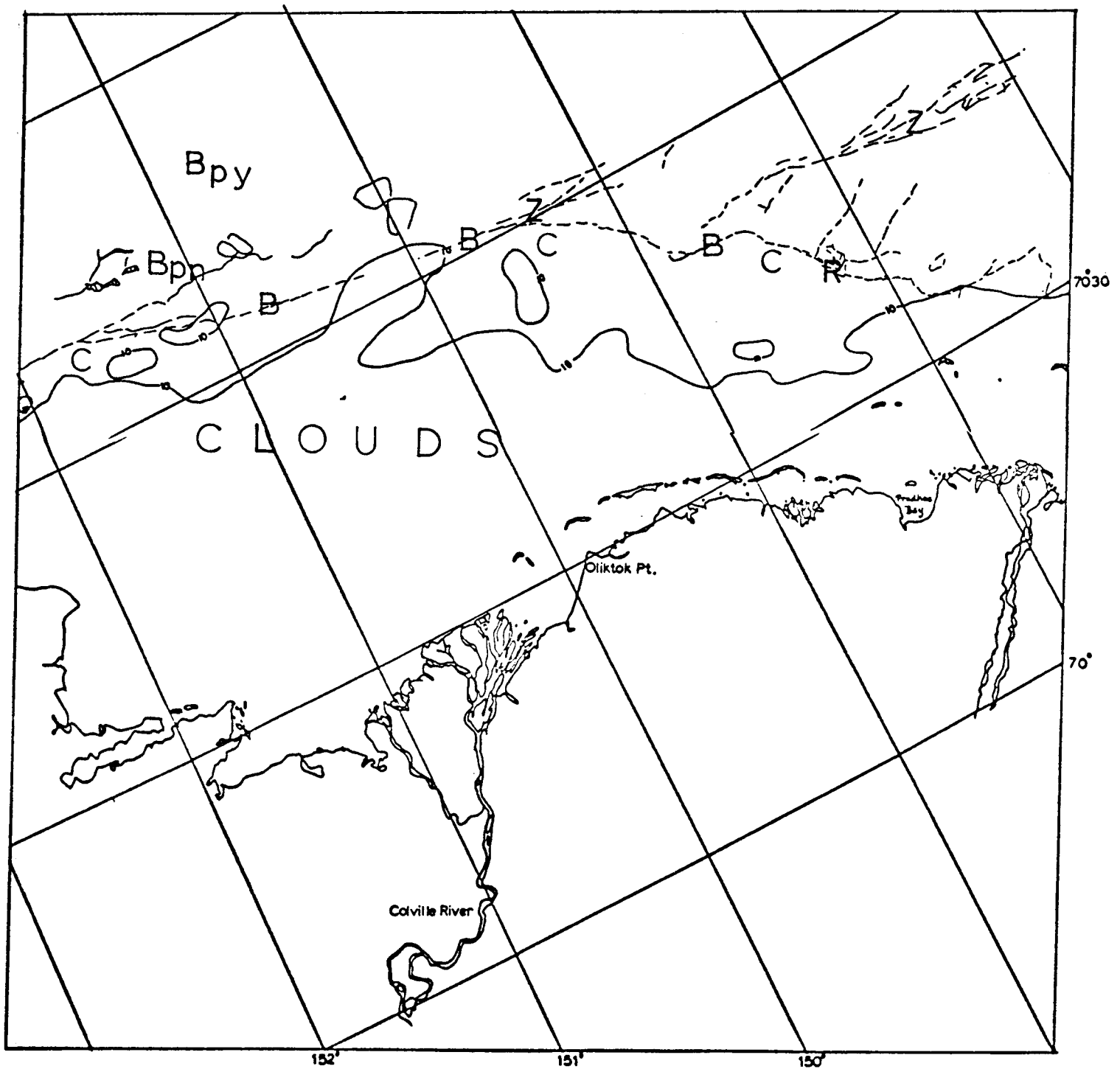
Figure 3a



E-2411-21074-7
 8 MARCH 1976

BEAUFORT SEA

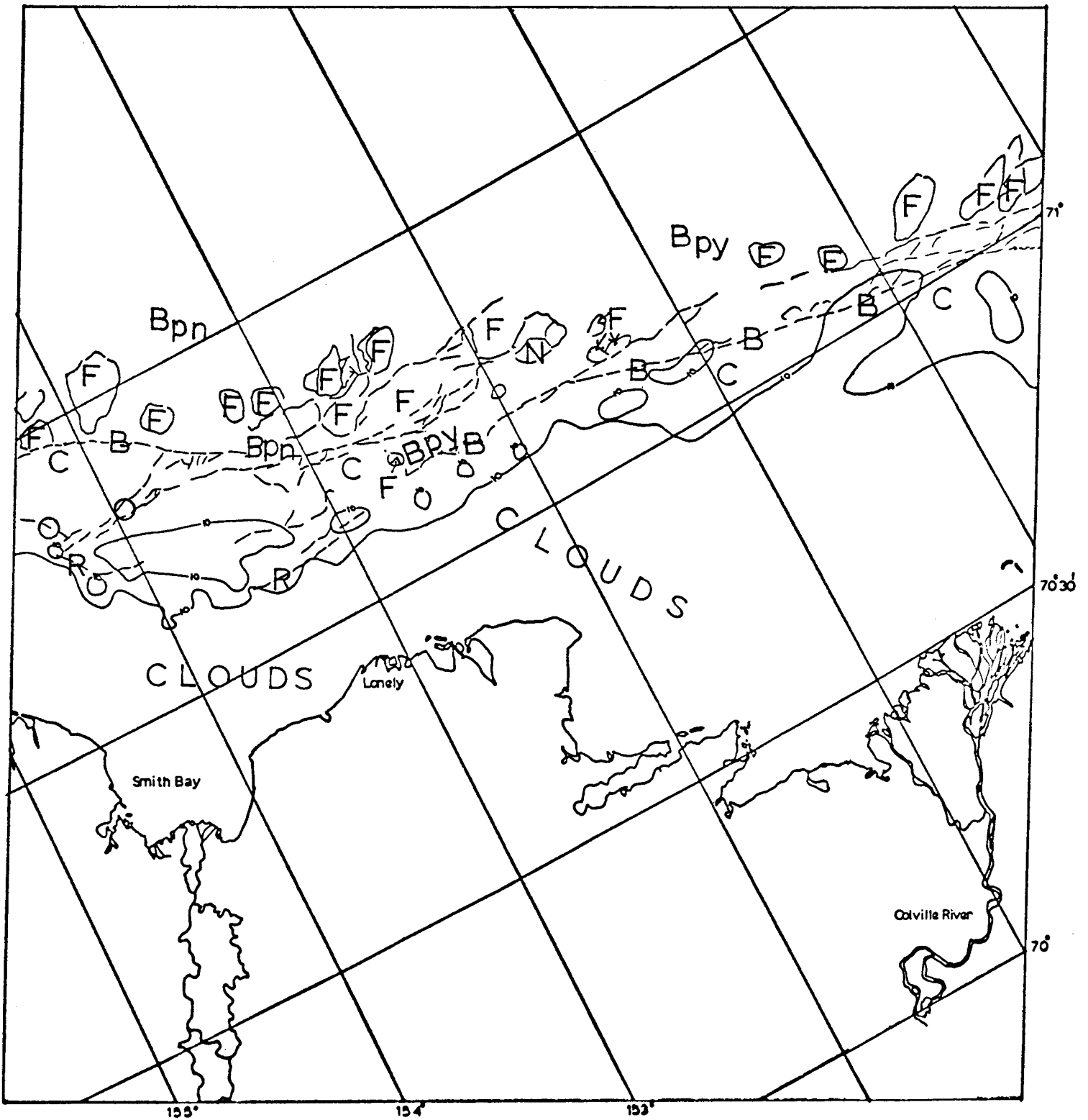
Figure 3b



E-2412-21132-7
9 MARCH 1976

BEAUFORT SEA

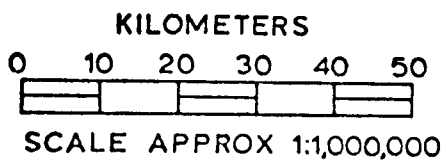
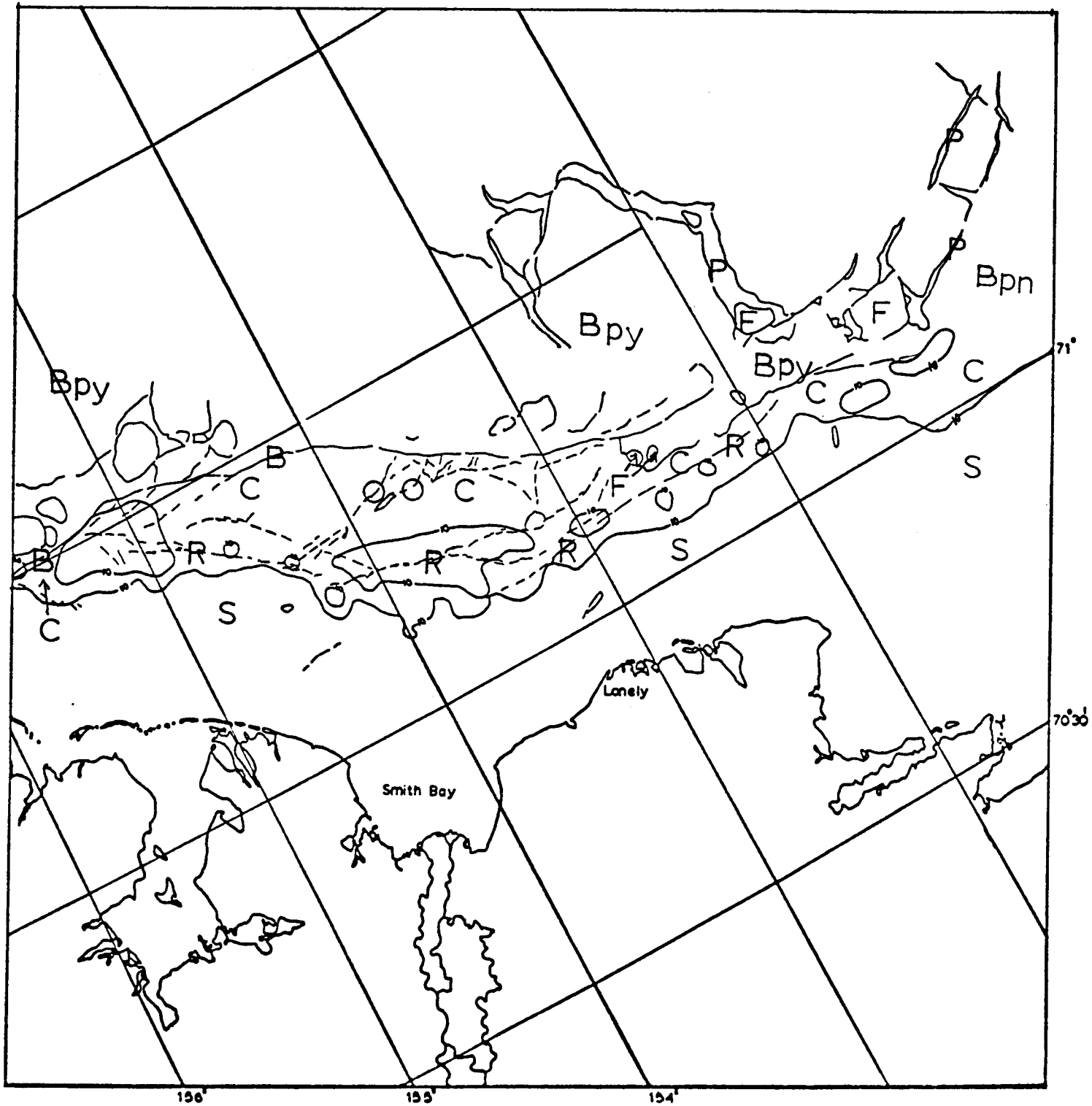
Figure 3c



E-2414-21242-7
 -21244-
 11 MARCH 1978

BEAUFORT SEA

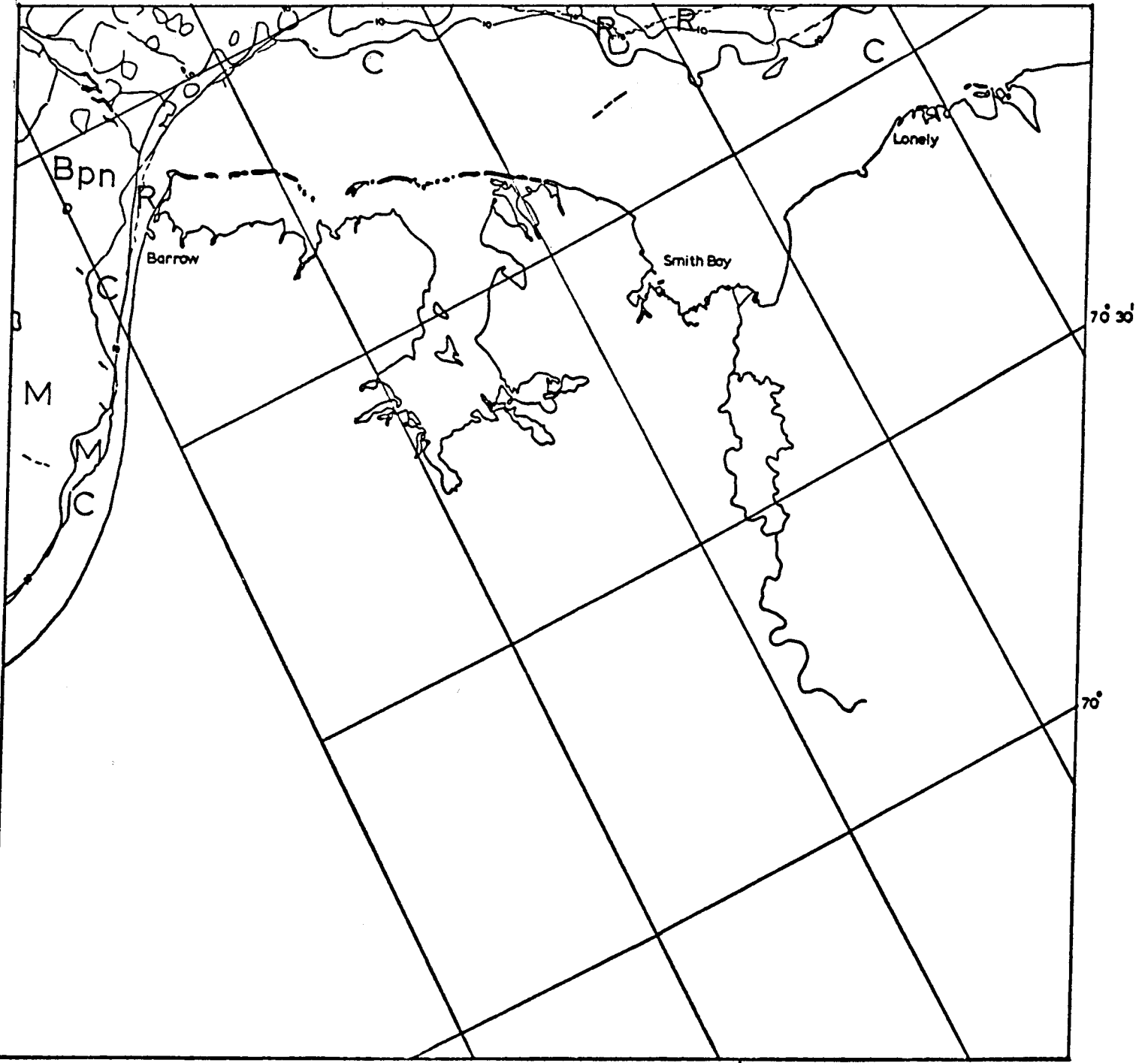
Figure 3d



E-2415-21300-7
- 21303-
12 MARCH 1978

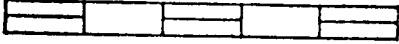
BEAUFORT SEA

Figure 3e



KILÔMETERS

0 10 20 30 40 50



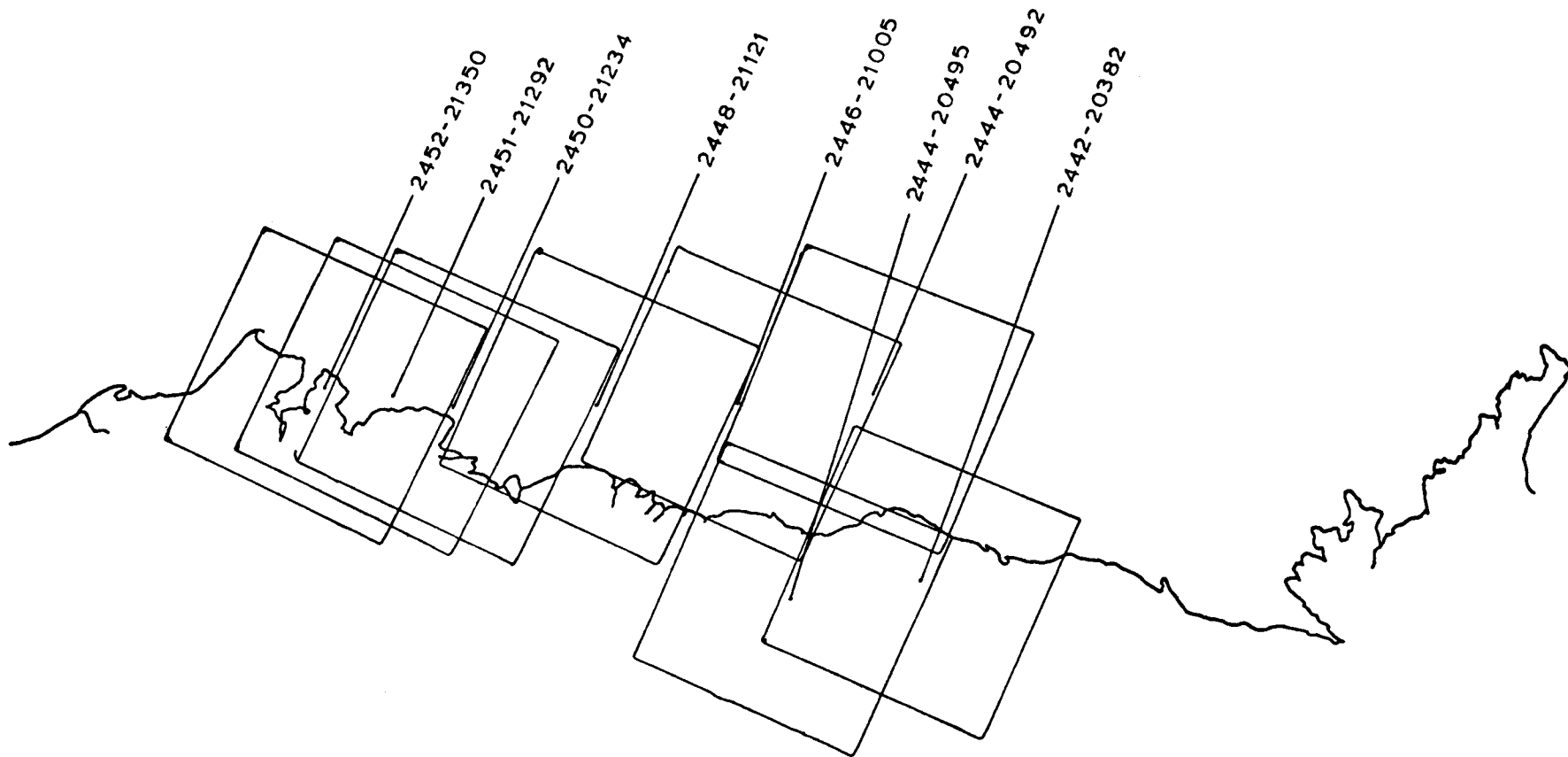
SCALE APPROX 1:1,000,000

E-2416-21361-7

13 MARCH 1976

BEAUFORT SEA

Figure 3f



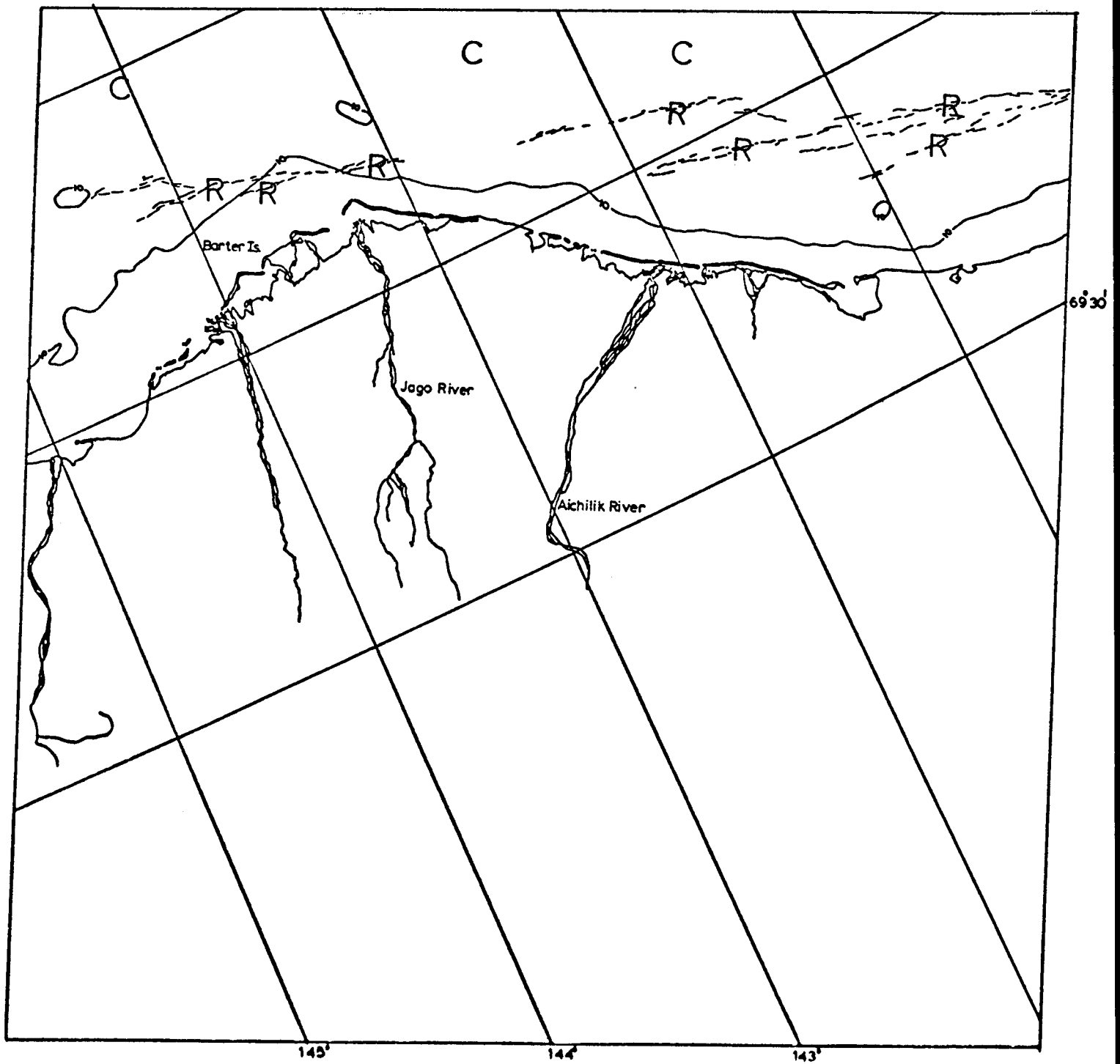
BEAUFORT SEA
31 MARCH to 17 APRIL 1976
IMAGES: 2435 - 2452

Figure 4

The eastern end of the Beaufort Sea is again frozen solid with no sign of the recent ice breaking event. Ridges formed before November remain in place. Between the 8th and 10th of April pack ice motion takes place. The resulting leads lie mainly far offshore except east of Barter Island where one small lead angles shoreward and then follows a previously existing ridge system to the east along a line close to the 10-fathom isobath.

Between Barter Island and Harrison Bay, the recently-formed lead systems remain quite far seaward until the fourteenth when new displacements take place. At this time, a large lead opens as a result of an eastward displacement of the pack ice. This lead continues to open, following the shoals above the 10-fathom isobath west of Harrison Bay quite closely.

Off Admiralty Bay this large lead is still opening on April 17 yet previously created portions have frozen over and thickened considerably. However, the next image, for the 18, shows that the lead has now closed again somewhat. Late spring aerial observations have often been made of large frozen leads in this area which have shown evidence of slight closing after formation of relatively thin ice.

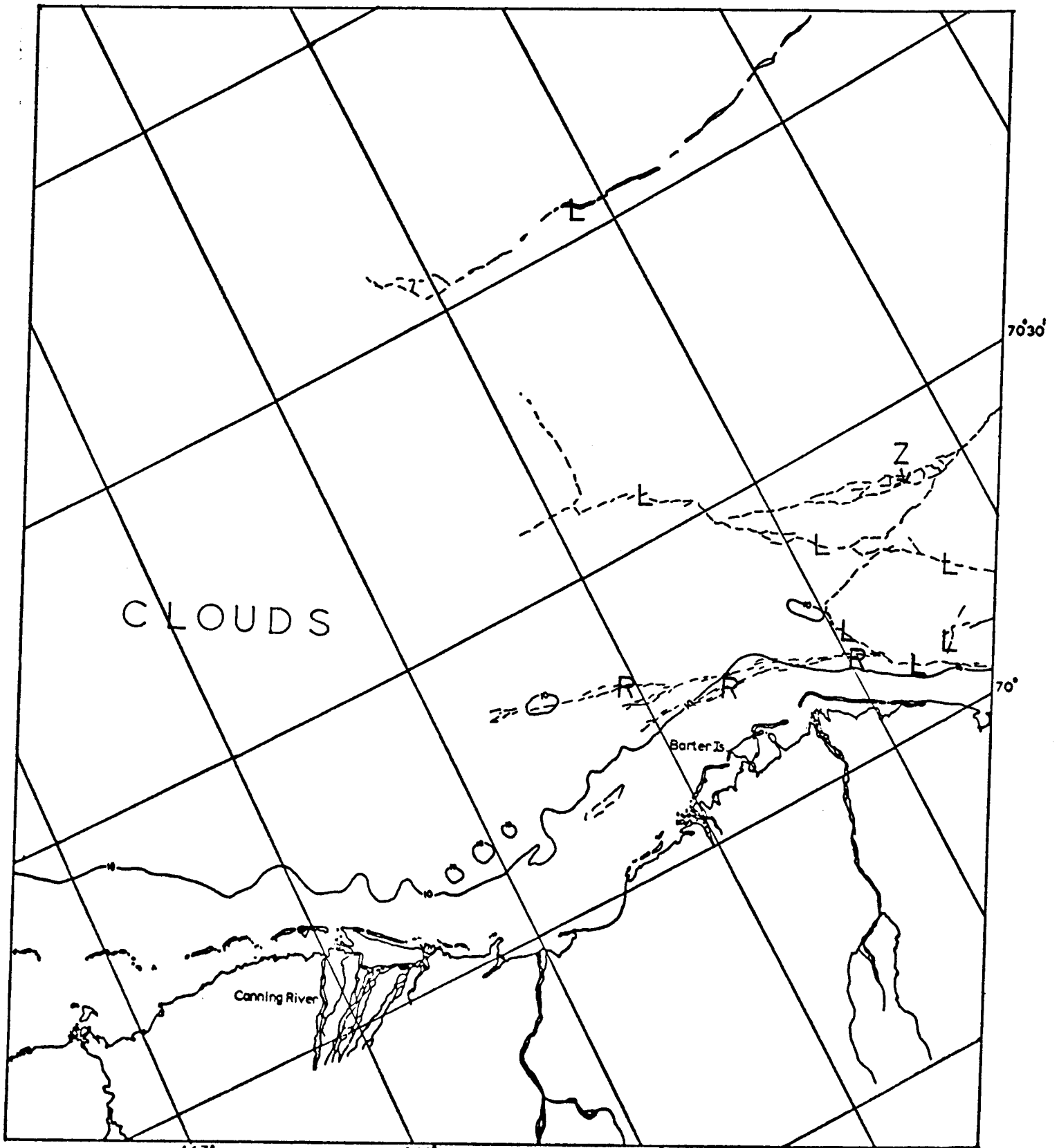


E-2442-20062-7
 8 APRIL 1976

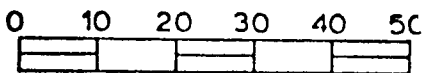
KILOMETERS
 0 10 20 30 40 50
 SCALE APPROX 1:1,000,000

BEAUFORT SEA

Figure 4a



KILOMETERS



SCALE APPROX 1:1,000,000

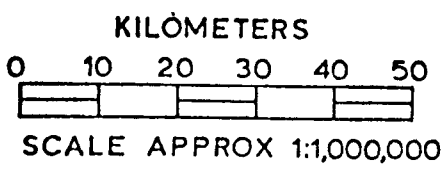
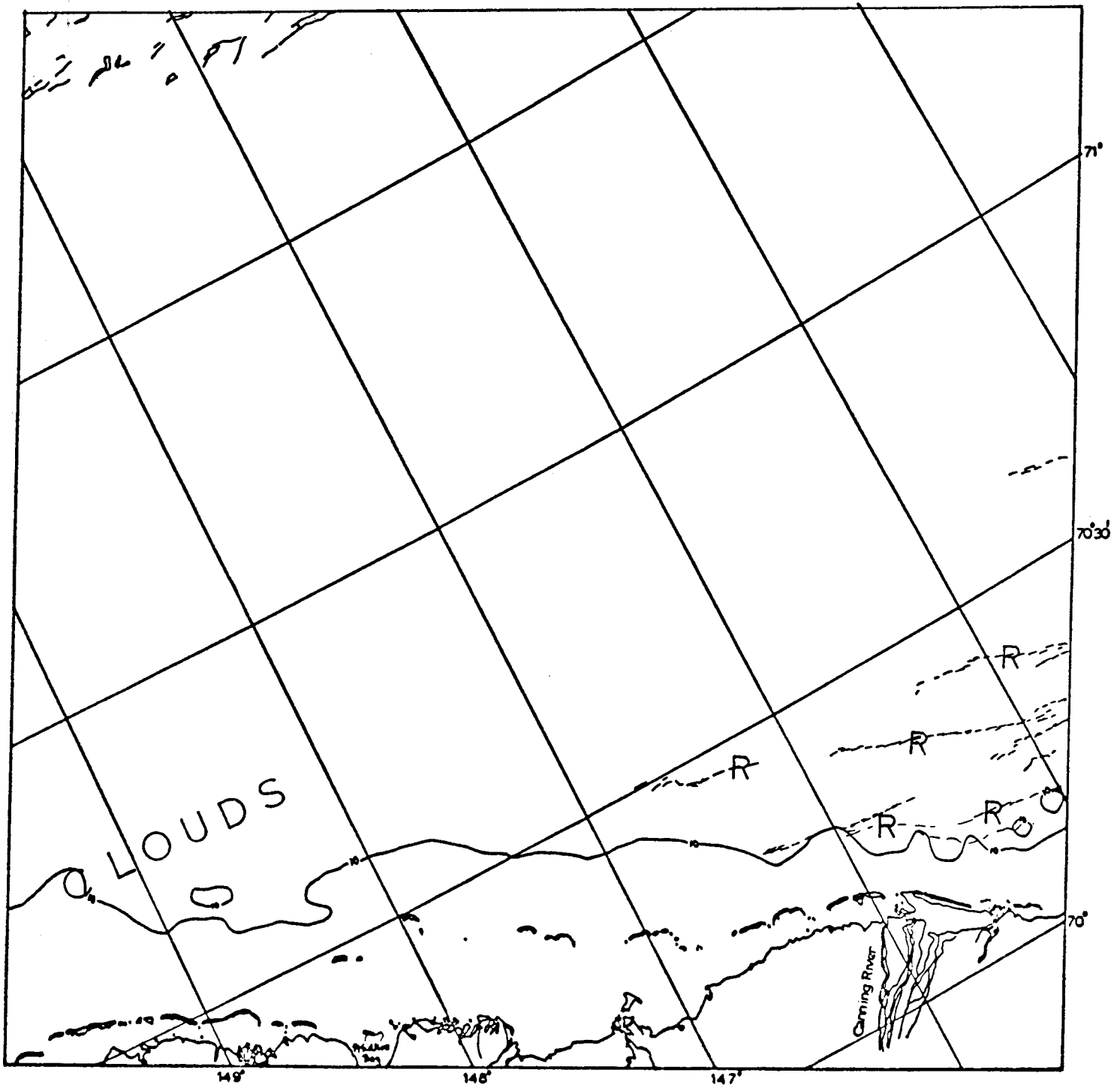
Figure 4b

BEAUFORT SEA

E-2444-20492-7

-20495-

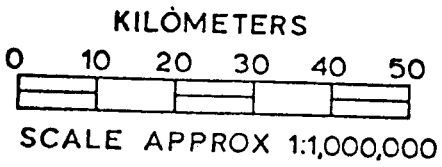
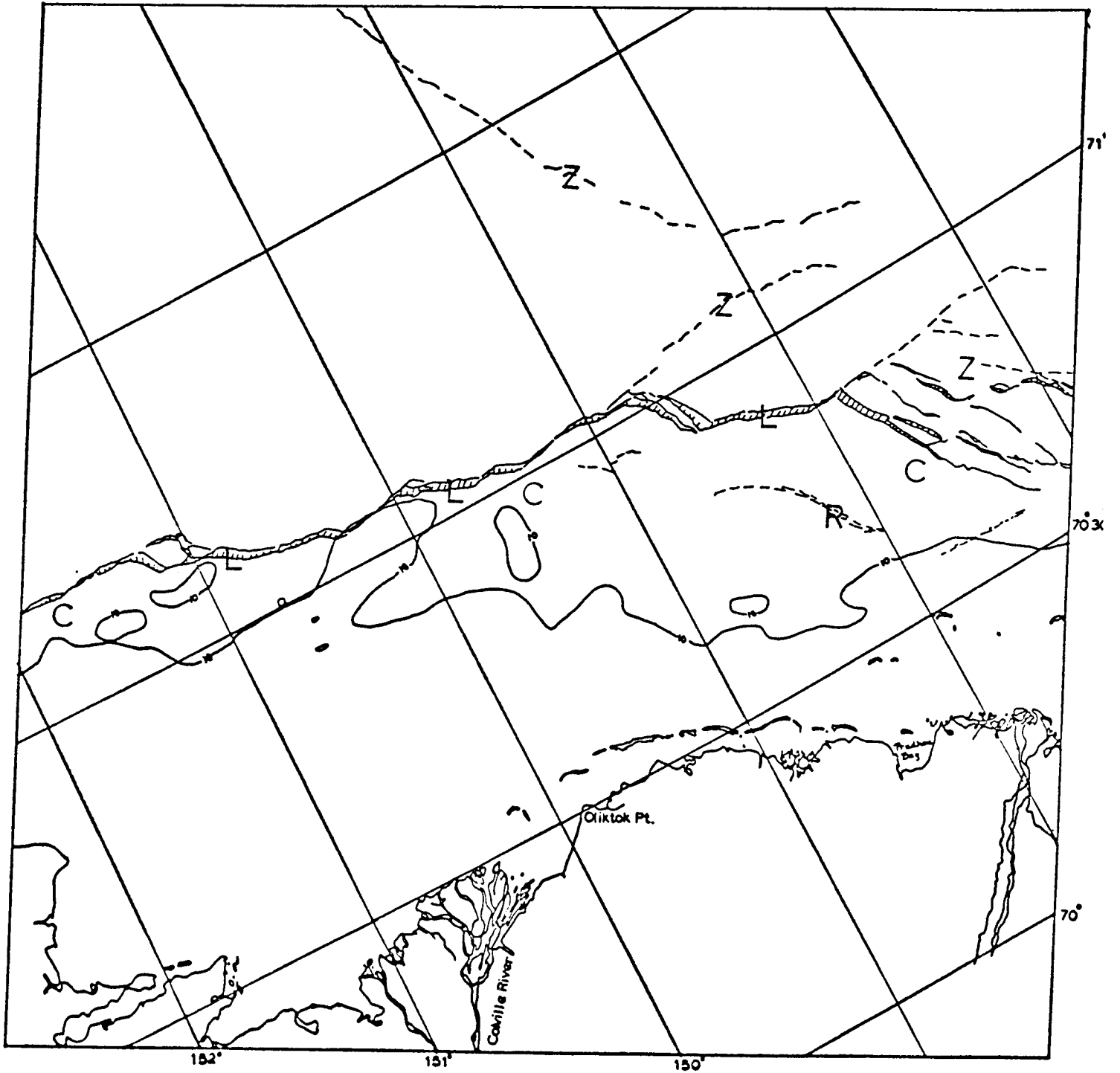
10 APRIL 1976



E-2446-21005-7
12 APRIL 1976

BEAUFORT SEA

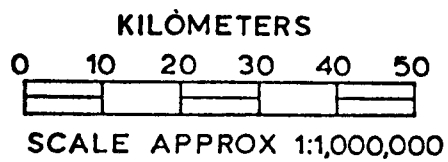
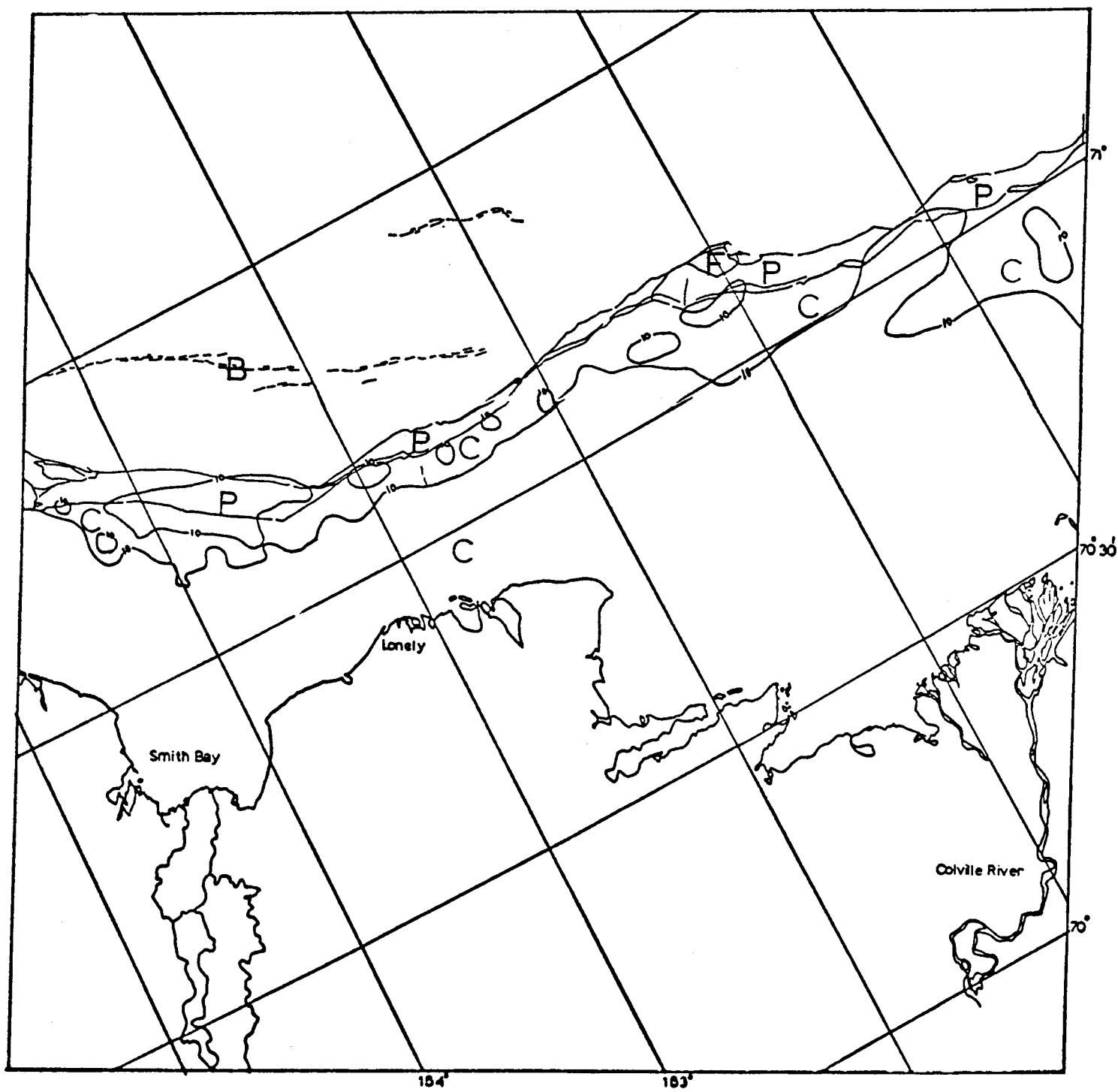
Figure 4c



E-2448-21121-7
14 APRIL 1978

BEAUFORT SEA

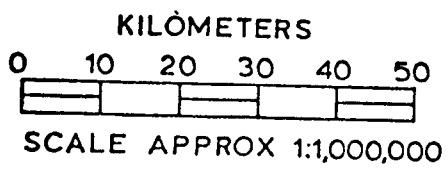
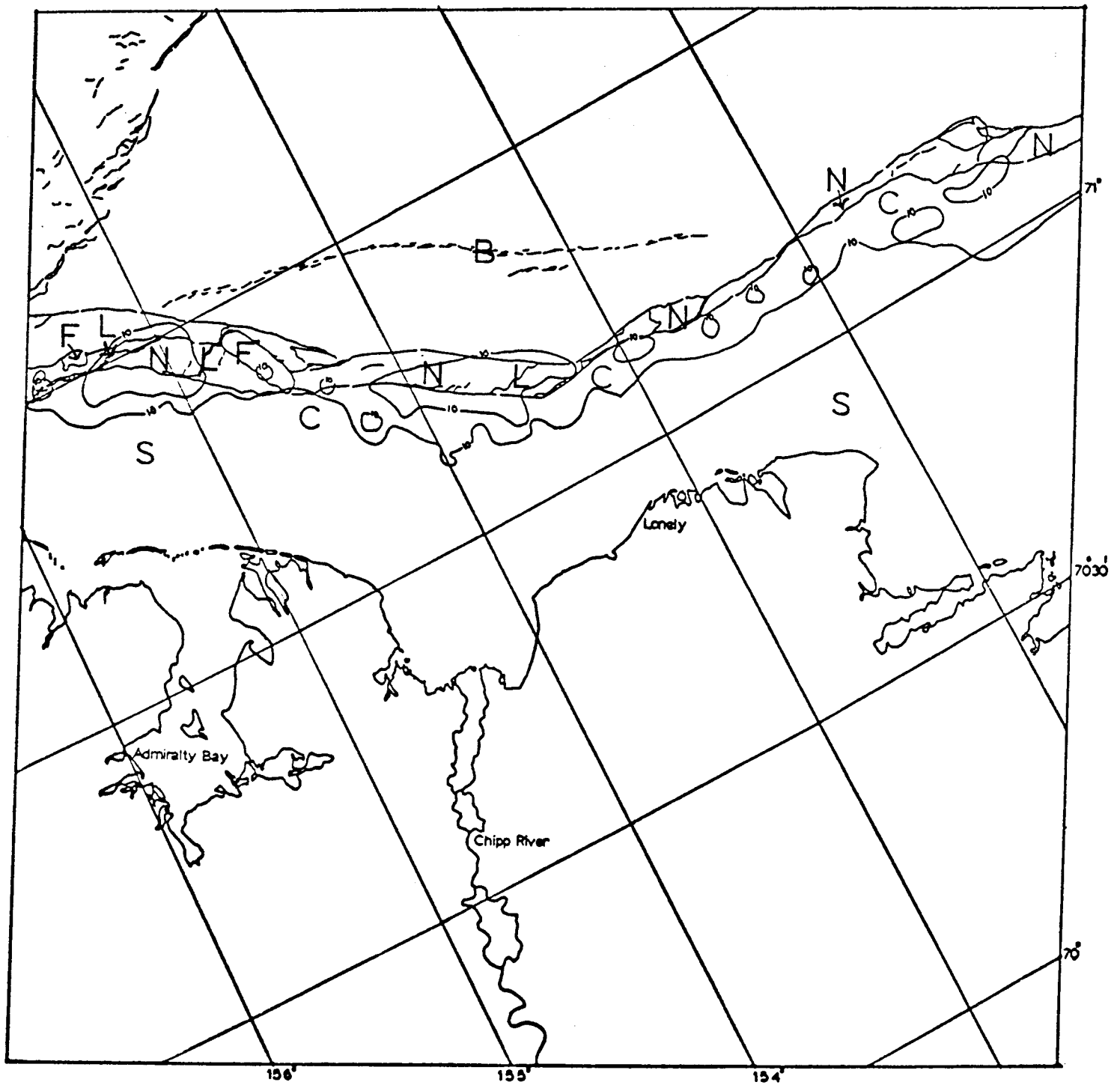
Figure 4d



E-2450-21234-7
16 APRIL 1978

BEAUFORT SEA

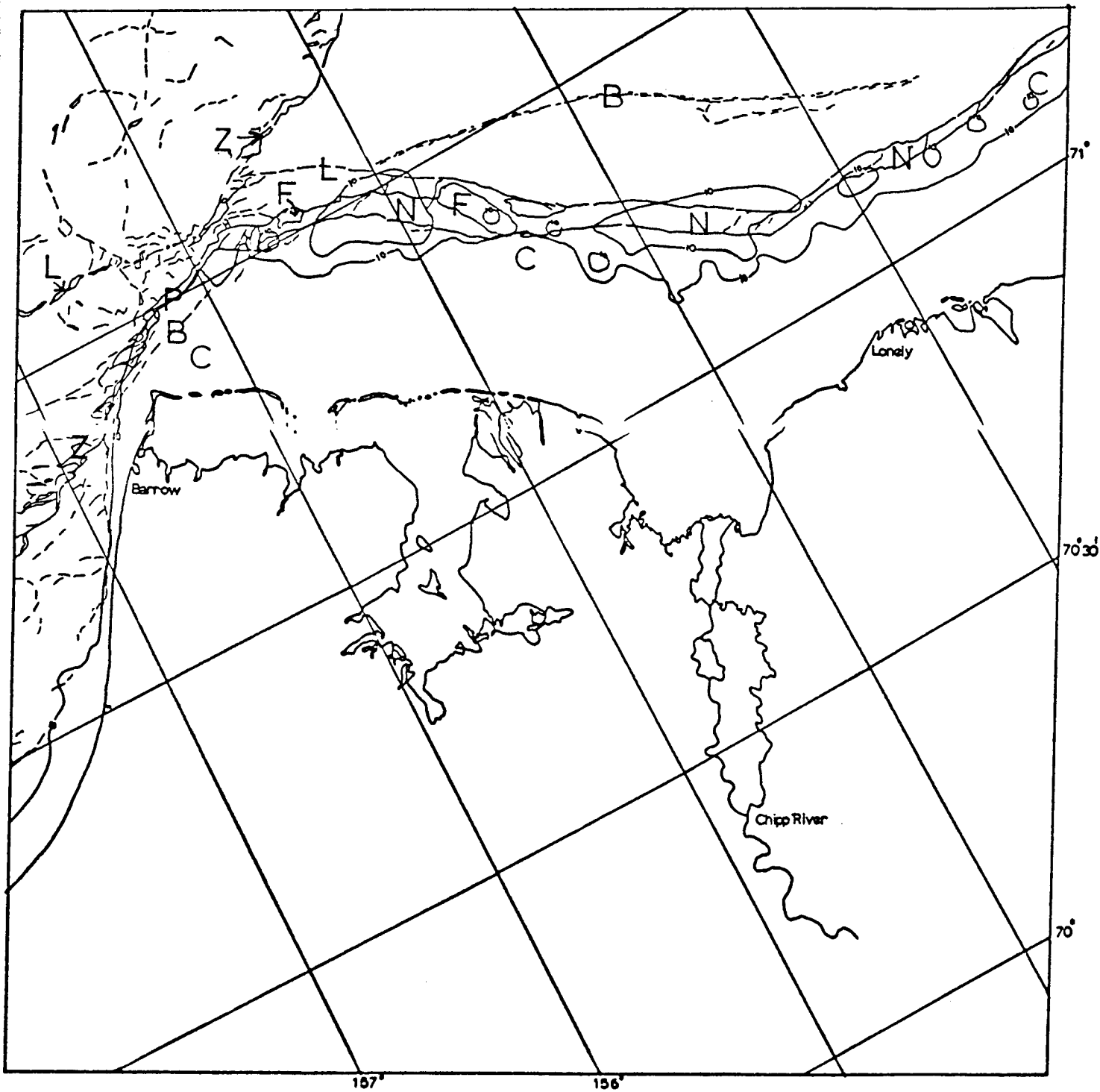
Figure 4e



E-2451-21292-7
17 APRIL 1976

BEAUFORT SEA

Figure 4f

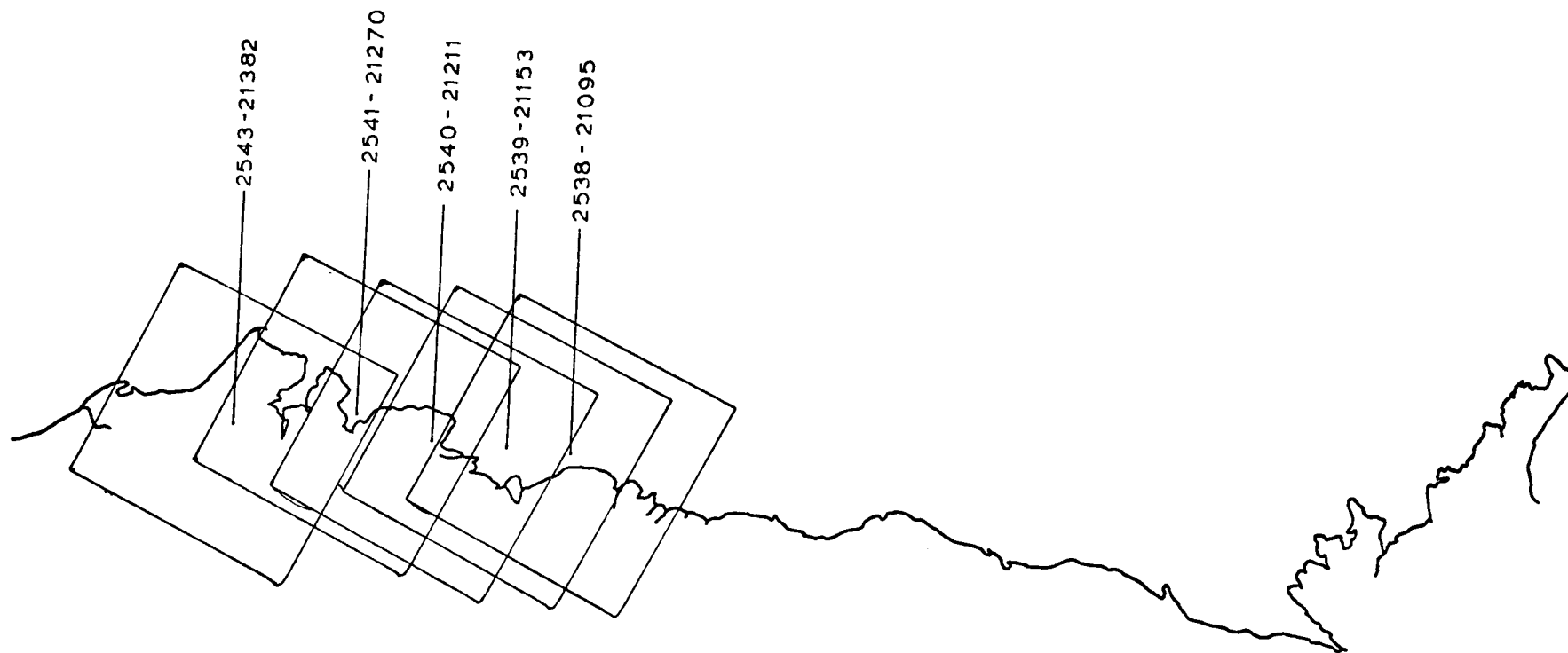


E-2452-21350-7
18 APRIL 1976

KILOMETERS
0 10 20 30 40 50
SCALE APPROX 1:1,000,000

BEAUFORT SEA

Figure 4g



BEAUFORT SEA

30 JUNE - 17 JULY 1976

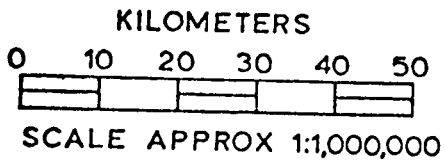
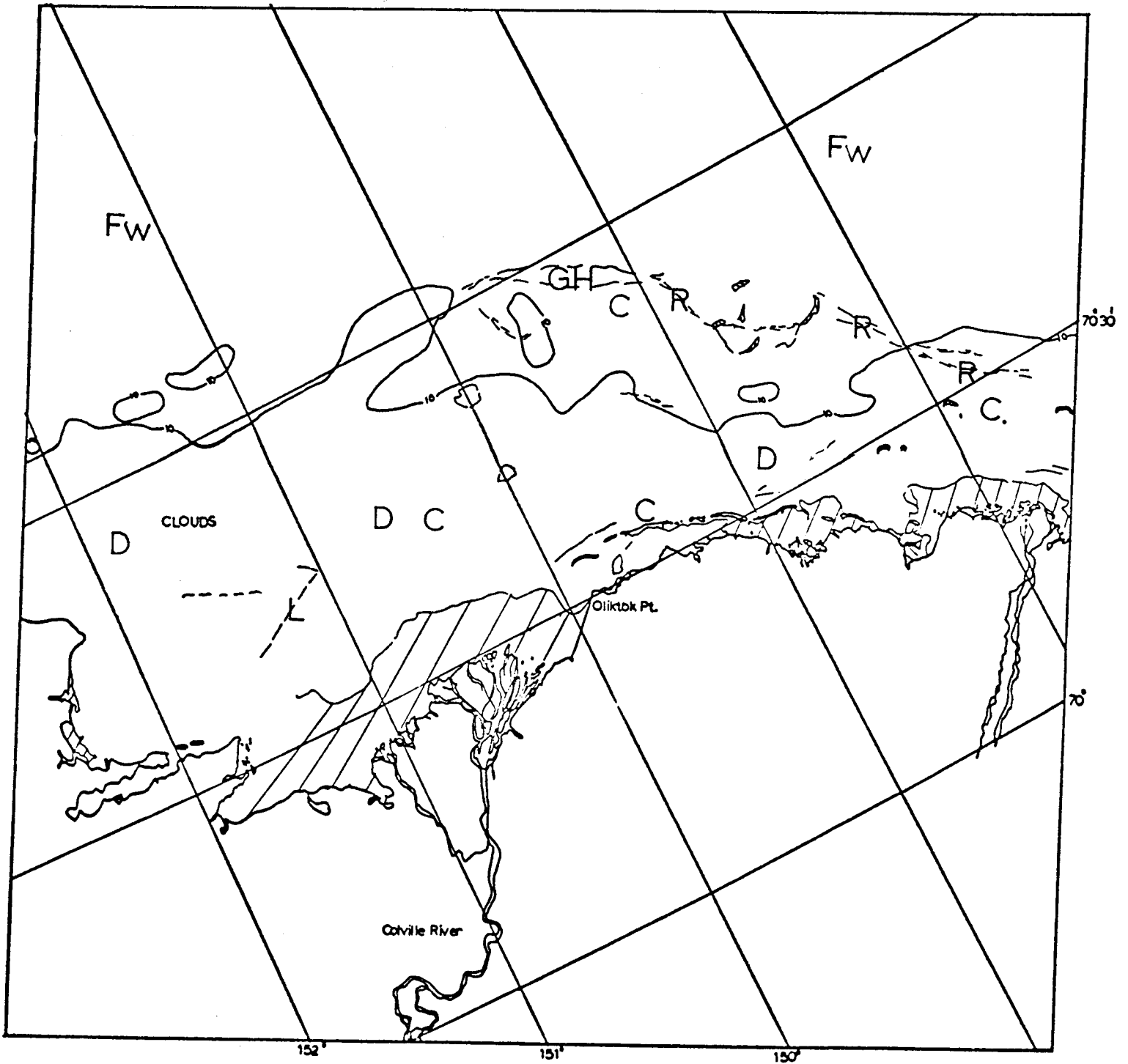
IMAGES: 2525 - 2542

Figure 5

Scenes 2538-21095 through 2543-21382

By this time (mid-July) the pack ice is highly fractured and contains many small open areas. At the same time, river overflows near shore have helped melt vast expanses of ice just adjacent to the coast. Although the large grounded hummock field in Harrison Bay is still in place, the ridge system extending from the hummock field toward Cross Island has been broken by several leads. This portion of the ridge system was located in waters over 10-fathoms. This event is further evidence that the 10-fathom isobath is near the limit of grounded ice.

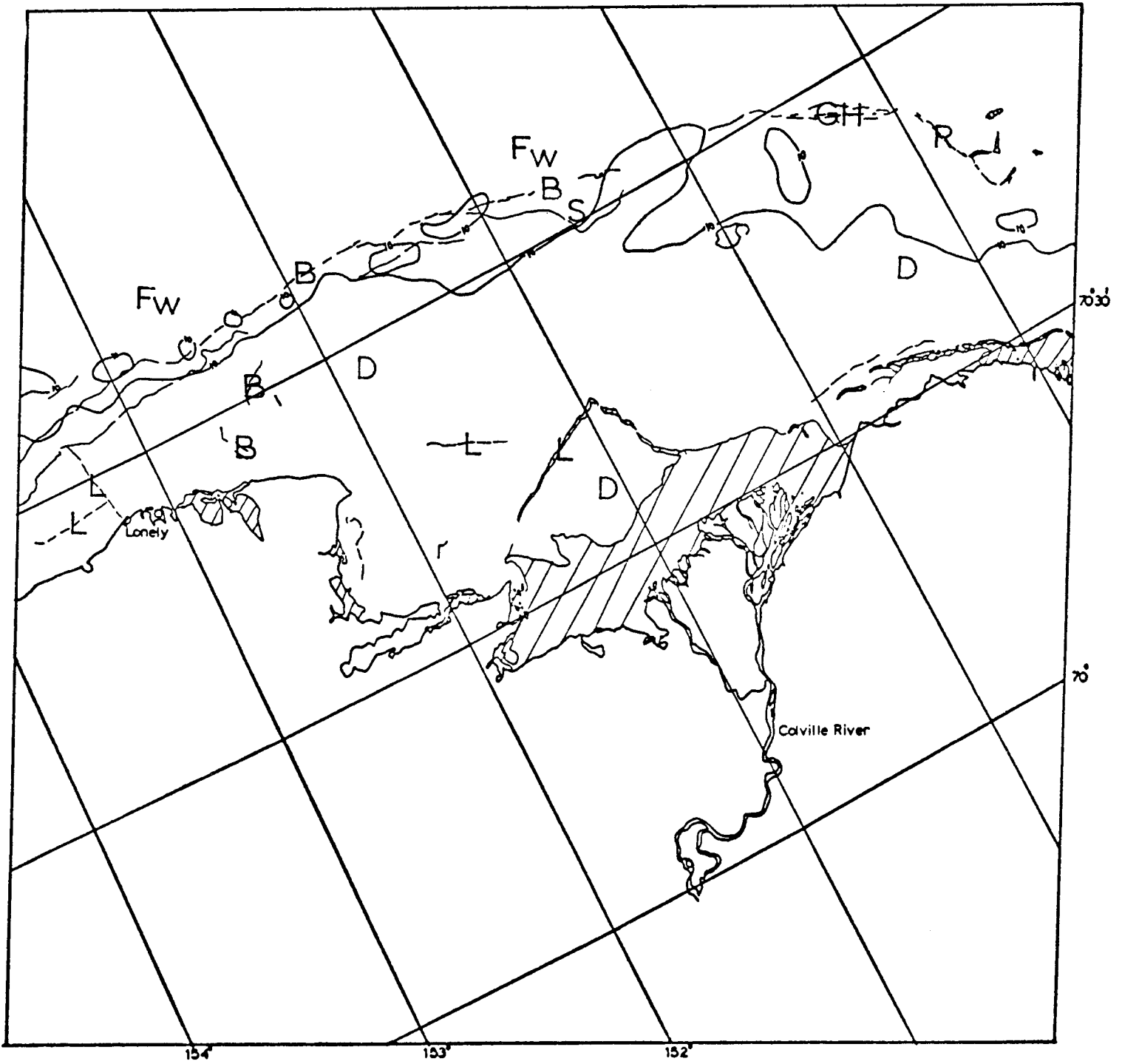
Between the pack ice and open water near shore is a considerable expanse of decayed ice held in place by the grounded ridges. Field observations showed that much of this ice consisted of very dirty floes which were very likely relics of the previous ice year. During the period of observation of this sequence several leads are opening in the decayed contiguous ice.



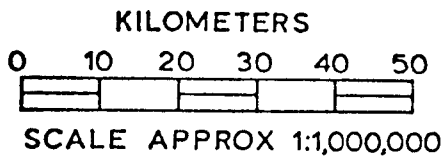
E-2538-21095-7
13 JULY 1976

BEAUFORT SEA

Figure 5a

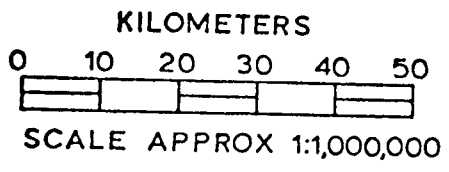
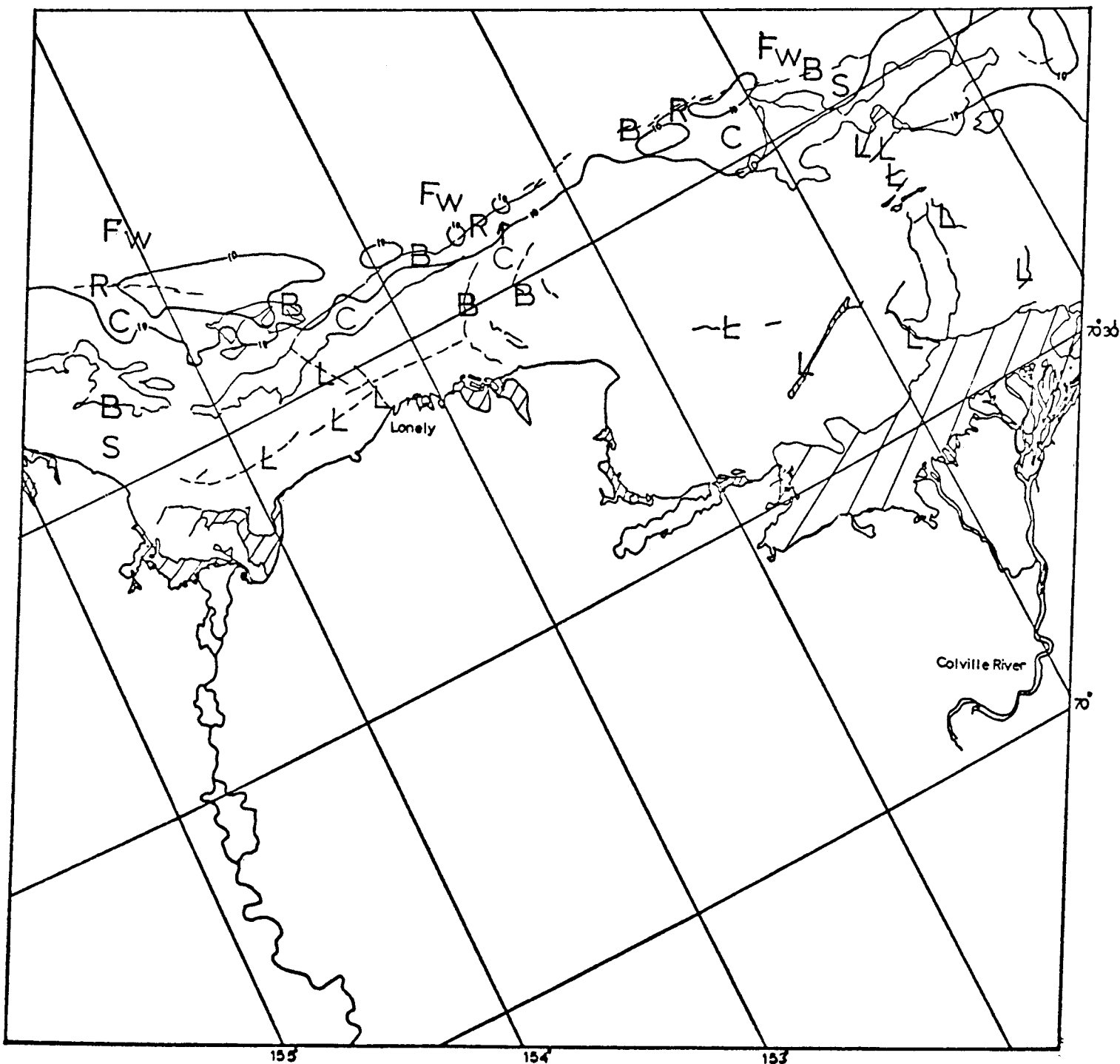


E-2539-21153-7
14 JULY 1976



BEAUFORT SEA

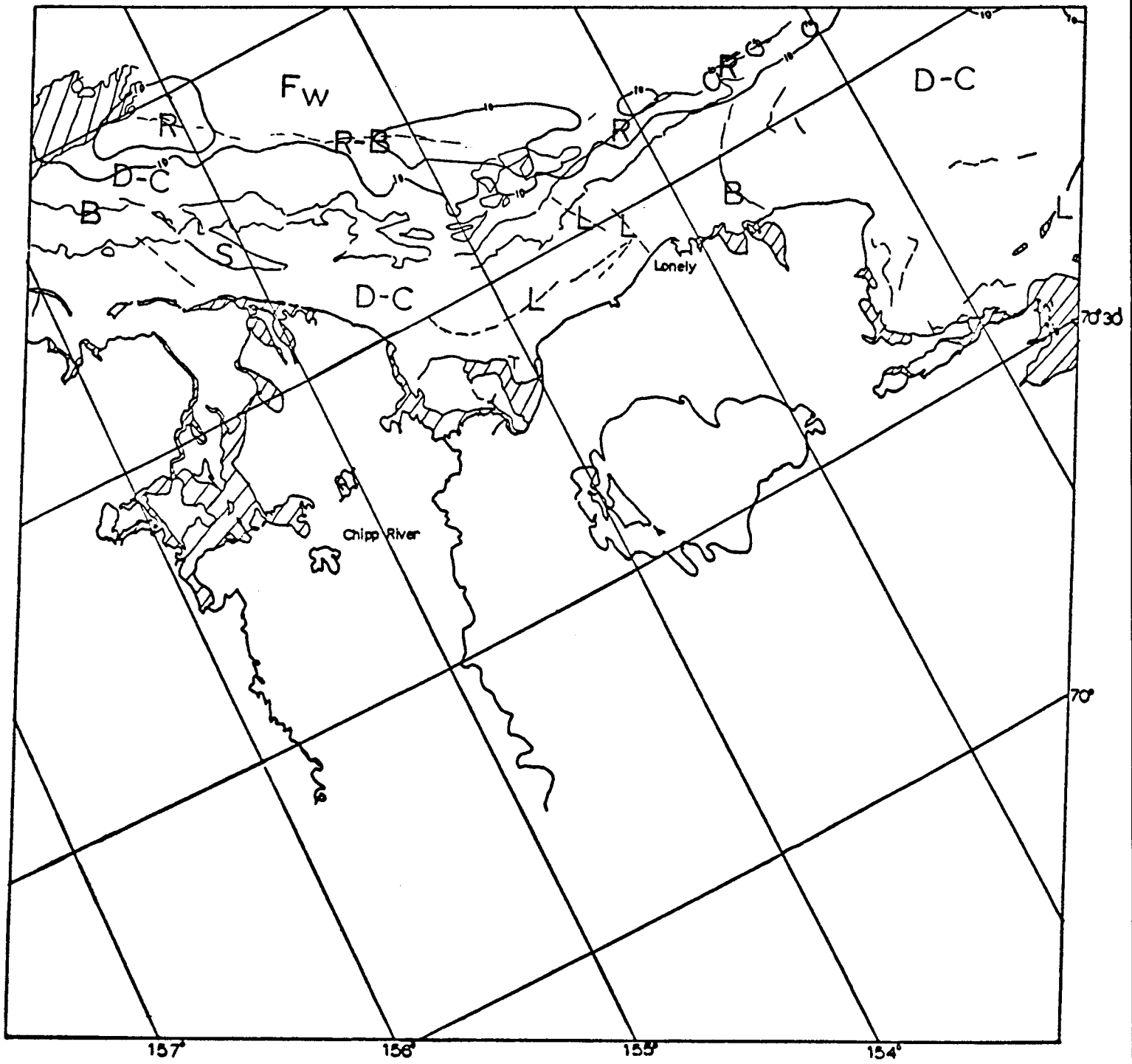
Figure 5b



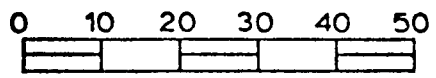
E-2540-2121-7
15 JULY 1976

BEAUFORT SEA

Figure 5c



KILÒMETERS



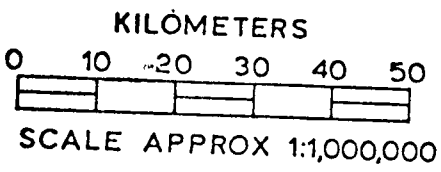
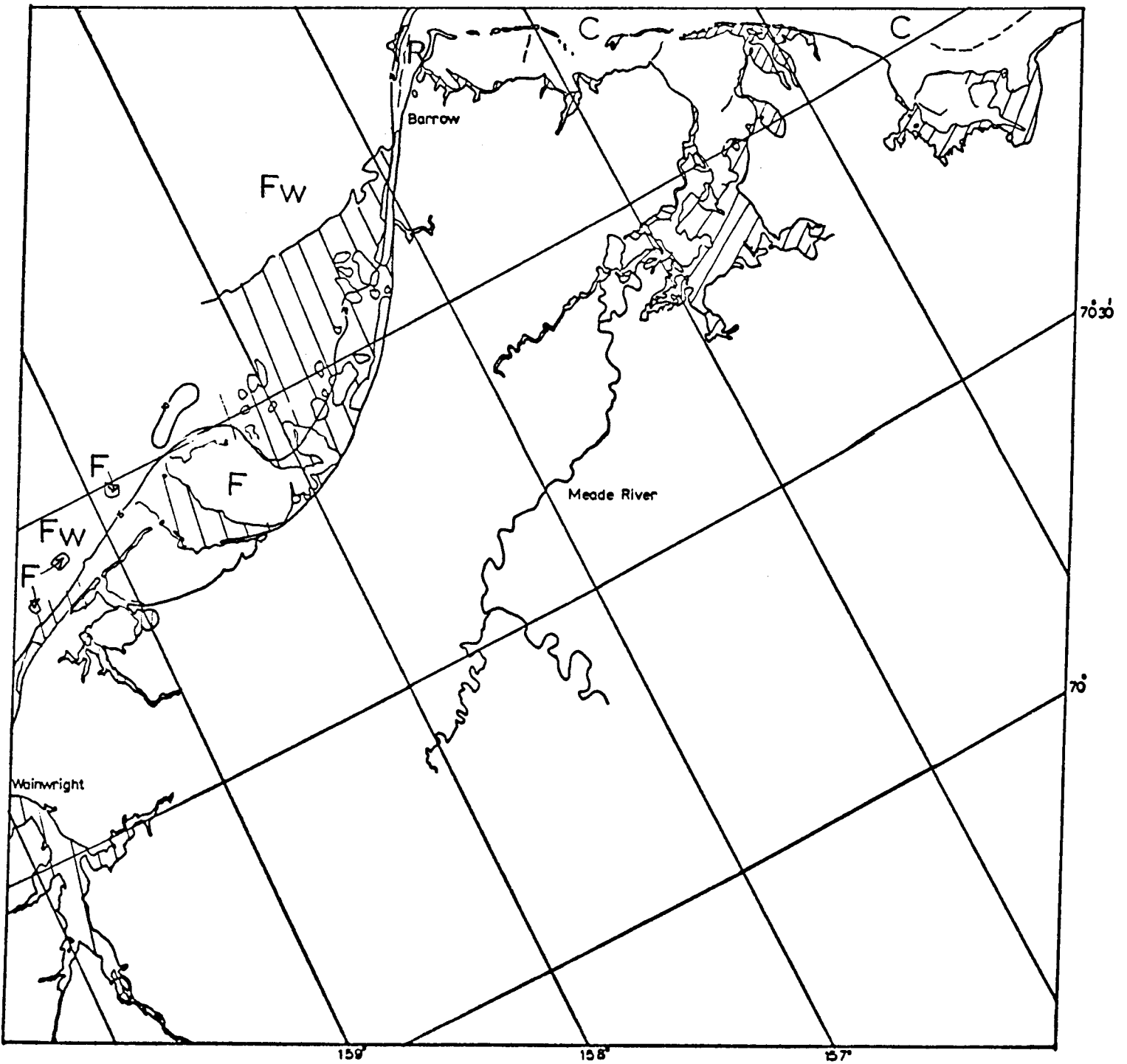
SCALE APPROX 1:1,000,000

BEAUFORT SEA

E-2541-21270-7

16 JULY 1976

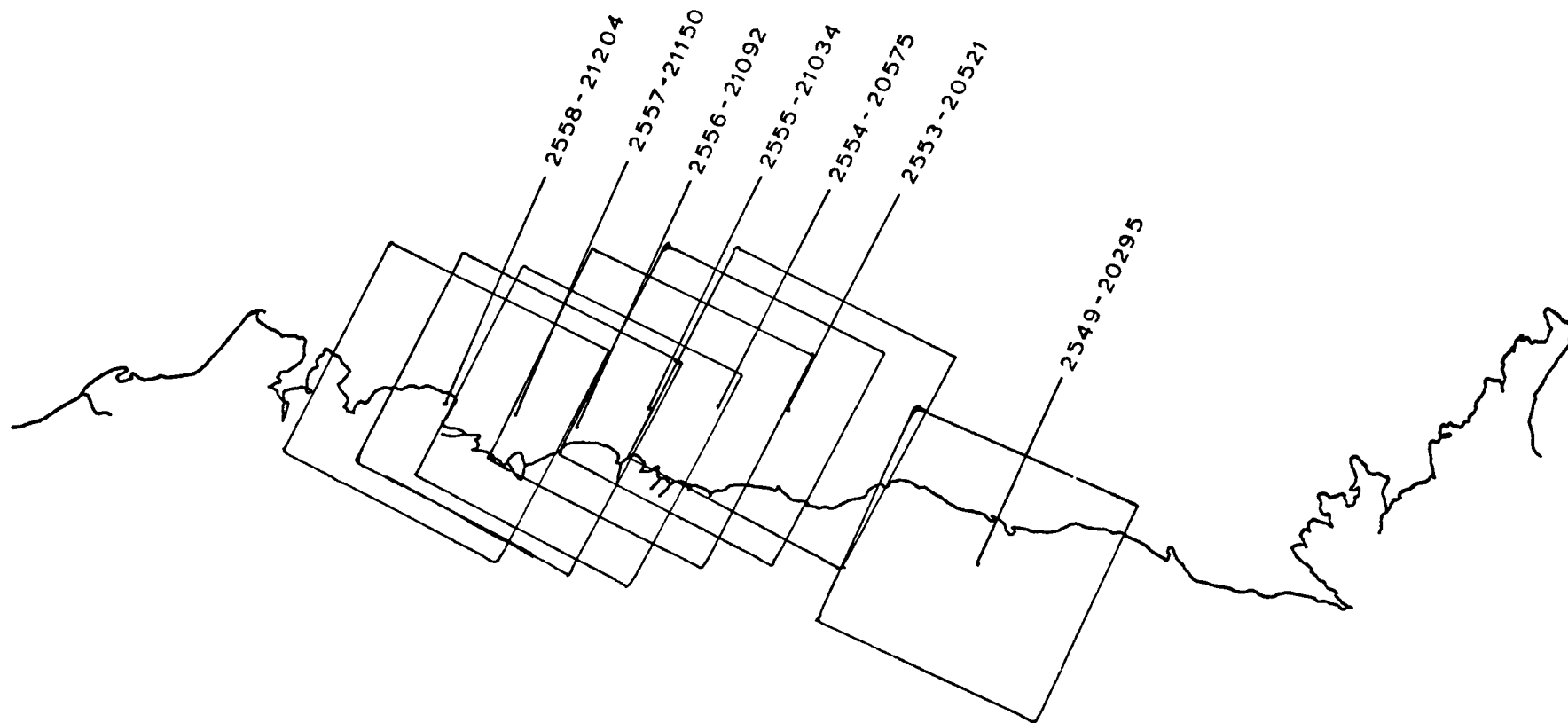
Figure 5d



E-2543-21382-7
16 JULY 1976

BEAUFORT SEA

Figure 5e



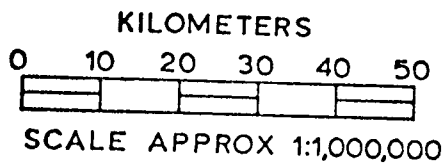
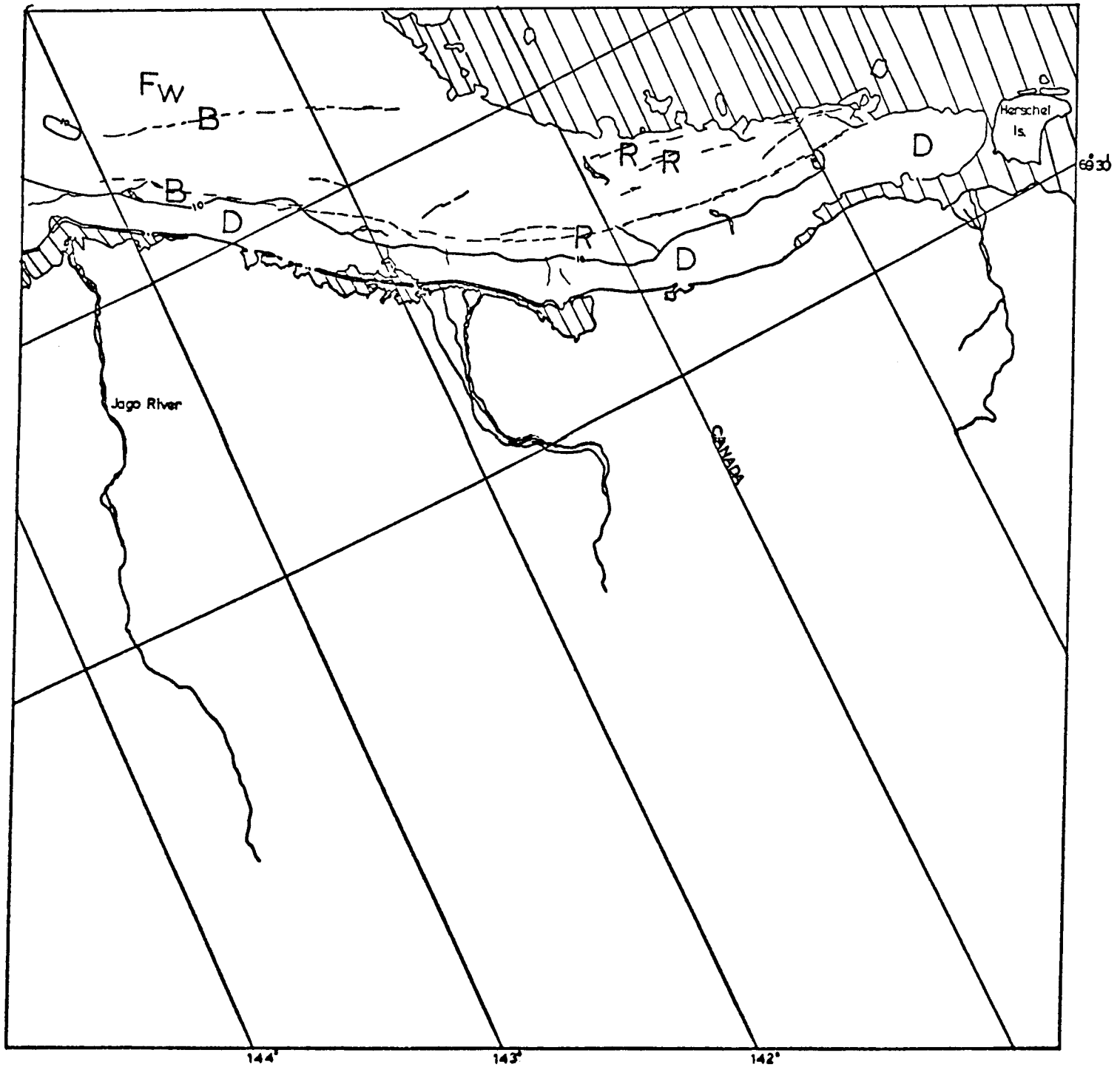
BEAUFORT SEA
18 JULY to 4 AUGUST 1976
IMAGES: 2543-2560

Figure 6

Scenes 2549-20295 through 2558-21204

These late July and early August scenes show the near shore ice in advanced stages of decay and break-up. Nearly all ice inshore of the grounded ridges has melted. Beyond the grounded ridges the ice is defined by the category "FW" - floes in water. The grounded ridges themselves show signs of breaking up and moving at least short distances. The extensive grounded ridges off Harrison Bay have broken up and are now drifting. A small area approximately 10 by 30 km in extent offshore between Harrison and Prudhoe Bays containing two major ridge systems appears to have not yet broken up.

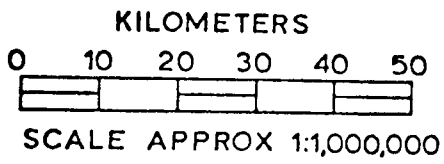
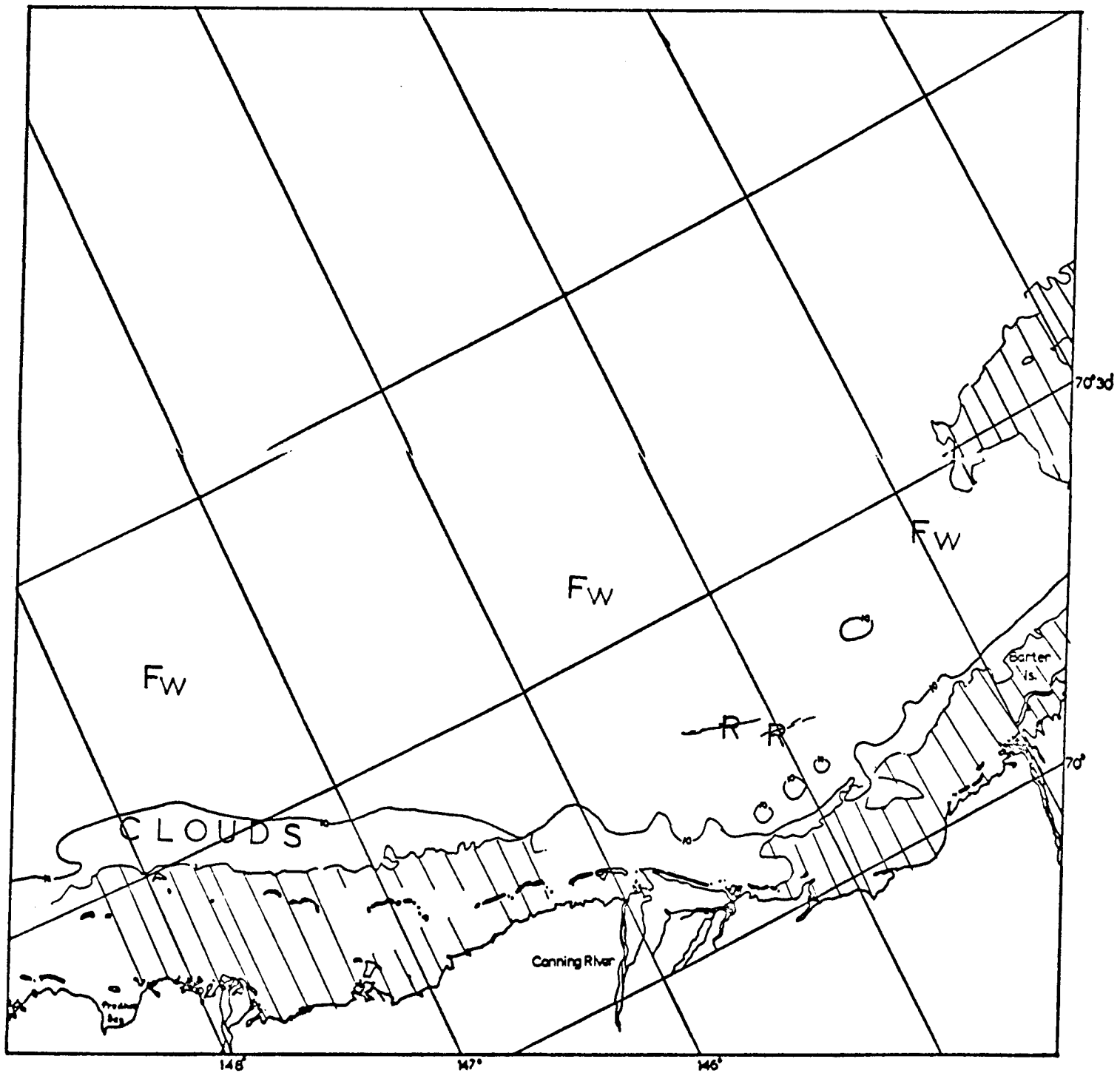
West of Harrison Bay the east-west ridge system lying just seaward of the line of shoals above the 10-fathom isobath has broken up and drifted away. Since the November sequence this ridge system had been the edge of contiguous ice.



E-2549-20296-7
24 JULY 1976

BEAUFORT SEA

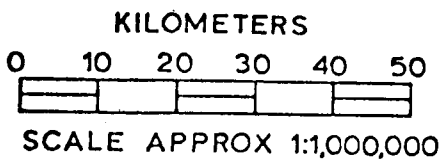
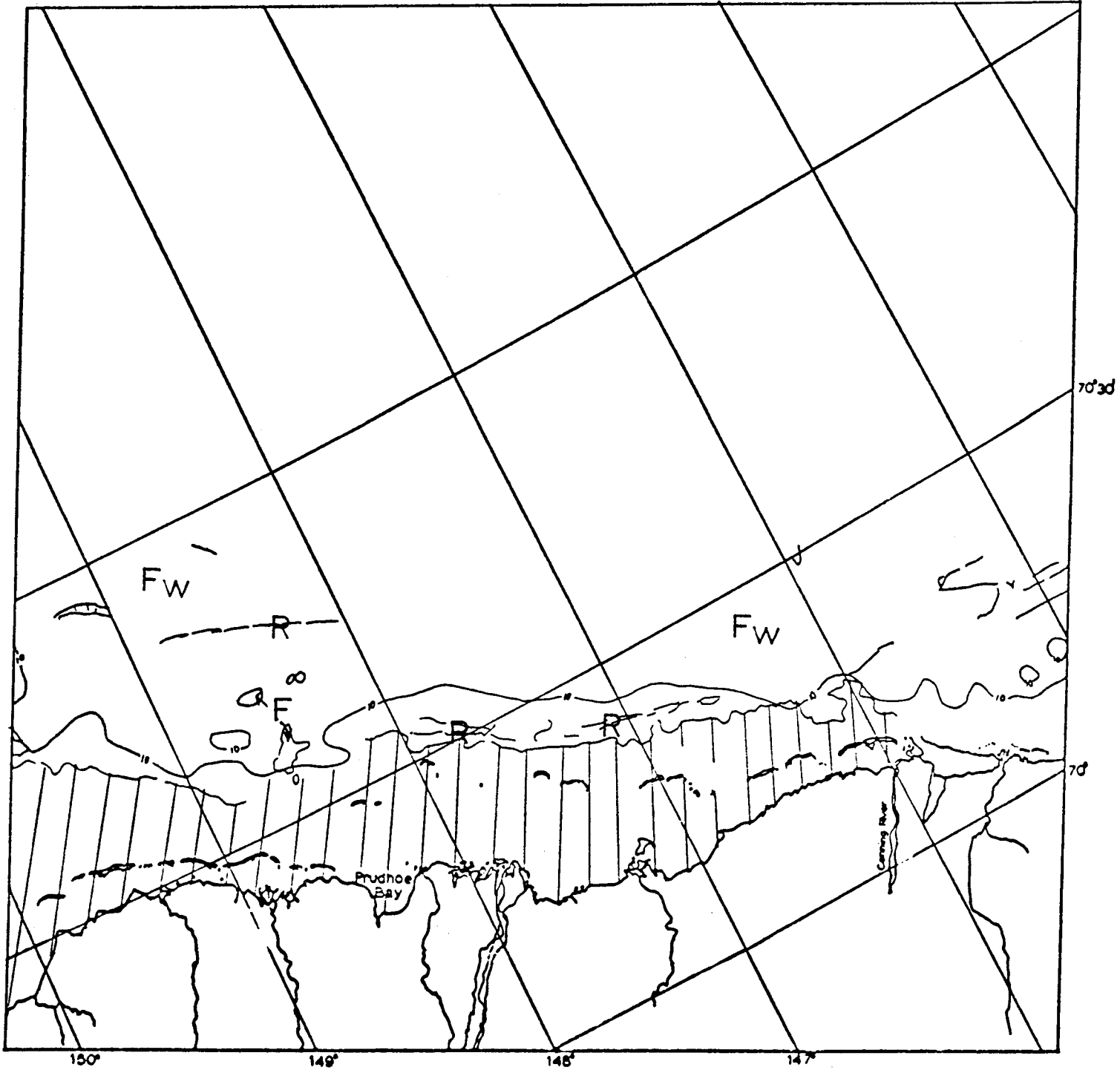
Figure 6a



E-2553-20521-7
 28 JULY 1976

BEAUFORT SEA

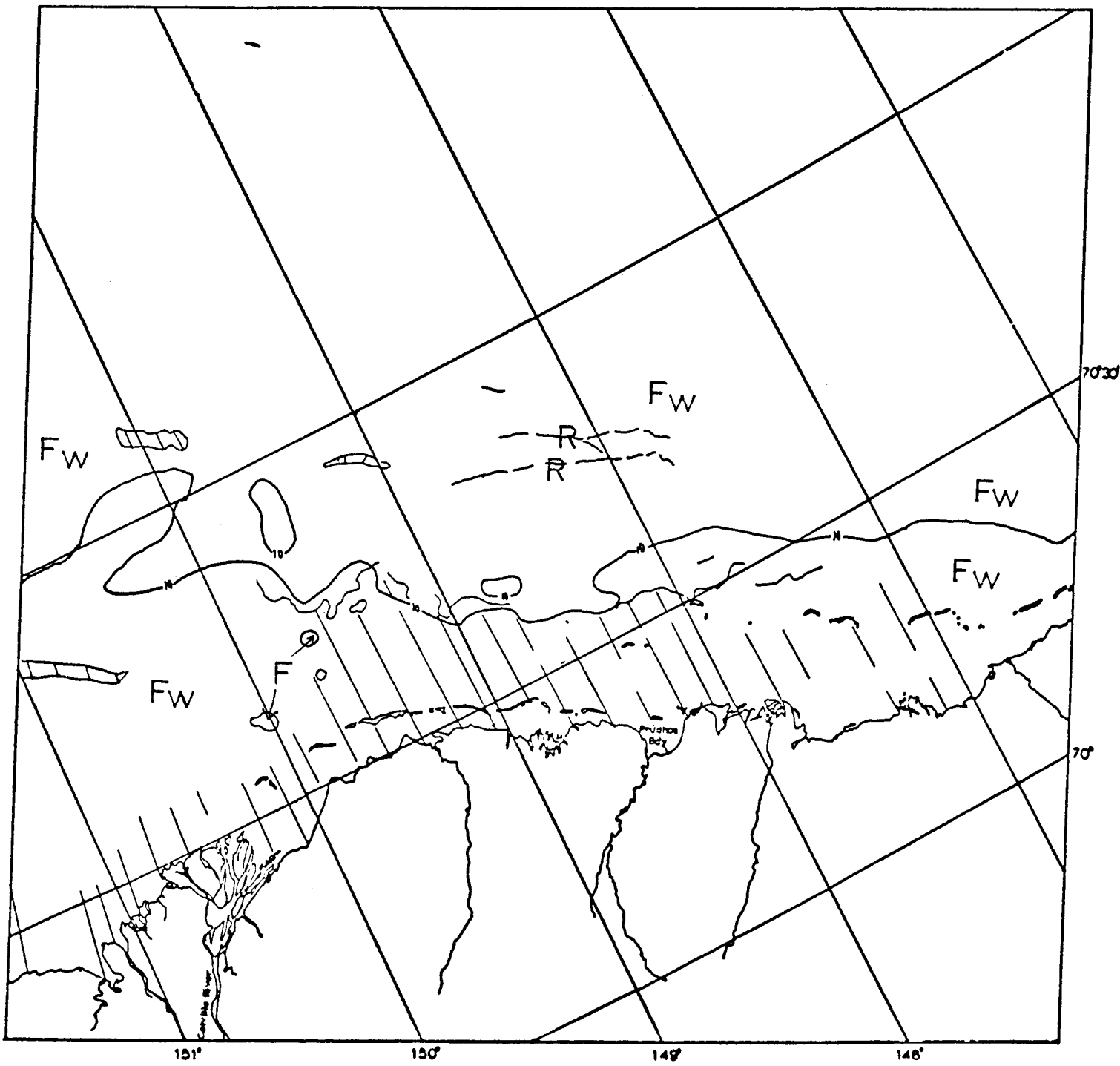
Figure 6b



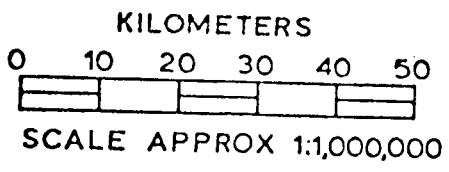
E-2554-20575-7
29 JULY 1976

BEAUFORT SEA

Figure 6c

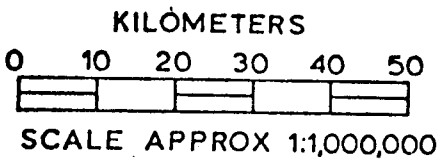
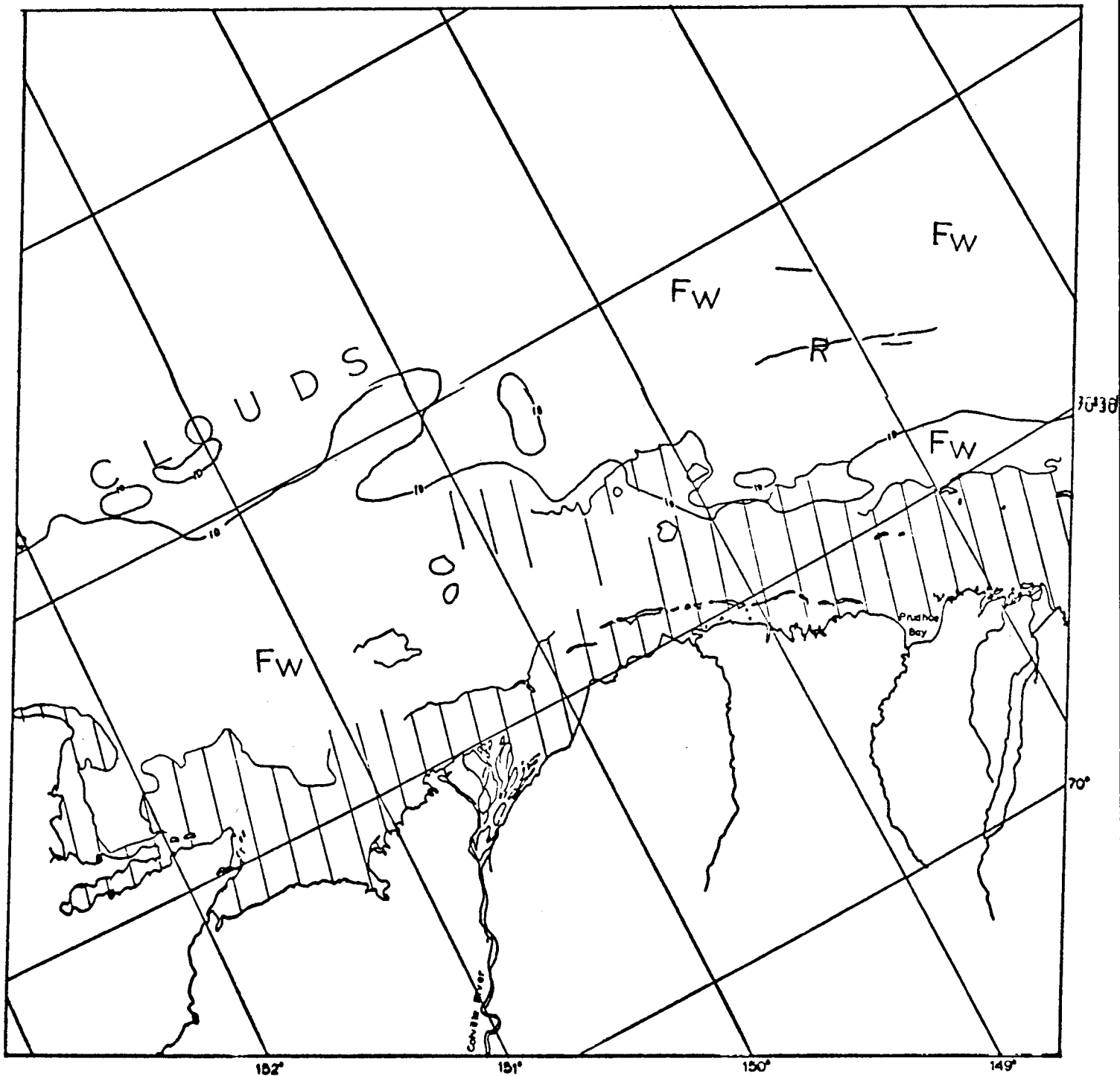


E-2555-21034-7
30 JULY 1976



BEAUFORT SEA

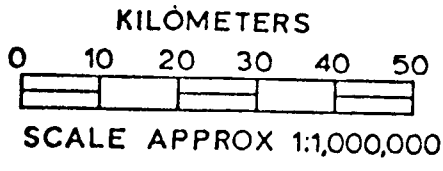
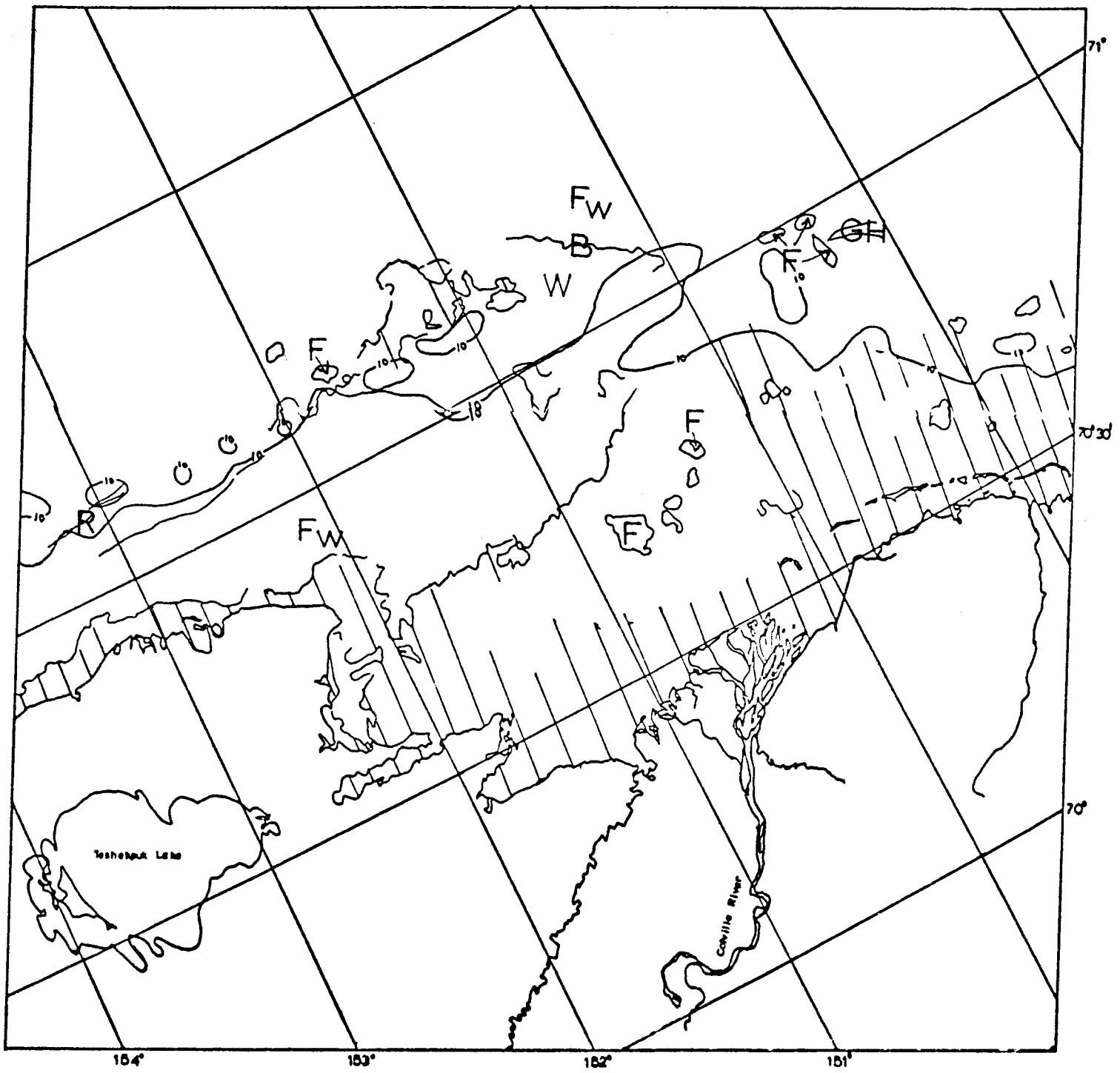
Figure 6d



E-2556-21092-7
31 JULY 1976

BEAUFORT SEA

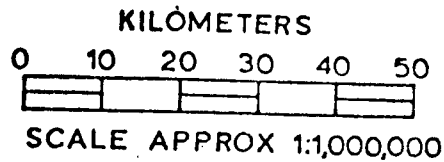
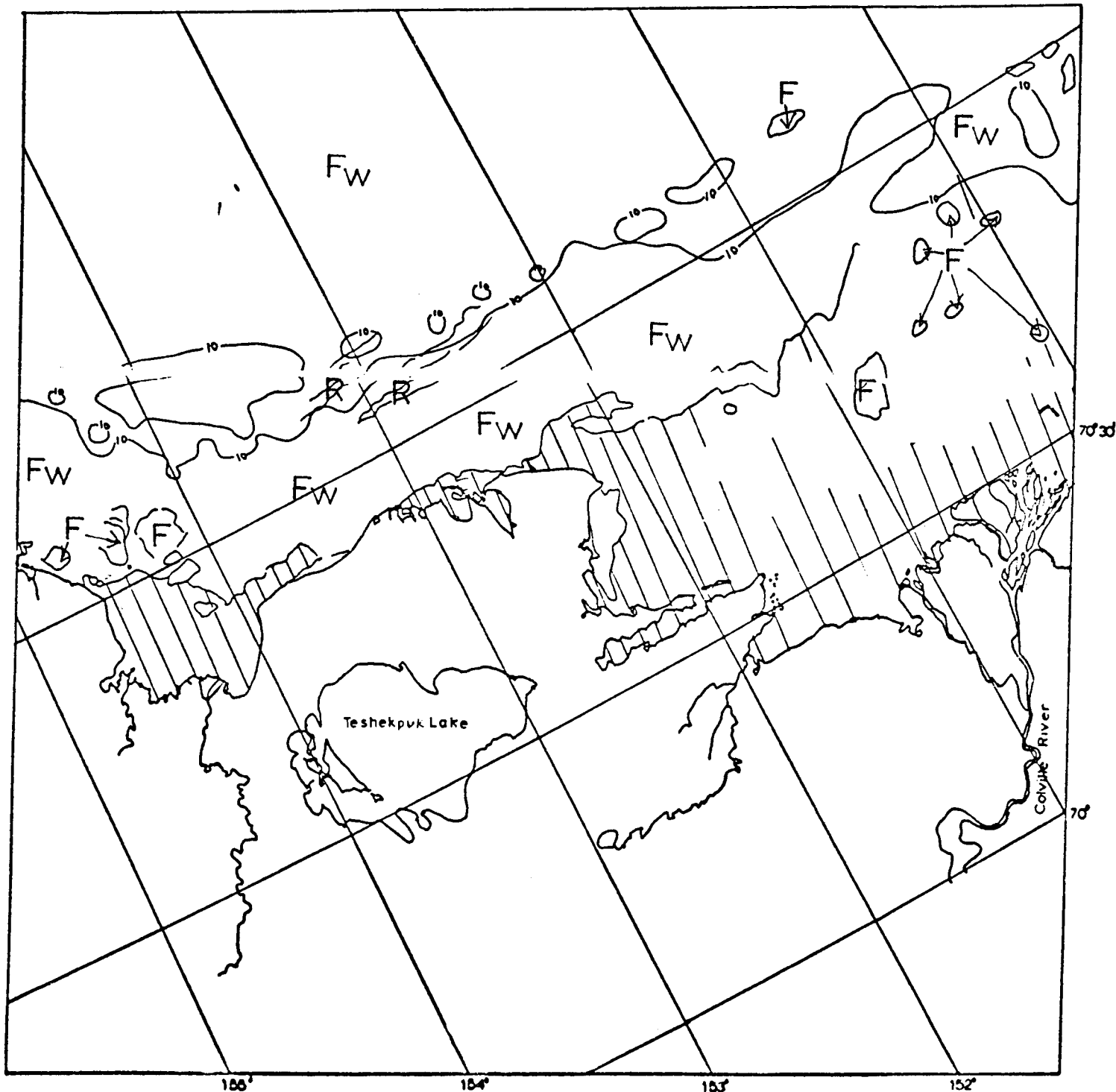
Figure 6e



E-2557-21150-7
 01 AUGUST 1978

BEAUFORT SEA

Figure 6f



E-2558-21204-7
 02 AUGUST 1978

BEAUFORT SEA

Figure 6g

BERING SEA
16 FEBRUARY
to
4 MARCH
1976

IMAGES: 2390 - 2407

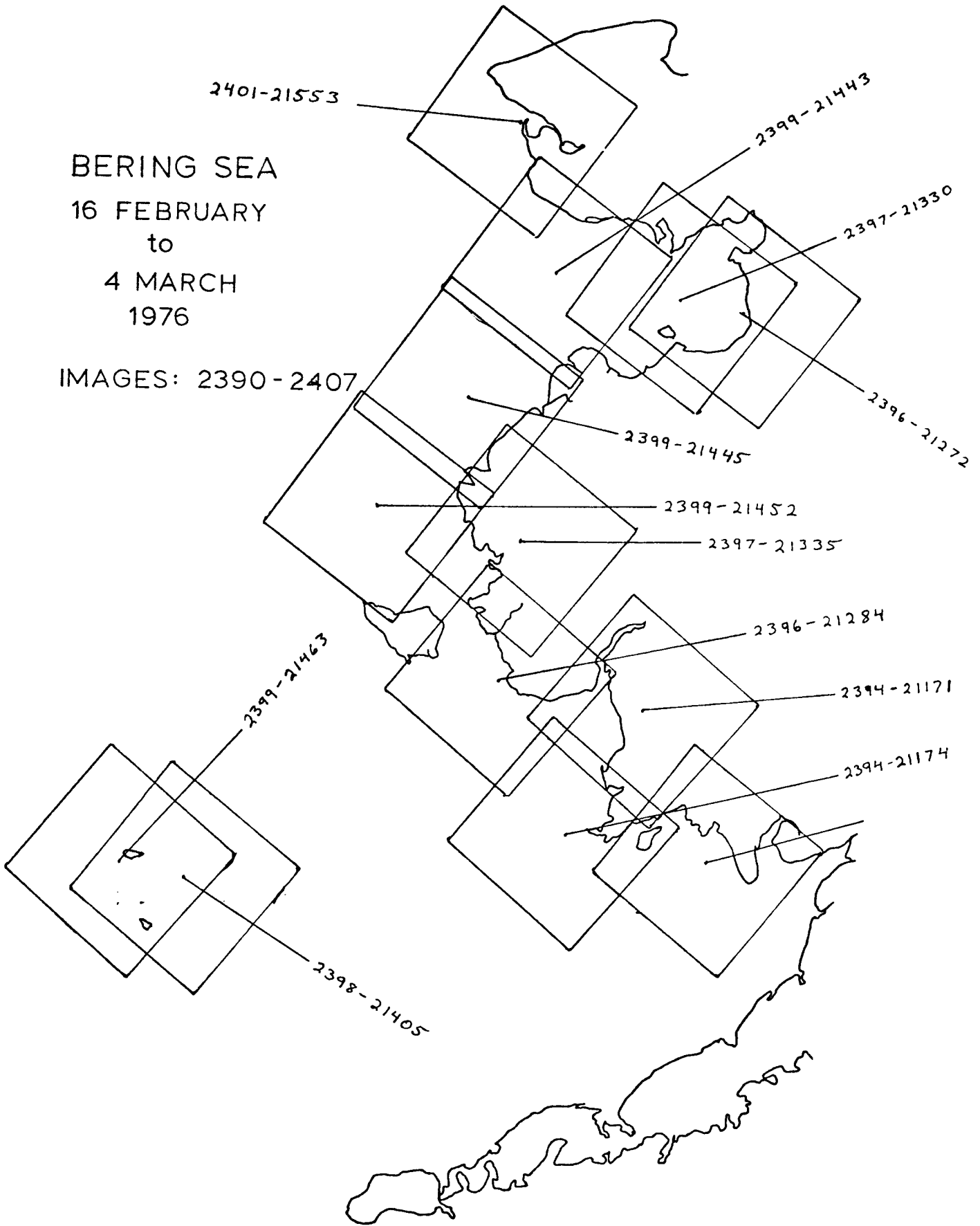


Figure 7

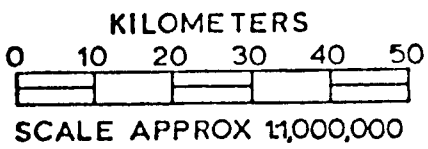
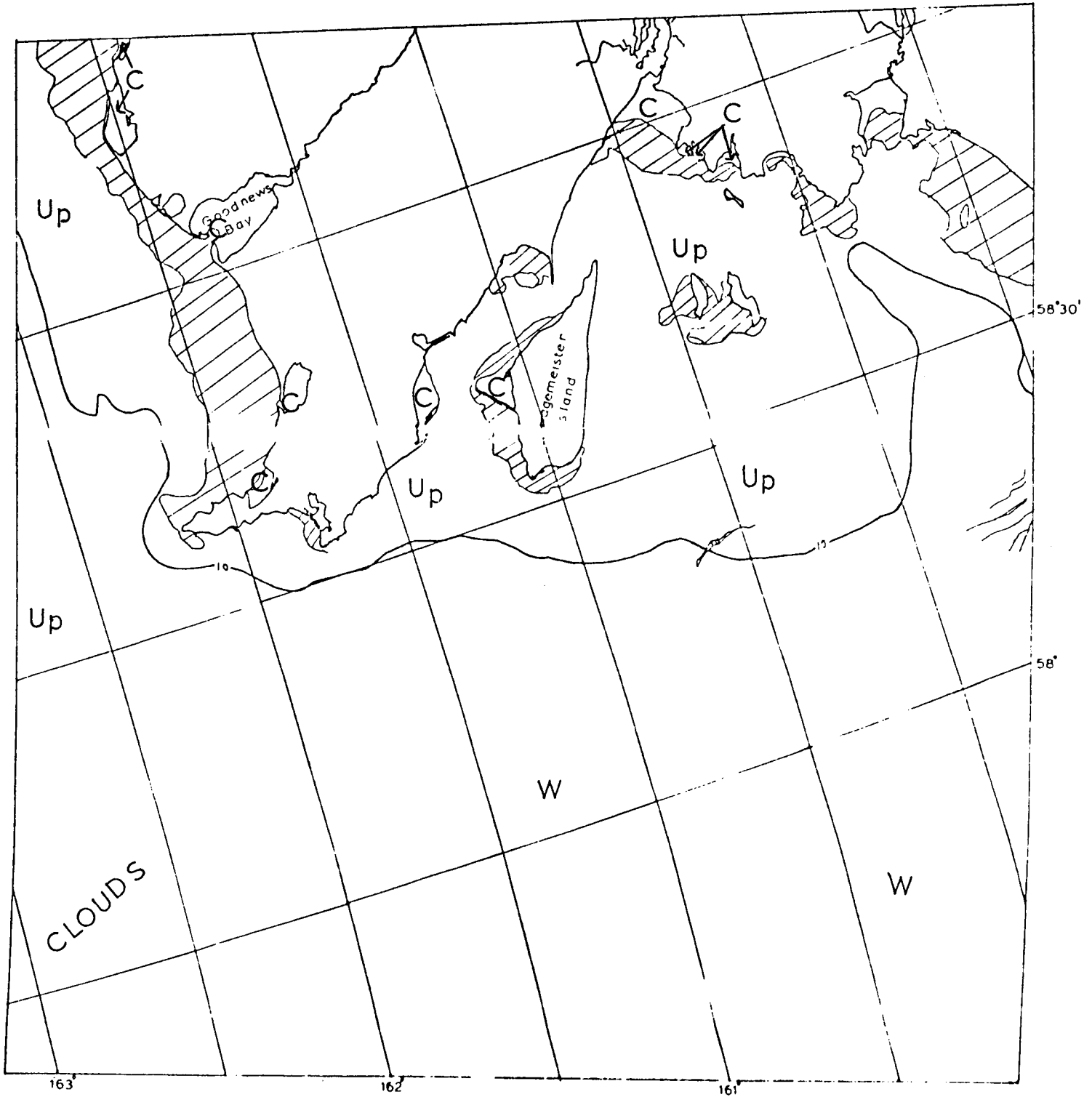
Scenes 2392-21051 through 2401-21553

This second sequence of Landsat scenes for 1976 was obtained two and one half weeks after the first sequence. During this interval the major change in near shore ice conditions along northern Bristol Bay has been growth of the contiguous ice in the shallow embayments.

Kuskokwim Bay shows contiguous ice only on very shallow mud flats and some indications of rafting away of ice in inlets. Norton Sound exhibits evidence of almost constant ice motion out of the Sound and into Bering Sea. Contiguous ice is not correlated well with Bathymetry - - - physical protection appears to be a much more important controlling factor. Most of the contiguous ice is young ice lying in protected embayments around the edges of the Sound. While the center of the Sound is filled with a column of very new ice originating at to open water at the head of the Sound, and growing to young ice at the entrance to the Sound. Apparently, this column has been moving seaward out of Norton Sound in increments for some time.

Although considerable ice motion appears to take place through Etolin Strait, no large grounded shear ridge systems appear to have been constructed and contiguous ice on both sides of the Strait is confined to shallow areas far inshore from the 10-fathom isobath.

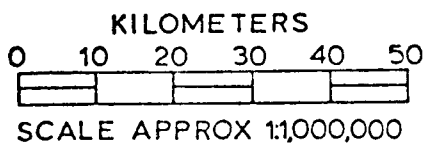
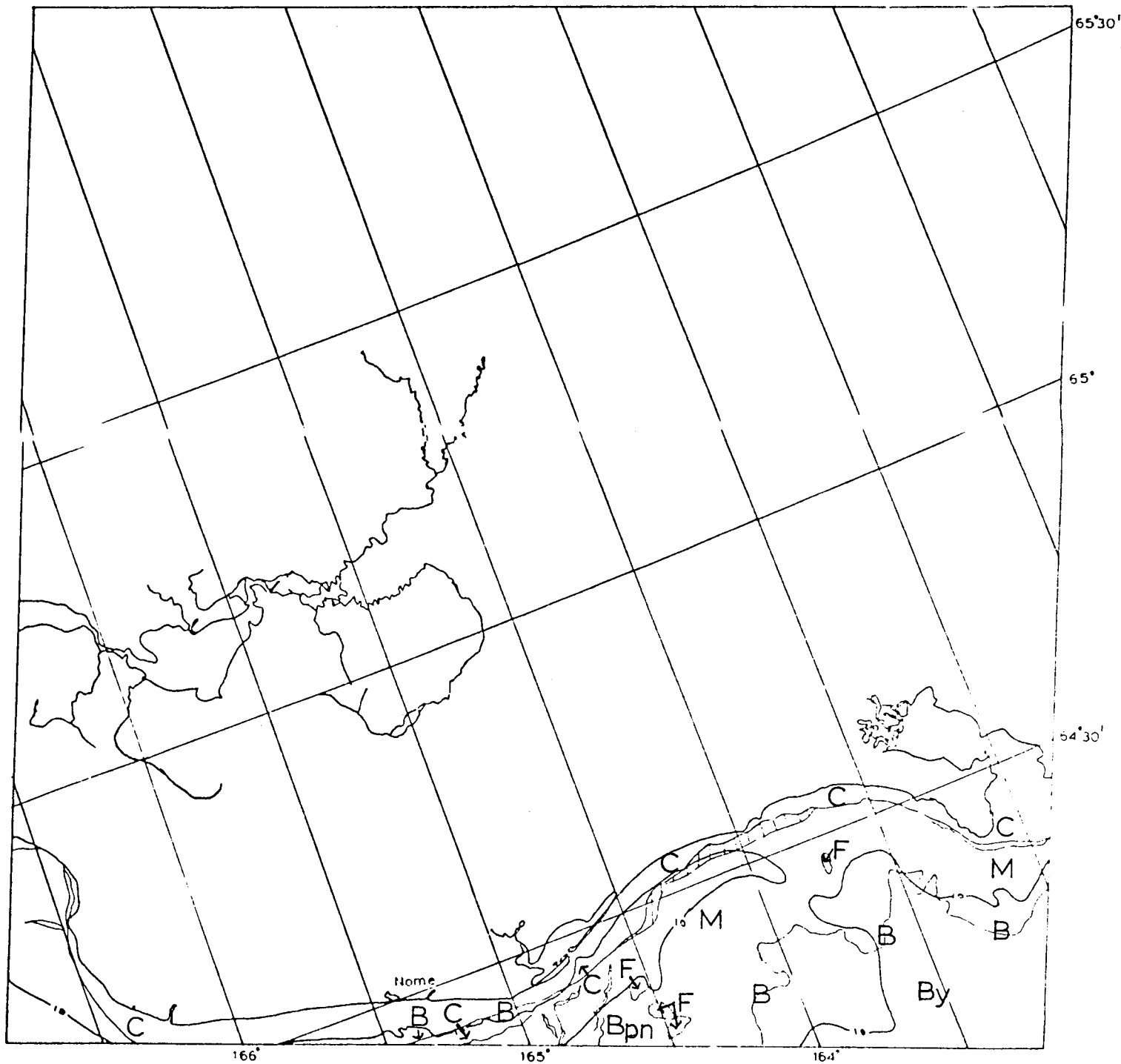
At the mouth of Norton Sound ice exiting the sound is encountering ice in Bering Sea. As a result, floe grinding is taking place in a rather narrow shear zone approximately 30 km north of the mouth of the Yukon River. Shear ridges are apparent on the imagery on both sides of this zone.



E-2375-21122-7
1 FEBRUARY 1976

BERING SEA

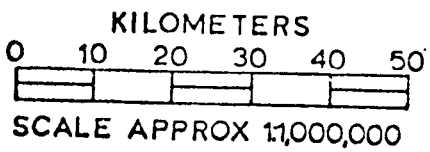
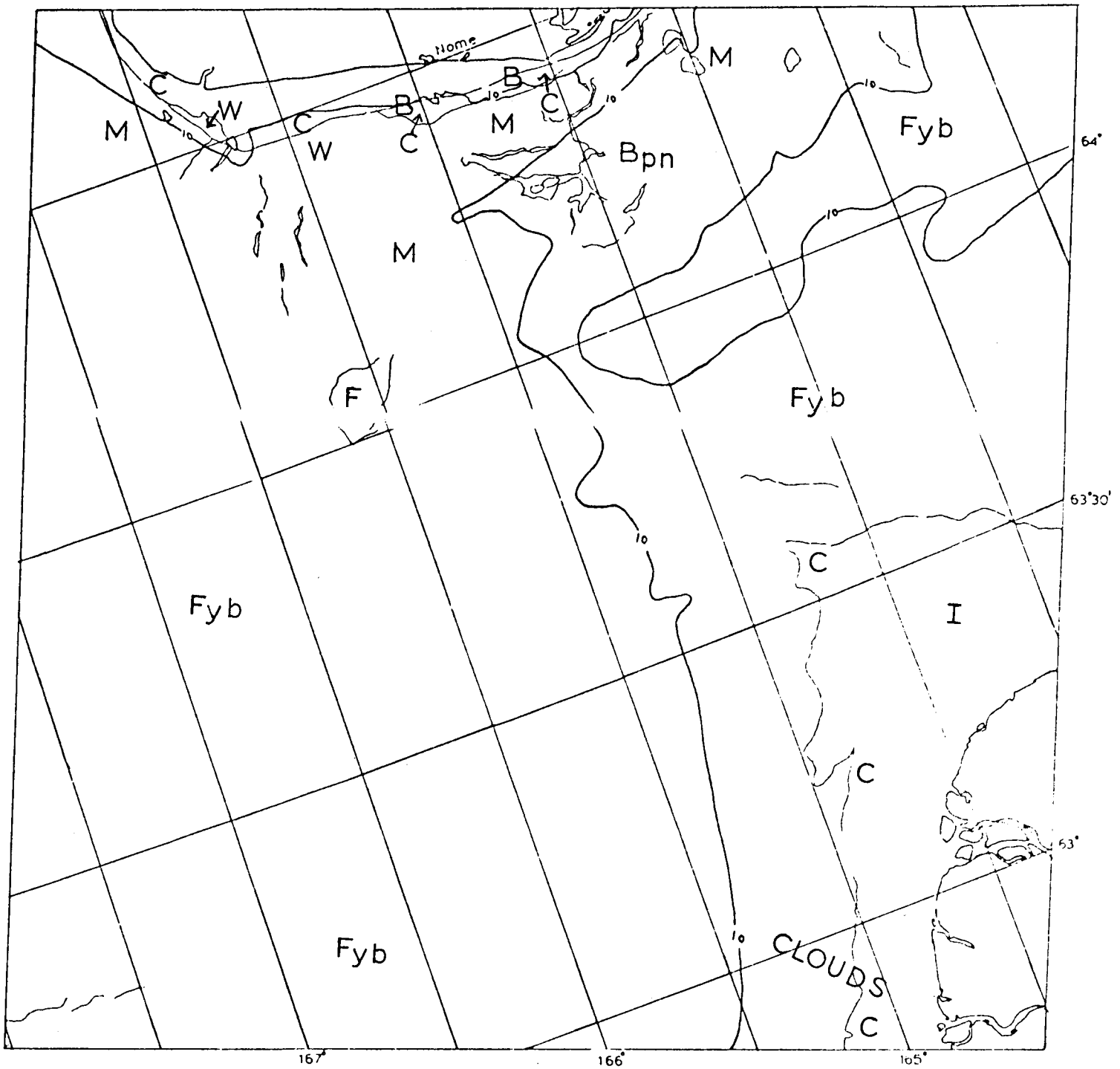
Figure 7a



E-2381-21443-7
7 FEBRUARY 1976

BERING SEA

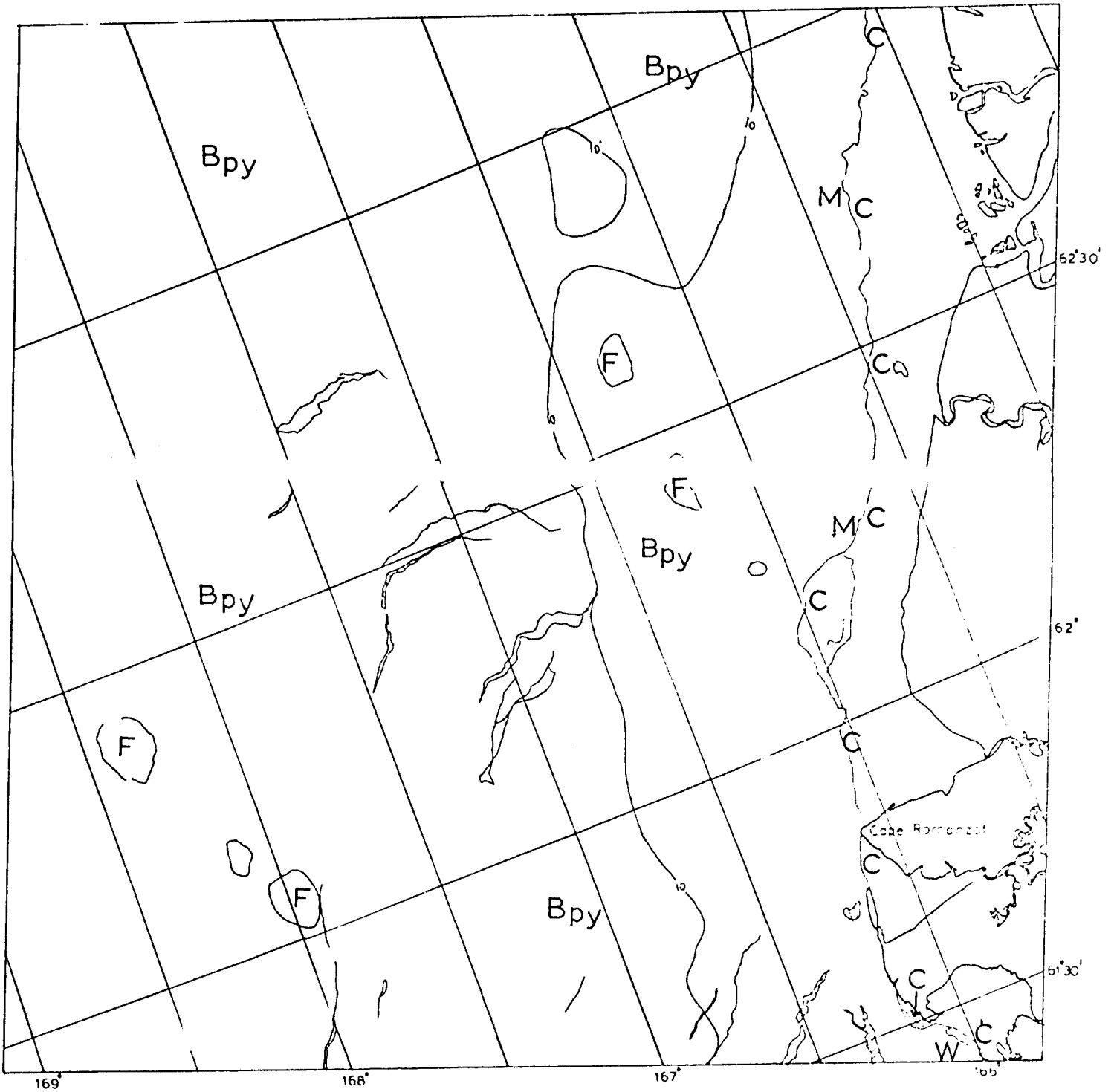
Figure 7b



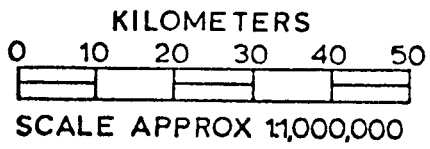
E-2381-21450-7
7 FEBRUARY 1976

BERING SEA

Figure 7c

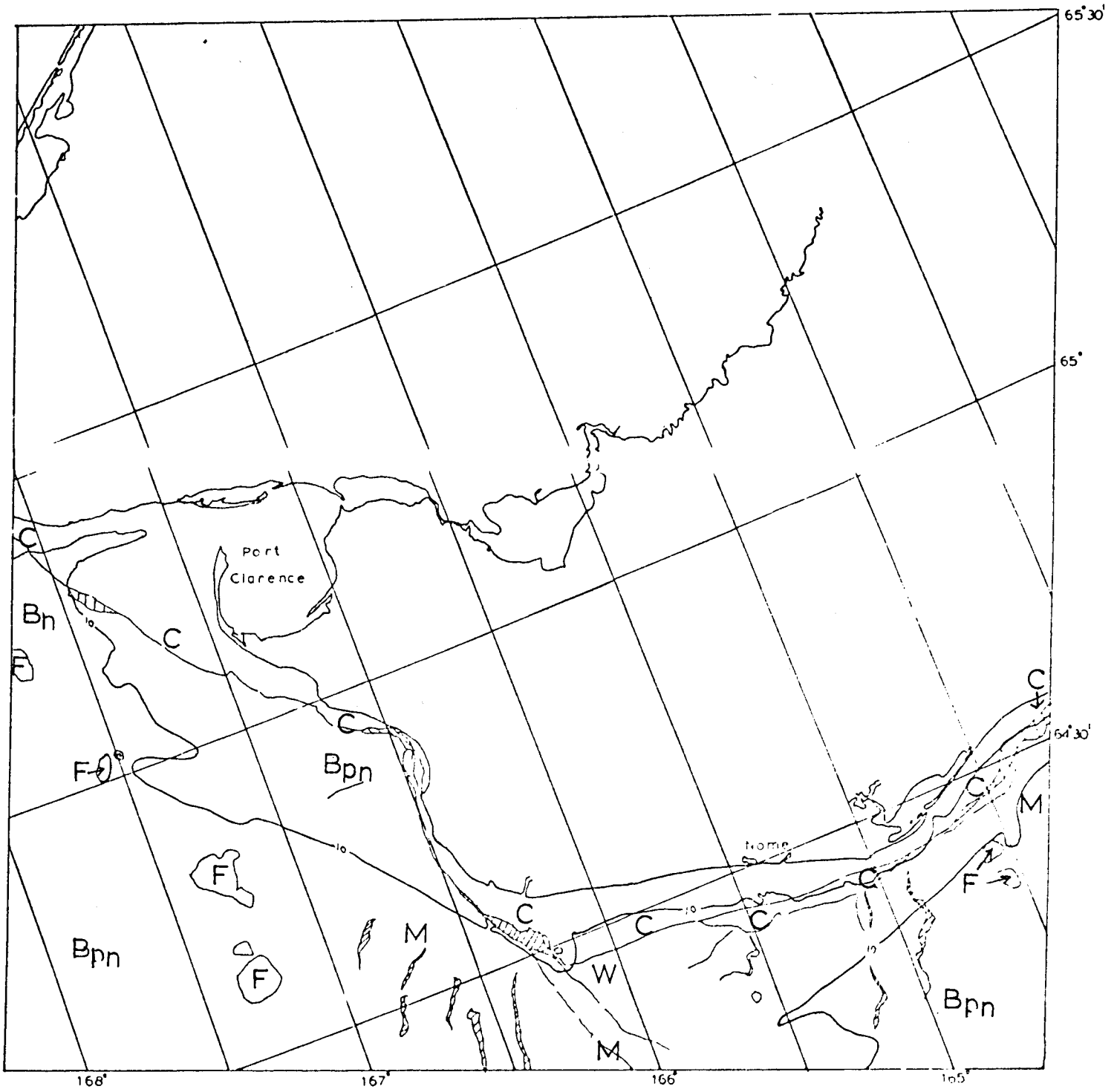


E-2381-21452-7
7 FEBRUARY 1978



BERING SEA

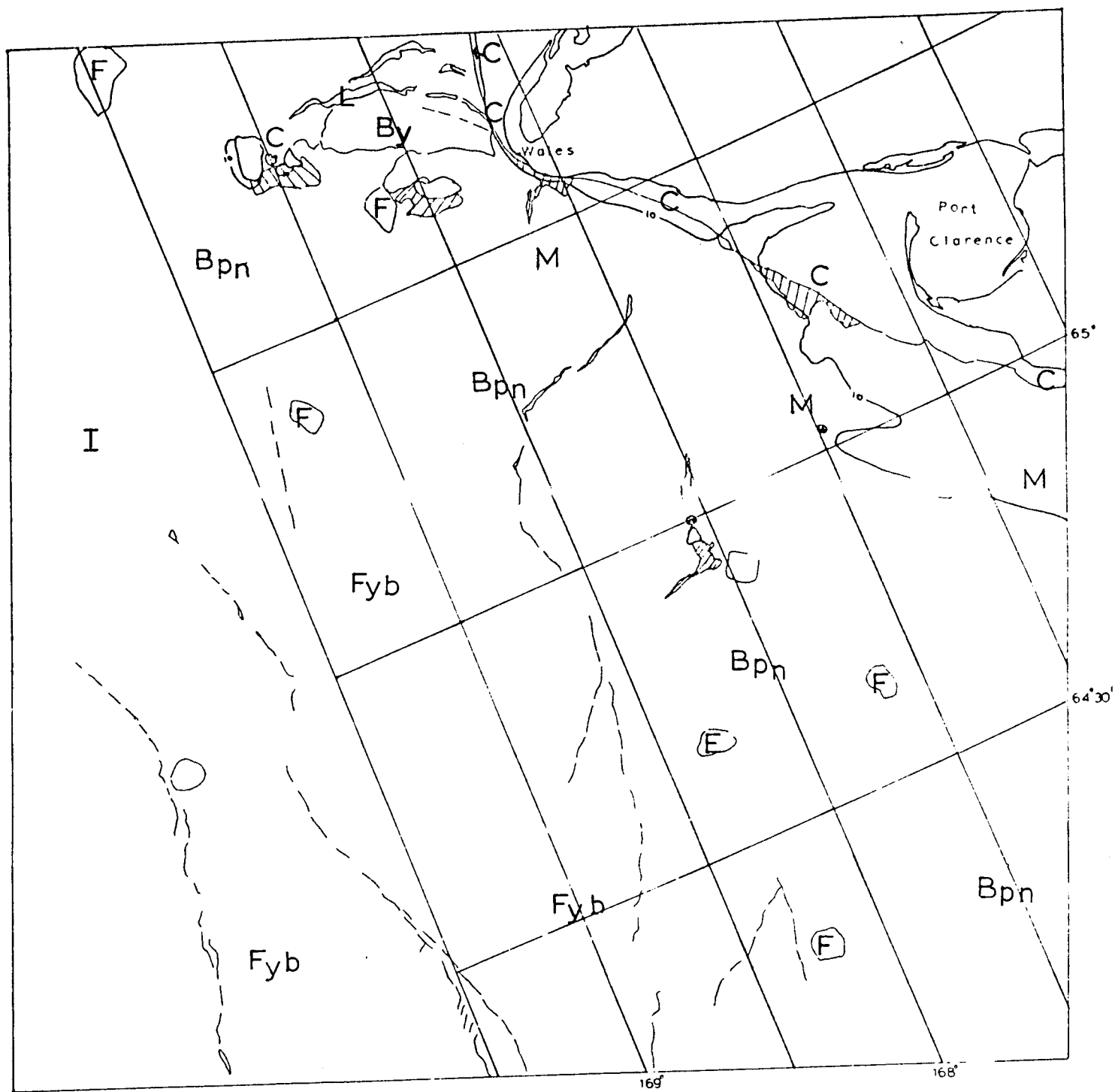
Figure 7d



E-2382-21502-7
8 FEBRUARY 1976

BERING SEA

Figure 7e

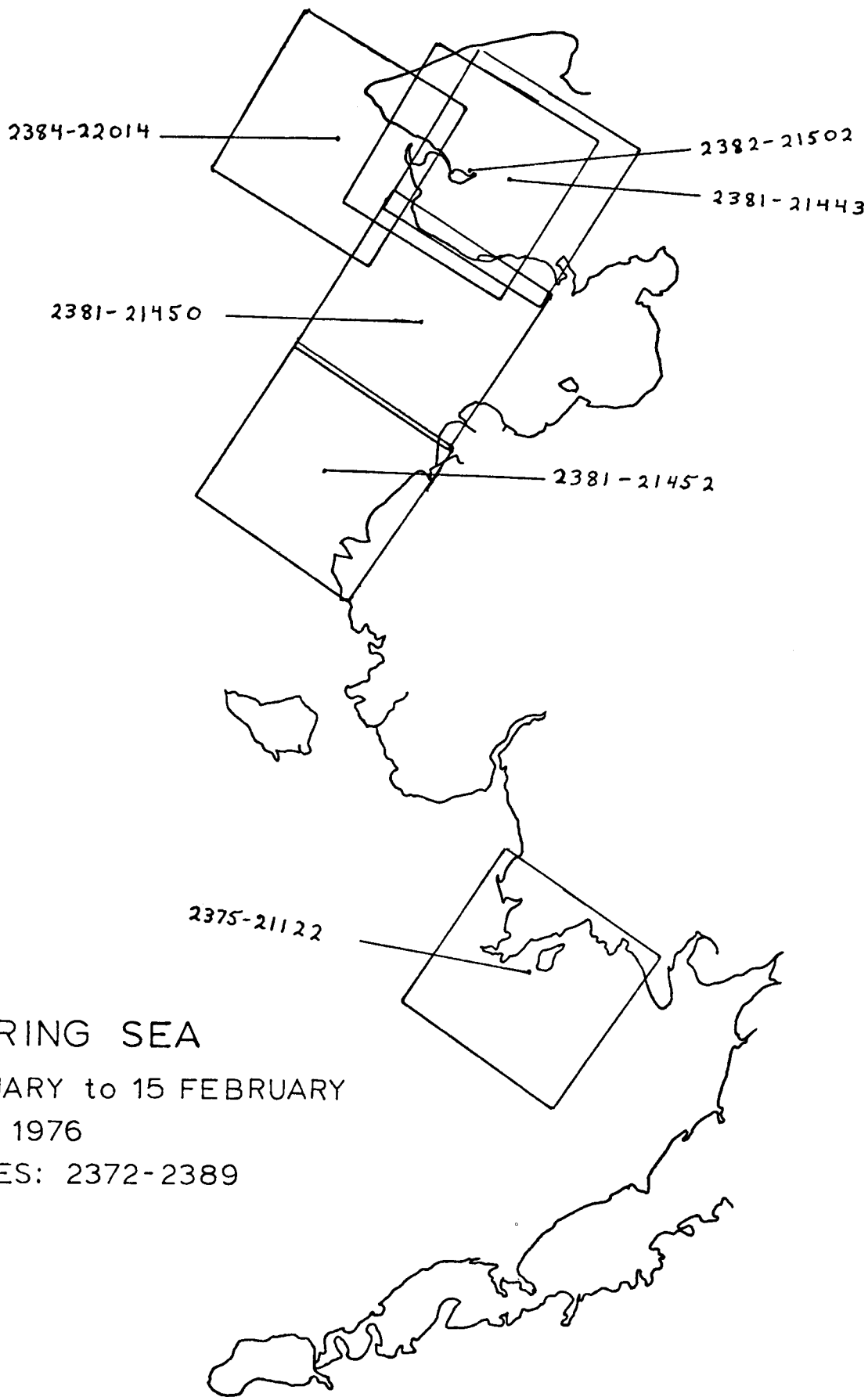


E-2384-22014-7
10 FEBRUARY 1976

KILOMETERS
0 10 20 30 40 50
SCALE APPROX 1,000,000

BERING SEA

Figure 7f



BERING SEA

29 JANUARY to 15 FEBRUARY

1976

IMAGES: 2372-2389

Figure 8

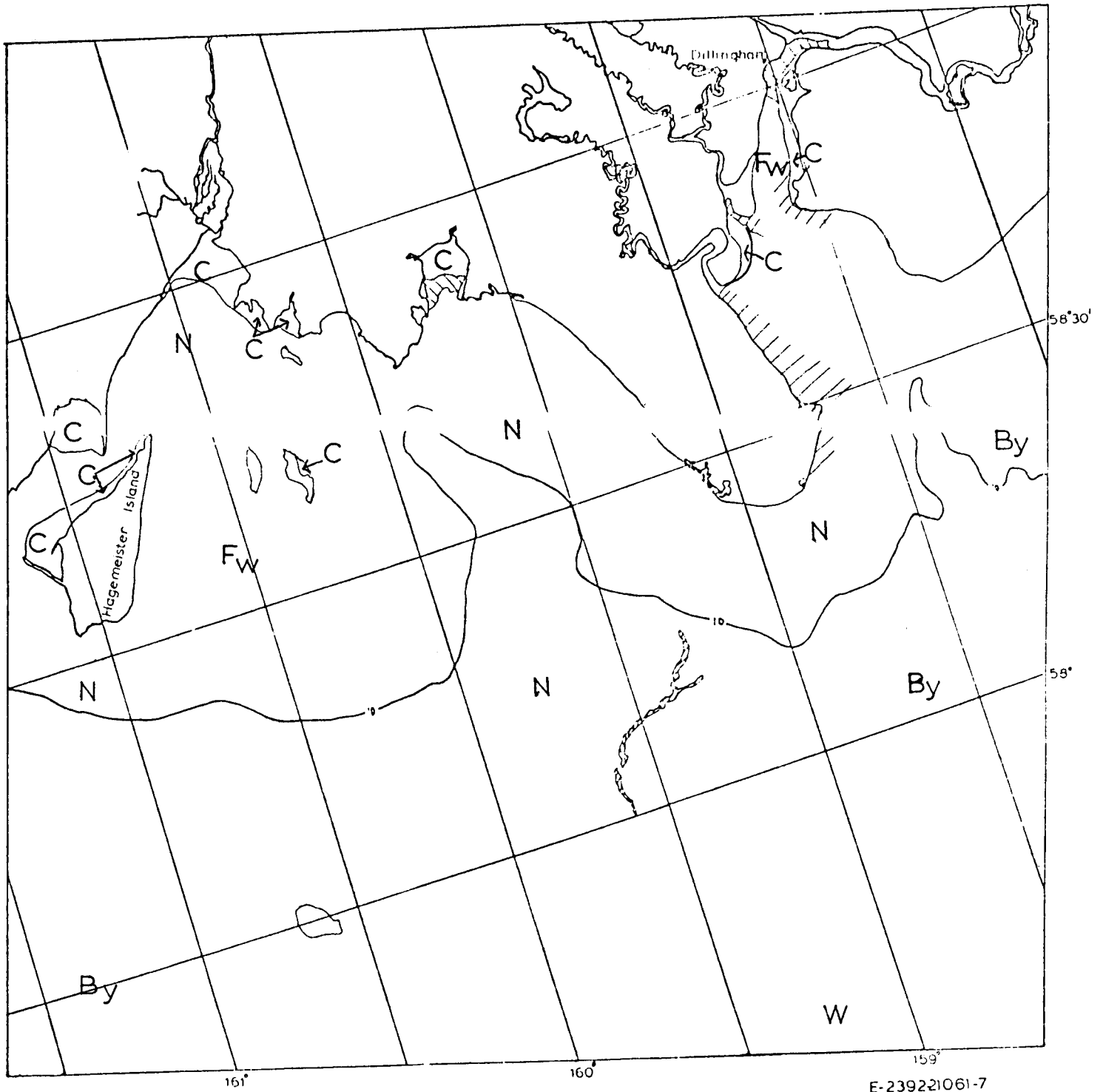
Scenes 2375-21127 through 2384-22014

These scenes show the Bering Sea coast during early February, 1976. Scene 2375 shows contiguous ice along the Northern Bristol Bay coast only in highly protected embayments where mean lower low water depths are on the order of one-fathom. Daily tidal variations in this area are on the order of three-fathoms.

In the Norton Sound area the correlation between the edge of contiguous ice and the 10-fathom isobath is rather poor; approximately 50 km east of Nome is a rather large embayment where depths are considerably less than 10-fathoms yet a polynya is open near shore and large expanses of new ice (M) are found seaward. At Nome, however, contiguous ice extends considerably seaward of the 10-fathom isobath. No signs of ridges can be seen on the imagery for this period.

South of the mouth of the Yukon River, contiguous ice is found on mud flats less than a couple of fathoms below mean lower low water - in some places extending 10 km or more seaward.

Farther west, similar non-correlations between depth and location of contiguous ice can be found - particulatly in the vicinity of Port Clarence. Scene 2382-21502 shows a very interesting feature worthy of note: Sledge Island and associated shoals located several km offshore at the point where the coastline bends from generally east-west at Nome to northwest -southeast, may be responsible for the shelf of contiguous ice in waters deeper than 10-fathoms off Nome.

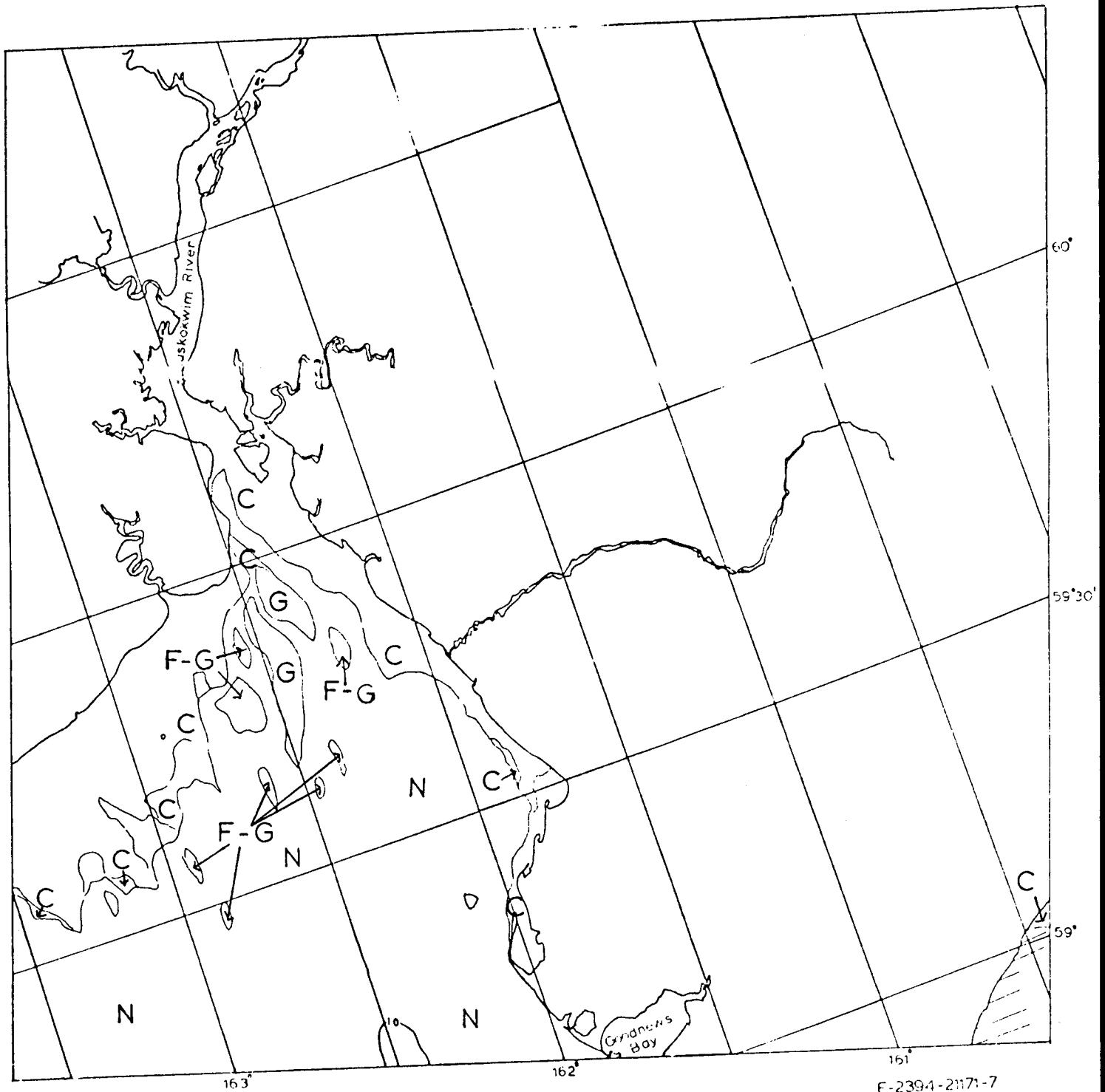


E-239221061-7
18 FEBRUARY 1976

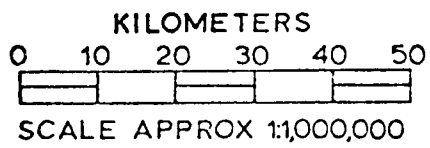
KILOMETERS
0 10 20 30 40 50
SCALE APPROX 1,000,000

BERING SEA

Figure 8a

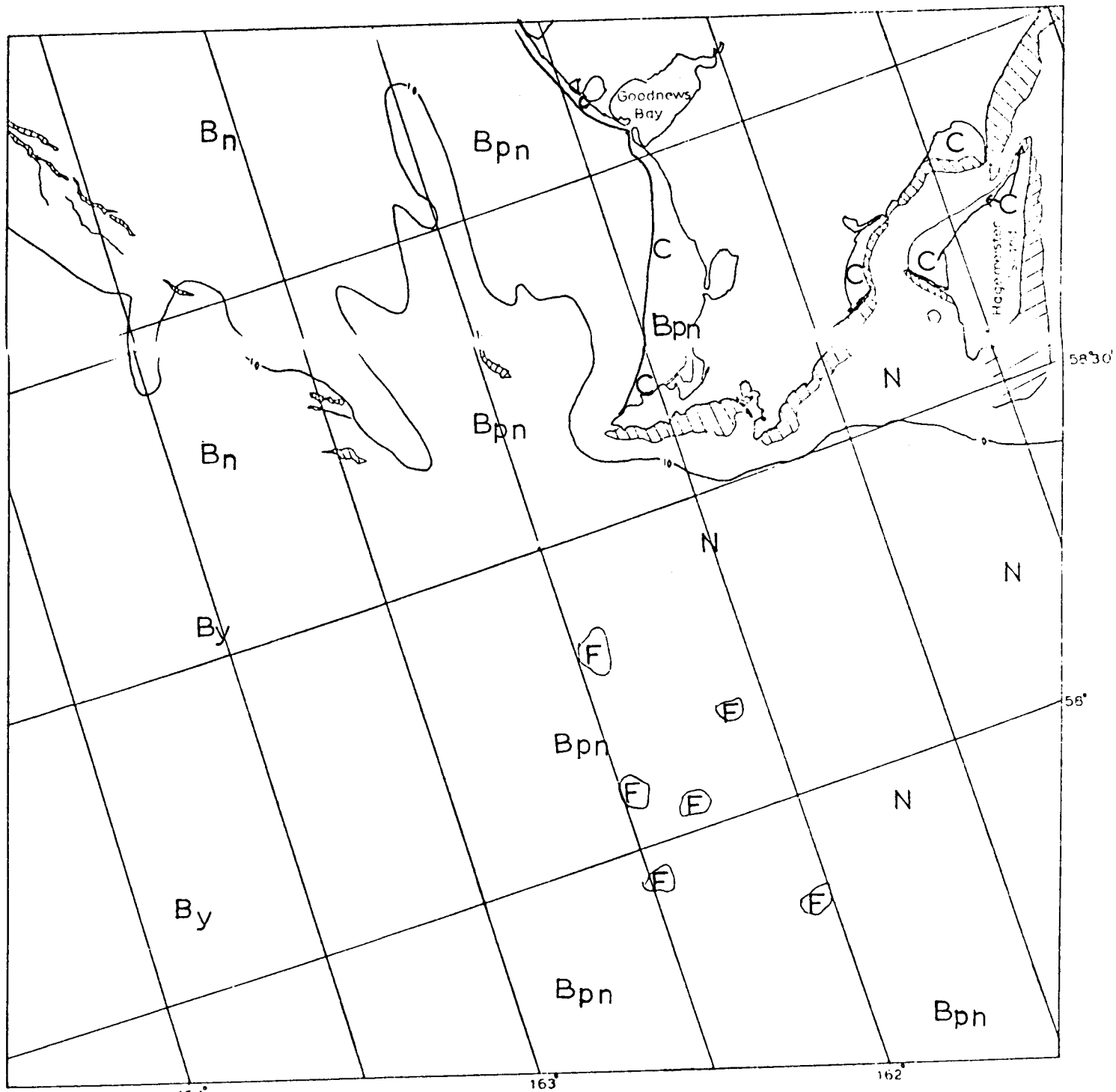


E-2394-2171-7
20 FEBRUARY 1976



BERING SEA

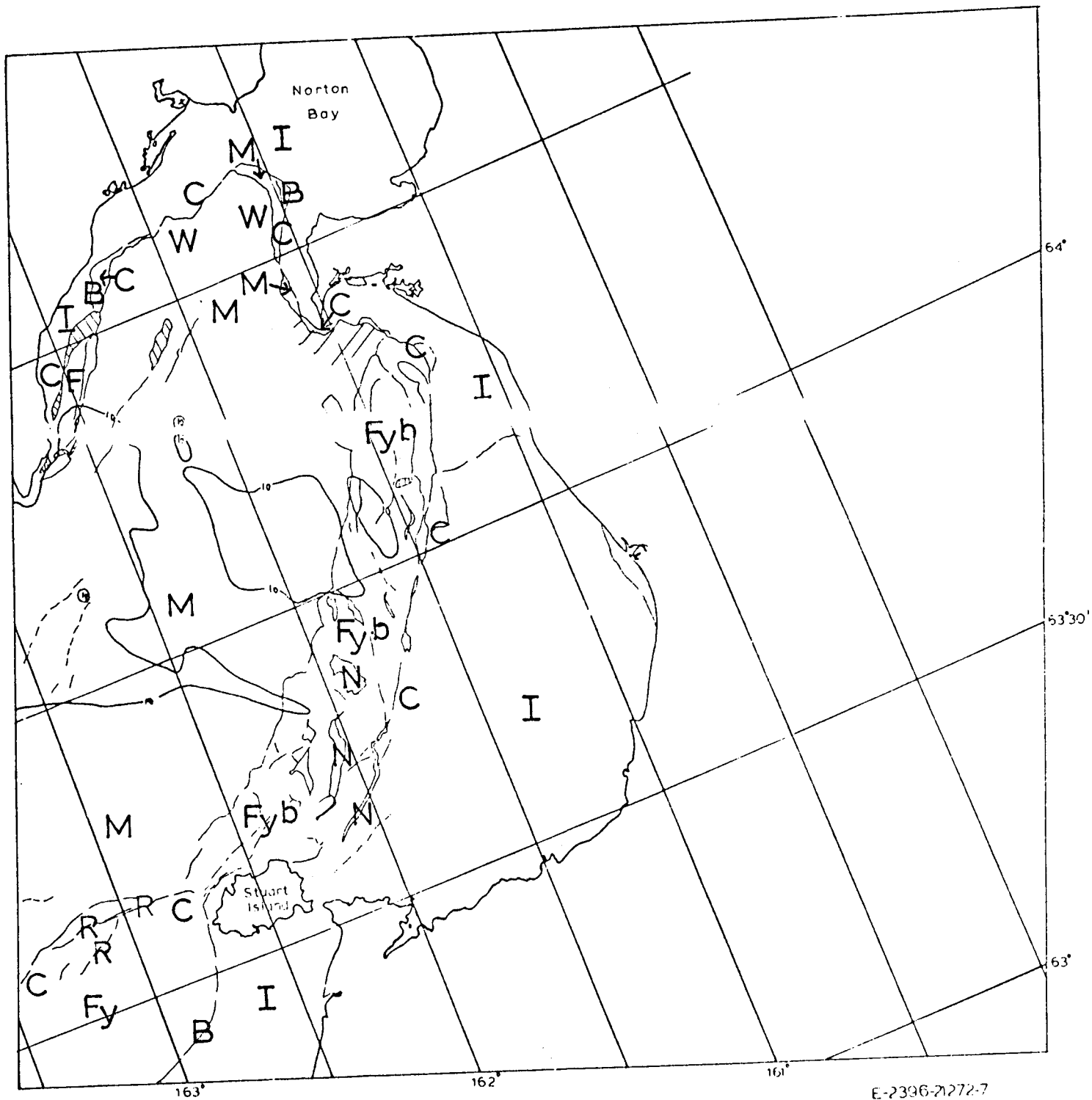
Figure 8b



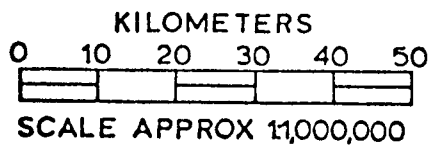
E-2394-21174-7
20 FEBRUARY 1976

BERING SEA

Figure 8c

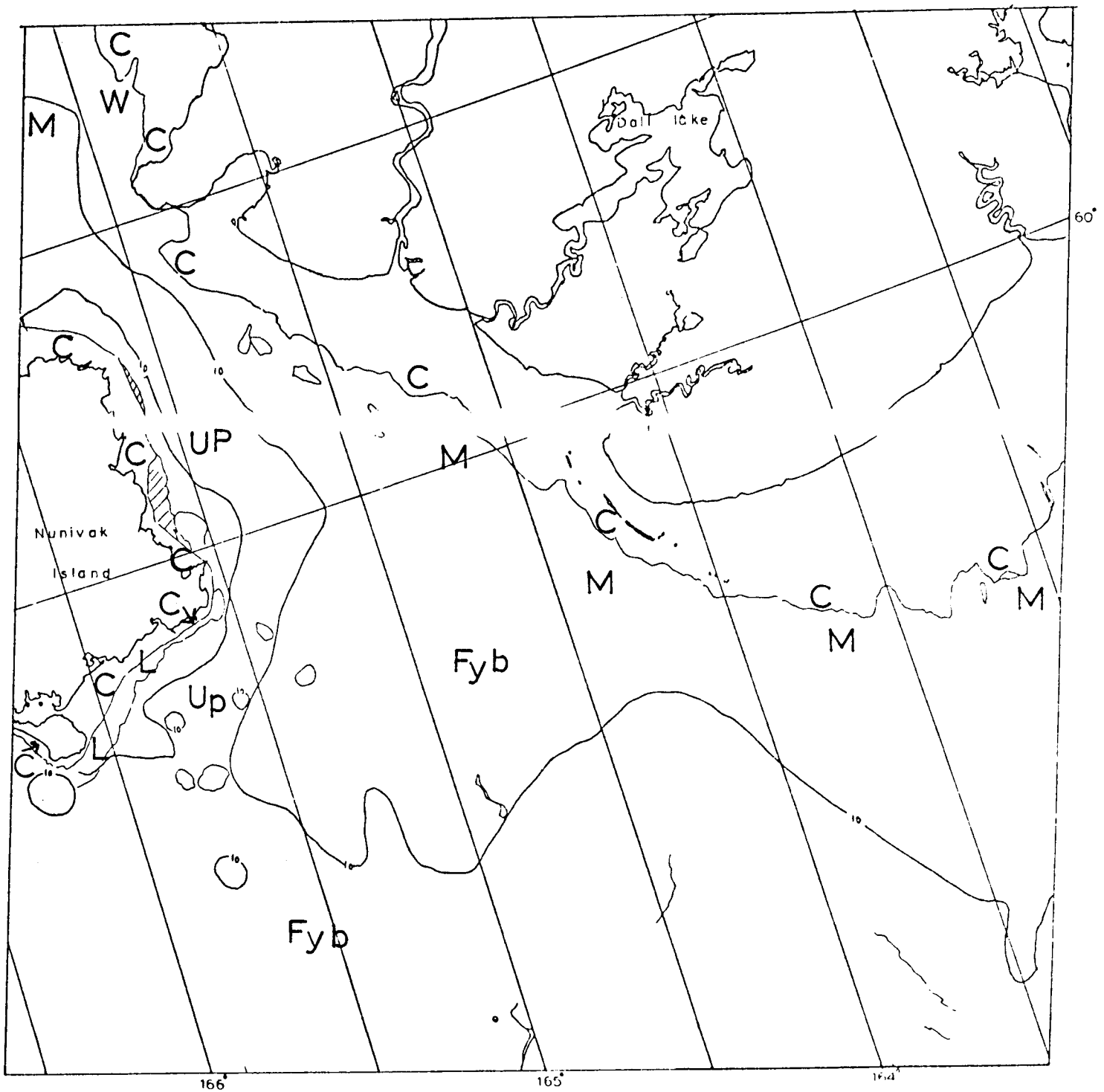


E-2396-21272-7
22 FEBRUARY 1976

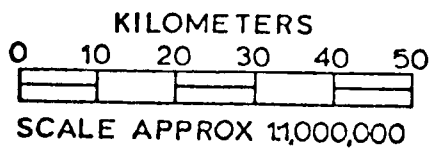


BERING SEA

Figure 8d

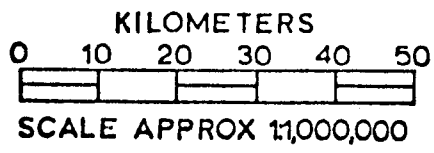
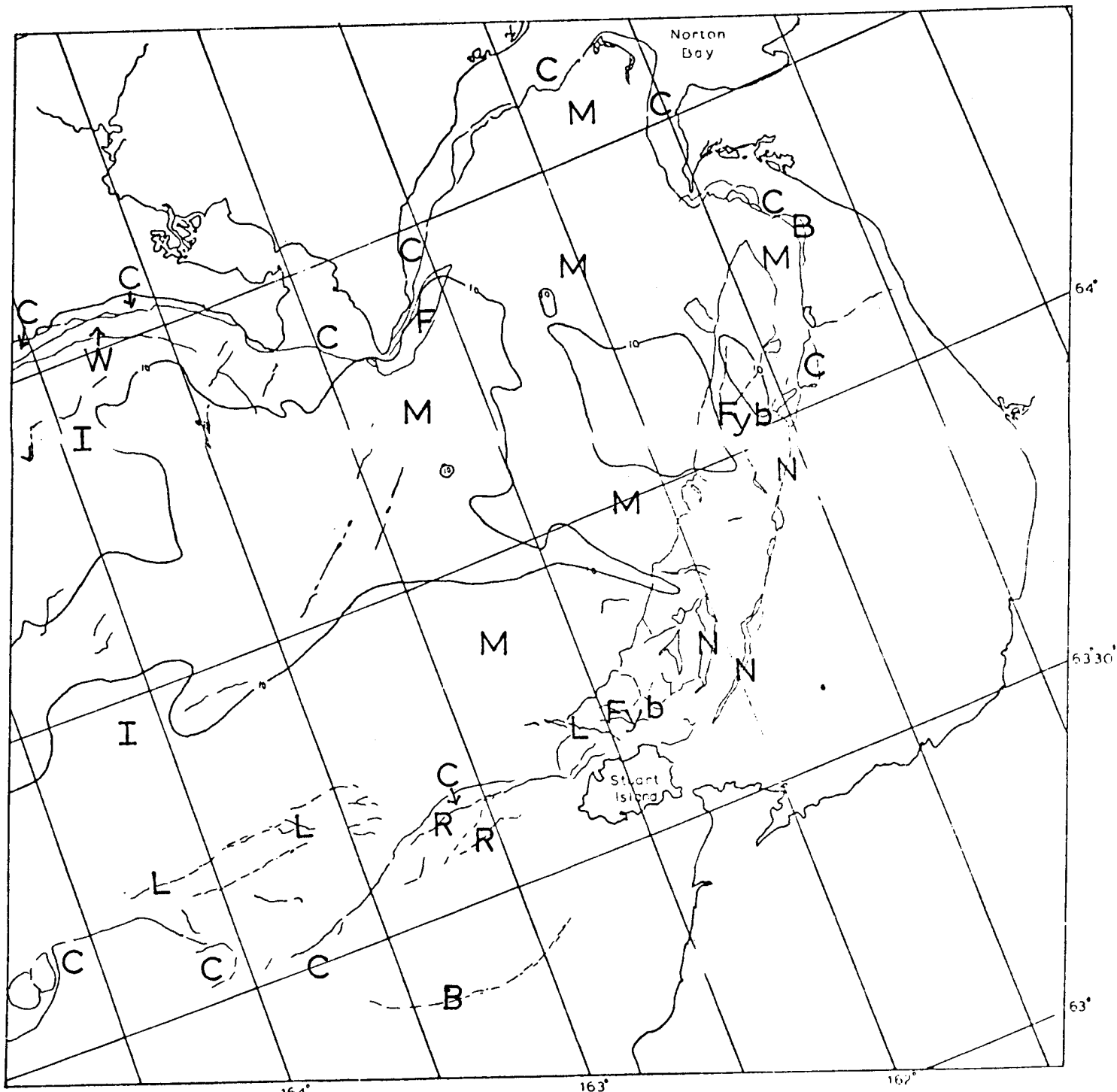


E-2396-212B4-7
22 FEBRUARY 1976



BERING SEA

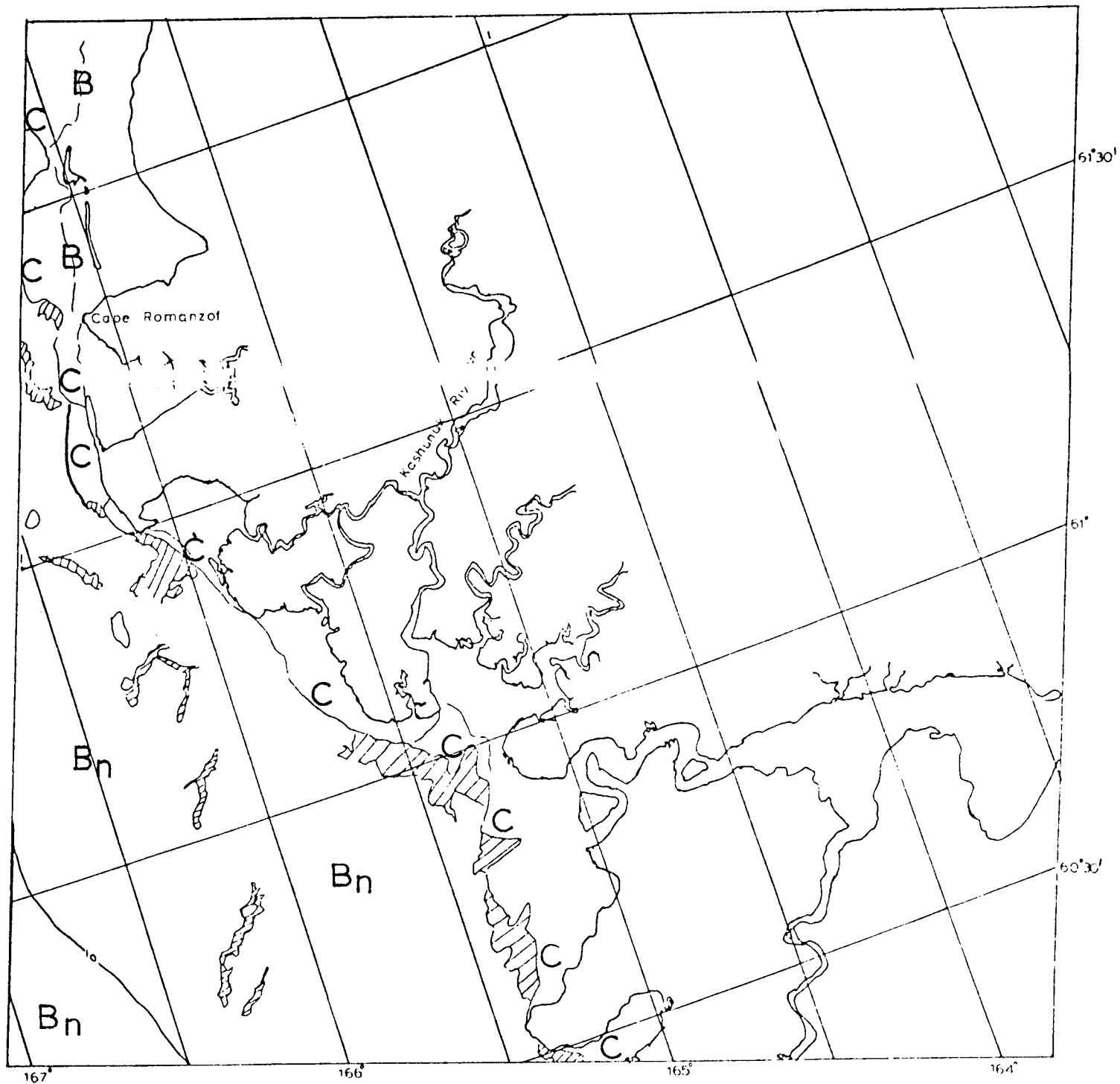
Figure 8e



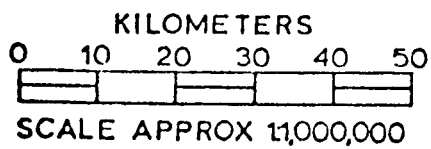
E-2397-21330-7
23 FEBRUARY 1976

BERING SEA

Figure 8f

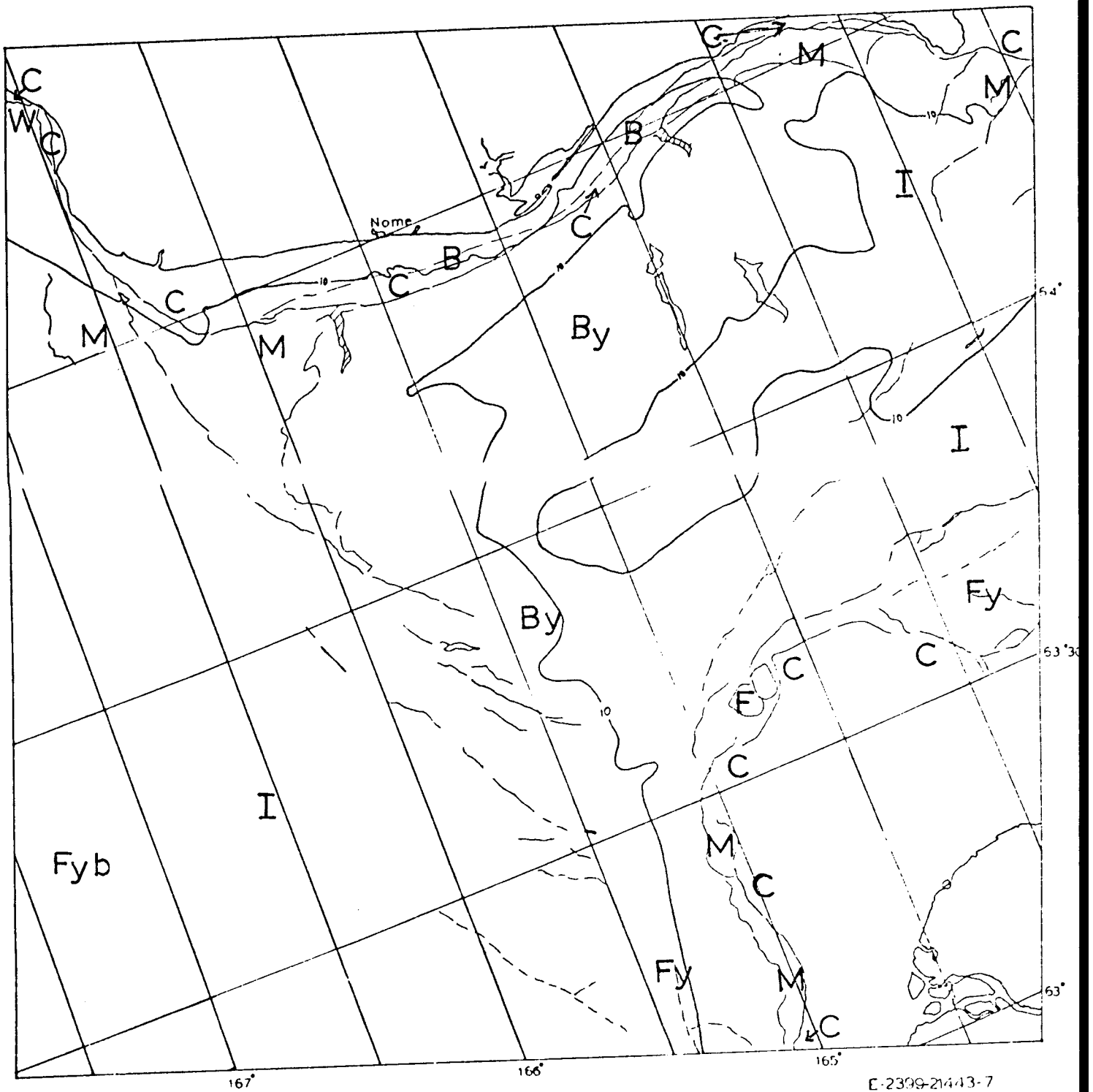


E-2397-213.65-7
23 FEBRUARY 1976

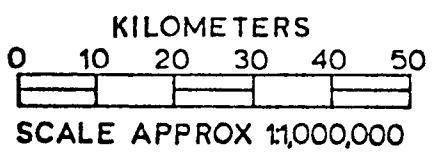


BERING SEA

Figure 8g

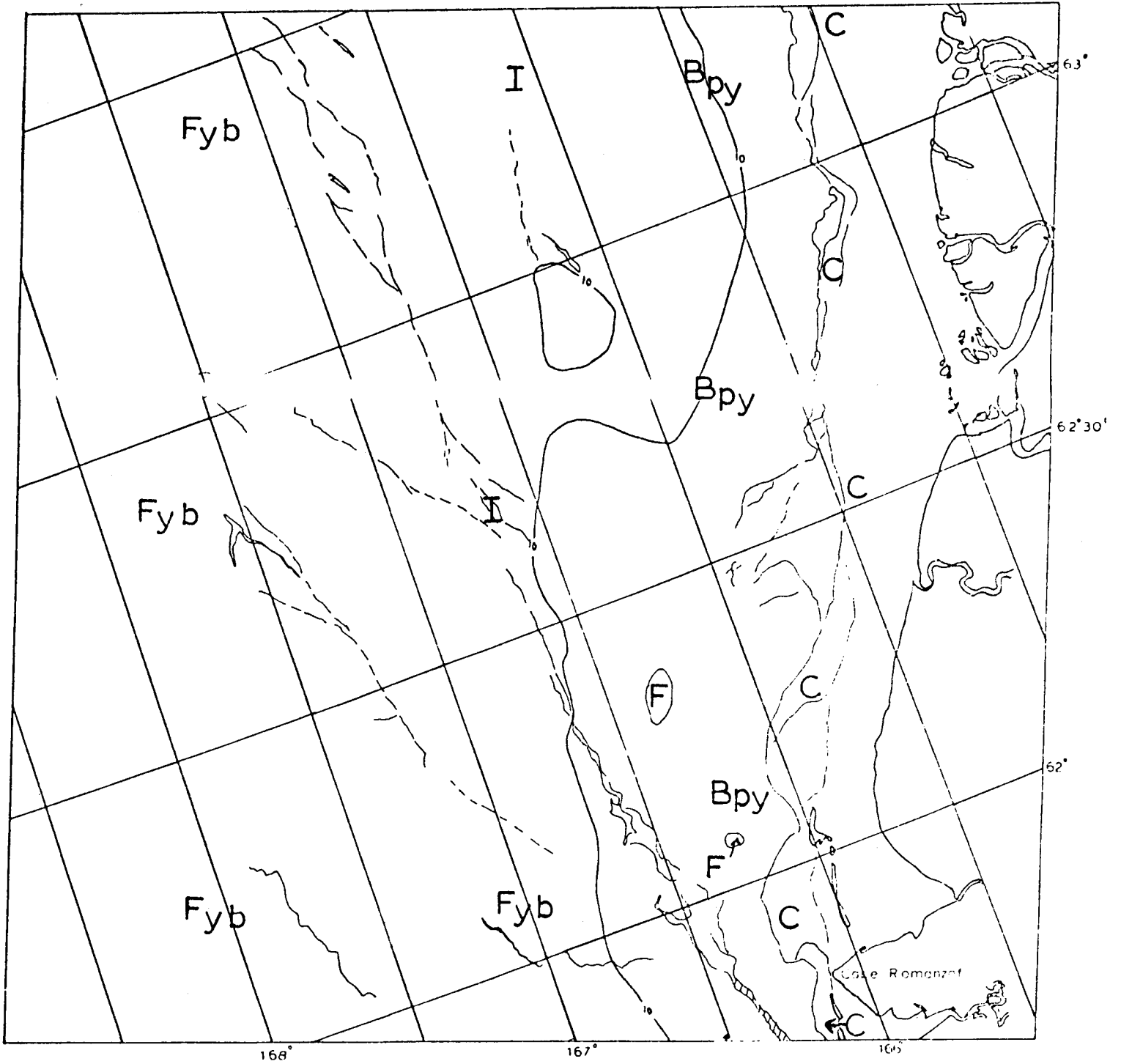


E-2399-2443-7
25 FEBRUARY 1976



BERING SEA

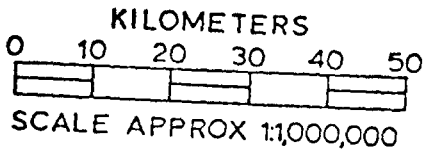
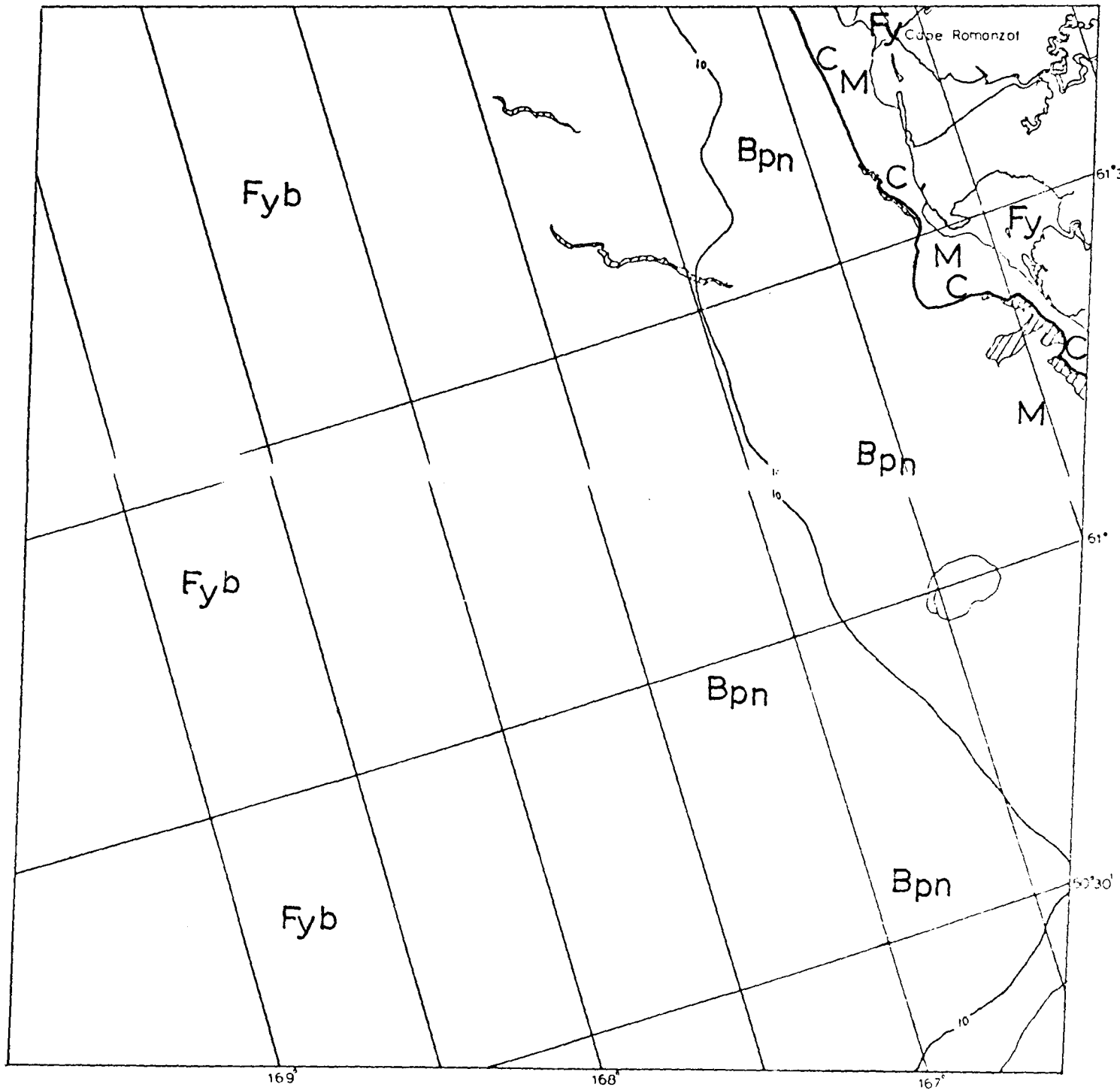
Figure 8h



E-2399-21445-7
25 FEBRUARY 1976

BERING SEA

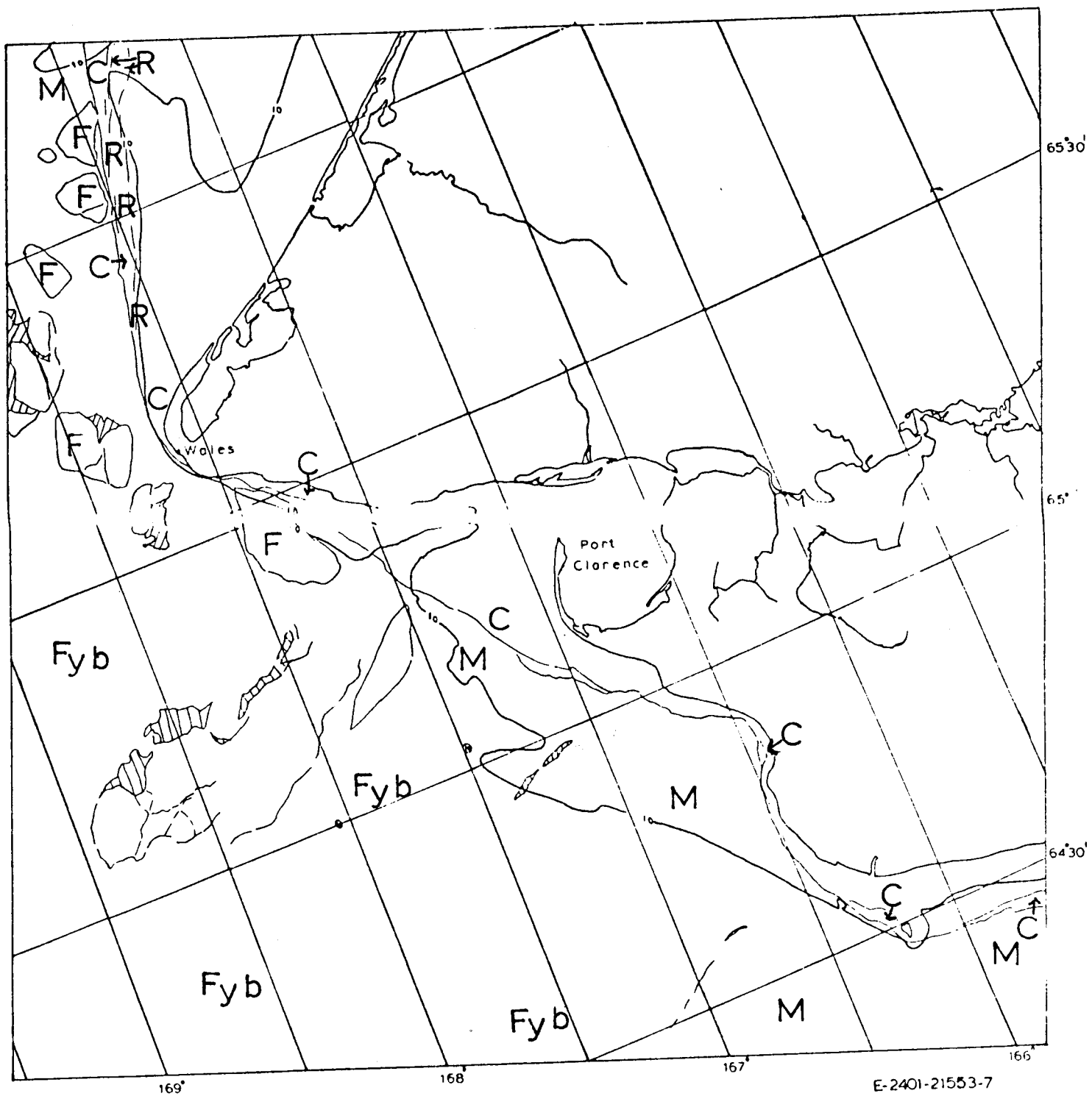
Figure 8i



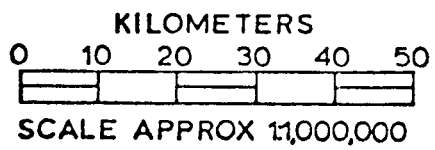
E-2399-21452-7
25 FEBRUARY 1976

BERING SEA

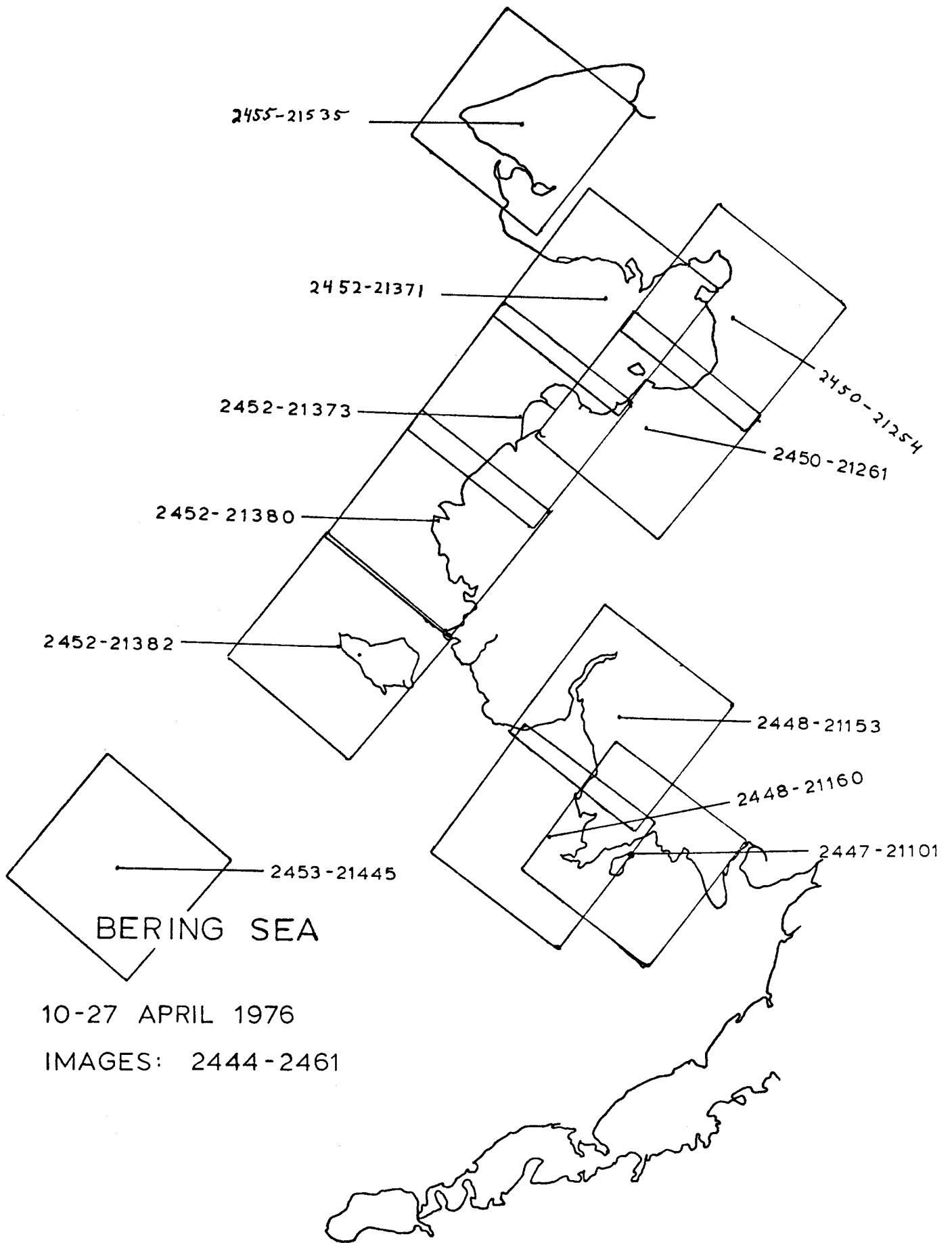
Figure 8j



E-2401-21553-7
27 FEBRUARY 1976



BERING SEA



10-27 APRIL 1976

IMAGES: 2444-2461

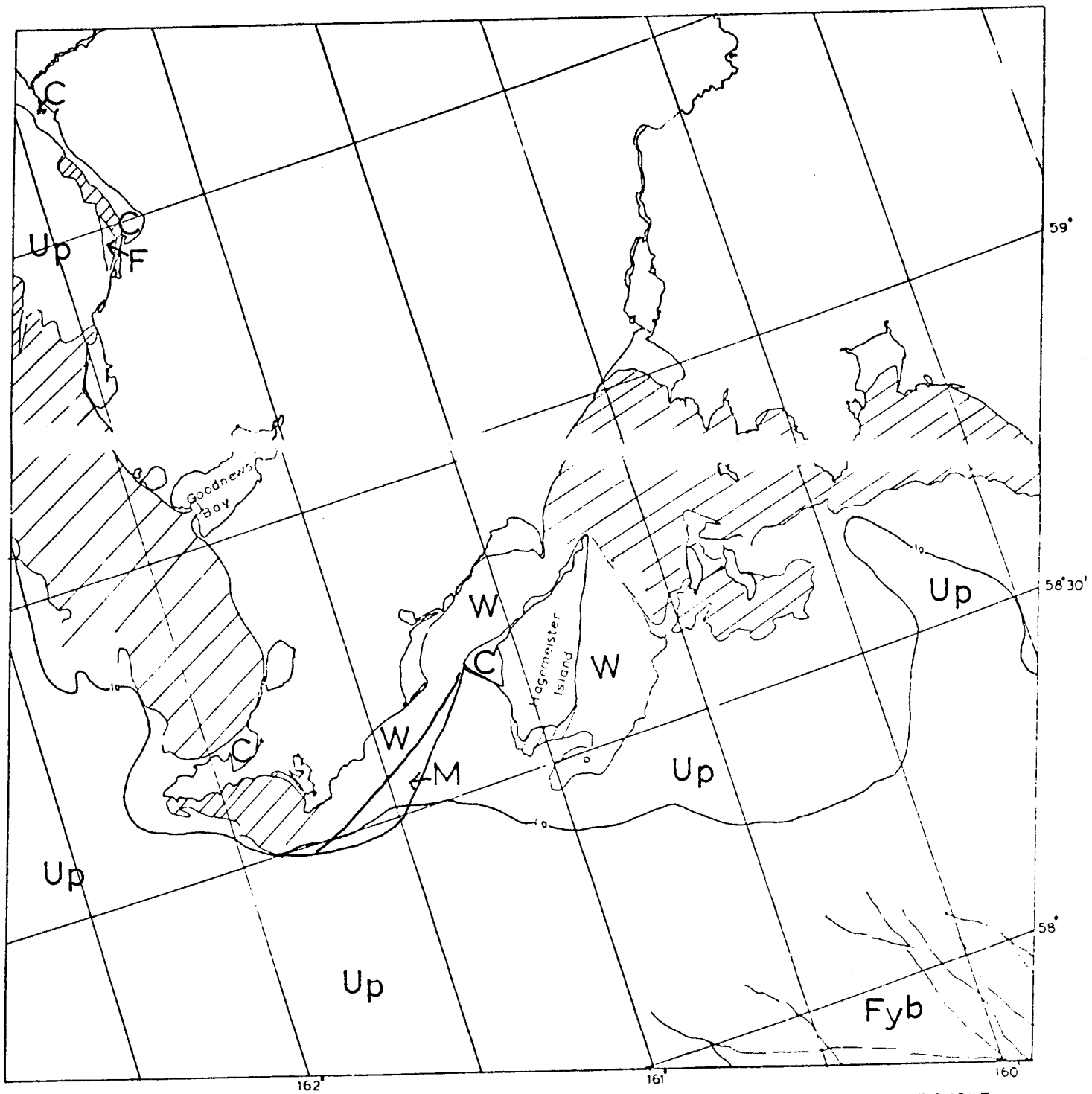
Figure 9

Scenes 2447-21101 through 2455-21535

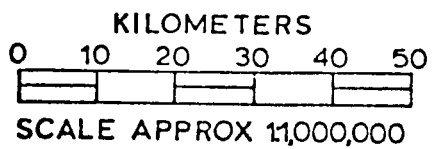
This sequence shows Bering Sea ice conditions for mid-April, 1976. Along the north coast of Bristol Bay contiguous ice is confined to very shallow areas (\sim 1-fathom) in well-protected inlets, and other protected areas such as the north coast of Hagemeister Island. In Kuskokwim Bay the situation is somewhat similar; contiguous ice is only found on mud flats barely below mean lower low water.

In Norton Sound the situation is similar to the previous two Landsat cycles described for this year; contiguous ice is located in protected areas while new ice is constantly being generated and moved outward from the sound. A large area of new ice (M) has just formed in a recently-formed open area at the head of the sound. In two days the ice at the head of the sound was driven considerably far toward the mouth of the sound creating considerable compaction in the area north of Stuart Island.

Around the mouth of the Yukon River, contiguous ice lies on the mud flats well within the 10-fathom isobath. This condition continues down the coast toward Nunivak Island. Around Nunivak Island contiguous ice is found in protected areas well within the 10-fathom isobath - with the exception of one area: This exception is found on the south side of the island where, protected by a large area of shoals and residing on the lee side of the island, contiguous ice extends seaward in an area where the 10-fathom isobath meets the shoreline.

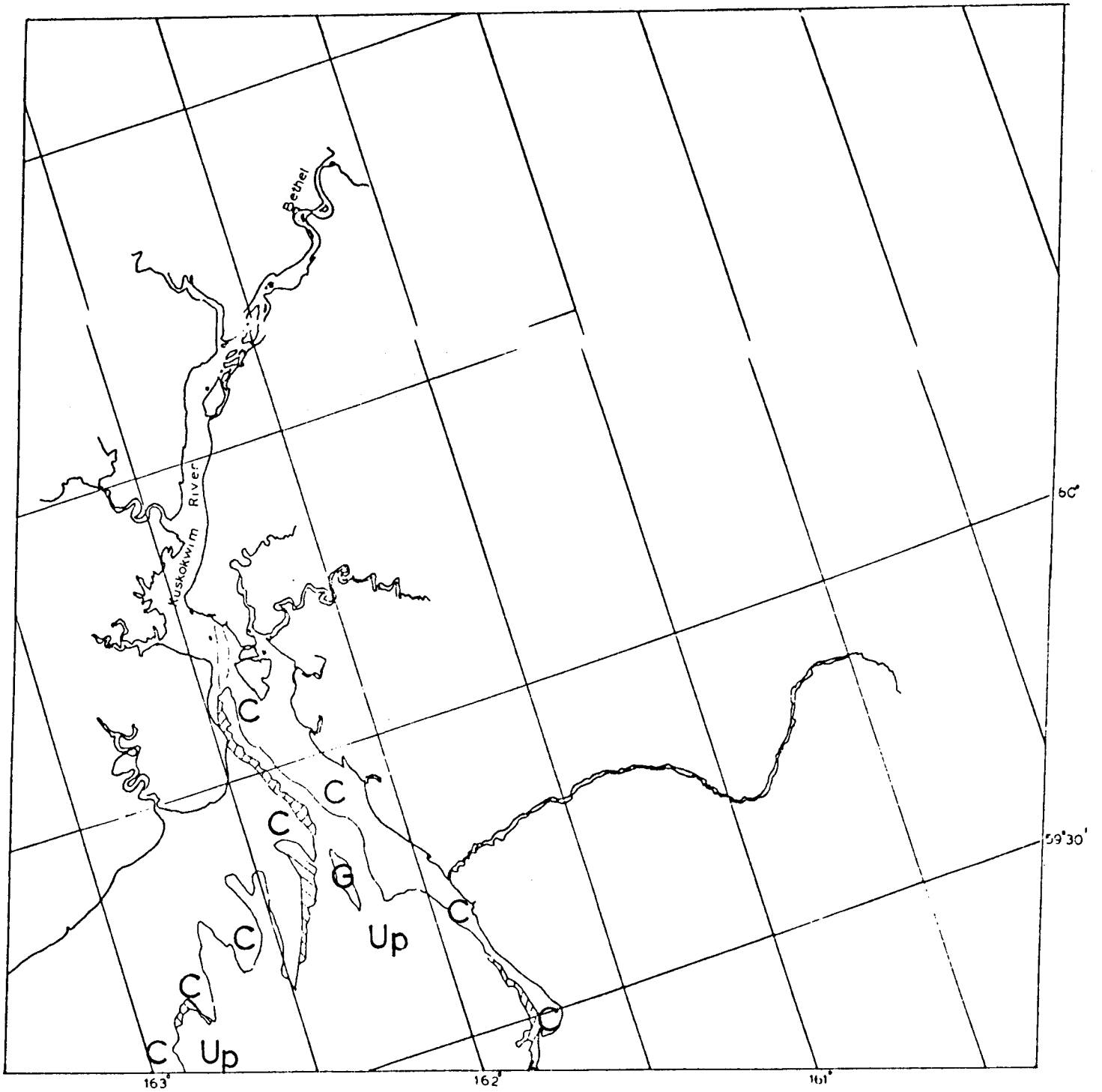


E-2447-21101-7
13 APRIL 1976



BERING SEA

Figure 9a

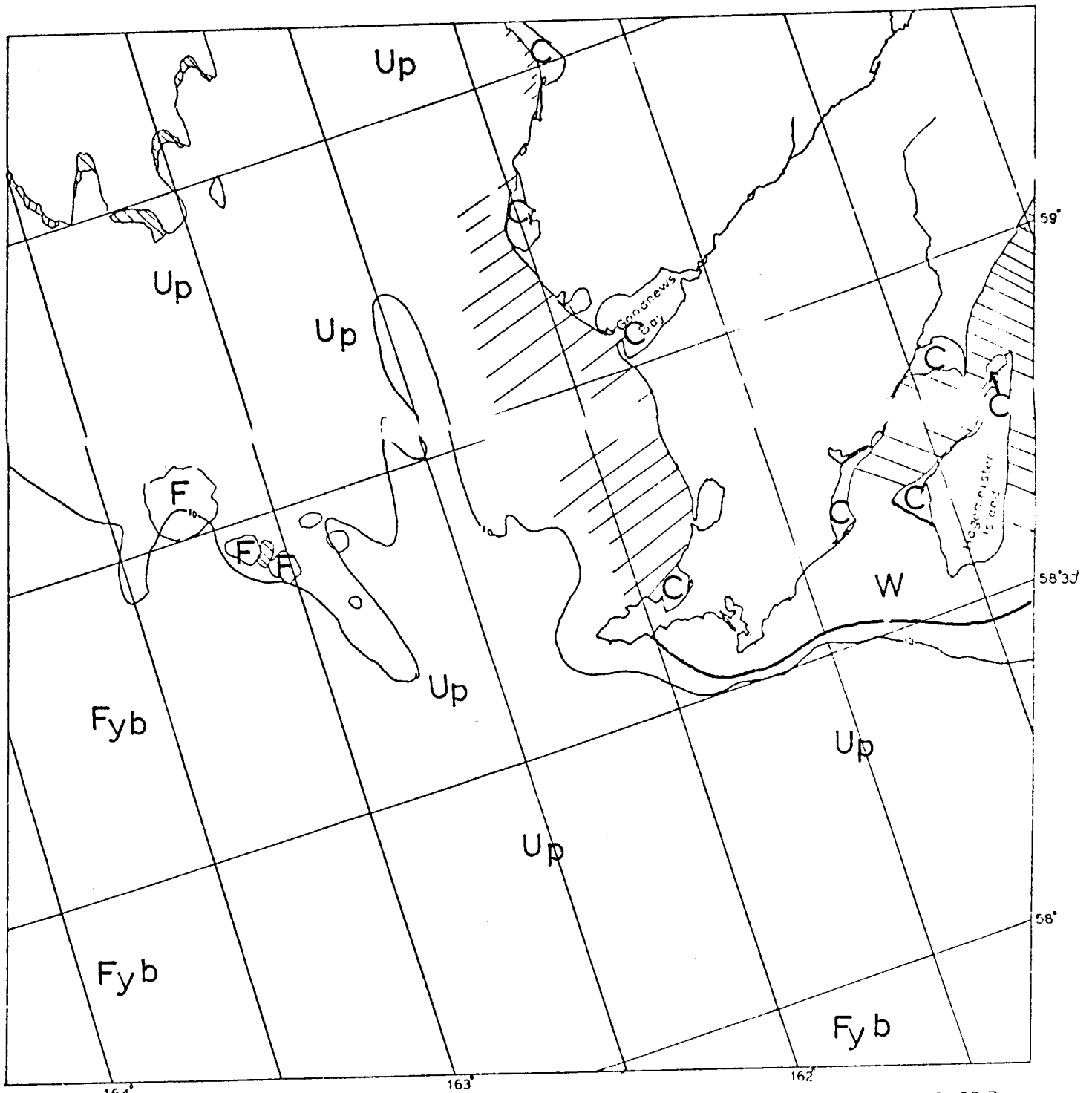


KILOMETERS
 0 10 20 30 40 50
 SCALE APPROX 1,000,000

E-2448-21153-7
 14 APRIL 1976

BERING SEA

Figure 9b



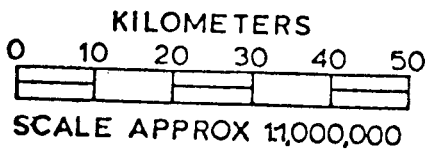
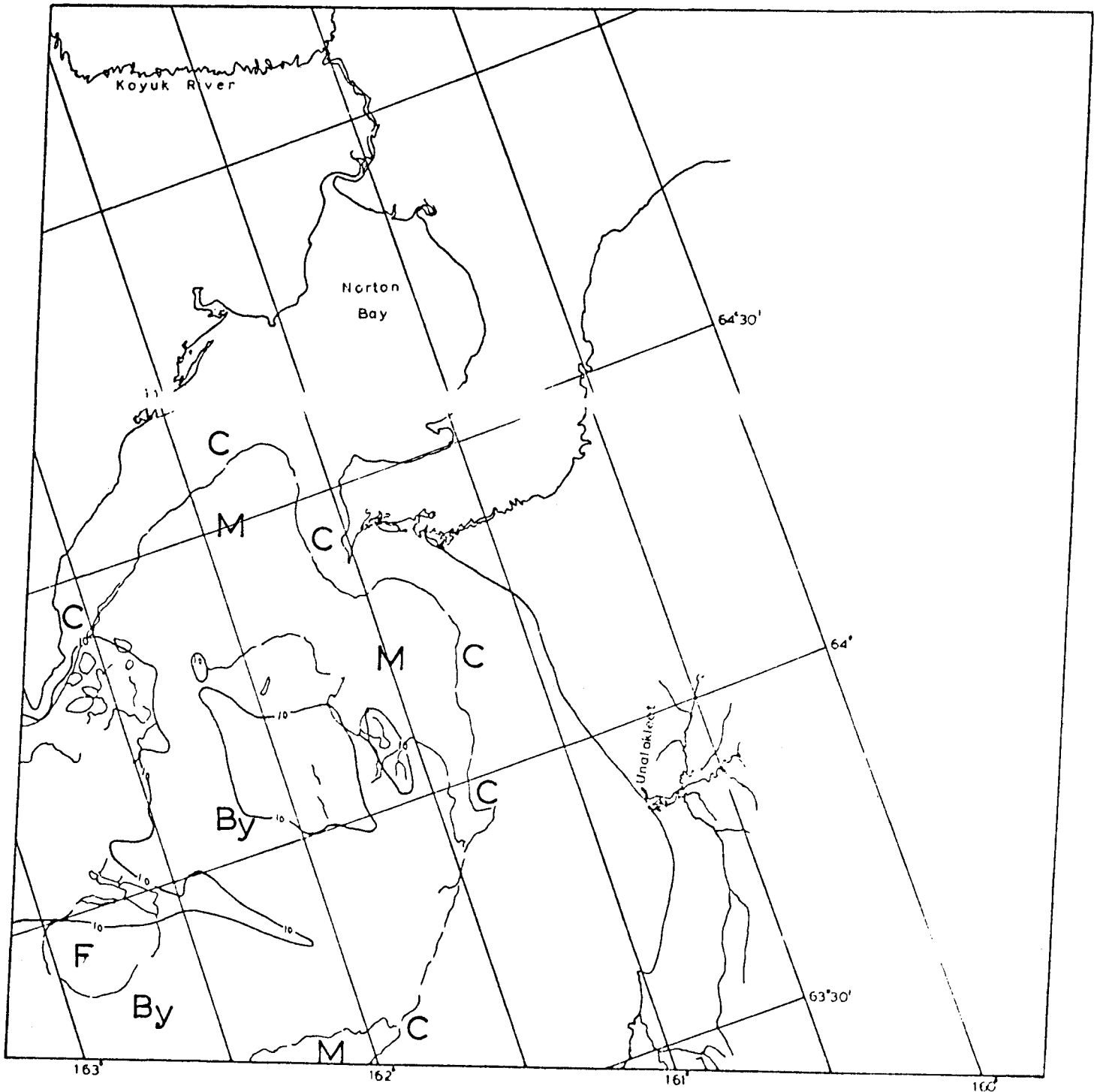
164° 163° 162°

KILOMETERS
 0 10 20 30 40 50
 SCALE APPROX 1:1,000,000

BERING SEA

E-2448-21160-7
 14 APRIL 1976

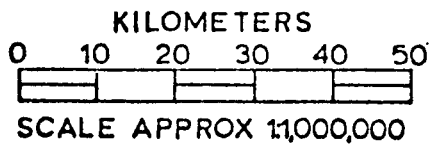
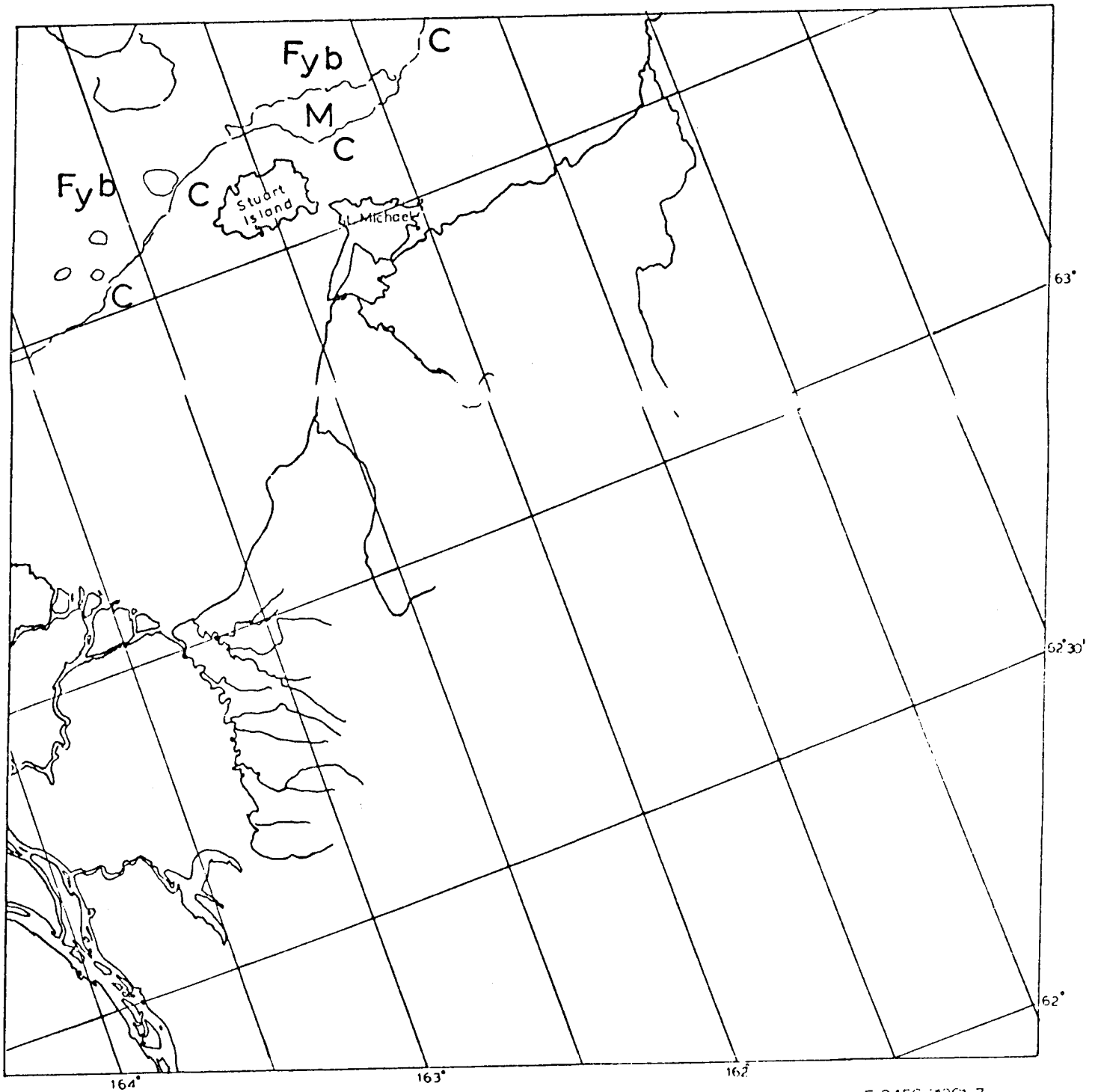
Figure 9c



E-2450-21254-7
10 APRIL 1976

BERING SEA

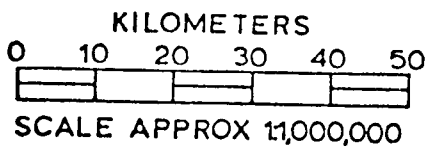
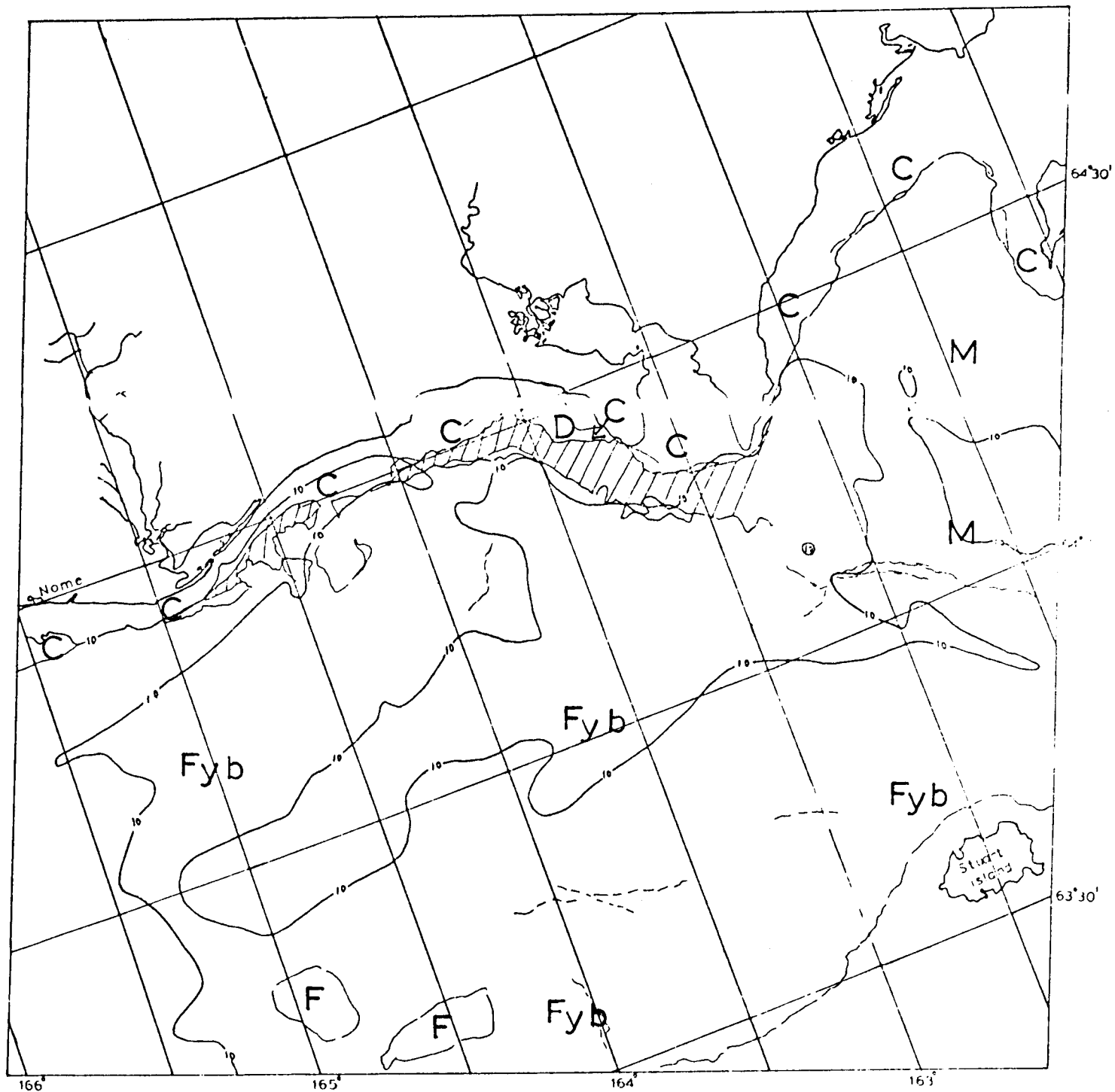
Figure 9d



E-2450-2261-7
16 APRIL 1976

BERING SEA

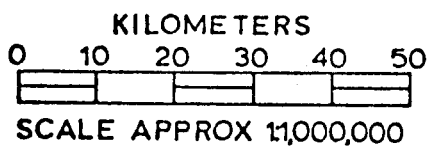
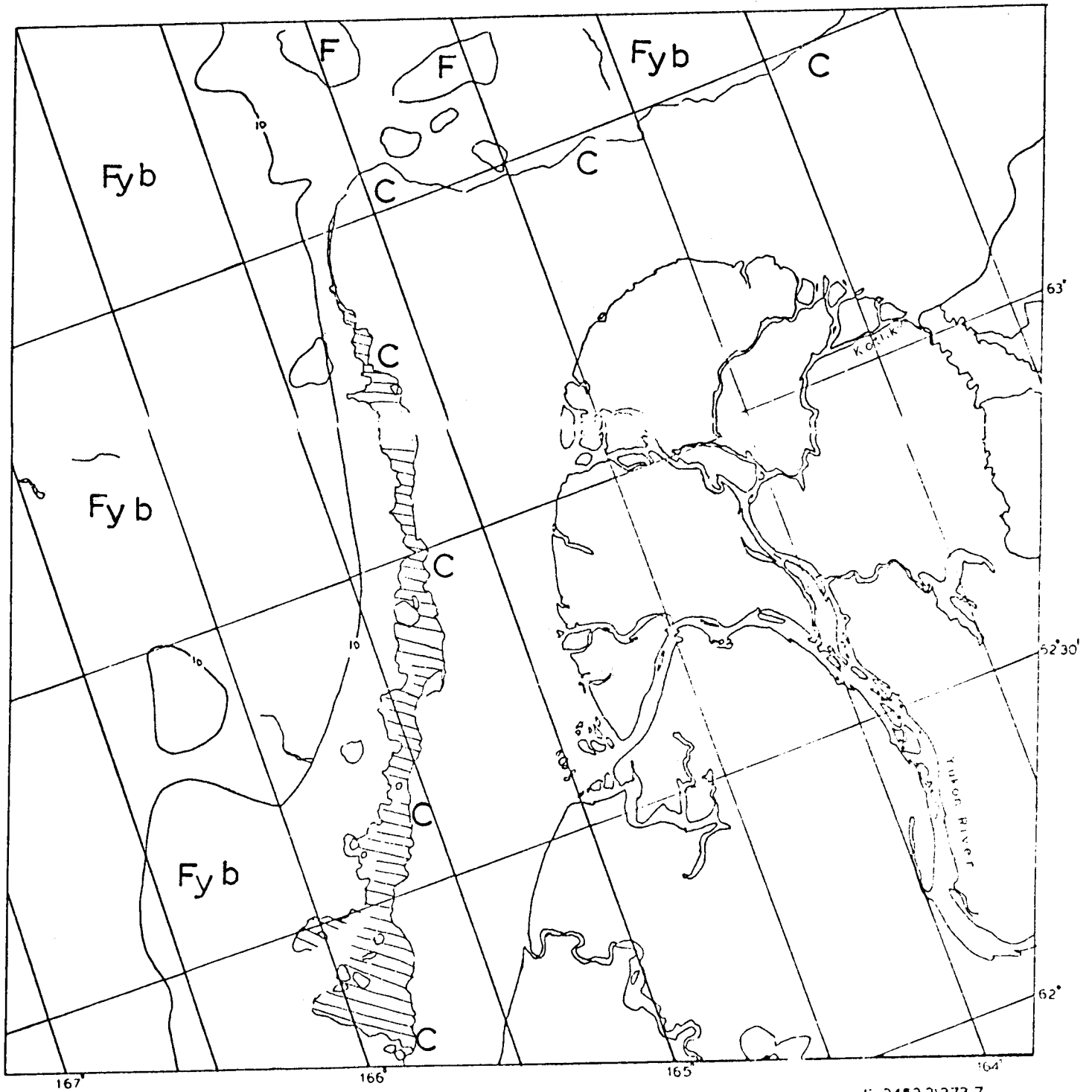
Figure 9e



E-2452-21371-7
18 APRIL 1976

BERING SEA

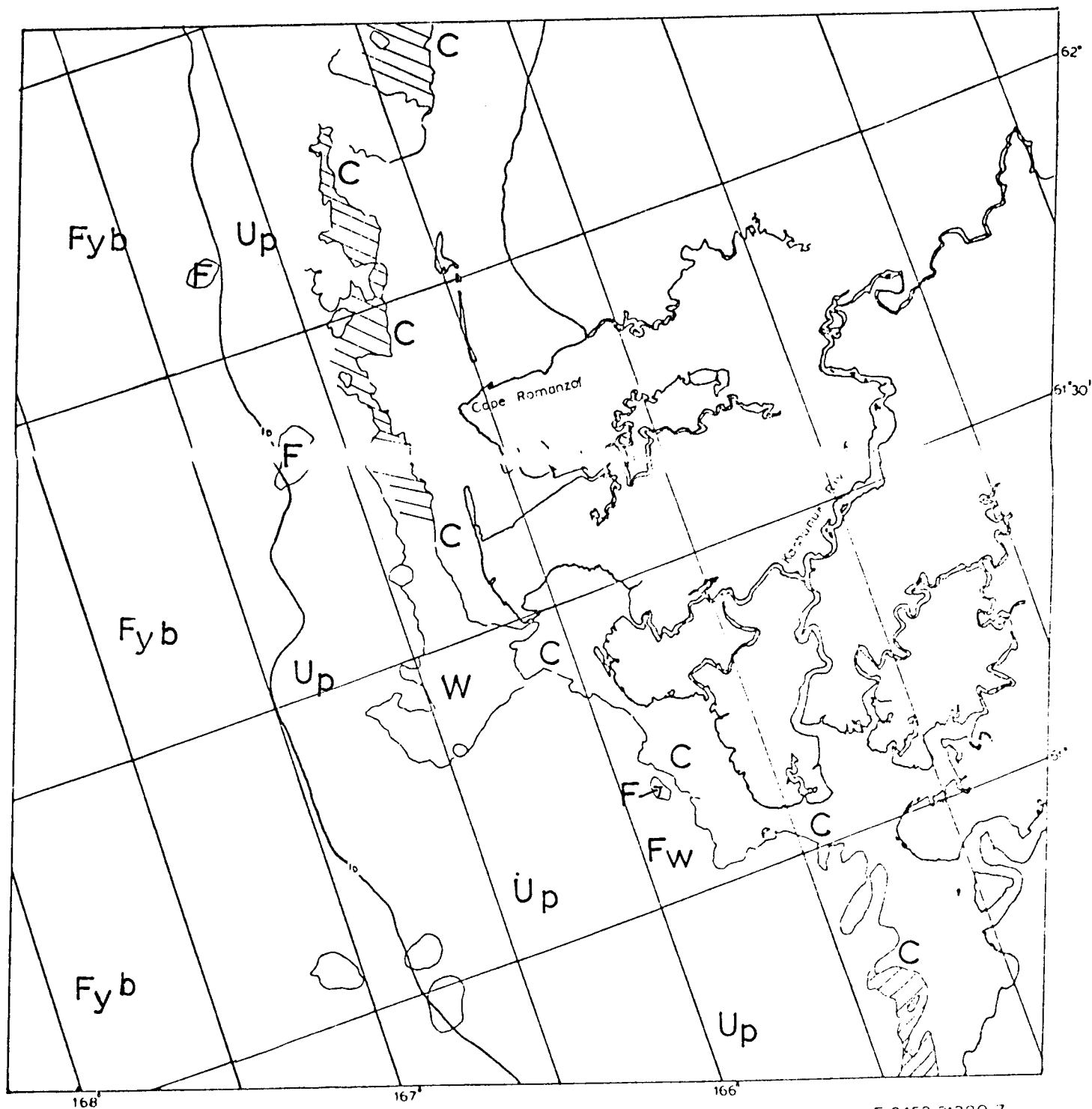
Figure 9f



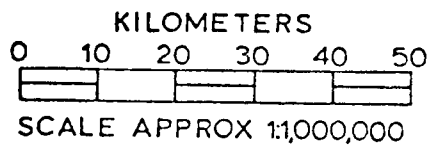
E-2452-21373-7
18 APRIL 1976

BERING SEA

Figure 9g

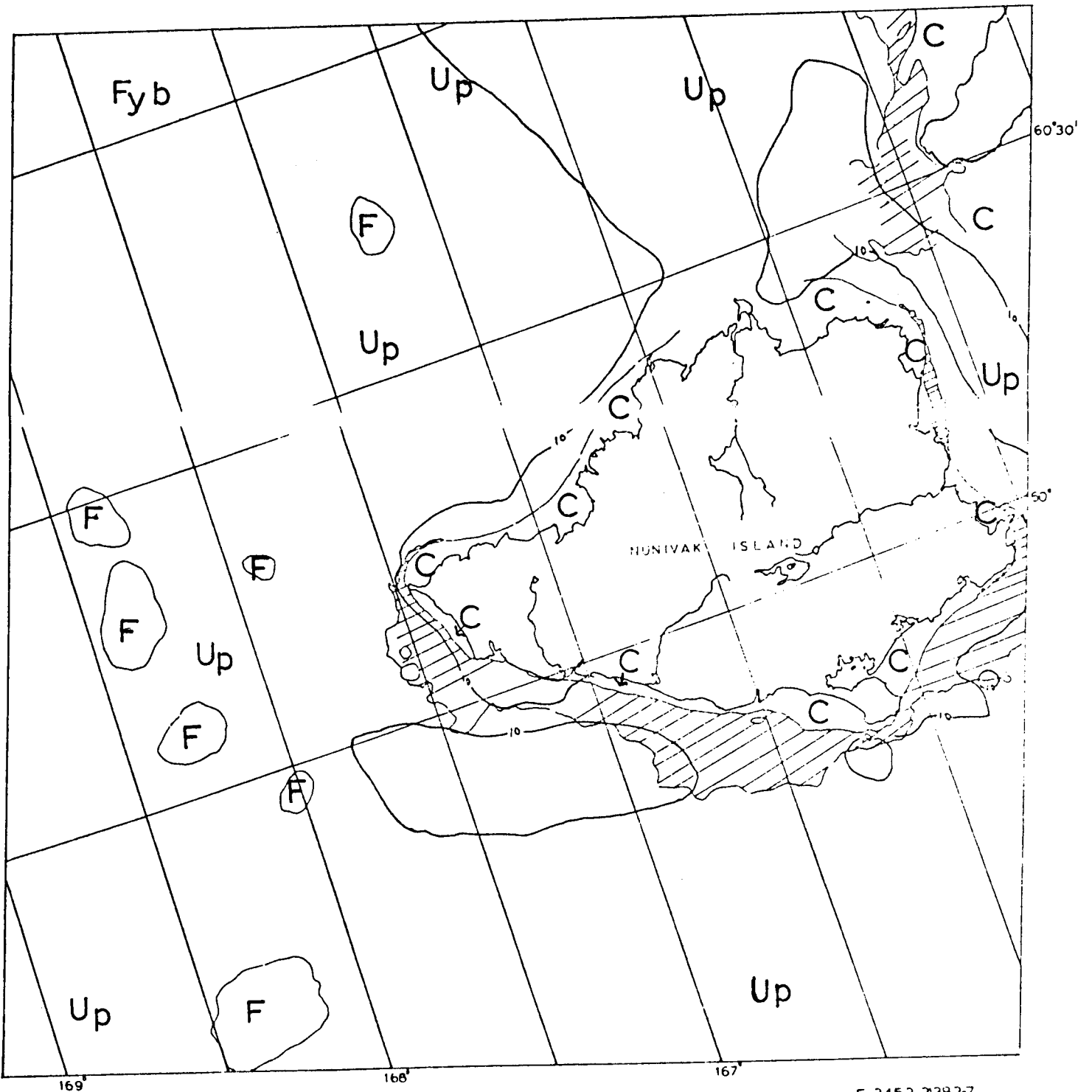


E-2452-21330-7
18 APRIL 1976

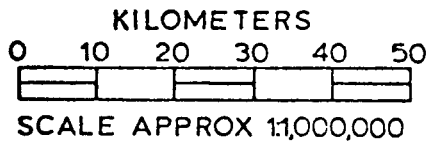


BERING SEA

Figure 9h

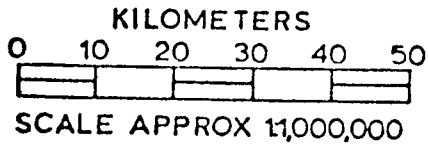
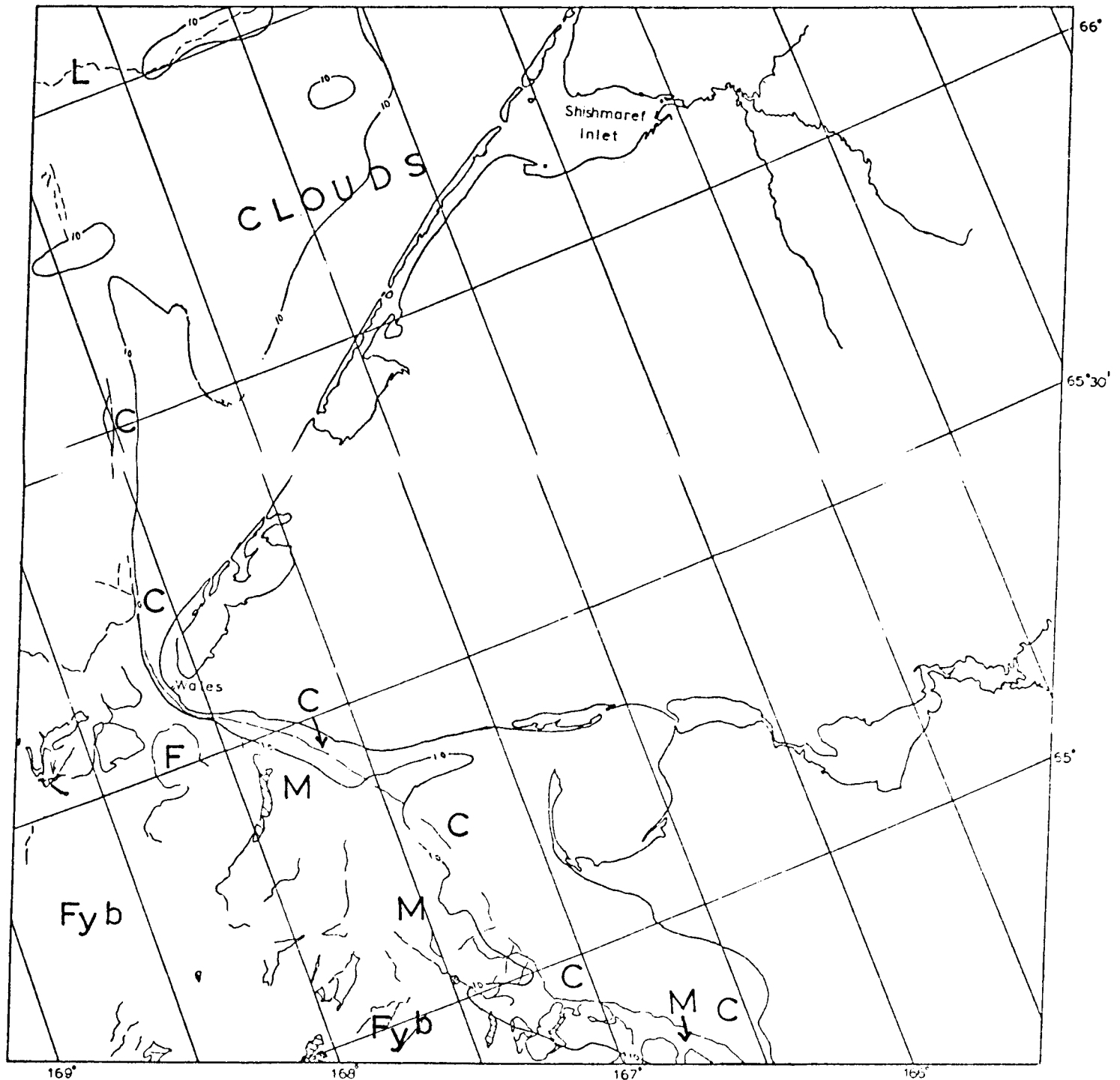


E-2452-2382-7
18 APRIL 1978



BERING SEA

Figure 9i



E-2455-21535-7
 21 APRIL 1976

BERING SEA

Figure 9j

ON THE FEASIBILITY OF A SHIP LOADING
FACILITY AT CAPE DYER OR CAPE THOMPSON, ALASKA

There are no ports along Alaska's northwest coast. Further, that coast is the site of rather severe ice conditions. There is a good possibility that in the near future resource exploitation in the northwest region will require year-round ship loading facilities.

In the absence of a suitable port, near-shore loading facilities for commodities such as coal and oil might be built in locations where deep waters are located sufficiently close to shore for such structures to be economically feasible. However, because of the severe ice conditions along this coast, it would seem that even this sort of loading facility would be out of the question.

Generally speaking, wind-driven ice builds massive shear ridges along coastal headlands parallel to ice motion. Many of these ridges are grounded in water 60-feet deep and extend over 20-feet above sea level. Maintenance of an offshore loading facility in the presence of these conditions would be difficult if not impossible. The most likely locations for offshore loading facilities are locations where deep water is found close to shore and severe ice conditions are at a minimum.

As part of an extensive near-shore ice survey two likely locations for such facilities have been located. Both of these locations are found at the extreme western end of the Brooks Range. They are: Cape Dyer, located between Cape Lisburne and Point Hope, and Cape Thompson, located southeast of Point Hope.

Cape Dyer is on a north-south oriented portion of coast open to the sea to the west and northwest. Cape Lisburne offers protection to the north while the large spit at Point Hope gives protection from the south and southwest. Steep cliffs at Cape Dyer apparently extend to a depth of 7 to 8 fathoms offering the possibility that ships could be loaded directly from boom-like structures extending from shore.

Examination of Chukchi Sea satellite images from 1973 to the present (1977) indicates that the normal ice motion in the vicinity of Cape Dyer is west of south following the tangent between Cape Lisburne and Point Hope. Water depths are too great along this tangent for grounding of any shear ridges to take place. Close examination of satellite images of Cape Dyer on seventy occasions shows that ice does form in this indentation but it is often carried out to sea with the ice pack, driven by east and northeast winds which push the ice pack out Bering Strait. Hence, even the shore-bound annual ice does not attain the six-foot thickness usually attributed to full-season annual ice.

Although shearing motion cannot take place along Cape Dyer, ice can be driven into the shore from the west and northwest. Fortunately, the extreme wind speeds from these directions occur less frequently than from other directions, and the sum of wind frequency from the west and northwest is only ten percent. Corresponding to this, one occasion was observed on satellite imagery when large pans of ice were driven into the shore at Cape Dyer. This episode certainly would have made ship loading operations difficult during the event. However, direct observations as well as wind records indicate that this is a rare occurrence.

Cape Thompson is located to the south, on the opposite side of Point Hope, on a northwest to southeast tending portion of the coast. It is even better protected from normal shearing events than Cape Dyer, but is open to ice motion from the west to southeast. Further, although Cape Thompson also consists of cliffs extending beneath the ocean, available charts indicate water depth there of less than thirty-feet. While ten percent of the winds at Cape Dyer could cause adverse ice conditions, at Cape Thompson twenty-two percent of the winds are in this category. Beyond that, the greatest winds observed in that area - 70 mph - have been from the southeast and could possibly cause shearing along the coast at Cape Thompson. During the five years of satellite observation, no such event was witnessed. However, although a large polynya exists just to the south of Cape Thompson (created by southward motion of the Chukchi ice) there is always a small shelf of ice at least a kilometer wide extending seaward from Cape Thompson. The nature of this ice is not obvious (first year smooth ice, shear ridges, etc.) from satellite imagery. It is quite possible that because of this near-shore ice and the shallow water that a ship loading facility at Cape Thompson would necessarily include a bottom-founded offshore structure.

Thus, of the two locations, it would appear that Cape Dyer is the better location for a shore line ship loading facility. However, during wind conditions that create the greatest hazards for approach to Cape Dyer, the polynya at Cape Thompson is enhanced - thus offering ships awaiting approach to Cape Dyer around Point Hope an ice-free place to wait.

CAPE DYER

<u>Date</u>	<u>Scene I. D.</u>	<u>Comments</u>
<u>1973</u>		
6 Mar.	1226-22160-7	Young ice - large pans offshore
7 Mar.	1227-22212-6	Not shown - large pans offshore
7 Mar.	1227-22214-6	Young ice - large pans offshore
8 Mar.	1228-22270-7	Young ice - large pans offshore
8 Mar.	1228-22273-7	Young ice
11 Mar.	1262-22160-6	Open water
12 Mar.	1263-22212-6	Still water
17 May	1298-22155-7	Even more open
19 May	1300-22265-6	Open water
19 May	1300-22271-6	Open water
4 June	1316-2253-7	Clouds
23 June	1353-22210-6	Open with occasional pans
24 June	1336-22262-7	Open
<u>1974</u>		
1 Mar.	1586-22104-7	First year ice frozen in place
2 Mar.	1587-22162-6	First year ice frozen in place
3 Mar.	1588-22214-7	N.S.
3 Mar.	1588-22220-7	First year ice frozen in place
4 Mar.	1589-22272-6	First year ice frozen in place
4 Mar.	1589-22275-6	First year ice frozen in place
5 Mar.	1590-22331-7	N.S.
19 Mar.	1604-22102-7	First year ice covered with dirt
20 Mar.	1605-22160-7	First year ice covered with dirt
23 Mar.	1608-22325-6	N.S.
6 Apr.	1622-22100-7	Narrow band of ice with water offshore
7 Apr.	1623-22154-7	Narrow band of ice with new ice offshore
8 Apr.	1624-22210-7	Narrow band of ice with new ice offshore
9 Apr.	1625-22264-6	Narrow band of ice with water offshore
27 Apr.	1643-22261-7	Narrow band of ice with broken ice offshore
13 May	1659-22144-6	Narrow band of ice with open water offshore
14 May	1660-22200-6	Narrow band of ice with open water offshore
17 June	1694-22080-6	Open water with pack ice offshore
18 June	1695-22134-7	Open water
7 July	1714-22182-7	Open water
<u>1975</u>		
24 Feb.	1946-21585-7	First year ice
25 Feb.	1947-22040-7	N.S.
25 Feb.	1947-22043-7	First year ice
26 Feb.	1948-22094-7	First year ice
26 Feb.	1948-22101-7	N.S.
27 Feb.	1949-22152-7	N.S.
27 Feb.	1949-22155-7	N.S.
14 Mar.	1964-21580-7	New ice
1 Apr.	1982-21571-7	New ice and large first year pans
2 Apr.	1983-22025-7	New ice and large first year pans

CAPE DYER (Cont'd)

<u>Date</u>	<u>Scene I. D.</u>	<u>Comments</u>
<u>1975 Cont'd</u>		
3 Apr.	1984-22080-7	New ice and large first year pans
3 Apr.	1984-22083-7	N.S.
10 Apr.	2078-22035-7	New ice with large pans offshore
12 Apr.	2080-22145-6	Young ice
12 Apr.	2080-22151-6	N.S.
28 Apr.	2096-22034-7	Narrow belt of first year ice with open water
29 Apr.	2097-22090-7	Narrow belt of first year ice with open water
29 Apr.	2097-22093-7	N.S.
30 Apr.	2098-22144-7	Narrow belt of first year ice with open water
16 May	2114-22033-7	Narrow belt of first year ice with open water
17 May	2115-2284-7	Clouds
3 June	2132-22034-7	Open water
5 June	2134-22151-7	N.S.
25 Oct.	2276-22021-6	Open water with pans offshore
27 Oct.	2278-22131-6	Open water with pans offshore
28 Oct.	2279-22185	Open water with pans offshore
<u>1976</u>		
10 Feb.	2384-22005-7	Young ice
11 Feb.	2385-22061-7	Young ice and older pans
11 Feb.	2385-22063-7	Young ice and older pans
12 Feb.	2386-22115-7	Dark image
29 Feb.	2403-22054-7	Narrow shelf first year with water offshore
29 Feb.	2403-22060-7	Narrow shelf first year with water offshore
1 Mar.	2404-22112-7	Narrow shelf first year with new ice offshore
1 Mar.	2404-22115-6	Narrow shelf first year with new ice offshore
2 Mar.	2405-22170-7	Narrow shelf first year with water offshore
2 Mar.	2405-22173	Narrow shelf first year with water offshore
17 Mar.	2420-21595-7	First year pans driven into coast
18 Mar.	2421-22053-7	First year pans driven into coast
19 Mar.	2422-22105-7	Pans driven into coast consolidate and break off, narrow shelf first year with green water offshore
19 Mar.	2422-22111-7	N.S.
20 Mar.	2423-22163-6	Narrow shelf first year with green water offshore
20 Mar.	2423-22165-6	N.S.
21 Mar.	2424-22221-6	N.S.
6 Apr.	2440-22101-7	Wide shelf of ice off coast with open leads
6 Apr.	2440-22104-7	Wide shelf of ice off coast with open leads
7 Apr.	2441-22155-6	Wide shelf of ice off coast with open leads
22 Apr.	2456-21584-6	Narrow shelf of ice off coast with open leads
23 Apr.	2457-22040-6	N.S.
24 Apr.	2458-22101-7	Narrow shelf of ice off coast with open leads
15 June	2510-21572-6	Open water and occasional pans
23 July	2548-22072-6	Open water with many pans
7 June	5415-21361-6	Narrow shelf of ice with broken pack ice

CAPE DYER (Cont'd)

<u>Date</u>	<u>Scene I. D.</u>	<u>Comments</u>
<u>1976 Cont'd</u>		
22 July	2547-2202	No ice
8 Aug.	2564-21555	No ice
8 Aug.	2564-21561	No ice
9 Aug.	2565-22013	No ice
25 Aug.	2581-21500	Too far south
26 Aug.	2582-21552	No ice
13 Sept.	2600-21545	No ice
14 Sept.	2601-22003	No ice
10 Oct.	2637-21592	No ice

CAPE THOMPSON

<u>Date</u>	<u>Scene I. D.</u>	<u>Comments</u>
<u>1972</u>		
1 Aug.	1009-22090	No ice
2 Aug.	1010-22145	No ice
6 Sept.	1045-22091	No ice
7 Sept.	1046-22145	No ice
<u>1973</u>		
6 Mar.	1226-22160	Broad band first year ice near shore new ice beyond
7 Mar.	1227-22214	Broad band first year ice near shore, new ice beyond
8 Mar.	1228-22273	Broad band first year ice near shore, new ice beyond
10 Apr.	1261-22104	Clouds
11 Apr.	1262-22160	Broad band first year ice near shore, lead beyond
17 May	1298-22155	Broad band first year ice near shore, new ice beyond
17 May	1298-22161	N.S.
2 June	1314-22041	Broad band first year ice near shore, open water beyond
2 June	1314-22043	Broad band first year ice near shore, open water beyond
4 June	1316-22153	Broad band first year ice near shore, open water beyond
22 June	1334-22155	N.S.
23 June	1335-22210	Coast clear, pack ice beyond
9 July	1351-22095	N.S.
13 Aug.	1386-22031	No ice N.S.
14 Aug.	1387-22090	No ice
14 Aug.	1387-22092	No ice
2 Sept.	1406-22142	No ice
3 Sept.	1407-22200	No ice
22 Sept.	1426-22252	No ice
7 Oct.	1441-22075	No ice
7 Oct.	1441-22081	No ice
29 Nov.	1494-22011	
<u>1974</u>		
9 Feb.	1566-21595	Too far south
10 Feb.	1567-22051	Broad band first year ice near shore, new ice beyond
10 Feb.	1567-22053	Too far south
1 Mar.	1586-22104	Large expanse first ice extending from shore
1 Mar.	1586-22110	N.S.
2 Mar.	1587-22162	Large expanse first year extending from shore broken by lead
18 Mar.	1603-22043	Large expanse first year extending from shore broken by lead.

CAPE THOMPSON (Cont'd)

<u>Date</u>	<u>Scene I. D.</u>	<u>Comments</u>
<u>1974 Cont'd</u>		
19 Mar.	1604-22102	Large expanse first year extending from shore broken by lead
19 Mar.	1604-22104	Too far south
20 Mar.	1605-22160	Large expanse first year extending from shore broken by lead
5 Apr.	1621-22041	Narrow shelf near shore, new ice beyond
5 Apr.	1621-22044	Too far south
6 Apr.	1622-22100	Narrow shelf near shore, new ice beyond
7 Apr.	1623-22154	Narrow shelf near shore, new ice beyond
10 May	1656-21580	Narrow shelf near shore, new ice beyond
13 May	1659-22144	Narrow shelf near shore, new ice beyond
28 May	1674-21573	Too far south
29 May	1675-22031	Too far south
30 May	1676-22090	Too far south
31 May	1677-22141	Can't find
17 June	1694-22080	
17 June	1694-22082	Too far south
18 June	1695-22134	Broad shelf decaying ice offshore
4 July	1711-22014	
4 July	1711-22020	Open water
23 July	1730-22064	No ice
3 Oct.	1802-22040	No ice
4 Oct.	1803-22094	No ice
22 Oct.	1821-22094	No ice
<u>1975</u>		
24 Feb.	1946-21585	Shelf of first year with new ice beyond
25 Feb.	1947-22043	Shelf of first year with new ice beyond
26 Feb.	1948-22101	Shelf of first year with new ice beyond
14 Mar.	1964-21580	Shelf of first year with young ice beyond
31 Mar.	1981-21512	Too far east
31 Mar.	1981-21515	Can't find folder
1 Apr.	1982-21571	Shelf of first year ice and young ice adjacent
2 Apr.	1983-22025	Shelf of first year ice and young ice adjacent
3 Apr.	1984-22083	Clouds
9 Apr.	2077-21580	Shelf of first year, young ice has broken away
10 Apr.	2078-22035	Shelf of first year, young ice has broken away
11 Apr.	2079-22093	Shelf of first year, young ice has broken away
12 Apr.	2080-22151	Shelf of first year, young ice forming adjacent
27 Apr.	2095-21580	No folder
28 Apr.	2096-22034	Shelf of first year, young ice forming adjacent
29 Apr.	2097-22093	Shelf of first year, young ice forming adjacent
14 May	2112-21520	Shelf of first year, young ice forming adjacent
15 May	2113-21574	Shelf of first year, young ice forming adjacent
16 May	2114-22033	Shelf of first year, young ice forming adjacent
2 June	2131-21580	Narrow shelf with floes adjacent
3 June	2132-22034	Narrow shelf with floes driven shoreward
5 June	2134-22151	Narrow shelf with floes drifting seaward

CAPE THOMPSON (Cont'd)

<u>Date</u>	<u>Scene I. D.</u>	<u>Comments</u>
<u>1975 Cont'd</u>		
14 Aug.	2204-22025	No ice
14 Aug.	2204-22031	Too far south
2 Sept.	2222-22023	No ice
24 Oct.	2275-21563	No ice
25 Oct.	2276-22021	
11 Nov.	2293-21561	Ice free
<u>1976</u>		
9 Feb.	2383-21551	Narrow shelf of ice, water beyond (narrowest part of shelf does not correspond to shallow area)
10 Feb.	2384-22005	Narrow shelf of ice, water beyond
11 Feb.	2385-22063	Narrow shelf of ice with new ice beyond
27 Feb.	2401-21544	Narrow shelf of ice with new ice beyond
29 Feb.	2403-22060	Narrow shelf of ice with new ice beyond
1 Mar.	2404-22115	Clouds
16 Mar.	2419-21541	Narrow shelf of ice with water beyond
17 Mar.	2420-21595	Narrow shelf with water beyond
18 Mar.	2421-22053	Narrow shelf with water beyond
19 Mar.	2422-22111	Narrow shelf with new to young ice beyond
2 Apr.	2436-21481	Narrow shelf with new to young ice beyond
3 Apr.	2437-21533	Narrow shelf with contiguous thick young ice
6 Apr.	2440-22104	N.S.
20 Apr.	2454-21474	N.S.
21 Apr.	2455-21532	Coastal lead opening up
22 Apr.	2456-21584	N.S.
22 Apr.	2456-21591	
23 Apr.	2457-22042	
24 Apr.	2458-22101	Coastal lead opening again
10 May	2474-21581	Nothing in folder
14 June	2509-21514	Narrow shelf with pack ice adjacent
15 June	2510-21572	Narrow shelf with water adjacent
16 June	2511-22030	Nothing in folder
	5415-21361	Narrow shelf with pack ice adjacent

OCS COORDINATION OFFICE

University of Alaska

Annual Report for Period Ending March 31, 1977

Project Title: Experimental Measurements of Sea Ice
Failure Stresses Near Grounded Structures

Contract Number: 03-05-022-55

Research Unit
Number: 259

Task Order Number: 7

Principal Investigators: W. M. Sackinger, R. D. Nelson

I. SUMMARY

The objectives of this study are to measure, in-situ, the stresses generated in a sea ice sheet as it fails in the vicinity of a static obstacle and the rate of approach of the ice sheet during this process.

The stresses in a floe of multi-year ice near a grounded floe-island were studied for 60 hours starting April 21, 1976. The instrumented floe was subjected to many compressive stress pulses during the first 26 hours of the experiment. The highest stress pulse recorded on the strip charts was 1.7×10^6 N/M² (250p.s.i.) compression. The length of this pulse was not adequately resolved by the recorder, but probably lay between 0.33 seconds and 32 seconds. It did not cause destruction of the ice at the transducer. A second installation in annual ice beyond a grounded pressure ridge in 20 meter water depth showed a tensile stress buildup to 0.68×10^6 N/M² (100 p.s.i.) which was followed by crack formation adjacent to the transducer.

Offshore structures subjected to multi-year ice floes must withstand ice stresses greater than 1.7×10^6 N/M² (250 p.s.i.). Impulse loading should be expected.

II. INTRODUCTION

Recently the mechanics of the interaction of large sea ice sheets with fixed obstacles has become of interest. This new interest has sprung up because of the need in the near future for fixed offshore structures in ice bound waters. Of major importance to the design of such structures is a knowledge of the forces which would be applied to the structure by sea ice moving past it. The magnitude of these forces depend on three general factors:

- a. The mechanics of elastic and plastic deformation of the quasi-continuum of ice floes in the ice sheet.
- b. The failure strength of the ice as found in nature.
- c. The nature of the forces driving the ice sheet and the associated strain rates during ice-structure interaction.

Each of these factors may be examined experimentally, but it is now known that the results are affected by the size of the ice sample and the degree to which natural conditions are preserved in the experiment. Because of this, the excellent work done on sea ice in the past 20 years has served to provoke nearly as many new questions as it has answered and there is the need for full scale in-situ experiments which preserve as many natural variables as possible. Tabata's large scale beam tests (1958), the plate bending tests performed by Hobbs et al. (1962) and the Aidjex experiments are examples of this development. When it comes to ice-structure interaction, full scale tests

are not so easily performed. For arctic conditions, almost any structure large enough to provide an adequate test would be quite expensive. For this reason, the present work has chosen to use natural occurring obstacles as "test structures." Four such static obstacles occur in the arctic environment:

1. Islands
2. Ice Islands
3. Grounded accumulations of ice
4. Grounded pressure ridges at the seaward edge of shore-fast ice

In order to examine the stresses when moving pack ice encounters a structure, we have made measurements near the grounded pressure ridges at Barrow, Alaska and near a grounded ice accumulation located in the open ocean 175 KM (109 miles) N.W. of Barrow 72° 3.4' N., 162° W. This accumulation of ice floes and ridges has been termed a "floeberg" by Stringer and others, but as pointed out by Kovacs is not a "floeberg" as the term has been classically used. In this report, the term floe-island will be used to indicate that it is a more or less permanent feature composed of ice floes and ice ridges. Our primary purpose is to measure the stresses present in a failing ice sheet near such an obstacle and this is being accomplished by the use of embedded load cells (stress transducers). A secondary objective is to measure ice motion and/or strain. At Barrow, this is provided by radar surveillance of the ice pack. For the experiments at the floe-island, no such instrumentation is available and ice motion must be inferred from satellite photography, on-site surveying or navigational data obtained from the helicopter used for logistics.

III. PRESENT STATE OF KNOWLEDGE

Several studies have been conducted in which instrumented pilings were used to measure forces imposed by moving ice when failure is of the crushing or "cutting" type. The study by Blenkarn (1970) is typical while that by Schwartz (1970) is the most complete in that 50 points were instrumented on the piling. Both of these studies dealt with warm, relatively thin ice. Theoretical studies have been performed on the interaction of ice with pilings and with piers whose surfaces slope in order to induce bending in the ice. No experimental data are available in the open literature for structures of an extended nature where the ice must fail by pressure ridging, although several proprietary studies have been done by Imperial Oil Limited. Artificial islands, ice islands, causeways, and docks are typical extended structures which would induce pressure ridging. In addition, multiple piling or single piling structures might have an effective radius much larger than the nominal radius if hummocked ice were to adfreeze to them, or if the cutting action were prevented by interaction with a deep or partially grounded moving pressure ridge. In this case, the structure would become an extended structure for which the ridging mechanism would apply.

IV. STUDY AREA

Near the grounded ice feature or floe-island located approximately 109 miles west of Barrow at $72^{\circ} 3.4'N$, $162^{\circ} W.$, and in the fast ice at Barrow, Alaska.

V. SOURCES, METHODS, AND RATIONALE OF DATA COLLECTION

A. Introduction

In previous work, we had used self contained remote data stations to measure stresses in land fast ice. An aerial reconnaissance of the floe island was made in May, 1975 and again in September, 1975. These flights disclosed several features of its morphology which dictated important changes in the data gathering techniques to be used there. We had previously envisioned laying cable from a safe location to several sites of ice activity where transducers would be emplaced. The size of the island and its extreme ruggedness make this impossible and require radio telemetry links for data transmission. Very little is known about the rapidity with which stresses fluctuate in breaking ice. However, it is known that the rate of stress application seriously affects the measured strength of sea ice in laboratory tests and Schwartz's (1970) results from an instrumented bridge pier include some variations at frequencies above 10 Hertz. A digital recording system using magnetic tape was selected as the one most likely to meet the requirements of power consumption and frequency response. In this system, which was designed and built at the University of Alaska, data acquisition is under the control of a micro-computer which makes decisions as to whether significant changes in stress have occurred within successive sampling periods. If so, the data is recorded, together with time reference data. During inactive periods, no data is recorded.

Equipment. The stress measuring technique used during the experiments has been described by Nelson (1974, 1975). While the electronics instrumentation used at the floe-island differed from that used at Barrow, the principle of stress measurement was the same in each case:

The stress transducers used in these tests are essentially load measuring devices. When embedded in a host such as ice, their output is directly proportional to whatever loading is transferred to them from the ice. If a transducer is stiff, it supports more than its share of the stress. In this case, the transducer output reflects both the magnitude of the ice stress and a stress concentration factor which depends on transducer geometry, transducer stiffness, and rheology of the ice. It has been shown (Hawkes, 1969; Nelson, 1975) that the stress concentration factor is reasonably constant for a given transducer, regardless of the effective ice stiffness (including creep), provided it is in fact stiff relative to the host. Therefore, such a load cell can be used as an embedded stress-measuring transducer. Nelson et al., (1972) have found that stiff transducers can be used to measure ice stresses close to compressive failure of the ice. In addition, stiff transducers should be capable of measuring initial stresses present at the time of transducer installation if the host material can creep. An in-situ emplacement usually involves removing a block of ice from an existing ice floe, making a small hollow in the ice to accept the transducer, and refreezing the block and

the transducer into the ice sheet. Subsequent creep in the ice should readjust the local stress field until the transducer and replaced block assume their full share of the load, a process which takes place most rapidly for warm, saline ice.

The transducer bodies are shown in Figure 1 with the protective copper sleeve removed. The brass slug is 5.08 cm (2 inches) in diameter by 16.9 cm (6.67 inches) long and 10.2 cm (4.0 inches) in the center section have been milled to a 2.54 cm X 3.56 cm (1 X 1.4 inches) rectangular cross section to make room for strain gages and electronics.

Because of the remoteness of the floe-island, its size, and the fact that destruction of the data gathering stations was likely, it was decided to tele-meter data from the stress transducers to a safe recording location at the center of the island. For this purpose, each transducer was equipped with an internal voltage controlled oscillator (VCO) to convert the amplified output of the 1000 ohm strain-gage bridge to a frequency modulated (FM) signal. Four FM signals were multiplexed into one transmitter (Monitron T-15F-13) whose signal was sent to the central receiving station. Standard IRIG center frequencies were used for the VCO's with $\pm 7 \frac{1}{2}\%$ modulation. At each transmitter three channels were used for stress transducers while the fourth was used for an auto-calibration signal. Each transducer was fitted with a 2.37 megohm resistor which could be shunted through a relay across one leg of the Wheatstone bridge to provide a known calibration signal. These relays were controlled by a central timing network which also controlled the signal level on the fourth channel. In the reduction of the data, a signal on channel four going from negative full scale to positive full scale was regarded as an indicator that the outputs of all channels during that period were to be regarded as calibration data. System sensitivity was 6.89×10^6 N/M² (1000 p.s.i.) full scale.

Because of the possible severe temperature changes during the experiments, close attention was paid to thermal compensation of the transducer systems. Since the strain bridge, amplifier, and VCO were all contained in the transducer shell a two point thermal compensation of the entire subsystem could be effected by including the thermistor (T). The system was balanced to zero output at 0° C by adjusting resistors (B) and (F). The system was then cooled to -20°C and rebalanced with resistor (T_c). This provided the desired thermal compensation and reduced temperature generated signals to less than 0.138×10^6 N/M² (20 p.s.i.) between the two calibration points. Thermally caused variations in the transmitter were specified by its manufacturer to be less than 0.005% of center frequency over the range of -40°F to +80°F. The transducers and transmitter are powered by lithium batteries placed in an insulated box on the ice.

Each transmitting channel uses a Monitron R15F-N receiver. The four signals on each channel are then separated and demodulated. The four data channels are then sequentially sampled and converted to digital information at a rate of one channel every 0.008 seconds. This permits recording data at frequencies up to 15 Hertz when eight data channels (two transmitters) are in use. The frequency response is limited by the digital panel meter which is used to digitize the analog data. Channel sampling is under the control of the central processor (CPU) which stores the signal level of each channel and the time only if the stress level is $\pm 0.689 \times 10^6$ N/M² (10 p.s.i.)

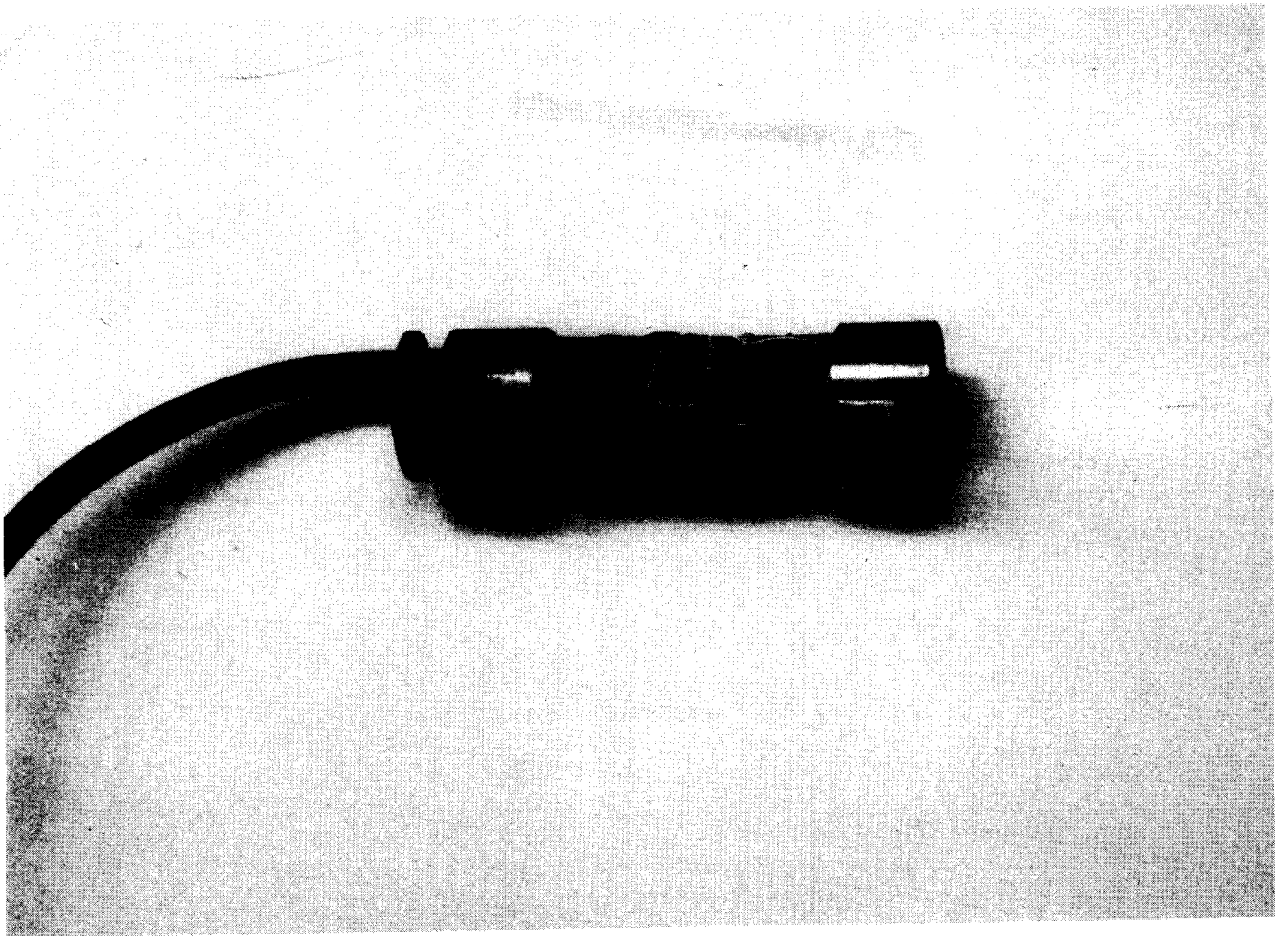


Figure 1 - Ice stress transducer with tubular cover removed.

different from the previously stored reading on that channel. When the CPU memory fills up, all recorded data are dumped onto the magnetic tape in B.C.D. code and the memory is reset for further data taking. Data is put on the tape at a density of 1.66×10^4 data points per tape. During the time the data is being dumped to the tape, frequency response is limited to 0.15 Hertz.

Since the equipment at the central data recorder was in a protected environment, its thermal sensitivity is less critical. The equipment was located in an insulated box inside a shelter at the center of the island. Lead/acid batteries were used to supply power.

After the initial deployment of the ice stress telemetry system at the grounded ice mass located 100 miles west of Pt. Barrow in 1976, plans were made for the 1976-77 winter season which would increase the time for data acquisition, provide for more exact detection of ice movement, and reduce the time required for initial data reduction. The essential focus of the experimental program, which was to measure the failure stresses in ice, in the vicinity of grounded obstacles, was examined to determine whether such data could be gathered within the range of the ice movement radar station at Pt. Barrow. Although ice ridgebuilding and failure is occurring virtually continuously at the grounded ice mass, which is exposed to the movement of the pack ice directly, the ice movements near the shoreline at Pt. Barrow can occur as seldom as a few times each winter, so that the fortuitous cooperation of nature is more essential, and provision should be made for data acquisition for as much of the winter as possible.

It was decided to install the ice stress telemetry transmitter beyond the farthest grounded pressure ridge at Pt. Barrow, and provide it with battery power sufficient for at least four months of the active ice season. The receiver and recorders, located at the radar site on the shoreline, could also be operated indefinitely from the line voltage available there. The grounded pressure ridge then serves as the static obstacle for the experiment. Movement of the ice is automatically recorded on film by the ice dynamics radar located there, so that ice ridging motions can be quantitatively described and related to ice stresses observed by the telemetry system.

Prior to the deployment, detailed laboratory checks of the system were made, which included load calibration, low-temperature calibration, and other tests. An analog recording system was implemented for the receiver station, since a heated and accessible location was available. Three Esterline-Angus chart recorders were driven from the output of the IRIG discriminators, at 730 Hertz, 1300 Hertz and 2300 Hertz, corresponding to the three channels of ice stress data. Because it was expected that data would only be obtained during a limited number of ice stress events, which could readily be analyzed from chart recordings, the provision for digitally-recorded data and subsequent computer processing was deemed unnecessary.

VI RESULTS

University of Alaska personnel arrived at Barrow, April 17, 1976,

prepared to set up two stress experiments at the floe-island. However, an aircraft was not available to escort the helicopter until April 19 and by this time the area was covered by low clouds and fog which made flying hazardous. The weather improved on April 20 and upon arriving at the floe-island we found that the instrument hut which had been placed on the island in March was still there and that the location was stable enough to place the data-gathering station there. A 4.6 meter (15 feet) high UHF antenna mast was installed on the hut roof with one antenna for receiving data, and a 91 meter (300 feet) long antenna was strung about two meters off the ground to provide a radio beacon for later navigation.

The following day, April 21, the data receiver and recorders were installed at the hut, and one station of three transducers was set out on the ice. The transducers were set in the middle of an ice floe approximately 16 nautical miles on a bearing of N15°E (magnetic) from the hut. These figures were obtained from the helicopter's air speed and magnetic compass heading and are therefore approximate. The site was selected to be well out into the dynamic region of the ice on the windward side of the island. The ice in this region was composed of many floes separated by three to seven meter-high recent pressure ridges, with short re-frozen leads in several places. The ice was generally continuous and considerably more compact than that on the sides of the island. The thickness of the ice blocks in the ridges surrounding the floe was about 50 cm.

Because of deteriorating weather, time did not permit a thickness measurement of the floe, and only shallow salinity samples were obtained. The salinity was 0.5 p.p.t. at 5 cm depth and 1.5 p.p.t. at 25 cm depth. Thus the floe was probably multi-year ice. Three ice stress transducers were set out on this floe near its center and buried about 30 cm deep in the ice. Twenty to forty centimeters of wind-packed snow covered the site. The three transducers were oriented in a 0°-45°-90° rosette with transducers #17 (1700 Hertz center frequency) oriented to measure stress along a North-South magnetic bearing, #8 (3000 Hertz) magnetic East-West, and #6 (960 Hertz) magnetic North-West/South-East. The approximate location and orientation of the transducers is shown in Figure 2. The 4.6 meter high antenna for the UHF transmitter was placed on the high point of an adjacent pressure ridge and secured with ice pitons screwed into ice blocks. A large red cloth marker was laid out over the ridge and weighted down with ice blocks to help identify the site later. The installation required two men working at top speed for two and a half hours. Once the transmitting site was in operation, it was necessary to return to the instrument hut to ascertain whether data was being received and to rotate the antenna for optimal gain. With this done, the unit was left to operate on its own with battery power to last for two days. Further deterioration in the weather prevented us from revisiting the site for about a week. When the weather had cleared enough to return, the computer, recorder, and beacon had all ceased to operate because their batteries had run down. These instruments were retrieved but the floe with the transmitting site could not be located.

As described previously, the telemetered data was recorded simultaneously on strip charts and on magnetic tape. Reduced copies of the strip charts for the three data channels and one unused channel are given in Figure 3, and

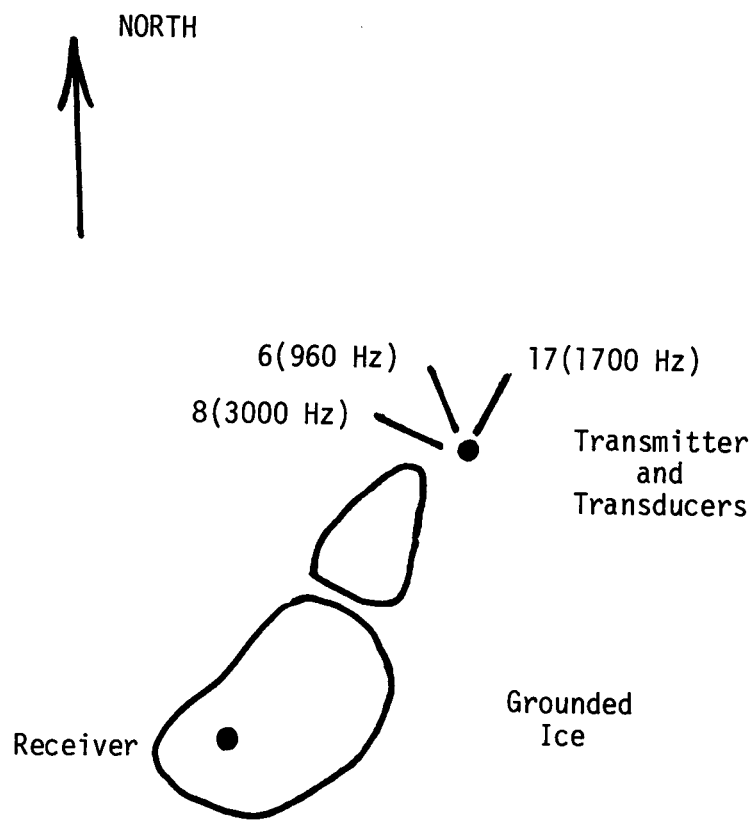


Figure 2 - Approximate location of ice stress transducers at grounded ice mass. Lines give orientations of stress measuring axes.

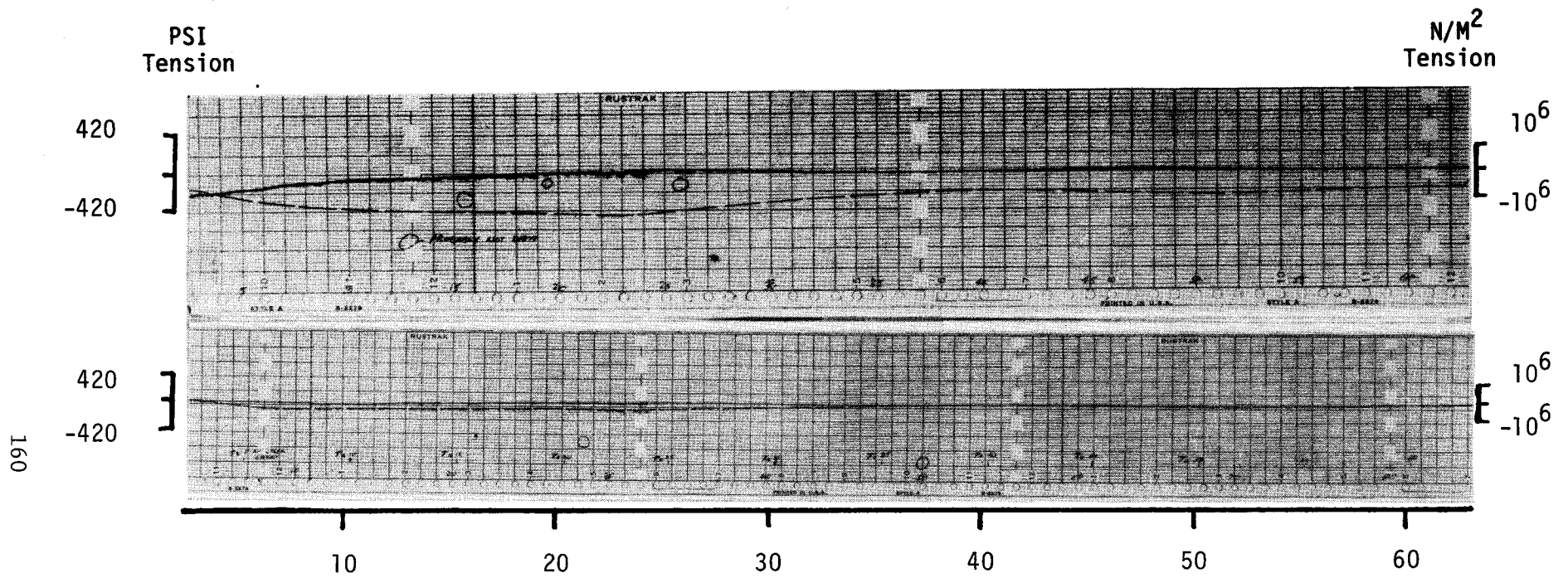


Figure 3 - Chart recordings of stress transducer signals at grounded ice mass. The initial and final few hours described in the text have been omitted. The upper solid trace is the 3000 Hz sensor; the upper broken trace was unused. The lower solid trace is the 960 Hz sensor; the lower broken trace is the 1700 Hz sensor.

details of some of the periods of activity are given in Figures 4-8. Because unregulated DC motors drive the strip charts, the time scale varies between the two charts. However, the beginning of the experiment and the time when the receiver batteries were exhausted are both clearly evident and allow justifying the time scale. Time data from a previous experiment with these recorders have provided the time scale which is superimposed on the charts and is estimated to be accurate to $\pm 5\%$. Since the stress transducers are essentially load measuring devices, it is necessary to convert the load sensed by them to stress in the nearby ice according to the following equation:

$$\text{ICE STRESS} = \frac{\text{Load}}{(\text{Transducer face area}) (\text{Stress concentration factor})}$$

For the 5.08 cm (2 in) diameter transducers used here the stress concentration factor in sea ice is 3.2. This was determined experimentally by embedding a transducer in a 0.61 meter (2 feet) block of annual ice cut near shore at N.A.R.L. (Barrow, Alaska), on April 19, 1976, and loading it with a flat-jack as shown in Figure 9. The block was split vertically to facilitate removal from the ice and installation of the transducer, then both halves were replaced in the hole with plastic sheeting on the bottom to prevent re-freezing. The saw cuts were filled with fresh water, and after they had re-frozen the sides were relieved with a chain saw so that applying pressure to the flat-jack closely simulated uniaxial compression in the horizontal plane. A stress concentration factor of 3.2 has also been determined for 3.81 cm (1.5 in) diameter stress gages with effective elastic modulus and length-to-diameter ratio identical to the gages used here (Nelson, 1974).

Analysis of the magnetic tape recording has been delayed because of compatibility problems between the cassette medium used and the Honeywell Computer at the University of Alaska. This problem is two-fold: First, peripheral equipment which will accept these cassettes is not yet on-line. Second, the software design for our data acquisition system was being done during a time when the Honeywell Computer was being acquired and installed. According to the information available at that time, the computer would accept unblocked character strings of any length. To save space on our tape, this data format was adopted. The Honeywell computer, as since installed, has not yet been able to accept unblocked data and this has hampered our efforts on automated analysis of digital data. A preliminary manual analysis of short portions of the magnetic tape indicates that the digital system did work properly and that stress variations of approximately $3.4 \times 10^6 \text{ N/M}^2$ (500 p.s.i.) were recorded. These variations were both tensile and compressive, and came in bursts with high frequency components. The strip chart records, however, have been analyzed and a discussion is presented below.

A second installation using two transmitting sites was planned for May 21, 1976. However, the ice proved to have too many areas of open water to allow safe operation of a helicopter without floats. Since no helicopter was available with floats at this time, the installation was cancelled. In June, a float-equipped aircraft became available, but at this time the weather was too warm to assure that the transducers would properly freeze into the ice, and hence no further experiments could be performed in 1976.

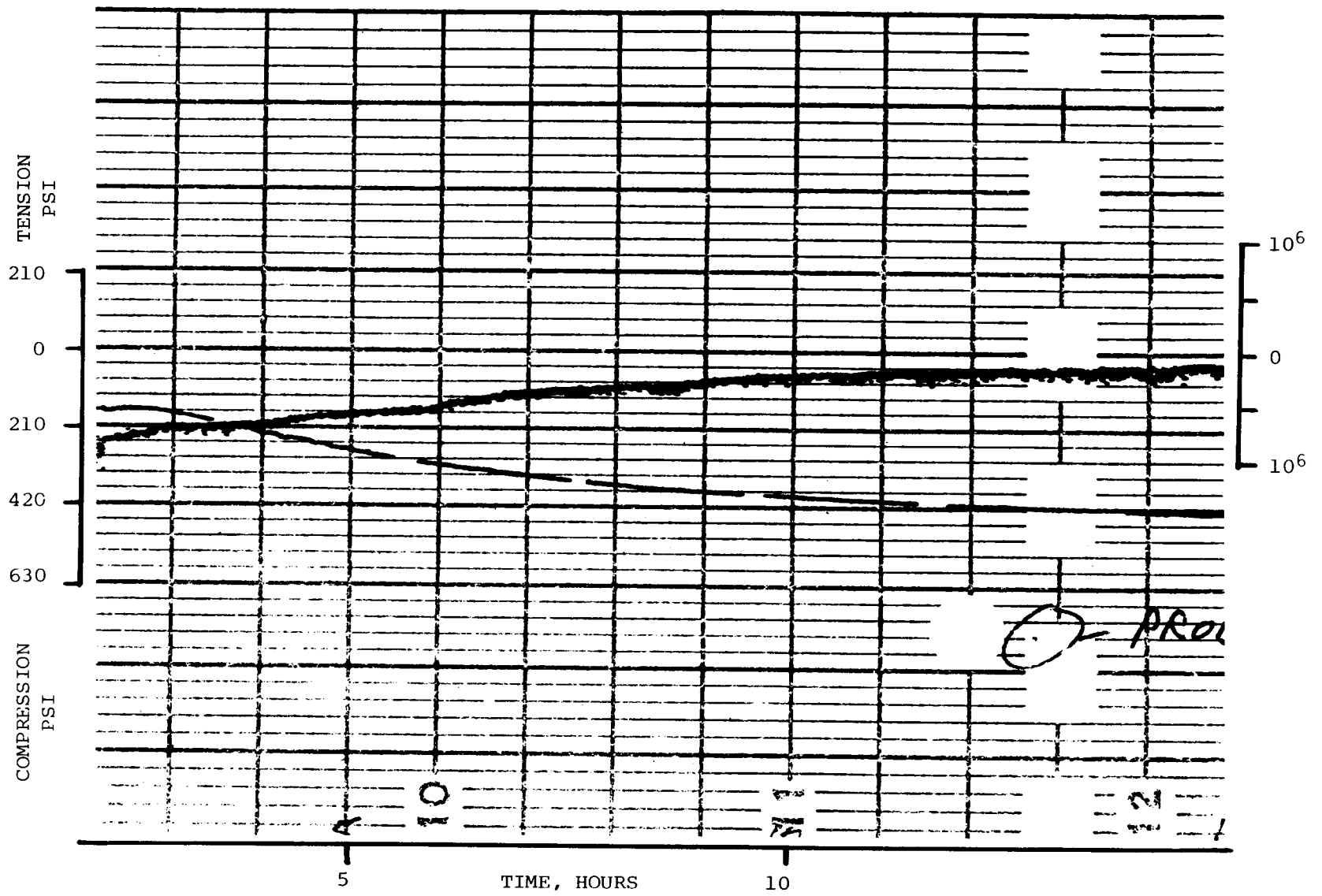


Figure 4 Detail of Stress data for 3000 Hertz transducer oriented East-West. Point A is probably not data. Broken trace was not used.

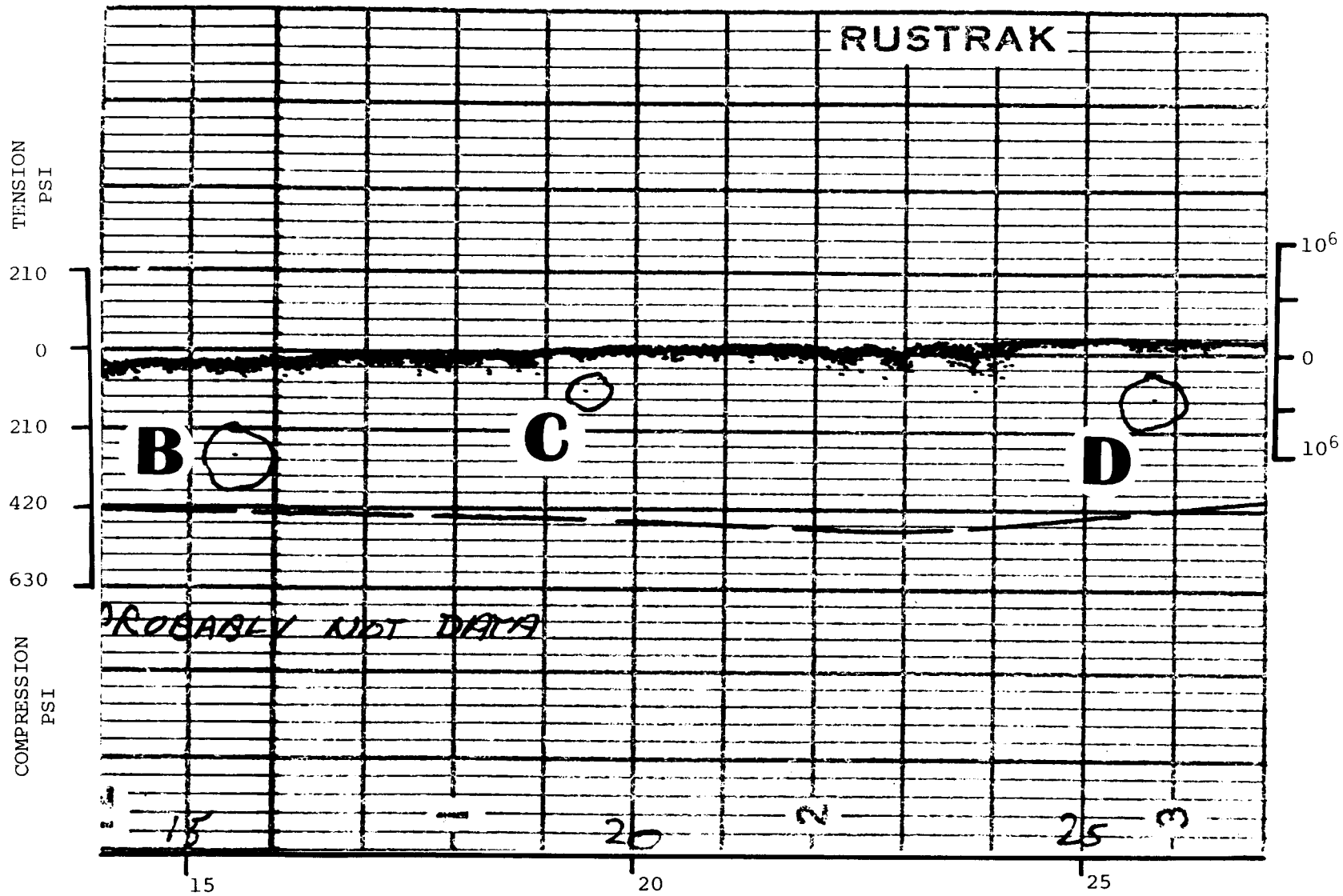


Figure 5 Detail of stress data for 3000 Hertz transducer oriented East-West.
Broken trace was not used.

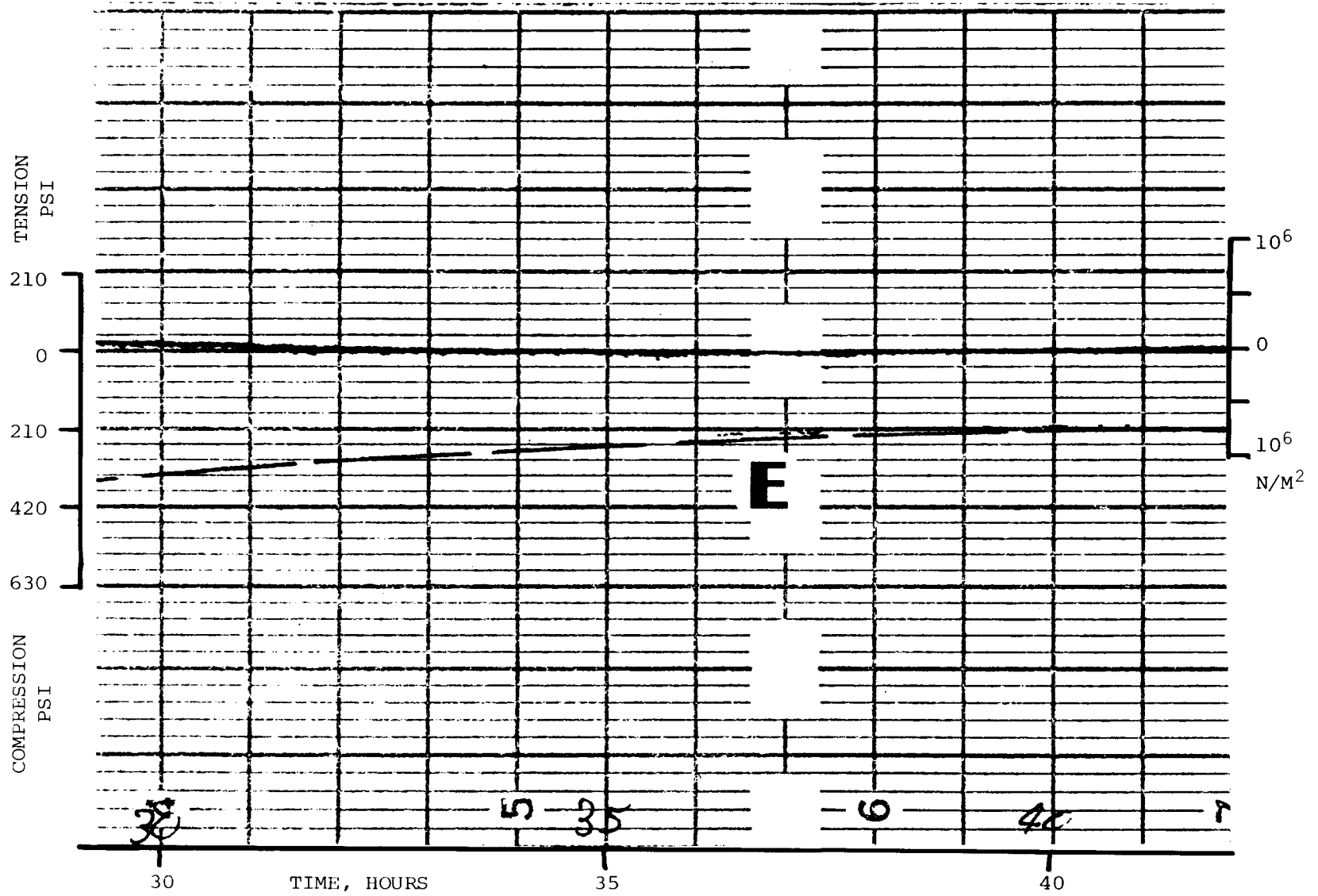


Figure 6 Detail of stress data for 3000 Hertz transducer oriented East-West.
Broken trace was not used.

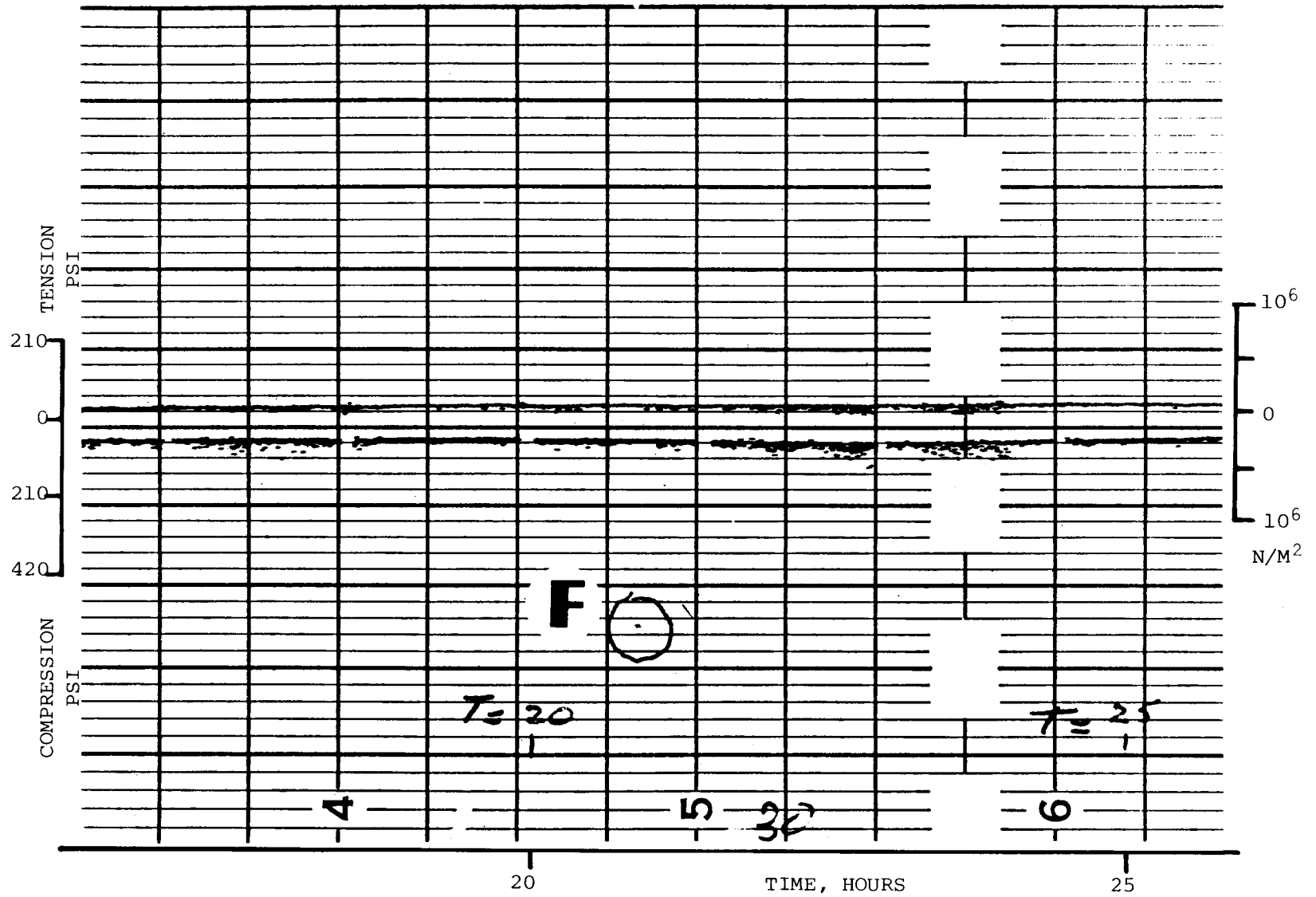


Figure 7 Detail of stress data. The solid trace is the 960 Hertz sensor oriented North-West to South-East. The broken trace is the 1700 Hertz sensor oriented North-South.

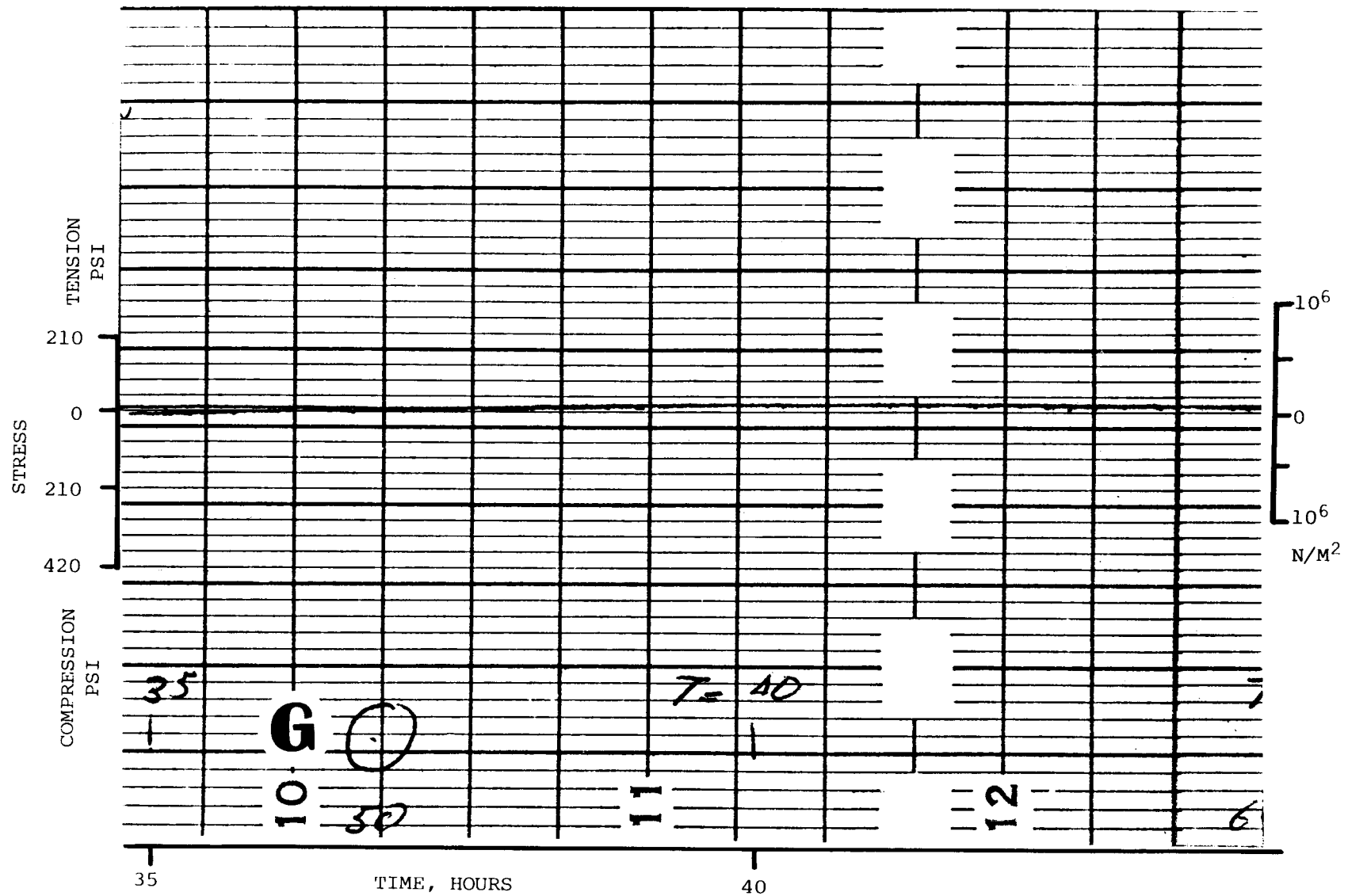


Figure 8 Details of stress data. The solid trace is the 960 Hertz sensor oriented North-West to South-East. The broken trace is the 1700 Hertz sensor oriented North-South.

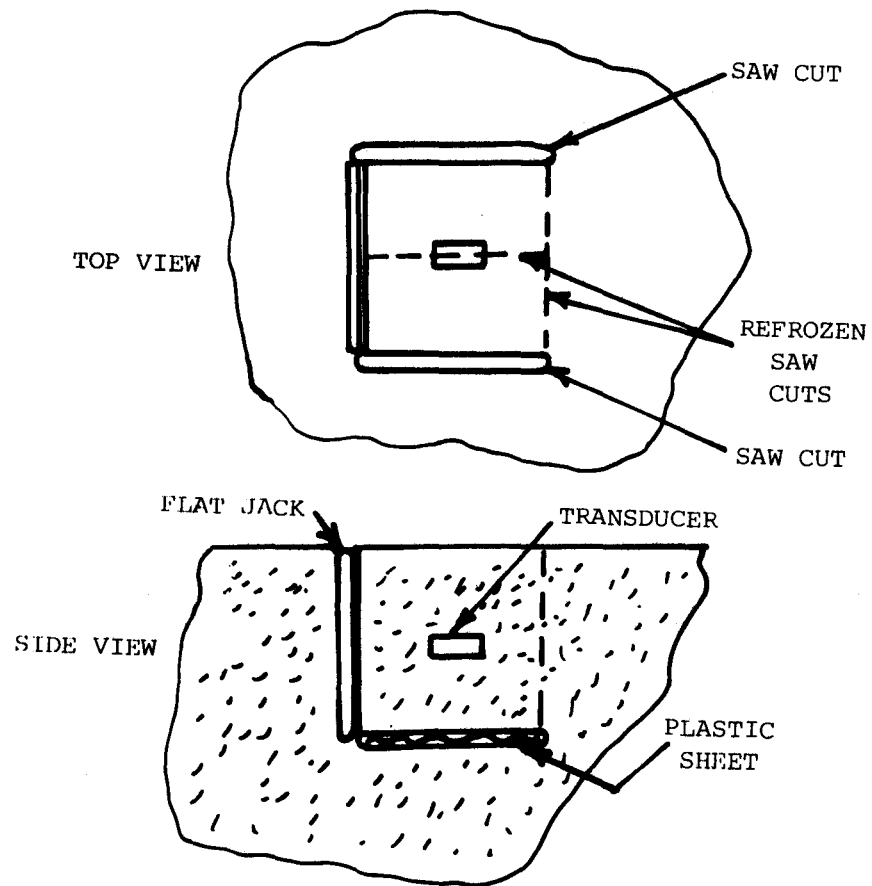


Figure 9 Calibration of stress gage. Pressure applied to flat jack puts the block in uniaxial compression.

Early in the winter of 1976-1977, the Alaskan North Slope was subject to the unseasonably warm weather which covered the rest of Alaska. Ice growth and ridgebuilding was minimal until early in December, when cold weather finally began. However, ridgebuilding did not progress to the stage where the ridge at the 20 meter water depth contour became grounded until midwinter. Helicopter operations were suspended, for equipment reasons, when temperatures colder than -35° F were encountered, so the deployment of the ice stress telemetry was scheduled for early in March 1977.

The ice stress telemetry transmitter, with three stress sensors, was deployed on March 12, 1977, in the location shown on the map in Figure 10. The farthest grounded pressure ridge, normally a prominent linear feature along the 20-meter water depth contour, was barely discernable in this anomalous year, and there were only a few separate locations along the ridge where ice piles were high enough to cause obvious grounding to the sea floor. Considerable activity had resulted in a random collection of ice fragments and piles throughout the shorefast ice zone. The number of points which were grounded to the seafloor could not be determined directly, but the qualitative impression of the height of the ridges and piles led one to believe that the grounding was much less than in previous years. The three ice stress sensors were installed in a refrozen pan of ice, of nominal thickness 70 cm, which was located beyond a large ice pile (of height 5 meters), part of the barely-discernable linear ridge feature at the 20 meter water depth contour described above. A detailed sketch of the installation site is given in Figure 11. The ice salinity was 9% to 10%, taken at 10 cm depth at sites #2 and #3. Snowcover varied from 10 cm over most of the refrozen pan, to 1 meter at the edges near the broken ice fragments around the boundary. These fragments around the boundary were only 1 meter to 1.5 meters in height. Transducers #1 and #2 were installed at a depth of 30 cm in the ice; sensor #3 was installed at a 25 cm depth. Freeze-in transient temperatures and stresses were not monitored, but a final field check indicated that all transducers were functioning satisfactorily. A strong signal was received at the recording station, and data collection began on March 12, 1977.

VII DISCUSSION

A. Experiment at the floe-island, April 17-25, 1976. The strip chart recordings contain four significant changes which should be discussed:

- 1) starting and ending behavior
- 2) long-term drifts
- 3) areas of clear stress events
- 4) isolated single data points of high stress

At the start of each data trace is a period of about 2-1/4 hours which contains a broad noise band. During this time the receiver was working, but the transmitters were not yet powered, and the receiving antenna was connected to the wrong receiver. This noise band is characteristic of data obtained when the telemetry link is broken, and indicates that transmission was adequate during the rest of the period. At the end of the

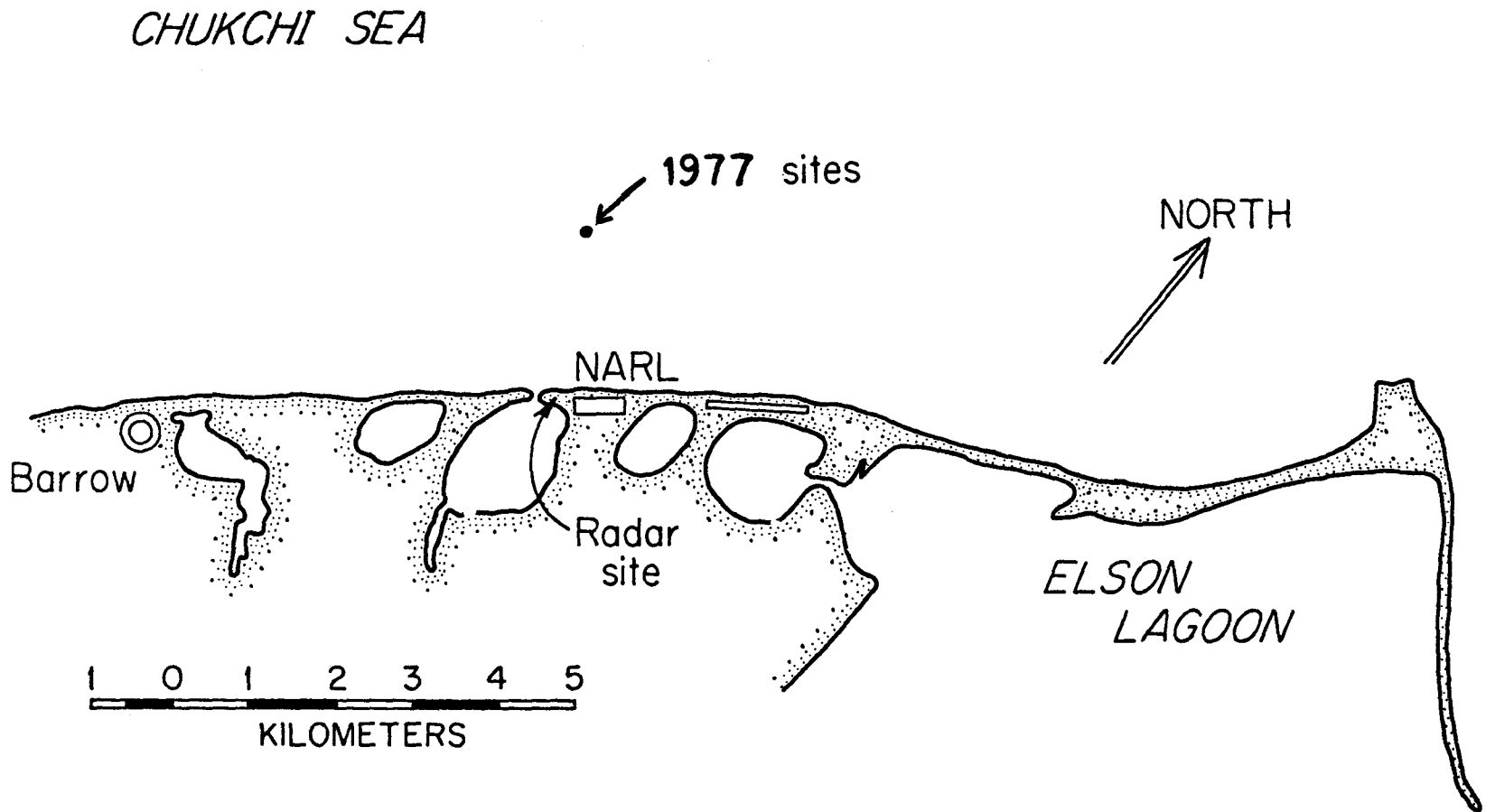


FIGURE 10. LOCATION OF TRANSMITTER AND ICE STRESS TRANSDUCERS FOR MARCH 12, 1977 INSTALLATION.

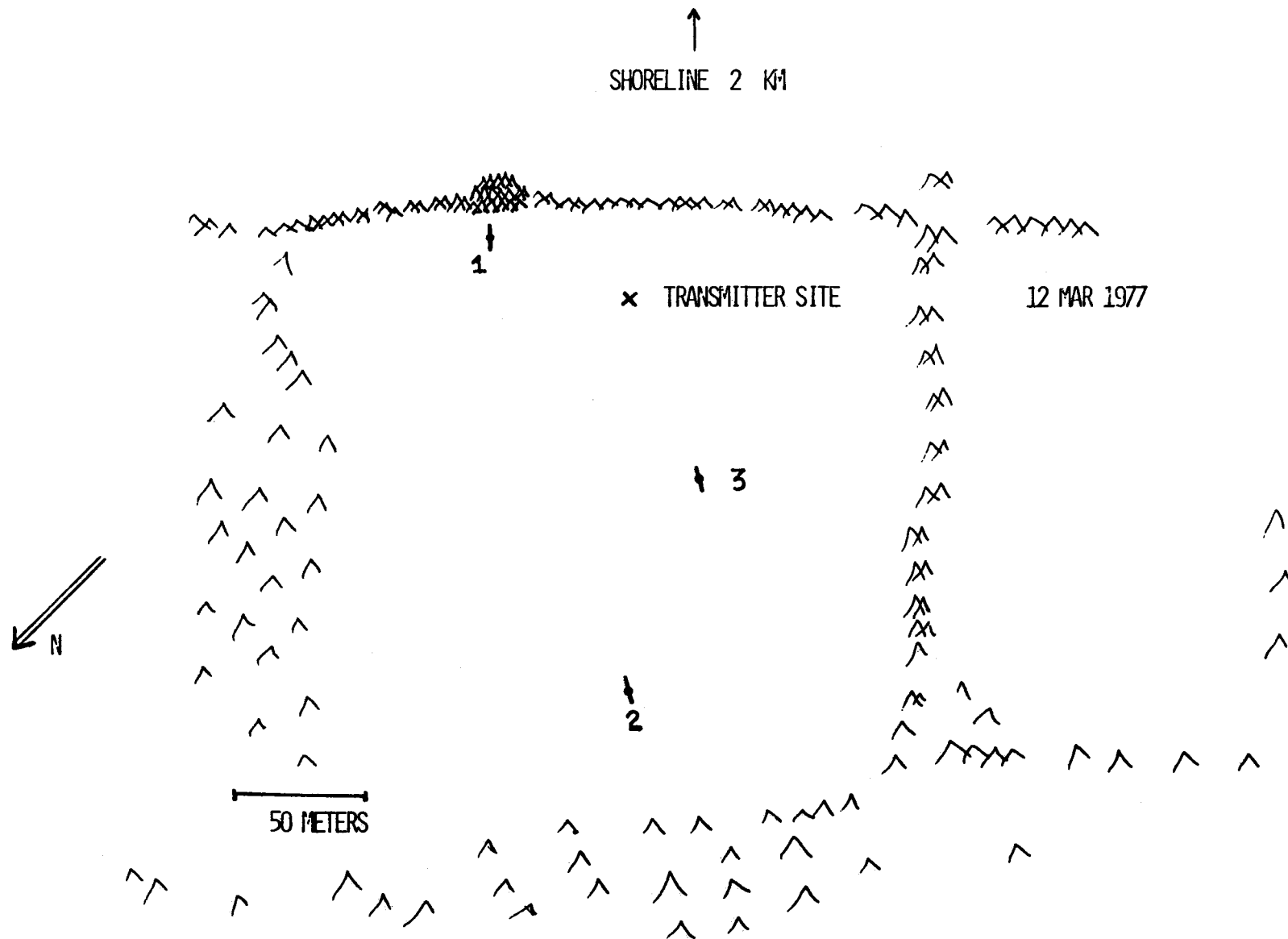


FIGURE 11. DETAILED LOCATION MAP
FOR ICE STRESS TRANSDUCERS,
MARCH 12, 1977 INSTALLATION.

chart each trace becomes noisy, then goes off scale as the battery voltage powering the receiver fell below that necessary to operate the DC-DC converter. A separate battery powered the chart recorders which continued to operate.

There are several factors which contributed to the long-term drifts evident in the data. First, a catalytic heater was used to heat the instrument hut, and its fuel supply was exhausted after about 24 hours. Thus, since the receivers and discriminators have some thermally-induced drift, this temperature change produced a drift which is most evident in the unused channel whose receiver was unpowered. Second, a compressive transient is usually found in the stress transducer outputs as it is frozen into the ice sheet. Much of this stress transient occurred during the initial noise period, and only the decay is evident, lasting about 20 hours. Third, diurnal variations are seen in the last 48 hours which could be either due to heating of the instrument hut, or due to thermally generated stress in the ice. As will be discussed later, we feel that there was little stress on the ice floe during the last twenty hours of operation, and therefore the zero stress scales have been placed at these levels.

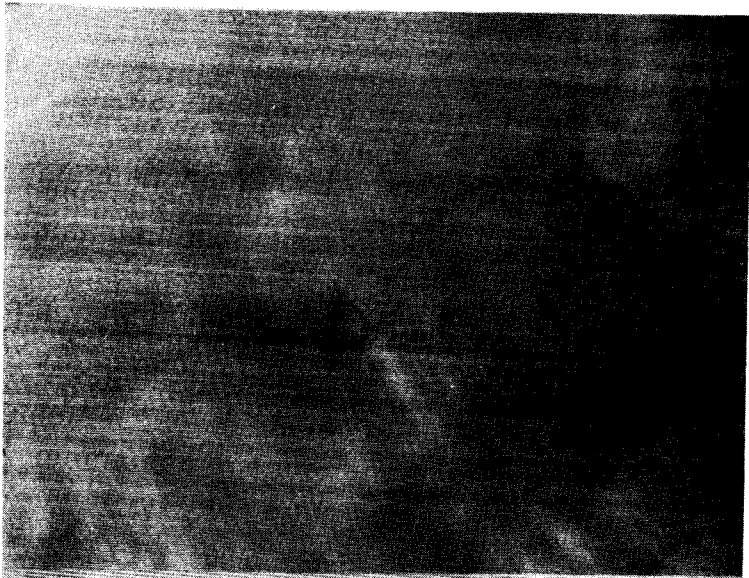
During the first 26 hours of the experiment, the floe on which the transducers were located appears to have been jostled about. Imagery of the region obtained by the NOAA II satellite for April 20, 21 and 22 is shown in Figure 12, and gives the impression that the location of maximum pressure on the island shifted from the Northeast edge on April 20 to North on April 21, and West on April 22. Thus, the location of the transducers may not have been at the point of maximum pressure during installation. However, it should be pointed out that only a few leads were encountered on the flight to the floe-island from Barrow and only one on the way to the transducer site. Thus, the apparent open water to the Northeast of the island, shown on satellite imagery, may in fact be warmer portions of the ice in a region of re-frozen leads. The change in direction of pack movement apparently is responsible for the random appearance of compression stresses in the traces for the first 26 hours of the experiment. Even in a position somewhat removed from the stagnation point, significant pressure could be expected as the pack moved past the fixed floe-island and the individual floes jostled one another, fracturing in areas of re-frozen leads and rearranging themselves. This seems to explain why the traces are discontinuous; the recorders sample one data point each 16 seconds, so they could not be expected to follow rapid events continuously. The bursts of high frequency stress found on the magnetic tape recording would also be characteristic of this jostling and fracturing. The event at about 24 hours, is most dramatic and seems to consist of several pulses. It is possible to calculate the magnitudes of the principal stresses during this period, but only if an assumption is made concerning the timing of the data points registered on all three traces. Because of the coarse time scale on the chart recorders, we do not feel that such an assumption is warranted. It is clear from the data, however, that the direction of maximum compression generally had a west to east orientation. This corresponds to the direction of ice motion which can be inferred from the patch of open water or loose ice adjacent to the floe-island. Apparently, sometime about the 26th hour of the experiment either the pack ice stopped moving or the stagnation region shifted so that the instrument floe was in the lee of the floe-island, as implied by the NOAA II photos. At any rate, the stress records indicate that the loads applied to the floe were much less severe after this time and we assume that it was essentially unstressed.

Many of the isolated data points marked A-G on Figures 4-8 appear to be portions of moderate-frequency high-intensity stress events. The points marked B, C, and D have the same elongated character as the pen marks in the main trace and are clearly data. Those marked A, F, and G are not the right shape and are probably scratches in the waxed paper surface of the chart record. Those marked E are data points, but it is unclear whether they are associated with the active channel or the inactive channel which they seem to follow with a slight off-set. The Rustrack recorders act as a two stage mechanical filter in reproducing the stress events.

First, since one data point per sixteen records is registered on the chart, it is difficult to resolve a pulse shorter than 64 seconds duration. Even for pulses of this length, a reasonably unrelated blurr of points results when several occur in a row, because the chart speed is 0.63 cm per hour. For shorter pulses, it is a matter of chance whether the peak is recorded, and for recordings where only one data point is recorded, the pulse length must have been less than 32 seconds. Nevertheless, instantaneous data will be reproduced without attenuation until the inertia of the galvanometry movement becomes effective. For these recorders, this corresponds to a pulse length of 0.33 seconds and attenuation is 0.1 for pulse lengths of about 0.08 seconds. The frequency response for these recorder movements is 3 db down at 1.5 Hz. and 20 db down at 6 Hz. Pulses are assumed to be half sine waves. Therefore we can say that the peak compressive stress during the interval of activity was at least as great as the values recorded and the duration of the isolated pulses B, C, and D were probably between 32 seconds and 0.33 seconds.

In view of the location of the instrumented floe and the fact that only one floe was instrumented, very little can be inferred about the pressure distribution around the floe island, or the total load imposed on it. In fact, the data are probably characteristic of stress levels in a floe located in a field of jostling floes anywhere in the dynamic pack. Even as such, these data are applicable to the design of offshore structures. First, the strength of sea ice is known to exhibit a significant size effect, and the degree to which full-scale strength is lower than small-scale strength has been a source of much confusion. Previously available data from fast ice protected by grounded ridges (Nelson et al., 1976) did not include compressive stress pulses greater than $0.138 \times 10^6 \text{ N/M}^2$ (20 PSI) while compressive strengths of $6.89 \times 10^6 \text{ N/M}^2$ (1000 PSI) have been measured for small specimens by Peyton (1966). The data obtained here implies that at least $1.72 \times 10^6 \text{ N/M}^2$ (250 PSI) compression (point B) was sustained, and possibly more, since we do not know where fracture occurred, the thickness of the ice there, or the duration of the stress pulse. Second, the resonant frequencies of actual offshore structures may be in the range 0.5 Hertz to 18 Hertz (see for example Reddy, et al. 1975 or Mänttinen, 1975). Since the stress pulses recorded here may also have been in this range of frequencies, future offshore structures will have to allow for dynamic excitation as well as static loading. Reddy et al. have discussed this, and much more information on ice behavior should be available before rational designs can be produced.

B. Experiment at Barrow, March 16-18, 1977. At the time of installation on March 12, 1977 the pack ice was close to the shoreline, and there were no open leads offshore. The wind was from 070°, at less than 15 km/hr. Since the shoreline is oriented at 043°, there was a wind component parallel to the shoreline, and a component perpendicular to the shoreline (offshore). This



April 20, 1976



Figure 12

Grounded ice mass photographed by NOAA II satellite. Ice mass is located at $72^{\circ} 3.4' \text{N}$, $162^{\circ} 4.6' \text{W}$. See Figure 2 for orientation of North.

April 21, 1976



April 22, 1976

wind increased until, on March 16, 1977, enough stress had developed in the pack to cause activity in the ice and data collection by the ice stress telemetry system. Although a more detailed analysis remains to be done after the ice radar photographic records are processed, it is possible to give a preliminary account of the ice motion and the resulting stresses here.

The wind direction and magnitude at Barrow are given for March 16, 1977, and March 17, 1977 in Table I. Since this wind direction, 070°, had prevailed for several days, the pack ice apparently was responding by moving in the same approximate direction. The shorefast ice began to develop tension cracks near the shoreline at 1500 AST on March 16, according to observers there. In particular, the tide crack near the shore opened to 10-20 centimeters, and a crack approximately 70 centimeters wide opened at about 200 meters offshore, beyond the ice mechanics research site of Dr. L. Shapiro. The tension developed at all three remote ice stress stations simultaneously, at 1951 AST, as can be seen in Figure 13. All sites recorded a rise in tension over a period of one hour, after being at equilibrium for four days. The tension field applied to the ice pan was smallest near the grounded ice pile, site #1, but was larger at site #3 and largest at site #2, which was the farthest from the grounded ice pile. The largest tensile stress recorded was at site #2 at 2200 AST, a value of 0.68×10^6 N./M.² (100 p.s.i.), after which the stress dropped quickly, reaching zero after six hours. A similar behavior was noted at site #3, but the maximum tensile stress there was 0.42×10^6 N./M.² (61 p.s.i.). The site #1, near the grounded ice pile, sustained a modest tension of 0.08×10^6 N./M.² (12 p.s.i.) during this interval and beyond, as shown in Figure 13. Both sites #2 and #3 briefly went into compression, then into tension again, then into compression, and finally back into tension. This behavior can best be understood by including an observation made of the site at 1515 AST on March 18, after the above action had occurred. The time of reconnaissance is indicated on Figure 13 by the vertical arrow. The reconnaissance showed that a new crack had developed as shown in Figure 14, and that it had refrozen. This new crack was between sites #2 and #3 and the transmitter, and obviously was a result of the tension developed during the time period of 16-18 March. It is wider near site #2, indicating that it initiated seaward of site #2 and propagated beyond site #3. Based upon the short distance (approximately 1.25m) from the crack to sensor #2, and the data shown on Figure 13, the following explanation is proposed, to relate the data to the crack formation.

The initial buildup of tension was sufficient to cause a crack to form at approximately 2200 AST on March 16, after which the tensile stress was relieved. This crack initiated seaward of site #2 and propagated through the ice pan, separating #2 and #3 from the grounded ridge. From 0400 to 0800 AST on March 17, some limited compression was observed which may have been due to refreezing of sea water in the very narrow crack. Then, from 0800 to 1030 AST, further pack motion caused an additional tension to develop, resulting in the widening of the original crack at 1030 AST. From 1200 AST on 17 March to 1000 AST on 18 March, both sites #2 and #3 recorded compression which may have been produced by the refreezing of water in the cracks after they were opened. Finally, on March 18, further ice motion in the pack caused tension to build once again. After the radar information is available, it should be possible to confirm the nature of the pack ice motion farther from shore which caused these tensile fields to develop. The direction of crack formation appears to be perpendicular to the wind direction, as might be expected.

VII CONCLUSIONS

1. The ice stress telemetry system was developed, which provides a method for recording the ice stress in hazardous locations during times of ice movement.

Table 1 . Wind at Barrow, Alaska

For March 16-17, 1977.

	<u>TIME</u> (AST)	<u>WIND</u> <u>DIRECTION</u> (°)	<u>WIND</u> <u>SPEED</u> (KM/HR)	<u>MAX</u> <u>GUST</u> (KM/HR)
16 MAR	1500	070	42.6	55.6
	1600	070	37.0	50.0
	1700	070	40.7	51.9
	1800	060	38.9	55.6
	1900	070	40.7	53.7
	2000	060	38.9	48.2
	2100	070	38.9	51.9
	2200	070	33.3	42.6
	2300	060	27.8	-
	2400	060	25.9	-
<hr/>				
17 MAR	0100	060	27.8	-
	0200	070	31.5	-
	0300	060	27.8	-
	0400	070	29.6	-

Similar direction and magnitude for the remainder of March 17.

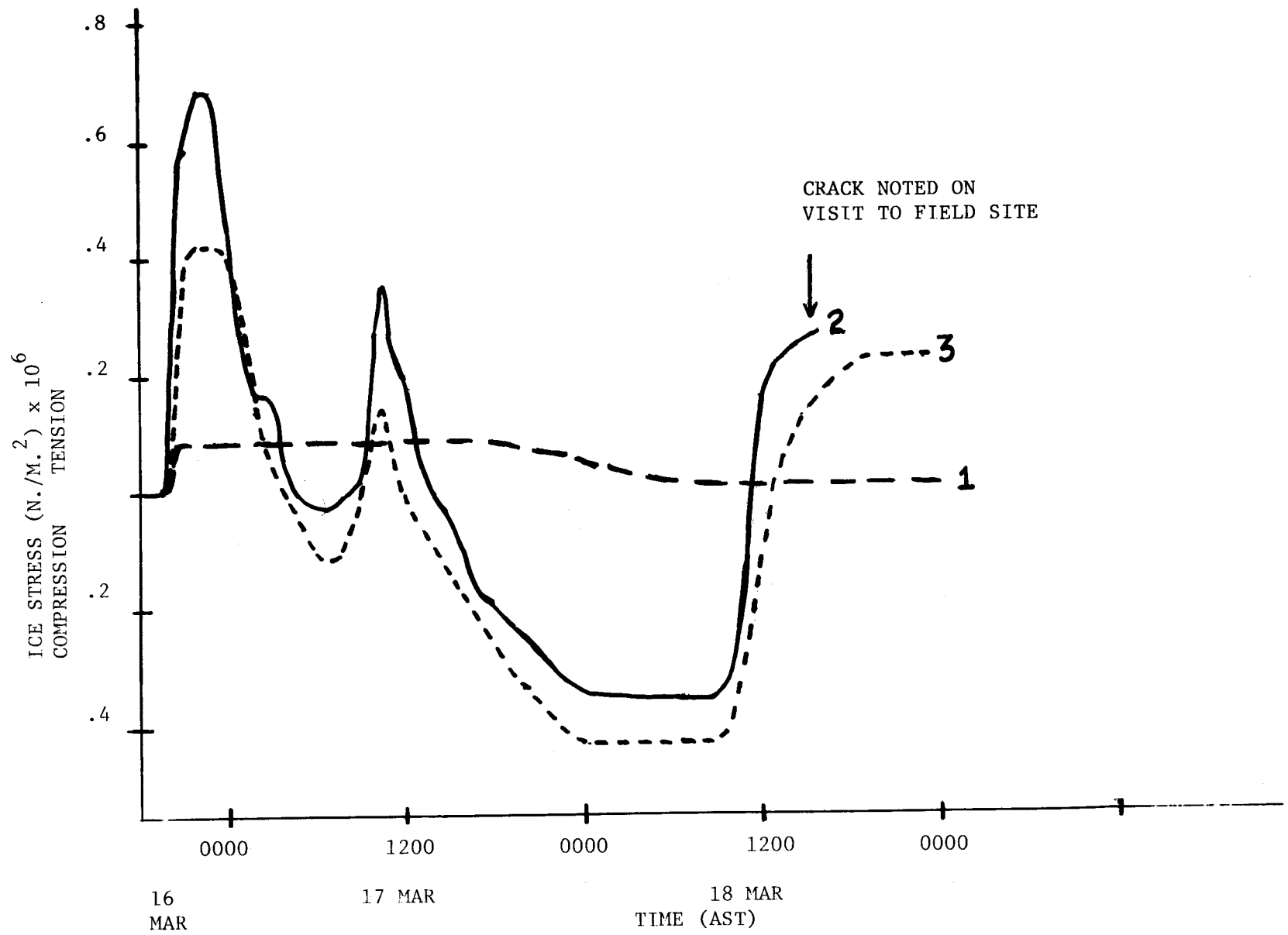


FIGURE 13. TIME VARIATION OF STRESSES AT BARROW SITES, MARCH 16-18, 1977.

↑
SHORELINE 2 KM

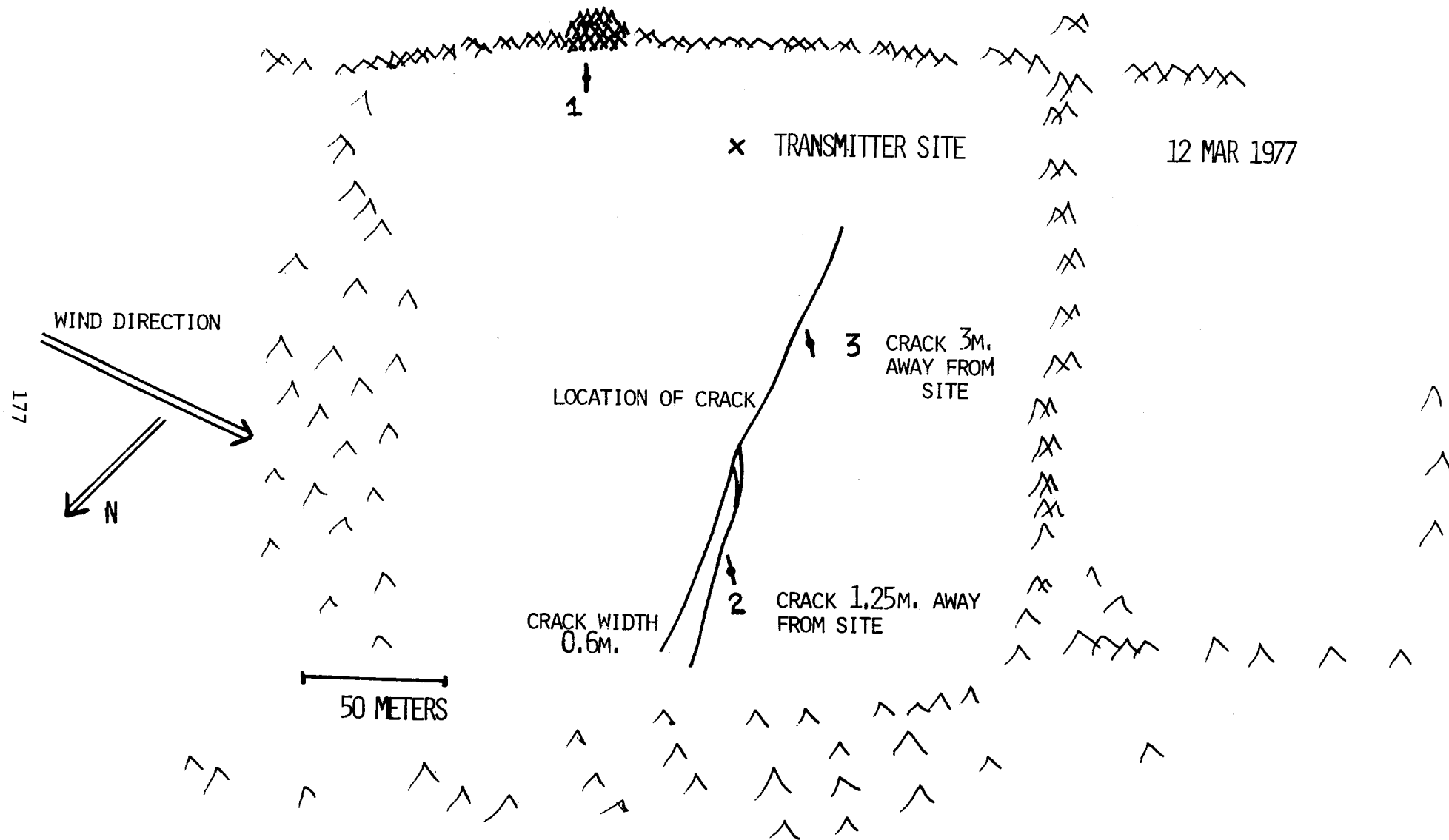


FIGURE 14. DETAILED LOCATION OF CRACK AFTER ICE STRESS EVENTS OF MARCH 16-18, 1977.

2. Stresses were measured in a floe of multi-year ice which was in the moving pack near a grounded accumulation of ice or floe island.
3. The highest compressive stress measured was $1.72 \times 10^6 \text{ N/M}^2$ (250 PSI) and we infer that the crushing strength of ice in the pack may have been higher.
4. The maximum compressive stresses recorded occurred as pulses whose duration was probably between 0.33 seconds and 32 seconds. Impulse loading of shorter duration may also have occurred but would not have been recorded.
5. Stresses were measured in a refrozen pan of annual ice beyond a grounded pressure ridge. A tensile field with stresses at least as high as $0.68 \times 10^6 \text{ N/M}^2$ (100 PSI) developed in response to a 40 km/hr wind.

IX. NEEDS FOR FURTHER STUDY

The radio telemetry system developed for the stress sensors provides a particularly convenient method of stress analysis. The study which is being performed here will only begin to answer questions about the failure of sea ice in situ. The apparent presence of high intensity pulses with frequency content above one Hertz at the floe island implies that future data acquisition systems should have a frequency response at least to 30 Hertz. The spectral distribution of ice stresses near grounded obstacles, as well as the maximum values of ice stress, should be measured for all of the ice conditions expected to be encountered at a particular offshore location. Maximum stresses which correspond to static failure in compression can be obtained by specific in-situ ice loading experiments, and it is recommended that such tests be included as part of Dr. L. Shapiro's program. Additional telemetered stations are required to record the spectral distribution of ice stresses during floe-floe interactions and ridgebuilding events near grounded structures.

X. SUMMARY OF 4th QUARTER OPERATIONS

A. Field Activities

1. Field Trip: March 11-13, 1977. NOAA Helicopter, NARL, Barrow.
2. Scientific Party: W. M. Sackinger, University of Alaska, Principal Investigator
W. J. Zito, University of Alaska, Electronics Technician
3. Method: Ice stress telemetry system installed.
4. Locality: 2 km offshore from NARL (Barrow, Alaska).
5. Data Collected: Data acquisition of ice stress begun.
6. Data Submission Schedule: In quarterly reports, as available.

B. Problems encountered: No logistic, scientific, or management problems were encountered during this quarter.

C. Estimate of total funds expended:
\$76,829

XI. REFERENCES

1. Blenkarn, K. A.; "Measurement and Analysis of Ice Forces on Cook Inlet Structures." Off Shore Technology Conference Paper OTC 1261, 1970.
2. Hawkes, I., 1969. "Stress Evaluation in Low-Modulus and Viscoelastic Materials Using Photoelastic Glass Inclusions. *Experimental Mechanics*, pp. 58-66, February, 1969.
3. Hobbs, H. A., Cutcliffe, J. L., and Kingery, W. D. "Effect of Creep and Temperature Gradients on Long-time Deformation of Ice Sheets," in Ice and Snow, W. D. Kingery Ed., M. I. T. Press, Cambridge, Mass., 1963.
4. Nelson, R. D., Taurianinen, M., and Borghorst, J.; 1972, "Techniques for Measuring Stress in Sea Ice," University of Alaska, Institute of Arctic Environmental Engineering. available as Alaska Sea Grant Report 76-18, Alaska Sea Grant Program, University of Alaska, Fairbanks.
5. Nelson, R. D., 1974. "Measurements of Tide and Temperature Generated Stresses in Shorefast Sea Ice," in The Coast and Shelf of the Beaufort Sea, J. Reed and J. Sater, Editors, Arctic Institute of North America, Arlington, Virginia.
6. Nelson, R. D., 1975. "Internal Stress Measurements in Ice Sheets Using Embedded Load Cells," Presented at Third International Conference on Port and Ocean Engineering under Arctic Conditions, University of Alaska, Fairbanks, Alaska.
7. Schwartz, J., 1970; "The Pressure of Floating Ice Fields on Piles," Proc. I.A.H.R. Symposium on Ice and Its Action on Hydraulic Structures, Reykjavik, Iceland.
8. Tabata, T. 1958; "Studies on Visco-Elastic Properties of Sea Ice," in Arctic Sea Ice, Nat. Acad. Sci./Nat. Res. Council Pub. 598, Washington, D.C., 1958.
9. Peyton, H. R., 1966. "Sea Ice Strength". University of Alaska Geophysical Institute Report UAG R-182. College, Alaska.
10. Nelson, R. D., Hanley, T. O'D., and Shapiro, L. H., 1976; "Ice Pressure in Grounded Ice Zones", University of Alaska, Geophysical Institute, Fairbanks, Alaska. In Press.
11. Reddy, D. V., Cheema, P. S., and Swamidas, A. S. J., (1975); "Ice Force Response Spectrum Model Analysis of Offshore Towers", Proc. Third Int. Conf. on Port and Ocean Engin. under Arctic Cond., University of Alaska, Institute of Marine Science, Fairbanks, Alaska.
12. Mähtänen, M. 1975; "Experiences of Ice Forces Against a Steel Lighthouse Mounted on the Seabed", Proc. Third Int. Conf. on Port and Ocean Engin. under Arctic Cond., University of Alaska, Institute of Marine Science, Fairbanks, Alaska.

ANNUAL REPORT

Contract No. 03-5-022-55
or 261/262

Reporting Period:
April 1, 1976 to April 1, 1977

BEAUFORT SEA, CHUKCHI SEA, AND
BERING STRAIT BASELINE ICE STUDY

William R. Hunt

and

Claus-M. Naske

April 1, 1977

ANNUAL REPORT

BEAUFORT SEA, CHUKCHI SEA, AND BERING STRAIT BASELINE ICE STUDY

I. Task Objectives:

The investigators are finishing work on a data supplement to the charts which show seasonal navigational conditions from 1870 to 1970. This supplement presents all pertinent ice information and navigational information found in ships logs.

II. Field Activities:

The investigators collected data showing seasonal navigational conditions from 1870 to 1970. The data was extracted from ship logs of whaling vessels, U. S. Revenue Marine Service and U. S. Coast Guard vessels as well as trading ships. The investigators spent four man months during the year researching in the Whaling Museum in New Bedford, Massachusetts, the Federal Record Center in Suitland, Maryland, the Fleet Weather Facility, Navy Department, in Suitland, Maryland, the U. S. Coast Guard Headquarters in Washington, D.C., and the National Archives in Washington D.C.

III. Results:

The investigators completed a number of maps which show the historic variations in ice conditions over a 100 year period. These maps were presented at the February, 1977 conference of principal investigators in Barrow, Alaska. They will be utilized in the preliminary report which the Arctic Project Office is preparing.

The investigators are continuing to transfer pertinent ice data to maps.

A sample of ice data that lends itself to chronological narrative rather than cartographic representation is included with this report.

EXCERPTS FROM THE LOG BOOK OF THE BARK HELEN MAR ON A CRUISE

TO THE ARCTIC IN 1872, 1873, 1875, 1877 AND 1878

SEASON 1872

- August 11, 1872, 5 of wrecked ships in sight, at noon, other wrecks in sight, at Point Belcher. All of them broke up but the Seneca, Minerva and Thomas Dickerson. The Seneca and Thomas Dickerson are in six feet of water their spars standing.
- August 12, Strong wind from NE working to the NE. Middle part laying aback, have seen several whales in the ice. Latter part steering S. Sea Horse islands bearing SSE.
- August 20, Picked up a dead whale. At anchor since 17th.
- August 25, Spoke to Bark Arctic. They told us of Bark Hlen, Snow, Roscoe, and Sea Breeze being lost in the ice to the eastward of Point Barrow.
- August 28, At 2 PM lowered for a bowhead, it being the first time this season. Have seen several going fast to the westward.
- October 9, Ship covered with ice.
- October 10, The ship one mass of ice.
- October 12, At 10 AM sighted Cape East.

SEASON 1873

- June 6, 1873, At 5 PM passed Cape East and entered Arctic Ocean.
- June 7, Steering NW at 7 PM hauled up NNE Cape Serdez bearing SW 30 miles, no ice in sight, something that has not been before in my recollection.

SEASON 1875

- June 21, 1875, Got 48 wall ruses. Ship in the open ice. Caught 7 wall ruses. Lat. 66.47
- June 24, Working to the N along the Western Ice. Got 11 walrus.
- July 12, At 3 PM tied the ship up to the Ice that had the walrus on. At 9 AM cast off and stood out of the Eice to the Eastward. Got 161 walrus.
- July 25, Scatering Ice. Got 60 walrus.
- July 27, Begins with a fresh SE wind at 3 PM, lowred and got 76 walruses have used up all the ammunition have got 1,250 all told.

Season 1875, continued

August 26, Got 1 whale, off Harrison Bay.

August 28, Got 1 whale off Colville River.

SEASON 1877

July 5, 1877, Working along the ice looking for walrus the ice is so scattered that the walrus have gone back to the main pack.

July 13, Working along the east shore saw several walrus and got 25 of them.

July 14, Ship among the scattering ice looking for walrus saw several and got 29 of them.

July 15, Steering to the north part a strong breeze from the S, raised several walrus and the captain shot 100 of them we went on the ice to skin them and it was so rough that the sea washed over the ice and broke it up we saved but of of them.

July 29, Ship steering to NE point Barrow in sight we found very heavy ice a ground all along the bank and the ice was packed on the land so that we could not get in to the point so went to the north until we came back to point Barrow.

August 11, Ship all at anchor and the boats cruising in the ice. Several whales struck but most of them tucked the lines under the ice.

September 18, Strong breeze from SE, ship cruising to NE of Herald Island. Got one whale and another one in the afternoon.

September 21, Freezing hard, ship cruising NE of Herald Island, Boats are badly iced up. Spoke to Bar Norman which reports that Bark Three Brothers abandoned frozen in the ice to the eastward of Point Barrow.

September 22, This day commences with a strong breeze from the NE. The ship under reef top sails, cruising to the NE of Herald island the weather very cold the ships and boats covered with ice saw several whales and looked for them the waist boat carted at one but did not get fast the starboard boat struck one got fast with one iron and the whale went into the ice and I had to hold on to him so hard that the iron draud out.

October 4, Pleasant weather and moderate breeze from westward. Herald island 15 miles of bearing SW by W. Plenty of whales in sight. Got 1 whale.

October 6, Cruising on NE side of Herald Island. Got 1 whale.

October 10, Ship steering ESE bound out of the Arctic.

SEASON 1878

- June 3, 1878, Ship laying in ice with all sail firtled getting water off the ice, 80 barrels of it.
- June 19, Pleasant weather and a light breeze from NE, ship under all sial beating through Berring Strates. Natives came on board from the Dimeads and we got sum boots and clothing.
- June 20, Got 50 walrus.
- June 22, Working in the ice of Cape Surge. Got 14 walrus.
- June 24 Slight breeze from NW. Ship under sail working through the ice scattrng ice. Got 11 walrus.
- June 27, Cruising along the ice of Cape Surge 11 sails in sight.
- June 28, Captan shot 32 walrus.
- June 30, Captan shot 126 walrus.
- July 1, Commences with a light breaze from the S.E. with foggy weather finished skinning the walrus this morning and had to leave them on the ice the walrus was so far in the pack that we could not get them of so we anchored the cacke of ice that they were on and left them thear.
- July 2, Commence with a calm and fog the ship laying of the ice latter part of the day clear with a light breaze from the SE we came to anchor close to the pack in 25 fathoms of water and haled the ice that the walrus was on out ot the edge of the pack and got the blubber on bord then got under way.
- July 6, Captan shot 28 walrus.
- July 9, Got 5 walrus.
- July 11, Got 52 walrus.
- July 12, Got 7 walrus.
- July 13, 12 sails in sight and walrus very scarce.

CRUISE OF THE U.S. REVENUE CUTTER SERVICE SHIP BEAR TO THE

ARCTIC IN 1911 UNDER THE COMMAND OF J.G. BALLINGER

SEASON 1911

August 1, 1911, 4 AM got underway for Barrow, arrived there 4:20 p.m.

August 2, 1911. During the entire trip to Point Barrow, no ice of any description, even grounded ice, was sighted until in about the latitude of the Seahorse Island, when a few pieces were seen, from the masthead well off-shore. Strong North-easterly winds prevailed for several days before and after our return from Barrow.

The present season in the Arctic has been one of the most remarkable, so far as ice conditions are concerned, within the memory of the oldest inhabitants. The ice left Point Hope the latter part of June, and early in July the Arctic was practically free of ice, and I was also informed that at Point Hope there had been no real Arctic pack during the entire winter. The whaling has been unsatisfactory this past year--one taken at Pt. Hope, two live and one dead at Icy Cape, one at Barrow. Many foxes trapped, but few polar bears taken.

WHALING SHIP BELVEDERE OF NEW BEDFORD, WINTERING
AT HERSCHEL ISLAND IN 1897-98 RECEIVED THE
FOLLOWING AMOUNTS OF DEER MEAT AND FISH

Deer Meat		Fish	
November 29	150 lbs.	November 29	250 lbs.
December 6	140 "	December 6	230 "
December 24	280 "	December 24	385 "
January 14	500 "	January 14	80 "
January 27	40 "	April 1	500 "
February 4	950 "	April 8	<u>500 "</u>
February 23	100 "		
March 13	845 "		
March 19	670 "		
April 4	275 "		
April 12	110 "		
April 15	600 "		
April 24	735 "		
April 30	1,000 "		
May 6	528 "		
May 15	437 "		
June 26	624 "		
July 11	173 "		
July 15	182 "		
July 19	<u>720 "</u>		
Total	9,059 lbs.	Total	1,945 lbs.

SOCIAL INFORMATION

Log of the Steamer Bear, under the command of First Lt. D. H. Jarvis, R.C.S.

Sunday, July 23, 1899

Off Cape Blossom, Kotzebue Sound

At 1:30 PM steamer "Arctic Bird" made fast alongside. Received 32 destitute miners suffering from scurvy. Delivered to "Arctic Bird" 28 sacks of coal. Lieut. Bertholf reported as follows. Found from 250 to 300 miners encamped on beach, north of Cape Blossom, alarming state of affairs existing, 32 men particularly helpless from scurvy, many other just recovering, about 15 had died during winter and spring from this disease and black-leg. Many others had no means of living and food and food supply exhausted. The steam launch being inadequate for transportation of so many, the master of the stern wheel steamer "Arctic Bird" brought off the sick, receiving in return the coal expended. 32 were brought off and put under surgeon's care. There had been much distilling of whiskey during winter by whites and natives, but no evidence was obtainable, Principal offenders having left the country.

Two brothers Roger and Al Pickering from Princeton, Ky, were killed between May 1-4 on portage between Selawik and Kuyukuk River by native named Kokonuck; reports state they first attacked the native; that Roger Pickering character was bad and had killed a man named Martex on the Nastuk River during the winter. In consequence of the killing no Selawik natives had come to the coast and Kokanuk could not be found. At 3:30 p.m. Lt. Bertholf left on "Arctic Bird" for purpose of transporting miners to this vessel. Sent in 3 cases canned tomatoes, case evaporated cream, crate of potatoes, 1 tin dissicated potatoes, 1 case canned fruit, to be left with the Rev. Robt. Samms, missionary at Cape Blossom, for the use of those at the encampment.

Names of miners received on board.

Geo. Sargent	B. Jaster	A. J. Haywood
J. F. Gordon	J. Johnson	C. J. Connely
J. H. Kilner	J. O. Eckles	W. R. Hastings
O. C. Ford	M. H. Walley	Thos. Meadow
J. H. Cole	H. S. DeLong	A. McGavitt
C. Hasse	E. W. Martin	J. Berquist
Frank Hanis	H. S. Bike	J. A. Steel
J. Meyer	G. W. Breed	Chas. Bush
Theo Francisco	J. Wilson	
Geo. Sinclair	F. Etzel	
J. M. Lane	Hans Basteau	
Sabin Hanis	A. Fahrenholt	

July 24, 1899

At 3:45 a.m. Arctic "Bird" came alongside with Lieut. Bertholf and 48 men, 2 women and one child, for transportation to St. Michaels. Between 150 and 200 people left at encampment. Extra rations, fruit and vegetables were left by cabin and wardroom messes for the care of sick.

July 24, 1899, continued

Names of persons received at Cape Blossom.

G. W. Berry	J. Maiden	A. Johnson
E. Humphrey	B. Anasi	C. S. Bushnell
M. Thomas	F. E. Smith	J. C. Hollister
S. M. Fuller	G. C. Bence	L. Junnelli
C. Schlumecher	W. H. Shaffer	F. Statsnell
H. B. Alzioth	E. W. Clark	G. W. Close
M. Kane	C. Ashley	F. Ramez
		A. Scott

W. Simmons	D. Sullivan	A. R. Jones
Thos. Russell	D. Deathe	A. Detzenhoff
A. Ahlers	F. Dickman	G. P. Blanchard
E. Ahlers	F. Sledder	F. Yamock
H. F. Masters	C. Murphy	C. Martinez
M. Premo	L. D. Morris	C. F. Webb
A. C. Thees	C. M. Smith	- Mockerzy
O. McCormick	H. Gould	H. E. Welb

Mrs. Alvis A. Herman (alias Bownraro) and infant,
Mrs. Alice Smith

July 26, 1899

Anchored off Sledge Island

4 - 8 AM. Lt. Bertholf went ashore with cutter crew and Master at Arms and brought off Diomedea native Nubarloo who killed the boy Nanoruk the 15th inst. on the Port Clarence sand spit. He was placed in irons and confined into the fore hold.

Mid. to 4 P.M. Watch making anchor, Mr. D. H. Smith, U. S. Deputy Marshal came on board for the arrest of Captain Jens B. Neilson of schooner General McPhersen for piracy. Sent Mr. Smith with an officer to schooner to serve warrant.

3:15 Lt. Berthold and Deputy Marshall Smith returned with Jens B. Neilson under arrest. Turned schooner over to Mr. Smith as managing owner. Received on board for transportation to St. Michaels wife and three children of Jens B. Neilson.

4 - 6 PM. Wm. Kjillman and Redemeyer came on board for passage to St. Micheals. [sic]

6 - 8 PM George Rowan and Nany Ford, stranded miners wishing to work there [sic] passage to St. Micheals [sic] were taken on board.

Jerimah Abramson assistant to Dr. Doty lately teacher at St. Lawrence Island left the ship at Anvil City.

July 27, 1899

8 AM to merid. The Commanding officer called upon Captain Walker, U.S.A. commanding Ft. St. Micheals, and turned over to same, destitute miners and their effects.

Merid. to 4 PM. Landing destitute miners on shore with their effects, having turned them over to U.S.A. authorities at St. Micheals. Deputy Marshal D. H. Smith left the ship with Jens Neilson, in custody. Mrs. Neilson and three children left the vessel.

July 29, 1899

Sent the following prisoners ashore and turned them over to the authorities Sablok, (alias Capt. Jack) Frank Temple of the "Mermaid," Ashuik, and Nubarlo and C. Crutchfield, received from "Mermaid" 19th instant for medical treatment and witness in case against Temple, left the vessel.

These cases were heard before the U. S. Commissioners. Sablok sentenced to 6 months imprisonment in the military jail at St. Micheals. The others were turned over to the District Court at Sitka, C. Crutchfield was sent ashore and held by authorities as a witness against Temple.

July 31, 1899

At anchor, St. Micheal, Alaska

4 PM to Mid. At 6:00 observed the American Bark "Agate" of San Francisco, Hansen, master, coal, flying International signal (DKR) mutiny. Sent officer and master of arms to her and found one man Geo. Muier, Seaman, refusing duty when ordered to man boat. At request of master put Geo. Muier in irons and confined him in fore hold.

August 8, 1899

4 to 8 AM. At 4:40 cutter returned with two native women Coonook and Pugenvik for transportation to St. Micheals witnesses to the killing of the boy Nanowk by the native Nubarloo 15th ultima.

Merid. to 4 PM. Upon interrogating the natives it was learned liquor had been traded by whale ships. The Commanding Officer then investigated, obtaining such evidence as warranted the detention on board of two natives, Kotoweena and Teekok. Later to serve as witnesses against the master of the steam whaler Bowhead.

August 11, 1899

At anchor Cape Blossom, Kotzebue Sound

4 to 8 AM. Some 15 miners were found still on the beach waiting to get out, while 40 were still up the river. No one seriously ill. A notice was posted at the mission House requiring all able bodied men who wished to leave the country had no means of doing so to be encamped on the bluff at Cape Blossom by August 20th to facilitate embarkation on the "Bear."

August 16, 1899

Lat. 71.06'00 N

Long. 157.10'00 W

Choppy to smooth. Numerous cakes of ice floating near ship.

August 17, 1899

At anchor near Cape Smyth, Alaska.

Occasional pieces of ice drifting near vessel. At 1 a.m. veered 25 fms of chain to steer clear of ice.

August 27, 1899

Merid. to 4 PM. At Cape Blossom. At 12.40 boats returned with miners and their effect for transportation to St. Micheals. At 2.20 steam launch left with cutters to bring off persons ashore and their effects.

Miners received on board.

A. Goetz

Henry Nobles

J. Bower

W. J. Phillips

F. Granholz

L. H. Northrup

J. W. Stevens

J. W. Sorsick

L. J. Ray

D. Stibi

A. Scott

C. Partridge

C. Aiken

J. W. Johnson

E. McTaggart

August 28, 1899

Miners received on board.

G. R. Porterfield

A. J. Hamilton

O. W. Holt

September 6, 1899

The native women Coonok and Pugennuk witnesses to the killing of the boy Nauwak, and Ahlooksuk witness in Boyd murder cases, delivered to authorities at St. Michaels.

ANNUAL REPORT

Contract Number: 03-5-022-55

Research Unit Number: 265

Reporting Period: 1 April 1976 to 31 March 1977

Number of Pages: 49

DEVELOPMENT OF HARDWARE AND PROCEDURES
FOR IN SITU MEASUREMENT OF CREEP IN SEA ICE

Lewis H. Shapiro
Richard D. Nelson

Geophysical Institute
University of Alaska
Fairbanks, Alaska 99701

Contributing Scientist:

Earl R. Hoskins

Department of Mining Engineering
South Dakota School of Mines & Technology
Rapid City, South Dakota

March 31, 1977

I. SUMMARY

The objectives of this project are to develop and test the procedures and hardware required for in-situ measurement of the mechanical properties of sea ice, and to conduct a program of such measurements. In addition, the results of the extensive series of laboratory tests of sea ice in creep and at constant loading rates which were done by Peyton (1966) are being reevaluated.

During the past year sufficient data has been acquired to verify the repeatability of results from the method of direct shear strength tests described below. Procedures developed for tests in uniaxial compression and indirect tension (Brazil test) appear to give reasonable results, but further work is needed. Finally, it has been demonstrated that the combination of loading the ice sheet with flatjacks and sensing strain with wire strain gauges embedded in the ice does produce good creep curves. However, numerical results for these tests are not yet available.

The analysis of Peyton's (1966) laboratory creep tests in compression is in progress, and a one-dimensional, non-linear viscoelastic stress-strain law has been developed which fits the creep curves generally with errors of less than 2% at each data point. In addition, the law describes the shape of Peyton's experimental curves relating strength to rate of loading.

Field work is in progress at the present time, with two primary objectives. The first is to conduct as many creep experiments as possible to obtain data with which to evaluate the constants of the stress-strain law noted above. The second is to further evaluate the uniaxial and biaxial compression tests described below. Incidental to these objectives, data on the elastic properties of sea ice are also being acquired, as well as information in the degree to which anisotropy resulting from preferred crystal orientation affects the measured parameters.

II. INTRODUCTION

A. General Nature, Scope and Objectives

The problem of translating results from laboratory tests to field conditions is well known in many branches of science, and forms an important aspect of studies of the mechanical properties of sea ice. It is difficult in the laboratory to simulate the effects of temperature and salinity gradients, continuous variations in grain size and ice fabric, and the presence of inhomogeneities on scales larger than laboratory samples. Further, mechanical properties of the ice can change during the processes of removal from the ice sheet, transport and storage. A program of determining the mechanical properties of sea ice in-situ, and with minimal disturbance to the ice, is thus needed to supplement and verify laboratory results.

The objective of this project is to develop the techniques, procedures and equipment necessary to measure as many as possible of the mechanical properties of sea ice in-situ, and further, to utilize these methods in a program of performing the relevant measurements.

B. Relevance to Problems of Petroleum Development

Any permanent or semi-permanent structure off the Arctic Coast of Alaska must contend with the hazard that sea ice presents to its stability. In order to properly design such installations it is necessary that reliable values of the mechanical properties of the ice be available both for establishing the design of the structure, and for the evaluation of that design by public agencies. In addition, significant savings in cost of construction can be realized if less conservative safety factors can be utilized.

III. CURRENT STATE OF KNOWLEDGE

Previous work on the determination of creep properties of sea ice was reviewed by Weeks and Assur (1967). The work of most direct interest

is that of Tabata (1958) who performed a series of in-situ tests using cantilever and fixed end beams. In these tests, a constant load was applied to the beam and the deflection at that point was measured as a function of time. The resulting curve of deflection vs. time has the form of a creep curve, and the constants for a 4-parameter, linear visco-elastic model were derived from it.

Peyton (1966) conducted a laboratory study in which cylinders of natural sea ice were subjected to constant tensile or compressive loads of different magnitudes to generate creep curves. Loads were removed after the creep curves were established, and the elastic components of the deformation were recovered. Unfortunately, for all but a very few of the tests, no information was given regarding the temperature, salinity, or crystal orientation of the test specimens. These parameters obviously influence the mechanical properties of the specimens and interpretation of the results, for the purpose of determining the parameters of a stress-strain law, is not possible without them. Note that Peyton did not include any analysis of the results of these tests in his final report. However, the unpublished notes and laboratory records of these tests, which include the necessary data, are archived at the University of Alaska, and with Dr. Peyton's permission we are using these in an analysis of the test data.

Creep curves for fresh ice show a pronounced increase in strain rate following the initial decrease leading to the secondary creep stage, for the case of loads above some threshold value (about 4 kg/cm^2). For sea ice, Peyton's (1966) data show a similar effect, but in some tests the increase in strain rate is restricted to a short time period, after which the rate decreases again. This introduces an obvious 'kink'

into the curve. Karlsson (1972) interpreted this effect as an example of strain rate dependent yield, and developed a three-dimensional visco-elastic-plastic stress-strain law from which good approximations to some of Peyton's one-dimensional, experimental curves have been calculated. Note that an alternative explanation of the significance of these 'kinks' to the deformational process is given below.

IV. SOURCES, METHODS AND RATIONALE OF DATA COLLECTION

Experimental methods for various types of tests were described in the last annual report of this project, and are reviewed briefly in other sections of this report.

One important change in the conduct of the program has been instituted since the last annual report. It was originally intended that the basic creep experiments would consist of generating a stress field in the ice sheet through the use of flatjacks. The stress at some point in that field was then to be measured with a stress transducer and the strain, at a geometrically similar point relative to the flatjack, with a strain gauge. However, after preliminary tests were run it was decided that because controlled uniaxial or biaxial stress fields of known magnitude could be developed in the ice using flatjacks alone, the use of stress transducers could be eliminated. This has the effect of simplifying the instrumentation and procedures required for the experiments.

The experimental program for the present year has been designed to evaluate the significance of mechanical anisotropy of the ice sheet resulting from preferred crystal orientation. In laboratory tests on small samples this anisotropy causes significant variations with load direction in measurements of mechanical properties. However, it is not clear that these results should apply to in-plane loading of the entire ice sheet. In that case, much

of the load is concentrated in the relatively strong upper part of the ice sheet, which should be nearly isotropic to such stresses.

In addition to the field test program, the results of the extensive series of laboratory tests done by Peyton (1966) are being re-examined. To date, this work has been concentrated on creep data only, and a report of preliminary results is included below. The major part of Peyton's work, involving tensile and compressive strength experiments at constant load rate are yet to be studied.

V. RESULTS

A. Introduction

Discussions of the results of investigations into procedures for conducting strength tests in uniaxial and biaxial compression, direct shear, and indirect tension are given below. In addition, a report of the results of the study of Peyton's (1966) data is also included. Part of this work involved the first steps in the formulation of a non-linear viscoelastic stress-strain law for sea ice.

The results of the preliminary creep tests conducted during the past field season can be summarized by noting that, although good creep curves were obtained for several tests, it was not possible to accurately determine the stresses which caused the deformation. Thus, no further analysis has been attempted. Tests are currently in progress, however, and these are discussed in the quarterly progress report below.

B. Review of Peyton's (1966) creep data and development of a viscoelastic stress-strain law for sea ice.

1. Review of Peyton's data.

The purpose of this work is to provide small-scale laboratory test data with which in-situ determinations of the creep properties of sea ice can be compared.

During the past year we have been reviewing the results of Peyton's (1966) creep tests on sea ice samples. Within the past quarter enough results became available to permit a preliminary report to be prepared. The preliminary nature of the following discussion is emphasized - much more data remains to be evaluated. The same is true of the derivations of the equations of the viscoelastic models presented below. As an example, the viscous components of the strain were assumed to follow a hyperbolic sine relationship between the stress and the strain rate. This appears to agree well with the data, but other functional relationships, which might fit better, remain to be investigated. In addition, in the interest of brevity, the derivations have not, in general, been presented with the degree of thoroughness or rigor which would be expected in a formal publication. Finally, the reader is referred to Peyton (1966) for description of sampling methods, preparation and description of test specimens and experimental techniques.

The total data set consists of approximately 190 creep tests in uniaxial compression. The curves for all of these have been plotted,

and the tests were sorted by sample orientation, test temperature and load. The groupings by temperature and orientation include from 1 to 9 tests, with most having less than 5. Thus, there is neither the range of loads nor the repetition of tests for averaging which would be needed in order for the mechanical properties of the ice to be determined for any given set of conditions. However, useful information and suggestions for additional work can be obtained as discussed below.

The following discussion is based upon the results of 70 of Dr. Peyton's experiments which represent most of the samples from groups of 4 or more tests. Samples from depths of 8, 17, 48 and 60 inches at temperatures from -6°C to -21°C are included. Those referred to below as "vertical" were loaded along a direction normal to the ice sheet and, therefore, normal to the c-axis orientation. "Horizontal" samples were loaded in the plane of the ice sheet at a specified orientation to the dominant c-axis direction. Orientation and temperatures are indicated in the figures where the data appears.

The quality of the data is generally good in the sense that the creep curves are smooth. In some cases, apparently irregular data points were found to be the result of errors in calculation or transcription of the data and these were corrected by reference to the original notes.

To the present, we have referred to the tests as "creep tests". However, examination of the curves shows that this description needs to be modified. Some of the tests were true creep tests, with steady-state creep approached closely. However, many of the tests were actually stress-rupture tests in which tertiary creep leading to failure was

initiated at some time during primary creep. Interpretation of this type of test is described in Grant and Mullendore (1965). The results of a series of stress-rupture tests on sea ice, by bending of simply supported beams, are given in Kingery and French (1963).

Finally, a peculiar feature of some of the data is the presence of one or more discontinuities in the creep curves. These are points at which the strain rate instantaneously increases, as if an incremental load was applied at that time as in a two-step creep test, then gradually decreases toward a steady-state creep rate which is higher than that just prior to the discontinuity. A typical example is shown in Figure 1. These features, termed here "jump points" were previously found in Peyton's data by Karlsson (1972) who considered them to be strain-rate dependent plastic yield points in the viscoelastic flow field, and modeled then as such following the theory suggested by Naghdi and Murch (1963). An alternative explanation is considered below.

ORGANIZATION OF THE DATA

A minimum value of the strain-rate was determined, by inspection, for each strain-time curve. For creep tests, this value is simply the slope of the "best fit" straight line to the linear portion of the curve; that is, the steady-state strain rate. For stress-rupture tests, it is the slope of the curve at the inflection point at the onset of tertiary creep. If the curve included a "jump" point, then the minimum strain rate was taken as the slope of the curve at the jump. The time to the minimum strain rate of stress-rupture tests was also measured, as were the time to the first jump point in any test and the total duration

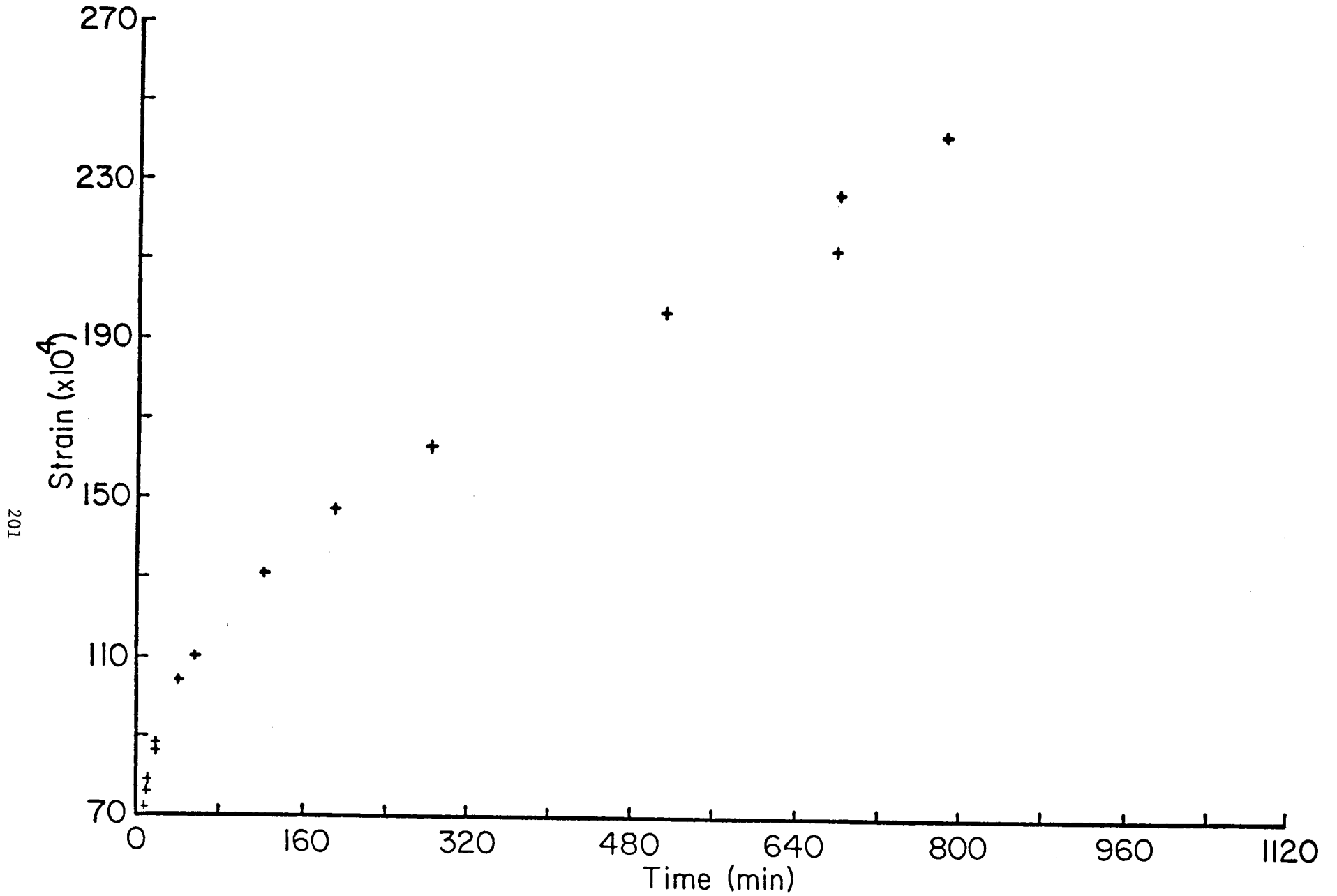


Figure 1. Typical jump point in a strain-time curve, from Peyton's (1966) experiment 37; 8" vertical sample at -18.7°C , and loaded at 16.9 kg/cm^2 .

of the test for creep tests in which neither rupture nor jumps occurred. The total strain of the sample at the minimum strain rate or at the end of a creep test was also recorded. Finally, the time to rupture of the stress rupture tests was taken as the time asymptote of the strain-time curve. Note that this was estimated in most cases because the samples were unloaded prior to total collapse. However, errors in these estimates probably do not exceed a few percent but, of course, cannot be accurately measured.

A plot of time to rupture vs. stress is given in Figure 2 for all of the vertical samples. Tests in which jump points occur are also indicated, as are the durations of the creep tests. Stress vs. time to minimum strain rate for the same tests is plotted in Figure 3. In both cases, the points fall into reasonably well-defined linear zones (compare with Kingery and French, 1963). Note that there is no clear separation with respect to temperature, but this may reflect the relatively small number of samples. Of particular interest, however, are the positions of the jump points. Clearly, these are not random occurrences, but instead, fall within the main trends of the plots. From the available data, the association with the minimum creep rate seems to be preferred, but in either case, it is clear that the jump points are associated with the failure process. This is discussed further below.

Finally, the value of the minimum strain rate for all the vertical specimens is plotted against stress in Figure 4. Note again that the minimum strain rates for those tests which include jump points fall within the trend. The scatter in this plot is somewhat greater than that of Figures 2 and 3, but this may be partially due to the fact that

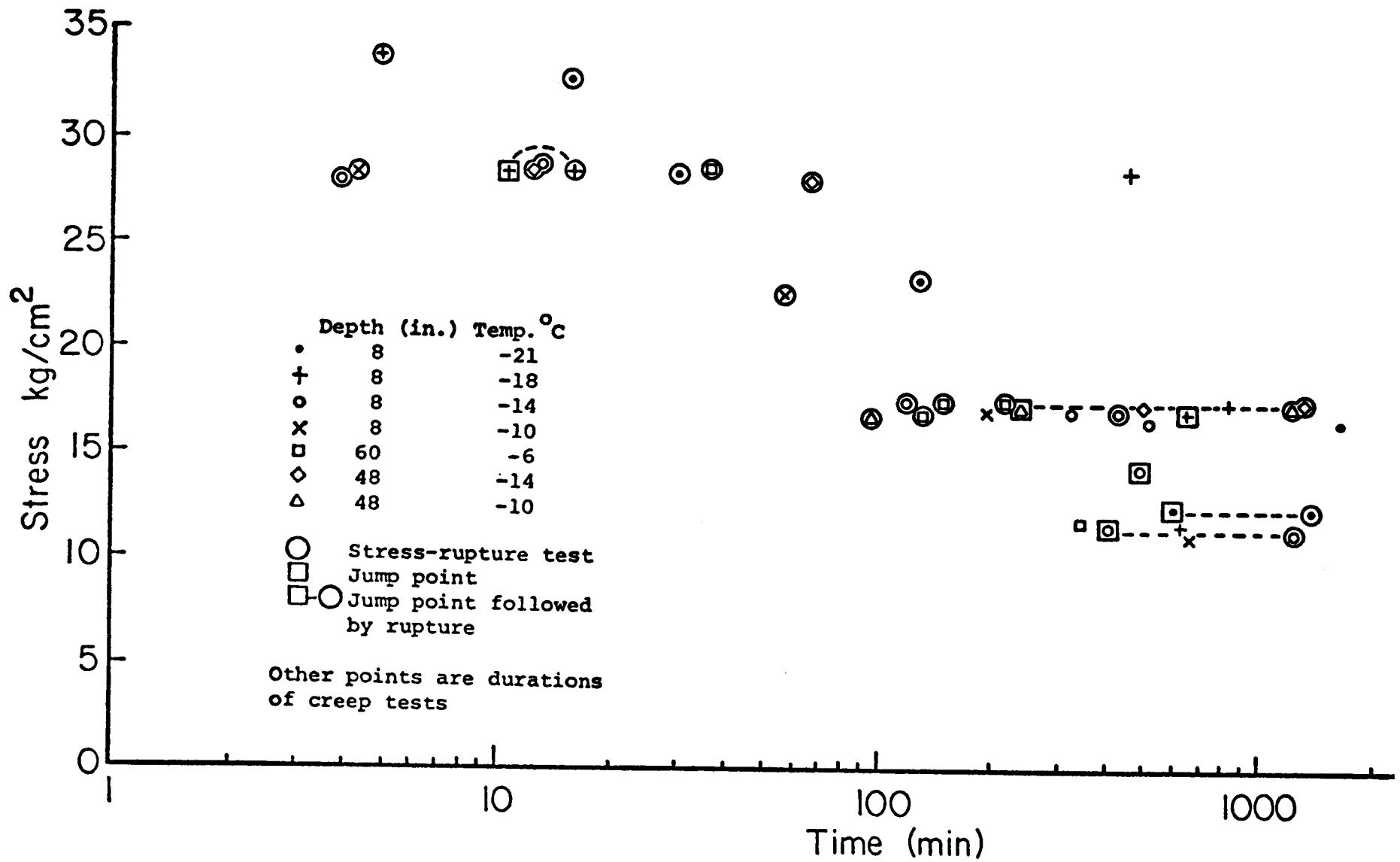


Figure 2. Stress vs. time to rupture for vertical samples.

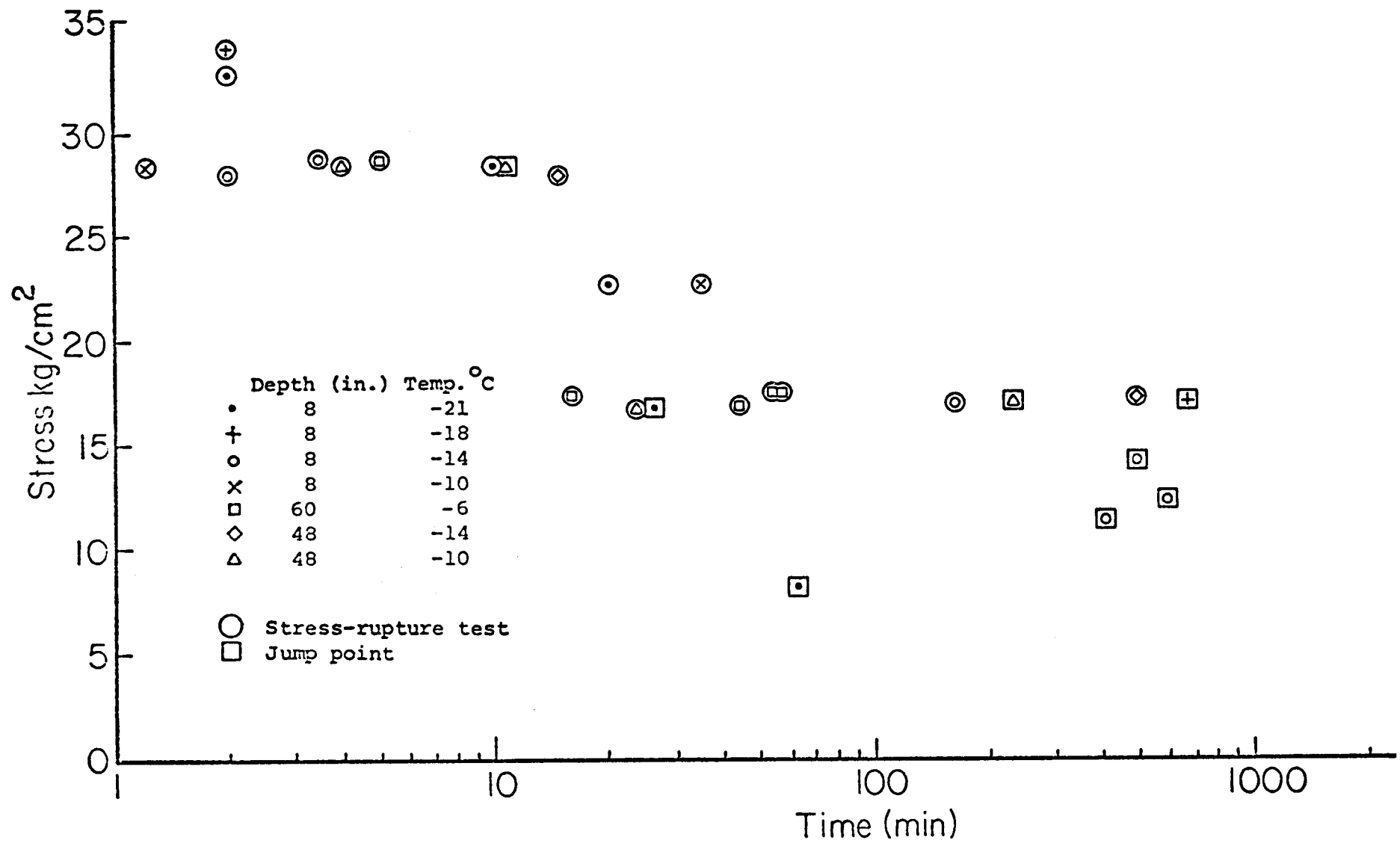


Figure 3. Stress vs. time to minimum strain rate for vertical samples.

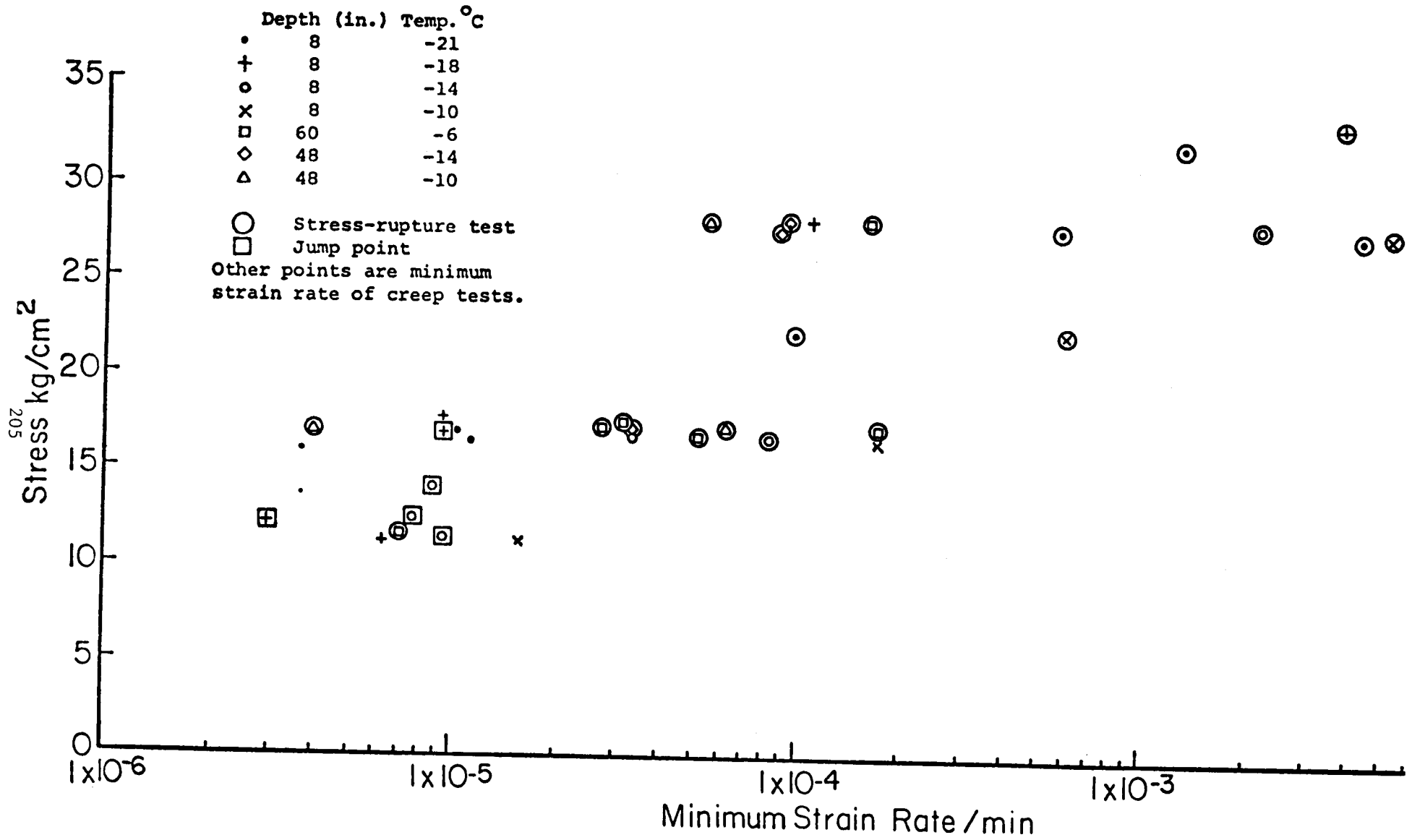


Figure 4. Stress vs. minimum strain rate for vertical samples.

the spacing between data points of the creep curves was often too great for the minimum strain rate to be measured with accuracy. Thus, errors must be present in some of the plotted values.

Figures 5 and 6 show the same plots for horizontal samples (loading in the plane of the ice sheet). These show a wider scatter with poorer definition of the trends. However, two sets of samples within this group are of particular interest: those from 60" depth at various orientations to the c-axis, and a set from 17" depth with randomly oriented c-axes.

The data from the 60" depth samples clearly shows the effect of orientation on the time to rupture. The samples loaded at 45° to the c-axes are obviously weakest, while the results from those loaded at 0° and 90° tend to overlap. Note that one of the tests at 0° orientation was run to rupture at about 2800 minutes at a load of 2 kg/cm², although a jump point appeared at about 160 minutes.

The results from the 17" horizontal samples represent the largest single group of tests under the same conditions of temperature and orientation, and clearly show the association between stress and time to rupture and minimum strain-rate.

DISCUSSION OF THE DATA

It is of interest to compare the plots of stress vs. time to rupture and time to minimum strain rate for the vertical samples (Figures 2 and 3). In the semi-log plots used, the zones defined by these appear to be sub-parallel, so that the time span between the occurrence of the minimum creep rate and of rupture may be some regular multiple of the time to minimum creep rate. It is obvious that there is insufficient

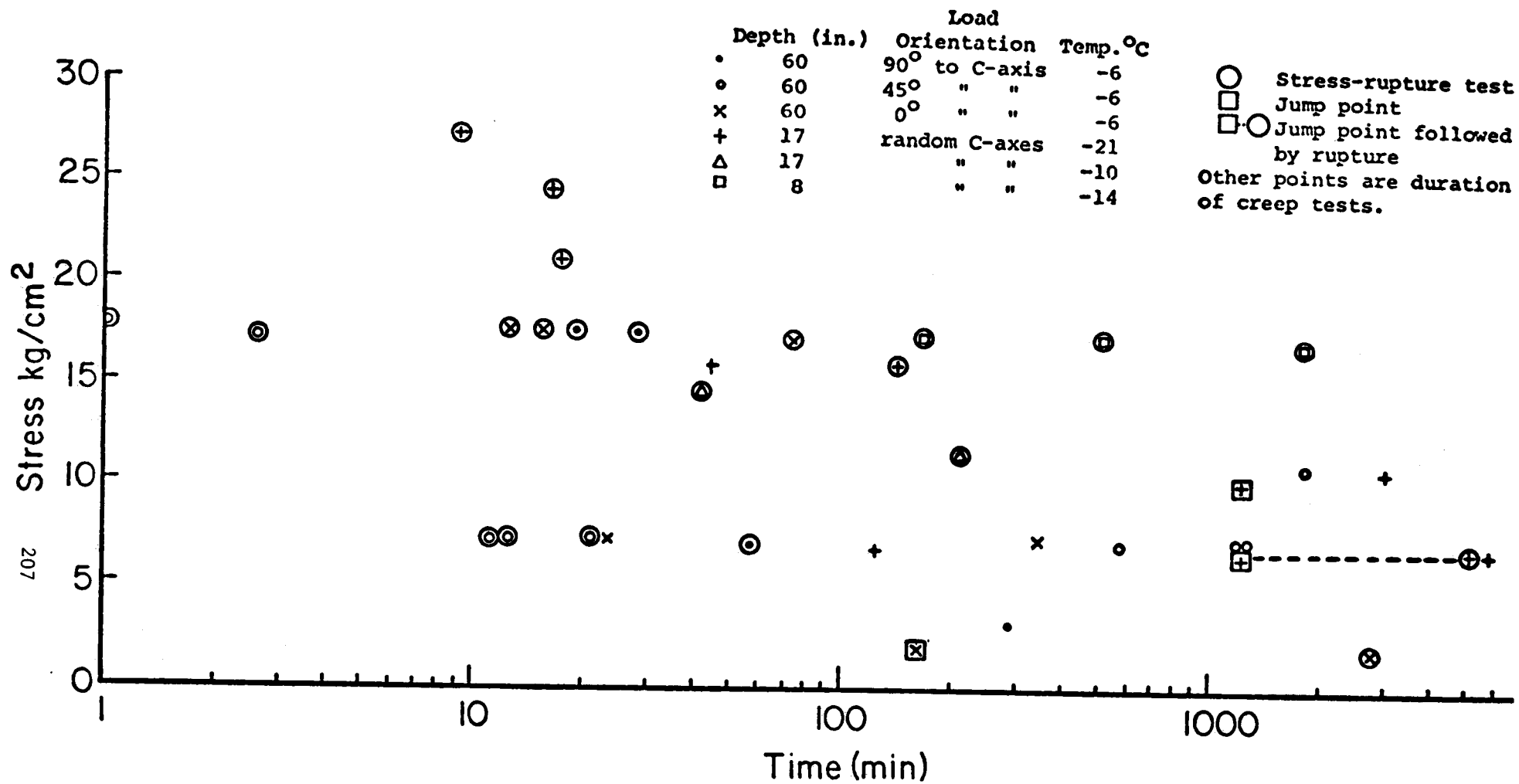


Figure 5. Stress vs. time to rupture-horizontal samples.

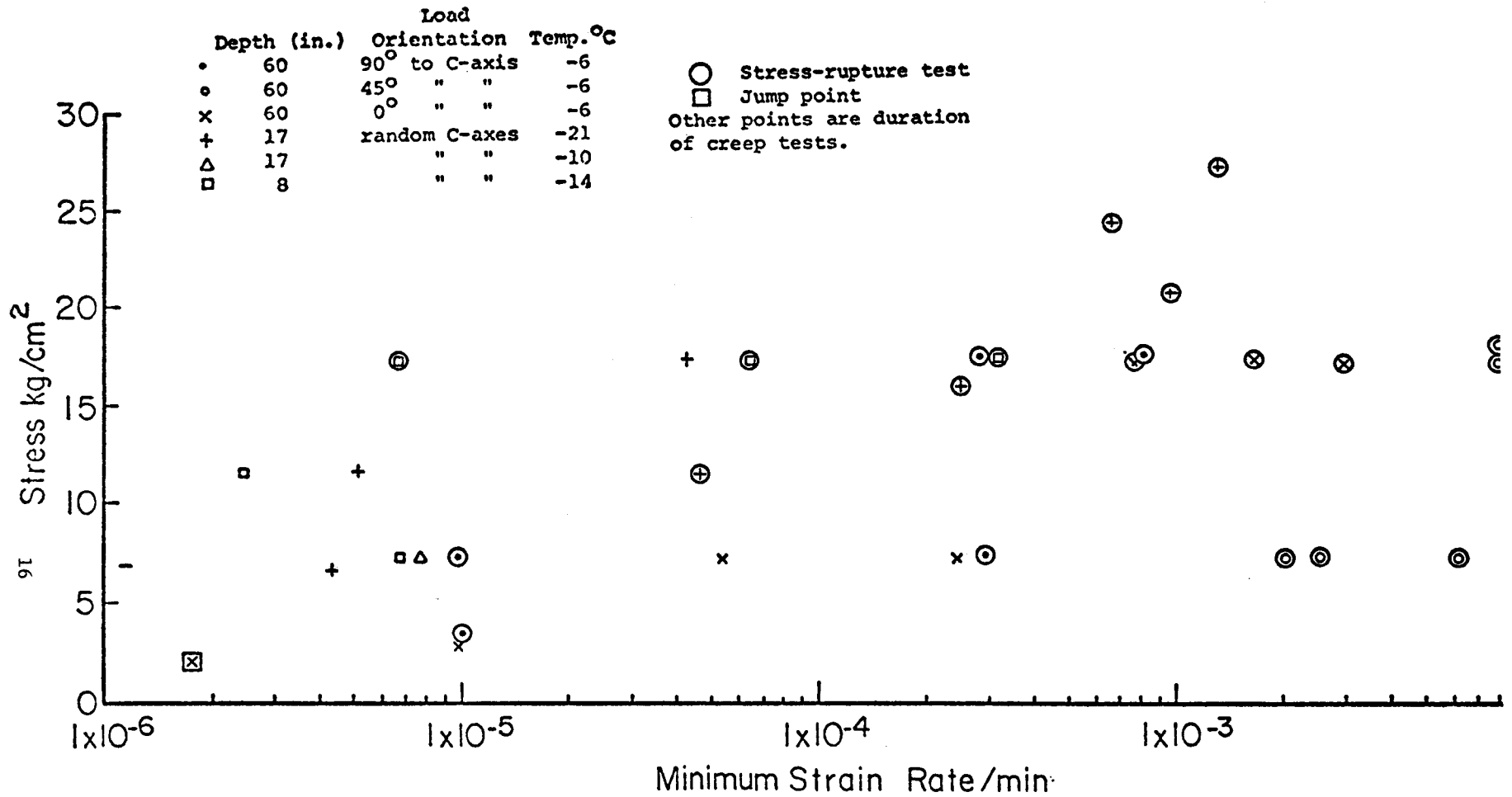


Figure 6. Stress vs. minimum strain rate for horizontal samples.

data to do more than suggest this as a possibility but, if verified (particularly for tension tests), this may have application in considering safety factors for offshore installations or for loads on floating ice sheets.

The relative lack of scatter in the vertical samples of Figures 2, 3 and 4 is somewhat surprising in view of the range of temperatures and ice types represented. It is possible that the number of tests is simply not large enough to represent the full range of typical values so that the lack of scatter is fortuitous. However, it should be noted that in all the tests shown, the loading direction was parallel to the basal planes and normal to the c-axis orientation. Thus, the relationship between the load direction and the directional properties of the sample were similar for all tests.

The apparent relationship between the stress and the minimum strain-rate and the stress and time to minimum strain-rate in the vertical samples suggests the possibility of some correspondence between the stress and the strain at minimum strain-rate. A plot of these is shown in Figure 7a, and a similar plot for the horizontal samples is shown in Figure 7b. In both data sets there is an apparent tendency to cluster, with a trend to increasing strain with increasing load. The data from Figures 7a and 7b are replotted in Figure 8 for purposes of comparison. These show a distinct overlap between the points for both data sets which is unexpected in view of the range of ice types, temperatures, loads and sample orientations represented. This is a potentially important result if it is accepted that the inflection point or first jump point in a strain-time curve represents the initiation of processes

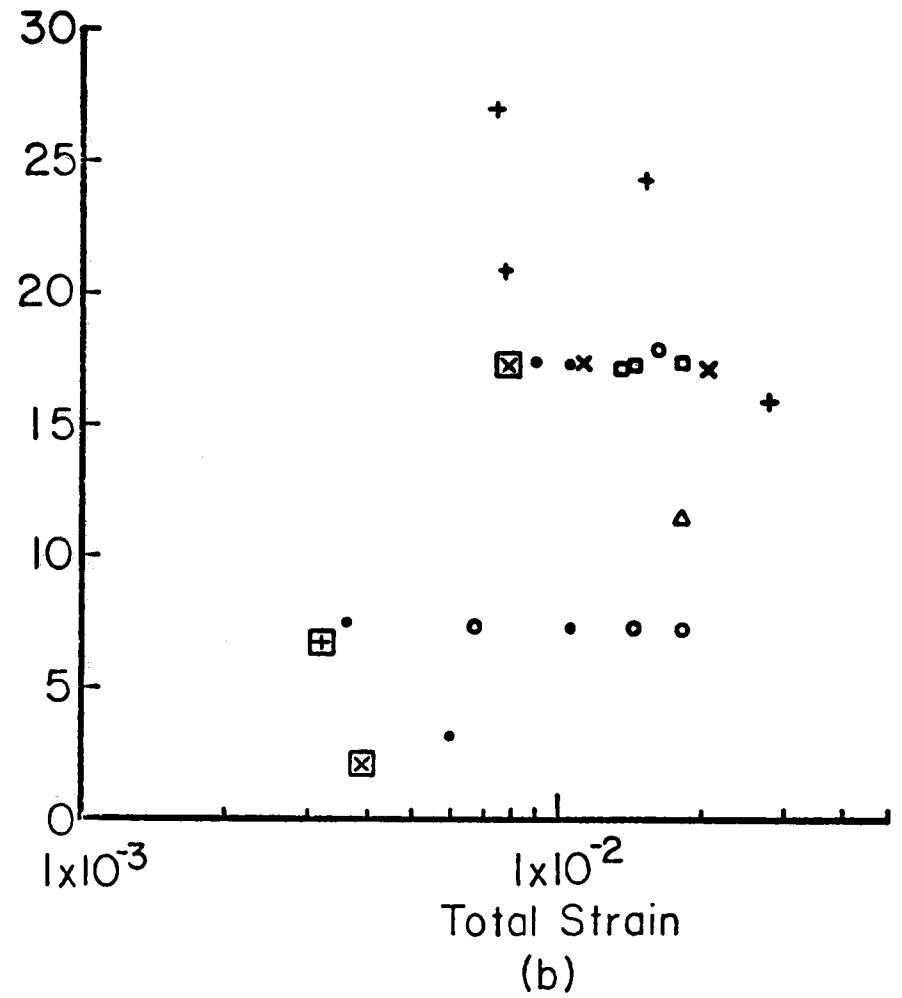
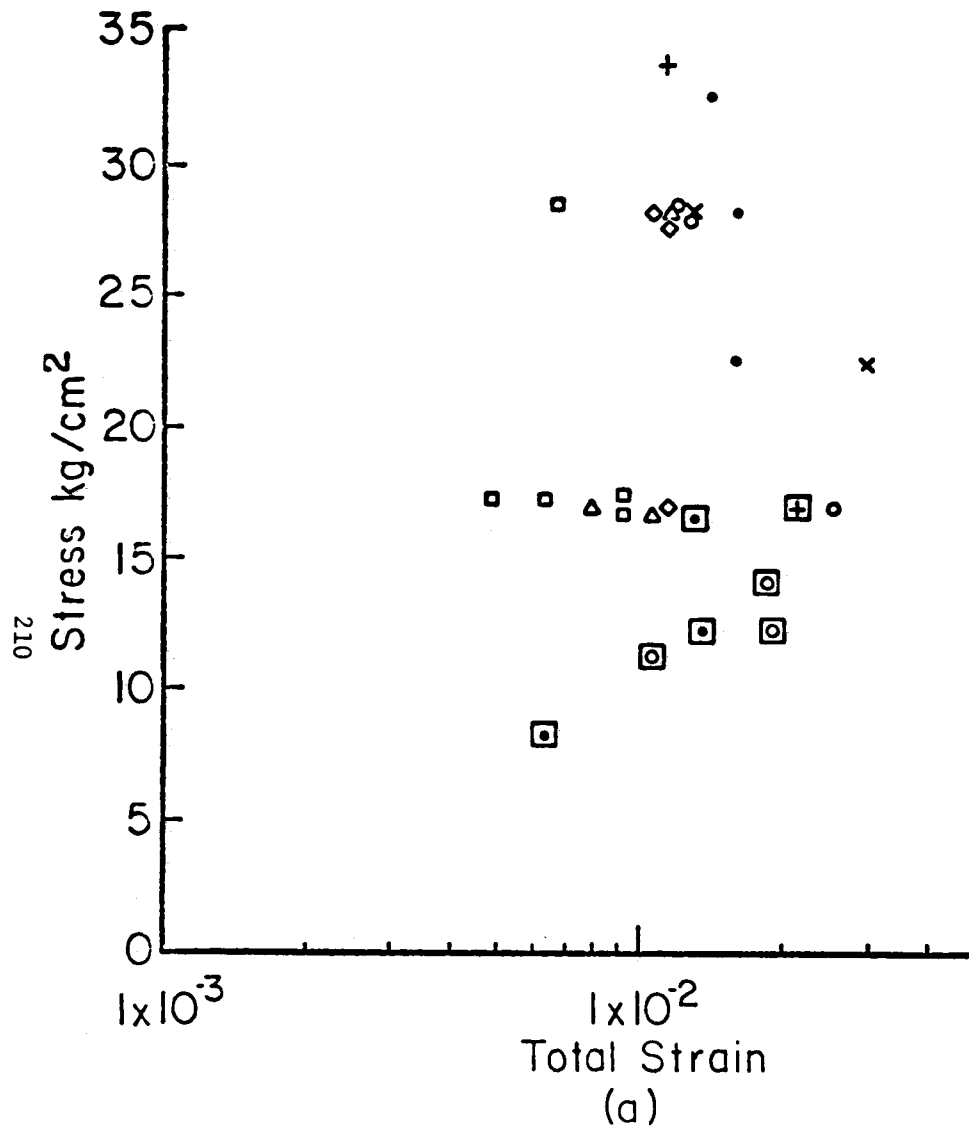


Figure 7a,b. Stress vs. total strain at minimum strain rate. (a) vertical samples; (b) horizontal samples. Points outlined by squares are jump points; the remainder are from stress-rupture tests. Symbols are the same as in previous figures.

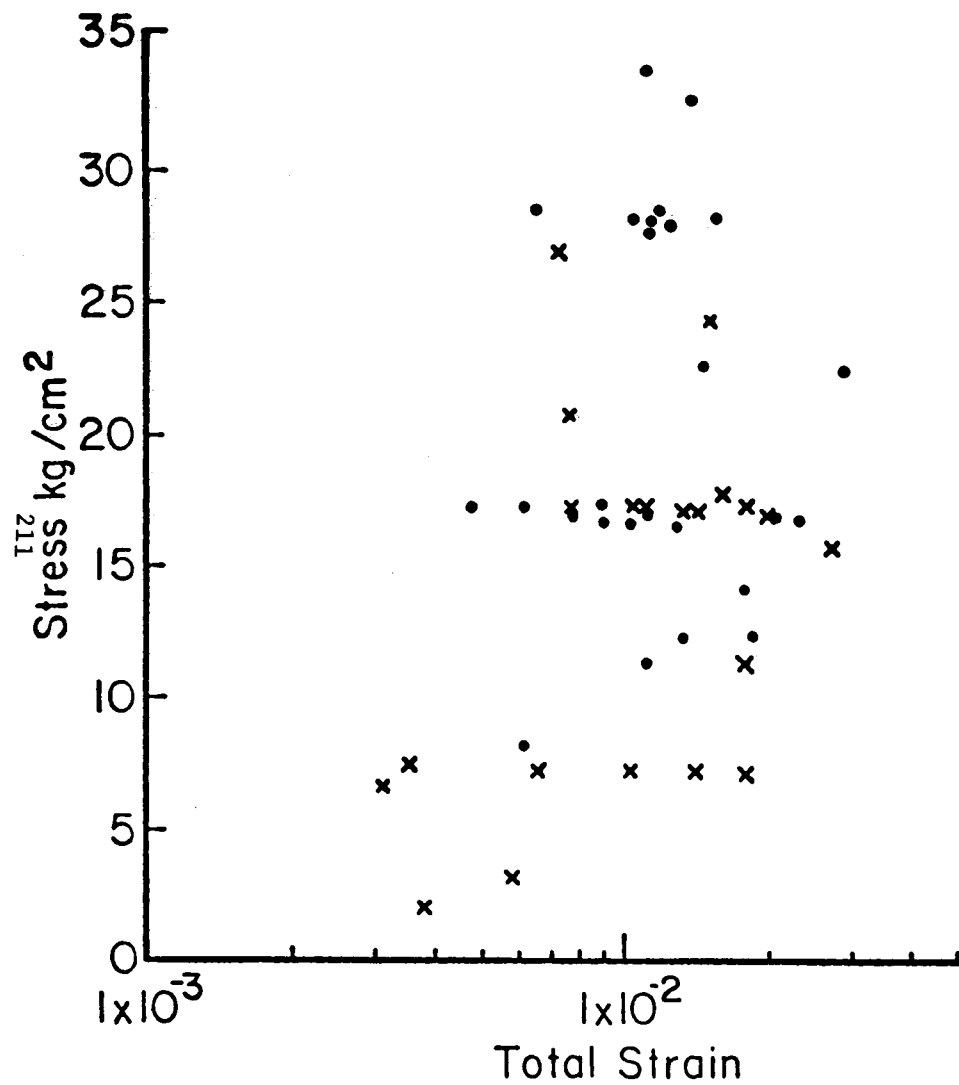


Figure 8. Stress vs. total strain at minimum strain rate for both horizontal (x) and vertical (•) samples.

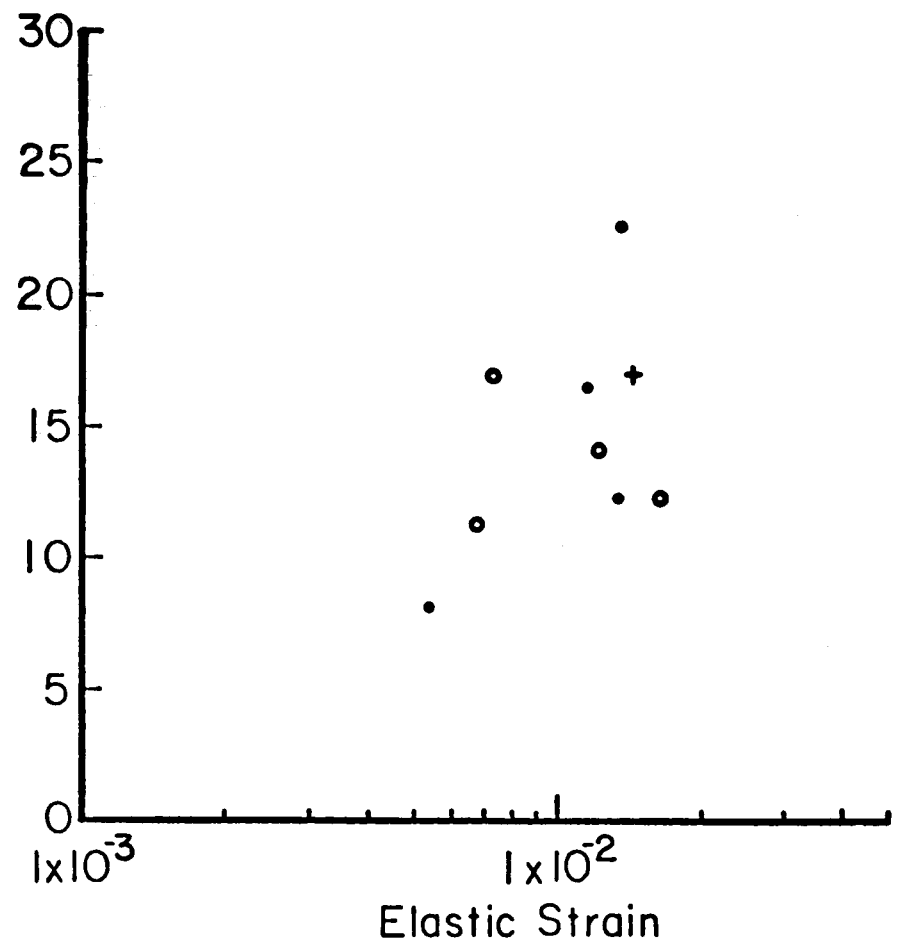


Figure 9. Stress vs. elastic strain at minimum strain rate for 8" vertical samples. Symbols as in previous figures.

leading to failure. The data in Figure 8 implies that the position of these points in the curve is primarily strain dependent and relatively independent of temperature and orientation with respect to load.

In fact, this cannot be strictly true, because sea ice is a visco-elastic material, so that some of the strain represents a dissipation of energy by flow. Thus, failure cannot depend upon the total strain, but instead, must depend upon the elastic component of the strain through which energy can be stored. Accordingly, using methods indicated in the next section, it has been possible to separate the viscous from the elastic strain for a few of the vertical samples. A plot of the results is shown in Figure 9, although there are too few points to indicate any decrease in scatter of the data. In addition, errors in the positions of these points could be as great as $3-4 \times 10^{-3}$ in the strain. These result from inaccuracies in the value of the initial elastic strain, which would tend to increase the calculated elastic strain, and from errors in measurement of the viscous strain which must, of necessity, be too great. This is discussed more fully below.

It should also be emphasized that elastic strain in a single direction in itself cannot provide a failure criteria. Instead, a full 3-dimensional description of the elastic strain is required, through which the strain energy density can be calculated. An approach to the problem is given in Reiner (1960).

Finally, further discussion of the significance of the jump points to the failure process is indicated. Figure 10 shows the stress-rupture curve of a horizontal sample from 60" depth, loaded parallel to the c-axis at -6°C . The dashed lines between the data points have been added

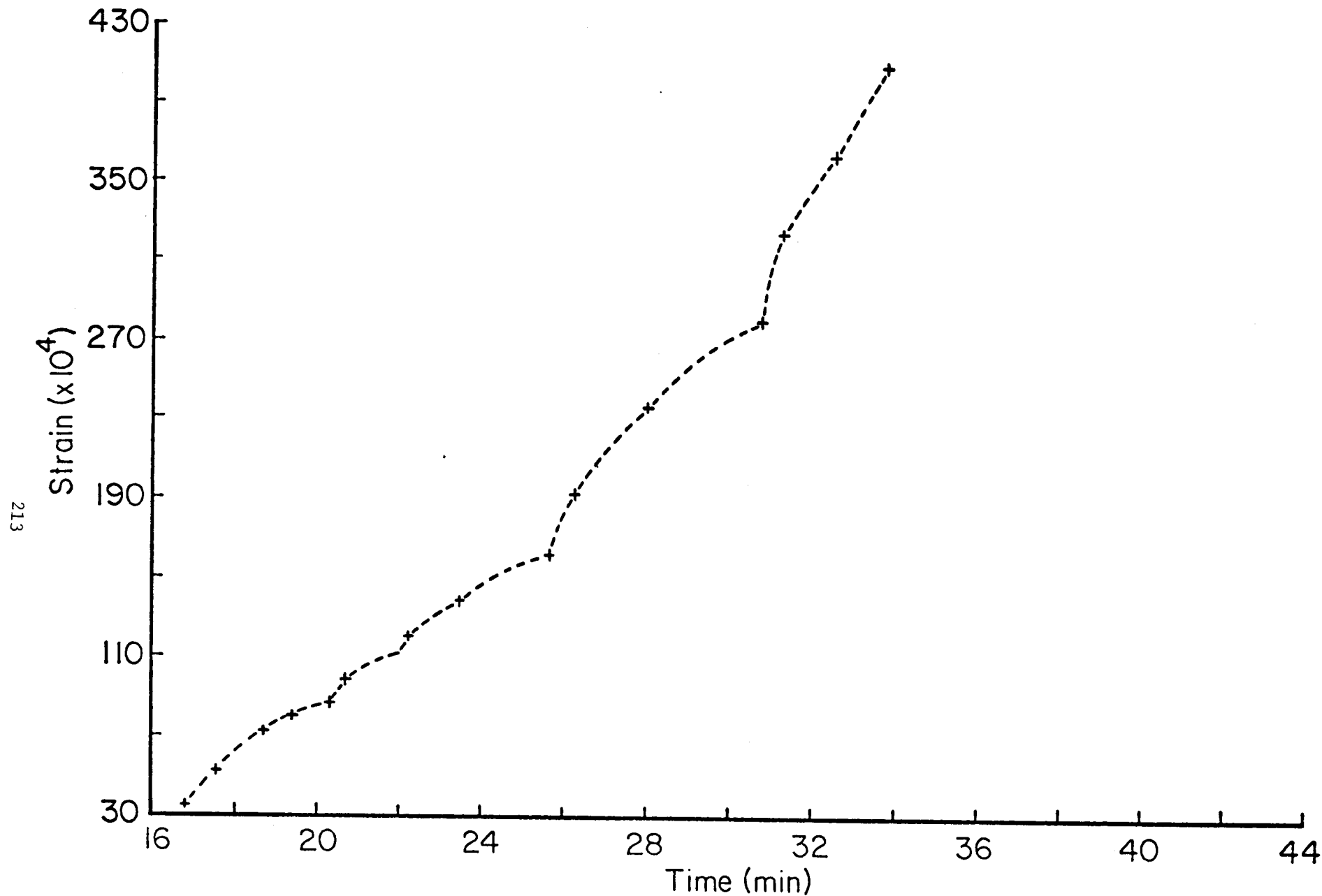


Figure 10. Stress-rupture curve points from Peyton's (1966) experiment 91; 60" horizontal sample at -6°C , loaded parallel to c-axes at 17.4 kg/cm^2 . Dashed line indicates possible interpretation of tertiary creep as a series of jump points.

to show a possible interpretation of the tertiary segment of the curve as a series of jumps. This suggests that tertiary creep may in some instances be considered to be a series of closely spaced jump points which, even if not true, may provide a means of modelling this part of the curve.

Considering Figure 1 to represent a typical jump point, it is apparent that it shows an initial elastic reaction followed by flow. As noted above, this part of the creep curve appears to be similar to those which result from two-stage creep tests so that, in effect, the stress on the sample appears to have been suddenly increased at that point. This is what would be expected if failure had occurred within some volume of the sample at the indicated time, so that the load carrying capacity of some fraction of the cross-sectional area of the sample was effectively reduced. The stress across the remainder of the cross-section of the sample then increases, thus leading to failure. This is essentially the process described in Maser (1972).

VISCOELASTIC STRESS-STRAIN LAWS FOR SEA ICE

The initial approach to analysis of the data from Peyton was based upon the work of Tabata (1958) who fitted the results of a series of creep tests on sea ice to a 4-parameter, one-dimensional model of a linear viscoelastic solid (Figure 11), and obtained values of the relevant constants. This is the simplest viscoelastic model which includes all the elements of a creep-recovery curve (except for tertiary creep leading to failure) and is thus a useful starting point.

The differential equation which describes the behavior of the model is

$$(1) \quad \dot{\epsilon} + \tau_2 \ddot{\epsilon} = \frac{1}{\eta_1} \dot{\sigma} + \left(\frac{1}{k_1} + \frac{\tau_2}{\eta_1} + \frac{1}{k_2} \right) \ddot{\sigma} + \frac{\tau_2}{k_1} \dddot{\sigma}$$

where σ and ϵ are stress and strain, the dot indicates differentiation with respect to time, $\tau_2 = \eta_2/k_2$, and η_1, η_2, k_1, k_2 refer to the constants of the model in Figure 11. The derivation of equation (1) can be found in standard textbooks of linear viscoelasticity (i.e., Bland, 1960). For creep tests, the load is given by

$$(2) \quad \sigma(t) = \sigma^* u(t)$$

where σ^* is a constant, and $u(t)$ is the unit step function. Substituting (2) into (1) and integrating gives the equation for strain as a function of time as

$$(3) \quad \epsilon(t) = \left(\frac{1}{k_1} + \frac{1}{k_2} + \frac{t}{\eta_1} - \frac{1}{k_2} e^{-t/\tau_2} \right) \sigma^*$$

The elements of the creep curve can readily be deduced from equation (3) and the model. Note that equation (1) can also be integrated for constant load rate or constant strain rate.

Attempts to fit equation (3) to Peyton's creep curves gave unsatisfactory results.

In order to obtain a better fit to the creep curves the dashpots in the model were assumed to obey a non-linear stress-strain law which was taken in the form of a hyperbolic sine relationship between the stress and strain rate. (Note that Krausz and Eyring (1975) describe the application of models of this type in studies of the deformation of textiles and polymers.) Then, letting $\epsilon_v(t)$ represent the strain in the Voigt model, the strain-rate is given by

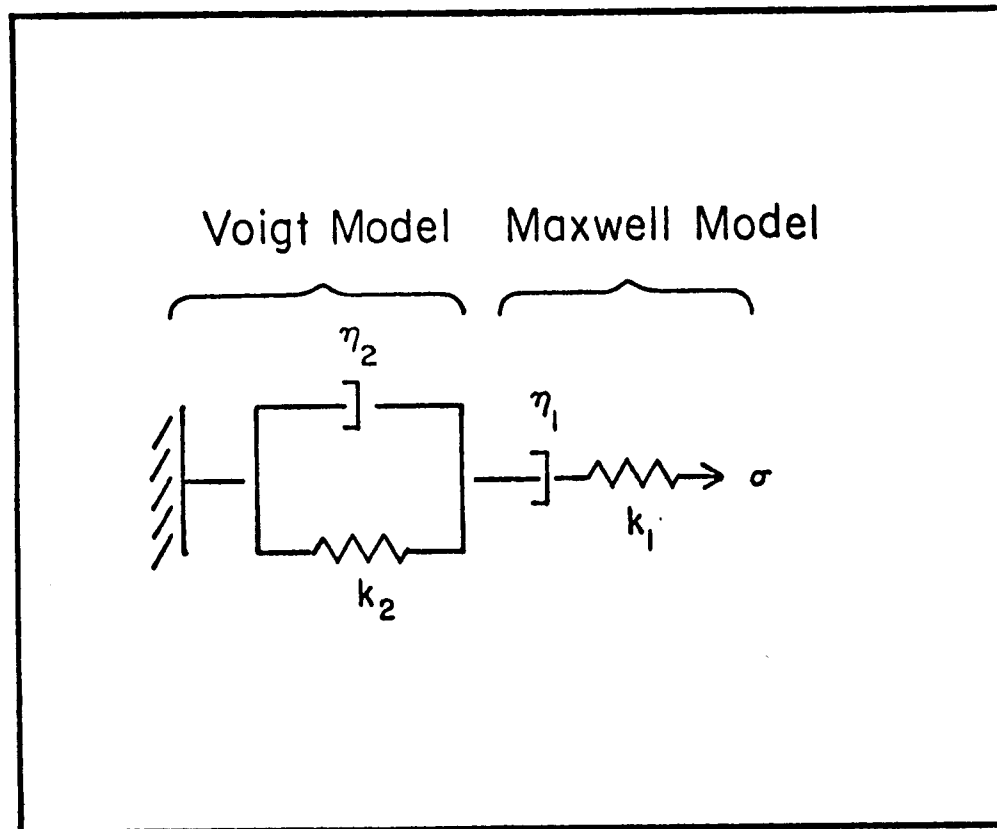


Figure 11. Spring-dashpot model of a 4-parameter linear-viscoelastic solid.

$$(4) \quad \dot{\epsilon}_V(t) = A \sinh \phi \sigma_1(t)$$

In which $\sigma_1(t)$ is the stress on the dashpot of the Voigt model and A and ϕ are constants. The strain on the element is simply

$$(5) \quad \epsilon_V(t) = \frac{\sigma_2(t)}{k_2}$$

where $\sigma_2(t)$ is the stress on the spring of the Voigt model. Then, equilibrium requires that, for a load $\sigma(t)$ applied to the total 4-parameter model,

$$(6) \quad \sigma(t) = \sigma_1(t) + \sigma_2(t)$$

Introducing (6) and (5) into (4) then gives

$$(7) \quad \dot{\epsilon}_V(t) = A \sinh \phi [\sigma(t) - k_2 \epsilon_V]$$

For a constant load ($\sigma(t) = \sigma^*$) equation (7) can be integrated and rearranged to give

$$(8) \quad \epsilon_V(t) = \frac{\sigma^*}{k_2} - \frac{2}{\phi k_2} \tanh^{-1} \left(e^{-A\phi k_2 t} \tanh \frac{\phi \sigma^*}{2} \right)$$

the creep curve of the Voigt model alone.

To extend the law to the total 4-parameter model, note that the strain in the spring of the Maxwell model is

$$(9) \quad \epsilon_1(t) = \frac{\sigma(t)}{k_1}$$

while the strain rate of the dashpot of the Maxwell model is assumed to be

$$(10) \quad \dot{\epsilon}_2(t) = B \sinh \theta \sigma(t)$$

where B and θ are constants.

The strain of the total 4-parameter model is simply the sum of the strains in the elements of the model arranged in series, which is

$$(11) \quad \epsilon_T(t) = \epsilon_V(t) + \epsilon_1(t) + \epsilon_2(t)$$

Then for $\sigma(t) = \sigma^*$, substituting (8), (9) and (10) into equation (11), and noting that $\dot{\epsilon}_2(t) = \dot{\epsilon}_2^* = \text{constant}$ when $\sigma(t) = \sigma^*$, gives

$$(12) \quad \epsilon_T(t) = \frac{\sigma^*}{k_1} + \dot{\epsilon}_2^* t + \frac{\sigma^*}{k_2} - \frac{2}{\phi k_2} \tanh^{-1} \left(e^{-A\phi k_2 t} \tanh \frac{\phi \sigma^*}{2} \right)$$

the creep curve of the total model.

In principal, the constants in equation (12) can be determined by fitting the equation to an experimentally determined creep curve. This is presently being done using Marquardt's (1963) maximum neighborhood method. To date, satisfactory fits to the data have been obtained for about 25 creep curves, but more are required before any results can be discussed. It is noteworthy, however, that creep curves calculated using the parameters determined by the fit seldom show errors of greater than 2% when compared with the original data points.

In fitting the curve, the modulus k_1 is not treated as a free parameter, but instead is calculated from the strain at the first data point of the creep curve if that point was measured within one minute of the application of the load. This is clearly in error, because the strain from the Voigt model and the dashpot of the Maxwell model are included in this value, although their combined contribution should be no greater than two orders of magnitude less than the strain in the spring of the Maxwell element. Note that a more significant error is indicated by comparison of the initial strain with the strain recovered

within the first minute after the specimen is unloaded. Unfortunately, there are few recovery curves in the data for non-rupture tests with no jump points, upon which to base a comparison. Those which are available, however, indicate that the initial strain is greater than the recovered strain by as much as 50% (i.e., magnitude of 1 to 4×10^{-3}). This affects the computation of the elastic strain in the total model as a function of time, so that the data points of Figure 9 would be translated to lower values. However, the error does not enter into the curve fitting process, and therefore does not affect the computed values of the remaining parameters.

In some of Peyton's tests, stress-strain data were taken during loading and, when available, these were plotted to determine k_1 . However, the errors in total strain are still present in the creep curves for these tests.

The source of this error is probably at least partially experimental, resulting from taking up "slack" in the loading system and the specimen. However, the possibility that some of the difference is due to strain dependent changes in the mechanical properties of the sample cannot be ignored based upon the available data.

From equation (12) and the model (Figure 11), it is apparent that the only viscous component of the strain at any time is that associated with the dashpot of the Maxwell model, represented by the second term on the right side of the equation. This quantity can be estimated for those experimental creep curves which appear to have nearly reached the steady-state creep phase by measuring the minimum strain-rate and multiplying by the time. Subtraction of this value at any time from the curve gives

the value of the elastic strain (including the errors above) at that time. The values of the elastic strain shown in Figure 9 were determined in this way. Note that the value of the strain-rate measured must be too large, so that the error introduced tends to compensate that in the estimate of the initial strain.

CONSTANT LOAD-RATE TESTS

The stress-strain law for the 4-parameter model with non-linear dashpots can also be derived for the case in which the specimen is loaded at a constant load rate. Fitting this model to experimental data would then, in principal, permit all of the parameters of equations (10) to be evaluated.

The derivation follows that for the constant load problem. Equation (4) is integrated and substituted into (5) to obtain an expression for $\sigma_2(t)$ in terms of $\sigma_1(t)$. Then, substituting into (6), gives

$$(13) \quad \sigma(t) = \sigma_1(t) + Ak_2 \int \sinh \phi \sigma_1(t) dt$$

For constant load rate tests, the load as a function of time is given by

$$\sigma(t) = \dot{\sigma}^* t$$

where $\dot{\sigma}^*$ is the constant rate of loading. Substituting into (13) and differentiating with respect to time then gives

$$\dot{\sigma}^* = \dot{\sigma}_1(t) + Ak_2 \sinh \phi \sigma_1(t)$$

or

$$(14) \quad \int_0^{\sigma_1} \frac{d\sigma_1'}{C - \sinh \phi \sigma_1'} = Ak_2 \int_0^t dt'$$

where the primes indicate dummy variables and the substitution $C = \dot{\sigma}^*/Ak_2$ has been used. Using the substitution

$$z = C - \sinh \phi \sigma_1'$$

and noting the limits on z as σ_1' gives from zero to σ_1 , (14) becomes

$$(15) \quad -\frac{1}{\phi} \int_{\beta}^{\beta - \sinh \phi \sigma_1} \frac{dz}{z(z^2 - 2Cz + C^2 + 1)^{1/2}} = Ak_2 t$$

In the quadratic term of the denominator $b^2 - 4ac = -4$, ($4ac > b^2$), so that (15) integrates to (Dwight, 1947, #380.111)

$$\frac{1}{\phi C^{1/2}} \sinh^{-1} \frac{bz+2c}{z(4ac-b^2)^{1/2}} \Big|_{\beta}^{\beta - \sinh \phi \sigma_1} = Ak_2 t$$

and

$$\frac{1}{\phi(1+C^2)^{1/2}} \left[\sinh^{-1} \left(\frac{1 + C \sinh \phi \sigma_1}{C - \sinh \phi \sigma_1} \right) - \sinh^{-1} \frac{1}{C} \right] = Ak_2 t$$

Then, introducing the substitutions

$$D = \phi(1 + C^2)^{1/2} k_2 A$$

$$E = \sinh^{-1} \frac{1}{C}$$

and solving for $\sigma_1(t)$ gives

$$(16) \quad \sigma_1(t) = \frac{1}{\phi} \sinh^{-1} \left[\frac{C \sinh (Dt + E) - 1}{C + \sinh (Dt + E)} \right]$$

The stress-strain law for the Voigt model can then be found from equations (5), (6) and (16), since

$$\epsilon_V(t) = \frac{\sigma_2(t)}{k_2} = \frac{\sigma(t) - \sigma_1(t)}{k_2}$$

so that [recalling that $\sigma(t) = \dot{\sigma}^* t$]

$$(17) \quad \epsilon_V = \frac{\sigma}{k_2} - \frac{1}{\phi k_2} \sinh^{-1} \left[\frac{C \sinh(D \frac{\sigma}{\sigma^*} + E) - 1}{C + \sinh(D \frac{\sigma}{\sigma^*} + E)} \right]$$

To extend the results to the 4-parameter model, note that from (9), the spring of the Maxwell model strains as

$$(18) \quad \epsilon_1(t) = \frac{\sigma^* t}{k_1}$$

while the strain-rate of the dashpot is (from 10)

$$\dot{\epsilon}_2(t) = B \sinh \theta \sigma^* t$$

The dashpot strain is therefore

$$(19) \quad \epsilon_2(t) = \frac{C}{\theta \dot{\sigma}^*} \cosh \theta \dot{\sigma}^* t$$

Then, substituting (17), (18) and (19) into (11) gives the stress-strain curve for the total model,

$$(20) \quad \epsilon_T(t) = \frac{\sigma(t)}{k_1} + \frac{C}{\theta \dot{\sigma}^*} \cosh \theta \sigma(t) + \frac{\sigma(t)}{k_2} - \frac{1}{k_2 \phi} \sinh^{-1} \left[\frac{C \sinh(D \frac{\sigma}{\sigma^*} + E) - 1}{C + \sinh(D \frac{\sigma}{\sigma^*} + E)} \right]$$

where, as above, the strain in the spring of the Maxwell model is given by the first term, while the second term is the strain in the dashpot of the same model.

One additional point should be noted here which provides a further test of the suggestion above that failure is dependent on the elastic strain. The only viscous strain represented in equation (20) is that given by the second term on the right, which describes the strain in the

dashpot of the Maxwell element. The elastic strain of the model is therefore given by the remaining three terms. It is thus possible to calculate the value of $\sigma(t)$, for any value of constant load rate $\dot{\sigma}^*$, at which the elastic strain reaches some specified value corresponding to failure. This has been done with the elastic strain fixed at a value of 6×10^{-3} and load rates ranging up to $500 \text{ kg/cm}^2/\text{min}$. The results are plotted to give the curve of "compressive strength" vs. load rate shown in Figure 12. The values of the parameters are arbitrary. For purposes of comparison, Figure 13 shows plots of experiment curves of strength vs. load rate taken from Peyton (1966). The similarity is apparent, and thus tends to reinforce the hypothesis of the elastic strain dependency of failure, at least over the range of values indicated.

It should be noted that because the model does not include any elements which would lead to a decrease in strength with increasing load rate, that hypothesis is not excluded by the result presented here.

CONSTANT STRAIN RATE TESTS

Finally, for the sake of completeness, the derivation of the stress-strain law for constant-strain rate tests of the non-linear 4-parameter model will be outlined.

Let $\dot{\epsilon}^*$ be the applied constant strain rate. Then, this must equal the sum of the strain rates in the individual elements, so that

$$\dot{\epsilon}^* = \dot{\epsilon}_v(t) + \dot{\epsilon}_1(t) + \dot{\epsilon}_2(t)$$

where $\epsilon_v(t)$, $\epsilon_1(t)$ and $\epsilon_2(t)$ are defined above. Then from (4), the derivative of (9), and (12)

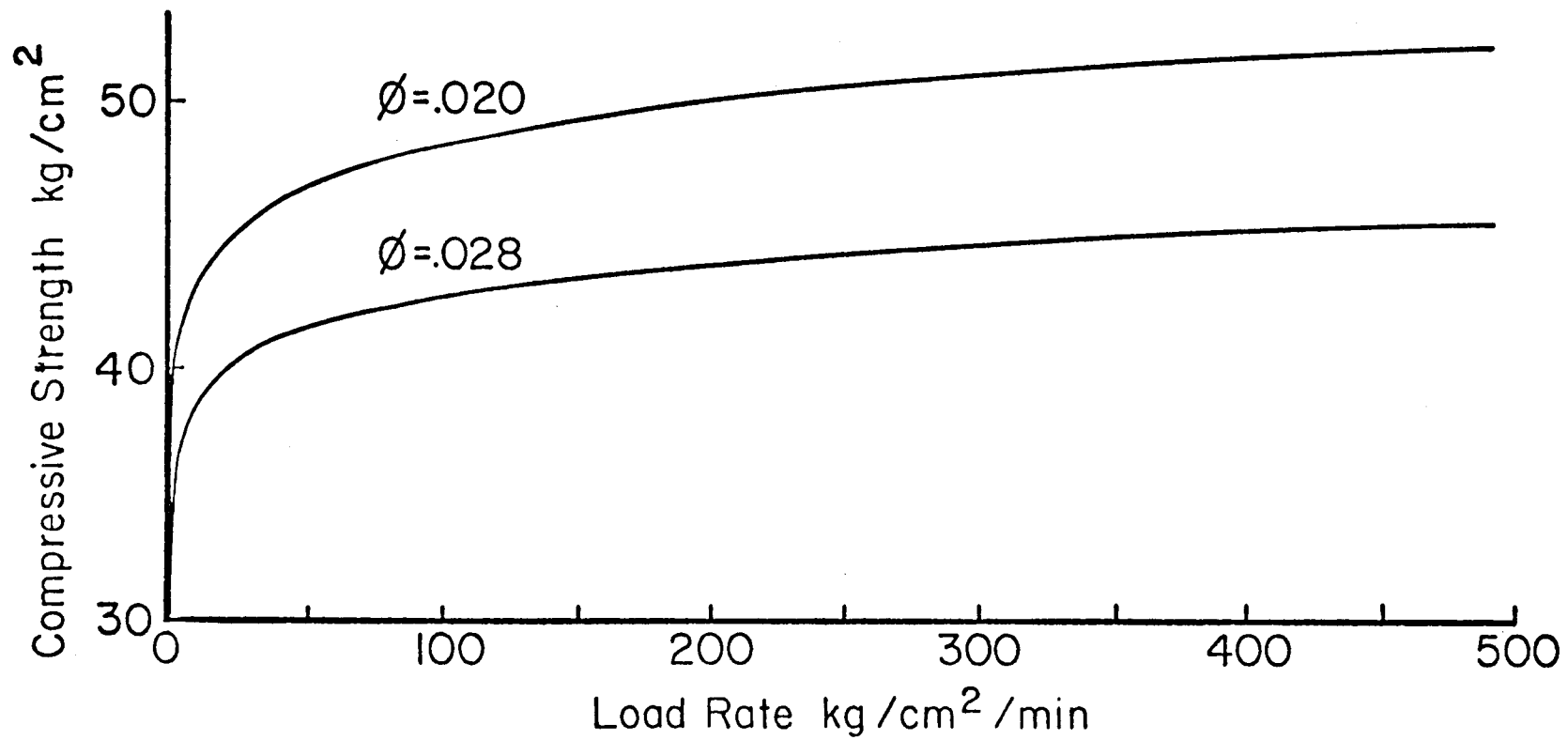


Figure 12. "Compressive strength" as calculated assuming failure occurs when the elastic strain in equation (20) reaches 6×10^{-3} . Values of the constants were $k_1 = 1.4 \times 10^4$ kg/cm², $k_2 = 7.02 \times 10^3$ kg/cm², $A = 5 \times 10^{-6}$ /min. Values of ϕ as indicated.

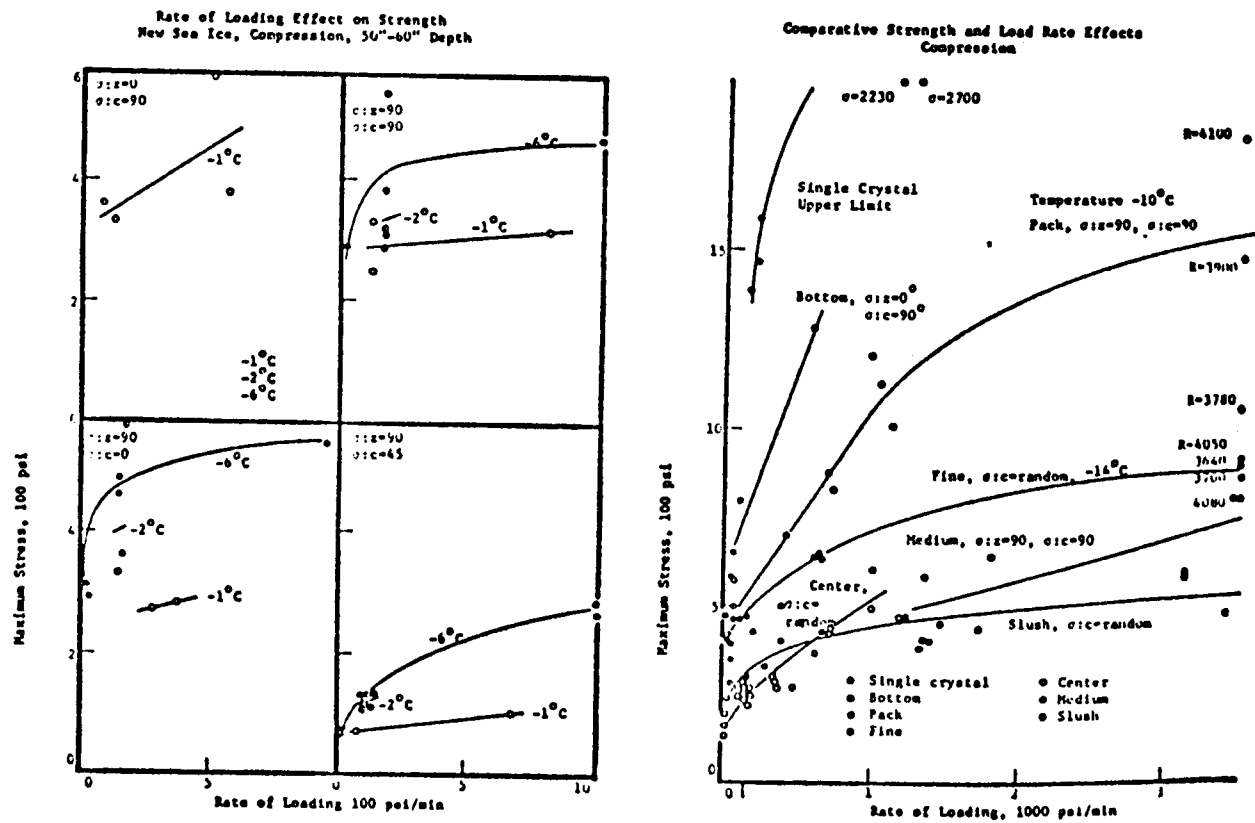


Figure 13. Experimental curves of compressive strength vs. loading rate from Peyton (1966).

$$(21) \quad \dot{\epsilon}^* = A \sinh \phi \sigma_1(t) + \frac{\dot{\sigma}(t)}{k_1} + B \sinh \theta \sigma(t)$$

Similarly, the strain at time t is

$$\dot{\epsilon}^* t = \epsilon_v(t) + \epsilon_1(t) + \epsilon_2(t)$$

or, from (5), (9) and the integral of (10)

$$(22) \quad \dot{\epsilon}^* t = \frac{\sigma_2(t)}{k_2} + \frac{\sigma(t)}{k_1} + B \int \sinh \theta \sigma(t) dt$$

Solving (21) for σ_1 and (22) for σ_2 , and substituting into equation (6) then gives

$$(23) \quad \sigma(t) = \frac{1}{\phi} \sinh^{-1} \frac{\dot{f}}{A} + k_2 f$$

where

$$f = \dot{\epsilon}^* t - \frac{\sigma(t)}{k_1} - B \int \sinh \theta \sigma(t) dt$$

Equation (23) can be differentiated to remove the inverse hyperbolic sine, and then rearranged to

$$\dot{f}^4 - \frac{2}{k_2} \dot{\sigma} \dot{f}^3 + \frac{\dot{\sigma}^2 + k_2^2}{k_2^2} \dot{f}^2 - \frac{2}{k_2} \dot{\sigma} \dot{f} + \frac{\dot{\sigma}^2}{k_2^2} = \frac{1}{\sigma^2 A^2 k_2^2} \ddot{f}^2$$

which is a complicated (algebraically) non-linear ordinary differential equation which should be solvable by numerical methods. However, the possibility of obtaining a closed form solution still has not been excluded.

DISCUSSION

It is important to note that introducing non-linear dashpots into the 4-parameter model removes the results from the firm foundation of

the theory of linear viscoelasticity. It is intuitively reasonable that such models may eventually be associated with the integrals of the stress-strain laws of non-linear viscoelasticity but we know of no examples of this in the literature. A possible approach to this problem is presently being examined. Further, the equations given are one-dimensional, and the form of the analogous 3-dimensional law is not established. This must be done before the anisotropy of the material can be considered. Thus, for the present, the models should be taken only as a means of examining the energy balance in the sample and for what information can be obtained regarding the changes in these quantities during deformation.

C. Direct Shear Test

In the last annual report of this project, a procedure for conducting direct shear tests in a horizontal plane in-situ was described. The method used is shown in Figure 14. At the time the report was written, only three tests had been run but subsequently, fifteen additional tests were conducted to further evaluate the procedure and assess the repeatability of the results. The following discussion gives a summary of these experiments.

The tests consist simply of loading the flatjack with air or hydraulic fluid until failure occurs at the base of the block. The shear strength is then calculated assuming the stress to be uniform across the failure plane. This is clearly not true, but is nevertheless the standard procedure in tests of this type. Thus, if the dimensions of the jack are "a" and "b", and the pressure at failure is "P", then the total force is Pab . This is assumed to be equal to τcd , where " τ " is the shear strength of the ice, and "c" and "d" are the dimensions of the block outlined by the relief slots. In the tests to date, c and d have been set equal to b, so that $\tau = (a/b) P$. Note that one criterion of validity of the test is that the results should agree for different values of the ratio a/b. To date, tests have been run at only two ratio's, 1/2 and 1/3, and the values of τ obtained are in reasonable agreement.

The results of all eighteen tests are shown in Table 1.

Tests in which square flatjacks were used (numbers 1, 3, 4, 5 and 6) gave distinctly lower strength values than the remaining tests. Further, the failure surfaces were smooth and wavy with only minor, scattered asperities, and no cracks penetrating the adjacent ice. Thus, these tests were not satisfactory, and should be interpreted perhaps as bending tests on thick cantilever beams loaded uniformly along their lengths, rather than as shear tests.

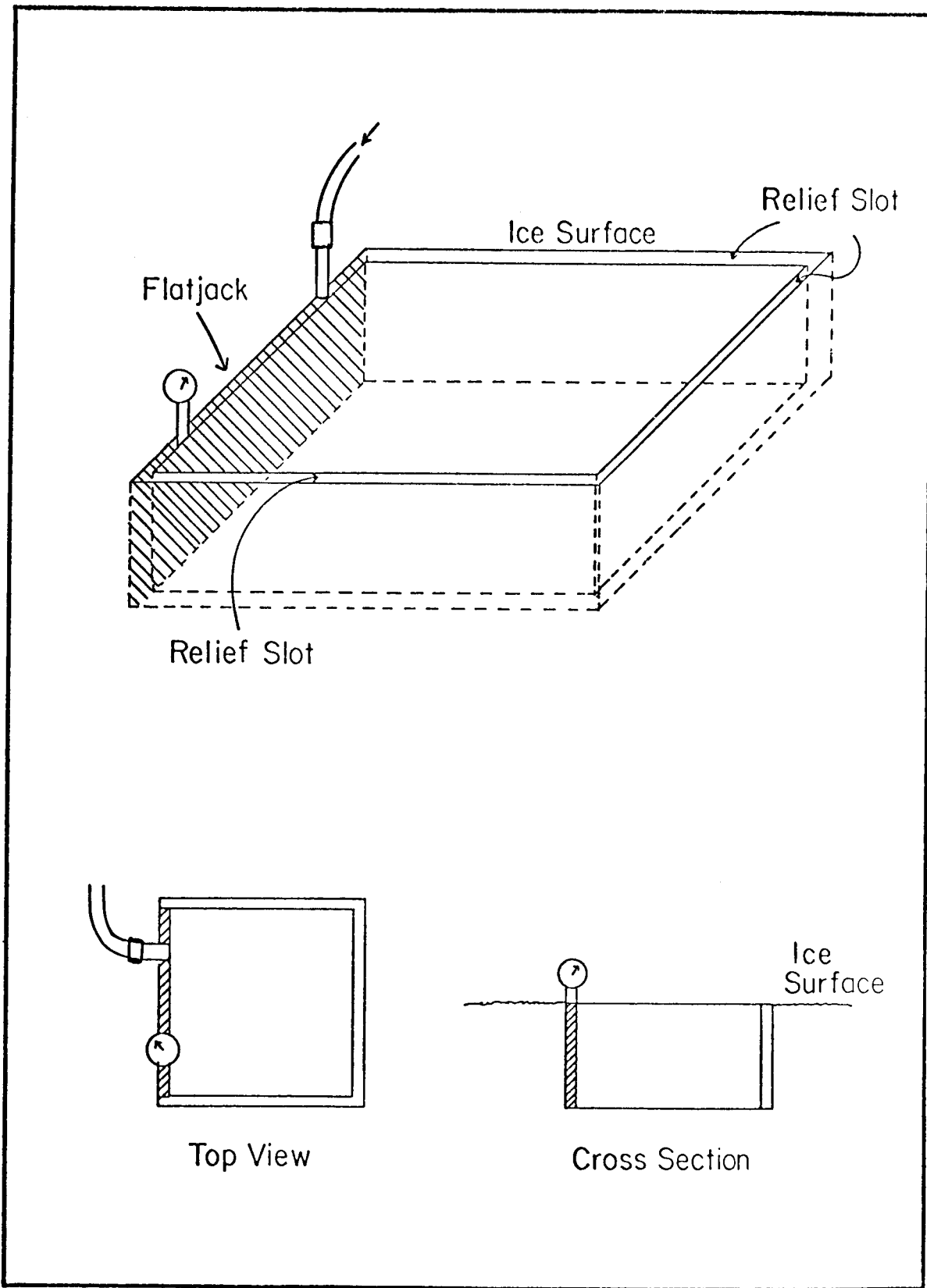


Figure 14. Direct shear test.

TABLE 1
SUMMARY OF DIRECT SHEAR TEST RESULTS

TEST #	FLATJACK DIMENSIONS (CM)	TEMP (°C)	τ (Pa)	Comments
1	15x15		4.48×10^5	Slow loading with hand pump
2	15x45		8.60×10^5	" " " " "
3	61x61		5.27×10^5	" " " " "
4	15x15	-13	4.14×10^5	Load rate approx. 14 kPa/Sec
5	15x15	"	2.76×10^5	" " " " "
6	15x15	"	4.27×10^5	Relief slots improperly cut Load rate approx. 14 kPa/Sec
7	15x30	"	5.65×10^5	" " " " "
8	15x30	"	5.79×10^5	" " " " "
9	15x30	"	6.55×10^5	Pressure held constant for 30 sec. after each 210k Pa load increment
10	15x45	"	5.72×10^5	Load rate approx. 14 kPa/Sec
11	15x45	"	5.72×10^5	" " " " " "
12	15x30	-10	5.17×10^5	" " " " " "
13	15x30	-7	8.27×10^5	" " " " " Extensive shattering at base of block
14	15x30	"	4.76×10^5	Load rate approx. 14 kPa/Sec
15	15x30	"	4.55×10^5	" " " " " "
16	15x45	"	6.07×10^5	" " " " " "
17	30x60	"	5.17×10^5	Pressure held at 20.69 MPa for 1 hr. then increased to 1.03 MPa. Failure occurred in 2 min.
18	60x122		4.07×10^5	Slow loading with hand pump.

With the exception of test #18, in which the broken block was not removed for examination, all of the remaining tests were verified to have failed in shear. This is based upon interpretation of the mode of failure. In all cases, the lower part of the block broke into irregular flat plates up to 1 cm in thickness with the lowest few (i.e., 2-4) centimeters of the block completely fragmented in this manner. An exception was test #13 which failed at a distinctly higher stress than usual. In this case, the shattered zone was about twice the normal thickness, suggesting the release of more strain energy at failure than in the remaining experiments.

The surface of the ice below the broken block typically showed irregular linear, "step" asperities oriented transverse to the direction of motion of the failed block, with the riser of the step facing the loading direction. Flat cracks extended into the ice from the base of each step, as evidenced by a distinct gray color of the ice in these areas. The failure mode represented in these tests is thus similar to that of failure by coalescence of interacting cracks which occurs during shear failure in uniaxial compression tests on both ice and rocks. Therefore, it is reasonable to conclude that the test does indeed produce failure in shear. However, the question posed above regarding the distribution of stress across the failure plane still remains.

In evaluating the repeatability of the tests, it should be noted that tests 7, 8, 10 and 11 were conducted on adjacent sites within about two hours. The test blocks had the same orientation, and salinity determinations from three samples at the base of the blocks gave values of 3.6, 4.1 and 4.2 ppt. The mean value of the shear strength for these tests is 5.72 MPa, with a standard deviation of .06. Tests number 13, 14, 15 and 16 constitute a similar

set, with only the temperature different from the conditions given above. Two (#13) was noted above to have failed in an anomalous manner, but no explanation is apparent for the variation of test 16. The other tests show a reasonable trend from high to low values with temperature. However, these are all single tests, and clearly, more data are needed to verify the trends.

Finally, test #9 was the loaded in increments of 2.1 MPa separated by 30 second pauses during which the pressure was held constant so that the ice could creep. This sample showed a marked increase in strength, but other tests are required to verify the result.

Several attempts were made to measure strain in the failure plane using wire strain gauges embedded in the ice. These gave unsatisfactory results, probably because of misalignment of the gauges. However, a load-displacement curve for one block was obtained using a structure of aluminum rods frozen into the block and adjacent stationary ice with one rod free to travel in a horizontal plane. The gap between the end of this rod and a similar, but stationary rod, was closed with a strain extensometer. The curve gives a modulus of 1.52 GPd.

In summary, the results to date indicate that repeatable results can be obtained from tests of the type described. However, there is some question regarding the validity of the test because the stress trajectories can curve around the lower edge of the flatjack, resulting in high stress concentrations in that area. Methods of overcoming this limitation have been devised and will be tested. In addition, a technique for conducting shear tests in a vertical plane is under study.

D. Compressive strength tests

A short series of tests were conducted in order to evaluate techniques and develop procedures through which the strength of sea ice can be measured in uniaxial and biaxial compression. In all tests loading was done with a hydraulic hand pump, and loading rates could not be controlled. Pressures were read from a pressure gauge which, unfortunately, had too great a range for accurate readings to be taken. This is an acceptable limitation, however, because the primary purpose of the tests was to evaluate the mode of failure of the ice.

In all but one of the tests the flatjacks used were in the form of equilateral triangles 38 cm on a side. These were installed in facing pairs, 60 cm apart, with one edge of each jack at the surface. In uniaxial tests a triangular prism with a flatjack at each end was prepared by making chain saw cuts at 60° from the horizontal along the boundaries of the block. These are parallel to the edges of the flatjacks, and meet beneath the block forming the prism.

A variation of the above configuration was also used. In this case, the flatjacks were installed as described above, but the relief slots were cut to isolate a rectangular prism 23 x 40 cm on each face in the center of the block between the jacks. One face of the prism was at the surface, so that it was not centered between the jacks with respect to depth.

In all cases, the relief slots were cut just prior to testing, so that disturbance to the ice by temperature changes and brine drainage were minimized.

Biaxial tests of two types were also run. In the first of these a pair of triangular flatjacks, installed as described above, were loaded without cutting relief slots, so that the ice provided the confining pressure. In the second, a 15 x 15 x 46 cm block was broken out of the ice sheet, the hole lined with plastic film, and the block replaced. 15 x 46 cm flatjacks were

installed along the sides of the block to provide confining pressure, and 15 x 15 cm flatjacks at the ends provided the axial load.

Five uniaxial tests were run on the full-size triangular prisms. The tests were run at various orientations so that they cannot be grouped to accurately assess repeatability. Temperatures during the first four tests were in the range of -12°C to -15°C . The fifth test was run at -8°C .

All of the tests produced failure in extension with one primary crack extending the length of the block close to the center line, and thus parallel to the maximum principal stress. The cracks were inspected after the tests by cutting vertical slabs through the blocks. These showed the cracks to be vertical with a tendency to splay near the base of the block. Other cracks with the same orientation were also formed. These originated at either jack and did not extend over the entire length of the block.

Breaking strengths measured in these tests ranged from 2.8 MPa to 3.5 MPa.

Attempts were made to produce shear fractures in the blocks by reducing the cross-section of the prism (i.e., "dog-boning" the test sample). These were unsuccessful, because the ice always failed around the flatjacks before fracture of the specimen occurred.

One uniaxial test was conducted using the reduced prism configuration described above. The test was run at an ice temperature of -8°C . The sample was loaded to about 4.1 MPa, but the pressure could not be increased beyond that value, because the creep rate of the ice became too great to resist expansion of the flatjack. At that time, the specimen showed a distinct whitish-gray color which appeared to be due to pervasive small-scale fracturing along planes oriented at 30° to 45° to the maximum principal stress direction. No macrocracking was observed.

Following completion of this test, the specimen was left unloaded for approximately 24 hours. It was then loaded again, until one of the flatjacks failed at 5.2 MPa. As in the earlier test, no macrocracking was observed.

Two biaxial compression tests were also run, one using each of the configurations described above. In the test involving the triangular jacks, failure occurred by extension fracturing at a load of 4.8 MPa.

In the second biaxial test, a constant confining pressure of 0.3 MPa was maintained along the sides of the specimen by loading the flatjacks with compressed N_2 gas through a pressure regulator. The flatjacks at the ends of the specimen were loaded with a hand-operated hydraulic pump. The maximum pressure reached was 6.21 MPa at which time the ice surrounding the ends of the test block failed, so that the load could no longer be applied to the block.

The results above suggest that triangular flatjacks provide a simple tool for measuring the uniaxial compressive strength of ice. Tests both with, and without, relief slots should be run. In addition, the use of reduced triangular prisms should be investigated further, particularly at colder temperatures, to determine whether shear failure can be induced by that method. Finally, further tests using confining pressure applied by flatjacks will require modification to decrease the stresses in the ice around the test specimen so that the tests can be run to completion.

E. Brazil Test

It was noted in the last annual report of this project that an indirect tension or Brazil test had been run in-situ on a vertical cylinder of ice 59 cm in diameter. In that test, loading was done using two 15 x 60 cm flatjacks installed at opposite ends of a diameter of the cylinder, with their 15 cm edges at the ice surface. When loaded, the cylinder failed with a single crack

along the diameter, and secondary cracking near the jacks. The tensile strength calculated for the test was .54 MPa, with a compressive stress along the loaded diameter of 1.62 MPa.

In order to investigate the possibility of eliminating the secondary cracking near the line of application of the load, the test was repeated using curved flatjacks. Two such flatjacks were prepared from 46 cm lengths of 7.6 cm diameter copper tubing. The tubing was flattened and then bent about the long axis to a radius of curvature of 29.5 cm. The ends were then sealed by silver soldering, and a threaded nipple installed at one end. Note that flatjacks of the size produced are capable of exerting a load over 15° of the surface of a test specimen of the above size.

The test was set up in the field as described above, and the relief slot, which defines the boundary of the test sample, was cut to a depth of 76 cm, or 30 cm deeper than the flatjacks extended into the ice. Loading was done by a hand-operated, hydraulic pump.

Failure occurred at a pressure of 3.7 MPa, which corresponds to a tensile strength of .47 MPa, with a compressive stress along the loaded diameter of 1.42 MPa. In contrast to the first test described above, failure in this test occurred by formation of a single crack extending between the flatjacks. No secondary cracking occurred. Further, following the test the block was sectioned vertically, and the crack was observed to extend vertically down with no indication of splaying or secondary cracking.

It can therefore be concluded that the technique of conducting the tests is established, but further work must be done to assess the repeatability of the results.

VI. ACTIVITIES DURING THE 8th Quarter

A. Results

Field work has been in progress since mid-February, but a series of problems (see below) have slowed the rate of experimentation. However, some preliminary results have been obtained:

A series of in-situ measurements of Young's modulus and Poisson's ratio have been made on a sample 30 x 30 x 60 cm at the top of the ice sheet. The block was broken loose from the ice sheet, the hole lined with plastic sheeting, and the block then replaced and frozen back. Flatjacks 30 x 60 cm in size were frozen along the sides of the block, and were used to apply confining pressure. Note that the block was thus confined even at zero pressure in the flatjacks. Axial loads were applied through flatjacks placed at the ends of the block. Strain was measured by strain gauges embedded in the ice.

The experiments were carried out over a two day period. The ice temperatures on the first day ranged from -14°C at the surface of the block to -9°C at the base. On the second day however they had changed to -19°C and -12°C respectively.

Axial loads and confining pressure were both applied using compressed N_2 gas through a pressure regulator and loading rates were about 6.9 k Pa/sec.

The value of Young's modulus for the first loading during which a confining pressure of .1 kPa was maintained was 10 GPa, which is high in the range of values of this parameter as determined by in-situ seismic methods (Weeks and Assur, 1967). The value of Poissons ratio for this test was 0.31. Subsequent loadings at various confining pressures up to 0.4 kPa produced progressively lower values of both parameters over the two day test period, with values for the tenth (and last) loading of 3.9 GPa and 0.19 for Young's

Modulus and Poisson's ration respectively. This clearly indicates the effect of strain softening.

A series of creep tests (2 - 3 stage tests and 1 - 2 stage tests) were also conducted using the same array, to evaluate the affect of confining pressure on creep rates. The results suggest little change in the secondary creep rate for a given value of differential pressure up to 0.8 MPa and condining pressures to .2 MPa.

Loading rates during the creep tests were about 20 k Pa/sec. for the initial loading as well as incremental loading during the tests. Values of Young's modulus were determined for each rapid loading sequence, and the resulting pattern of decreasing modulus with repeated loading was again observed. The maximum value of Young's modulus measured during the series of tests was 12.8 G Pa. Of interest also, is the fact that at the completion of each creep test, all of the instantaneous elastic strain associated with the loading phases of the test was recovered. This is in marked contrast to the problem of apparent loss of elastic strain in laboratory tests.

In addition to the above experiments, an array of 6 test samples, each 60 x 60 x 120 cm has been installed in the ice. These are oriented with 2 parallel to the dominant c-axis orientation, 2 perpendicular, and 2 at 45°. An attempt was made to conduct experiments with these blocks, but this was delayed as discussed below. In addition to these, several experiments to determine stress-strain curves during loading to failure in uniaxial compression are set up, as well as test specimans for creep experiments on small (i.e., 30 x 30 x 60 cm and 45 x 45 x 90 cm) blocks. These will be run shortly.

B. Problems Encountered

1. Failure of a component of the strain recording system delayed the start of the program for about 2 weeks.

2. Unusually warm weather persisted in the area through February, so that the ice thickness was only about 1m when the program began, and ice temperatures were several degrees above normal. This necessitated an extensive revision in the test program, because the experiments could not be conducted as designed under these conditions.

3. Installation of the 6 - sample array noted above required the installation of long (about 75 m) cables from the test site to the recording location. These are apparently acting as antennas, and are receiving substantial noise from the local radio station. A solution to the problem was found, but a delay of about one week was involved.

REFERENCES CITED

- Bland, D. R., 1960, The Theory of Linear Viscoelasticity, Pergamon Press, New York, 125 p.
- Dwight, H. B., 1957, Tables of Integrals and Other Mathematical Data, Macmillan Co., New York, 288 p.
- Grant, N. J. and Mullendore, A. W., 1965, Deformation and Fracture at Elevated Temperatures, M.I.T. Press, Cambridge, Mass., 211 p.
- Karlsson, T., 1972, A viscoelastic-plastic material model for drifting sea ice, in Sea Ice, Proc. Conf. Reykjavik, Iceland, May 10-13, 1971, p. 188-195.
- Kingery, W. D. and French, D. N., 1963, Stress-rupture Behavior of Sea Ice, in Ice and Snow - Processes, Properties and Applications, (W. D. Kingery, ed.), M.I.T., Cambridge Mass., p. 124-129.
- Krausz, A. S. and Eyring, H., 1975, Deformation Kinetics, John Wiley and Sons, New York, 398 p.
- Marquardt, D. W., 1963, An algorithm for least-squares estimation of non-linear parameters, J. Soc. Indust. Appl. Math., 11, p. 431.
- Maser, K. R., 1972, An analysis of the small-scale strength testing of ice, M.I.T. Sea Grant Office, Rept. No. MITSG 72-6, 137 p.
- Naghdi, P. M. and Murch, S. A., 1963, On the mechanical behavior of viscoelastic-plastic solids, J. Appl. Mech., 30, p. 321-328.
- Peyton, H. R., 1966, Sea Ice Strength, Geophysical Institute, University of Alaska, Report UAG R-182, 273 p.
- Reiner, M., 1960, Plastic Yielding in Anelasticity, J. Mech. Phys. Solids, 8, p. 255-261.
- Tabata, T., 1958, Studies on viscoelastic properties of sea ice, in Arctic Sea Ice, U.S. National Academy of Sciences, National Research Council, Pub. 598, p. 139-147.

Weeks, W. F. and A. Assur, 1967, The mechanical properties of sea ice,

CRREL Monograph II-C3, 94 p.

ANNUAL REPORT

Contract # 03-5-022-55
Research Unit #267
Reporting Period: April 1, 1976
to March 31, 1977
Number of pages: 26

OPERATION OF AN ALASKAN FACILITY
FOR APPLICATIONS OF REMOTE-SENSING DATA TO OCS STUDIES

Albert E. Belon
Geophysical Institute
University of Alaska

April 1, 1977

TABLE OF CONTENTS

Page

I	SUMMARY OF OBJECTIVES	
II	INTRODUCTION	
	A. General Nature and Scope of Study	
	B. Specific Objectives	
	C. Relevance to Problems of Petroleum Development	
III	CURRENT STATE OF KNOWLEDGE	
IV	STUDY AREA	
V	SOURCES, METHODS AND RATIONALE OF DATA COLLECTION	
	A. Remote-Sensing Data Acquired for the OCS Program	
	1. Landsat data	
	2. NOAA satellite data	
	3. USGS/OCS aircraft remote-sensing data	
	4. NASA aircraft remote-sensing data	
	5. NOS aircraft remote-sensing data	
	6. Army aircraft remote-sensing data	
	7. Preparation and distribution of remote-sensing data catalogs	
	B. Remote-Sensing Data Processing Facilities and Techniques	
	C. Consultation and Assistance to OCS Investigators	
	1. General Assistance	
	2. Individual Assistance	
VI	RESULTS	
	A. Establishment of a Remote-sensing Facility for OCS Studies	
	B. Disciplinary Results of the Applications of Remote-Sensing Data to OCS Studies	
VII, VIII +		
IX	DISCUSSION, CONCLUSIONS, AND NEEDS FOR FURTHER STUDY	
X	SUMMARY OF FOURTH QUARTER OPERATIONS	
	A. Laboratory Activities During the REporting Period	
	1. Operation of the remote-sensing data library	
	2. Operation of data processing facilities	
	3. Development of data analysis and interpretation techniques	
	4. Consultation and assistance to OCS investigators	
	B. Problems Encountered/Recommended Changes	
	C. Estimates of Funds Expended	

OPERATION OF AN ALASKAN FACILITY
FOR APPLICATIONS OF REMOTE-SENSING DATA TO OCS STUDIES

1976/77 Annual Report

Principal Investigator: Albert E. Belon
Affiliation: Geophysical Institute, University of Alaska
Contract: NOAA # 03-5-022-55
Research Unit: # 267
Reporting Period: April 1, 1976 - March 31, 1977

I - SUMMARY OF OBJECTIVES

The primary objective of the project is to assemble available remote-sensing data of the Alaskan outer continental shelf and to assist OCS investigators in the analysis and interpretation of these data to provide a comprehensive assessment of the development and decay of fast ice, coastal geomorphology and ecology, sediment plumes and offshore suspended sediment patterns along the Alaskan coast from Yakutat to Demarcation Bay.

Four complementary approaches are used to achieve this objective. They are, 1) the operation of a remote-sensing data library which acquires, catalogs and disseminates satellite and aircraft remote-sensing data; 2) the operation and maintenance of remote-sensing data processing facilities; 3) the development of photographic and computer techniques for processing remote sensing data; and 4) consultation and assistance to OCS investigators in data processing and interpretation.

Thus, the project has primarily a support role for other OCS projects, and in itself does not usually generate disciplinary conclusions and implications with respect to OCS oil and gas development. Such results will be generated by the various disciplinary OCS projects, most of which are users of remote-sensing data and services provided by our project. At this time at least two dozen OCS projects are utilizing remote-sensing data routinely, six of them (RU #88, 99, 248, 249, 257, 289A) almost exclusively. In addition, the availability of near-real-time remote-sensing data (NOAA satellite) and delayed repetitive data (Landsat and aircraft) provides a continuous monitoring of environmental conditions along the Alaskan continental shelf for research and logistic support of the OCSEAP Program.

II - INTRODUCTION

A. General Nature and Scope of Study

The outer continental shelf of Alaska is so vast and so varied that conventional techniques, by themselves, are unlikely to provide the detailed and comprehensive assessment of its environmental characteristics which is required before the development of its resources is allowed to proceed during the next few years. The utilization of remote-sensing techniques, in conjunction with conventional techniques, provides a solution to this dilemma for many disciplinary investigations. Basically the approach involves the combined analysis of ground-based (or sea-based), aircraft and satellite data by a technique known as multistage sampling. In this technique, detailed data acquired over relatively small areas

by ground surveys or sea cruises are correlated with aerial and space photographs of the same areas. Then the satellite data, which extend over a much larger area and provide repetitive coverage, are used to extrapolate and update the results of the three-way correlations to the entire satellite photograph. Thus, maximum advantage is taken of the synoptic and repetitive view of the satellite to minimize the coverage and frequency of data which have to be obtained by conventional means.

B. Specific Objectives

The principal objective of the project is to make remote-sensing data, processing facilities and interpretation techniques available to the OCS investigators so that the promising applications and cost effectiveness of remote-sensing techniques can be incorporated in their disciplinary investigations. The specific objectives of the project are: 1) the acquisition, cataloging and dissemination of existing remote-sensing data obtained by aircraft and satellites over the Alaskan outer continental shelf, 2) the operation and maintenance of University of Alaska facilities for the photographic, optical and digital processing of remote-sensing data, 3) the development of photographic, optical and computer techniques for processing remote-sensing data for OCS purposes and 4) the active interaction of the project with OCS users of remote-sensing data, including consultation and assistance in disciplinary applications, data processing and data interpretation.

C. Relevance to problems of petroleum development

The acquisition of remote-sensing data, specially satellite data, has proved to be a cost-effective method of monitoring the environment on a synoptic scale. Meteorological satellites have been used for over a decade to study weather patterns and as an aid to weather forecasting. The earth resources satellite program, initiated in 1972, offers a similar promise to provide, at a higher ground resolution, synoptic information and eventually forecasts of environmental conditions which are vital to petroleum development on the continental shelf. For instance the morphology and dynamics of sea-ice which are relevant to navigation and construction of offshore structures, the patterns of sediment transport and sea-surface circulation which will aid to forecast trajectories of potential oil spills and impact on fisheries, the nature of ecosystems in the near-shore regions which can be changed by human activity, are among the critical development-related environmental parameters which can be studied, in conjunction with appropriate field measurements, and eventually routinely monitored by remote-sensing.

III - CURRENT STATE OF KNOWLEDGE

The utilization of remote-sensing techniques in environmental surveys and resource inventories has made great strides during the last few years with the development of advanced instruments carried by aircraft and satellites. The early meteorological satellites had a ground resolution of a few miles and a broad-band spectral response which made them well-suited to meteorological studies and forecasting but inadequate for environmental surveys. The ground resolution of the sensors has been gradually much improved over the years and thermal sensors were added for cloud and sea temperature measurements, but generally the relatively low ground and spectral resolution of the meteorological satellites is a limitation for environmental surveys.

The initiation of a series of Earth Resources Technology Satellites (now renamed Landsat) in July 1972 was intended to fill the need for synoptic and repetitive surveys of environmental conditions on the land and the near-shore sea. With a ground resolution of about 80 meters and sensitivity in four visible spectral bands, Landsat-1 and 2, have fulfilled that promise beyond all expectations. Landsat-3, scheduled to be launched in fall 1977 will have a higher ground resolution (40 meters for the RBV system) and a thermal spectral band which will improve its capabilities enormously. The Seasat satellite, to be launched in 1978, will have all weather capabilities through the use of imaging radars and, as the name implies, has been specially designed for environmental surveys of the sea.

The development of techniques for analyzing and interpreting Landsat have proceeded at an even more rapid pace than the satellite hardware. While in 1972 much of the Landsat data interpretation was done by visual photointerpretation, the last four years have seen major developments in photographic, optical and, in particular, digital techniques for processing and interpreting the Landsat data. Some of these techniques, applicable to OCS studies, will be discussed in section V and VI of this report.

Through the impetus provided by the national commitment to satellite observations of the earth, the aircraft remote-sensing program has also made great strides in the last few years. While in the early 1960's airborne platforms were mostly used for aerial photography, the late 1960's saw the development of advanced multispectral scanners, thermal scanners, side-looking radars and microwave radiometers, partly for the testing of future satellite hardware and partly because the airborne observations serve for middle-altitude observations between ground and satellite measurements as part of the multistage sampling technique. Two philosophies are apparent in the airborne remote-sensing program: the first, exemplified by the NASA program as well as several universities and industrial agencies, involves relatively large aircraft and sophisticated instrumentation which produce vast quantities of data usually processed by computer techniques. The costs of data acquisition and data processing are quite high and for this reason this approach is usually applied to intensive, non-repetitive surveys of relatively small areas. The second approach uses airborne remote-sensing in a truly supporting role for ground-based or satellite measurements. The aircraft are smaller and the instrumentation usually consists of proven, simpler instruments such as aerial cameras, single-band thermal scanners, and single wavelength side-looking radars which usually generate data only in photographic format. The costs of data acquisition and data processing, while they are not small, are sufficiently low that the approach is often used for repetitive surveys of relatively large areas. In our opinion the second approach fulfills best the needs of the NOAA/OCSEAP program and we have been working very closely with the NOAA Arctic Project Office toward the implementation of such a remote-sensing program.

IV - STUDY AREA

The study area for the project includes the entire continental shelf of Alaska, except for the southeastern Alaska panhandle. This area includes the Beaufort, Chukchi and Bering Sea and the Gulf of Alaska shelves and coastal zone. Temporal coverage is year-around, although the data coverage from November 1 to February 15 is limited owing to the very low solar illumination prevailing at high latitudes during winter.

V - SOURCES, METHODS AND RATIONALE OF DATA COLLECTION

A remote-sensing data library and processing facility was established in 1972 on the Fairbanks campus of the University of Alaska as a result of a NASA-funded program entitled "An interdisciplinary feasibility study of the applications of ERTS-1 data to a survey of the Alaskan environment". This experimental program, which covered ten environmental disciplines and involved eight research institutes and academic departments of the University, terminated in 1974, but the facility which it established proved to be so useful to the statewide university and government agencies that it has continued to operate on a minimal basis with partial funding from a NASA grant and a USGS/EROS contract. In view of the large potential demand of the OCS program on these facilities, a proposal was submitted to NOAA in March 1975 for partial funding of the facility for OCS purposes. This proposal resulted in a contract from NOAA on June 12, 1975, and the work performed since that time is the basis for the present report.

As a result of the NASA-funded program, the remote-sensing data library had total cloud-free and repetitive coverage of Alaska by the ERTS-now renamed Landsat-satellite from the date of launch (July 29, 1972) to May 1974 (about 30,000 data products), 60 rolls of imagery acquired by NASA aircraft (NP3 and U-2) some of which includes coverage of the Beaufort Sea, Cook Inlet and Prince William Sound, and substantial facilities for photographic, optical and digital processing of these data. Through a NOAA-funded pilot project, which studied applications of NOAA satellite data in meteorology, hydrology, and oceanography, the remote-sensing data library also had nearly complete coverage of Alaska by the NOAA satellites since February 1974.

A. Remote-Sensing Data Acquired for the OCS Program

1) Landsat data

At the initiation of the project we performed searches of the EROS Data Center (EDC) data bank for Landsat and aircraft remote-sensing data obtained over the four areas of interest to the OCSEAP program. From the several thousand scenes so identified, we selected the scenes which we did not have in our files and which had satisfactory quality and 30% or less cloud cover. As a result of this search 566 Landsat scenes (2830 data products) were ordered from the EROS Data Center in the following data formats:

- 70mm positive transparencies of multispectral scanner (MSS) spectral bands 4, 5 and 7
- 70mm negative transparency of MSS spectral band 5
- 9½ inch print of MSS spectral band 6

During the first year of the project 265 additional cloud-free scenes (1325 data products) were acquired by the satellite and purchased from EDC. Throughout the second year of the project (current reporting period 1976-77) we continued to search the EDC data bank weekly for cloud-free Landsat scenes of the OCS areas acquired in the intervening period. As a result, 841 scenes were selected and ordered from EDC as of 31 March 1977.

2) NOAA satellite data

With the termination of a NOAA pilot project, sponsored by NOAA/NESS, in October 1975, our acquisition of NOAA satellite scenes stopped after having accumulated 1320 images since February 1974. Following an interim arrangement with the National Weather Service, which turned out to be inconvenient for both parties, funding was provided by OCSEAP, starting on 1 February 1976, to purchase NOAA satellite imagery directly from the NOAA/NESS Satellite Data Acquisition Facility at Fairbanks. Under this purchase order we are receiving two NOAA scenes daily from the Bering Sea pass of the satellite (covering the Beaufort, Chukchi and Bering Seas) and one scene daily from the interior Alaska pass (covering the Gulf of Alaska) in both the visible and infrared spectral bands (6 images daily except in winter) for a total of 1232 images received during the reporting period.

In addition we have made arrangements with the NOAA/NESS facility to save digital tapes of the thermal infrared data, upon request and for the cost of tape replacement, for scenes which are specially cloud-free or of high interest to OCS investigators. These tapes allow the precise mapping of sea-surface temperatures at locations and at times of special interest to OCS investigators.

3) USGS/OCS aircraft remote-sensing data

In November 1975, we started receiving the remote-sensing data acquired by USGS aircraft under a NOAA/OCS contract, along the Alaskan arctic coast since July 1975. These data consist of six 250 ft rolls of black and white aerial photography and 42 strips of side-looking radar imagery. This program terminated in December 1975.

4) NASA aircraft remote-sensing data

Over the last few years the NASA Earth Resources Aircraft Program has flown several missions over preselected test sites within Alaska. The program is directed primarily at testing a variety of remote-sensing instruments and techniques and to support NASA-sponsored investigations. However, black and white and color-infrared aerial photography were obtained on most missions and in particular during the May 1967, July 1972, June 1974, and October 1976 missions which include flights over portions of the Alaskan coast and coastal waters. We have acquired copies of these data from NASA.

The U-2 imagery of the Beaufort Sea obtained in June 1974 is of particular interest to OCS investigators because it was obtained during the sea-ice break-up period, it covers a large area (20x20 mi.) in a single frame with good ground resolution (~10 ft), and nearly concurrent Landsat data are available. Similarly, the U-2 imagery of the northern Gulf of Alaska and Prince Williams Sound, acquired in October 1976, is of excellent quality.

We have a request pending with NASA for the U-2 aircraft to acquire aerial photography of the entire Alaskan coastal zone (except the Seward Peninsula), weather permitting, during June 1977.

5) NOS aircraft remote-sensing data

In spring 1976 we learned that the National Ocean Survey's (NOS) Buffalo aircraft was scheduled to obtain aerial photographic coverage of Shelikof during summer 1976. Knowing that this area is frequently covered by clouds, we requested NOS to acquire aerial photography of other areas of the Alaskan coastal zone on a non-interference basis with their primary mission. NOS agreed to do so for the cost of the raw film. As a result 1316 frames of color aerial photography were acquired, covering the entire coast from the Yukon delta to Cape Lisburne and several isolated areas in the Gulf of Alaska. This aerial photography fills a serious gap in color coverage of the Alaskan coastal zone; it is of excellent quality, and it has been heavily used by OCS investigators.

6) Army aircraft remote-sensing data

With the termination of the USGS/OCS remote-sensing data acquisition program in December 1975, an important need developed for all-weather remote-sensing coverage of the Beaufort and Chukchi coasts during critical periods (end of winter and end of summer). We worked closely with the OCSEAP Arctic Project Office and with a major user (Dr. Cannon, RU #99) in investigating various options culminating in a contractual arrangement with the U.S. Army remote-sensing group at Ft. Huachuca, Arizona. Under this contract an Army Mohaw aircraft equipped with an all-weather side-looking radar (SLAR) flew two missions in Alaska in May and August 1976 resulting in complete SLAR coverage (51 flights) of the Beaufort and Chukchi shelves during the critical periods. These data have been heavily used, particularly by OCSEAP RU #88 (Weeks) and RU #99 (Cannon).

Contractual and technical arrangements have been made for another mission of the Army Mohawk aircraft in April 1977

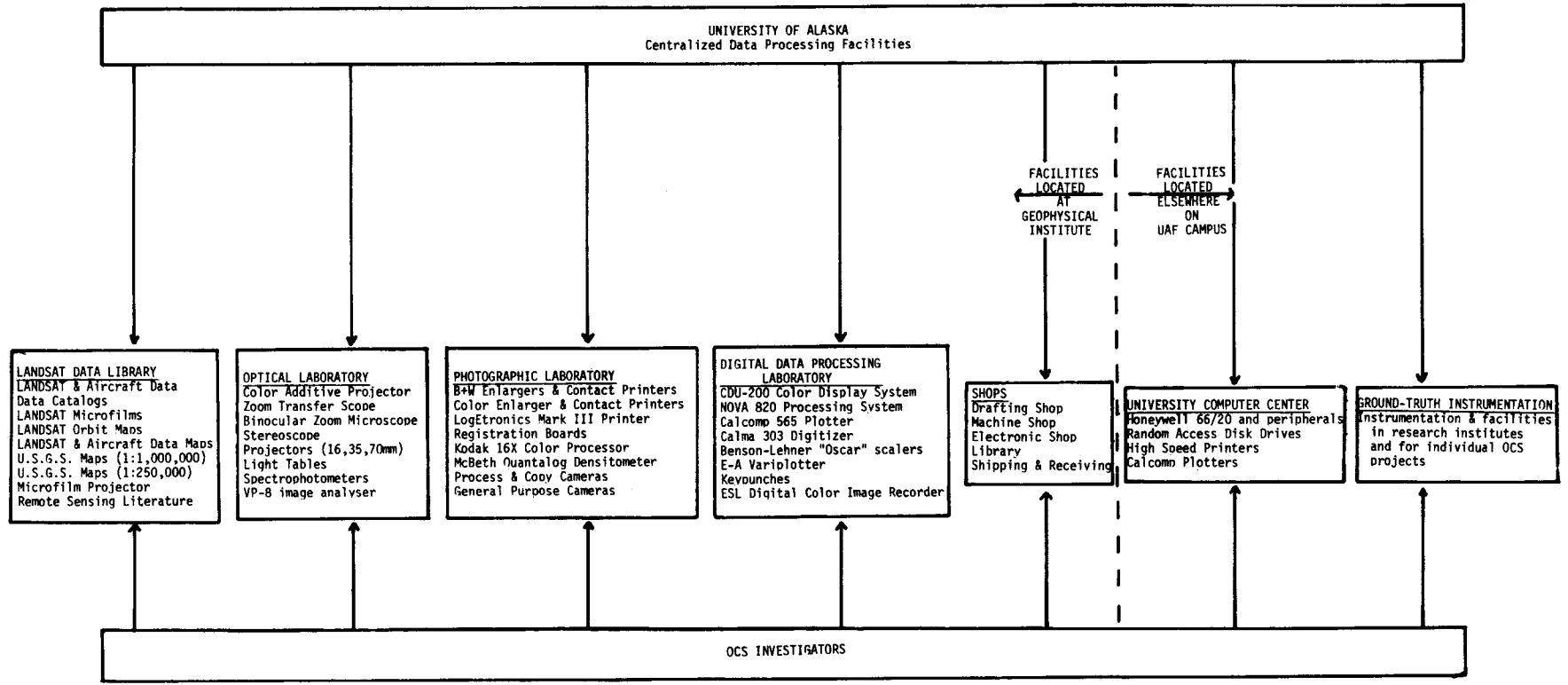
7) Preparation and distribution of remote-sensing data catalogs

All the remote-sensing data available in our files for the Alaskan continental shelf have been indexed and plotted on maps. Catalogs summarizing the availability of these data and providing instructions for selecting and ordering data have been prepared and distributed to all OCS investigators as appendices to the series of Arctic Project Bulletins (Nos. 6, 9, 10 and 12). In addition we have developed a file of catalogs and photo indices of aerial photography obtained by federal, state and industrial agencies in Alaska, and we attempt to stay informed on plans for future aircraft photographic missions.

B. Remote-Sensing Data Processing Facilities and Techniques

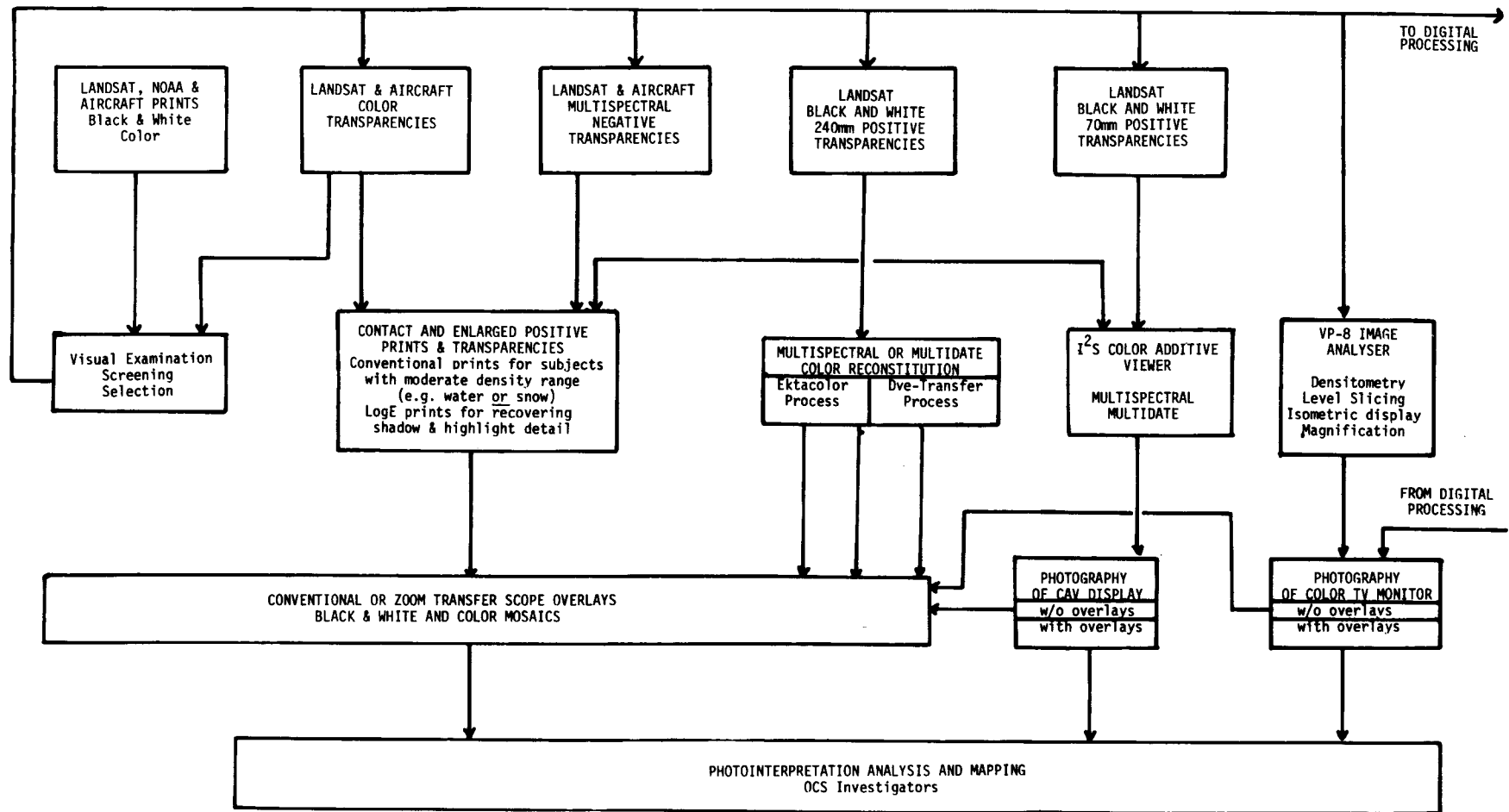
The facilities and equipment commonly used for remote-sensing data processing are listed in Figure 1. Most of this equipment is not devoted exclusively to remote-sensing data processing but arrangements have been made to support the needs of the OCS investigators on a share-time and work-order basis, and to take into account the needs of the OCS program in any planned modifications or expansions.

The optical and photographic processing techniques developed for the remote-sensing program are described in the flow diagram of figure 2.



Centralized Data Processing Facilities

Figure 1



Optical and Photographic Processing

Figure 2

Photographic processing probably needs no further explanation. The full range photographic laboratory of the Geophysical Institute is well adapted to the generation of custom, as distinct from production run, photographic products. However the available equipment limits photographic enlargements to 16x20" maximum size from 4x5" maximum size originals. Electronically dodged prints or transparencies are produced by contact printing only.

Optical processing revolves around the use of specialized equipment such as the multiformat photo-interpretation station, the zoom transfer scope, the color additive viewer and the VP-8 image analyzer in addition to conventional light tables, stereoscopes and a binocular zoom magnifier.

Multiformat Photo Interpretation Station - Analysis of aerial imagery in roll form is a cumbersome task and is likely to damage the original material even with careful handling if one uses ordinary reel holders and a light table. With stereo coverage, it is impossible to achieve stereo viewing with the frames appearing on the roll format unless one uses the photo interpretation machine. It can accommodate either 5-inch or 9-inch film formats and the film transport adjusts to permit stereo viewing with varying amounts of forward lap between frames. The viewing turret includes zoom binoculars with up to 5X magnification.

Zoom Transfer Scope - The time-consuming process of transferring information from images to maps is made considerably easier by the use of the zoom transfer scope. This table-top instrument allows the operator to view simultaneously both an image and a map of the same area. Simple controls allow the matching of differences in scales (up to 14X) and provide other optical corrections so that the image and the map appear superimposed. In particular a unique one-directional stretch capability (up to 2X) allow the matching of computer print-out "images" to a map or photograph.

Color Additive Viewer/projector/tracer - This instrument is primarily intended for the false-color recomposition of Landsat images from 70mm black and white transparencies and tracing information contained on these images at scales of 1:1,000,000 and 1:500,000. However it has proved to be very useful also for superimposing and color-coding Landsat images acquired on different dates and looking for change or movement and for viewing any other enlarged image on 70mm film format.

VP-8 Image Analysis System - The VP-8 image analysis system provides an electronic means of quantizing information contained in a photograph when the sought information can be expressed in terms of density ranges. It consists of:

- a light table having uniform brightness and a working surface of 15x22 inches
- a vidicon camera which transforms the photographic (transmittance) data to electrical signals
- an electronic image analyser which quantizes and formats the vidicon signals
- a CRT oscilloscope
- a color television monitor as an output device

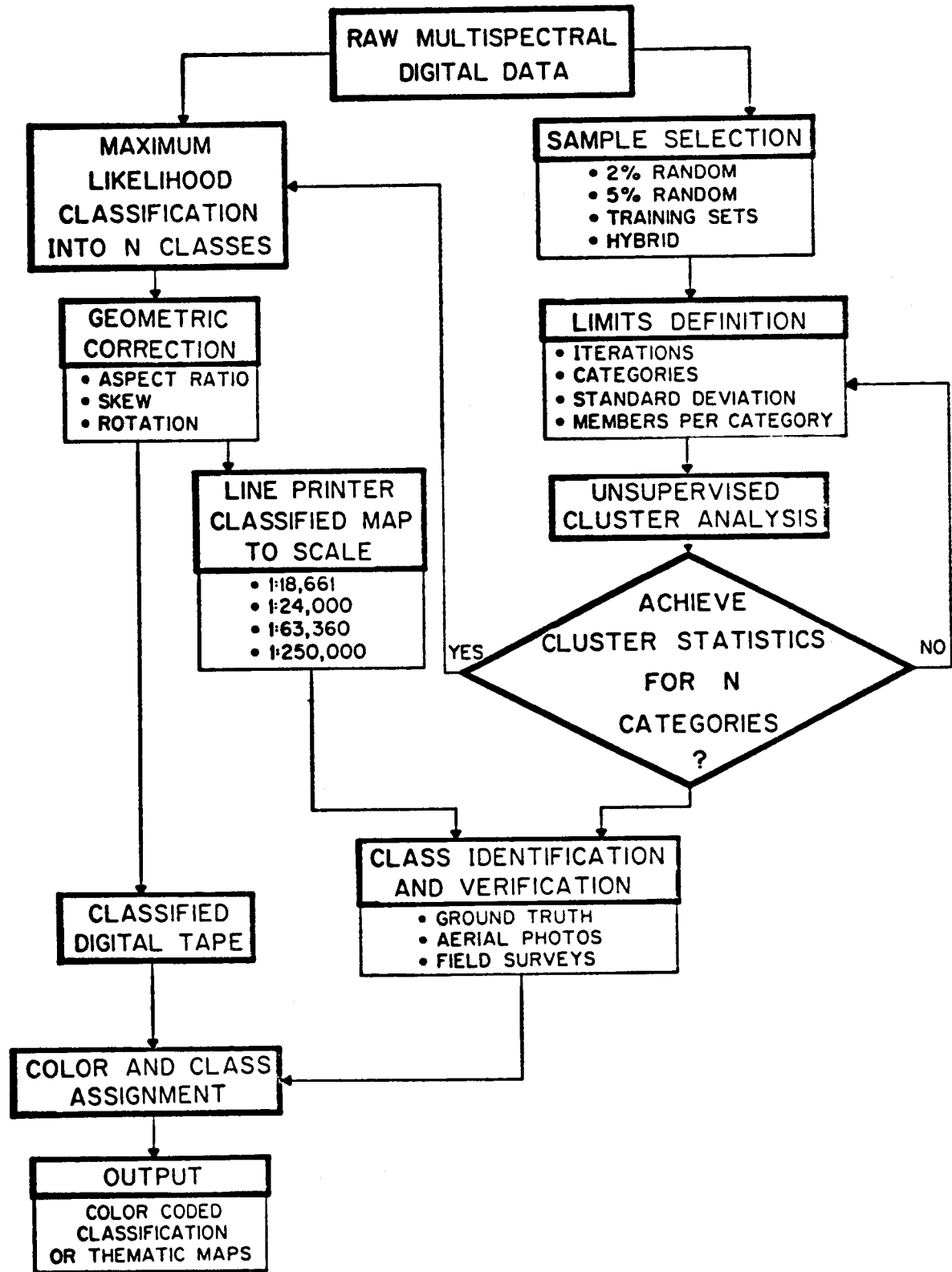
The capabilities of the VP-8 image analysis system include:

- density level slicing. This feature allows lines of uniform density on the input image to be displayed as contours. These contours form the boundaries of density bands which are displayed as up to 8 color bands on the color television monitor. The base density levels and the density range of the bands are individually as well as collectively variable. An example and illustration of the density slicing technique applied to coastal sedimentation studies was provided in the OCSEAP Arctic Project Bulletin No. 7, Appendix C, "Environmental Assessment of Resource Development in the Alaskan Coastal Zone based on Landsat Imagery" by A.E. Belon et al, University of Alaska.
- single scan line display. Any single horizontal scan line of the vidicon camera can be selected for display on the CRT oscilloscope by positioning a horizontal cross-hair on the image. This display of a single scan line is effectively a microdensitometer trace.
- digital read-out of point densities, selected by adjustable cursors or of total area of the image having a given (color-coded) density range. For instance the VP-8 image analysis system is well adapted to the area measurement of sea-ice, newly refrozen ice, and open water in any area of the Beaufort Sea imaged by Landsat.
- 3-D display. This mode of operation allows a three-dimensional presentation where the X and Y coordinates of the original image are displayed in isometric projection and intensity information is shown as a vertical deflection. Subtle features of the image, which are often lost on level-sliced displays, become obvious in 3-D displays.
- 5X magnification. This feature allows the expansion of a small part of the image to full screen size.

The digital data processing equipment available to the OCS investigators include the main University computer, a Honeywell model 66/20 with 1M bytes of core memory, which has a remote time-share terminal at the Geophysical Institute, a NOVA 820 data preprocessing computer as well as conventional typewriter printers, plotters and digitizers. Most remote-sensed imagery in digital format is reformatted, classified or otherwise processed on off-line computing systems. An overall flow diagram of digital processing of Landsat imagery is illustrated in figure 3 and discussed later in this report. Once the digital data have been processed, they are displayed on two specialized systems available at the Geophysical Institute.

The CDU-200 digital color display system is described by the simplified block diagram of figure 4. The CDU-200 performs three primary functions:

- 1) it provides a capability, similar to the VP-8 image analysis system for density slicing up to 3 bands of Landsat data in digital format. The accuracy of digital density-slicing is greater and more reproducible than with the VP-8 system because digital Landsat data have a more accurate radiometric calibration than photographic data and because up to 127 levels of intensity can be sliced (in groups of 16). Furthermore three digital images can be stored at once on the disc of the CDU-200 system and displayed sequentially for multispectral or multi-date signature determination.



FLOW CHART FOR GENERATING ECOSYSTEM MAPS

Figure 3. Digital processing of Landsat imagery

Flow chart of the unsupervised classification algorithms used for generating ecosystem maps of the Alaskan coastal zone from Landsat digital imagery.

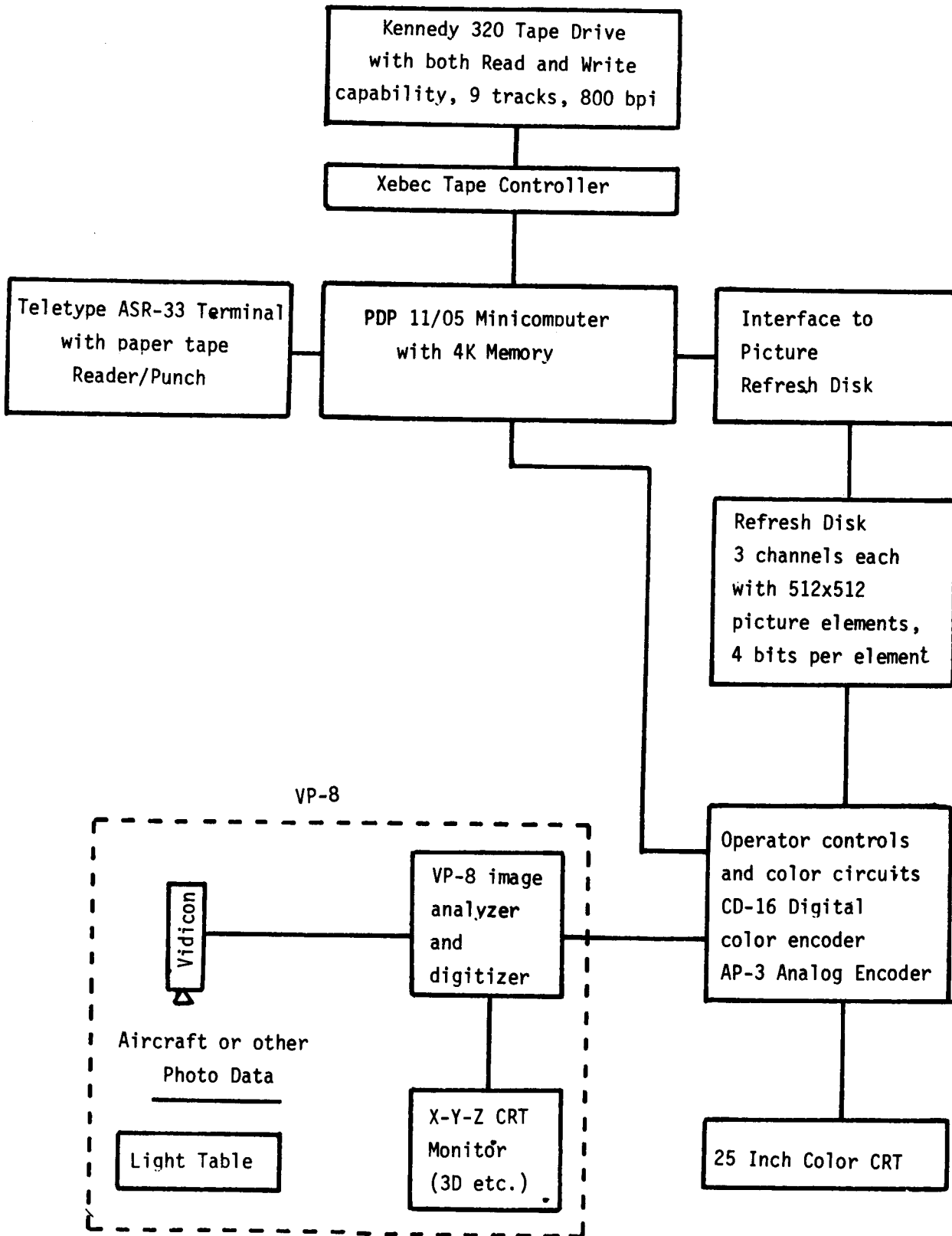


Figure 4 - CDU-200 digital color display system and VP-8 image analyzer

2) it provides a capability, similar to the color-additive viewer, for registering and combining three black and white digital images into a false-color image (displayed on the color television monitor) which has a larger scale, spatial and intensity resolution than the images displayed on the color-additive viewer.

3) it provides a capability to generate color-coded thematic displays from the output of classification processing techniques performed by off-line computer systems. An example of the application of the CDU-200, as well as the digital color image recorder, to the mapping of coastal zone ecosystems is provided in the OCSEAP Arctic Project Bulletin No. 7, Appendix C.

The digital disk memory of the CDU-200 has required considerable maintenance during the past year and it is still unreliable owing to design defects. Consequently we are currently utilizing the technical and financial resources of several Geophysical Institute projects to replace the disk memory with a random-access solid state memory which will provide greater reliability and, in conjunction with new electronic interfaces and software, a much greater capability for interactive data processing.

Digital Color Image Recorder - it often is necessary to reconstitute an image from the processed digital data in order to convey information in the most suitable form to the human mind. Also, if one deals with multi-spectral data it is impossible to convey the density of information required without the use of color. A digital image recorder with the capability of reconstituting color products was procured and installed during the past year using State of Alaska funds appropriated to the University of Alaska Geophysical Institute. Basically it is a rotating-drum film recorder which will produce four simultaneous standard images on film up to 8x10" in size. Density resolution is 64 levels of gray, and spatial resolution is 500 lines per inch and 500 samples per inch. Recording rate is 3 lines per second. Any combination of the four negatives so produced can be registered and printed with suitable filters to produce a reconstituted color negative which can be processed and enlarged photographically using standard techniques.

Remote-Sensing Data Interpretation Techniques - the basic techniques for remote sensing data reduction and interpretation are described in flow diagram format in figure 2 (optical and photographic data processing) and figure 3 (digital data processing). The techniques for visual photointerpretation, as applied to sea-ice mapping; for density slicing, as applied to sea-surface suspended sediment mapping and transport; and for digital data processing, as applied to ecosystem thematic mapping, are described in the OCSEAP Arctic Project Bulletin No. 7, in particular its Appendix C "Environmental Assessment of Resource Development in the Alaskan Coastal Zone based on Landsat Imagery" by A.E. Belon, J.M. Miller and W.J. Stringer.

Variations of these techniques offer considerable promise of effective applications to OCS studies, but are too numerous and varied to be discussed in detail here. Usually they are developed in cooperation with individual OCS investigators for application to a specific project. Therefore we refer to the reports of other OCS investigators for detailed descriptions of applications of remote-sensing data to disciplinary studies.

C. Consultation and Assistance to OCS Investigators

This activity may be subdivided into two parts: general assistance to all OCS investigators provided through the Arctic Project Bulletins, program planning and negotiations and meetings/workshops; and individual assistance through consultation, training sessions on the use of remote-sensing data and equipment and cooperative data analyses.

1. General Assistance

In order to familiarize OCS investigators with the available remote-sensing data, processing equipment, and interpretation techniques, we prepared five substantial reports which were included as appendices to the OCSEAP Arctic Project Bulletins Nos. 6, 7, 9, 10 and 12, and distributed to all OCS investigators active in studies of the Beaufort, Chukchi and Bering Seas and the Gulf of Alaska.

The appendix to Arctic Project Bulletin No. 6 described the operation of the remote-sensing data library, provided catalogs of Landsat and aircraft data available in our files and provided instructions to OCS investigators on the selection and ordering of these data.

The appendix to Arctic Project Bulletin No. 7 described the facilities and techniques available for analyzing remote-sensing data and included a scientific report in which these facilities and techniques were used to analyse and interpret remote-sensing data in three representative investigations of the Alaskan continental shelf: sea-surface circulation and sediment transport in the Alaskan coastal waters, studies of sea-ice morphology and dynamics in the near-shore Beaufort Sea, and mapping of terrestrial ecosystems along the Alaskan coastal zone.

The appendix to Arctic Project Bulletin No. 9 provided a cumulative catalog of all available OCS remote-sensing data including Landsat and NOAA satellite data, USGS/OCS aircraft data and NASA aircraft data.

Arctic Project Bulletin No. 10 provided a catalog of the SLAR (Side-looking radar) imagery obtained by the Army Mohawk remote-sensing aircraft in May 1976.

The Appendix to Arctic Project Bulletin No. 12 provided an updated catalog of satellite and aircraft remote-sensing data acquired since the issuance of the cumulative catalog of Bulletin No. 9.

Although the existing remote-sensing data base is very useful in supporting OCS disciplinary projects, there is also a vital need for an airborne remote-sensing data acquisition program dedicated to OCS purposes. To this end we have worked very closely with the NOAA Arctic Project Office in attempting to implement such a program. We participated in several meetings at the Geophysical Institute and one at Barrow in an attempt to set the USGS/OCS airborne remote-sensing data acquisition program on the right course, and took over responsibility for cataloguing, reproducing and disseminating these data. When this program failed and was terminated in January 1976, we studied alternatives and recommended several options to NOAA, one of which was a contractual arrangement with the U.S. Army remote-sensing squadron at Ft. Huachuca Arizona. This recommendation was implemented, and two missions of the Army Mohawk remote-sensing aircraft were conducted in May and August 1976, resulting in high quality SLAR imagery of the Beaufort, Chukchi and Gulf of Alaska

shelves at critical period. Another mission is scheduled for April 1977. In parallel with these activities we have negotiated with NASA for the acquisition of high altitude (U-2, 65000 ft) aerial photography of the entire Alaskan coastal zone. This program was approved by NASA at no cost (so far) to NOAA/OCSEAP. The first attempt to acquire the requested data, in June 1975, failed because of prevailing heavy cloud cover during the 3 weeks the U-2 aircraft was in Alaska. A second attempt, unfortunately delayed until October 1976, was partially successful and acquired high quality aerial photography of the Gulf of Alaska and Prince Williams Sound. A third attempt is currently scheduled for June 1977, but NASA is considering a policy requiring cost-reimbursement (\$2800 per hour flight time) which would be prohibitively expensive. We also participated in successful negotiations with the National Ocean Survey for acquisition of color aerial photography of the Bering and Chukchi Sea coasts during a previously scheduled mission of their Buffalo aircraft to Alaska in summer 1976. Excellent medium altitude photography was acquired from the Yukon delta to Cape Lisburne, as well as isolated areas of the Gulf of Alaska coast.

While the OCSEAP Arctic Project Office and our project have been fairly successful in negotiating remote-sensing data acquisition by other agencies on an irregular basis, such arrangements are not wholly satisfactory on a long-term basis because the type and format of the data vary from one mission to another and the frequency of data acquisition is insufficient to provide timely observations and good statistical information on coastal zone conditions and processes. For this reason we have worked with the Arctic Project Office on a plan which would utilize a Naval Arctic Research Laboratory (NARL) C-117 aircraft, remote-sensing equipment available from several sources, and local processing of the data to provide more frequent and more relevant data on a consistent format. Following this plan, the Arctic Project Office has requested a proposal from NARL for a remote-sensing data acquisition program, and from our project (RU #267) for the photographic processing of the data acquired by NARL. In anticipation of the acceptance of these two proposals the Cold Regions Research Laboratories (CRREL) is providing a Motorola side-looking radar and a laser profilometer to NARL, and we have located and secured approval for transfer of the following equipment from government laboratories in Alaska, Nevada and Mississippi:

- | | |
|---|-----------------|
| 1. KC-6 aerial camera (9" focal length) | value \$120,000 |
| 2. KC-1B aerial camera (9" focal length) | value \$10,000 |
| 3. KS-72 aerial camera (5" focal length) | value \$25,000 |
| 4. I ² S multispectral camera (6" focal length) | value \$10,000 |
| 5. Versamat continuous processor (5" to 9½" film or paper) | value \$30,000 |
| 6. LogEtronic SP1070B strip printer (5" to 9½" film) | value \$25,000 |
| 7. LogEtronic Mark III step and repeat printer (5" to 9½" film) | \$35,000 |
| 8. Omega B+W and color enlarger (10"x10" film) | value \$10,000 |

We are confident that the availability of this equipment, and the combined expertise and facilities of NARL and the Geophysical Institute will provide a good local capability for a remote-sensing data acquisition responsive to OCS needs and at relatively small cost to NOAA/OCSEAP.

At the request of the Arctic Project Office the principal investigator attended the OCSEAP Bird Investigator's Workshop in Anchorage on October 20-22,

1976 and presented a lecture on remote-sensing applications and capabilities, as part of a panel of physical scientists convened for the purpose of discussing data and services available from meteorology, climatology, and remote-sensing that can be of use to OCS bird investigators. An attempt was also made to identify major environmental events or conditions that could have had a bearing on bird phenology and reproductive success in summer 1976. (see Arctic Project Bulletin No. 12 for a summary of the meeting). As a result of general and individual discussions held at this meeting several OCSEAP bird biologists are now using remote-sensing data through the facilities provided by our project. Three of the major users in this group are George Divoky and his assistants (RU #196 and RU #330) who spent numerous hours analyzing remote sensing data in our facility, Leonard Peyton (RU #458) who is using NOS color aerial photography to map bird habitat in the Norton Bay region, and George Hunt (RU #83) who requested our project to perform analyses of sea-surface temperatures from NOAA satellite data, and ice-edge locations from Landsat data in the vicinity of the Pribilof Islands. Arrangements have also been made with George Hunt to perform similar analyses on suitable future NOAA and Landsat data during the 1977 season. Discussions were also initiated with Peter Myers (RU #172) concerning bird habitat mapping from Landsat digital data.

At the request of the OCSEAP Arctic Project Office the principal investigator of our project attended the Beaufort/Chukchi Sea Synthesis Meeting held at NARL, Barrow on February 7-11, 1977 and participated in most sessions, but particularly the disciplinary sessions on sea-ice morphology and dynamics and the interdisciplinary sessions on the environmental effects of artificial offshore islands and causeways. Previously prepared Landsat mosaics of sea-ice conditions and sea-surface suspended sediments on the Beaufort and Chukchi Sea shelves (see figures 5-10), as well as selected satellite and aircraft remote-sensing imagery contributed significantly to this highly successful meeting. A report of the meeting is in preparation by the OCSEAP Arctic Project Office.

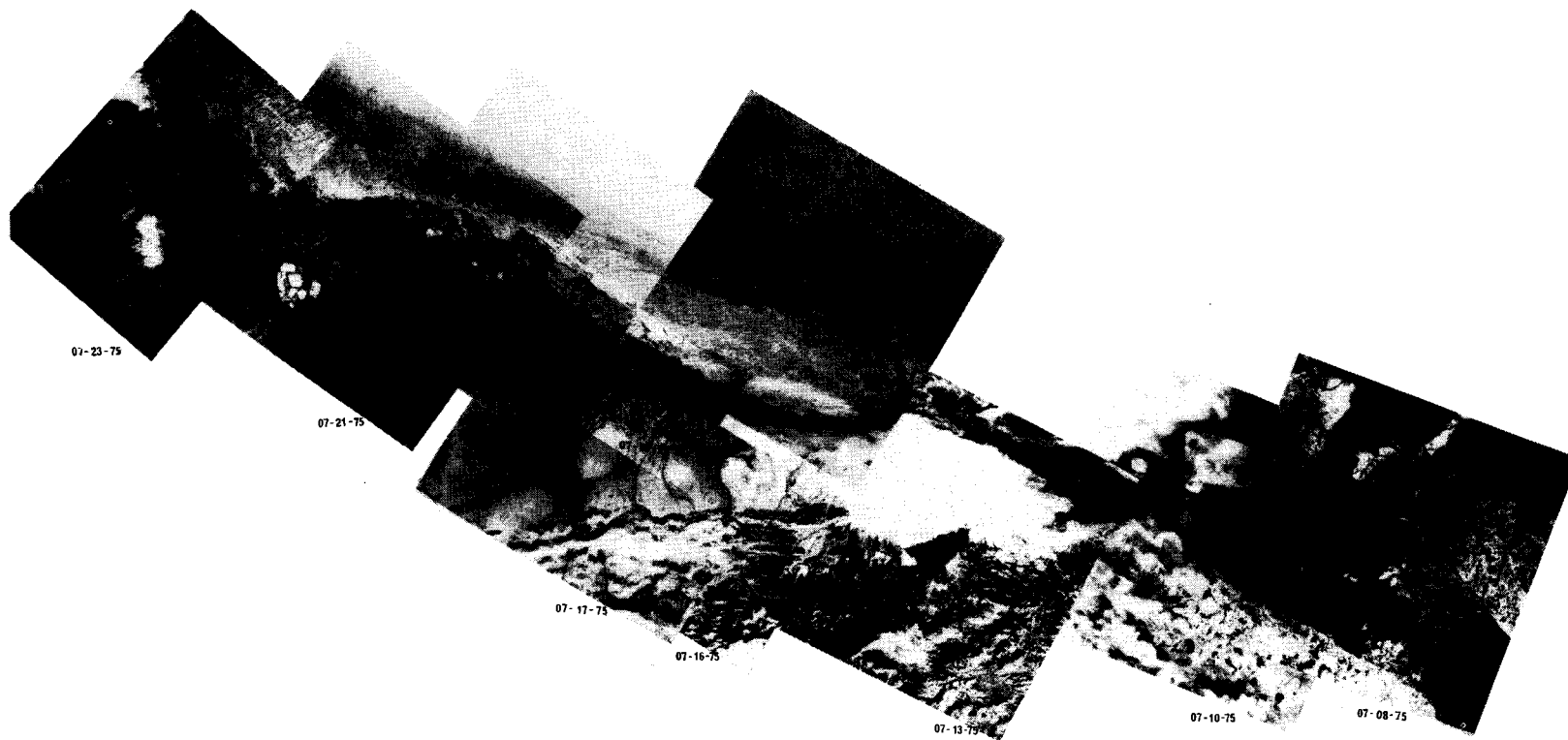
2. Individual Assistance

Individual assistance to OCS investigators involves consultations on the applicability of remote-sensing data to specific studies, data selection and ordering, preparation and supervision of work orders for custom photographic products and data processing, training in the use of remote-sensing data processing equipment and techniques, development of data analysis plans and sometimes participation in or performance of data analysis and interpretation.

This individual assistance has gradually increased in number and scope over the past year and we expect that it will continue to increase. 115 OCS investigators utilized our facilities during the past year, most of them for several hours, and some of them repeatedly. In addition numerous contacts occurred by mail or telephone correspondence. Therefore it is not possible to describe in detail these individual activities, but their scope is illustrated by listing the user projects: RU's nos. 3, 4, 31, 34, 81, 83, 88, 98, 99, 111, 140, 146, 149, 149, 172, 196, 205, 208, 231, 239, 244, 248, 249, 250, 251, 257, 258, 259, 289, 335, 337, 338, 339, 340, 341, 342, 343, 407, 458, 460, 461, 473, 483, 488. Of these about 20 projects are using remote-sensing data routinely, and six of them (RU's nos. 99, 248, 249,

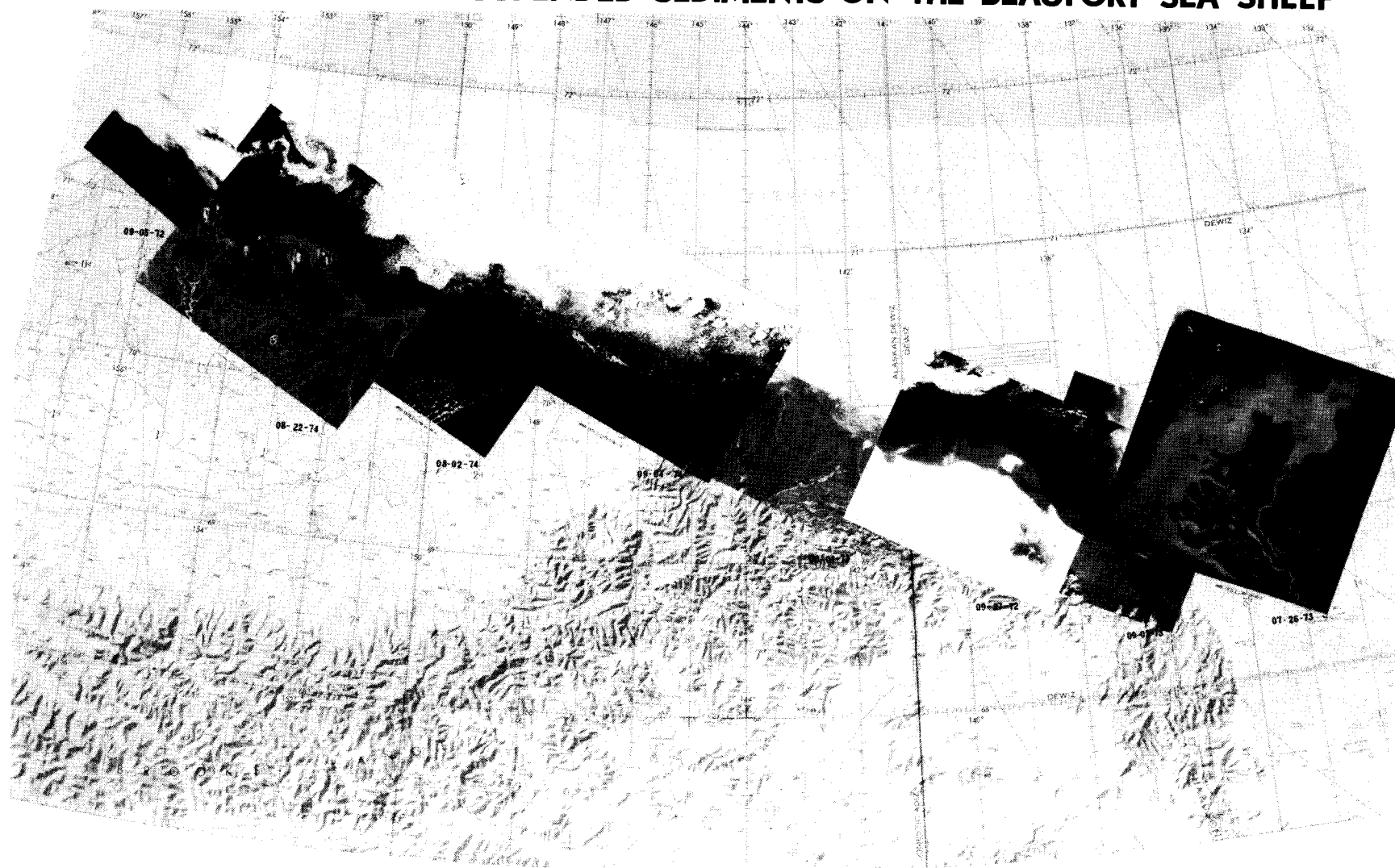
LANDSAT IMAGERY OF SEA-ICE ON THE BEAUFORT SEA SHELF

SUMMER 1975



260

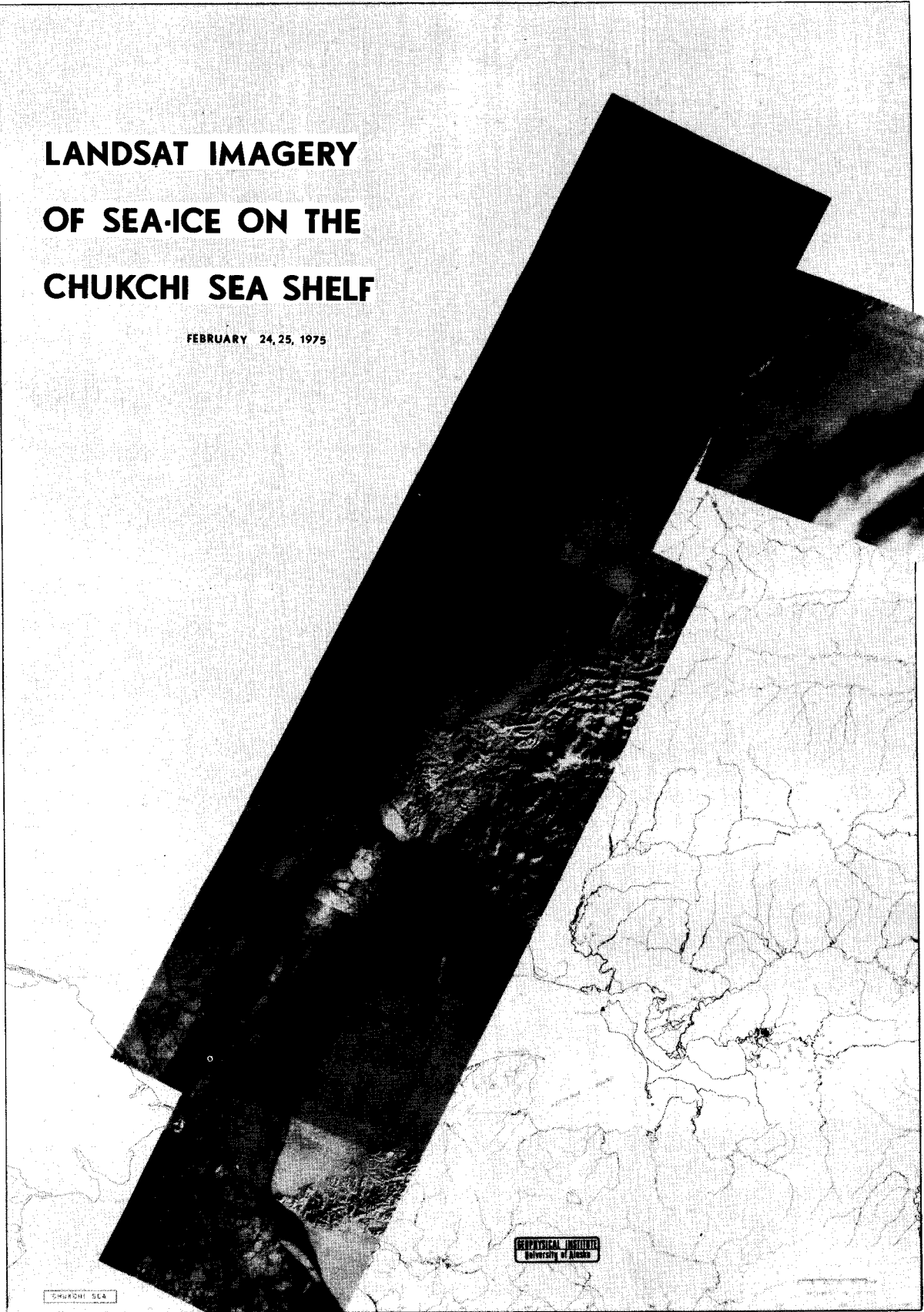
LANDSAT IMAGERY OF SUSPENDED SEDIMENTS ON THE BEAUFORT SEA SHELF



SUMMER, JULY- SEPTEMBER

**LANDSAT IMAGERY
OF SEA-ICE ON THE
CHUKCHI SEA SHELF**

FEBRUARY 24, 25, 1975



LANDSAT IMAGERY OF SEA-ICE ON THE CHUKCHI SEA SHELF

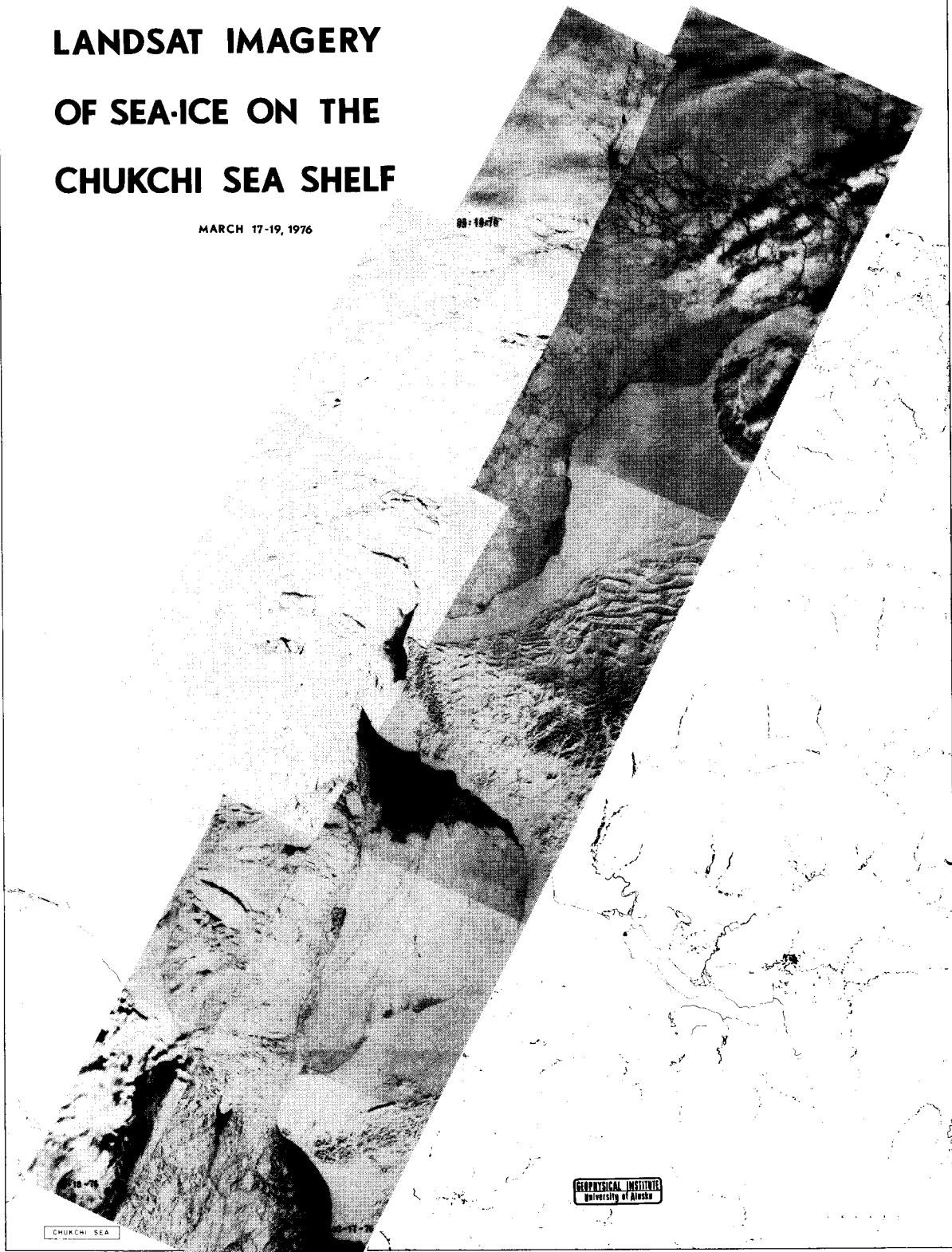
APRIL 27-30, 1975



LANDSAT IMAGERY OF SEA-ICE ON THE CHUKCHI SEA SHELF

MARCH 17-19, 1976

88-18-76

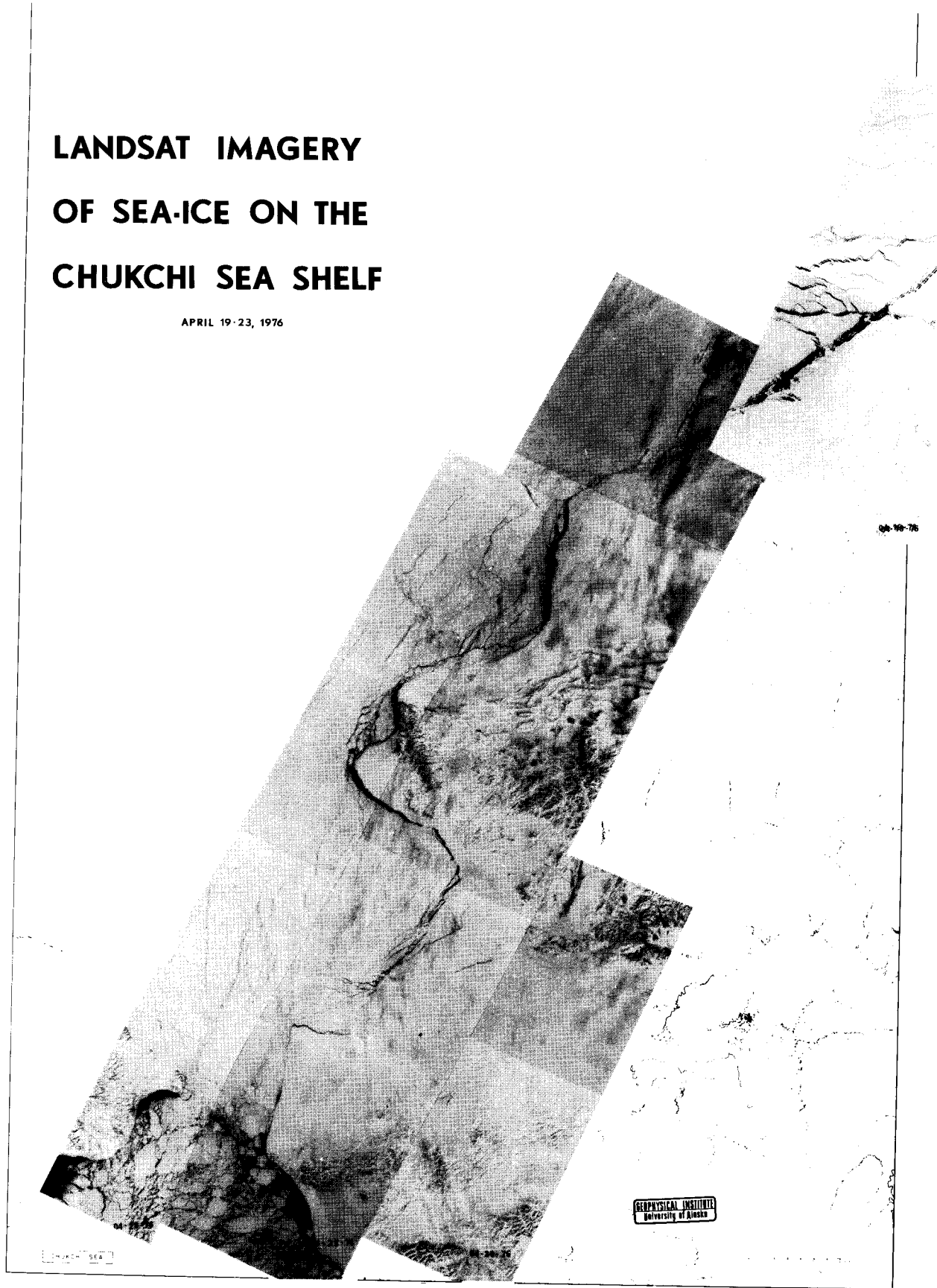


CHUKCHI SEA

GEOLOGICAL INSTITUTE
University of Alaska

LANDSAT IMAGERY OF SEA-ICE ON THE CHUKCHI SEA SHELF

APRIL 19-23, 1976



257, 258, 289A) almost exclusively. The principal applications are sea-ice morphology and dynamics, coastal geomorphology and geologic hazards, sea-surface circulation and sedimentation, sea-mammals habitat, and bird habitat mapping.

VI - RESULTS

The results of the project so far can be separated into two categories: the operational results (establishment of a remote-sensing data facility) and the research results (disciplinary applications of remote-sensing data to OCS studies).

A. Establishment of a Remote-sensing Facility for OCS Studies

The principal result of the project, as specified in the work statement of the contract, is that there now exists at the University of Alaska an operational facility for applications of remote-sensing data to OCS studies. This facility and its functions have been described in detail in the previous section of the report. Briefly it consists of:

- 1) A remote-sensing data library which routinely acquires, catalogs and disseminates information on Landsat and NOAA satellite imagery and aircraft imagery of the Alaskan continental shelf.
- 2) A remote-sensing data processing laboratory which provides specialized instrumentation for the photographic reproduction and optical or digital analysis of remote-sensing data of various types and formats.
- 3) A team of specialists that generates and develops techniques of remote-sensing data analysis and interpretation which appear to be particularly well-suited for OCS studies.
- 4) A staff that is continually available to OCS investigators for consultation and assistance in searching for, processing and interpreting remote-sensing data for their disciplinary investigations.

As a result of the establishment of the remote-sensing facility established by our project, about twenty OCS projects are routinely using remote-sensing data, six of them almost exclusively, and many more OCS investigators are occasional users of remote-sensing data.

B. Disciplinary Results of the Applications of Remote-Sensing Data to OCS Studies

In general, the results of applications of remote-sensing data to OCS studies will be contained in the annual reports of the individual projects and need not be repeated here. However as part of our function to develop techniques of remote-sensing data analysis and interpretation, we did prepare a scientific report entitled "Environmental Assessment of Resource Development in the Alaskan Coastal Zone based on Landsat Imagery" which illustrates the applications of Landsat data to three important aspects of the OCSEAP program: studies of sea-surface circulation and sediment transport in Alaskan coastal waters, studies of sea-ice morphology and dynamics in the near-shore Beaufort Sea, and mapping of terrestrial ecosystems in the Alaskan coastal zone. This report was presented at the NASA Earth Resources Symposium, Houston, Texas, June 1975 where it was

acclaimed as one of the best presentations. It was also distributed to OCS investigators as part of Arctic Project Bulletin No. 7 and is now out of print due to heavy demand in spite of the fact that 250 copies were made.

VII, VIII + IX - DISCUSSION, CONCLUSIONS, AND NEEDS FOR FURTHER STUDY

The principal objective of the contract, as specified in its work statement, has been achieved: a facility for applications of remote-sensing data to outer continental shelf studies has been established at the University of Alaska and is now fully operational.

The remote-sensing data library has acquired all available cloud-free remote-sensing imagery of the Alaskan continental shelf, catalogued it and provided information on its availability to all OCS investigators through the series of Arctic Project Bulletins.

Existing instrumentation for analysing remote-sensing data has been consolidated into a data processing laboratory and techniques for its use have been developed with particular emphasis on the needs of the OCSEAP program. New instrumentation is being acquired and new analytical techniques are continually being developed from this contract and other funding sources.

The staff of the project is interacting with a gradually increasing number of OCS investigators, providing consultation and assistance in all aspects of remote-sensing applications from data searches and ordering to advanced analyses of the data in photographic and digital format. We have also worked very closely with the NOAA Arctic Project Office in designing an interim remote-sensing data acquisition program using contract and aircraft missions by other agencies, as well as developing a plan in conjunction with NARL for a remote-sensing data acquisition program dedicated to OCS needs.

At this time about twenty OCS projects are using remote-sensing data and processing facilities routinely, some of them almost exclusively of other research activities, and many more OCS investigators are occasional users of remote-sensing data. The number of user projects has gradually increased over the last year. We expect that this trend will continue, specially as OCS investigators extend their localized intensive field studies to a synoptic scale where the benefits and cost effectiveness of remote-sensing attain their greatest impact.

It is clear from the foregoing discussions and from consultations with OCS investigators, regarding their study plans for the next year, that there will be a continuing need for the research support that our project provides. We intend to submit a continuation proposal to NOAA for this purpose.

X - SUMMARY OF FOURTH QUARTER OPERATIONS

This quarterly report covers the period January 1 to March 31, 1977

A. Laboratory Activities During the Reporting Period

1. Operation of the remote-sensing data library

We continued to search periodically for new Landsat imagery of the Alaskan coastal zone entered in the EROS Data Center (EDC) data base. As a result, 100 cloud-free Landsat scenes were selected and ordered from EDC at a total cost of \$732. The relatively small number of scenes ordered during the period reflects the fact that the satellite does not acquire data of Alaska during January and early February, owing to the very low solar illumination.

We continued to receive three daily scenes from NOAA satellite for a total of 367 images at a cost of \$1926. Again, owing to the low solar illumination during January and February, images in the visible spectral band were not acquired by the satellite for the first six weeks, but the thermal IR images which depend on emitted, rather than reflected radiation, were received throughout the reporting period.

No new aircraft remote-sensing data were received in the reporting period.

Thirty-five OCS investigators utilized our facilities during the reporting period and thirteen of them placed orders for satellite and aircraft remote-sensing data totalling \$3440. Most of them also utilized data available in our files and local data analysis equipment.

2. Operation of data processing facilities

All the data processing equipment (see section V.B of the annual report) was kept operational during the reporting period, with the exception of the CDU-200 Digital Color Display System which is undergoing substantial modifications. The replacement of its troublesome digital disk memory with a solid-state random access memory will improve greatly its reliability and, in conjunction with new electronic interfaces and software, will substantially increase its capabilities for digital data processing. Completion of the basic system is expected to occur during the next reporting period.

3. Development of data analysis and interpretation techniques

No new photographic or optical techniques were developed during the fourth quarter of the contract. However, existing techniques continue to be improved as time allows.

Computer programs for cluster analysis and maximum likelihood classification of multispectral satellite data (see figure 3 of annual report) were acquired and converted for use on the University of Alaska's Honeywell 66/20 computer. At present these programs are operational for analysis of relatively small areas. We plan to acquire and convert other programs (random sampling, geometric correction etc..) so that applications to large area mapping will be possible locally.

One of the OCS investigations (RU #172, Peter Myers) has identified a need for bird habitat mapping which will require simultaneous multispectral and multitemporal analysis of Landsat digital data with high location accuracy. This will represent a major effort, but the technique appears to have sufficiently wide applications to OCS studies that we are developing

an analysis strategy which will probably have to use outside computing facilities.

4. Consultation and assistance to OCS investigators

Thirty-five OCS investigators requested our assistance in searching for, obtaining or analysing remote-sensing data. RU's nos. 99, 248, 249, 257 and 289A continued to be very heavy users of our facilities. In addition RU #83 (George Hunt) and RU #172 (Peter Myers - see above) requested substantial assistance in digital analysis of NOAA and Landsat data for sea-surface temperatures and bird habitat mapping, respectively.

At the request of the OCSEAP Arctic Project Office the principal investigator of our project attended the Beaufort/Chukchi Sea Synthesis Meeting held at NARL, Barrow on February 7-11, 1977 and participated in most sessions, but particularly the disciplinary sessions on the environmental effects of artificial off-shore islands and causeways. Previously prepared Landsat mosaics of sea-ice conditions and sea-surface suspended sediments on the Beaufort and Chukchi Sea shelves (see figures 5-11), as well as selected satellite and aircraft remote-sensing imagery contributed significantly to this highly successful meeting. A report of the meeting is in preparation by the OCSEAP Arctic Project Office.

A plan was developed in cooperation with the OCSEAP Arctic Project Office for a program of remote-sensing data acquisition utilizing a C-117 NARL aircraft, equipment obtained on loan from various government laboratories, and photographic processing facilities at the Geophysical Institute (see section V.C.1 of annual report). As a result two companion proposals by NARL and our project (amendment to RU #267), respectively, were submitted to OCSEAP in January for implementation of the cooperative program.

B. Problems Encountered/Recommended Changes

The proposals discussed above were submitted in February and requested a starting date of March 1, 1977. A decision had not been made by OCSEAP as of 31 March, 1977. If the decision is postponed beyond April, it probably will not be possible to acquire the needed remote-sensing data during the critical sea-ice break-up period (June/July).

C. Estimates of Funds Expended

Expenditures of the project were \$5,341.58 in January 1977, \$10,976.79 in February, and an estimated \$20,000 in March (including \$14,000 in outstanding obligations for future purchases of remote-sensing data from NOAA/NESS and the EROS Data Center) for a total of \$36,317.

ANNUAL REPORT

CONTRACT # 03-5-022-56
TASK ORDER #19
RESEARCH UNIT #289
REPORTING PERIOD 4/1/76-3/31/77
NUMBER OF PAGES 102

CIRCULATION AND WATER MASSES IN THE GULF OF ALASKA

Dr. Thomas C. Royer

Institute of Marine Science
University of Alaska
Fairbanks, Alaska 99701

31 March 1977

TABLE OF CONTENTS

LIST OF FIGURES.

LIST OF TABLES

I. SUMMARY OF OBJECTIVES, CONCLUSIONS AND IMPLICATIONS WITH
RESPECT TO OIL AND GAS DEVELOPMENT

II. INTRODUCTION

III. CURRENT STATE OF KNOWLEDGE

IV. STUDY AREA

V. SOURCES, METHODS, AND RATIONALE OF DATA COLLECTION

VI. RESULTS.

VII. DISCUSSION

VIII. CONCLUSIONS.

IX. NEEDS FOR FURTHER STUDY.

REFERENCES

X. SUMMARY OF 4TH QUARTER OPERATIONS.
Ship Activities.
Problems Encountered

XI. APPENDIX I - CROSS SECTIONS OF SALINITY, TEMPERATURE AND
DENSITY VERSUS DEPTH FOR THE GULF OF ALASKA, SEPTEMBER 1975. . .

XII. APPENDIX II - LOW FREQUENCY SHELF FLUCTUATIONS IN THE GULF
OF ALASKA.

LIST OF FIGURES

- Figure 1. GASSE station locations with flow regimes and transect names
- Figure 2. GASSO station locations with flow regimes and transect names
- Figure 3. Dynamic topography.
- Figure 4. Dynamic topography.
- Figure 5. Dynamic topography.
- Figure 6. Dynamic topography.
- Figure 7. Dynamic topography.
- Figure 8. Dynamic topography.
- Figure 9a. Progressive vector diagram for station 9 at 20 m, April - July, 1976.
- Figure 9b. Progressive vector diagram for station 9 at 20 m, July - November, 1976
- Figure 10. Dynamic height gradients for Seward line.
- Figure 11. Dynamic height for Cook Inlet line.
- Appendix I
Cross sections of salinity, temperature and density versus depth for the Gulf of Alaska, September 1975 - 41 figures.
- Appendix II
- Figure 1. Bathymetry of northern Gulf of Alaska continental shelf study area.
- Figure 2. Wind and current vectors, temperature, salinity and sigma-t time series
- Figure 3. Isohalines at sea surface and 20 m depth, R/V *Acona* cruise 193, 2-4 July 1974
- Figure 4. Geostrophic currents calculated from R/V *Acona* cruise 193, hydrographic data.

LIST OF FIGURES (CONTINUED)

- Figure 5. Surface current vectors computed by numerical model . . .
- Figure 6. Schematic representation of inner gyre displacement . . .
- Figure 7. ERTS/LANDSAT-1 image of Gulf of Alaska, 14 August 1973. .

LIST OF TABLES

- Appendix Table I. Statistics for low pass filtered data
- Appendix Table II. Comparative statistics for calculated and observed winds

I. SUMMARY OF OBJECTIVES, CONCLUSIONS AND IMPLICATIONS WITH RESPECT TO OIL AND GAS DEVELOPMENT

The objectives of this study are to define the physical-chemical environment, transports of pollutants and to establish the long-term monitoring of the physical-chemical environment in the Gulf of Alaska.

The main conclusion from this year's work is that the shelf region around the Gulf of Alaska has many identifiable local circulation regimes, that is, distinctions in shelf flow can be made from one location to another. Four different regimes have been identified in the Northeast Gulf of Alaska. The Western and Aleutian regimes comprise two additional regimes for the western Gulf of Alaska. All of the regimes are connected physically, but represent areas where the flow has different characteristics. It has also been found that the areas of highest biological activity are usually regions of small net transport. For example, the productivity is relatively high to the west of Kayak Island, within Prince William Sound and on the shelf east of Kodiak Island, all of which are regions of small net transport.

Apparently, the Alaska Current and Stream acts as a dynamic boundary in the entire Gulf of Alaska. This allows the separation of shelf and deep ocean circulation with less interaction between them than was previously assumed. In addition to the identification of this dynamic boundary, it has been found that for the shelf area between Middleton Island and somewhere to the west of Kodiak Island, the circulation is characterized by eddies and counter currents, that is, to the northeast. The time dependence of this flow is presently unclear but will be clarified with further analysis.

The implications of the findings of this research unit with respect to oil and gas development are that the shelf flows in the Gulf of Alaska are spatially variable but yet interconnected. This variability allows currents in excess of 2 knots to be found in the vicinity of counter currents of low speed. For example, the area west of Middleton Island might retain pollutants for quite lengthy periods unless the pollutant entered the coastal jet or the Alaska Current. The high probability of flow into Prince William Sound has implication to development since this is a region with high biological productivity. This inflow has been implied by the hydrographic data gathered by this research unit and confirmed with the satellite tracked drifter study. Since regions of low flow are often identified with high biological productivity and long residence times, these represent especially critical region in terms of oil and gas development.

II. INTRODUCTION

This study is devoted to determining the ocean transports in the Gulf of Alaska and the distribution of water masses within the region. It is concerned with both the steady state currents and shorter term variations such as seasonal changes. A specific objective is the acquisition of hydrographic data both on the shelf and in nearby deep water to determine the water mass distributions and density fields from which flows and hence pollutant movement can be determined. Current meter data is being gathered at selected sites for the proper evaluation of the flow field. Satellite imagery is used to extend this study in both time and space. The study is relevant to both the short term and chronic pollution problems

posed by development of the natural resources of the region. It provides input to numerical models which produce trajectories of surface water in the Gulf of Alaska. Direct current meter measurements, water mass analysis and satellite imagery are used to verify the model trajectories.

III. CURRENT STATE OF KNOWLEDGE

Prior works which summarize the knowledge of the physical oceanography of the Gulf of Alaska include Dodimead, Favorite and Hirano (1963), Royer (1975) and Galt and Royer (1975). In the past year, several new papers on the gulf have been published. Hayes and Schumacher (1976), Royer and Muench (1977) and Favorite, *et al.* (1976) discuss work conducted under OCS sponsorship. In addition, Favorite, Dodimead and Nasu (1976), have updated the previous report by Dodimead, Favorite and Hirano (1963). Reid and Mantyla (1976) have discussed the use of sea level in the region for the determination of current speeds. While this past knowledge gives the general character of the physical processes in the region, the most important source of information in the region are the present OCS investigators. Broad generalizations to other coastal areas cannot be made until the important forcing mechanisms in the Gulf of Alaska have been evaluated. As mentioned previously, it is becoming apparent that these mechanisms differ from region to region in the Gulf of Alaska.

IV. STUDY AREA

The study area includes the continental shelf and adjacent deep waters of the Gulf of Alaska from Yakutat to Unimak Pass (Figs. 1 and 2).

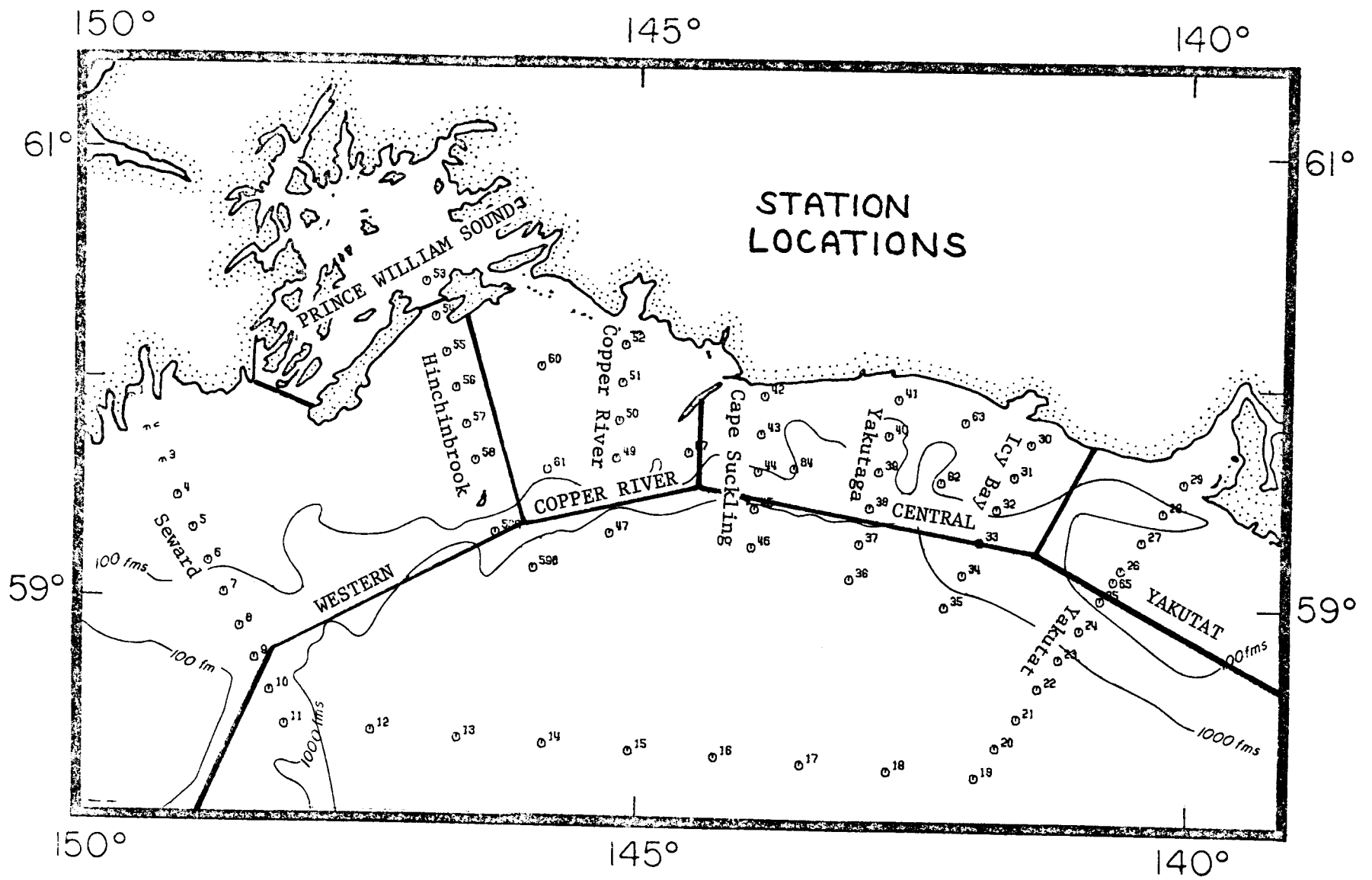
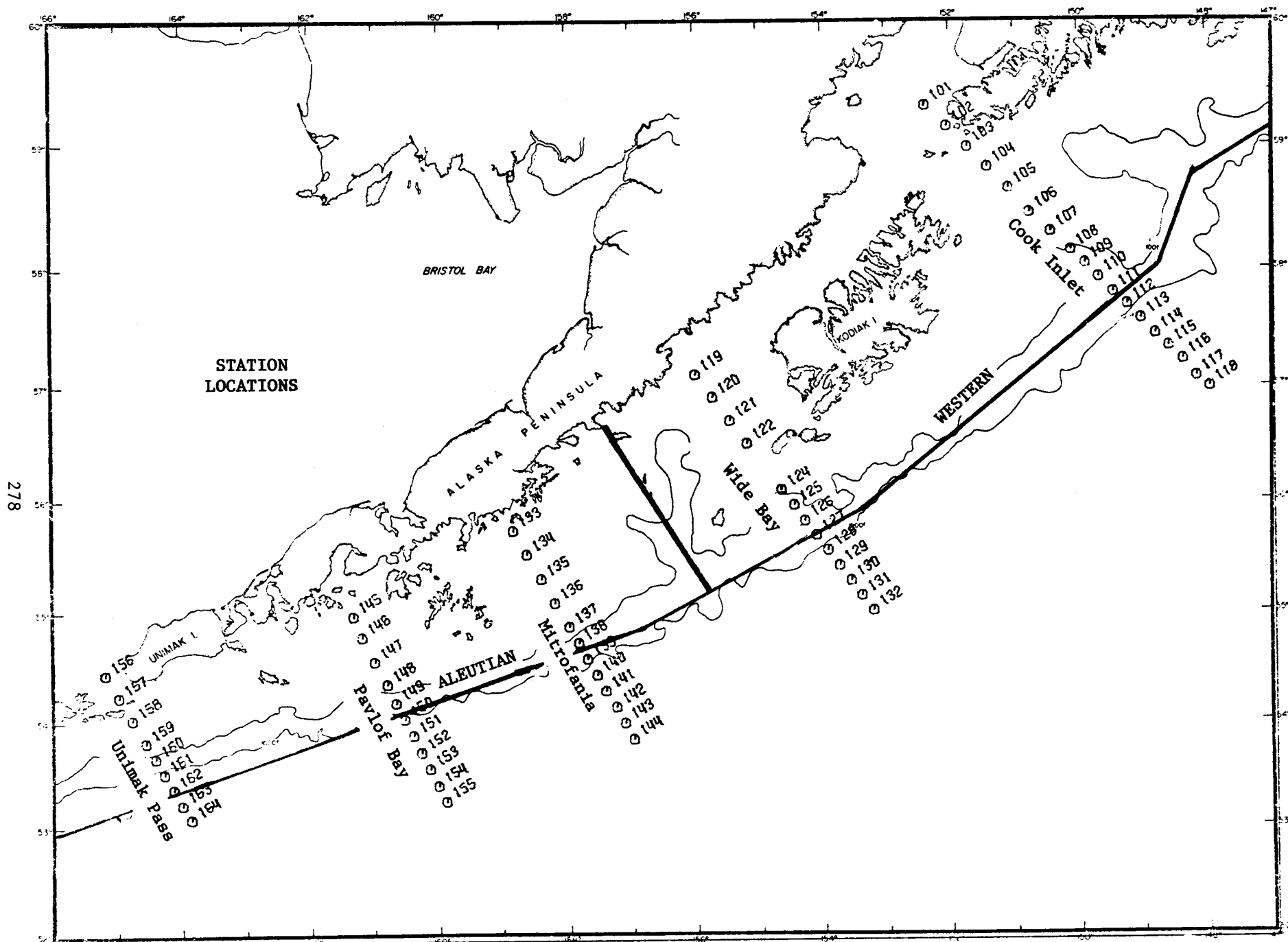


Figure 1. GASSE station locations with flow regimes and transect names.



278

Figure 2. GASSO station locations with flow regimes and transect names.

V. SOURCES, METHODS, AND RATIONALE OF DATA COLLECTION

To obtain seasonal description of transports, currents and water masses, the sampling program must be carried out on a seasonal basis. A quarterly sampling scheme is preferred. It is also necessary to obtain an adequate spatial distribution of currents and water mass characteristics. To achieve these goals, the grids in Figures 1 and 2 are occupied on a quarterly basis. Both temperature and salinity versus depth are measured at each grid point. The temperature and salinity value are recorded aboard ships through the use of an STD or CTD system that electronically measures salinity or conductivity and temperature versus depth. The system is calibrated both in the laboratory and the field. The field calibration consists of a comparison of the STD/CTD values with collected samples. These collected sample values are in turn compared with international standards. From these data both vertical and horizontal cross-sections are produced. The density and geopotential fields are calculated from which the baroclinic (or density driven) flow field can be determined. These same hydrographic data are being used by J. Galt at PMEL as input for his numerical model. However, since the model uses data which are integrated to some extent, with depth, these data contain a great deal more information than is apparent in the model results. For example, while surface flows are in one direction, subsurface flows can be in the opposite sense. In addition to describing the dynamics, the hydrographic data can be used to trace water masses throughout the region. A vivid example is the tracing of Icy Bay and Copper River water to various positions in the western Gulf of Alaska through their salinity and temperature characteristics.

The rationale for the various types of data gathering for estimating currents was presented in the 1976 annual report but will be repeated for emphasis at this point. Fofonoff (1962) presents the total current as the sum of the baroclinic and barotropic geostrophic components and the Ekman wind drift component. The baroclinic current field can be determined from the density field which is derived from the hydrographic measurements. The barotropic current field can be determined from the sea level slope. A satisfactory method of measuring the sea level slope over a large region is not yet developed. Instead, the barotropic current must be estimated at a point with a current meter array. The Ekman component is generally determined directly from the available surface wind data.

A combination of wind measurements, hydrographic data and current meter arrays is necessary for the complete description of currents in a particular region. For example, the density field might indicate an eastward flow over a particular region but the barotropic flow might be westward. Whether the net flow is eastward or westward is dependent on the relative magnitude of these two components. For total transport the Ekman wind drift must also be considered. Current meters are used to measure this entire flow but they only evaluate it at single points. Lagrangian drifters avoid this problem of point measurement but are difficult to interpret properly. Careful analysis must be employed in combining the various current components to yield the net flow. Such an analysis is presented later in this report with the evaluation of flow near Kodiak Island.

This year (April 1976-March 1977) STD/CTD data have been obtained for the eastern grid GASSE once, a modified eastern grid twice, the western

grid (GASSO) four times and the Kodiak Island small scale grid three times. A total of twelve cruises have been conducted for the GASSE grid and six for the GASSO grid over the past three years. However, these are not necessarily complete coverages of either grid. This is especially true of the western grid (GASSO) where complete occupation has only occurred once because of the higher priority placed on the data in the Kodiak Island region.

The cross-sections of salinity, temperature and density versus depth for the complete grid for September 1975 are included in Appendix I. The cross-sections for all other cruises through November 1976 are available upon request. These data are to be incorporated into a technical report.

In addition to hydrographic data gathered by project personnel, data from other sources such as NODC and the U.S. Coast Guard are being used. The latter supplies information on the deep water properties in the central Gulf of Alaska. Meteorological data from the U.S. Weather Service are being used for local conditions. Regional wind fields are determined from Bakun's work at the Fleet Numerical Weather Central in Monterey, California. Data are now being received from the Middleton Island weather station and EB-03 buoy on a continuing basis. The Middleton data represent one of the few truly marine weather observations and is of great importance in evaluating wind conditions west of Kayak Island near the entrance to Prince William Sound. The EB-03 data are valuable in providing a "ground truth" to the large scale wind field computations by Bakum.

The Institute of Marine Science is both providing and using NOAA 4 and 5 satellite data. Part of the work involves the monitoring of all NOAA visible and IR satellite data for the Alaskan coastline. Useable

images are retained and provided to other OCS investigators upon request. These data afford opportunities to map the distribution of sea surface temperature over vast regions.

VI. RESULTS

One of the most important results of the year's study was the development of the dynamic topography for the hydrographic data acquired in the Gulf of Alaska. From the dynamic topography the baroclinic flow can be inferred. These topographies are presented in Figures 3 to 8. The contours can be used as streamlines with the speed dependent on contour spacing (see insets). Regions of high and low speed flow are easily identified along with seasonal changes.

An analysis of the hydrographic and current meter data to the west of Kayak Island in the area of the Copper River has been conducted. This analysis is presented in Appendix II.

Current meter data for the period April–November 1976 at GASSE 9 (Fig. 1) give evidence of flow reversals (west to east). In general, there is southwesterly flow approximately along the direction of the shelf break contours at all depths with the exception of the meter at 273 m (10 m above the bottom) which was generally directed off the shelf. However, from about July to October the flow became irregular with significant flow reversals. The progressive vector diagrams indicate trajectories of several hundred kilometers to the northeast during this time (Fig. 9). Later, the flow once again was directed to the southwest. Current speeds at this mooring were extreme, greater than 100 cm/s (~ 2 kts.) on several occasions. The dynamic height gradients (Fig. 10) for stations 1–11 (Seward Line) indicate the possibility of very low speed baroclinic flow with baroclinic

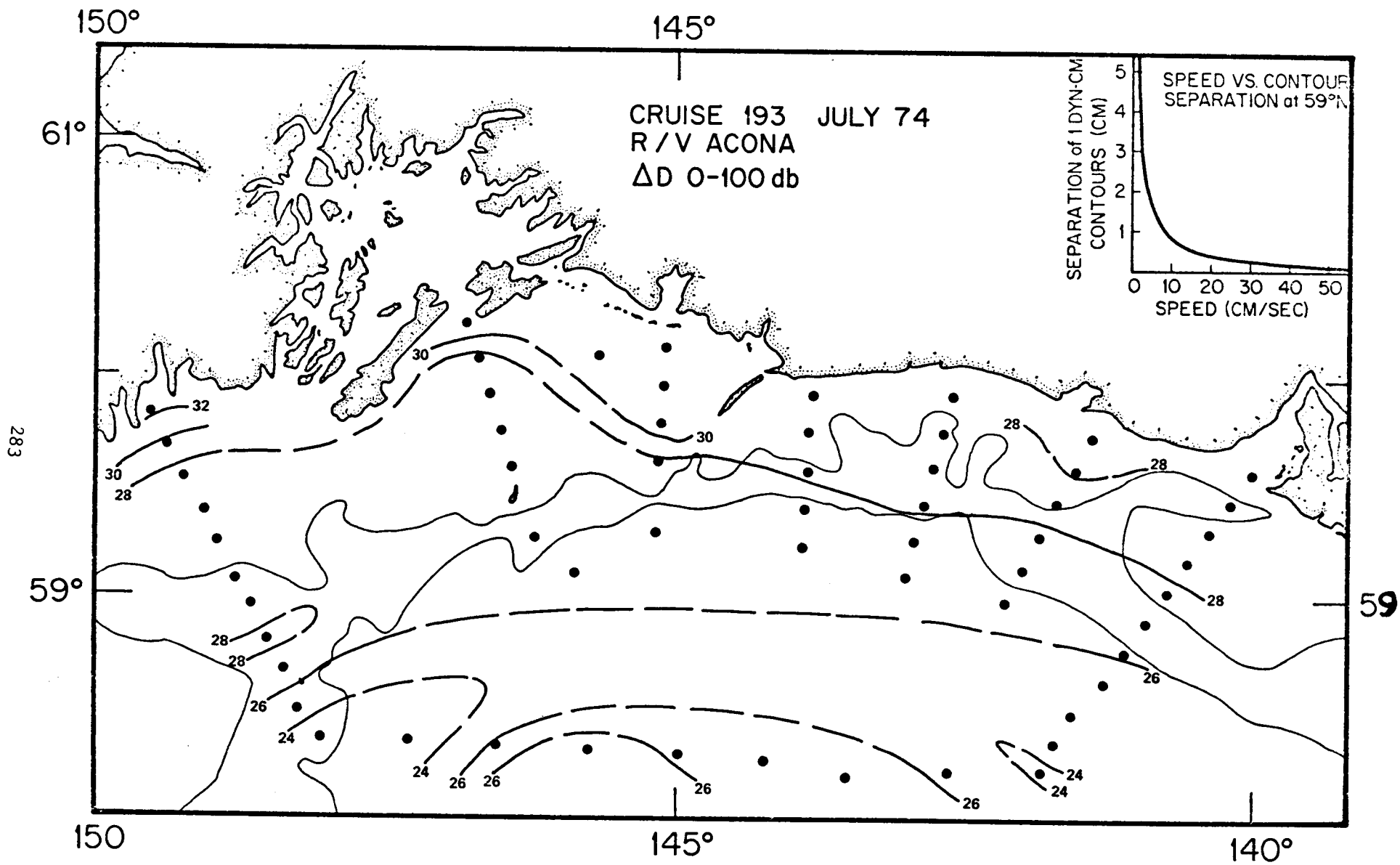


Figure 3. Dynamic topography.

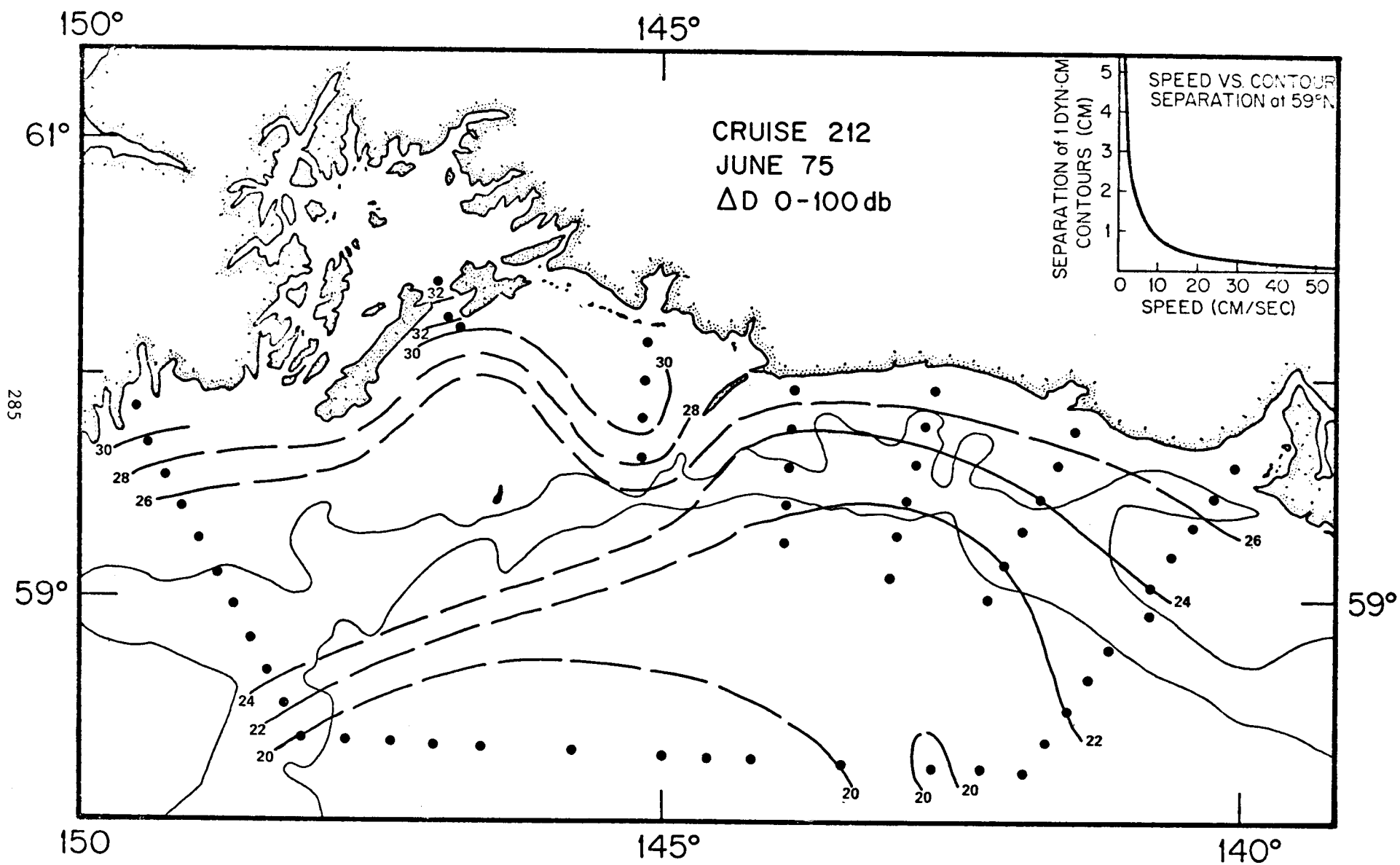


Figure 5. Dynamic topography.

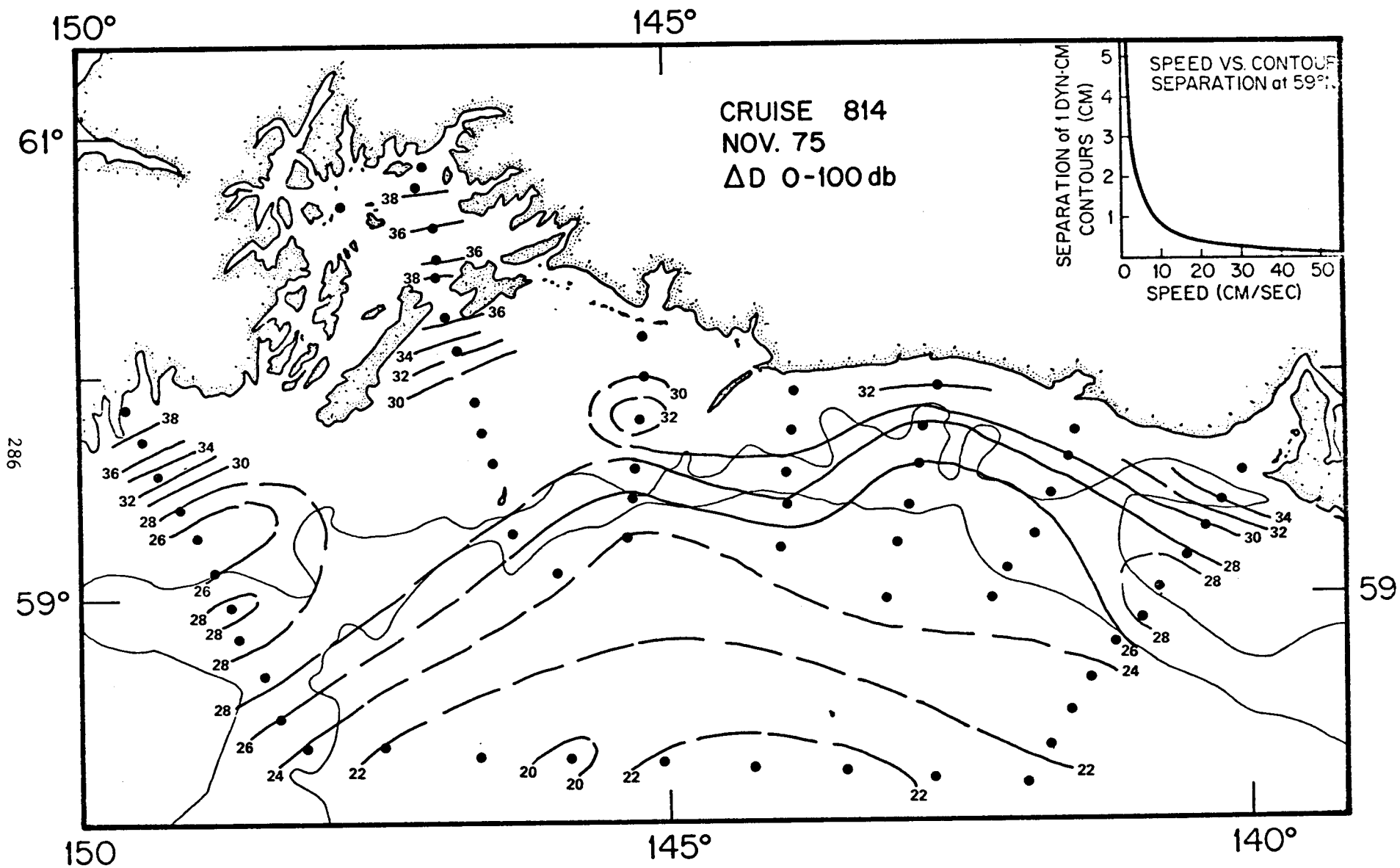


Figure 6. Dynamic topography.

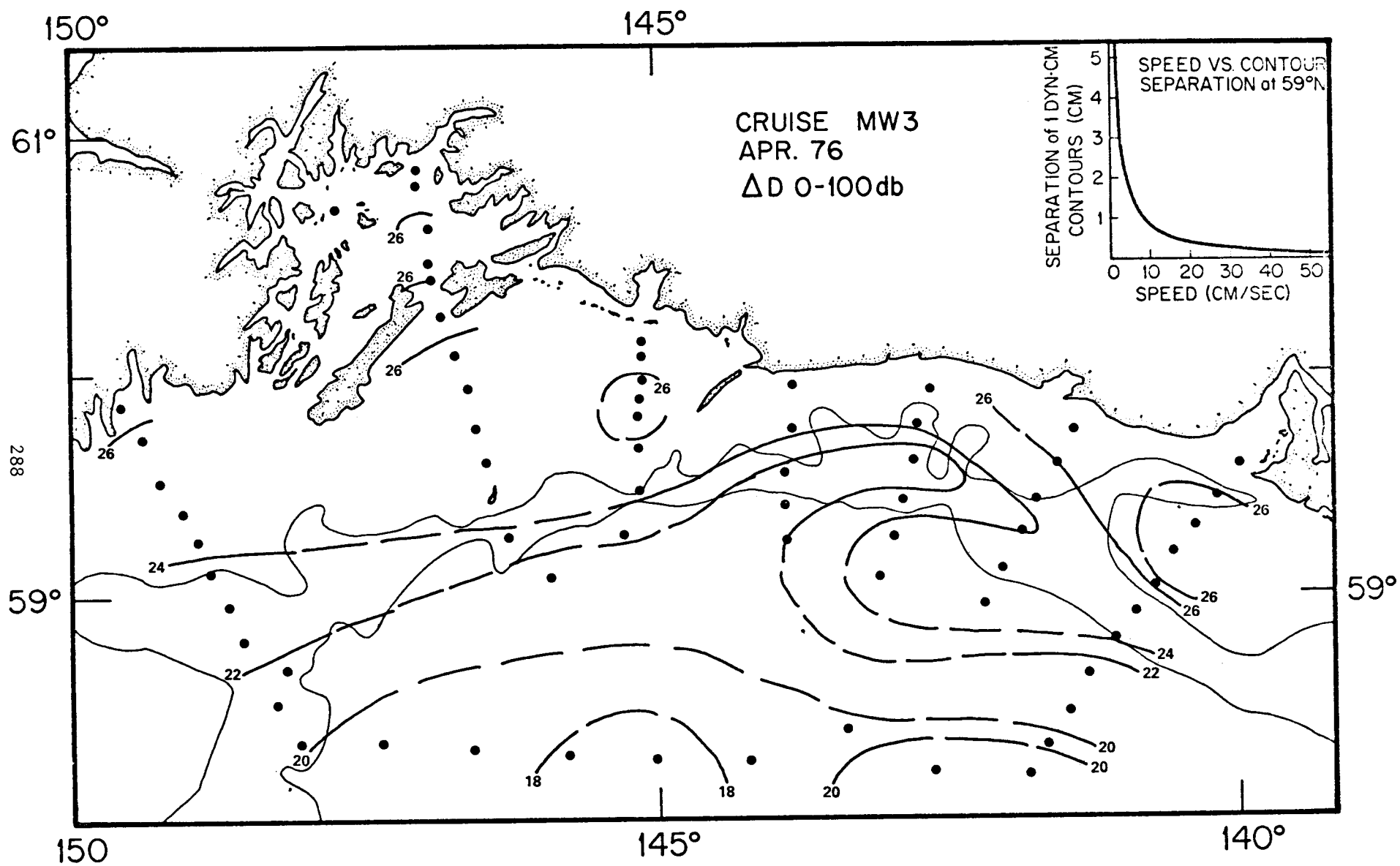


Figure 8. Dynamic topography.

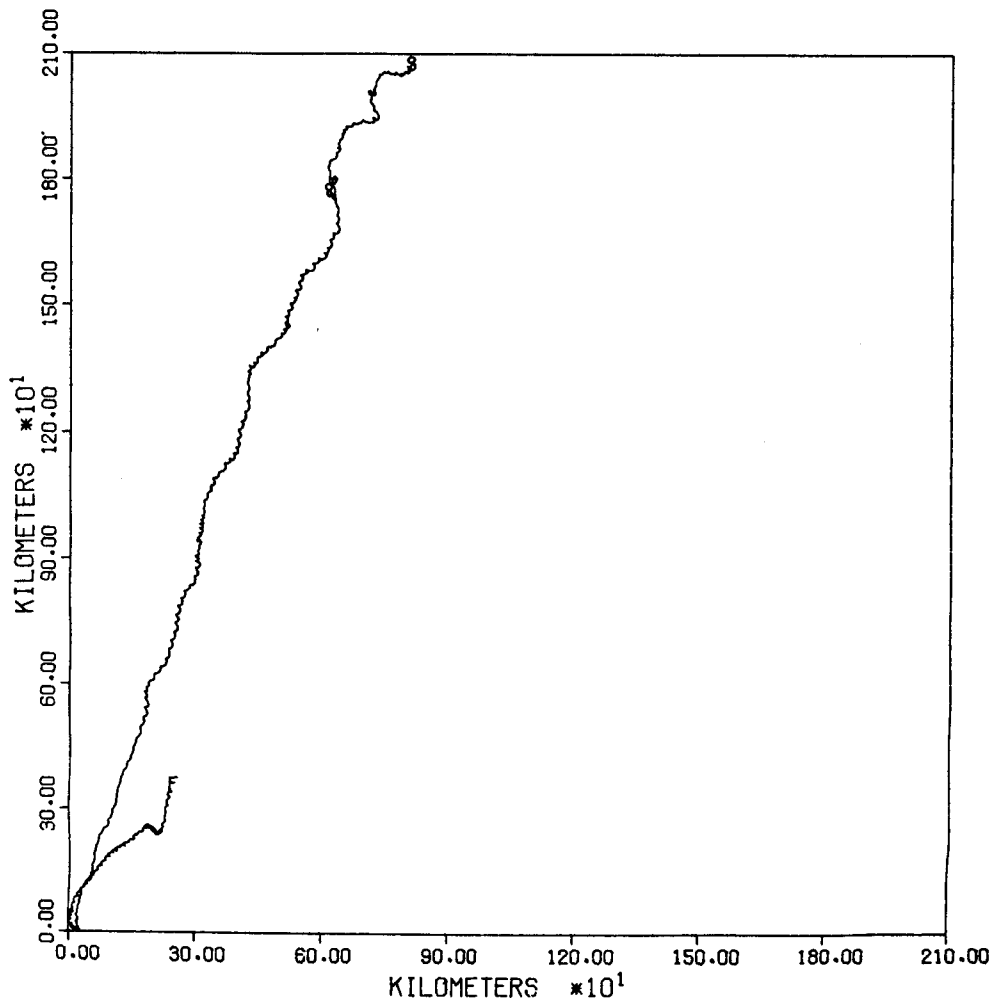
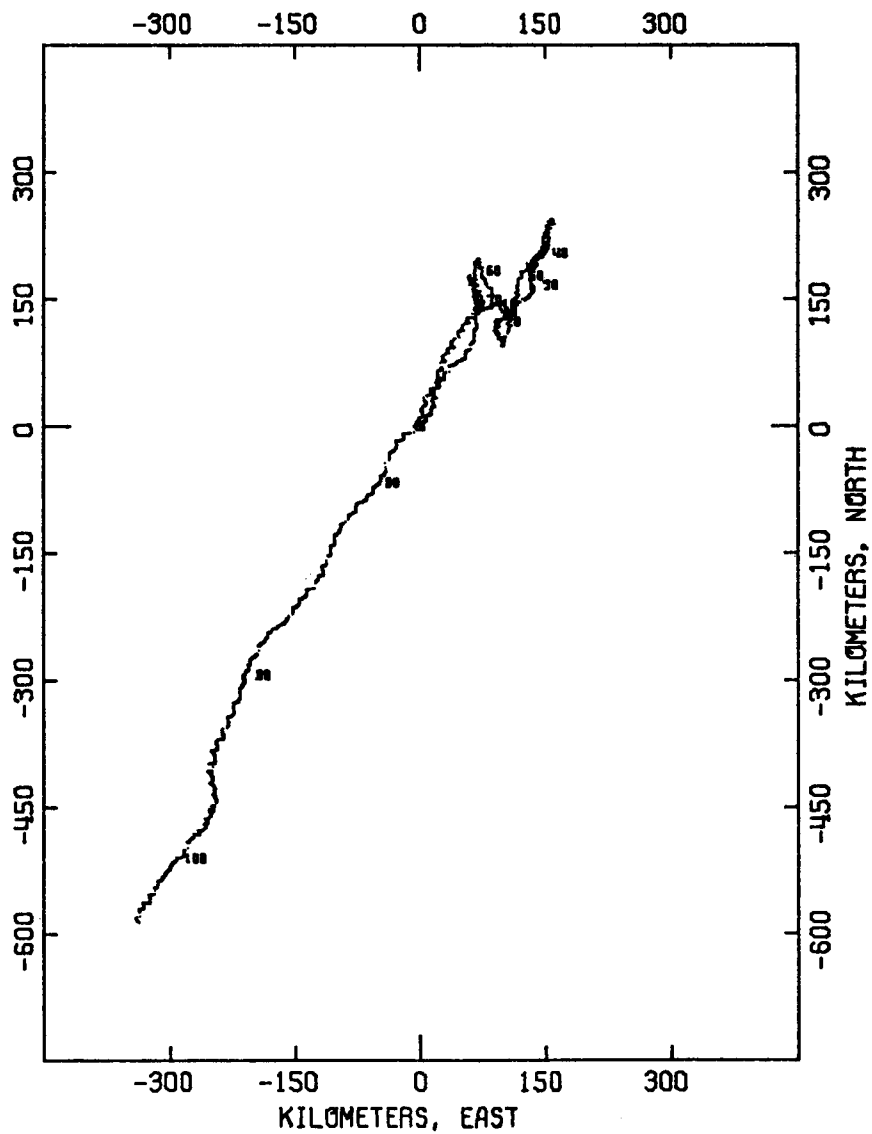


Figure 9a. Progressive vector diagram for station 9 at 20 m, April - July, 1976. Southwesterly flow until July when it became northeasterly.



METER NO. 1770 AT 54 M.

STATION GASS-9C, 58 44.76 N, 148 25.13 W.

RECORD FROM 2224 UT 23 JUL TO 0224 UT 4 NOV 1976.

Figure 9b. Progressive vector diagram for station 9 at 20 m, July - November, 1976. North-easterly flow until October when it became southwesterly.

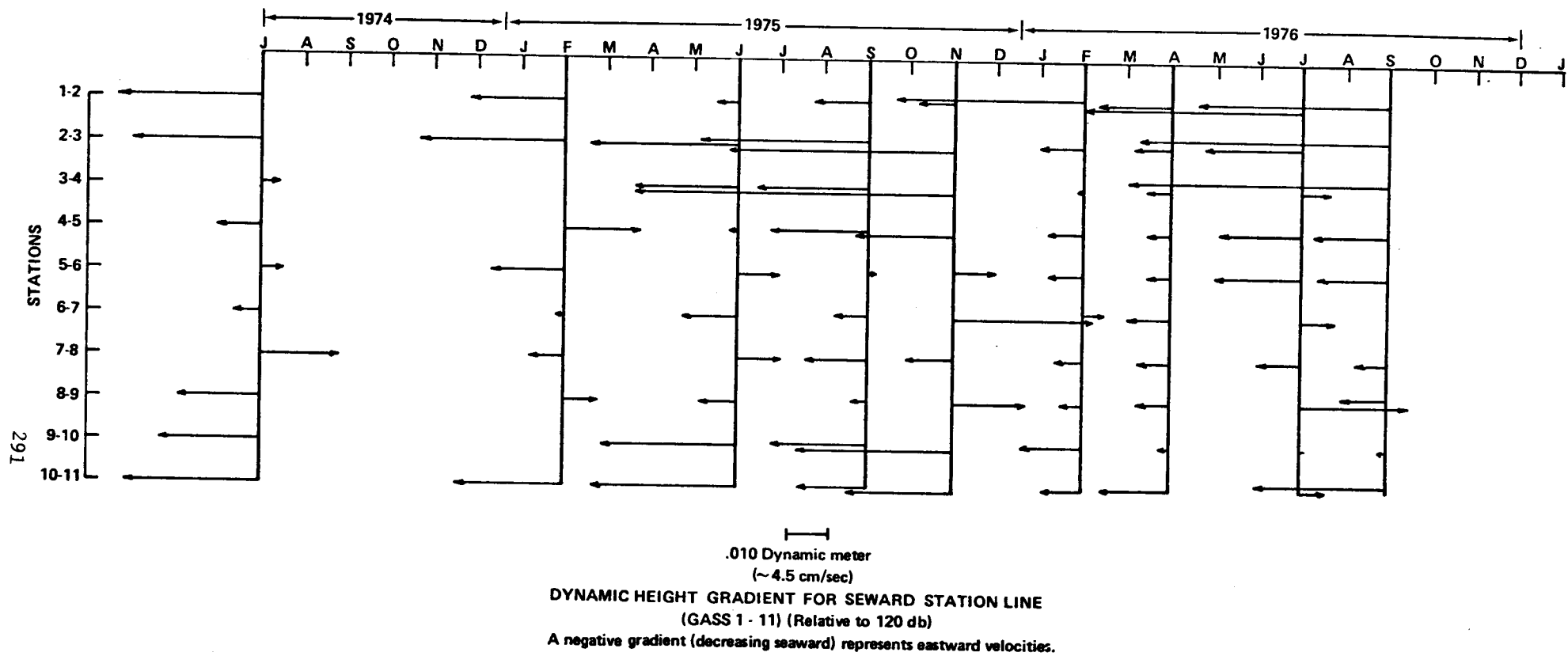


Figure 10. Dynamic height gradients for Seward line.

reversals somewhere in the middle of the transect. Actual current meter data were required on this line to confirm the actual current reversals. Unusual oceanographic conditions existed in the deep water adjacent to Seward and Kodiak in July 1976. It is not believed that these conditions are responsible, however, for this reversal in flow. These offshore conditions did result, though, in a dramatic increase in the baroclinic flow in the Alaska Stream off Kodiak from the usual flow of about 7 Sv (1 Sv= $10^6 \text{ m}^3/\text{s}$) to about 13 Sv (Fig. 11).

Numerical model experiments are presently being carried out using a non-linear, n-layered two dimensional time dependent cross-sectional model of the Seward line on the Alaskan Shelf. The model has been adapted from Great Lakes work (Bennett, 1973; Niebauer, 1976) and includes Coriolis force, vertical and horizontal viscosities and diffusivities, stratification and bottom topography. Given the appropriate initial and boundary conditions, the model generates temperature, salinity, and velocity fields in time and space. These data allow direct comparison with the collected hydrographic and current meter data. At present, the emphasis is on modeling "events" of duration 7-10 days. The model is being used to evaluate the relative importance of the forcing functions over the region, such as wind stress, topography and runoff.

The results of a study using sea level to determine offshore currents shows that the sea levels at Seward are directly related to the dynamic height at GASSE 1. Also shown was the fact that the dynamic height variations at GASSE 1 are independent of the variations at GASSE 11 on a seasonal basis. This indicates that the flow variations at the coast and offshore are independent, that is shelf circulation is separable from deep ocean circulation in the region of Seward.

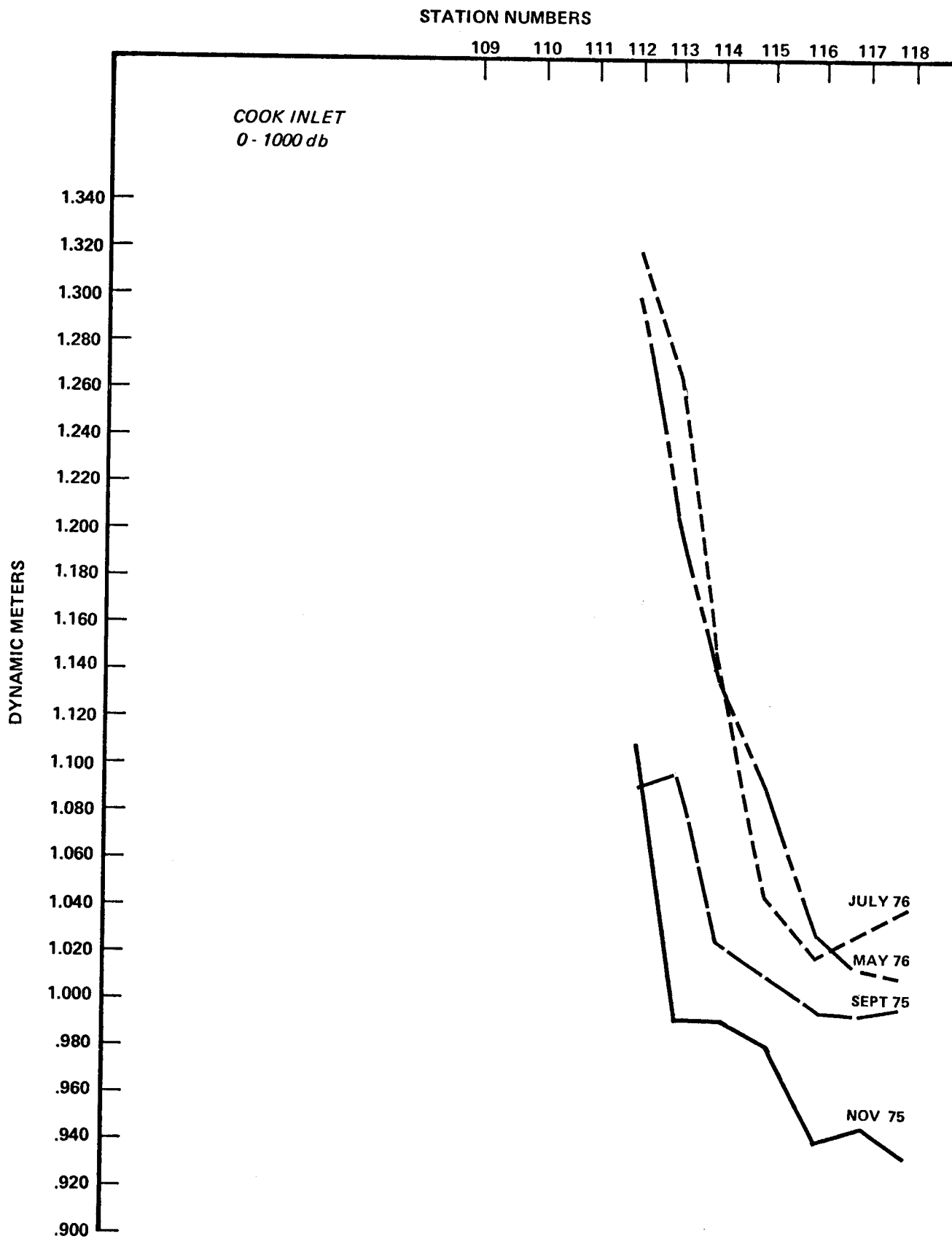


Figure 11. Dynamic height for Cook Inlet line.

Those hydrographic data gathered primarily as input for J. Galt's numerical model have been briefly analyzed to evaluate flow around Kodiak Island. These data appear to contain some information not fully utilized in the modelling effort. For example, extreme baroclinic shears exist in some of the data but are masked by a depth integration within the model. Although, surface and subsurface flows have been occasionally found to be in opposite directions, this fact will be hidden by the model. The data show that most of the shelf area east of Kodiak Island has very low speed baroclinic flow with possible reversals and/or eddies. On the other hand, the Alaska Stream along the shelf break is a swift (1-2 kts.) current flowing to the southwest and seems to form a dynamic boundary.

In support of the main objectives of the satellite work, a background archive has been set up to continually review all NOAA-VHRR daytime passes covering the coast of Alaska. This archive is based on special work, predominantly IR enhancements, completed during the experimental Alaska environmental satellite research in 1974 and 1975. The archive consists of negatives, contact prints and enlargements. The negatives have been cataloged.* Unreleased specially enhanced negatives for 1976 are stored at Gilmore CDA station. Prints are filed in ring binders that can easily be studied by other investigators without disturbing the others. They contain the following main groups in chronological order starting with 1974:

1. Arctic Ocean and Bering Sea
2. Gulf of Alaska to Aleutians

* A running catalog is also kept of the IR enhancements showing the temperature ranges used.

The above areas are continually monitored. Enlargements and IR enhancements are made of any features thought to be of interest. When ocean areas are clear temperature enhancements of the IR grey scale are made to emphasize surface currents, upwelling and ice cover.

During the course of the NOAA satellite project certain digitized tapes containing data of special interest were saved by different investigators in the project. These tapes have been cataloged to show features of interest, geographical coverage and location of storage.

When requested, assistance in interpretation of the satellite data, copies, selected temperature enhancements, and enlargements have been supplied to other investigators. Minor projects have been undertaken to provide answers to specific questions like: "Why is there a delay in bird migration to St. Paul Island as compared to nearby St. George Island in the Pribilof Islands". The interested investigator, upon request, has been supplied with appropriate satellite data and comments.

Satellite images are being used to extend the hydrographic observations to define surface features (see Royer and Muench, 1977). They have been used to help establish flow regimes in the Gulf of Alaska. For example, they give indications of eddies or localized flows near Kodiak Island.

In addition to the routine processing of current meter and pressure gauge data from our moorings, procedures are being established for the integration of these data with the hydrographic data. The baroclinic and barotropic current components will be estimated from these data. This includes the incorporation of sea level and atmospheric pressure data with the pressure gauge data. The weather observations at EB-03 (58°W 147°W) are being compared with local observations at Middleton Island and Kodiak for possible correlation. They are also being used as a "ground

truth" for the larger scale wind computations. The oceanographic data from EB-03 and elsewhere will also be used to determine anomolous conditions.

VII. DISCUSSION

Hydrographic data are now available to other OCS principal investigators in the Gulf of Alaska upon request. These are in the form of vertical profiles for individual stations and cross-sections across the shelf. Baroclinic currents and transports are also available.

A major accomplishment of this study during the past year has been the identification of flow regimes for various regions in the Gulf of Alaska. These regimes are (Figs. 1, 2):

- A. Yakutat
- B. Central
- C. Copper River
- D. Prince William Sound
- E. Western
- F. Aleutian

The Yakutat regime is characterized by small net transports with possible eddies and reversals. The Central regime has consistant flow and is under considerable influence of the Alaska Stream offshore and fresh water sources along the coast. Near Kayak Island, the flow on the shelf separates with part entering the gyre west of Kayak Island and part flowing along the shelf break south of Middleton Island. Beyond this point, the Alaska Stream is characterized by a fresh water filament at the surface as it flows along the shelf break. The other portion of the flow around Kayak Island passes to the north of Middleton Island with some unknown percentage entering Prince William Sound as evidenced by the satelllite tracked Lagrangian drifter study. The Copper River regime is found between Kayak Island and Hinchinbrook Entrance and it is discussed

in detail in Appendix II. The Prince William Sound regime is discussed in a recent work by Schmidt (1977). West of Middleton Island there is a baroclinic coastal jet, weak midshelf flow with reversals, and an outer dynamic boundary formed by the Alaska Stream. This is the Western regime. It extends from Middleton Island to the west beyond Kodiak Island. The point at which the flow once again becomes a uniform longshore flow is not clear. However, the Aleutian regime has characteristics similar to that of the Central regime where there is influence from the Alaska Stream and fresh water outflow along the coast. This results in a uniform longshore flow over the shelf. Apparently, the Alaska Stream forms an outer boundary for all of these regions but most directly influences the shelf circulation in the Central and Aleutian areas. Local effects over the shelf are probably more important in areas other than the Central and Aleutian regimes.

The fact that flow is continuous between these regions should be emphasized. Water and/or pollutants in one region will be found in "downstream" regimes. The residence time will vary from regime to regime with the Central and Aleutian regions having the shortest residence time. Prince William Sound or the Western regime might have the longest residence time. It also might be possible that Prince William Sound is occasionally "downstream" from Kodiak Island.

Other ramifications of this continuity of flow are that the outflow from Icy Bay is found with the Alaska stream off Kodiak Island and that the Copper River outflow is contained in the coastal jet which flows adjacent to the coast. Sediments from the Copper River are found in Cook Inlet. Fresh water added to the coastal current forces the sediment-laden Copper River water to disappear from the surface between Prince William Sound and Cook Inlet.

The Western regime appears to be very complex and deserves more attention. It has two strong westward flows with a region of variable, low velocity flow between them. It is not expected that the entire shelf flow in the Western regime reverses as might be interpreted from current meter data at GASSE 9. Instead, the circulation is probably characterized by filaments of reverse flow. The data may show a north-south movement of a boundary between east and west flow when the current reverses at GASSE 9. This would allow reverse flow at all times of the year. It should be possible to determine the validity of this assumption with the data at hand.

Another aspect of the division of the region into various flow regimes is that the annual changes in the water mass properties on the Seward line might be typical only of that regime. Once again, evaluation of the existing data will be used to answer this question. Wind stress probably has a relatively large influence in these regions of low flow and the results of the numerical modelling should be able to evaluate the effects of wind stress on the ocean over this region.

Evaluation of seasonal changes in the currents in the Gulf of Alaska is being done in this program. The absence of a strong seasonal trend in the baroclinic flow in the Alaska Stream was a surprising result. There is, however, a large seasonal cycle in dynamic height at the coastline. This indicates that the maximum flow in the coastal jet occurs in October or November. However, the midshelf flow does not have as strong a seasonal signal as the coastal area.

VIII. CONCLUSIONS

The circulation over the continental shelf region in the northern Gulf of Alaska from Yakutat to Unimak Pass can be divided into at least six

regimes (seven if Cook Inlet is included). These regimes are characterized by different transports and driving mechanisms. That the area can be divided into regimes is a reasonably firm conclusion, though the boundaries and the important driving mechanisms are tentative. Strong evidence exists to support the concept of long residence times in the Copper River, Prince William Sound and possibly the Western regimes. Of all the regimes, the least is known about the circulation of Prince William Sound, because little data is available for this region. It is also probably the most likely area to be impacted by oil and gas development. Evidence for a coastal jet from the Copper River area to Cook Inlet is reasonably strong. The circulation in the area of the gulf east of Middleton Island is probably known well enough to forego further field efforts at this point. The possibility of eastward flow in the Western regime links the Kodiak lease area with Prince William Sound. This must be stated as a very tentative conclusion until further data analysis is accomplished. However, strong evidence exists for slow currents on the shelf east of Kodiak Island with numerous baroclinic eddies in the system.

The movement of drifters into Prince William Sound must be viewed with reservations. The drifters would lead one to believe that nearly all flow goes through the sound after remaining behind Kayak Island for several weeks. We know that this is not possible. However, the need for better information of flow into and out of Prince William Sound is obvious, especially in light of the expected long residence times. The coastal jet in this vicinity could rapidly carry pollutant not entering the sound to the western Gulf.

The knowledge of flow near Kodiak is limited. The weak baroclinic flow with possible reversals can be masked entirely if one assumes a large

enough barotropic component. An overestimate of the barotropic current to the southwest would give an improper conclusion that all transports are toward the southwest.

The research in circulation and water masses of this region has reached the point where interactions with other disciplines can be mutually beneficial. For example, since the water masses are nearly continuous around the Gulf of Alaska, highly productive regions might represent areas of low net flow where organisms are not swept out of the area. The biologists could help the physical oceanographers identify low velocity regions by defining high productivity areas. Of course, other factors in some cases might be more important than low velocities alone. Finally, input from geologists has been helpful in strengthening the coastal jet concept through the tracing of sediments.

IX. NEEDS FOR FURTHER STUDY

Of primary importance are detailed studies of the Kodiak Island shelf region and Prince William Sound. Both studies require direct current measurements and hydrographic work. The inflow and outflow of Prince William Sound should be monitored along with identification of the water masses entering and leaving the sound. The baroclinic flow on the shelf east of Kodiak Island should be monitored on a seasonal basis and these data combined with direct current measurements from arrays. In both of these detailed studies it will be necessary to measure the local winds. The duration of these studies should be at least one year. The Kodiak Island study should be combined with a general study of the circulation of the Aleutian region for which insufficient data is now available. This particular study will allow the better definition of the boundaries

of regimes as mentioned previously in this report. In order to determine the regimes boundaries and to monitor flow reversals between the NE Gulf of Alaska and the Kodiak Island region, the Seward transect should continue to be occupied on a seasonal basis. The Seward transect data is the longest hydrographic time series for the region and is of value in detecting anomalous conditions.

Attempts should be made in the following year to integrate the physical oceanography between regions. It is apparent that the lease area boundaries do not represent flow regimes and the interaction between regions is extremely important. In this sense, care should be taken not to ignore regions between lease areas such as the northwest Gulf of Alaska. Also, the Aleutian area should be connected with the Bering Sea leases since it possibly represents an upstream region.

REFERENCES

- Bennett, J. R. 1974. On the dynamics of wind-driven lake currents. *J. Phys. Oceanogr.* 4:400-414.
- Dodimead, A. J., F. Favorite and T. Hirano. 1963. Review of Oceanography of the Subarctic Pacific Ocean. *In* Salmon of the North Pacific Ocean. International North Pacific Fisheries Commission, Bulletin No. 13. 195 pp.
- Favorite, F., *et al.* 1976. Annual report to BLM/OCS.
- Favorite, F., A. J. Dodimead and K. Nasu. 1976. Oceanography of the Subarctic. Pacific region, 1960-1971. International Fisheries Commission, Bulletin No. 33. 187 pp.
- Fofonoff, N. P. 1962. Dynamics of ocean currents. *In* M. N. Hill (ed.), *The Sea*. Vol. I, Interscience, New York. pp. 323-395.
- Galt, J. A. and T. C. Royer. 1975. Physical oceanography and dynamics of the N.E. Gulf of Alaska. Paper presented at Arctic Institute Symposium on the Gulf of Alaska, Anchorage, October 1975. 14 pp.
- Hayes, S. and J. Schumacher. 1976. Description of wind, current and bottom pressure on the continental shelf in the northeast Gulf of Alaska from February to May 1975. 81(36):6411-6419.
- Niebauer, H. J. 1976. Wind driven coastal upwelling in Lake Superior. Ph.D. Thesis, Univ. Wisconsin, Madison. 264 pp.
- Reid, J. L. and A. W. Mantyla. 1976. The effect of geostrophic flow upon coastal sea elevations in the northern North Pacific Ocean. *J. Geophys. Res.* 81(8):3100-3110.
- Royer, T. C. 1975. Seasonal variations of waters in the northern Gulf of Alaska. *Deep-Sea Res.* 22(6):403-416.
- Royer, T. C. and R. D. Muench. 1977. On the ocean temperature distribution in the Gulf of Alaska, 1974-1975. *J. Phys. Oceanogr.* 7(1):92-99.
- Schmidt, M. 1977. The exchange of water between Prince William Sound and the Gulf of Alaska. M.S. Thesis, University of Alaska. 114 pp.

X. SUMMARY OF 4th QUARTER OPERATIONS

Ship Activities

1. Ship schedule
27 March-1 April 1977, *Miller Freeman*, NOAA
2. Scientific Party
William Kopplin, IMS, University of Alaska
3. Methods - Standard CTD sampling
4. Ship tracklines - occupied Seward and Cook Inlet lines and recovered the current meter array at IMS9 (58°41'N, 148°21.6W).
5. Data collected - (Unknown at the time of this writing, but will be included in next quarterly report.)
6. Milestone chart

Problems Encountered

The funding delay for this project has caused some serious delays in producing some of our data products. The primary effect was a delay in the purchase of a graphics terminal and the development of the associated software. We are at about six months behind our original schedule. The graphic products for the Annual Report are therefore more limited than originally planned.

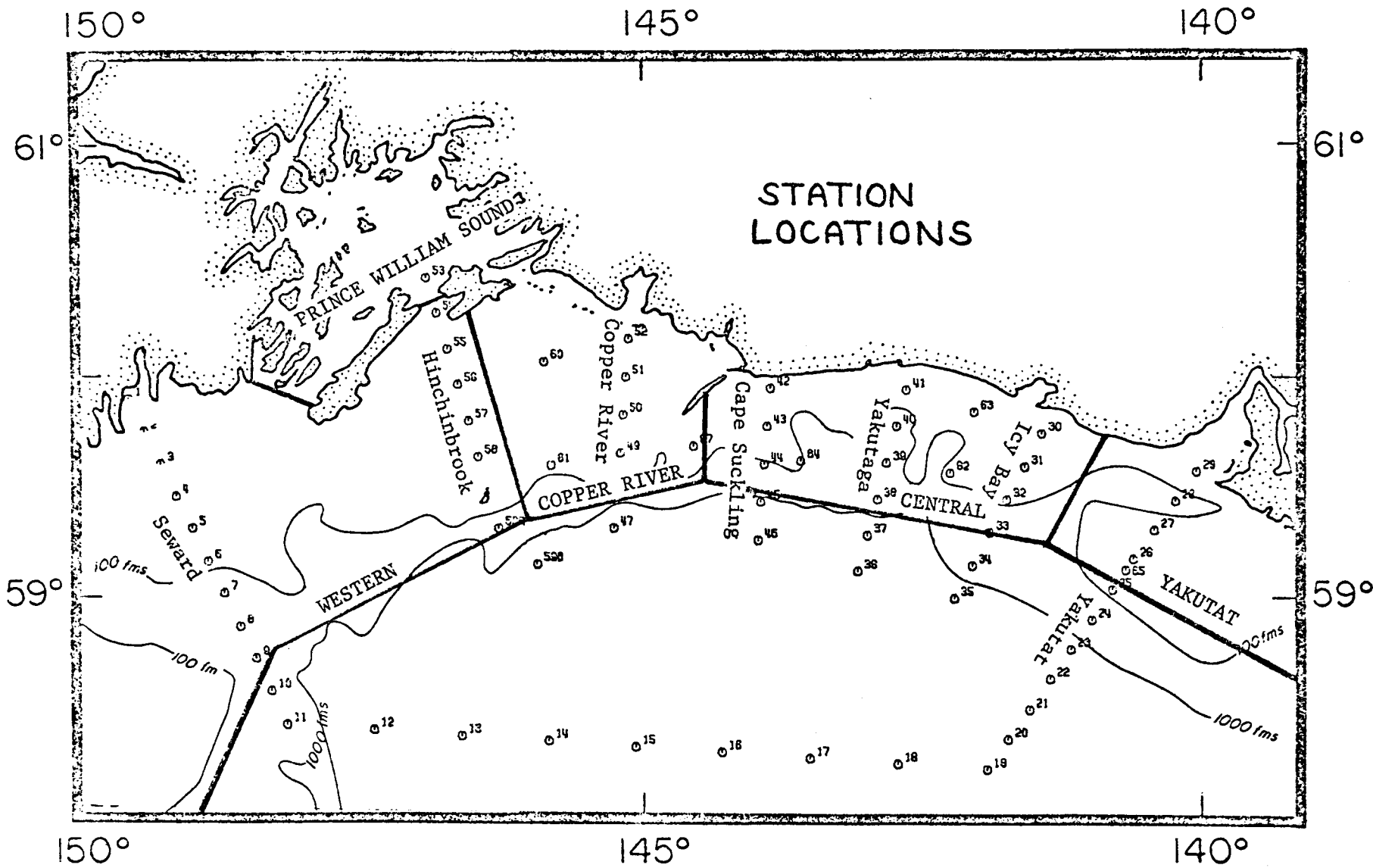
There is considerable concern over the role of project personnel aboard the NOAA vessels. The concern is brought about by the use of PMC CTD manual and an apparent change in the chief scientist position as reflected in the recent ship project instructions. We have forwarded a critique of the manual but have had no feedback nor have we seen a copy of the revised manual. While it may be agreed upon at some point in the future that the NOAA ships could gather the CTD data without project personnel aboard,

this change in policy should come from the participants. The entire program is based on data whose quality must be defended by the Principal Investigator. The data control has now been removed from the PI without relieving him of the responsibility for its quality.

Delays are continually encountered in receiving current meter data from PMEL. Neither printout nor magnetic tapes of the current meter data sent to PMEL in August 1976 have been received. This is in contrast to the data from the mooring recovered in November 1976, for which data was received prior to 1 January 1977. The latter tapes were sent to Aanderaa in British Columbia for processing since it was correctly anticipated that the results would be important to the NEGOA synthesis meeting.

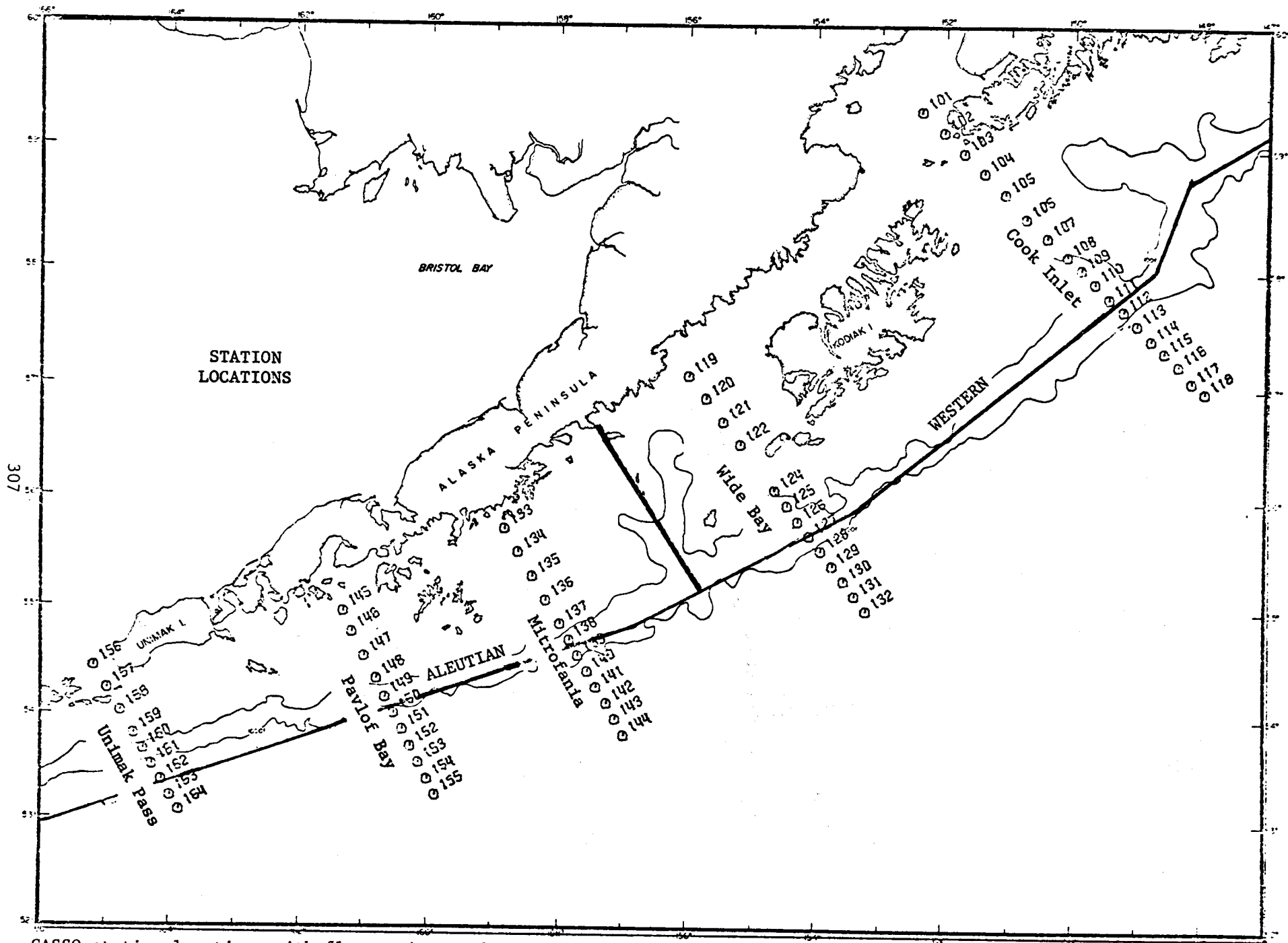
XI. APPENDIX I

CROSS SECTIONS OF SALINITY, TEMPERATURE AND DENSITY VERSUS DEPTH
FOR THE GULF OF ALASKA, SEPTEMBER 1975

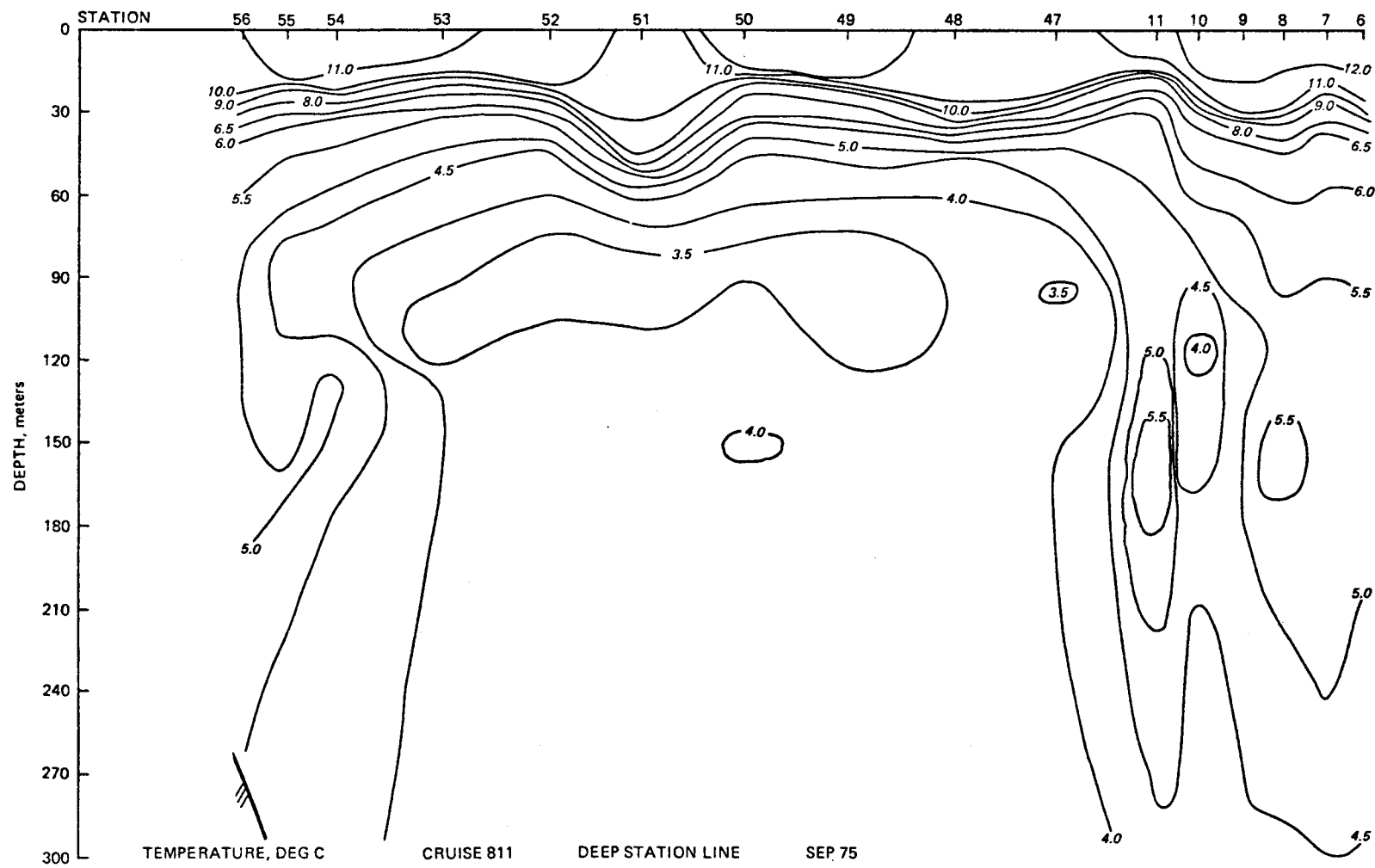


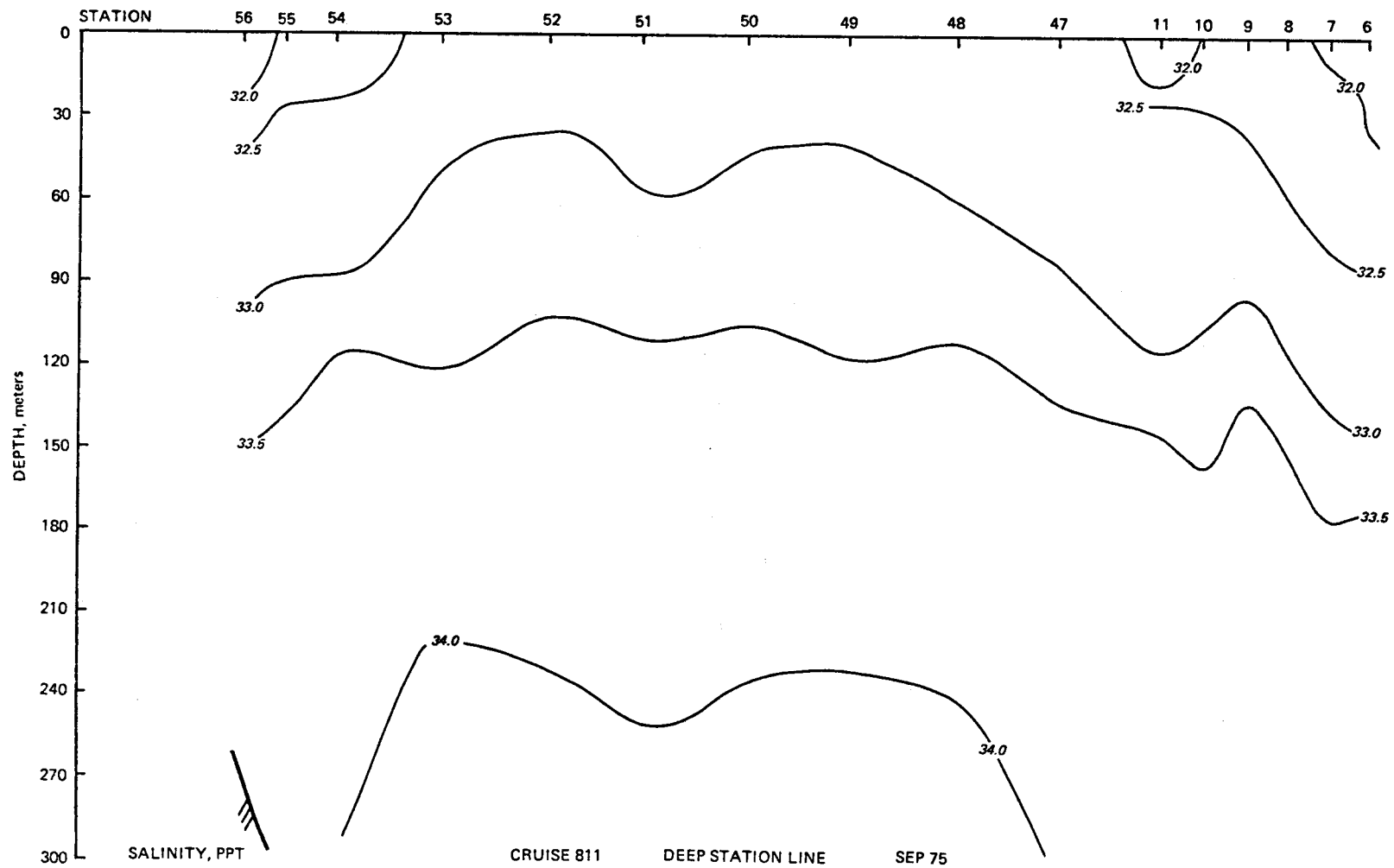
306

GASSE station locations with flow regimes and transect names.

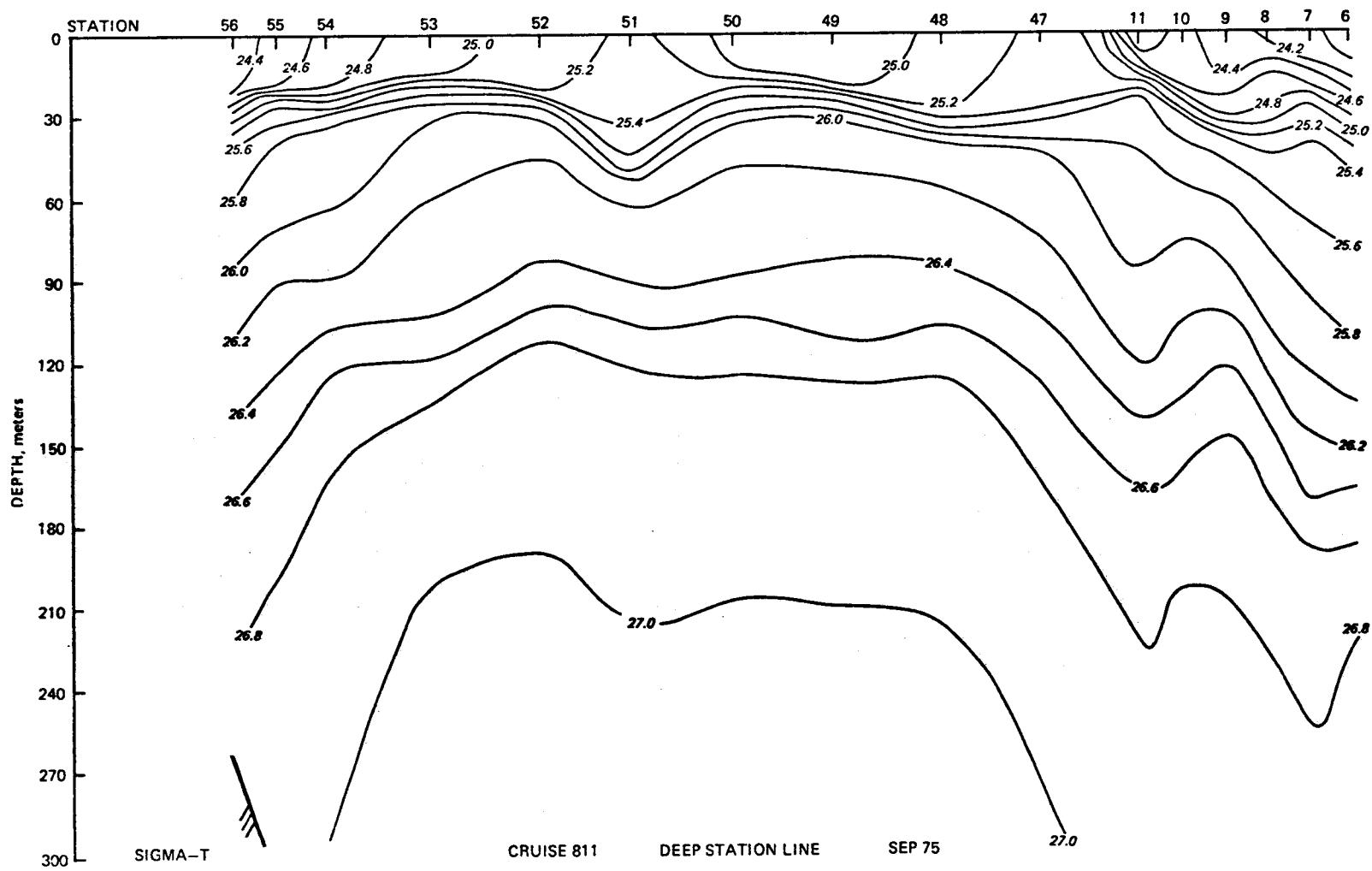


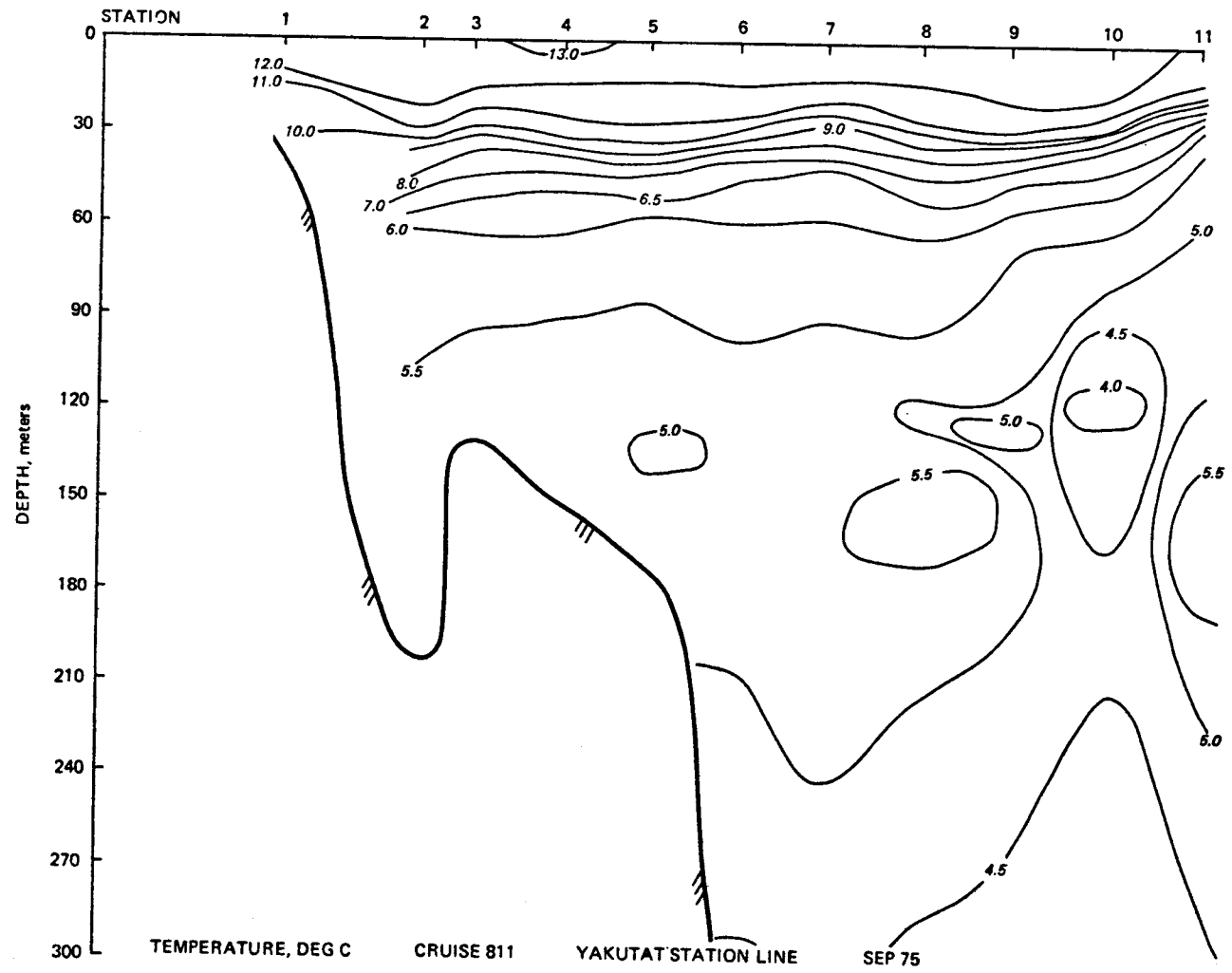
GASSO station locations with flow regimes and transect names.

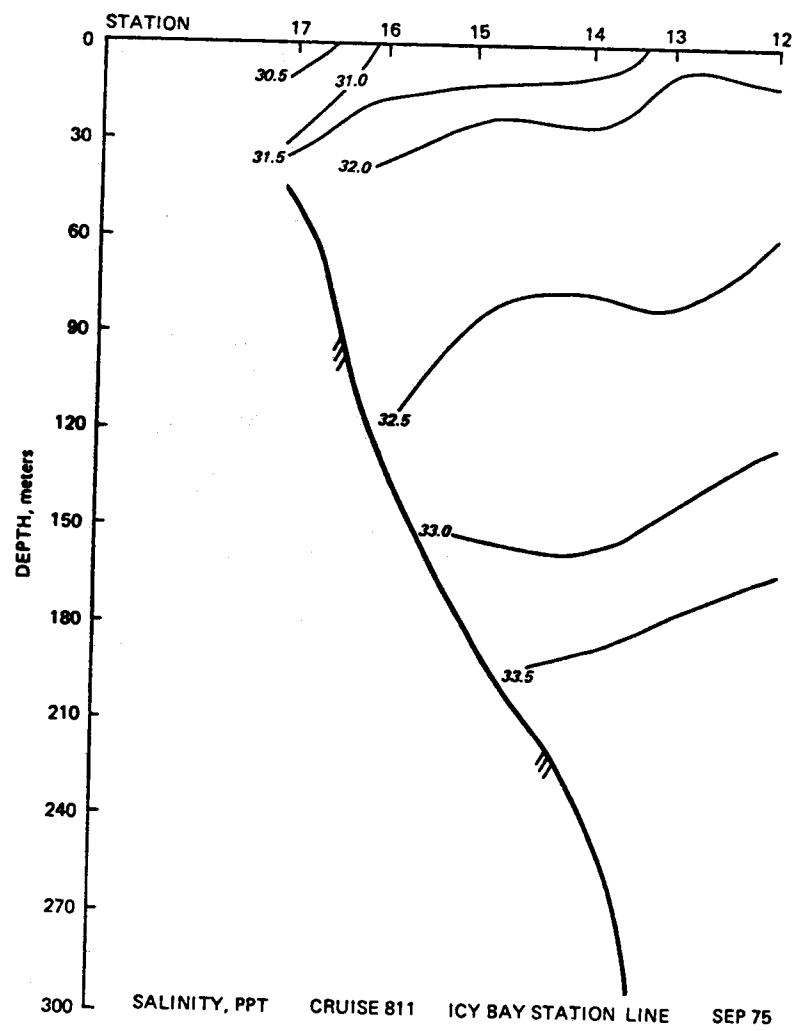


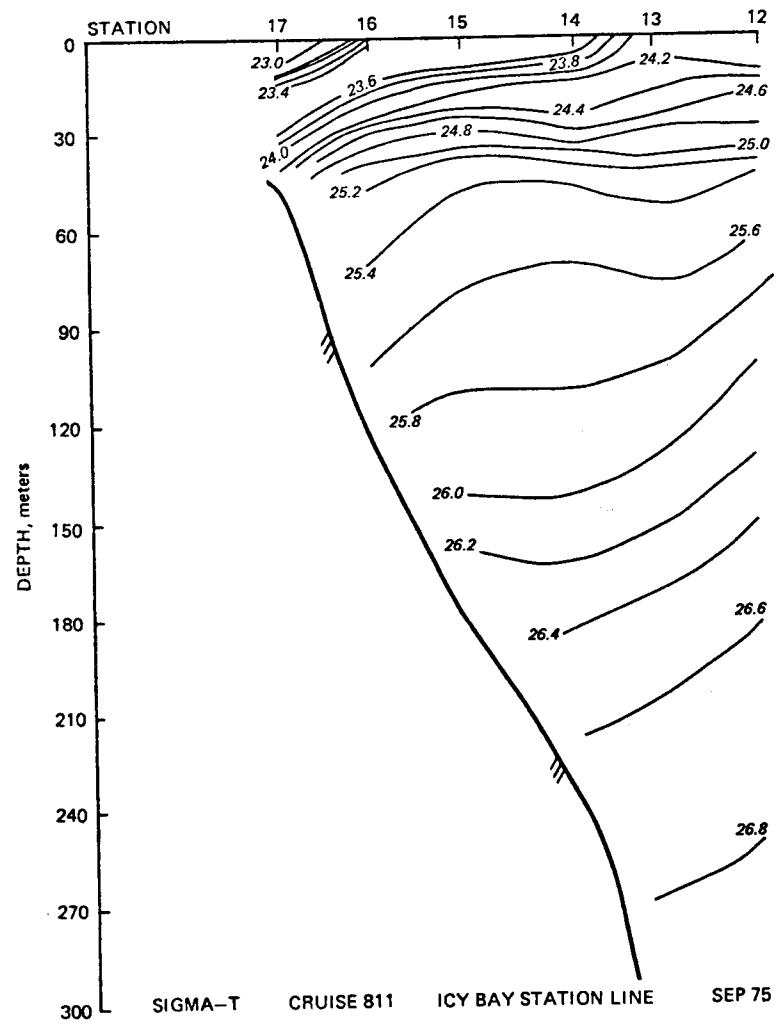


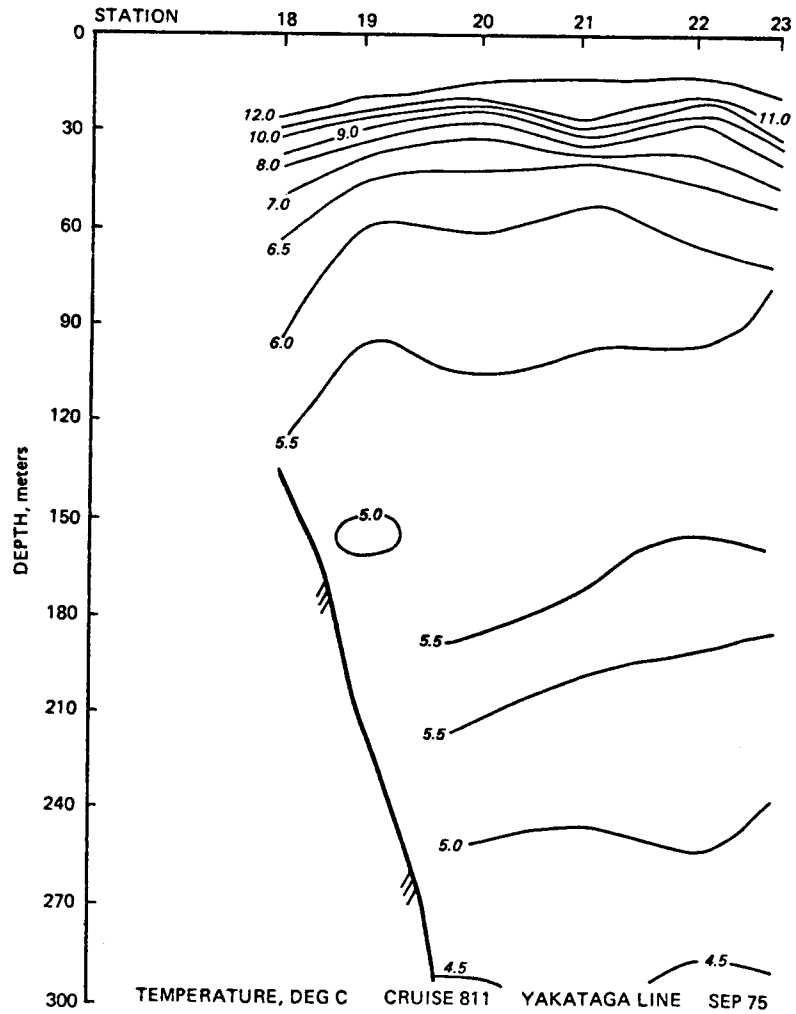
310

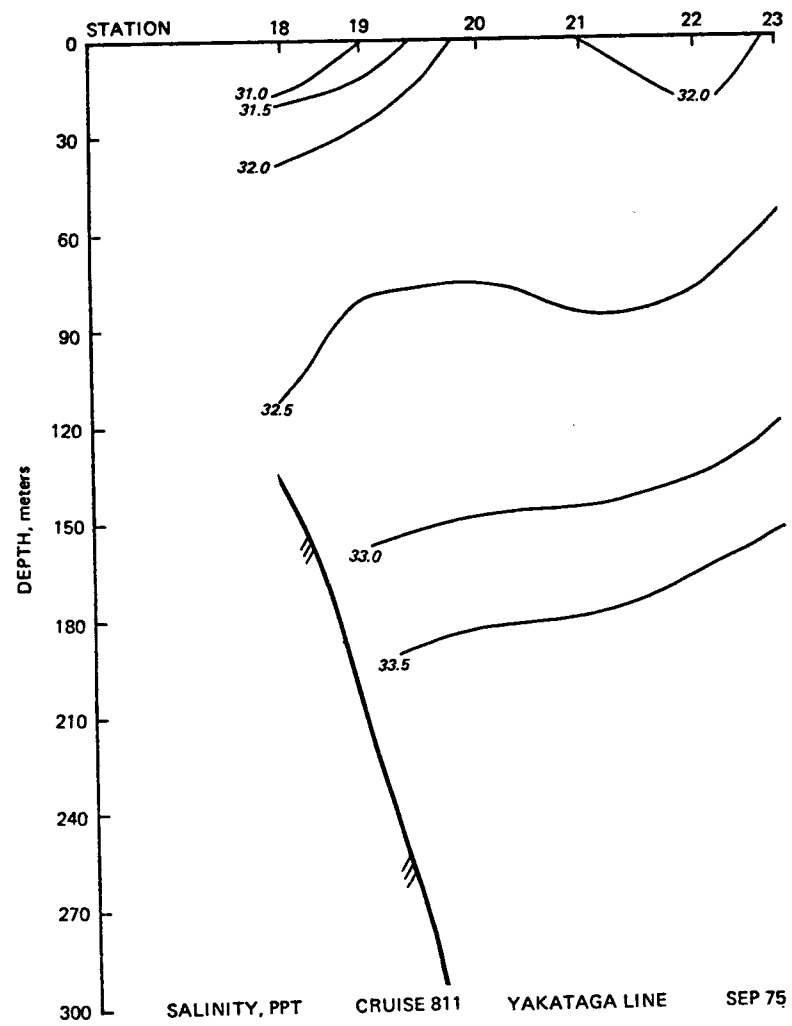


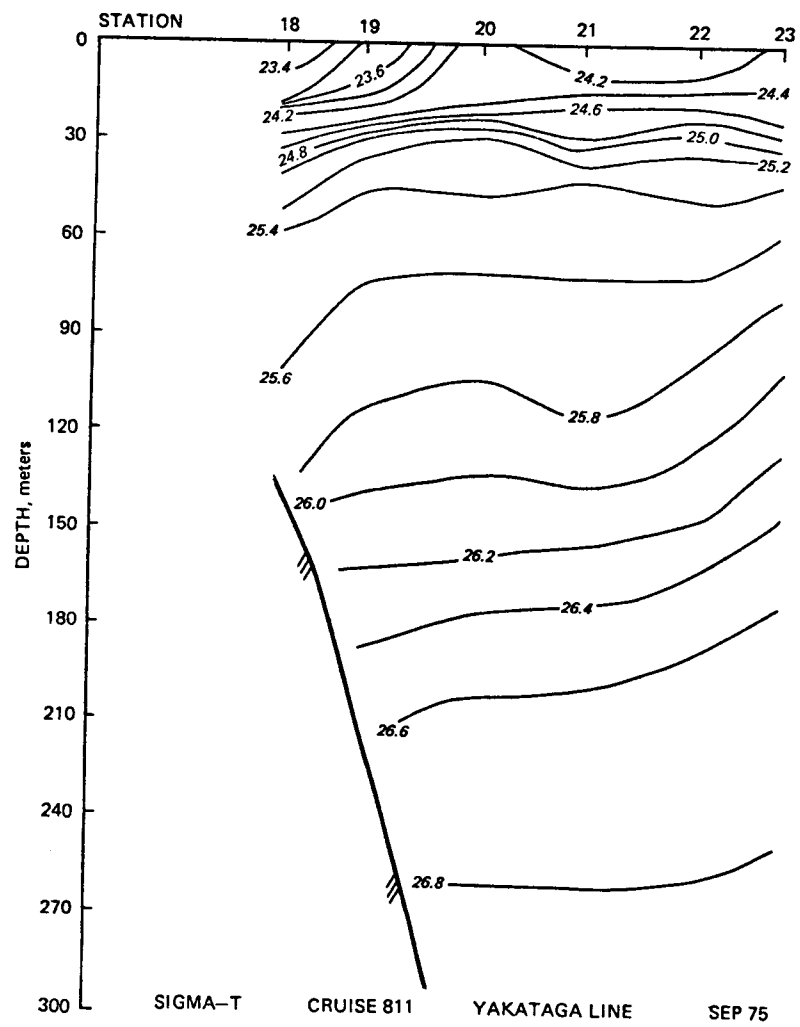


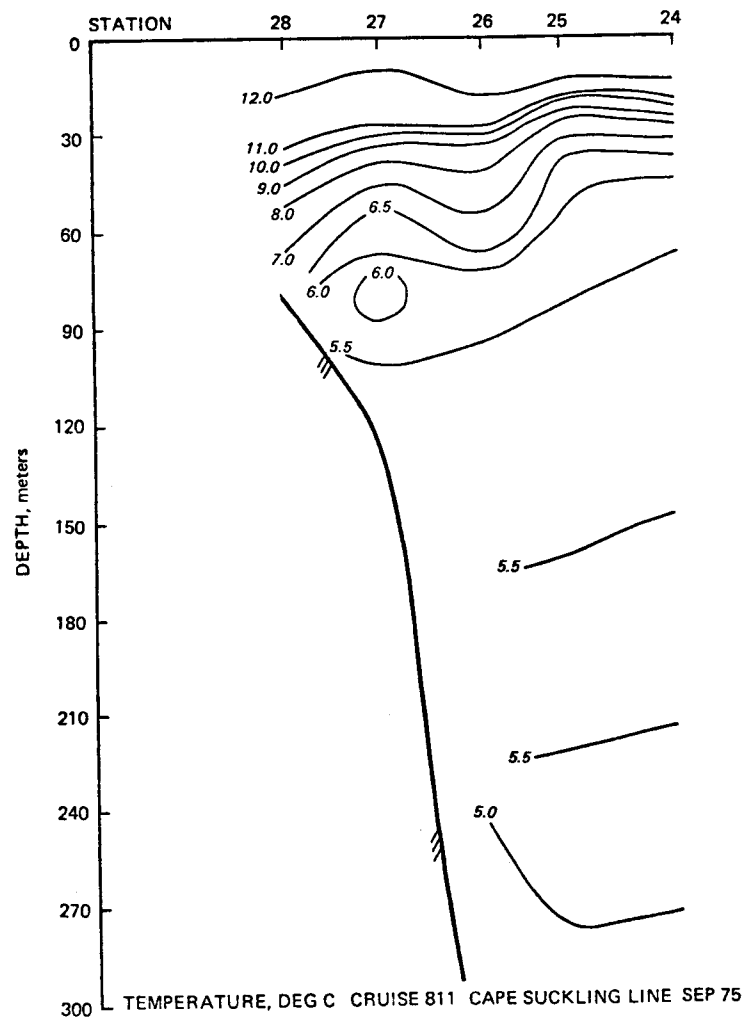


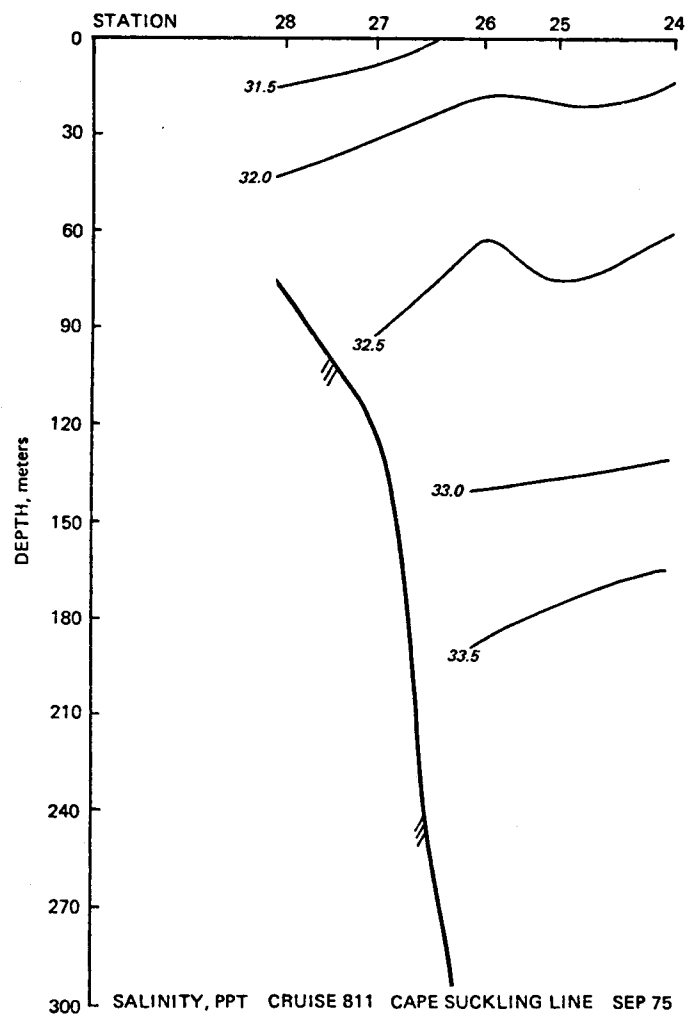


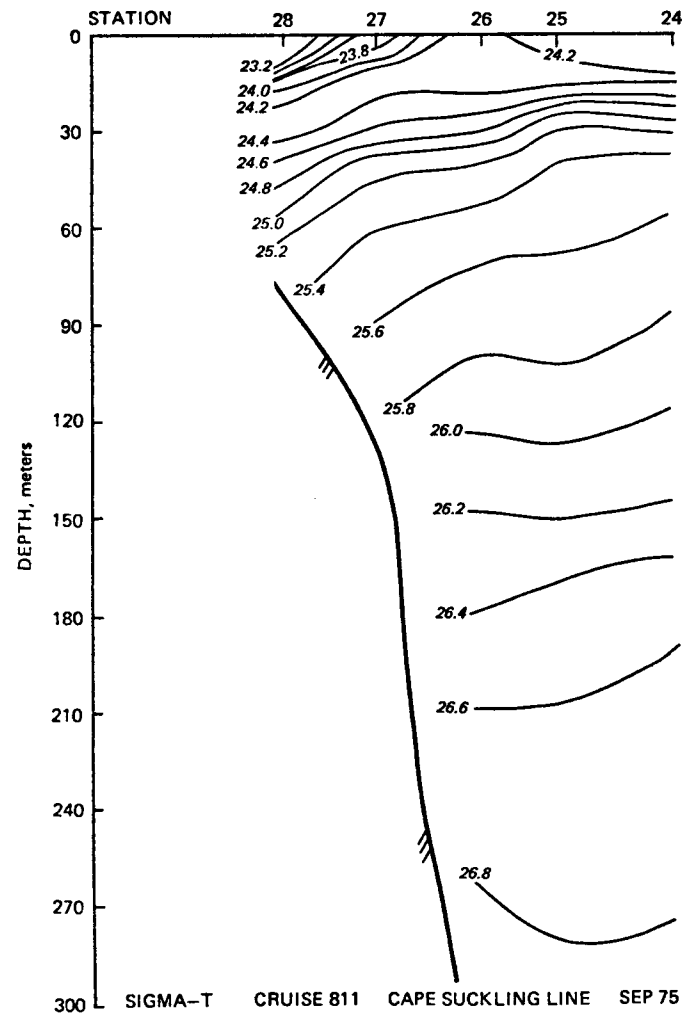


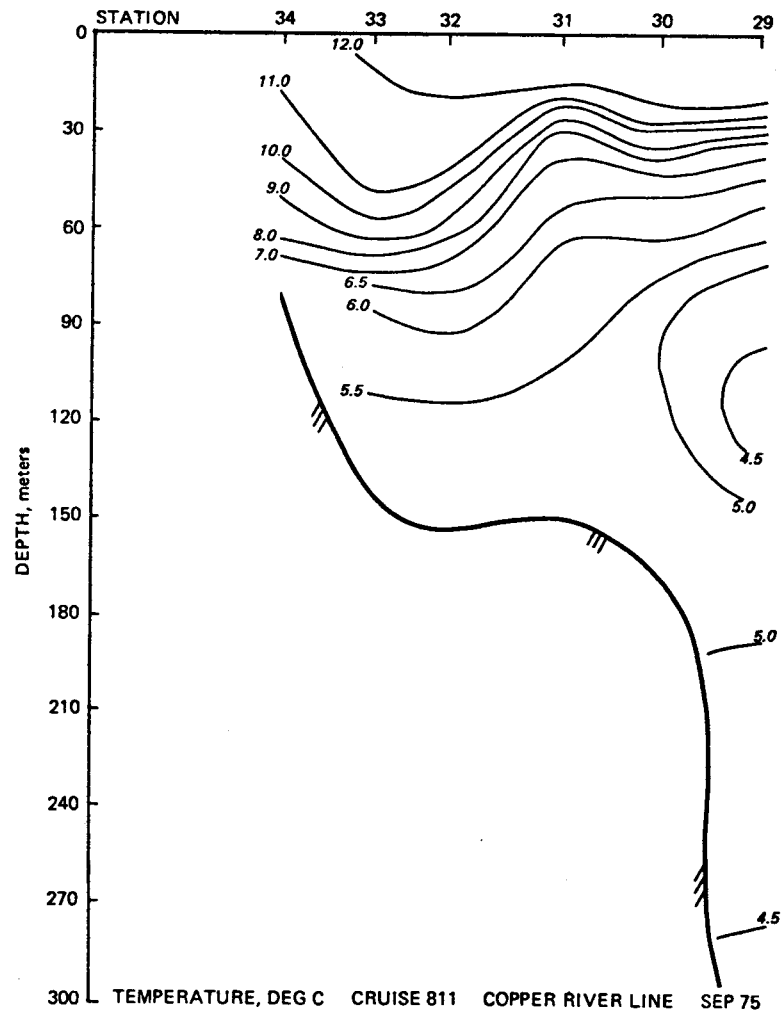


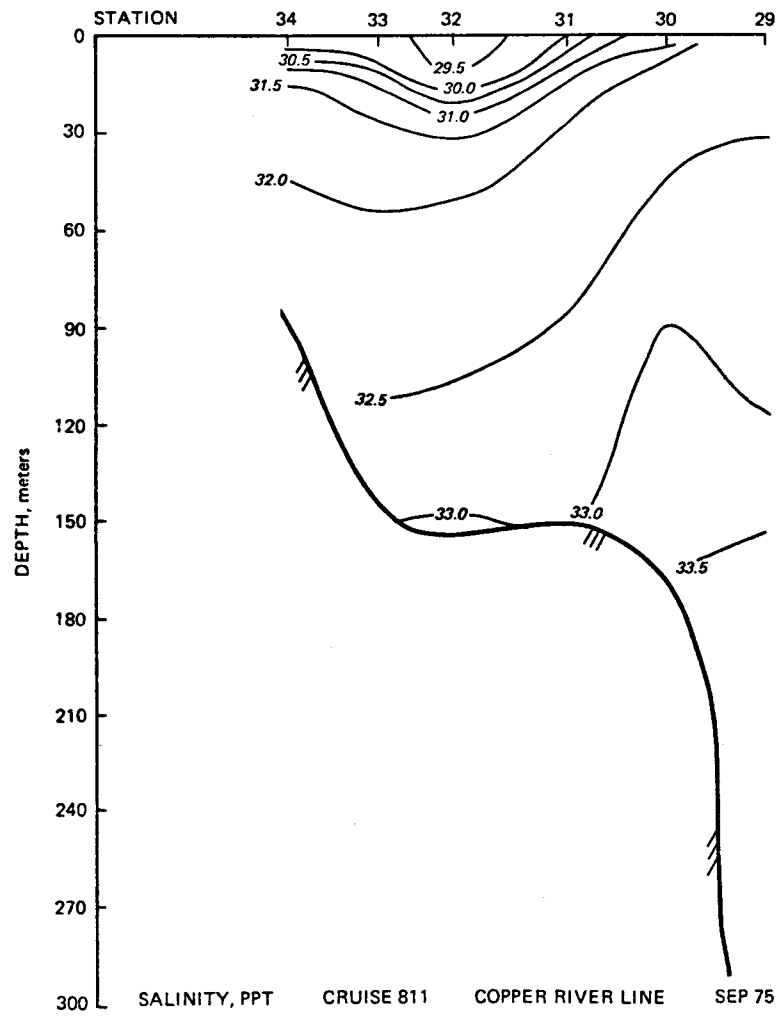




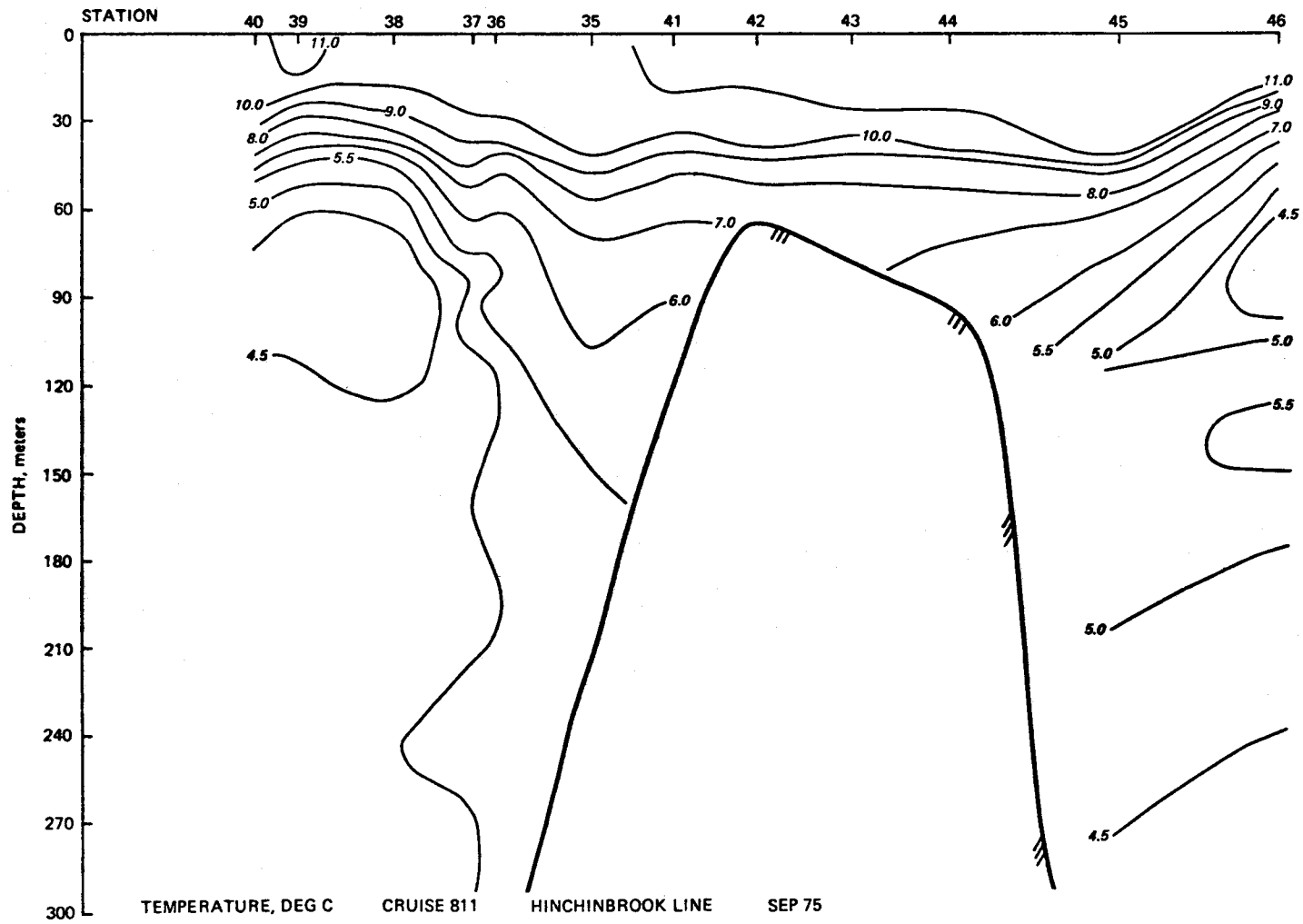




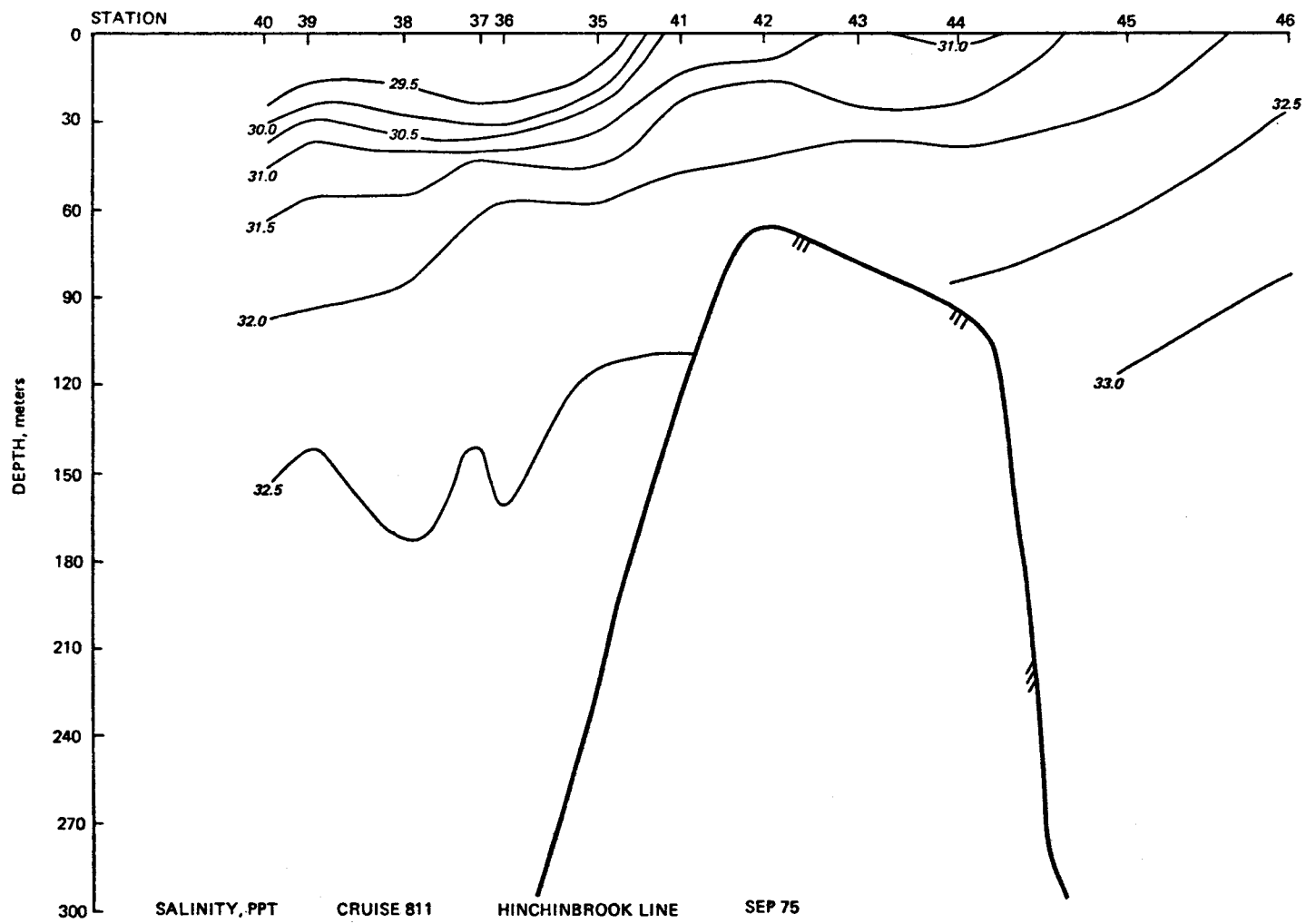


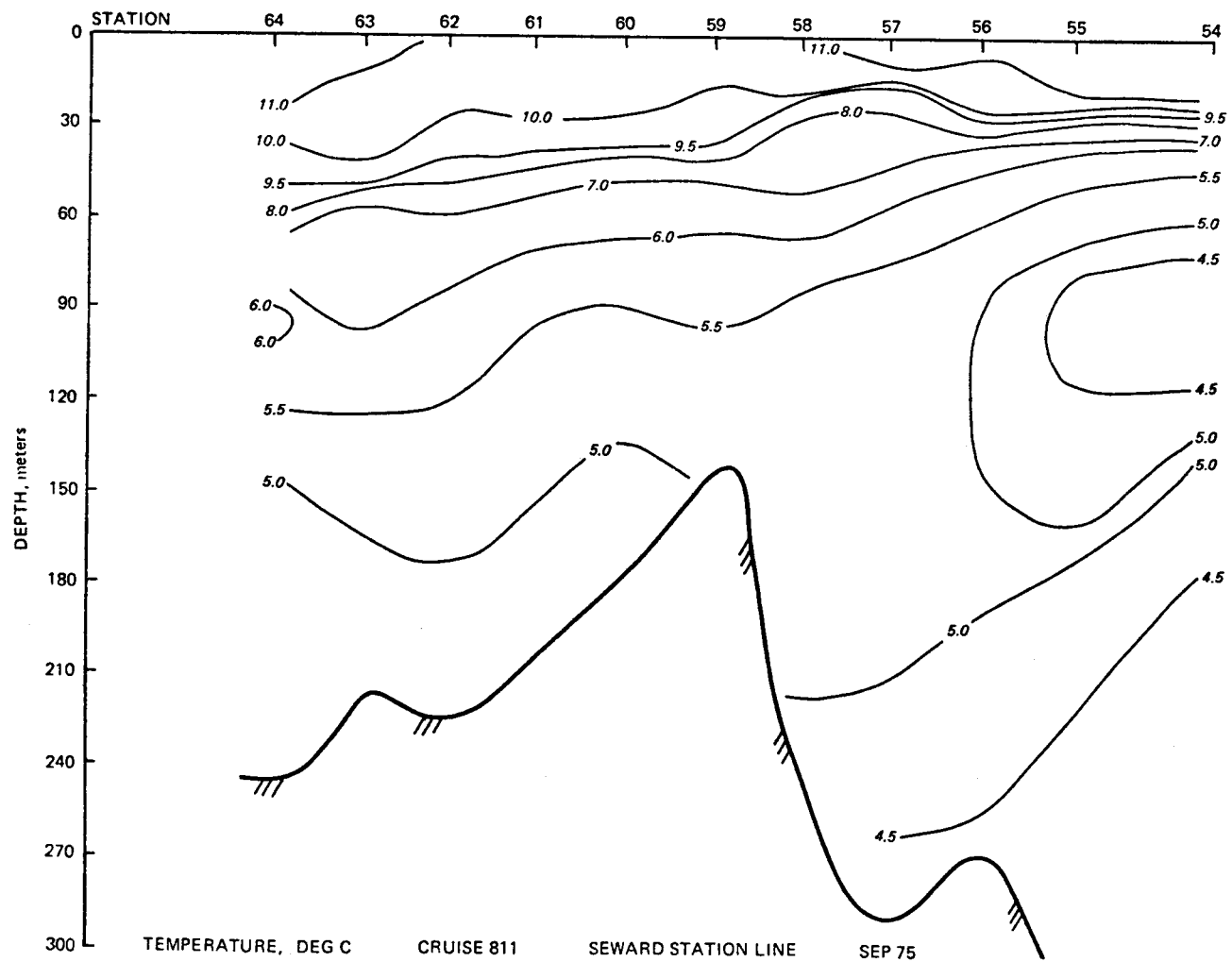


326

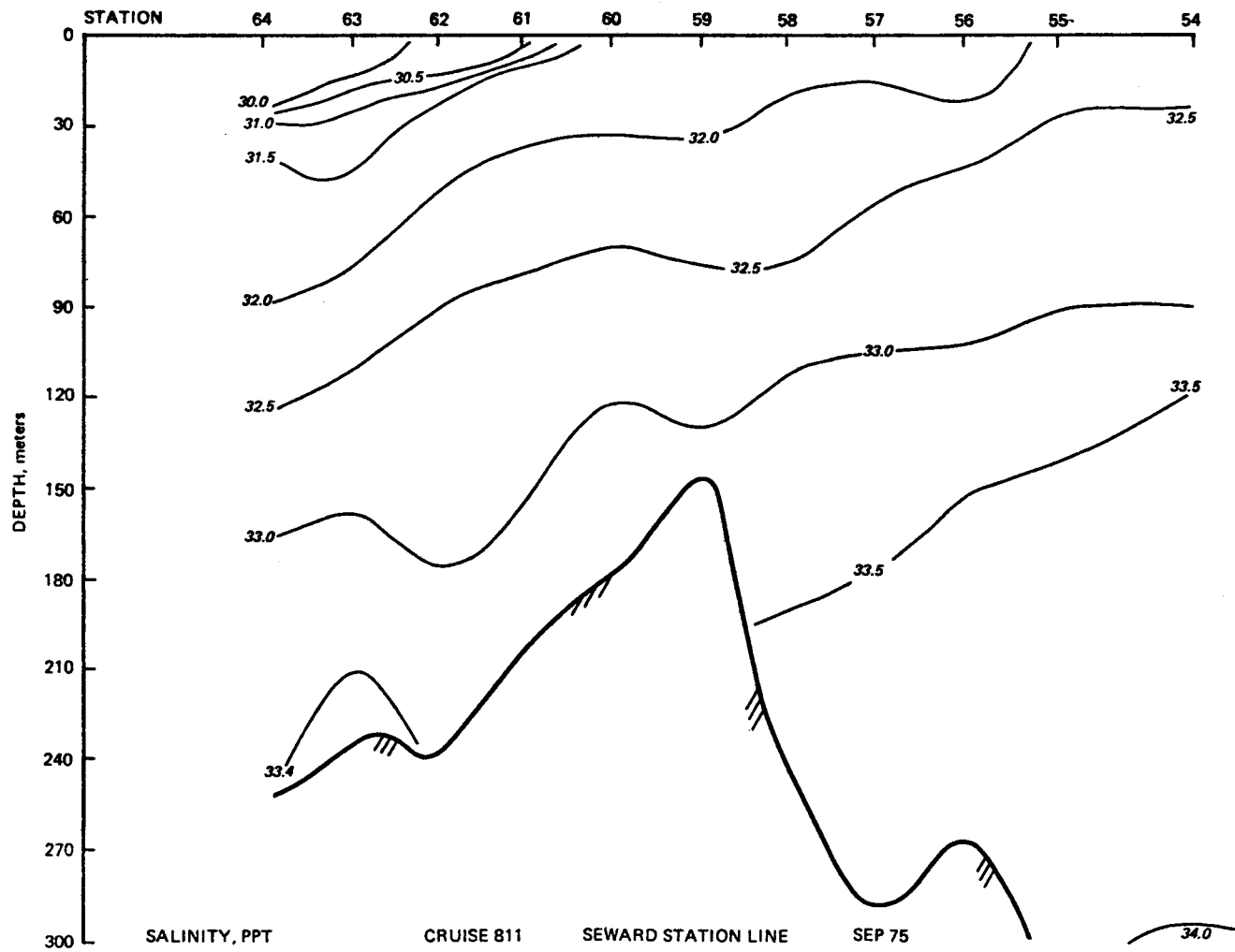


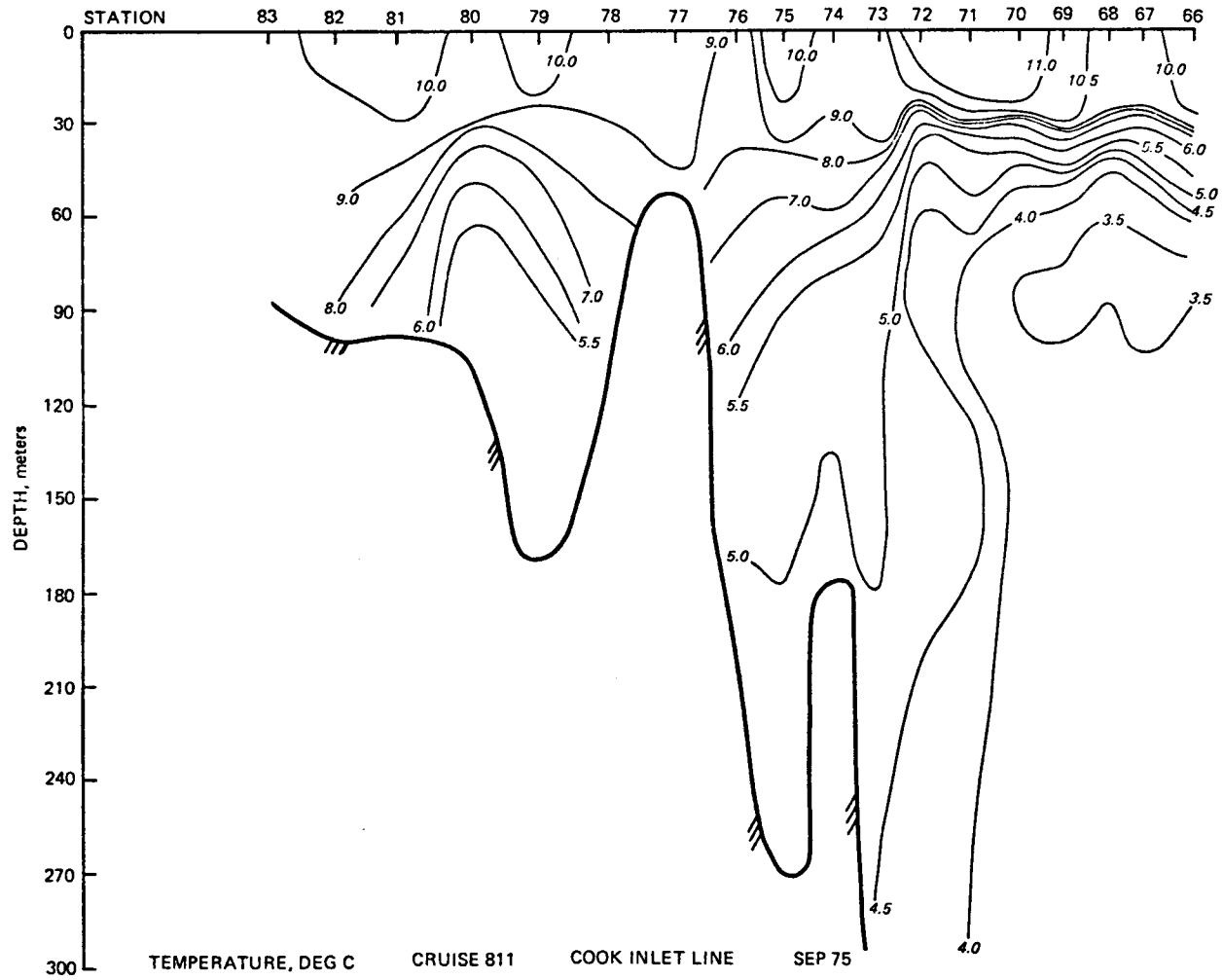
327

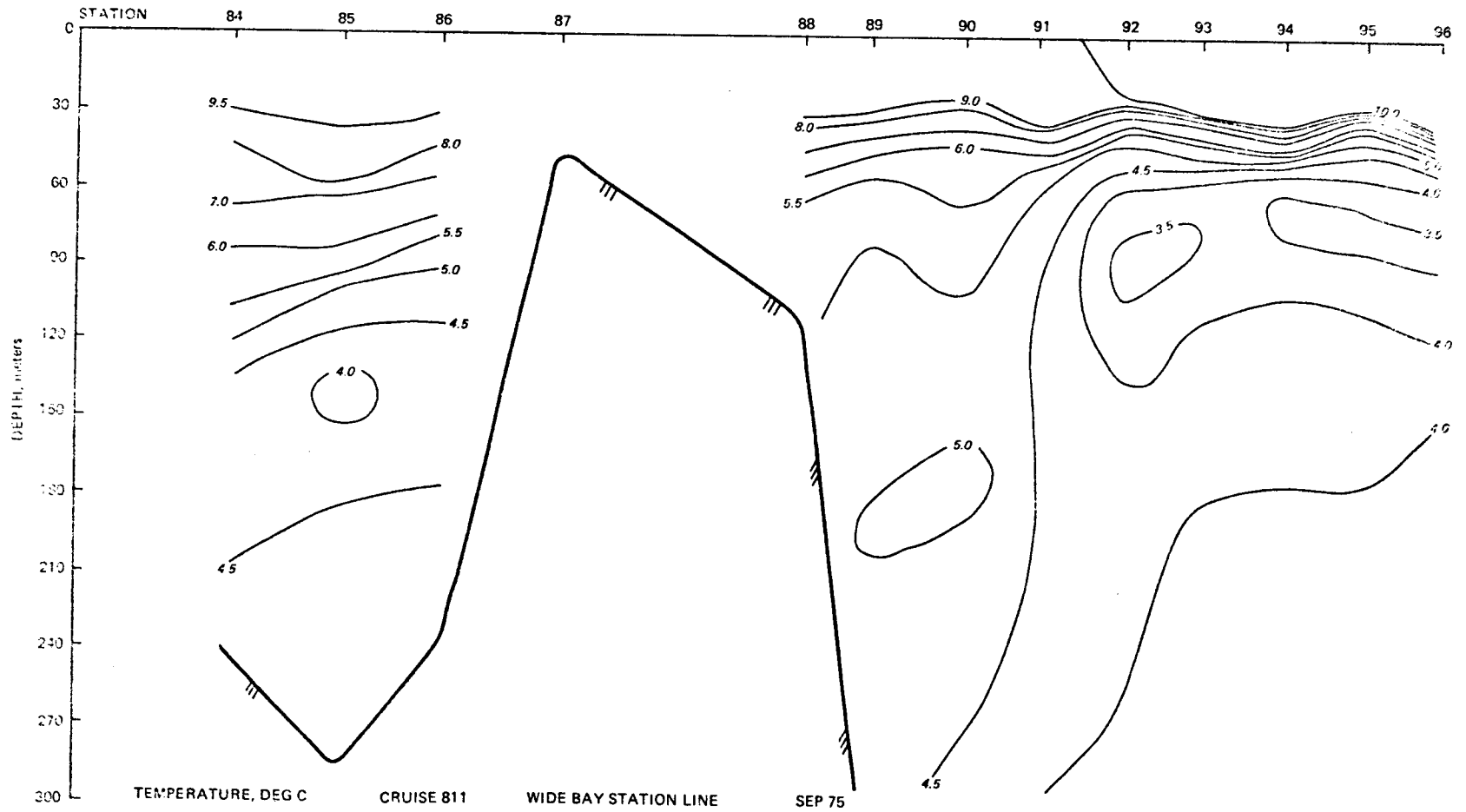


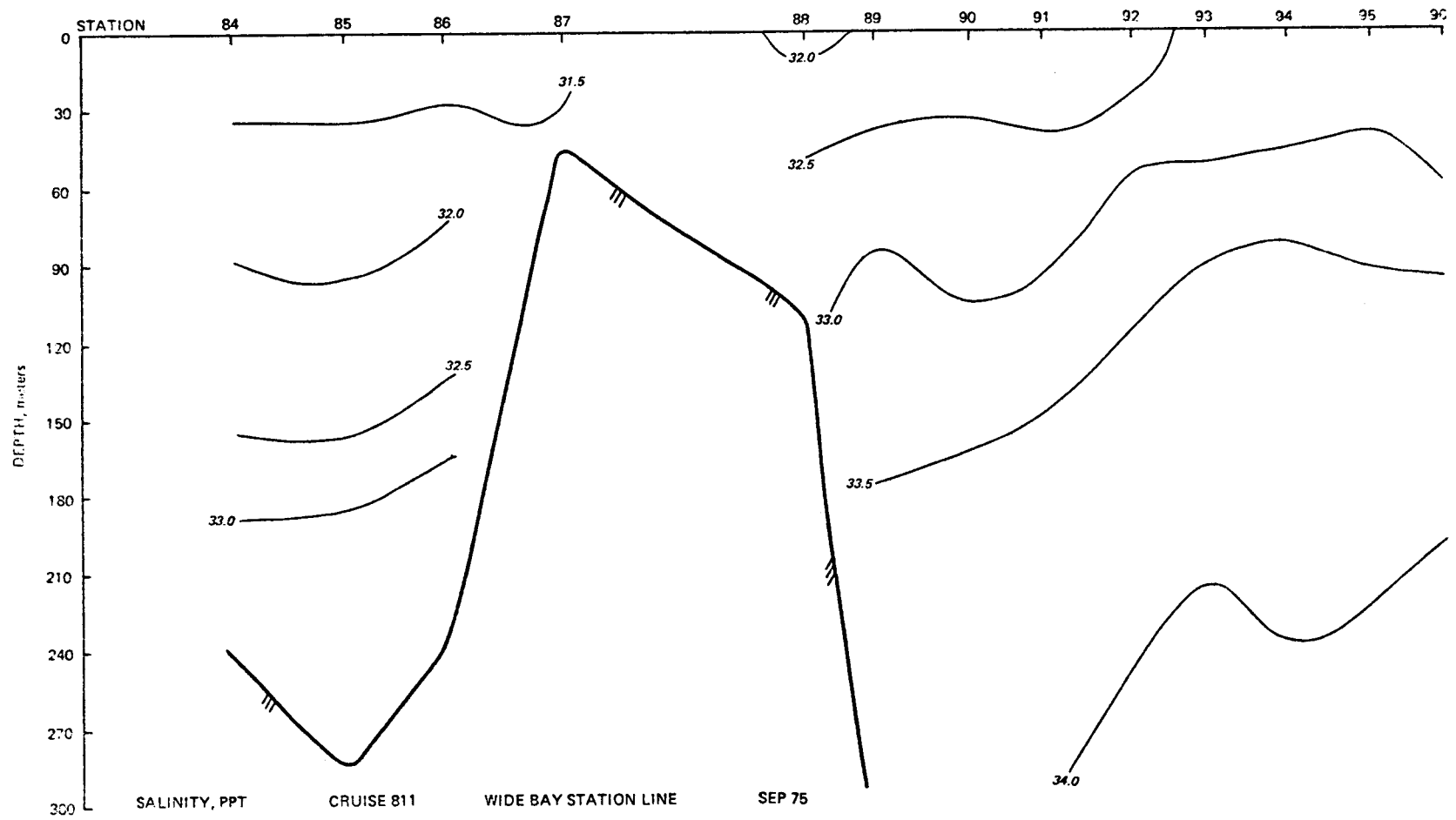


330

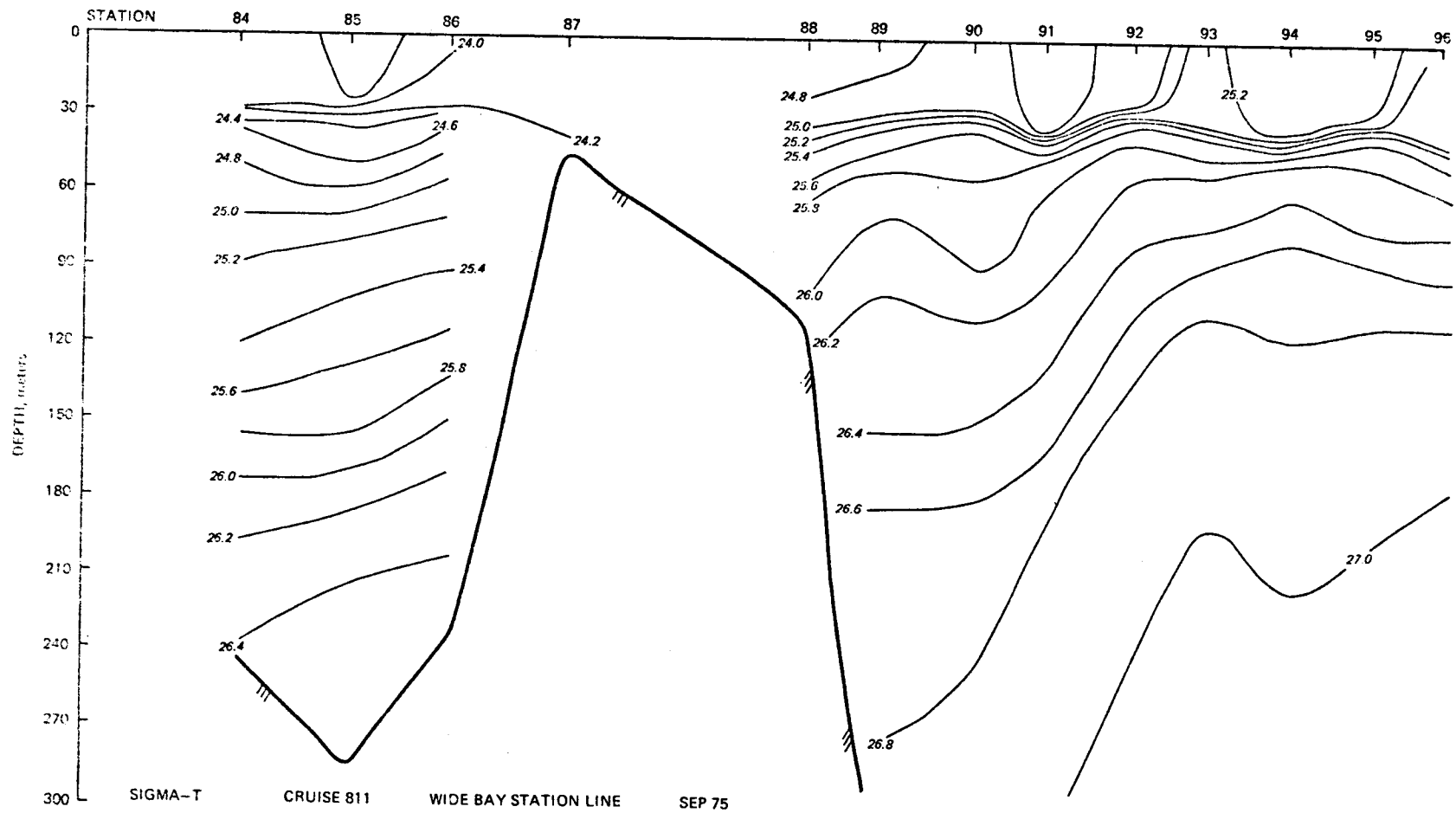


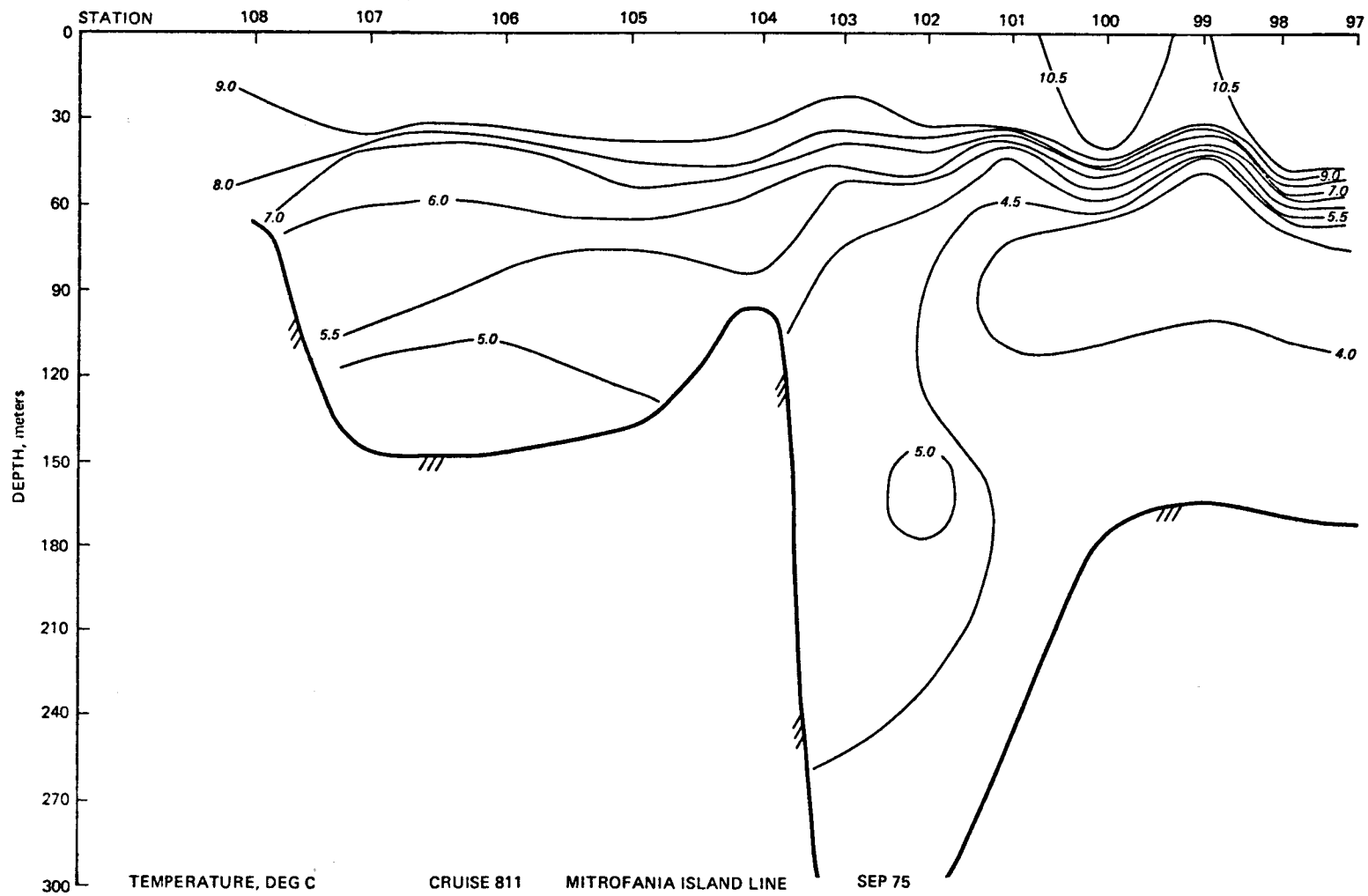




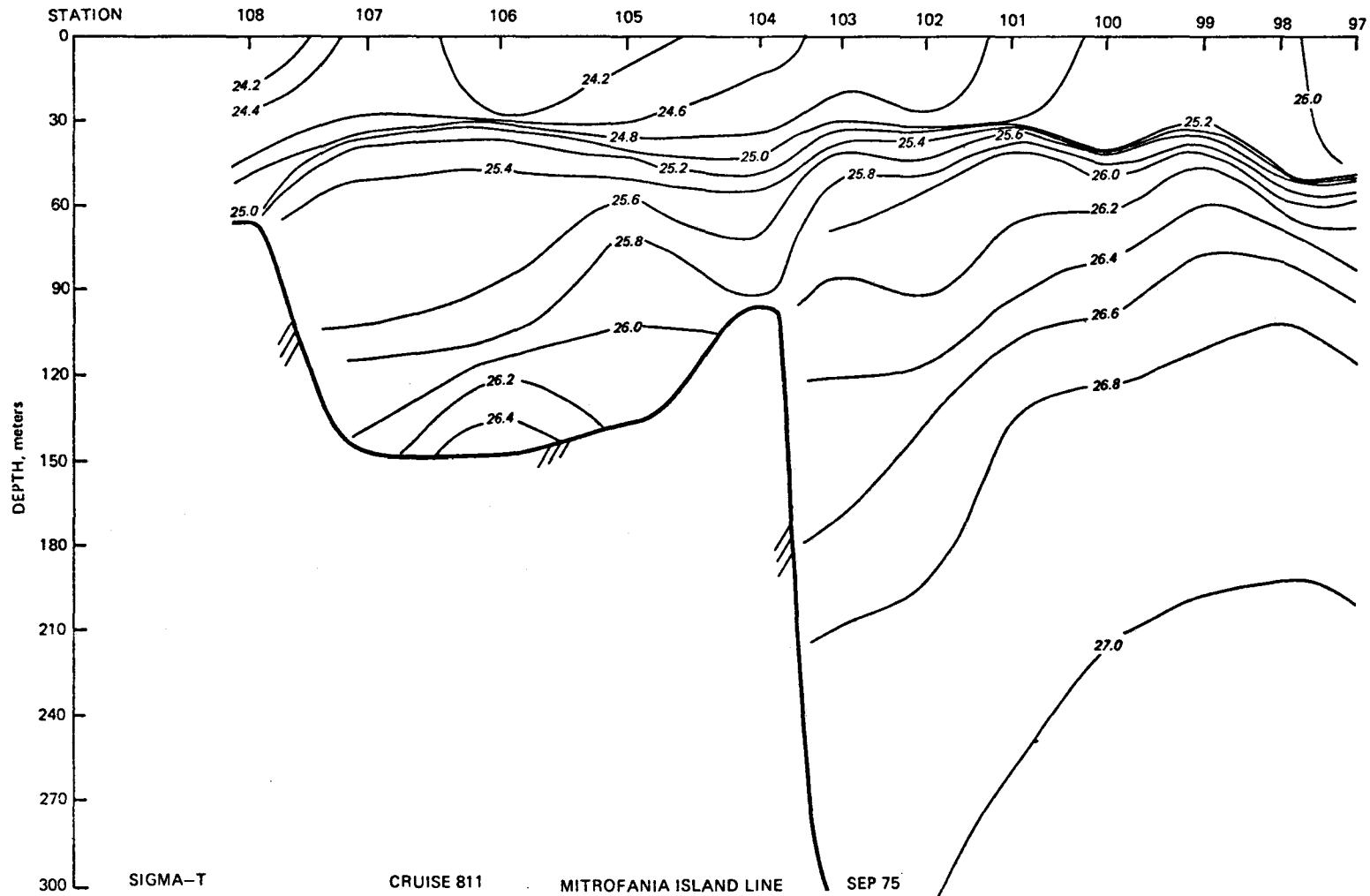


337

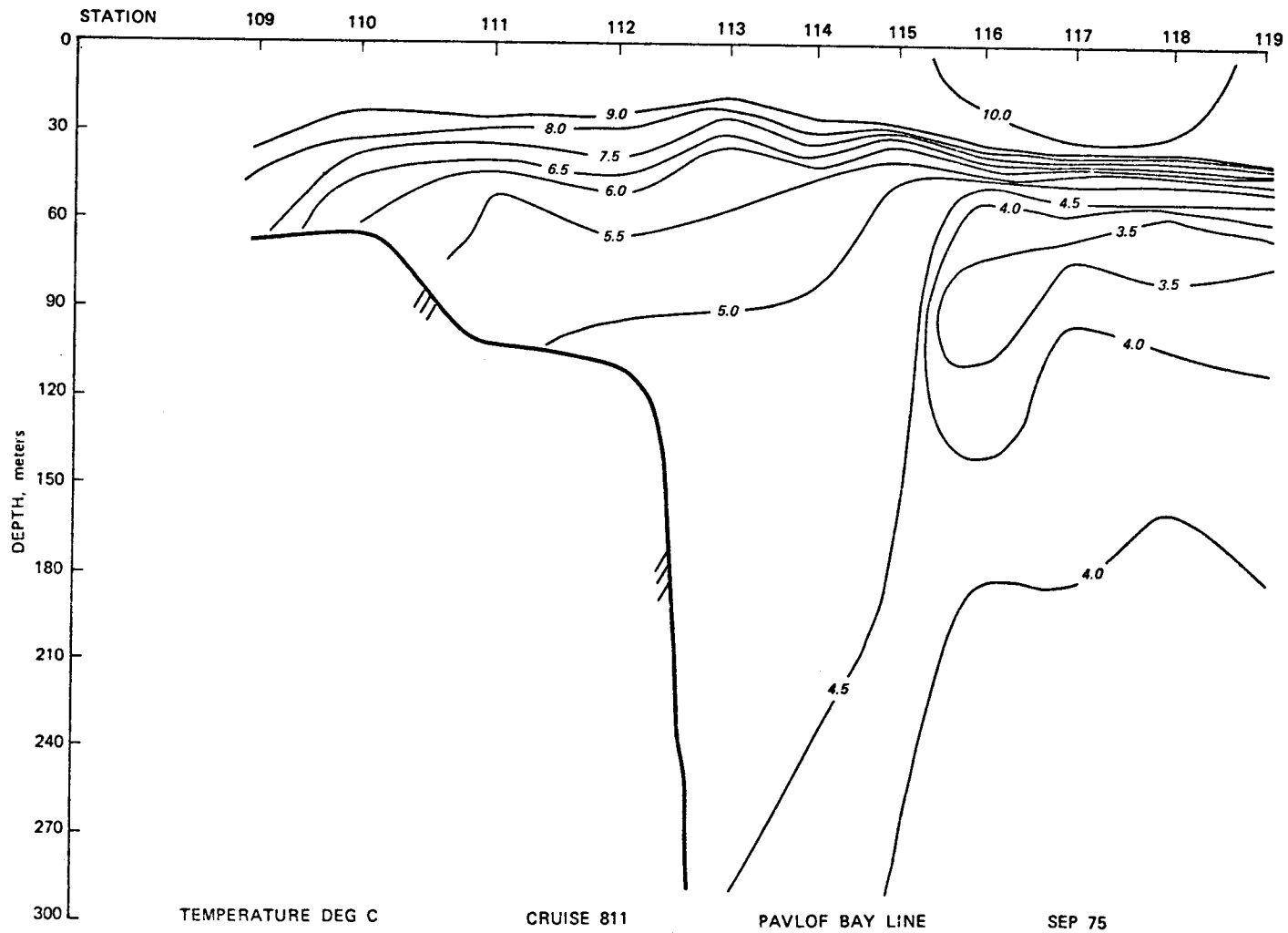




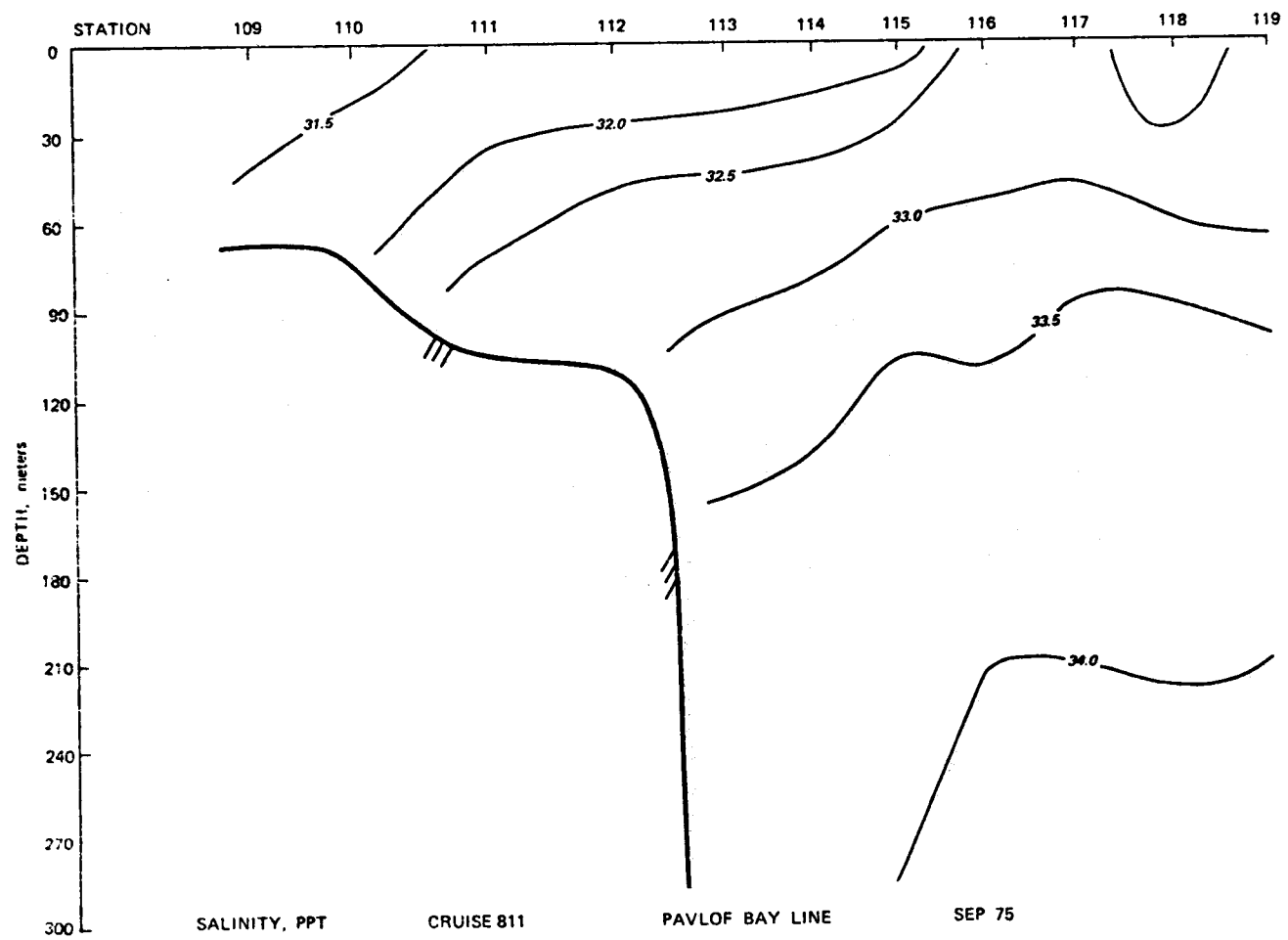
340

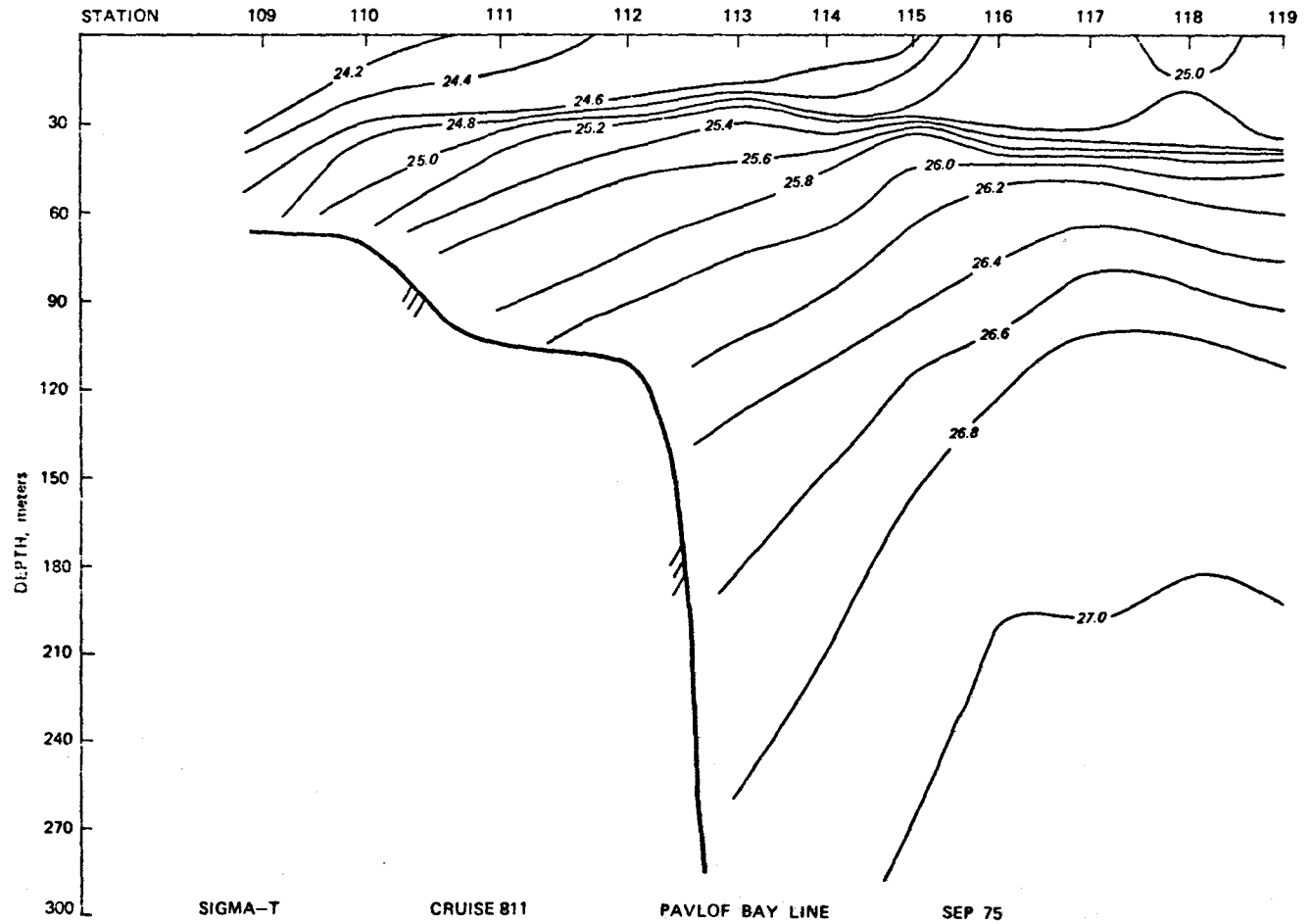


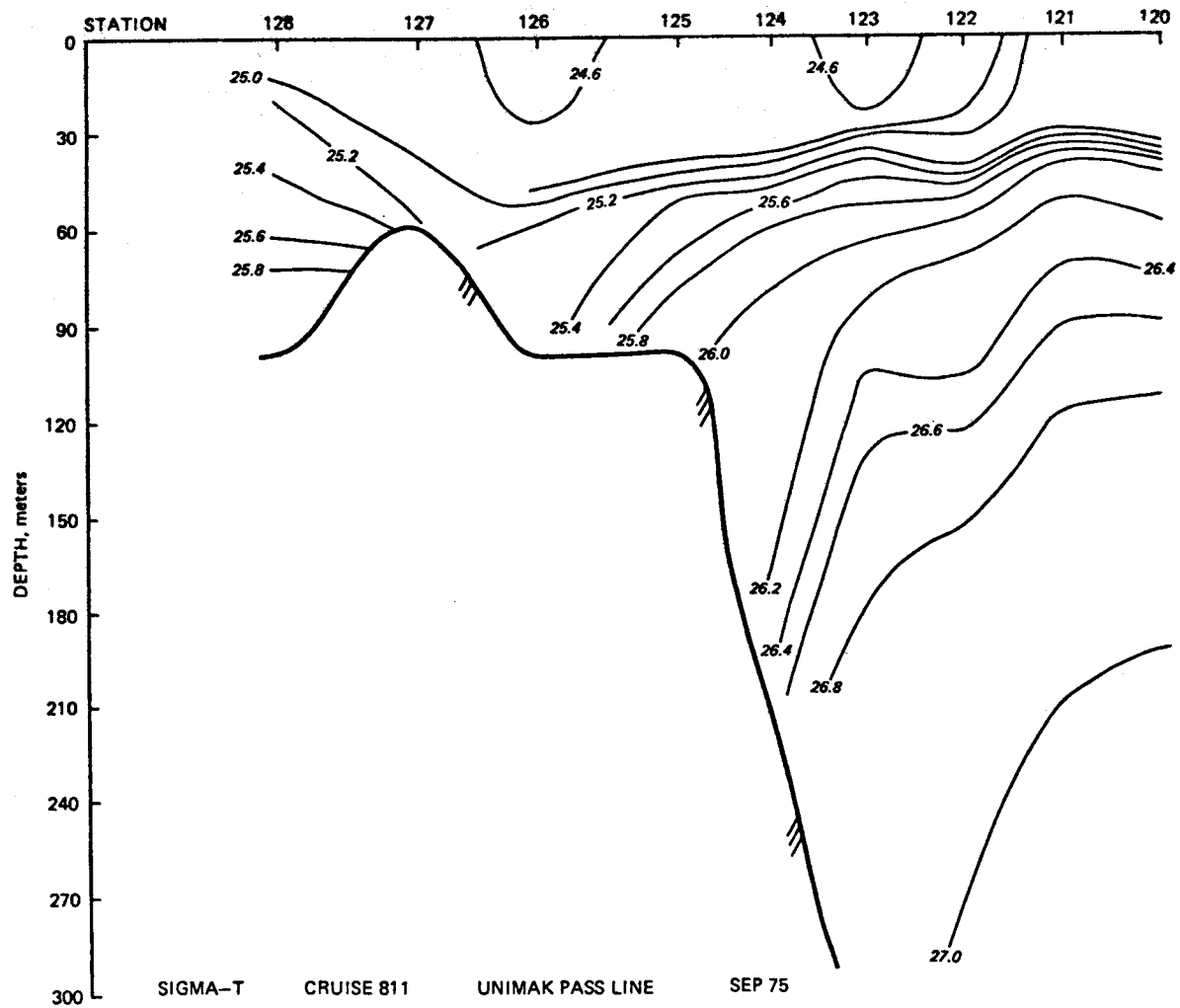
341



342







XII. APPENDIX II

LOW FREQUENCY SHELF FLUCTUATIONS
IN THE GULF OF ALASKA

S. Worley and T. Royer

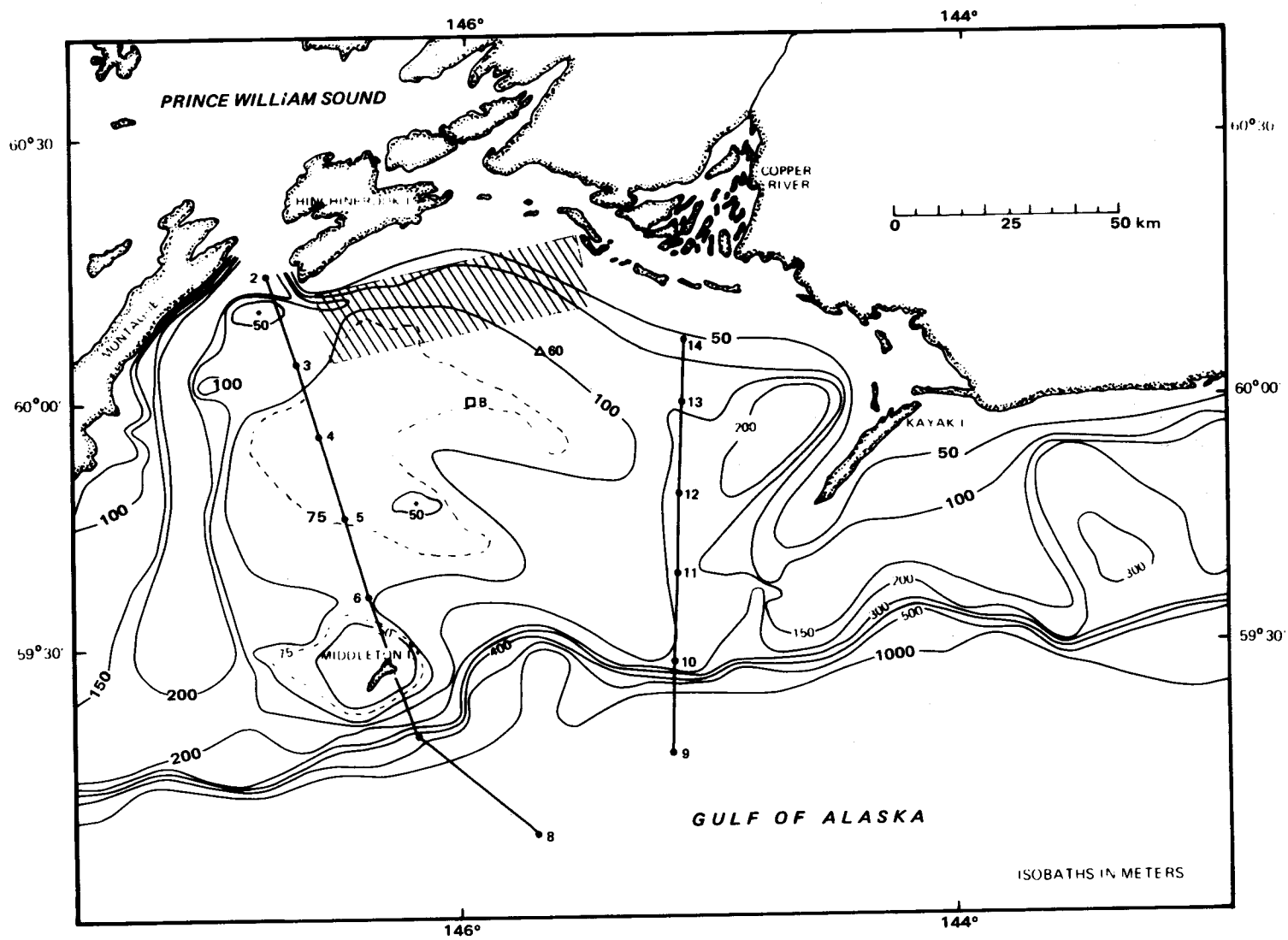
ABSTRACT

A general oceanographic study of a shelf region in the Gulf of Alaska has revealed low frequency current fluctuations. A current meter mooring was located approximately 20 km offshore, in a water depth of 100 m. The time dependent flow is found to be baroclinic and semi-systematic. The effects of local bottom topography, nearshore dilution by river discharge, orographic coastal features, and an island barrier are important to the shelf circulation in this region. The movement of the fresh water boundary from the Copper River is seemingly an important process in controlling the water motion at the mooring site.

INTRODUCTION

Current meter observations were performed at a location on the continental shelf of the northern Gulf of Alaska during the summer of 1974. The mooring, designated as Station 60, was the first of a series of current meter arrays to be used for direct measurement of flow in the region (Fig. 1). These measurements were obtained under the Outer Continental Shelf (OCS) study with the primary goal being one of environmental assessment. Our analysis utilizes the current measurements of the OCS study as well as data made available from unaffiliated sources.

The Gulf of Alaska circulation is under the general influence of the sub-Arctic cyclonic gyre, part of which is described by the northward Alaska Current and westward Alaska Stream (Tabata, 1975). Prior estimates of currents there have been restricted to baroclinic geostrophic computations and a few Lagrangian-type drifter measurements (Favorite, 1970). The shelf area of the gulf is subject to net surface dilution from the runoff and excess of precipitation over evaporation (Tulley and Barber, 1960). Other characteristics of the local study area are a complex local bottom topography (an abrupt rise to the north and more gradual shoaling to less than 75 m to the south forms an asymmetrical saddle where the mooring was located), an upstream barrier (Kayak Island), and a fresh water source (the Copper River) (Fig. 1). The precise influence of the Alaska Current on the study region is unknown. However, in light of the large shoal north of Middleton Island and the upstream barrier it is reasonable to assume that only a fraction of the mean flow of the Alaska Current directly affects the shelf region. A considerable portion of the mean flow is expected to follow the shelf break and move westward south of Middleton Island.



Appendix Figure 1. Bathymetry of northern Gulf of Alaska continental shelf study area.

During summer the wind regime is variable. Synoptic surface pressure maps (Arctic Weather Central Office, Edmonton, Alberta) indicate the alternating influences of low pressure systems, which develop over the Bering Sea and Aleutian Island arc, and high pressure systems originating from the mean summer position of the North Pacific High (150°W, 38°N) (Dodimead *et al.*, 1963). The time scale of alternation is 5 to 10 days with the high pressures usually exhibiting longer residence time.

This discussion focuses on the observed low frequency current variations at Station 60. The role of meteorological forcing and the hydrographic structure of the shelf water are utilized in the generation of a plausible explanation for the observed currents.

OBSERVATIONS

Observations from four Aanderaa (RCM-4) current meters at depths of 20, 30, 50, and 90 m for the period 2 July through 8 October 1974 form our primary data set. Current speed and direction, and water temperature were recorded at all four depths. Conductivity was recorded at the top and bottom meters and depth (pressure) at the top meter. All meters sampled on a 10 minute interval and a useable record of 56 days (2 July through 26 August) was obtained.

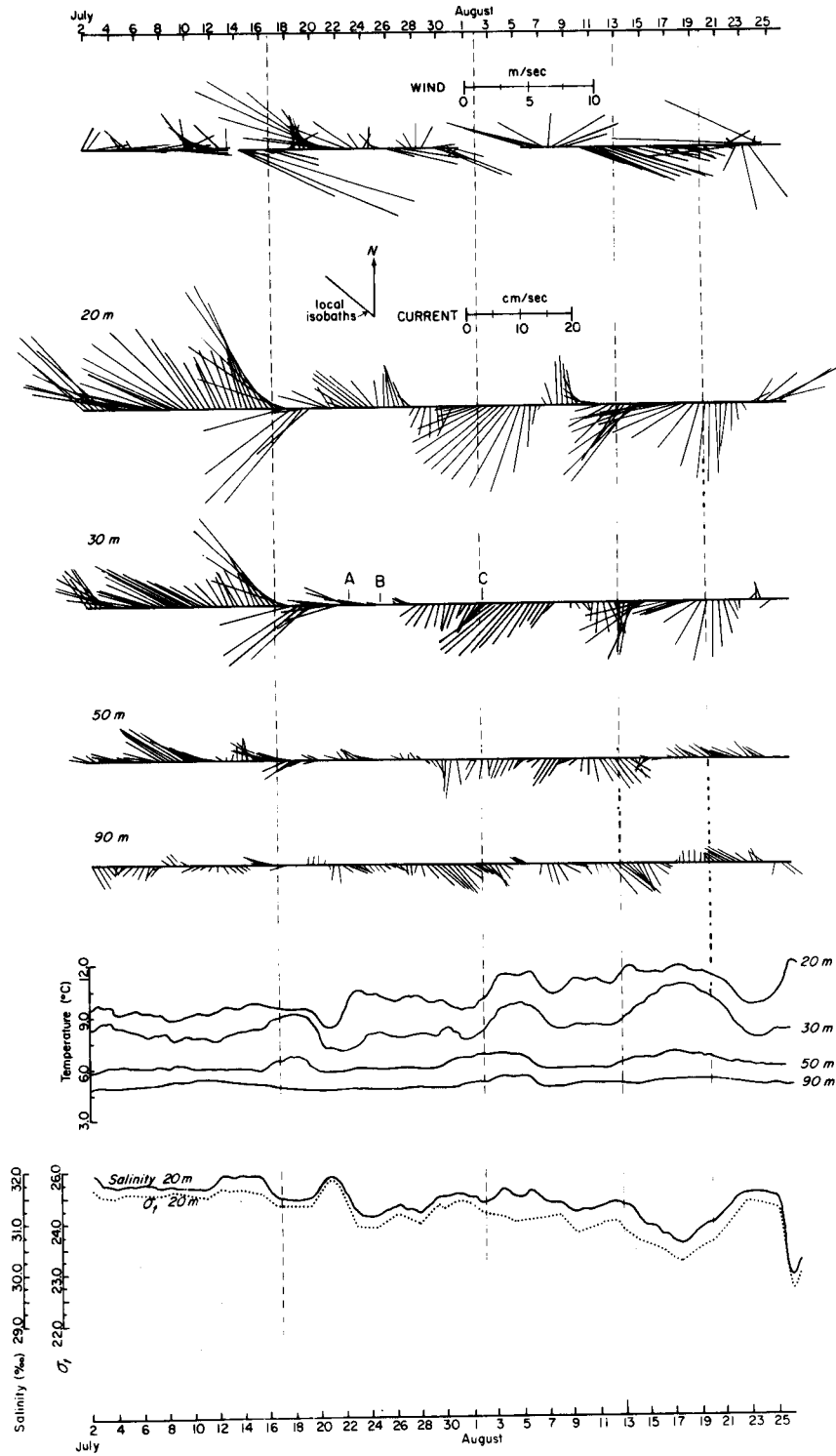
Hourly time series from the current meter data were obtained by using an approximate low-pass Butterworth filter, half power point 3 hours (half amplitude at 0.43 cycles per hour, 90% power at 0.18 cycles per hour) (Stearns, 1973), and then selecting every sixth point. Tidal and inertial oscillations were suppressed by using a similar Butterworth digital filter, half power point 50 hours (half amplitude at .025 cycles per hour, and 90% power at .014 cycles per hour) (Stearns, 1973).

The mean values and standard deviations of the E-W and N-S current components were obtained from the low-pass filtered data (Table I). The mean values are small and standard deviations are relatively large. These elementary statistics show that the flow is unsteady at the mooring location. The current vector diagrams (every tenth vector was plotted for clarity in presentation) further illustrate the transient nature of the flow at all levels (Fig. 2). Variations with time of direction and magnitude are most pronounced in the 20 and 30 m records. Our discussion will concentrate on the four sections of the record centered at 17 July, and 2, 13 and 20 August where large variations in direction occurred. The similarity of low frequency current velocity variation within these sections is indicative of a semi-permanent flow regime. The four events are highly baroclinic and exhibit some vertical correlation. The first occurrence is well defined at 20, 30 and 50 m with only the slightest indication of a correlated veering at 90 m. The second and third events are also well defined at the upper three current meters. However, in these cases the 90 m flow intensifies and veers in the same sense as in the upper layers. The final event has a smaller vertical scale. In this case, the flow veers counterclockwise only in the uppermost layers (20 and 30 m) while the 50 and 90 m currents seem relatively unaltered.

Hydrographic data (R/V *Acona* cruise 193, July 1974) were collected after the deployment of the current meter array at Station 60. Eight transects running normal to the coastline at different locations were sampled. Two of these transects, designated as Hinchinbrook and Copper River, provide temperature and salinity data to characterize the shelf water and reveal some subtle circulation features of this study (Fig. 1).

TABLE I
STATISTICS FOR LOW PASS FILTERED DATA

	U(eastward)		V(northward)		Speed	
	Mean	S.D.	Mean	S.D.	Mean	S.D.
Wind m/sec	1.13	4.22	.11	1.81	3.91	2.65
Current cm/sec						
20 m	-7.27	11.75	.94	12.68	17.36	8.03
30 m	-5.89	8.91	-.65	9.25	13.24	5.69
50 m	-2.57	6.30	-.06	8.28	10.70	3.63
90 m	.50	5.64	-1.11	8.56	9.63	3.88

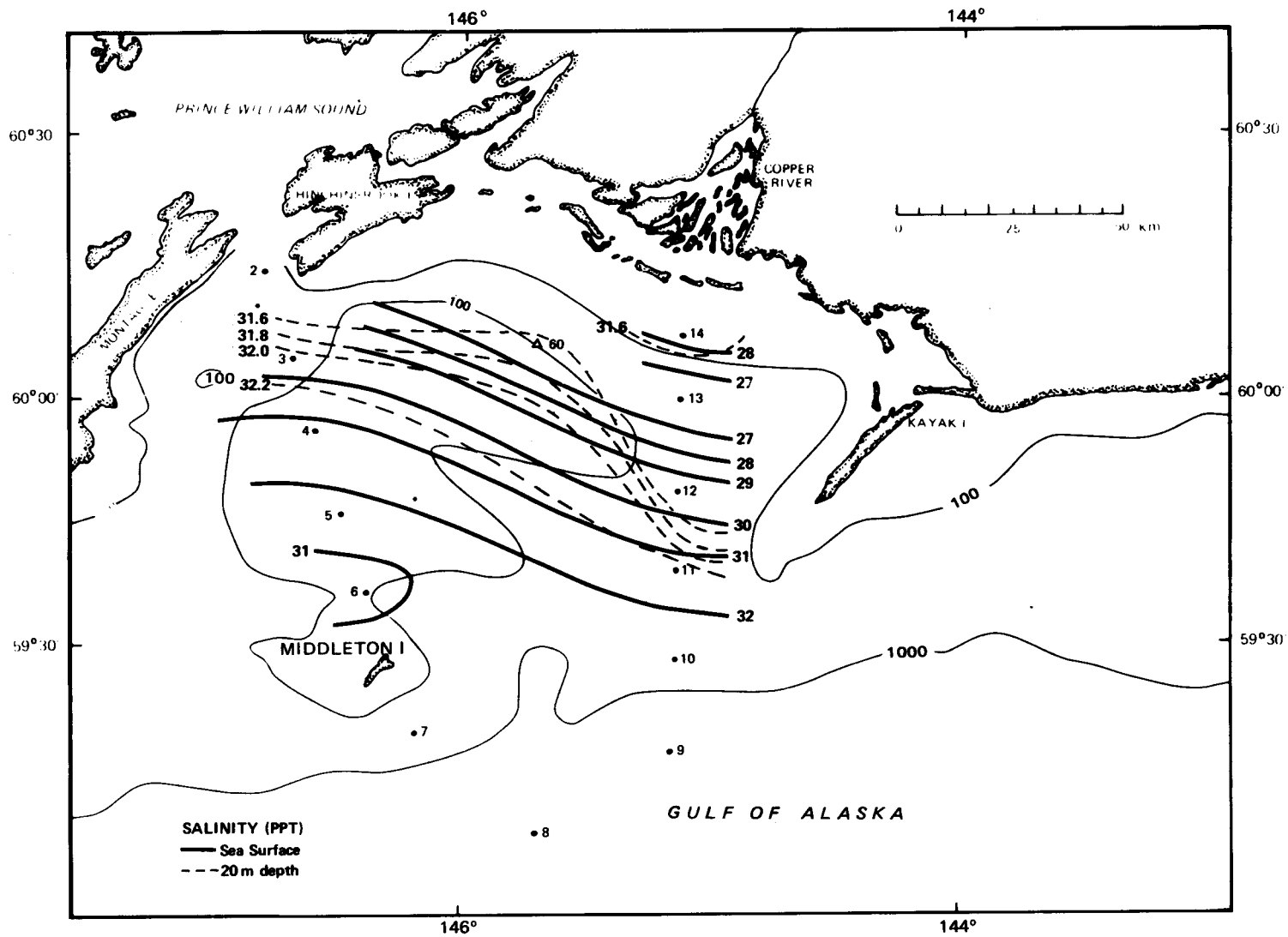


Appendix Figure 2. Wind and current vectors, temperature, salinity and sigma-t time series.

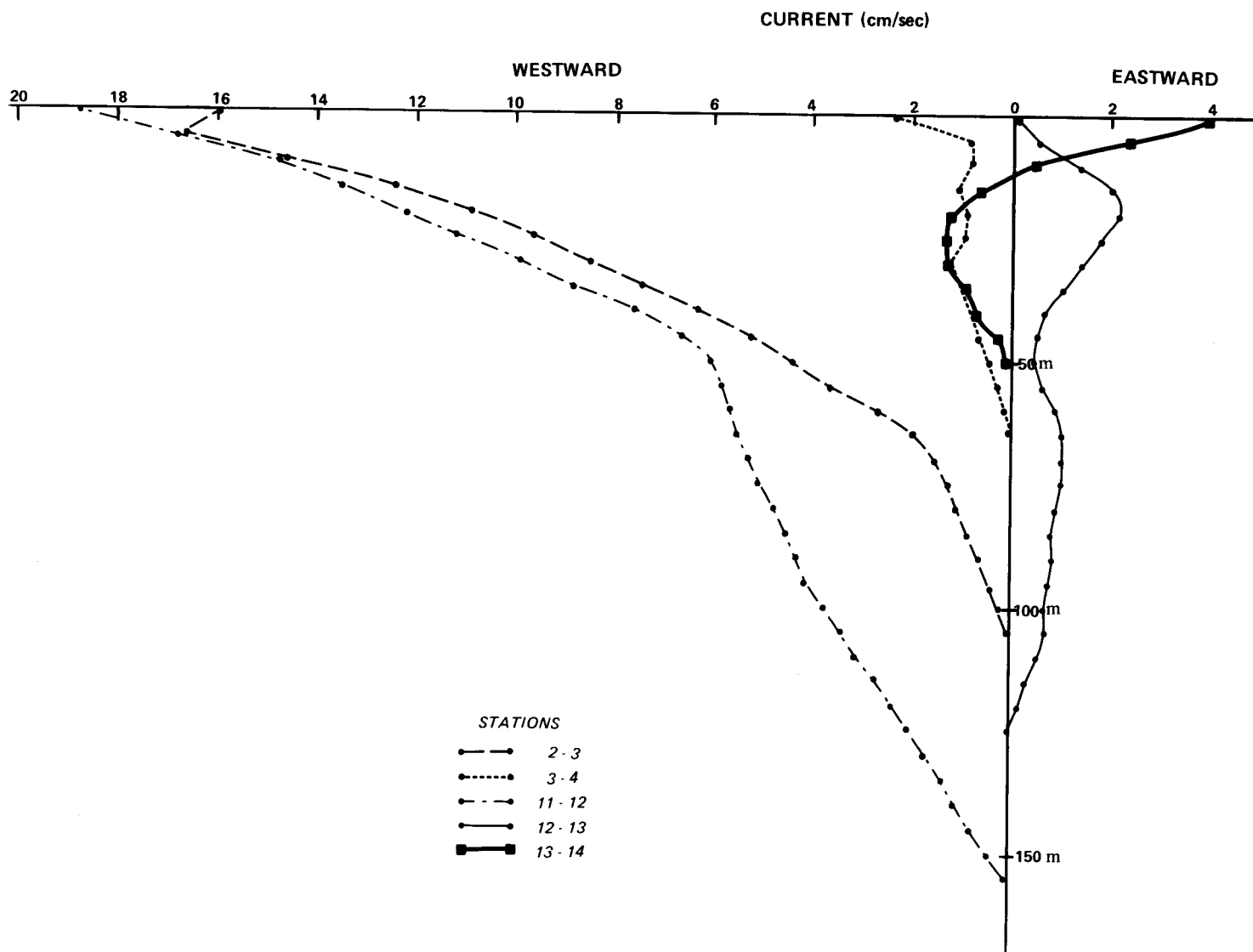
Salinity at the sea surface and at 20 m depth (Fig. 3) show the pronounced freshening of the surface and nearshore water, which is a distinctive feature for the Gulf of Alaska during summer (Royer, 1975). The Copper River with runoff typically equal to $3000 \text{ m}^3/\text{sec}$ (Ingraham, 1976) during July and August makes the major contribution to the observed low salinity of this region.

Baroclinic geostrophic current calculations indicate that westward flows with magnitudes of 20 to 45 cm/sec (relative to the 1350 decibar (db) surface) occur along the shelf break, whereas weak non-uniform westward flows of 0 to 20 cm/sec, and occasional eastward flows (1 to 2 cm/sec) are found on the shelf. The calculated currents along the Hinchinbrook and Copper River lines, determined relative to the maximum common depth between stations, indicate several interesting features. The maximum calculated baroclinic geostrophic currents occur in narrow bands coincident with concentrated salinity gradients. Elsewhere, the flow is weak and in one case (between Station 12 and 13) is directed eastward throughout the water column (Fig. 4).

Two sources of wind data are available for this region. Hourly wind data were recorded at the U.S. Weather Service AMOS facility on Middleton Island. This wind record has two missing data gaps for the period 2 July through 26 August (shown as gaps along time axis, Fig. 2). One is a minor gap of 27 hours in July and the other of 6 days, 1 to 6 August. A second data source is the 6-hourly calculated surface winds (Bakun, A., National Marine Fisheries Service Pacific Environmental Group, Fleet Numerical Central, personal communication) for grid point B (60°N , 146°W) (Fig. 1). The computation of these winds is based on surface atmospheric pressure distribution and geostrophic wind computation. To compensate for



Appendix Figure 3. Isohalines at sea surface and 20 m depth, R/V *Acona* cruise 193, 2-4 July 1974.



Appendix Figure 4. Geostrophic currents calculated from R/V *Acona* cruise 193, hydrographic data.

friction effects the geostrophic velocity is reduced 30% in magnitude and rotated 15° to the left to approximate surface wind velocity (Bakun, personal communication).

Initially, the correlation of measured and calculated wind was assumed to be good, however, hypothesis tests on linear regression and correlation coefficients at the 95% confidence level indicate otherwise. The analysis of the regression and correlation coefficients, which are a measure of the functional relationship and degree of association between variables, respectively, was done in three groups to bypass data gaps in the Middleton Island record. The results for north-south (N-S) and east-west (E-W) components of the wind velocity, treating the observed wind as the independent variable are shown in Table II. A Kolmogorov-Smirnov goodness of fit test indicates that the two unfiltered data sets are normally distributed on the 95% confidence level, therefore establishment and application of confidence intervals is reasonable (Sokal and Rohlf, 1969). The regression coefficients (Table II) indicate that the magnitude of the calculated wind is less than that of the observed wind. Furthermore, hypothesis tests at the 95% confidence level reveal that the functional relationship varies (Ostle, 1963) It was found that the RC(E-W) for 17-31 July and RC(N-S) for 1-15 July are different from the other coefficients in the respective groups.

The ramification of these results are twofold. First, the placement of calculated surface winds in observed record gaps is unsatisfactory. Second, the upwelling indices (Bakun, 1975) computed from the calculated surface winds must be used with caution. There is a plausible explanation for the above observations. The summer wind regime over the Alaskan

TABLE II

COMPARATIVE STATISTICS FOR CALCULATED AND OBSERVED WINDS
THE 95% CONFIDENCE INTERVAL IS INDICATED BY (\pm)

	# Points	RC(E-W)	CC(E-W)	RC(N-S)	CC(N-S)
1-15 July	59	.15 \pm .14	.29	.23 \pm .14	.38
17-31 July	61	.35 \pm .10	.67	.57 \pm .19	.61
6-31 August	102	.18 \pm .09	.32	.68 \pm .16	.66

continental shelf is variable. It is influenced by mesoscale atmospheric phenomenon, orographic coastal features, cloudiness and long periods of incident solar radiation. Consequently, a relationship between the observed and calculated winds may not be consistent since the model, employed by Bakun, relies primarily on the large scale pressure distribution. This led to the use solely of low-pass filtered (half power point 50 hours) observed wind records. Again, only every tenth vector was plotted for clarity in presentation (Fig. 2).

DISCUSSION

The horizontal flow in our study area may be adequately described by the equation,

$$\frac{\delta \vec{V}}{\delta t} + (\vec{V} \cdot \nabla) \vec{V} = \frac{-1}{\rho} \nabla P + f \vec{V} \times \vec{k} + g \vec{k} + \vec{F} \quad (1)$$

where \vec{i} , \vec{j} , \vec{k} are unit vectors in the x(+ eastward), y(+ northward) and z(+ upward) directions, respectively. Also P is pressure, ρ is fluid density, $f = 2\Omega \sin \phi$ where f is the Coriolis parameter, Ω is the angular frequency of earth's rotation, ϕ is the latitude, $\vec{V} = U\vec{i} + V\vec{j}$ is the horizontal velocity, g is gravity, and $\vec{F} = \vec{i}F_x + \vec{j}F_y + \vec{k}F_z$ are the combined frictional forces. Our data prohibit the evaluation of each term in equation (1), however, orders of magnitude can be determined which reveal the relative importance of the various terms.

Sea surface wind stress is a possible dominant frictional force in our situation. Two responses to this force must be considered, indirect changes in velocity through changes in isobaric surface inclination, and direct changes in current velocity due to drift currents. In general the

first response has the largest effect in a stratified nearshore region where upwelling and downwelling are most significant, whereas, the direct effect does not require coastal proximity.

These effects will be evaluated by applying the theory of Ekman (1905). Steady wind stress over a horizontally homogeneous and vertically stratified ocean will induce barotropic and baroclinic currents as responses to sea surface slope and tilting of isobaric surfaces, respectively. The mechanism generating this sea surface slope and internal horizontal pressure gradient is Ekman transport. This transport is directed 90° to the right of the wind stress vector in the Northern Hemisphere. Some of Ekman's initial assumptions: homogeneous, unbounded, infinitely deep, non-sloping oceans, are violated in a stratified continental shelf area. Nevertheless, qualitative application of this theory is useful.

The approximation of the effects of wind stress will be based on the fact that the coastline in the study area is oriented northwest-southeast and in general the intense and persistent winds flow parallel to the coast (Figs. 1 and 2). Northwestward wind stress (onshore Ekman transport) will create a rising sea surface in the onshore direction and cause the accumulation of low density surface water nearshore. The sea surface slope and redistribution of mass will lead to baroclinic and barotropic currents. In this situation, both baroclinic and barotropic current components will be directed toward the northwest as geostrophy is approached. Under southeastward wind stress, offshore Ekman transport would theoretically induce barotropic and baroclinic flow in the opposite sense, toward the southeast.

A visual correlation between wind and current records indicate the existence of a current response contrary to classical Ekman theory (Fig. 2). The strong southeastward wind event centered at 16 July and northwestward event centered at 21 July corresponded to an increase then a decrease in the observed westward current component, respectively. Similarly measured winds that bracket the August missing data gap show that southeastward winds on 31 July and northwestward on 6 August led to intensification followed by attenuation of the westward current component. Finally, southeastward winds beginning 10 August show identical correlation, that is the westward current component increased. These observations contradict elementary baroclinic and barotropic geostrophic theory. Hence, the observed variations in the flow cannot be explained in terms of simple geostrophic flow theory.

Since the upper two current meters were located relatively near the surface the direct frictional influence through pure wind drift currents on the records must be considered. The Ekman depth of frictional influence, D , for a homogeneous unbounded ocean without pressure gradient accelerations and nonaccelerated horizontal flow is (Ekman, 1905),

$$D = \pi \left(\frac{2A_z}{\rho f} \right)^{1/2}$$

where A_z is the vertical eddy coefficient of viscosity. The magnitude of the surface water velocity, V_o , induced by a uniform, steady state wind stress T_o is,

$$V_o = \frac{T_o D}{\pi A_z \sqrt{2}} = \frac{T_o}{(\rho f A_z)^{1/2}}$$

In order to predict the maximum effect of direct wind induced flow T_o and A_z were selected such that the limiting value of V_o may be approximated.

T_0 was estimated to be 33 dynes/cm² using an empirical relationship and a relatively large wind speed for the area ($T_0 = \rho_a C_D U^2$, where air density $\rho_a = 1.2 \times 10^{-3}$ (g/cm³), empirical drag coefficient $C_D = 1.15 \times 10^{-3}$ (Suthuraman and Raynor, 1975), and wind speed $U = 10$ m/s). Further, ρ and A_z were taken equal to 1.024 g/cm³ and 100 (gm cm⁻¹ sec⁻¹). Following these estimations the depth of frictional influence and wind induced surface velocity was found to be 40m and 29 cm/sec. According to Ekman's theory the magnitude of pure drift current falls off exponentially with depth, $\exp[\pi z/D]$, the maximum wind induced current components at 20 and 30 m would be 6.0 and 2.8 cm/sec, respectively.

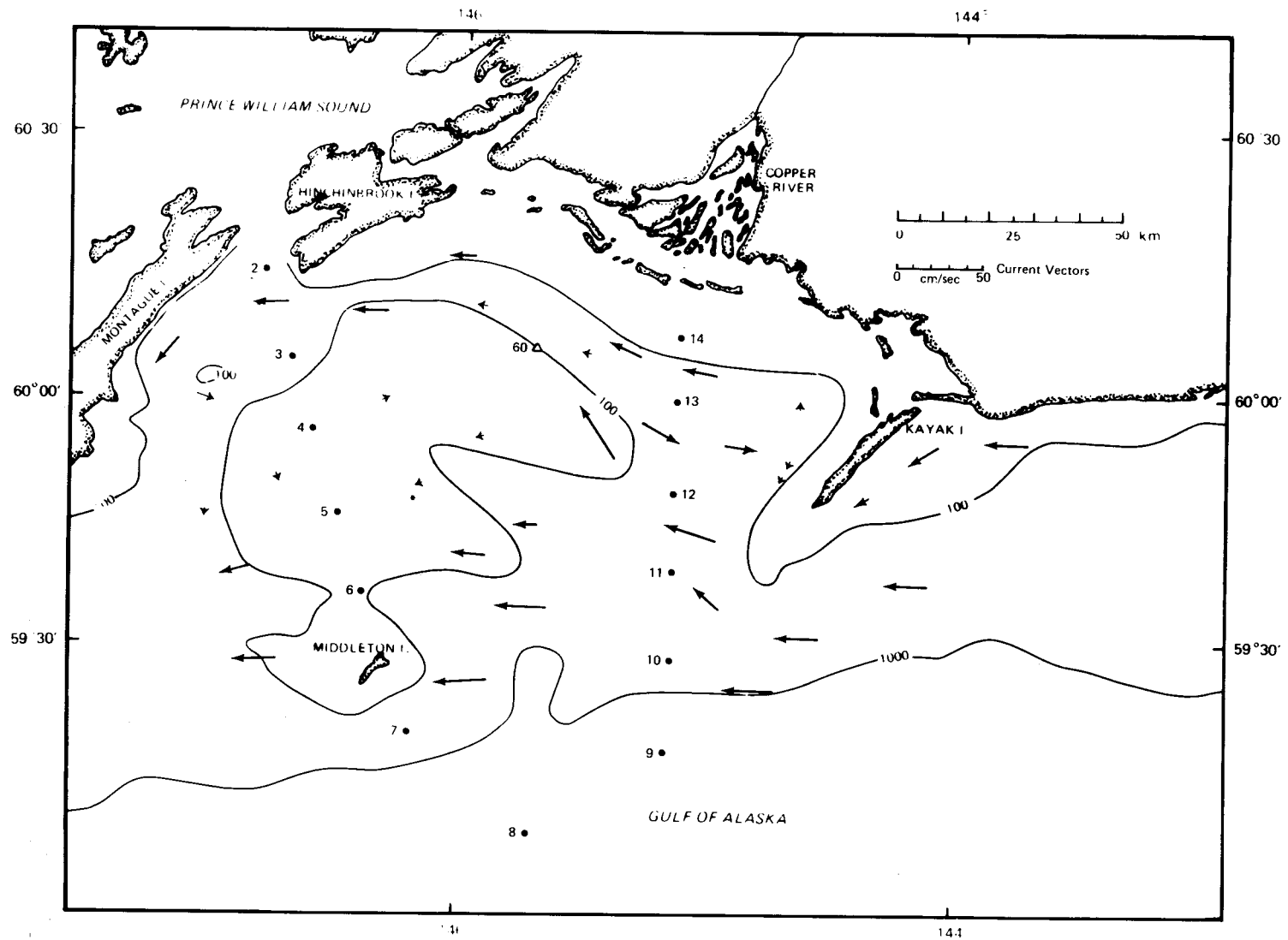
During the four current events (17 July, and 2, 13, and 20 August) there was a change in magnitude and direction of flow. Using the 20 m record as an example, we find that changes in current velocity to be at least 15 cm/sec directed southward (Fig. 2). The discrepancy between calculated wind drift current at 20 m and this observation indicate that the current veering events are not directly attributable to wind stress.

Furthermore, there is not much difference between a pure drift current in infinitely deep water and in a water layer where the total depth $H = 1.25 D$ or greater (Ekman, 1905). Stratification of the water column would tend to decrease D , that is, restrict the flow to a shallower surface layer. If D were decreased by 25% and V_0 was increased twofold (58 cm/sec) the maximum current component due to wind stress at 20 m would still be only 7.1 cm/sec. For the purpose of this study there is no significant difference created by stratification or finite depth.

Therefore the observed baroclinic phenomenon at Station 60 does not show any obvious link to conventional steady state meteorological forcing theories. Hence, in the first order approximation the frictional force

term in equation (1) can be neglected. It follows then, that the southward veering of flow is likely a result of a mesoscale scale feature, non-stationary in time or space. Numerical modeling efforts have predicted several mesoscale features in the area. The model which includes wind stress, Ekman dynamics, geostrophic and continuity of flow principles was initialized with hydrographic data (R/V *Acona* cruise 193, July 1974) and calculated current shear (Galt, 1976). The results of this time independent model indicate that a two gyre system might exist in the study region. The model predicted an inner (cyclonic) gyre which is linked to nearshore horizontal density gradients. The outer (anticyclonic) gyre, found north of a line between the southern tip of Kayak Island and Middleton Island, is linked to the mean westward flow of the Alaska Current that is deflected offshore by Kayak Island (Fig. 5 reproduced from Galt, 1976). Under ideal conditions, NOAA-3 satellite infrared spectral images support the existence of a gyre system (Galt, 1976).

Assuming the circulation is tending toward geostrophy, the observed changes in density with time at the mooring can be employed to characterize the flow events. A time series of sigma-t [$\sigma_t = (\rho - 1) \times 10^3$] was calculated from the hourly temperature and salinity series at 20 m depth using nine, a term third order polynomial (Cox *et al.*, 1970). Salinity governs the water density in the N.E. Gulf of Alaska (Royer, 1975). This is verified within the study region by comparing the low-passed (50 hour cutoff) sigma-t and salinity time series at 20 m (Fig. 2). Further, a comparison of temperature and density indicates that these two parameters are inversely proportional throughout the records (Fig. 2). This occurs because salinity and temperature are inversely proportional for this region, that is, the fresh upper



Appendix Figure 5. Surface current vectors computed by numerical model, reproduced from Galt, 1976.

waters are warmer than the dense deeper layers. Hence, the temperature records may be used in conjunction with salinity and σ_t to facilitate the recognition of density changes at Station 60.

The long term trends observed in the σ_t , temperature, and salinity series are consistent with surface warming and freshening of the summer season. Caution must be exercised when interpreting these records, because mixing and restratification will influence temperature and salinity at 20 and 30 m.

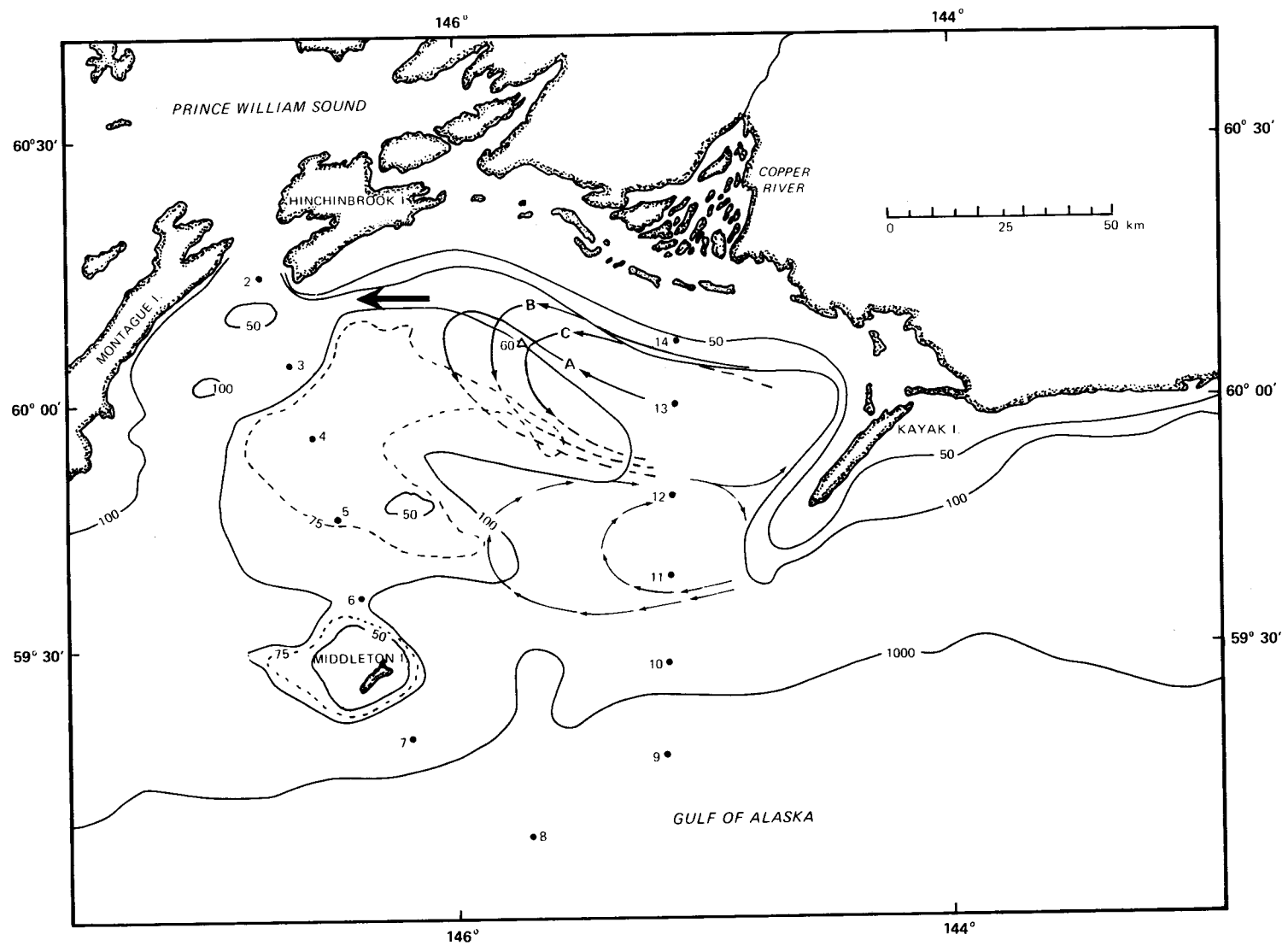
Three major events occur in the temperature records. These events are approximately centered at 17 July, 4 and 17 August, and are defined by temperature maximums (density minimums) (Fig. 2). The 20 m record is considerably contaminated by lateral and vertical surface layer phenomena (wind drift currents and mixing). The variations at 90 m are very subtle, therefore the three events are most clearly defined in the 30 and 50 m records. These three events in the temperature records are well correlated with the occurrence of southward current veering (cross-isobath flow) previously defined (Fig. 2).

Considering all available data, two explanations for the observed cross-isobath flow can be suggested. One is based on a numerically predicted two-gyre system (Galt, 1976), and the other on satellite (ERTS/LANDSAT-1) images. The current and wind records are time dependent data, whereas the numerical modeling efforts, hydrographic sections, and single satellite images are time independent data. Precise verification of one data set with the other is impossible. Therefore, the combined use of these data must be regarded as speculative.

Galt's model predicts a two gyre system at the surface. Semi-periodic displacement of the inner (cyclonic) gyre may have produced the

observed variations in current velocity. The dynamics of a cyclonic baroclinic gyre in the Northern Hemisphere require a relatively dense water core. Taken in conjunction with the observed density (temperature) changes, this high density core allows a plotting of the positions of the gyre with respect to the mooring location. That is, current variations at the meter location can be explained by expansion, contraction or repositioning of the gyre. In this context the higher salinity at hydrographic station 14 is indicative of the gyre core.

The current veering events (17 July, 2, 13, and 20 August) coincide with the appearance of relatively warm (less dense) water at mooring 60 (Fig. 2). This situation could prevail if the mooring was originally located on the interior of the gyre and southeastward movement or contraction occurred bringing about warmer temperature, changes in current direction, and increases in current speed. In general, increasing temperature is associated with the increase of southerly flow, while decreasing temperature is linked to reduction in flow speed. A *schematic* representation of the hypothesized eddy movement which would provide the observed flow in the vicinity of mooring 60 is shown in Figure 6. Situation A depicts northwestward flow, B relatively quiescent conditions, and C southwestward velocity. These situations are also illustrated in the 30 m vector series (Fig. 2). The vertical extent of observed temperature changes is variable. The 3 August event shows the maximum (temperature rises took place at all levels), and the last half of the 17 August event, the minimum (temperature decrease occurred most dramatically in the 20 and 30 m records) response (Fig. 2). These observations are coherent with the previously noted variations in depth of current veering.



Appendix Figure 6. Schematic representation of inner gyre displacement.

The vertical variations between events reflect the importance of direct topographic control at 90 and 50 m depth. The narrowing of the channel and saddle-like bathymetry cause convergence in the deep layer flow and current reversals can result if mass continuity is not sufficiently compensated by increases in current speed (Fig. 1).

Another, and perhaps simpler, explanation for the cross-isobath flow can be seen in a display of surface flow in a satellite photograph. ERTS/LANDSAT-1 images (Band 4, .5 to .6 micrometers wavelength) from the summer season visually delineate, via suspended sediment, boundaries between shelf water and water originating from land sources. Cloud free photographs for the summer of 1974 are not available, however, images from 1972, 1973, 1975, and 1976 indicate that the situation illustrated in Figure 7 (14 August 1973) is typical for this region.

Assuming that the boundaries defined by sediment-laden water are also dynamic boundaries, several major features of the summer flow regime are shown. These features are the cross-isobath flow along the seaward edge of the Copper River plume (southwest of the river mouth), water of coastal origin forced southwest and then offshore by Kayak Island, and an anticyclonic gyre between Middleton and Kayak Island. Further, as geostrophy is approached it is reasonable to assume that baroclinic currents, caused by density gradients, flow along these boundaries.

A simple box model calculation can be used to determine the effect of the Copper River discharge on the near coast density gradients. The dimensions of the box are 60 km (longshore), 15 km (cross-shelf), and 50 m deep. The horizontal dimensions of the box are illustrated (shaded area) in Figure 1. The horizontal dimensions were chosen to represent typical scale lengths of the Copper River discharge plume (Fig. 7).



Appendix Figure 7. ERTS/LANDSAT-1 image of Gulf of Alaska, 14 August 1973 (Band 4, 0.5 to 6.0 micrometers).

Similarly, the vertical scale represents that portion of the water column diluted directly by river discharge, wind mixing, and coastal downwelling due to onshore surface transport under wind stress. The model assumptions are (1) incoming seawater is completely mixed with river discharge within the volume, (2) changes in flow velocity result from volume continuity only, and (3) initially the salinity of the box is identical to the surrounding shelf water. A solution to the volume flux and salt conservation equations yields a time dependent salinity for the box. Under these conditions with an inflow of 10 cm/sec, a time interval of 10 days is required to reduce a initial salinity of 32 parts per thousand (PPT) to 31 (PPT). The difference between July and August Copper River discharge rates should not cause a significant variation in the time interval.

This magnitude of dilution is similar to that found in the hydrographic data (Fig. 2). This horizontal salinity gradient of 1 (PPT) over 15 km, under isothermal conditions between 5 and 8°C, would induce geostrophic flows of 22 and 12 cm/sec at the surface and 20 m depth, respectively. Only those motions caused by the salinity gradient in the upper 50 m have been considered. The estimates using a box model and geostrophic computations give evidence that the Copper River discharge plays an important role in near-shore dynamics.

Under actual conditions involving wind stress, non-uniform mixing, and mean advection along the coast, the Copper River freshwater input should have a similar influence. However, some obvious differences may occur. First, wind stress could move freshwater out of the nearshore area in the surface layer. This effect can generally be considered small because offshore winds seldom occur and local sheltering from wind stress by local orographic features reduces offshore transport (Figs. 1 and 2).

Second, horizontal salinity gradients are probably more concentrated, due to non-uniform mixing, than those considered in the calculation. The concentrated gradients would result in flow speed greater than 22 cm/sec. Unfortunately hydrographic station lines did not transect the hypothesized boundary so the model computation must be regarded as speculation. Nevertheless, the magnitude of the estimated flow from the box model is comparable to that measured at mooring 60 during cross-isobath flow, however it does not account for the observed transient flow. The horizontal component of the equation of motion (1), neglecting the frictional forces, offers insight to this observation. The local time rate of change term is estimated to be relatively small $O(10^{-5} \text{ cm/sec}^2)$ compared to the pressure and Coriolis terms which are $O(10^{-3} \text{ cm/sec}^2)$. Therefore, it will be neglected in the following analysis. While the geostrophic approximation does yield a realistic magnitude of flow along the hypothesized boundary it contains no forcing mechanism. The non-linear field acceleration term, $(\vec{V} \cdot \vec{\nabla}) \vec{V}$, becomes increasingly important if divergence occurs along the axis of flow or if flow curvature exists. From our observations the non-linear accelerations are predicted to be an order of magnitude less than either of the geostrophic terms. However, if the scale length is decreased and curvature is considered the term becomes of the same magnitude. The observations of current velocity and density at mooring 60 suggest the movement of the dynamic boundary between the Copper River plume and ambient shelf water. It is reasonable, here, to expect curvature of the boundary and divergence of flow. Since southeastward winds lead current veering events by 24 to 48 hours, it could be that wind stress is associated with horizontal movement of the boundary (Fig. 2). The mechanism that would account for near uniform horizontal translation of this boundary with depth is unclear.

A study with smaller length scales is required to delineate further these broadly described features on the Gulf of Alaska shelf. Of possible importance is the local wind stress curl (second order frictional forces) in the region between Hinchinbrook and Kayak Island. The orographic effect of these islands might be significant because they rise to height of 850 and 500 m above sea level, respectively. During southeastward winds there will be an area in the lee of Hinchinbrook Island where wind stress is relatively small and to the southeast wind stress will increase. Additional horizontal shear is expected along the lateral boundary. Local divergence of surface water created by this wind stress regime might account for the movement of internal boundaries. Similarly, northwestward winds encountering Kayak Island are expected to cause local convergence.

Experiments using satellite tracked Lagrangian drifters during the summer of 1976 were carried out by Donald Hansen at AMOL, NOAA (personal communication). Several of the drifters became involved in the anticyclonic gyre and eventually escaped moving northward along Kayak Island. Near the northern coastal boundary they all moved alongshore, westward, and out of the study area. These Lagrangian traces support a theory for an outer gyre and longshore flow induced by nearshore dilution.

CONCLUSIONS

The analysis of four filtered current meter records reveals that time dependent flow exists on the continental shelf of the Gulf of Alaska. Occasional southward current veering (cross-isobath flow) is the dominant feature of the records (Fig. 2). The duration and baroclinicity of the current events is variable. Wind records, water density, observations at the mooring location, and satellite imagery have been used to suggest

two explanations for the observed flow. The basis of the first is a time independent numerical model (Galt, 1976). The circulation, based on the hydrographic data for July 1974, includes a two gyre system at the surface (Fig. 5). The observed low frequency current fluctuations could have been associated with the inner (cyclonic-dense core) gyre if the current meter array had a position interior relative to the gyre edge. In this situation the displacement eastward or contraction of a geostrophic baroclinic gyre would have the potential for creating the observed changes in density and current velocity. An alternate explanation relies on flow features inferred from ERTS/LANDSAT-1 photography. The satellite images reveal, via suspended sediment, that a cross-isobath boundary exists between shelf water and water discharged from the Copper River (Fig. 7). A simple box model indicates that the volume of river discharge is capable of creating a horizontal density gradient of sufficient magnitude to justify geostrophic current velocities comparable to those observed. The movement of this mesoscale dynamic boundary eastward would also create the observed density and current responses at the mooring location. Wind records indicate that wind stress in the same direction as required for gyre displacement or boundary movement in the two theories, leads the observed current events by 24 to 48 hours. The relationship between this fact and the observed vertical coherence of current fluctuations remains unclear.

REFERENCES

- Bakun, A. 1975. Wind-driven convergence-divergence of surface waters in the Gulf of Alaska (abstract). *EOS Trans. AGU*, 56. pp. 1008.
- Cox, R. A., M. J. McCartney and F. Culkin. 1970. The specific gravity/salinity/temperature relationship in natural seawater. *Deep-Sea Research* 17(4):679-689.
- Dodimead, A. J., F. Favorite and T. Hirano. 1963. Review of oceanography of the sub-arctic Pacific region. *In* Salmon of the North Pacific Ocean, Bulletin. International North Pacific Fisheries Commission, 13. pp. 195.
- Ekman, V. W. 1905. On the influence of the earth's rotation on ocean currents. *Ark. Mat., Astr. Fysik* 2:1-53.
- Favorite, F. 1970. Fishery Oceanography - VII Estimation of flow in Gulf of Alaska. *Commercial Fisheries Review* 32:23-29.
- Galt, J. A. 1976. Circulation studies on the Alaskan continental shelf off the Copper River delta. NOAA Tech. Rept. ERL.
- Ingraham, W. J., Jr., A. Bakun and F. Favorite. 1976. Physical Oceanography of the Gulf of Alaska. Rept. RU-357, Northwest Fisheries Center. pp. 132.
- Ostle, B. 1963. *Statistics in Research*. Iowa State University Press, Ames. pp. 585.
- Royer, T. C. 1975. Seasonal variations of waters in the northern Gulf of Alaska. *Deep-Sea Research* 22:403-416.
- Sokal, R. R. and F. James Rohlf. 1969. *Biometry*. W. H. Freeman and Company, San Francisco. pp. 757.
- Stearns, S. D. 1973. Digital filter design routines. Rept. SLA-73-0871, Sandia Lab., Albuquerque, New Mexico. pp. 123.
- Suthuraman, S. and G. S. Raynor. 1975. Surface drag coefficient dependence on the aerodynamic roughness of the sea. *Journal of Geophysical Research* 80(36):4983-4988.
- Tabata, S. 1975. The general circulation of the Pacific Ocean and a brief account of the oceanographic structure of the North Pacific Ocean. *Atmosphere* 13(4):133-168.
- Tully, J. P. and F. G. Barber. 1960. An estuarine analogy in the subarctic Pacific Ocean. *J. Fish. Res. Bd. Canada* 17:91-112.

OCS COORDINATION OFFICE

University of Alaska

ENVIRONMENTAL DATA SUBMISSION SCHEDULE

DATE: March 31, 1977

CONTRACT NUMBER: 03-5-022-56

T/O NUMBER: 19

R.U. NUMBER: 289

PRINCIPAL INVESTIGATOR: Dr. T. C. Royer

Submission dates are estimated only and will be updated, if necessary, each quarter. Data batches refer to data as identified in the data management plan.

<u>Cruise/Field Operation</u>	<u>Collection Dates</u>		<u>Estimated Submission Dates</u> ¹		
	<u>From</u>	<u>To</u>	<u>Batch 1</u>	<u>2</u>	<u>3</u>
Acona #193	7/1/74	7/9/74	submitted	None	None
Acona #200	10/8/74	10/14/74	submitted	None	None
Acona #202	11/18/74	11/20/74	submitted	None	None
Acona #205	2/12/75	2/14/75	submitted	None	None
Acona #207	3/21/75	3/27/75	submitted	None	None
Acona #212	6/3/75	6/13/75	submitted		
Oceangrapher #805	2/1/75	2/13/75	submitted	None	None
Silas Bent #811	8/31/75	9/28/75	Submitted		
Discoverer #812	10/3/75	10/16/75	(a)		
Surveyor #814	10/28/75	11/17/75	submitted		
Discoverer #816	11/23/75	12/2/75	(b)	None	None
Station 60	6/2/74	9/10/74	None	(c)	None
Station 64	4/28/75	5/20/75	None	(c)	None
Station 9	-	-	-	(c)	
Station 9	-	-	-	(c)	
Moana Wave MW 001	2/21/76	3/5/76	submitted		
Moana Wave MW 003/004	4/20/76	5/21/76	submitted		
Moana Wave MW005	9/22/76	8/1/76	4/15/77		
Surveyor SU 003	9/7/76	9/17/76	4/15/77		

<u>Cruise/Field Operation</u>	<u>Collection Dates</u>		<u>Estimated Submission Dates</u> ¹		
	<u>From</u>	<u>To</u>	<u>Batch 1</u>	<u>2</u>	<u>3</u>
Surveyor	9/20/76	10/2/76	4/15/77		
Miller Freeman	11/1/76	11/19/76	4/15/77		
Moana Wave	10/7/76	10/16/76	4/15/77		

- Note: ¹ Data Management Plan and Data Formats have been approved and are considered contractual.
- (a) Parent tapes were coded in PODAS format, tapes were submitted to F. Cava as requested.
 - (b) Data useless due to malfunction of shipboard data logger.
 - (c) See following memo; copy enclosed, and problems section of Report.

UNIVERSITY OF ALASKA
INSTITUTE OF MARINE SCIENCE

M E M O R A N D U M

TO: Ray Hadley, Data Manager for Sea Grant

FROM: Dave Nebert, IMS Data Management *DN*

DATE: 25 March 1977

SUBJECT: Forwarding Current Meter Data to NODC

Current meter data to be forwarded to NODC under contractual agreement are:

<u>IMS Designation</u>	<u>Dates of Mooring</u>	<u>Translated by</u>	<u>Anticipated Completion Date</u>
GASS 60	2 July-26 Aug 74	Aanderaa, Norway (PMEL)	2 May 77
GASS 64	28 Apr-11 Jun 75	PMEL	Unknown
GASS 9B	21 Apr-23 Jun 76	PMEL	Unknown
GASS 9C	23 Jun-4 Nov 76	Aanderaa, B.C.	2 May 77

We are presently developing current meter processing programs and IMS data files. Those data that have been translated by Aanderaa and subsequently processed by IMS should be delivered to you in NODC format by 2 May 1977. This will include documentation on processing. Lack of documentation from PMEL preclude forwarding data translated by that organization. We are able to forward GASS 60 data because original data tapes were returned to us after processing by PMEL. They were subsequently translated by Aanderaa, Norway and processed by IMS. We cannot forward data from GASS 64 or GASS 9B until we either receive adequate documentation from PMEL or they return the original data tapes for subsequent translation by Aanderaa.

DN/sr

ANNUAL REPORT

Contract 03-5-022-56
Task Order #25
Research Unit #347
Reporting Period 4/1/76 - 3/31/77
Pages: 11

MARINE CLIMATOLOGY OF THE GULF OF ALASKA,
THE BERING AND BEAUFORT SEAS

James L. Wise
Arctic Environmental Information and Data Center
Anchorage, Alaska

March 31, 1977

UNIVERSITY OF ALASKA

March 18, 1977

ANNUAL REPORT

For the Period Ending March 31, 1977

Project Title: Marine Climatology of the Gulf of Alaska, the
Bering and Beaufort Seas

Contract Number: 03-5-022-56

Task Order Number: 25

Principal Investigator: James L. Wise*
Associate in Climatology
Arctic Environmental Information and Data Center
University of Alaska
707 A Street
Anchorage, Alaska 99501

I. Summary of objectives, conclusions and implications with respect to
OCS oil and gas development.

The objective of the project is to provide detailed marine and coastal climatology for input into the planning and operational phases of oil and gas development on the continental shelf. Conclusions normally resulting from a project will not result from this one. Decisions coming from private industry relating to their projects will use the climatological information as a partial basis for their conclusions. The same reasoning applies for implications.

II. Introduction.

A. All available climatological data for the Gulf of Alaska, Bering and Beaufort Seas will be used in determining and publishing the present state of the knowledge in this area. To best do this an atlas will be produced and published for each of the three areas mentioned above. Summarized data for period of record for coastal stations will also be included.

*This project is being conducted jointly with the National Climatic Center (NCC), a part of NOAA's Environmental Data Service. Principal Investigator for the NCC is William A. Brower, Jr., D5312. Much of this data summary work mentioned above will be done in Asheville, North Carolina, at the NCC.

- B. Specific objectives are to present information on temperature, precipitation, wind, and how they relate to such things as cloud cover, wave heights, and visibility (fog). Storm tracks and frequencies, storm surges and coastal flooding will be part of the presentation. Such things as potential superstructure icing, tides, surface currents, immersion hypothermia and topography of both land and sea will also be included. More detail on content is found in the original proposal.
- C. Extremely severe weather conditions can and do occur over all of the continental shelf areas of Alaska as well as coastal and interior portions. This makes it important that the intensities and durations of storms are known and available for use in planning, design and actual operations.

III. Current state of knowledge.

It is not necessary or practical timewise to acquire new data through field programs. It is necessary, however, to combine large quantities of raw data that have been acquired in recent years. Knowledge of the specific parameters mentioned in II above is already in a published form, but for some areas is based on small amounts of data. It is not only possible but probable that much of the present shelf material will change substantially with the addition of more recent data.

IV. Study area.

Included in the study area is the outer continental shelf of all of Alaska, and the entire coast. The area is to be covered by three volumes of the atlas. Title of the atlas will be "Climatic Atlas of the Outer Continental Shelf Waters and Coastal Regions of Alaska" Volume I, Gulf of Alaska; Volume II Bering Sea, and Volume III Chukchi and Beaufort Seas.

V. Sources, methods and rationale of data collection.

No new data will be collected through field programs. The data used are those already in the files of one of Environmental Data Service's numerous data centers. These data come from many sources. The marine data consist of observations made by "ships of opportunity" traversing Alaskan waters. The land data have been acquired from the National Weather Service through its various observational programs.

UNIVERSITY OF ALASKA

VI. Results.

Results for this project will be in the form of the completed volumes of the atlas. At this time all data have been gathered and formatted. Data are both tabulated and graphic with emphasis on graphic and only limited text. All data, legends, isopleth descriptions and text for preparation of the atlas have been received here at AEIDC from the NCC. Merging of the text and figures from NCC with those prepared at AEIDC is nearly complete. Final coordination and joint editing of the text, front material, etc of each of the three volumes is scheduled for the first half of April. Mr. Brower, the co-author, from the NCC will be here the week of April 4 for this purpose. After coordination final typesetting, page numbering, etc are expected to be complete sometime in May. All three volumes are expected to go to the printers by the first of June. Requests for bids on the printing have gone out. Table of contents and the list of maps, tables and figures, and areas covered by each volume are attached.

VII. Discussion.

Although increased knowledge is expected to result from this project, portions of the study area, because of their isolated nature, will have insufficient data for an accurate determination of all weather conditions. The resulting summaries will be qualified to show this.

VIII. Conclusions.

The summary work done for this project will update previous summaries and in addition add several new ones. It will also place together in one publication what has previously been spread through several publications. Both time and money will be saved by users.

IX. Needs for further study.

Considerable attention has been given to developing a history of storm surges. However, the scope of this study in terms of funds and time is such that more work needs to be done on this particular item. A fairly extensive bibliography can be put together on storm surges, but the ones surveyed by the principal investigator so far do not make a study of the storm itself. If this were done, it would be possible to more accurately predict the occurrence of storms having a potential for causing damage. A better knowledge of the stresses resulting from such storms will help in the engineering of equipment and structures used in the development of the outer continental shelf.

Much work has been done on the fate and effects on the environment of oil spills. Nearly all of this work has treated the oil that remains on the surface of the water, mixes into the water, sinks to the bottom or is deposited on beaches. What of the hydrocarbons which escape into the atmosphere? There are several mechanisms involved, evaporation of the lighter hydrocarbons, windblown minute droplets as aerosols or spray, and spray containing soluble hydrocarbons. These were referred to in Philip Abelson's editorial in the 14 January 1977 issue of Science. More study is needed into the effects of hot hydrocarbons introduced into the atmosphere by burning of spills or explosions, which later condense and return to the surface similar to rain. In this manner relatively large areas of the surface can be coated with oil. The resulting coating will be nuisance at the least, and may be fatal to plants and animals in the affected areas. There is a need for research into the probable and possible effects of hydrocarbons introduced into the atmosphere.

X. Summary of the 4th quarter operations.

Because there is no field work in this program, this section is not applicable.

CONTENTS

Maps, Figures and Tables

Acknowledgements

Abstract

Introduction

Selected Topics in Marine and Coastal Climatology

by James L. Wise and Harold W. Searby

Storm Surges

Superstructure Icing

Sea Ice

Immersion Hypothermia

Extremes Data

Wind Chill

Marine and Coastal Climatic Atlas

by William A. Brower, Jr., Henry F. Diaz, and Anton S. Prechtel

References

Maps

1. Bathymetry and topography
2. Storm surge occurrences
3. Summer sea surface currents
4. Winter sea surface currents

Figures

1. Tide data
2. Sea ice coverage
3. Sea ice distribution
4. Climatic means and extremes
5. Annual and extreme precipitation intensities
6. Annual and extreme snowfall and snow depth
7. Type of precipitation and obstructions to vision

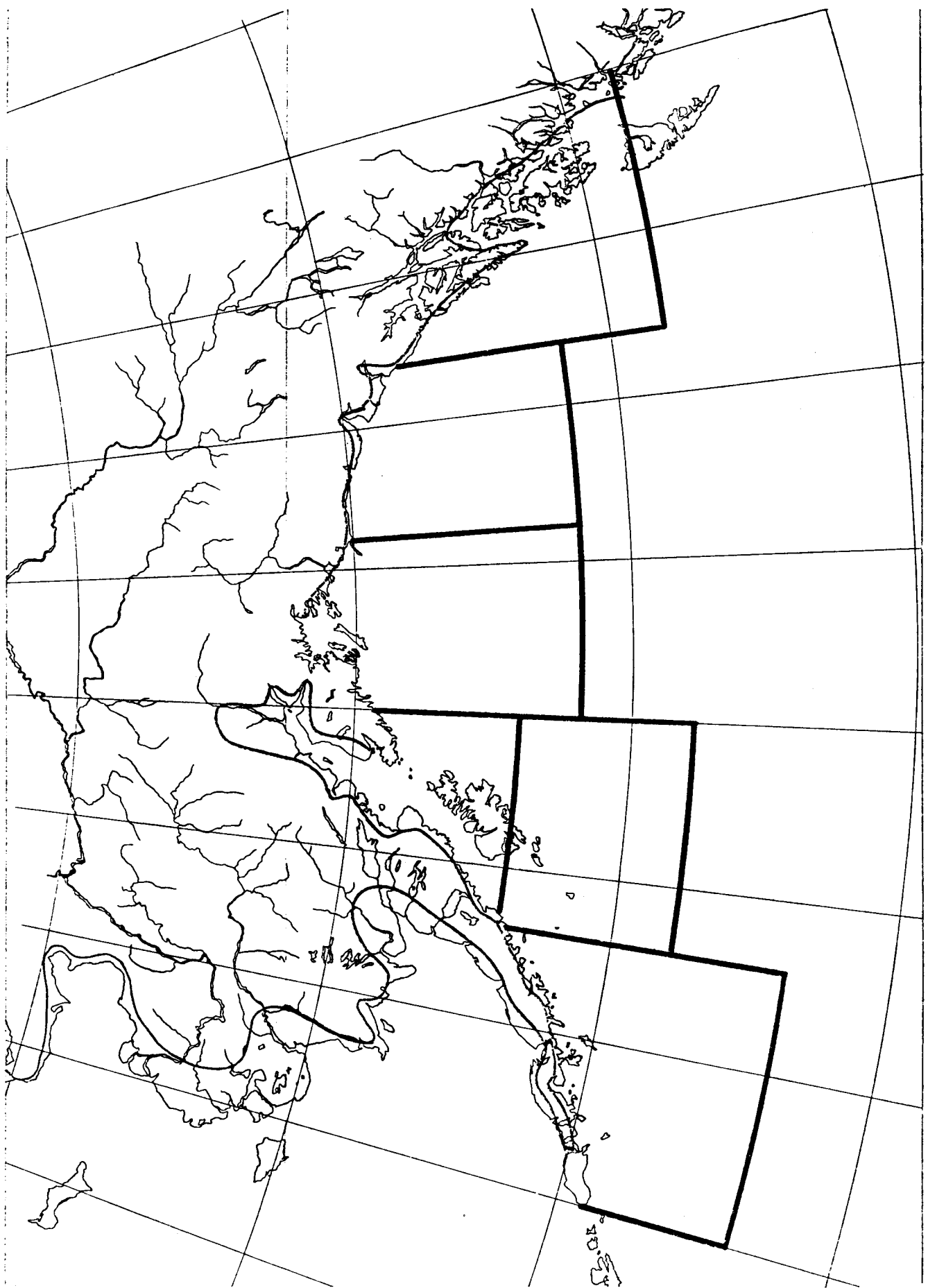
Tables

1. Guidelines for forecasting spray ice accumulation
2. Severity index and sea ice data
3. Survival time versus water temperature
4. Ceiling and visibility data
5. Equivalent wind chill temperature

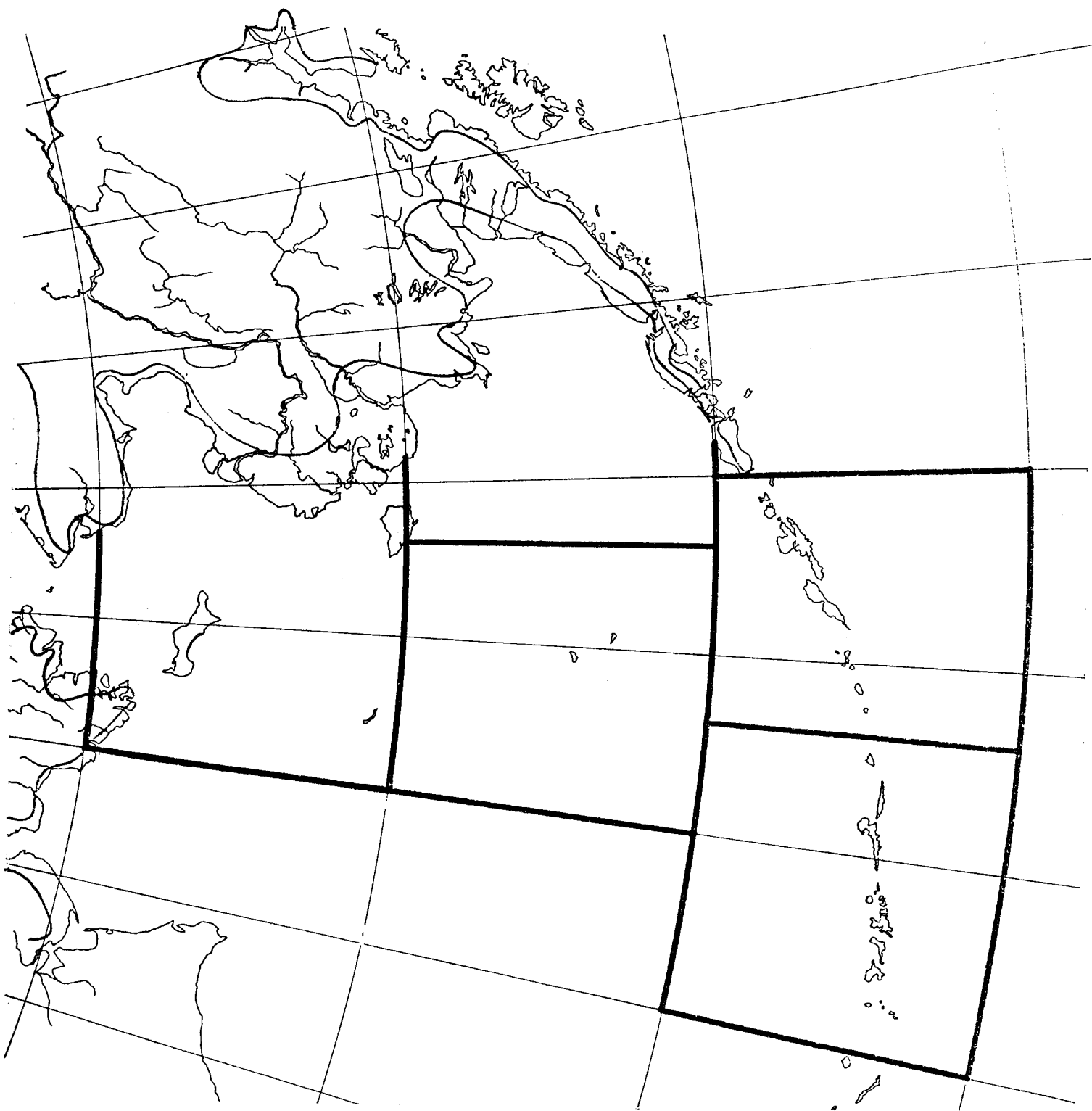
Marine and Coastal Climatic Atlas -- Page Index (cont'd)

Set No.		Jan	Feb	Mar	Apr	May	Jun	Jul	Aug	Sep	Oct	Nov	Dec
13	Sea level pressure - Graphs Mean sea level pressure - Maps												
14*	Fog/air-sea temperature difference - Graphs Mean sea surface temperature - Maps												
15*	Sea surface temperature - Graphs Sea surface temperature extremes - Maps												
16*	Wave height/direction - Graphs Wave height thresholds (nonhazardous) - Maps												
17*	Wave height/period - Graphs Wave height thresholds (hazardous) - Maps												
18	Low pressure center movement - Roses Storm track - Maps												
19	Persistence of visibility < 2 nmi - Graphs (Coastal stations)												
20	Persistence of visibility ≥ 10 knots - Graphs												
21	Persistence of wind ≥ 20 knots - Graphs												
22	Annual return periods of wind - Graphs/Tables (Coastal stations)												
23	Annual return periods of wind and waves - Tables (Marine areas)												

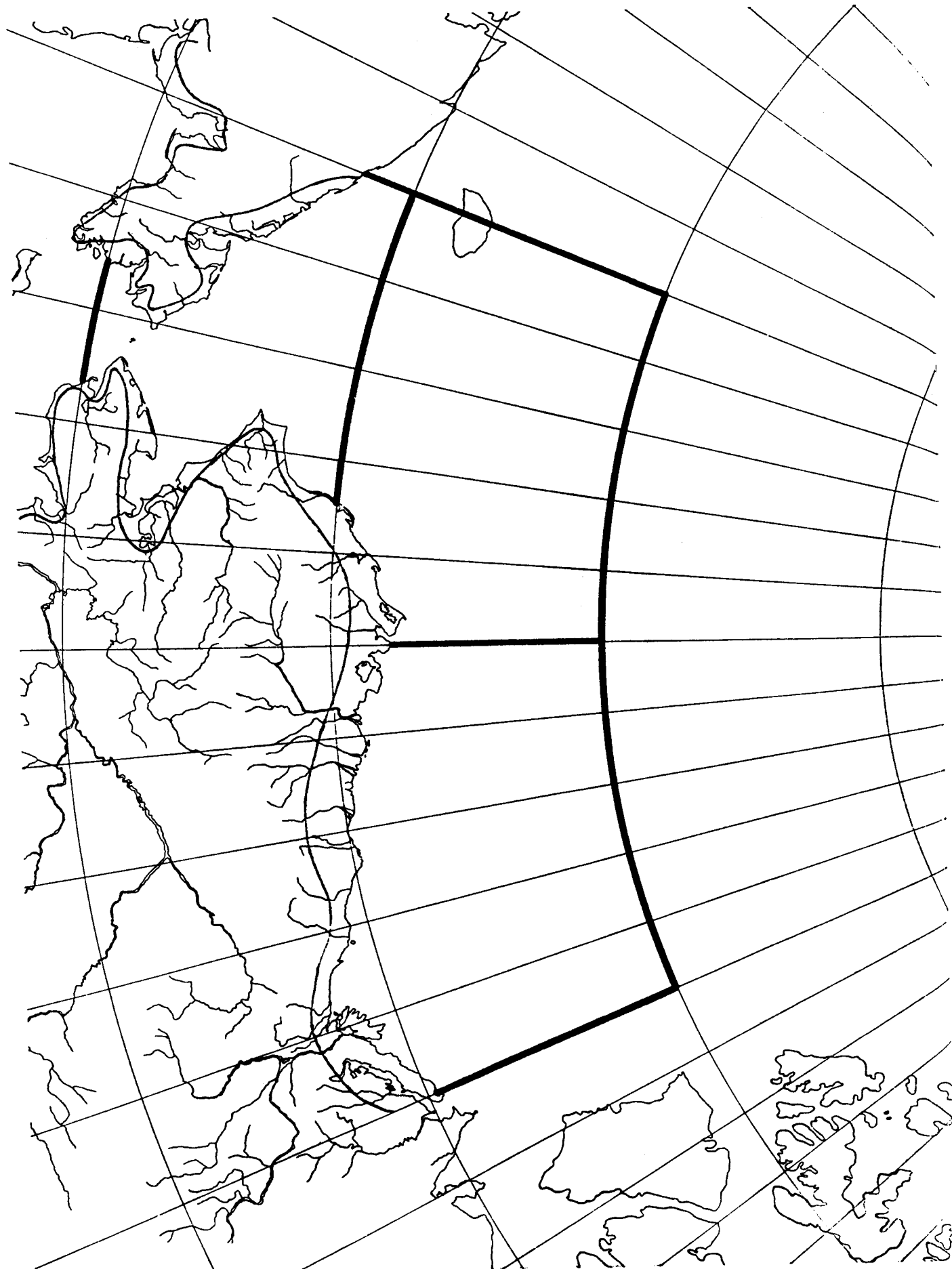
* Maps contain sea ice information



Volume I Gulf of Alaska



Volume II Bering Sea



OCS COORDINATION OFFICE

University of Alaska

ENVIRONMENTAL DATA SUBMISSION SCHEDULE

DATE: March 31, 1977

CONTRACT NUMBER: 03-5-022-56 T/O NUMBER: 25 R.U. NUMBER: 347

PRINCIPAL INVESTIGATOR: Mr. James Wise

No environmental data are to be taken by this task order as indicated in the Data Management Plan. A schedule of submission is therefore not applicable¹.

NOTE: ¹ Data Management Plan has been approved and made contractual.

OCS COORDINATION OFFICE
 University of Alaska
 ESTIMATE OF FUNDS EXPENDED

DATE: March 31, 1977
 CONTRACT NUMBER: 03-5-022-56
 TASK ORDER NUMBER: 25
 PRINCIPAL INVESTIGATOR: Mr. James L. Wise

Period July 1, 1975 - March 31, 1977 (21 mos.)

	<u>Total Budget</u>	<u>Expended</u>	<u>Remaining</u>
Salaries & Wages	56,086	45,736	10,350
Staff Benefits	10,080	8,224	1,856
Equipment	-0-	-0-	-0-
Travel	2,045	1,346	699
Other	<u>3,226</u>	<u>4,086</u>	<u>(860)</u>
Total Direct	71,437	59,392	12,045
Indirect	<u>29,461</u>	<u>24,033</u>	<u>5,428</u>
Task Order Total	<u>100,898</u>	<u>83,425*</u>	<u>17,473</u>

*Preliminary cost data, not yet fully processed.

ANNUAL REPORT

US Department of the Interior's Bureau of Land Management (BLM)
Alaskan Outer Continental Shelf Environmental Assessment Program (OCSEAP)

Contract No: N.A.

Research Unit No: 347

Number of Pages: 5

Climatic Atlas of the Outer Continental Shelf Waters
and Coastal Regions of Alaska

Vol. I Gulf of Alaska
Vol. II Bering Sea
Vol. III Chuckchi - Beaufort Sea

Principal Investigators

James L. Wise
Harold W. Searby
Arctic Environmental Information
and Data Center
University of Alaska
Anchorage, Alaska 99501

William A. Brower, Jr.
Henry F. Diaz
Anton S. Prechtel
National Oceanic and Atmospheric
Administration
Environmental Data Service
National Climatic Center
Asheville, North Carolina 28801

COMM: (907) 279-4523

FTS : 672-0266
COMM: (704) 258-2850 ext 266

March 21, 1977

ANNUAL REPORT

- I. Summary of objectives, conclusions and implications with respect to OCS oil and gas development.

This study is to establish descriptive climatology and data analysis of surface marine and atmospheric parameters for the outer continental shelf waters and coastal regions of Alaska. It is to serve as an environmental guide in assessing potential impact of oil and gas exploration and development and in influencing leasing and operating regulations and design of monitoring programs to permit resource development with the necessary environmental protection.

- II. Introduction

Because weather plays a governing role in determining the nature of offshore activities, knowing what kind of weather to expect is important in planning for efficient and safe operations. Evaluation of extreme weather conditions is essential before designing, constructing, and operating permanent platforms and structures in the ocean. Such information is also important in developing onshore supporting activities and assessing the onshore impact of offshore activities.

The NCC and AEIDC are involved in a joint study to determine and publish a descriptive climatology for those Alaskan waters and coastal regions that are important to resource development of the outer continental shelf (OCS). The evaluation is to be in the form of a climatic atlas for each of three marine and coastal areas; the Gulf of Alaska, the Bering Sea, and the Chuckchi-Beaufort Seas. The maps, graphs and tables in each atlas will present a detailed climatic profile of the marine and coastal

regions of Alaska. Statistics include means, extremes, and percent frequency of occurrence of threshold values for these elements: wind, visibility, present weather, sea level pressure, temperature, clouds, and waves.

III. Current state of knowledge

The U.S. Navy Marine Climatic Atlas of the World, Vol. II, North Pacific Ocean (1959), one of eight volumes in a series of atlases of the world which is currently being updated by the Navy, has had wide acceptance as an authoritative reference for large scale operational planning and research.

The present study will provide three atlases to represent the total of the Alaskan waters and each will be based on more than 20 years of additional marine data. Also, as marine data are typically sparse in the near coastal zone, a zone of sharp gradients and complex climate, data for 49 coastal stations will be included.

IV. Study area

The study area covers the Alaskan waters and coastal areas within 50° - 75° N and 130° - 180° W. The total area will be presented in three climatic atlases: the Gulf of Alaska, 50° - 65° N, 130° - 155° W; Bering Sea, 50° - 65° N, 155° - 180° W; and Chuckchi-Beaufort Sea, 65° - 75° N, 130° - 180° W.

V. Sources, methods and rationale of data collection

The marine observations used in computing the statistics for the maps, graphs, and tables in this atlas were taken from the National Climatic Center's (NCC) Tape Data Family 11 (TDF-11), containing surface marine observations collected by ships of various registry

traveling through the study area. Because the near-coastal zone is relatively data-sparse, observations for 49 coastal land stations were combined with the marine data to present the best possible climatological picture of the outer continental shelf waters and coastal regions of Alaska.

The stations' data were taken from the edited digital files of NCC and the U.S. Air Force's Environmental Technical Applications Center (Asheville, NC). The marine data were subjected to thorough computer and visual quality control before processing; this included elimination of duplicate observations and elimination or adjustment of elements detected during internal consistency and extreme value checks.

The percentages of the 600,000 marine and 2 million land observations that contained basic weather elements are:

	Marine	Coastal Stations
wind	98.5	98.2
visibility	97.8	97.4
present weather	96.9	98.2
sea level pressure	96.2	97.2
air temperature	99.1	99.4
wet bulb temperature	64.9	96.6
sea surface temperature	86.1	-
total cloud amount	95.6	97.8
low cloud amount	79.1	70.1
waves	70.8	-

With a TDF-11 inventory of the number of ships' observations by 1.0° squares, a polar projection grid was defined to give an approximate equal geographic area coverage: 1° latitude by 2° longitude for the latitude belt 50° - 61°N; 1° by 3° for 61° - 70°N; and 1° by 4° for 70° - 80°N. Element statistics (with observation counts) for each of 445 marine squares and 49 coastal stations for each month were then computed and plotted on maps. Meteorologists drew isopleths (lines connecting points of equal magnitude) on 324 element maps, making subjective

adjustments when data biases or insufficient observations were evident. They also performed consistency checks in monthly patterns for each element and between elements as well as comparative checks with other marine atlases and publications.

To supplement the isopleth analyses, over 10,000 statistical graphs were produced for 39 of the coastal stations and for 14 representative marine areas. The graphs represent the objective compilation of available data; they were not adjusted for suspected biases, and differences may be found when comparing the graphic data with the isopleth analyses. Attachment 1 defines by atlas the land stations and representative marine areas having data plotted for analysis and graphs.

VI. Results

The climatic data in each atlas are to be represented monthly, by isopleths on charts and by statistical graphs (see attachment 2, Legends).

Each atlas will be 11" x 11" in size and contain some 480 pages, of which 228 will be 3-color charts, each page having an opposing page of graphs for the particular set of coastal stations and marine areas pertinent to each atlas volume. The remaining pages will consist of statistical tables and a descriptive narrative of the atlas content.

VII. Discussion

A special effort was undertaken to digitize surface marine observations for the Alaskan area for the period 7/73 - 12/74. However, because there were still insufficient marine data available north of 60° latitude, data for 16 additional Alaskan and for six Russian coastal stations were processed to supplement the data of the originally proposed 27 coastal stations and marine areas.

Interaction continues between NCC and AEIDC to refine atlas specifications in order to provide as comprehensive a product as time and funds permit.

VIII. Conclusion

As of March 15, 1977, NCC has expended the \$10K funded for FY-77, and all materials that NCC was to provide for use in the atlases have been completed and mailed to AEIDC. This includes some 10K statistical graphs, 360 isopleth charts, and a text describing these products. AEIDC is to provide extremes of all weather elements and information on coastal damage resulting from wind generated weather elements, check the analysis work done by NCC and prepare all materials for print. Graphics preparation by AEIDC of the combined NCC/AEIDC materials is about complete, and NCC's Principal Investigator, Bill Brower, is scheduled to visit Anchorage the week of April 3 to assist AEIDC in the editing of these materials. (AEIDC will provide an independent annual report).

IX. Need for further study

This research task is to be completed with the publication in FY-77 of the Climatic Atlas of the OCS Waters and Coastal Regions of Alaska, Vols. I - III. It is important, however, that the digital files processed for these atlases be maintained and updated to continue providing the best possible data products and services for OCSEAP tasks (see RU # 496 for recommendations).

X. Not applicable.

ATTACHMENT 1

GULF OF ALASKA (VOL. I)

<u>Land Stations</u>	<u>Lat.(°N)</u>	<u>Lon.(°W)</u>	<u>Data Processed</u>	<u>No. of Obs.</u>	<u>Avg. No. Obs./Day</u>
Anchorage	61.2	150.0	Nov 1952-Dec 1974	61,834	8
Annette Island	55.0	131.6	Jul 1948-Dec 1974	77,419	8
Cold Bay	55.2	162.7	Jul 1955-Dec 1974	56,985	8
Cordova	60.5	145.5	Jan 1945-Jan 1971	74,809	8
Homer	59.6	151.5	Jul 1945-Dec 1974	76,366	8
Kenai	60.6	151.3	Jul 1948-Jan 1971	69,454	8
Kodiak	57.8	152.3	Nov 1945-Dec 1974	84,630	8
Middleton Island	59.5	146.3	Jul 1948-Jun 1963	43,216	8
Sitka	57.1	135.4	Jul 1948-Jan 1971	65,989	8
Yakataga	60.1	142.5	Jul 1948-May 1968	52,982	8
Yakutat	59.5	139.7	Aug 1948-Dec 1974	77,101	8

Representative Marine Areas

A	52-Coast	156-165	1872-1974	41,097
B	54-57	150-156	1872-1974	12,491
C	57-Coast	150-Coast	1872-1974	11,703
D	56-Coast	144-150	1872-1974	20,016
E	56-Coast	138-144	1872-1974	13,480
F	54-Coast	Coast-138	1872-1974	18,891

BERING SEA (VOL. II)

<u>Land Stations</u>	<u>Lat.(°N)</u>	<u>Lon.(°W)</u>	<u>Data Processed</u>	<u>No. of Obs.</u>	<u>Avg. No. Obs./Day</u>
Adak	51.9	176.6	Jan 1949-Dec 1974	75,956	8
Bethel	60.8	161.8	Jul 1948-Dec 1971	66,789	8
Buhta Providenija	64.4	173.2	Jan 1959-Jun 1971	27,320	4-8
Cape Newenham	58.7	162.1	Jul 1953-Dec 1970	46,471	6-8
Cape Romanzof	61.8	166.0	Mar 1953-Nov 1968	44,624	8
Driftwood Bay	54.0	166.9	Jul 1959-May 1969	28,896	8
Gambell	63.8	171.8	Jul 1949-Jun 1953	14,588	8
King Salmon	58.7	156.7	Jan 1949-Dec 1974	75,919	8
Moses Point	64.2	162.1	Jul 1948-Jun 1967	51,723	8
Nikolski	52.9	168.8	Jun 1959-Nov 1968	27,453	8
Nome	64.5	165.4	Jan 1945-Dec 1974	87,331	8
Northeast Cape	63.3	160.5	Jun 1959-Nov 1968	27,466	8
St. Paul Island	57.2	170.2	Jan 1956-Dec 1974	51,606	8
Unalakleet	63.9	160.8	Jul 1948-Dec 1964 Apr 1968-Dec 1974	44,624	8

Representative Marine Areas

A	60-65	Coast-175	1872-1974	8,526
B	55-60	167-175	1872-1974	31,892
C	55-60	Coast-167	1872-1974	46,971
D	50-55	172-180	1872-1974	62,391
E	50-55	165-172	1872-1974	68,020

CHUCKCHI - BEAUFORT SEA (VOL. III)

<u>Land Stations</u>	<u>Lat. (°N)</u>	<u>Lon. (°W)</u>	<u>Data Processed</u>	<u>No. of Obs.</u>	<u>Avg. No. Obs./Day</u>
Barrow	71.3	156.8	Jul 1948-Dec 1974	76,307	8
Barter Island	70.1	143.6	Jan 1949-Dec 1974	75,878	8
*Camden/Pow-D	70.0	144.8	Mar 1958-Jul 1963	2,782	1-2
*Cape Beaufort/Liz-A	69.0	163.8	Oct 1957-Aug 1963	4,123	2
Cape Liz-B	68.9	166.1	Aug 1952-Dec 1971	52,635	8
*Cape Simpson/Pow-A	71.1	154.8	Nov 1957-Aug 1963	4,386	2
*Flaxman Isl/Pow-3	70.5	149.9	Aug 1957-Jun 1971	9,750	2
*Humphrey/Bar-A	70.0	142.3	Apr 1958-Aug 1963	2,821	1-2
*Icy Cape/Liz-B	70.4	161.7	Nov 1957-Aug 1963	3,745	2
*Kogru River/Liz-B	71.6	152.2	Jan 1958-Aug 1963	3,966	2
Kotzebue	66.9	162.6	Jan 1945-Dec 1974	87,129	8
Lonely Point/Pow-1	70.9	153.2	Jul 1957-Nov 1975	26,790	4
*McIntyre/Pow-C	70.4	138.7	Mar 1958-Jun 1963	3,524	1-2
Mys Smidta	68.9	179.5	Jan 1959-Jun 1971	27,506	4-8
Mys Uzlen	66.2	169.8	Jan 1959-Jun 1971	27,403	4-8
Oliktok/Pow-2	70.5	149.9	Aug 1957-Nov 1975	26,493	4
Ostrov Kolyvchino	67.5	174.6	Jan 1959-Dec 1963	13,954	4-8
Ostrov Vrangolja	71.0	178.5	Jan 1959-Jun 1971	27,144	4-8
*Pearl Bay/Liz-C	70.8	158.3	Aug 1957-Jun 1963	3,896	2
Point Lay/Liz-2	69.7	163.0	Aug 1957-Nov 1975	26,510	4
Tin City	65.6	167.9	May 1953-Dec 1971	51,701	8
Wainwright/Liz-3	70.6	159.9	Aug 1957-Nov 1975	26,613	4
*Zaliv Kresta	66.4	179.1	Jan 1960-Jun 1971	20,687	4-8

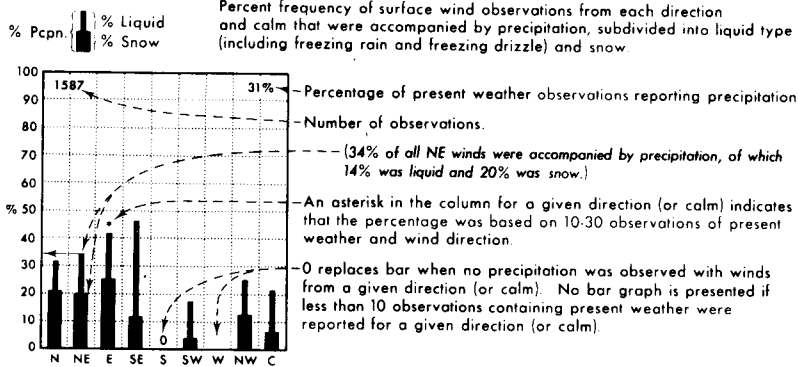
Representative Marine Areas

A	70-75	155-180	1872-1974	6,031
B	70-75	130-155	1872-1974	5,644
C	65-70	Coast-180	1872-1974	6,693

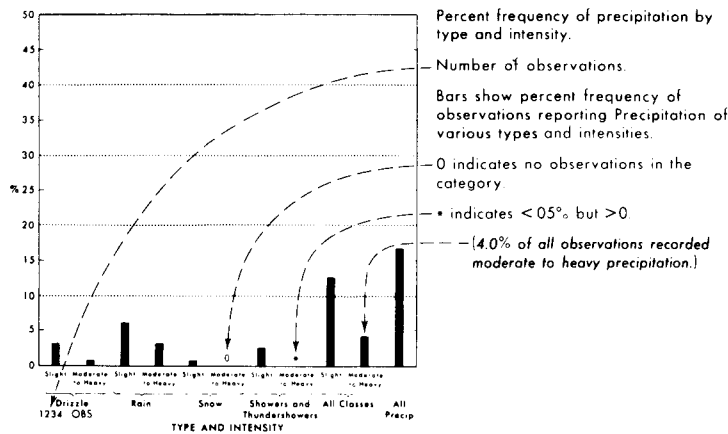
* There were insufficient observations to produce graphs; the stations' data were included to supplement the relatively few available marine observations, and were plotted and analyzed to permit a best estimate of the marine climatology of the coastal zone.

The land and marine data used in producing the maps and graphs are at the NCC in a separate file designated the Alaskan Waters Atlas work tapes. Also on file are computer tabulations of monthly statistical tables for the above stations and marine areas.

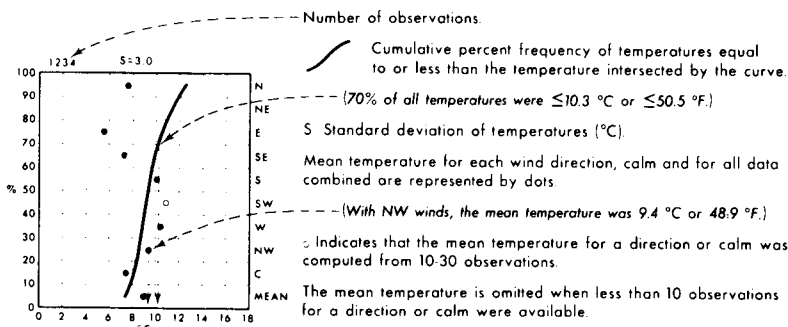
Precipitation/wind direction



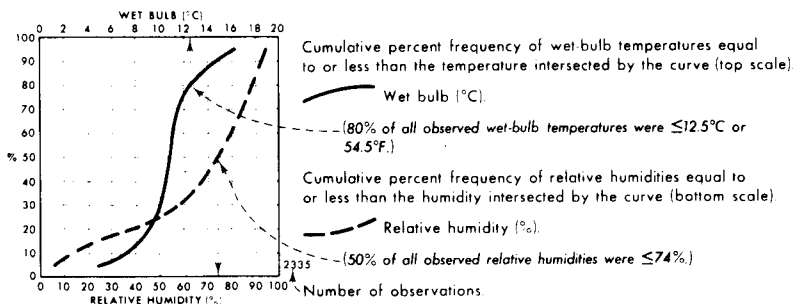
Precipitation types



Air temperature/wind direction



Wet bulb/relative humidity



Map - Precipitation

BLACK LINE - Percent frequency of observations reporting precipitation

Of all the elements recorded in historical marine observations, precipitation is one of those most subject to interpretation error, from coding practices, observers preference for certain present weather codes, and other biases.

Map - Snow

BLACK LINE - Percent frequency of precipitation observations reporting snow

The percent frequency of observations reporting snow for a given point can be determined by multiplying the percent frequency of observations reporting precipitation (map 1) with that of precipitation observations reporting snow (map 2).

Map - Air temperature mean and thresholds

BLACK LINE - Percent frequency of temperature ≤ 0°C (≤ 32°F)

RED LINE - Mean air temperature (°C)

BLUE LINE - Percent frequency of wind chill temperature ≤ -30°C (≤ -22°F)

Air temperature readings recorded on transient ships in warm, sunny weather appear biased toward high temperatures, apparently because of improper instrument exposure and ventilation. Despite the inaccuracies, the large-scale patterns and mean gradients of the isopleth analyses are relatively accurate.

The temperature scale of the graph may vary in both range and class interval. The percentage of temperature observations greater than a given value can be obtained by subtracting the cumulative percent frequency of that value from 100%. The number of observations and the standard deviation plus the plotted points on the graphs are based on those observations reporting both temperature and wind direction. The cumulative curve is based on all observations reporting temperature with or without wind direction.

Map - Mean dew point temperature

BLACK LINE - Mean dew point temperature (°C)

The observation count of the graph reflects those observations reporting both air and wet bulb temperatures; both are required in computing the relative humidity. The percentage of observations of either element greater than a given value can be obtained by subtracting the cumulative percent frequency of that value from 100%.

Air temperature/wind speed

WIND SPEED (kts)	
Temp (°C)	0 2 4 10 11 21 22 33 ≥34
4.5	18 8 7 1 1
2.3	17 8 7 1 1
0.1	13 6 5 1 1
2.1	1 0 0 0 0
4.3	0 0 0 0 0
6.3	0 0 0 0 0
8.2	1 0 0 0 0
10.9	0 0 0 0 0
12.11	1 0 0 0 0
14.13	1 0 0 0 0
16.15	1 0 0 0 0
3550	

Percent frequency of simultaneous occurrence of specified temperature (°C) and wind speed (knots).

(1% of all observations reported temperature 2-3°C simultaneously with wind speed of 22-33 kts.)

Indicates < .5% but > 0.

Number of observations.

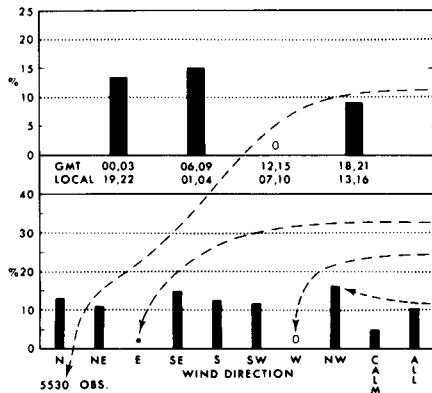
Map - Air temperature extremes (°C)

BLACK LINE - Maximum (99%) air temperature (1% of temperatures were greater than the given value)

BLUE LINE - Minimum (1%) air temperature (1% of temperatures were equal to or less than the given value)

The graph can be used to determine the extent of human discomfort from the combined effects of extreme heat or cold and winds or to estimate the likelihood of superstructure icing. Icing potential increases as the air temperature drops below freezing and the winds increase above 10 knots (12 mph) and may become quite severe with temperatures equal to or less than -9°C (16°F) and winds equal to or greater than 34 knots (39 mph).

Fog/time and fog/wind direction



Number of observations.

Bar graphs represent percent frequency of Fog (without precipitation) for various hour groupings and wind directions. Data are based on 100% for each hour-group and direction category.

* indicates < 0.5% but > 0.

0 indicates no fog occurred with the wind direction.

(Data show that 17% of all NW winds were accompanied by Fog (without precipitation).)

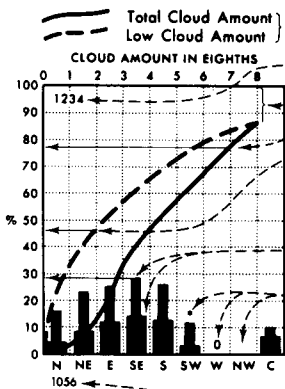
Map - Fog

BLACK LINE - Percent frequency of occurrence of all fog

BLUE LINE - Percent frequency of fog occurring without precipitation

The percent frequency of observations reporting fog with precipitation for a given point can be determined by computing the difference between the two analyses.

Cloud cover/wind direction



Total Cloud Amount

Low Cloud Amount

Cumulative percent frequency of indicated cloud amount equal to or less than the amount intersected by the curve.

Number of total cloud observations.

Observations.

(77% of all total cloud amounts were ≤ 7/8.)

(46% of all low cloud amounts were ≤ 2/8.)

Low cloud amount: Percent frequency of observations from each direction and calm that were accompanied by low cloud amounts ≥ 5/8 and ≥ 7/8. Low clouds are clouds with bases < 8000 feet.

(28% of all SE winds were accompanied by low cloud amounts ≥ 5/8 and 14% by low cloud amounts ≥ 7/8.)

An asterisk indicates that the percentage is based on 10-30 observations of wind direction, total and low cloud amount. 0 replaces bar graph when no low cloud amounts ≥ 5/8 were observed with a wind direction or calm. 0 or bar is omitted when number of observations of total and low cloud amount from a wind direction or calm is less than 10.

Number of low cloud observations.

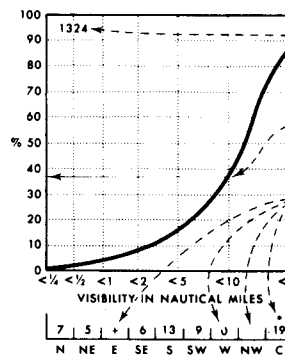
Map - Cloud amount thresholds

BLACK LINE - Percent frequency of total cloud amount ≤ 2/8

BLUE LINE - Percent frequency of low cloud amount ≥ 5/8

Since the number of observations reporting low cloud amount is usually less than that for total cloud amount, somewhat different samples may be used to compute the two curves on the graph. This may lead to inconsistencies where low cloud amount appears higher than the total cloud amount. Where this occurred the graph was adjusted in favor of the total cloud by making the curves coincide. The frequency of obscured conditions may be determined by subtracting the cumulative percent frequency corresponding to 8/8 coverage from 100%. In computing the bar graph, obscurations are considered as 8/8 coverage.

Visibility/wind direction



Number of observations.

Cumulative percent frequency of visibilities less than the visibility intersected by the curve.

(37% of all visibilities reported were < 10 nautical miles.)

The table below the graph indicates percent frequency of occurrence of visibility < 2 nautical miles versus wind direction.

* indicates < .5% but > 0. 0 indicates that no visibilities < 2 nautical miles were observed with winds from a direction or calm. No percentage is given if less than 10 observations were available for visibility and wind direction. An asterisk indicates that the percentage was based on 10-30 observations of visibility and wind direction.

(13% of all S winds were accompanied by visibilities < 2 nautical miles.)

Map - Visibility thresholds

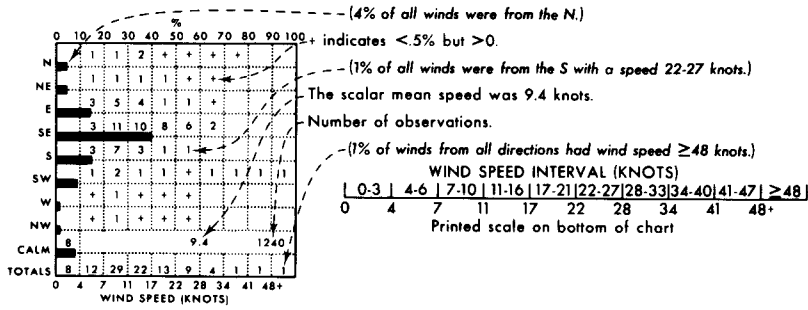
BLACK LINE - Percent frequency of visibilities ≥ 5 nautical miles

BLUE LINE - Percent frequency of visibilities < 2 nautical miles

The percentage of visibility equal to or greater than a given value can be obtained from the graph by subtracting the cumulative percent frequency of that value from 100%. Visibility at sea is difficult to measure because of the lack of reference points. Also, some observers seem to report reduced visibilities at night because of darkness, though this tendency has abated in recent years. The coarseness of the coding intervals, however, tends to minimize serious biases in the summarized data. Visibilities greater than 25 nmi. should be interpreted cautiously because the earth's curvature makes it impossible to see 25 nmi. horizontally from the bridges of most ships.

Wind speed/direction

Direction frequency (top scale): Bars represent percent frequency of winds observed from each direction. Speed frequency (bottom scale): Printed figures represent percent frequency of wind speeds observed from each direction.



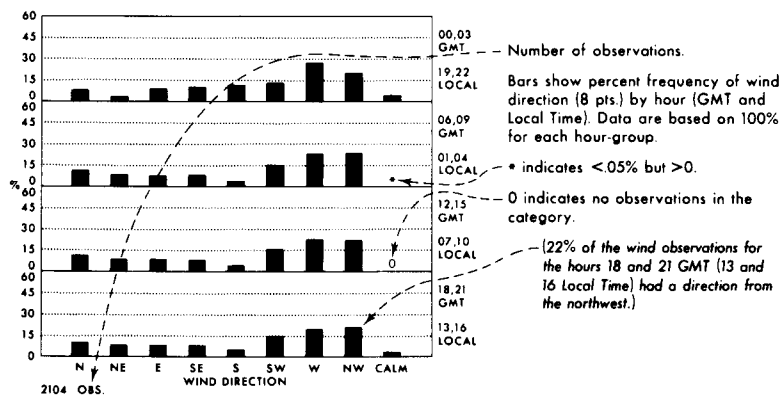
Map - Wind speed thresholds

BLACK LINE - Percent frequency of wind speed ≤ 10 knots (≤ 12 mph)

BLUE LINE - Percent frequency of wind speed ≥ 34 knots (≥ 39 mph)

The scalar mean wind speed on the graph is based on the number of observations reporting a wind speed with direction. The sum of the totals line provides the cumulative percent frequency of wind speed below a selected threshold value. In the example graph, 71% of all winds were less than 17 knots (20 mph).

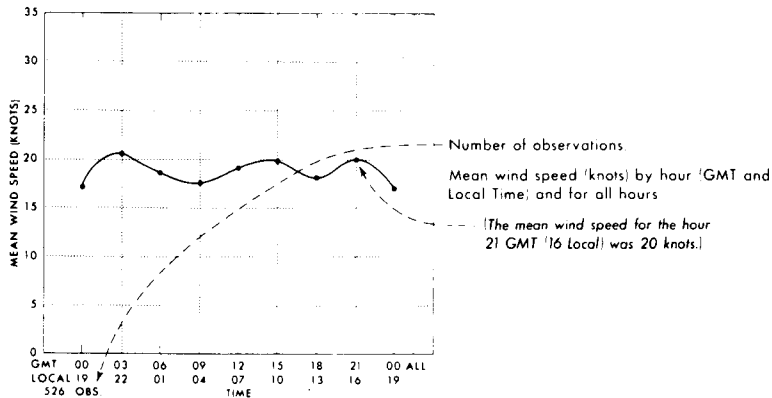
Wind direction/diurnal variation



Map - Vector mean wind

10.2 Direction of flow toward station dot; vector magnitude in knots (example: vector mean wind is from northeast at 10.2 knots or 11.7 mph)

Wind speed/diurnal variation

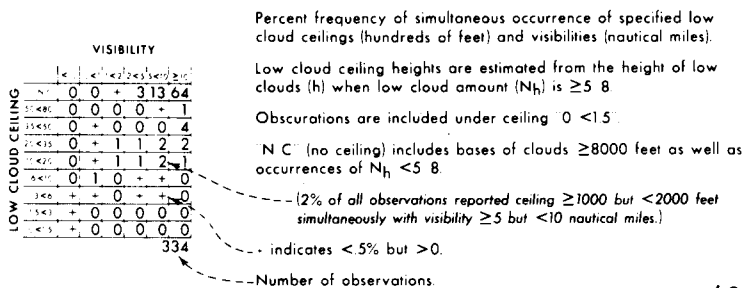


Map - Scalar mean wind

BLACK LINE - Scalar mean wind (knots)

In areas of high persistence of direction, the magnitude of the vector mean winds should closely approach that of the scalar mean winds. As most of the marine observations are recorded at six hour intervals, disregard the plots for other than 00, 06, 12, 18, GMT hours on the marine area graphs.

Low cloud ceiling/visibility

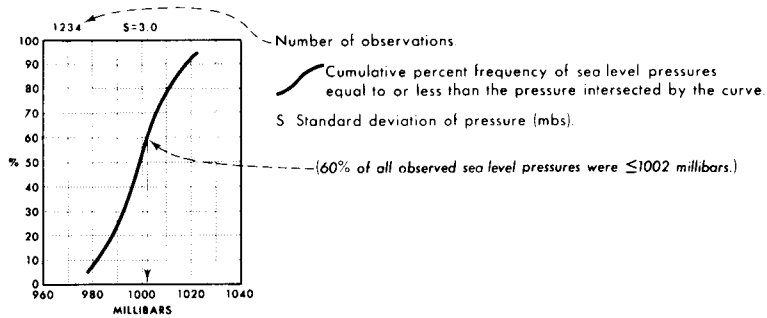


Map - Low cloud ceiling and visibility thresholds

BLACK LINE - Percent frequency of low cloud ceiling ≥ 1000 feet (or no low cloud ceiling) and visibility ≥ 5 nautical miles

BLUE LINE - Percent frequency of low cloud ceiling < 600 feet and/or visibility < 2 nautical miles

Sea level pressure

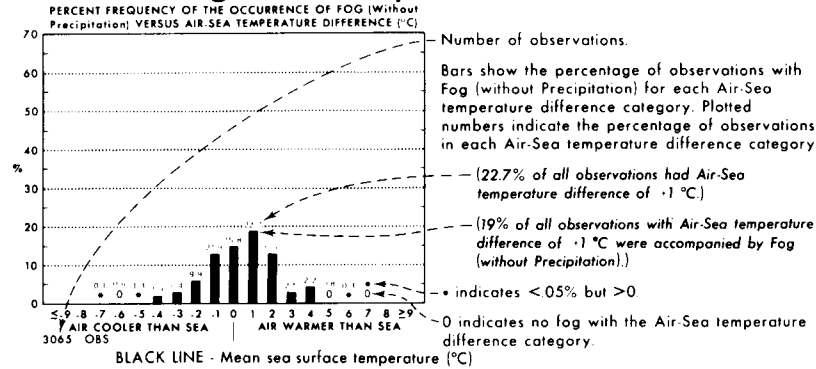


Map - Mean sea level pressure

BLACK LINE - Mean sea level pressure (millibars)

Sea level pressure is one of the most frequently recorded elements but one of the least accurate because of instrument and coding errors. Despite the inaccuracies of the individual readings, however, the large-scale patterns and mean gradients of the isopleth analyses are relatively accurate.

Fog/air-sea temperature difference



BLACK LINE - Mean sea surface temperature ($^{\circ}$ C)

Map - Mean sea surface temperature

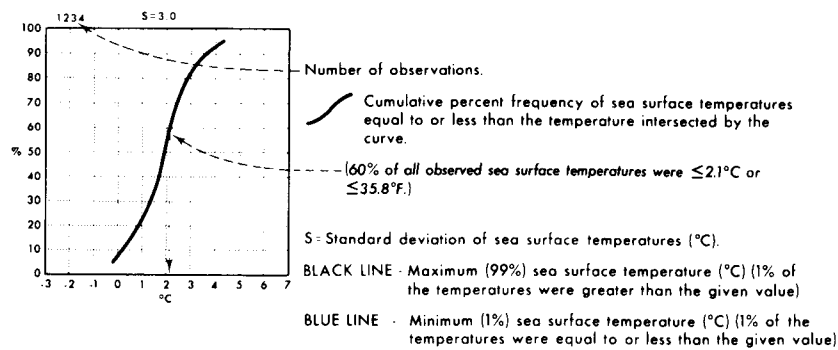
BLACK LINE - Mean sea surface temperature ($^{\circ}$ C)

Sea surface temperature is recorded frequently in marine observations; the various methods of recording tend to decrease the reliability of individual values. Despite the inaccuracies, the large-scale patterns and mean gradients of the isopleth analyses are relatively accurate.

Sea surface temperature may be used to estimate the length of time a person in ordinary clothes and life preserver may be expected to survive if washed overboard. The approximate survival time as a function of water temperature is shown in the following table:

Water Temperature $^{\circ}$ C	Water Temperature $^{\circ}$ F	Exhaustion or Unconsciousness	Expected Survival Time
<0	<32	<15 min	<15-45 min
0-5	32-41	15-30 min	30-90 min
5-10	41-50	30-60 min	1-3 hr
10-15	50-59	1-2 hr	1-6 hr
15-20	59-68	2-7 hr	2-40 hr
20-25	68-77	3-12 hr	3-indefinite hr
>25	>77	indefinite	indefinite

Sea surface temperature



BLACK LINE - Maximum (99%) sea surface temperature ($^{\circ}$ C) (1% of the temperatures were greater than the given value)

BLUE LINE - Minimum (1%) sea surface temperature ($^{\circ}$ C) (1% of the temperatures were equal to or less than the given value)

Map - Sea surface temperature extremes ($^{\circ}$ C)

BLACK LINE - Maximum (99%) sea surface temperature (1% of the temperatures were greater than given value)

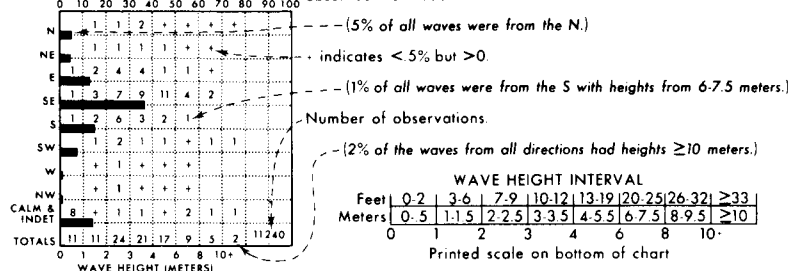
BLUE LINE - Minimum (1%) sea surface temperature (1% of the temperatures were equal to or less than given value)

The percentage of temperatures greater than a given value can be obtained from the graph by subtracting the cumulative frequency of that value from 100%. The number of observations and the standard deviation are based on all observations reporting sea surface temperature. The isopleths representing extreme conditions show the maximum (99%) and the minimum (1%) levels of sea surface temperature. The various methods of recording the sea surface temperature tend to decrease the reliability of the individual values. Gradients and relative values of the isopleths, however, are considered reliable.

Wave height/direction

Direction frequency (top scale): Bars represent percent frequency of waves from each direction.

Height frequency (bottom scale): Printed figures represent percent frequency of wave heights observed from each direction.



BLACK LINE - Percent frequency of wave height <1.5 meters (<5 feet)

BLUE LINE - Percent frequency of wave height <2.5 meters (<8 feet)

Map - Wave height thresholds (nonhazardous sea conditions)

BLACK LINE - Percent frequency of wave height <1.5 meters (<5 feet)

BLUE LINE - Percent frequency of wave height <2.5 meters (<8 feet)

Indeterminate directions are combined with calms in the direction scale of the graph (they can be distinguished by consulting the height scale). The number of observations is from all observations reporting both wave heights and directions. The higher of the sea wave or swell wave was selected for summarization. If the heights were equal, the wave with the longer period was selected. Wave height estimates are very subjective and depend upon the observer's experience and the size of the ship from which the observation is taken. Wave heights tend to be slightly underestimated by observers on transient ships. A correction factor of 1.1 was suggested (Hogben and Lumb 1967) and has been verified by preliminary work at NCC. Data in this atlas, however, have not been adjusted.

Wave height/period

HEIGHT METERS	PERIOD (Seconds)										NO.
	<6	6-7	8-9	10-11	12-13	14-15	16-17	18-19	20-21	>21	
0-1	21	3	1	+	+	+	+	+	+	+	0
1-1.5	22	16	6	2	+	+	+	+	+	+	0
2-2.5	3	6	4	3	1	+	+	+	+	+	0
3-3.5	+	1	1	1	1	+	+	+	+	+	0
4-5.5	+	+	+	+	+	+	+	+	+	+	0
6-7.5	0	+	+	0	0	+	+	+	+	+	0
8-9.5	0	0	0	0	0	0	0	0	0	0	0
≥10	0	0	0	0	0	0	0	0	0	0	0
4010											

Percent frequency of occurrence of wave period and height.

(2% of observed waves had a height of 1-1.5 meters and a period of 10-11 seconds.)

+ indicates <.5% but >0.

Number of observations.

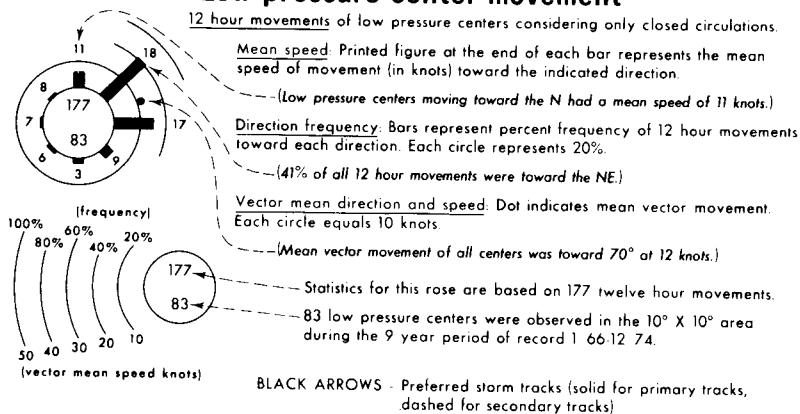
Waves are selected on the basis of the higher of sea and swell when both are reported. If both heights are equal, the wave with the longer period is selected.

BLACK LINE - Percent frequency of wave height ≥ 3.5 meters (≥ 12 feet)

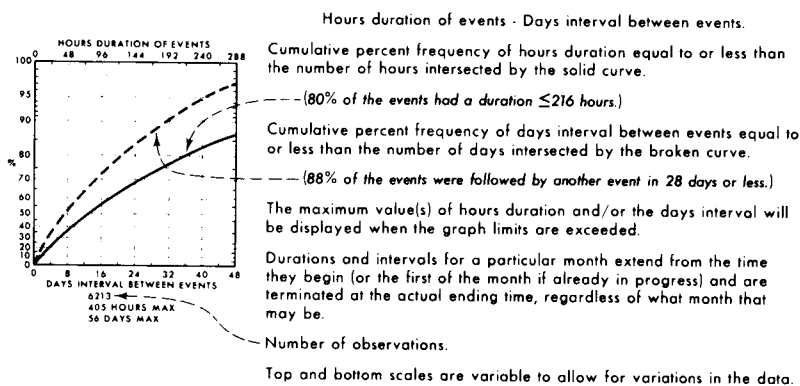
BLUE LINE - Percent frequency of wave height ≥ 6 meters (≥ 20 feet)

BLUE NUMBER - Maximum observed wave height (meters)

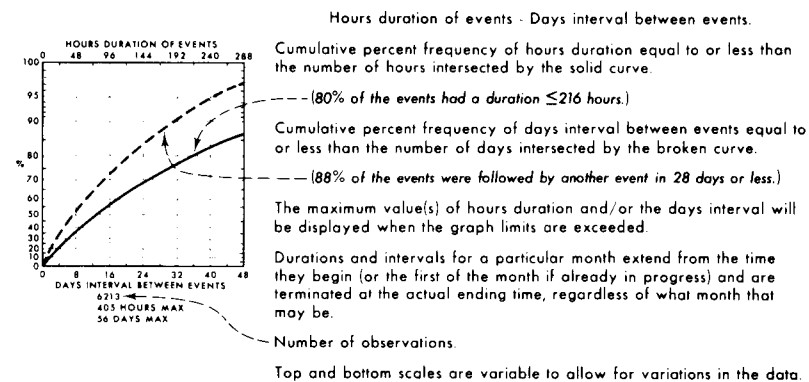
Low pressure center movement



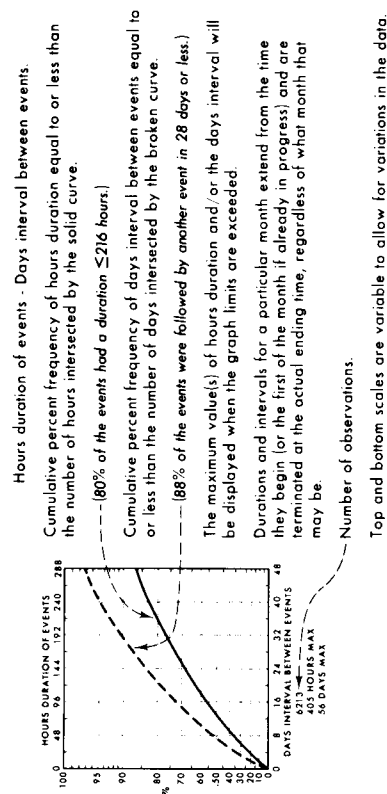
Persistence of visibility <2 n. mi.



Persistence of wind ≥ 10 kts.



Persistence of wind ≥ 20 kts.



ANNUAL REPORT

Contract #: R7120848

Research Unit: 367

Reporting Period: April 1, 1976-
April 1, 1977

No. of Pages: 52 plus Appendix

NEAR-SHORE METEOROLOGY

R. Michael Reynolds

and

Bernard Walter

April 1, 1977

CONTENTS

	Page
1. SUMMARY OF OBJECTIVES	1
2. INTRODUCTION	3
A. General Nature and Scope of Study	3
B. Specific Objectives	3
C. Relevance to Problems of Petroleum Development	5
3. CURRENT STATE OF KNOWLEDGE	6
4. STUDY AREA	8
5. RATIONALE, SOURCES, AND METHODS OF DATA COLLECTION	11
6. RESULTS	18
A. Results from Earlier Field Trips to NEG OA	18
B. Preliminary Results from Field Trip to Norton Sound-- October 1976	18
C. Preliminary Results from Field Trip to NEG OA-- February-March 1977	35
D. Model Results	44
REFERENCES	52
APPENDIX	

1. SUMMARY OF OBJECTIVES

Many near-surface meteorological processes act to modify the surface winds in the coastal regions of Alaska. The modification is generally extensive enough to seriously affect any attempts at relating synoptic weather maps to surface conditions. A typical example is the case of a predicted mild easterly wind which, in actuality, is a strong northerly near the coast, principally due to drainage from the interior. Further from shore, the lower continental air becomes modified by both the warmer seas and upper-level entrainment of the air above, thus altering its speed and direction.

The oceanic water near the surface is strongly influenced by the surface stress. As the wind makes a change in speed or direction, the water near the surface is strongly affected almost immediately. Then, with time, the momentum change diffuses downward, modifying the interior flow on a much larger time scale. The flow at depth in the oceanic mixed layer is thus related to a weighted average of past winds; in effect, its response is analogous to a low-pass filter whose cutoff frequency increases as the surface is approached.

The above comments indicate that a thorough knowledge of coastal wind conditions are an important consideration in offshore industrial development through its effects both on mean flow and the trajectory of surface contaminants.

The work under R.U. 367 is designed to define which processes are acting to modify coastal winds, how prevalent they are, and how far off shore they act. Aircraft and shipboard measurements, coupled with all available meteorological data, have been utilized in this goal. In addition, a study of computer simulation of coastal meteorological conditions has been undertaken to assess the applicability of a numerical model in making predictions of coastal winds.

The work is a necessary compromise between describing larger scale flows and detailing the energetics of the planetary boundary layer. Both ends of this spectrum are important contributions to the study, due to the juxtaposition of different processes.

2. INTRODUCTION

A. General Nature and Scope of Study

As outlined in the summary, the study is aimed at defining those processes on the Alaskan coastline which control the magnitude and direction of surface winds. Also, the horizontal variability of coastal effects, both offshore and longshore, are considered. Many of the concepts treated in this report were described in detail in our first annual report (Reynolds et al., 1976).

There appear to be three main processes which can act to modify coastal winds. At various times any of these three can be significant. First, the mountainous terrain interacts with the superimposed geostrophic flow to produce a complex wind field which is evident on land and which often extends a significant distance offshore. Second, slope winds (katabatic flow), the downhill movement of cold air during clear-sky periods, can cause significant winds along the Alaskan coast, especially at the mouths of estuaries. Third, a strong land-sea difference in air temperature in the boundary layer produces a force capable of modifying surface winds from predictions based only on pressure and friction. This baroclinic shear (thermal wind) acts to enhance the westerly component of the mixed layer wind in a rather complicated way.

One of the principal activities of this contract is to develop an accurate predictive numerical model capable of describing surface winds in the Icy Bay-Yakutat area. Field data will shed light on dominant processes and attest to the accuracy of a numerical model.

B. Specific Objectives

The meteorological program in the Gulf of Alaska is presently concentrating on the development of a numerical model capable of predicting coastal

surface winds based on synoptic maps. Field instrumentation is utilized for appraising the accuracy of the model as well as detailing active physical processes.

After a review of several numerical models, a simple slab model developed by Lavoie (1972) was selected. This model is simple, yet appears to incorporate sufficient physics to describe surface wind conditions. During the past year, this model was run several times and has undergone extensive revision; so much so that the term "Lavoie model" is used in a descriptive sense--a name for a boundary layer model incorporating simple mixed-layer profiles.

The field program includes the examination of continuous measurements of several coastal and offshore meteorological stations, including NWS data, NDBO data buoys, and two remote coastal stations established by PMEL as part of this contract. An intensive set of measurements was made during the period 21 February-8 March when both an instrumented aircraft and a ship were used to provide several detailed data sets for a variety of synoptic situations. The response of the surface current to winds was measured during this period by moored and profiling current meters which were deployed by the ship.

In October, a study was made in Norton Sound. This study was primarily motivated from the desire to field check several new instruments before the Yakutat study. However, the data is interesting in its own right, and blends itself nicely to the story developed for the Gulf of Alaska. For this reason it will be preliminarily discussed in this report.

At the time of the last annual report, we had just finished a major field trip; thus data included in that report were brief. Further analysis of those data has resulted in a paper which is included at the end of this report. The situation this year is little different in that we can only prepare a brief outline of our most recent field trip in time for this publication.

C. Relevance to Problems of Petroleum Development

Knowledge of surface winds is an important consideration in predicting wave development, surface currents (thus oil spill trajectory), and aircraft safety. Persistent coastal winds will have longer term effect on the general shelf circulation, possibly modifying midwater and bottom currents. As circulation models develop with our understanding of the meteorology, better wind fields can be used to improve the models.

3. CURRENT STATE OF KNOWLEDGE

General concepts and definitions concerning atmospheric boundary layer physics used in this study were summarized in the last annual report (Reynolds et al., 1976). Hence this section will deal with a description of the model, including a physical interpretation of some of its results. The model, a highly modified version of a model by Lavoie (1972), includes three layers: a constant flux surface layer, a well-mixed planetary boundary layer topped by an inversion, and a deep stratum of overlying stable air. Figure 3.1 is an example of the expected mixed layer profiles. The surface layer ($z < z_1$), mixed layer ($z_1 < z \leq h$), and overlying stable air mass ($z > h$) are shown. As long as the sea surface temperature exceeds the mixed layer potential temperature ($\theta_s > \theta_b$), then a positive flux of heat acts to generate turbulence in the mixed layer by buoyant production. At the inversion base, turbulence acts to entrain warmer air from above, resulting in growth of the mixed layer.

No figure provided

Figure 3.1. Schematic of expected vertical profiles in a convective mixed layer.

The model assumes that the atmospheric response on the mesoscale is dictated primarily by the behavior of the mixed layer as a whole with only secondary dependence upon the detailed vertical structure of the surface layer or upon the vertical structure of the overlying stable layer. The model is applied to mesoscale phenomena whose characteristic wavelength is of the order of tens of kilometers in the horizontal and less than 5 km in the vertical.

A detailed description of the numerical techniques used in solving the model equations will be given in the annual report of the Modeling and Simulation Studies (MASS) group of PMEL; RU#'s 140/146/149/31. Hence only specific applications with physical interpretation will be given here.

4. STUDY AREA

The study area is shown in figure 4.1. The Icy Bay-Yakutat area was selected due to its overlap with physical oceanography programs in the area. It is typical of coastal conditions all along the Gulf of Alaska in that it has deep estuaries, glacial troughs and fans, and strong mountainous relief. Figure 4.2 is a computer plot of the digitized topography in the study area. Evident in this figure are the high peaks of Mt. St. Elias (18,008'), Mt. Logan (19,850'), Mt. Augusta (14,070'), and Mt. Cook (13,760'). Each grid square in the figure is 5 x 5 km, which is the minimum grid scale to be treated numerically.

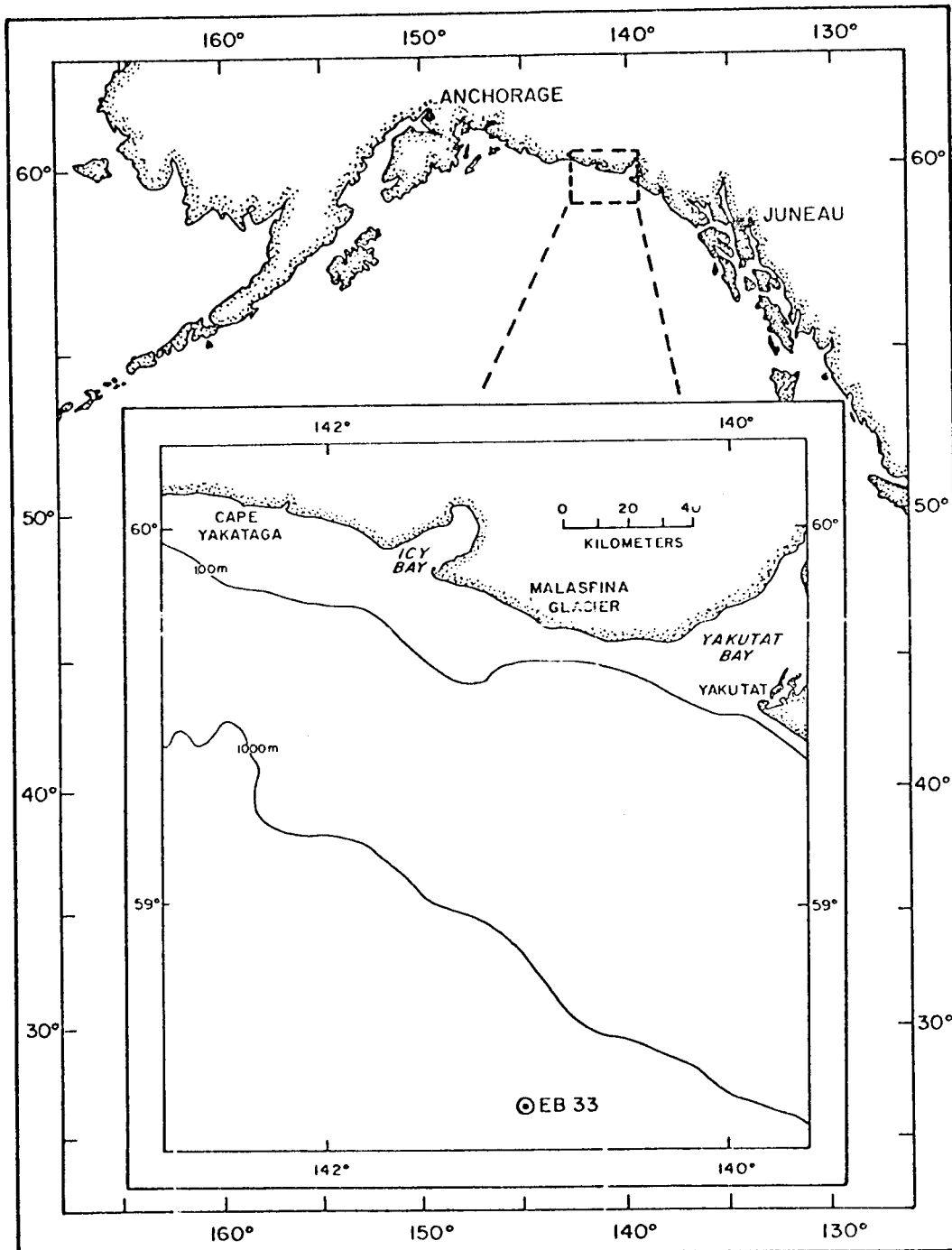


Figure 4.1. Map of study area in Northeast Gulf of Alaska (NEGOA).

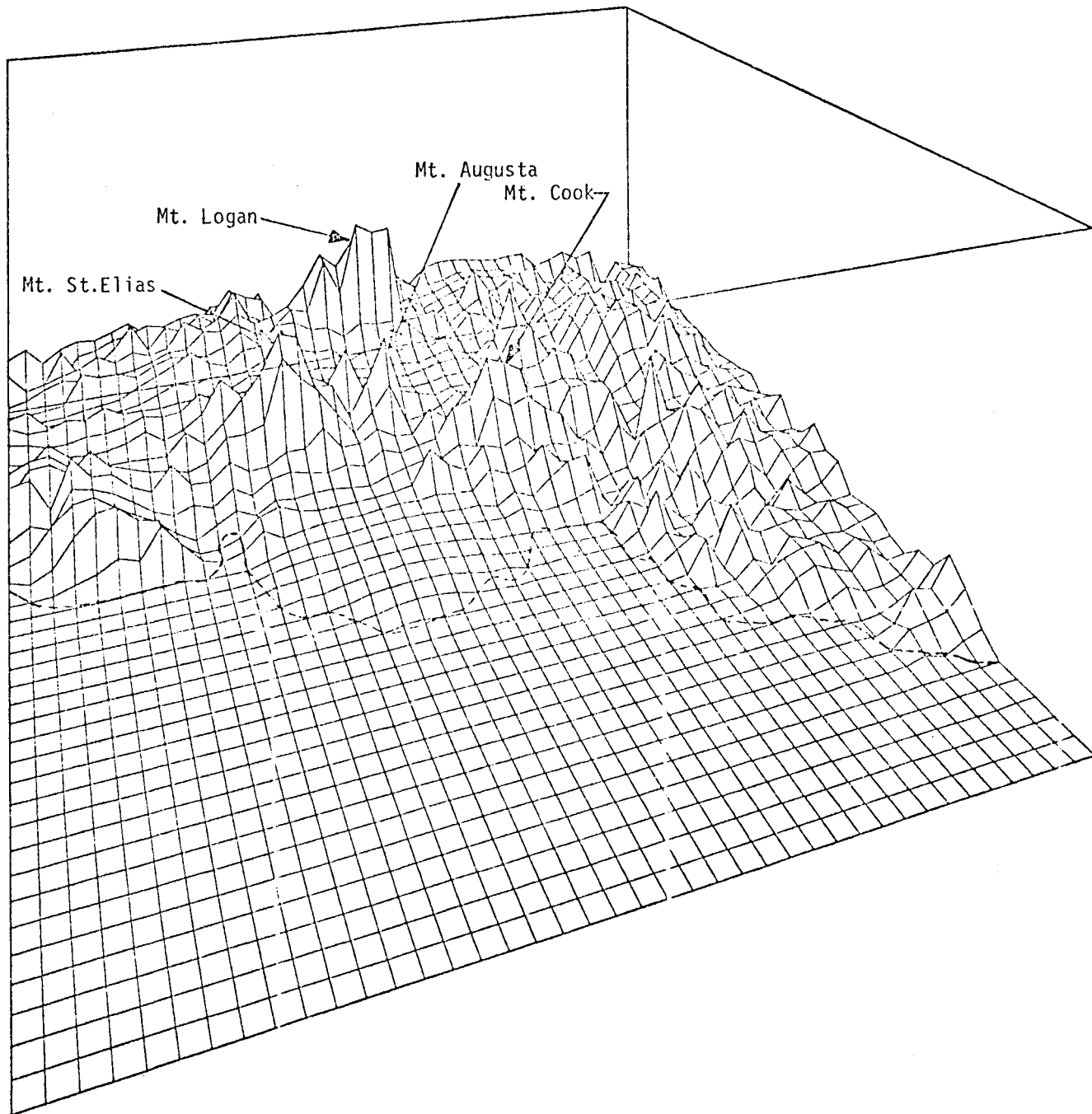


Figure 4.2. Computer-generated and isometric projection of the study area. Dashed line is the coastline. Significant peaks are noted.

5. RATIONALE, SOURCES, AND METHODS OF DATA COLLECTION

The rationale of data collection will be treated first in this section, since rationale, with associated priorities, dictates the sources and methods utilized in the overall study. One of the foremost objectives of the meteorology study is to develop a working numerical model capable of predicting surface winds in the very dynamic coastal environment. Fundamental to this objective is a field study aimed at verifying the model for a variety of synoptic conditions. Aside from simply measuring winds, an intensive study of the boundary layer structure was made so that identification of active dynamical processes would be possible. This knowledge can be used later to diagnose computational errors, even for modifying the model to better handle the imposed environment.

Several sources of data now exist which should provide an excellent long-term data set for describing the winds in the study area. Figure 5.1 is a summary of the meteorological stations which will be included in data analysis. Other sources of data include satellite photographs, synoptic weather maps with analysis, and upper-air profiles from the Yakutat rawinsonde.

During the intensive study period, several additional measurement techniques were employed to provide detailed information of the boundary layer structure. The most significant set of data was taken by an instrumented aircraft, a twin-engine Queen Air, which is operated by the National Center for Atmospheric Research (NCAR), Boulder, Colorado. Figure 5.2 is a photograph of the Beechcraft Queen Air (foreground). By combining exceptionally high quality instrumentation, a high speed data logger, and a precision inertial navigation system (INS), data collection sufficient to describe the turbulent behavior of the boundary layer is possible (Lenshow, 1972). Up to 64 data words are recorded at rates of 8 Hz. The three-dimensional wind field, temperature, humidity, and sea surface temperature are among the many measured quantities.

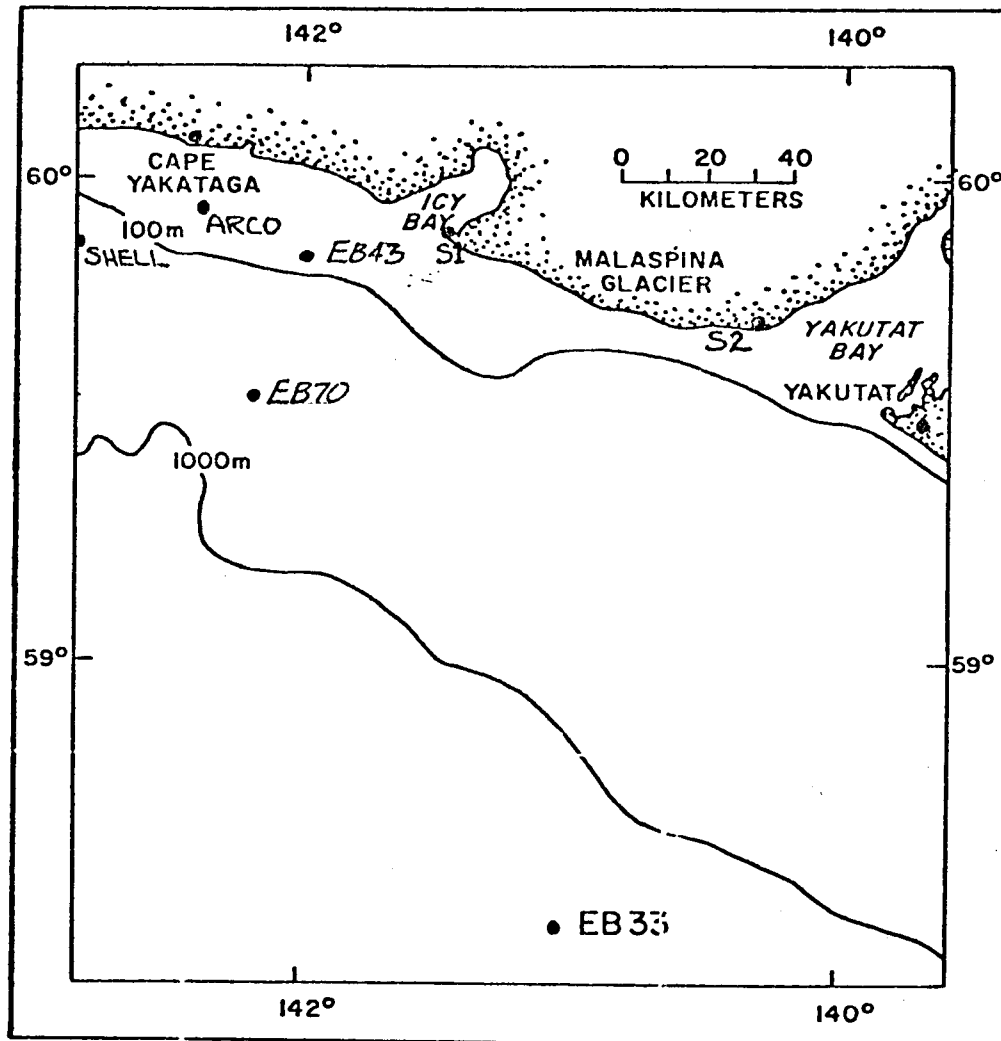


Figure 5.1. Sources of meteorological data. Yakutat is an NWS upper air station, Yakutaga is an NWS surface station. EB43 and EB70 are NDBO buoys. S1 and S2 are remote weather stations installed on 6 March 1977. The ARCO and Shell drilling platforms will occupy various sites over the next year. The positions shown are the most recent. EB33 was occupied during 1975 and early 1976. It no longer exists.

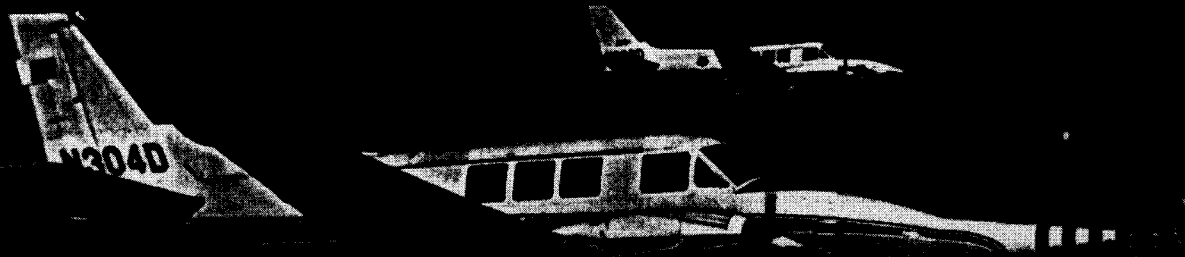


Figure 5.2. Photograph of the NCAR Queen Air 304D used during the intensive study (foreground).

Previous field investigations attempting to examine the spatial structure of the coastal meteorological processes in the Yakutat area have been handicapped by the time necessary for a ship to move between stations. Any temporal changes occurring interfered with the interpretation of the spatial structure. At an airspeed of 140 knots, the Queen Air can easily accomplish a flight plan with two primary objectives in 3-1/2 hours, weather permitting. A typical flight plan is shown in figure 5.3 and summarized in table 1.

The first objective is to obtain a survey of the surface wind velocity field from a height of 60 m and roughly 10 km offshore. The longshore wind distribution is measured twice, once flying each direction along the coast in order to provide redundancy in sampling and to provide measurements of opposite headings. The latter point is valuable in the determination and elimination of possible instrumental biases in the gust probe system. The flight directly over EB43 is to provide a geographical check on any drift present in the INS and thereby to provide a more accurate measurement of the mean wind field. Having obtained the longshore distribution of meteorological variables, both the orographic and thermodynamic effects of the nearby coast upon the surface winds will hopefully be evident. Certainly such a distribution will provide a critical test of theoretical or numerical schemes applied to the Yakutat region.

The second objective is to obtain a complete picture of the planetary boundary layer structure from the coast out to 60 km offshore. Such a picture provides boundary conditions in the case of onshore flow or reveals the effects of air modification upon the wind velocity field in the case of offshore flow. Offshore legs flown at several levels, along with vertical soundings at each end of the track, are used to satisfy this objective.

Table 1. Summary of flight plan shown in figure 5.3.

Way Points	Altitude (feet)	Remarks
1-2-3	200	Longshore wind distribution
6-7	50-600	Vertical sounding at coast-- lower level
7-6	600-3,000	Vertical sounding at coast-- upper level
8-9	100	} Offshore wind distribution and vertical structure including upper level (environment) conditions
9-8	330	
8-9	660	
9-8	1,300	
8-9	3,000-4,500	
9-8	200	
3-4	200	Longshore variation
4-5	200	Check INS and EB43 comparison
5-3-2-1	200	Return home, repeat measure- ments allow improved error analysis

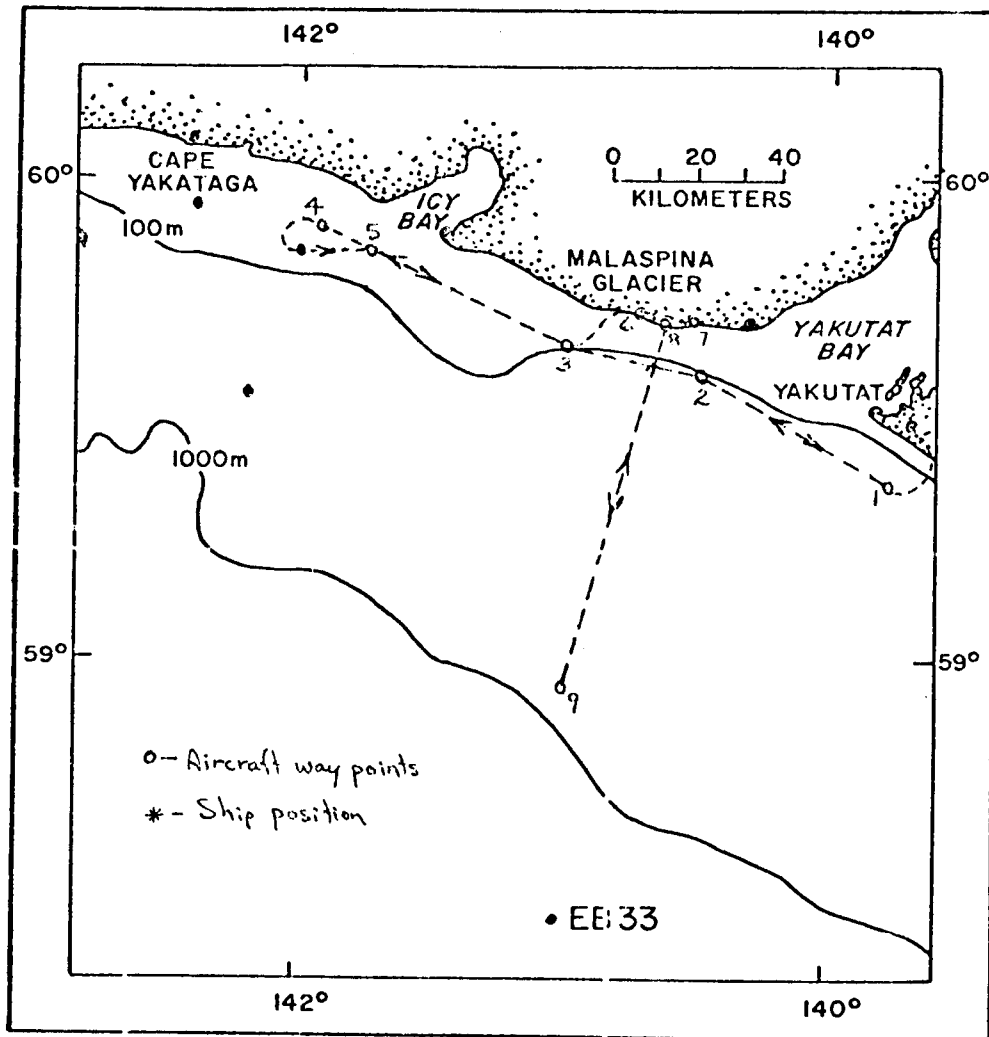


Figure 5.3. Typical flight plan for the NCAR Queen Air.

In addition to the aircraft measurements, the NOAA ship Surveyor made many measurements of surface conditions. Because of scheduling problems, only a small overlap period was possible between ship and aircraft. As luck would have it, a major storm disrupted hoped-for intercomparisons, allowing only two overflights and these under conditions which could only be described as trying. During overflights, radiosonde ascents and surface observations were made by the ship. Later, when operating alone, the ship made a sequence of radiosonde ascents, tethered BLP flights and detailed surface meteorological observations.

Additionally, measurements of surface currents were made by several independent techniques. A spar buoy was deployed at site 10 km offshore (*in fig. 5.3) and collected data for the period 1-7 March, which included at least two major storms and a period of calm. Profiles of current and temperature were made to depths of 50 m by a direct readout Aanderaa current meter. Finally, on two occasions orange 4 x 4' sheets of plywood were deployed as surface drifters to be photographed by aircraft observers. This latter exercise was principally a feasibility study for future aircraft-ship programs.

6. RESULTS

A. Results from Earlier Field Trips to NEGOA

Data from field trips taken during 1975 and 1976 have been analyzed in some detail. A paper on this analysis is appended to this report (Appendix A).

B. Preliminary Results from Field Trip to Norton Sound--October 1976

The main objective of this field trip was to test and calibrate the meteorological surface boom acquired from the GATE experiment. In addition, it was hoped that the synoptic field would provide offshore winds, enabling process studies of modification of the continental Alaskan air mass similar to the Yakutat Bay-Icy Bay experiments.

Data were collected using surface layer meteorological instruments on the bow boom interfaced to the ship's data collection system (PODAS). Information on the mixed layer was gathered from radiosonde and boundary layer profiler (BLP) ascents, while radiosondes also provided additional data on the free atmosphere above. Supporting surface and upper-level meteorological observations have been collected from both the Nome and Kotzebue National Weather Service.

The bow boom system proved most reliable and operational. The system is mechanically sound, easy to assemble and easy to swing inboard for maintenance. The RF interference to the temperature signals encountered during GATE was also experienced here, but a shielding error was discovered which may alleviate future problems. Data recording with PODAS worked well, although insufficient software preparation made shipboard processing of the acquisition tape impossible. As a result, the acquisition tapes are just now undergoing processing.

Two cyclonic storms passed south of the Norton Sound area (fig. 6.1) during the cruise period, furnishing the anticipated offshore winds; the first occurred on the last days of September before the meteorology program was in operational readiness. The second, however, occurred on October 3 and 4, 1976, and was observed in two ways: On the 3rd of the month, the ship steamed a six-station trackline offshore from Nome and oriented in the direction of the surface wind, allowing resolution of the spatial scale of the modification process. On the 4th, the ship occupied the third station outward from the coast for a 12-hour period in an attempt at resolving the temporal scale of the modification process. A summary of observations is provided in tables 2 and 3.

Nome is geographically situated such that with respect to the general circulation of the Northern Hemisphere it often lies just to the north of the upper level trough associated with the semipermanent Aleutian low-pressure cell at the surface. As a result, most North Pacific cyclonic storms are transported well to the south of the Norton Sound region.

Such was the case during this field activity. On September 28, the upper-level trough was centered just north of the Aleutians at about 56° N, 167° W, with the trough axis oriented nearly NW-SE. This position is shown in the 500-mb storm track, figure 6.2. With the passage of the storm, the trough center moved in a general northeast direction, lying above Cook Inlet near 62° N, 152° W at 12Z on September 30. Another upper-level trough was at this time centered over west Siberia, and Norton Sound lay in the column between the two systems. With the decay of the system moving over Alaska, the upper-level trough reaffirmed itself just off the tip of the Aleutians at 52° N, 173° E at 00Z on October 1, 1976. Over the next 4 days, the upper-level pattern rotated eastward, with the trough center tracing its way up the Aleutians,

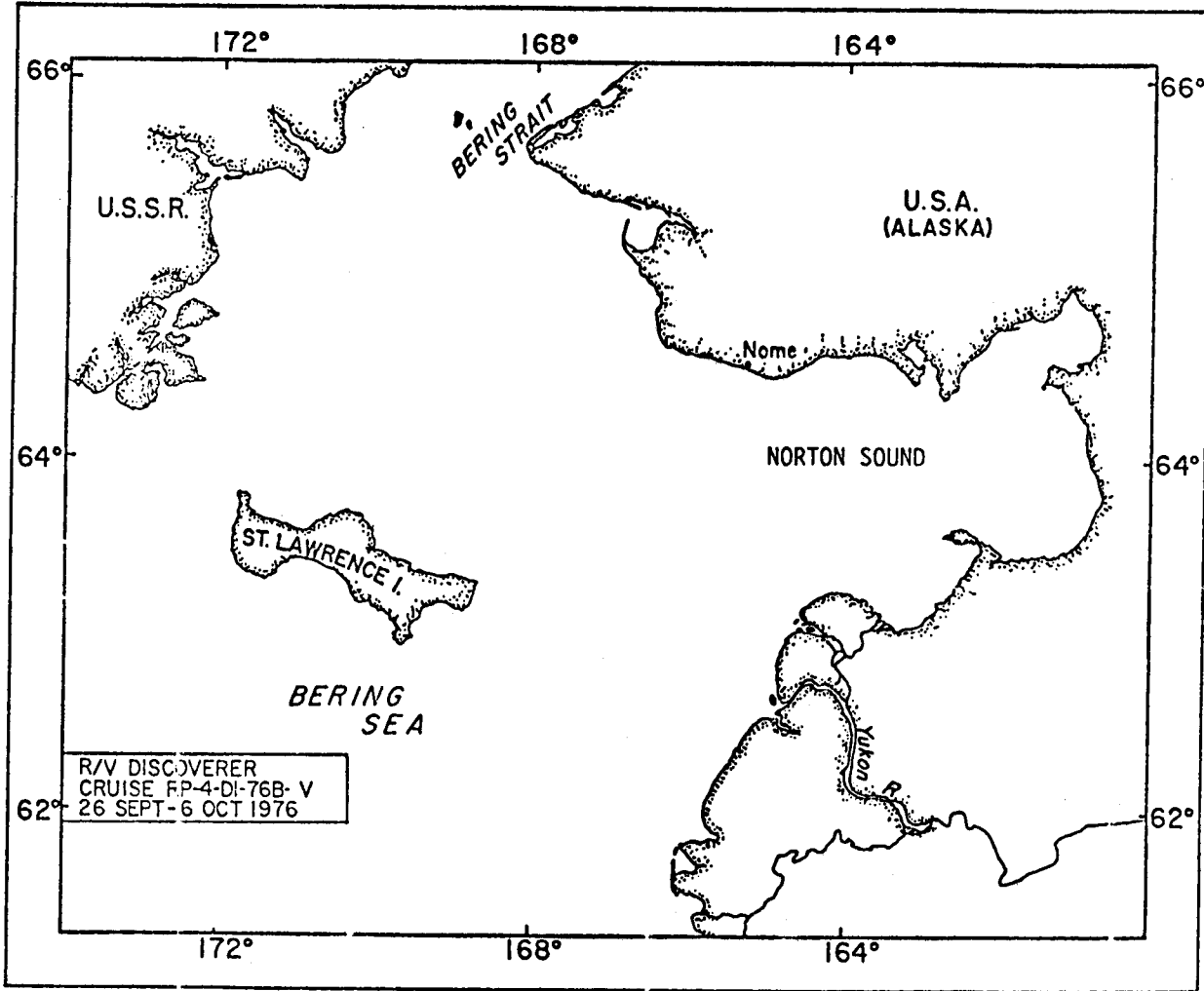


Figure 6.1. Norton Sound with Nome and Seward Peninsula to the north.

Table 2. Meteorological station summary--trackline.

Station	Time-GMT	Approximate Position	Radio-sonde	Tether-sonde	Surface Weather	Remarks
	09/30-0036	162°10' 64°17.3'	NS1		9.2 68	957 Eastern Norton Sound
	10/01-0011	165°31.3' 64°25.7'	NS2		8.1 80	035 Approx. 5 mi. fm Nome
	10/02-0007	165°24.3' 64°11.2'	NS3		6.7 74	113 Approx. 19 mi S. of Nome
	02-1814	" " " "	NS4		7.1 73	" " " " 072
N1	03-2354	165°25.0' 64°29.1'	NS5	N-BLP-1	7.9 61	071 One mile off Nome
N2	0210	165°28.0' 64°27.0'	NS6	N-BLP-1	8.8 54	060 BLP line broke
N3	0418	165°30.31' 64°27.18'	NS7		8.8 60	056 Four mi. off Nome
N4	0525	165°37.2' 64°23.8'	NS8		7.0 67	055 Eight mi. off Nome
N5	0643	165°50.5' 64°18.1'	NS9		7 68	054 Sixteen mi. off Nome
N6	0847	166°16.6' 64°06.8'	NS10		6.5 72	050 Thirty Two mi. off Nome
N5B	1042	165°51.1' 64°18.1'	NS11		.4 68	052 Sixteen mi. off Nome
N4B	1222	165°35.8' 64°25.0'	NS12		2.8 68	052 Eight mi. off Nome
N3B	1415	165°30.3' 64.27.4	NS13		1.5 70	050 Four mil off Nome
N2B	1505	165°25.92' 64°28.08'	NS14		.5 84	049 Met Boom Orientation Test
N1B	2045	165°25.0' 64°29.0'		N-BLP--2		Test Flight with BLP#2 Sonde
N2C	2145	165°36.2' 64°28.0'	NS15		4 50	041

Table 3. Meteorological station summary--anchor station N3C.

Time-GMT Radiosonde	Radio- sonde	Tether- sonde	Surface Weather	Remarks
10/03-2327	NS16		5.1 036 41%	
10/04-0001	NS17	NS-BLP-3	4.7 030 47	
0425	NS18	NS-BLP-4	3.0 023 64	
0625	NS19		2.9 026 64	BLP Sonde antenna broke, Sonde lost
0713	NS20		2.7 029 68	
0753	NS21		2.9 029 67	
0848	NS22		2.9 031 67	
0950	NS23		2.1 028 68	

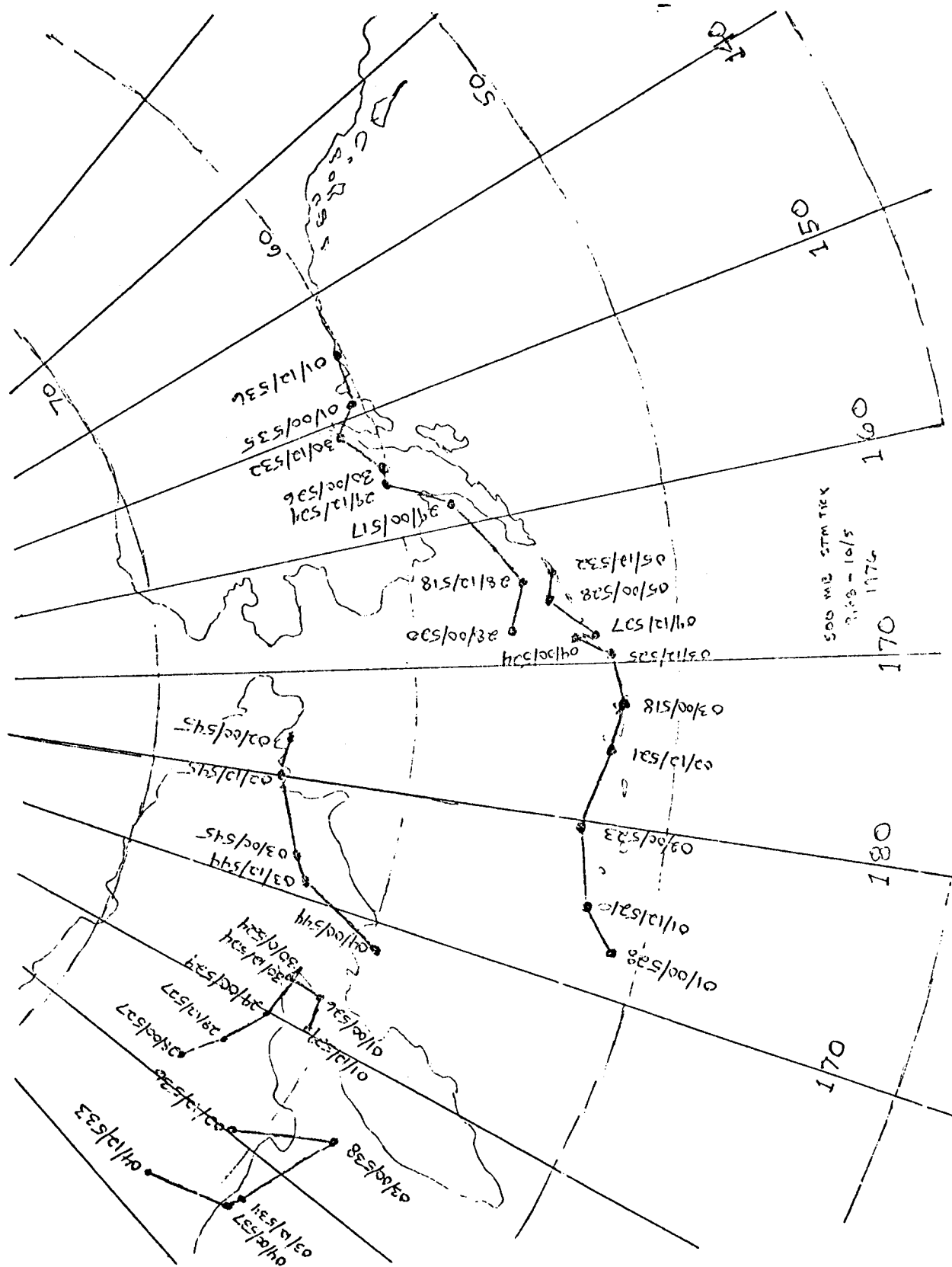


Figure 6.2. 500 mb stormtrack for the period 9-28-76 00Z to 10-5-76 12Z. Entries show day/GMT/thickness (from 12-hour program).

arriving just off the Alaska Peninsula at 12Z on October 5. The resulting surface pressure pattern from this synoptic system generated the offshore flow that was observed during this experiment.

The surface storm tracks that accompanied the upper-level patterns just described are shown in figure 6.3. The first storm exhibited a highly complex pressure pattern. On September 28 at 00Z, two cells are already evident, one at 54° N, 170° W, the other just north of Cook Inlet. The main cell of the storm tracked its way across the heart of Alaska and into Northern Canada. By the 29th, two low-level spinoff cyclones are evident. The first traveled into the Gulf of Alaska and slowly filled. The other moved generally northward and then retrograded into Norton Sound, filling by October 1. Nome reported light rain on September 30; Nome's surface winds varied from northerly on the 28th to easterly and southeasterly on the 30th.

The next storm began approaching Alaska on the 30th of September. By October 2, it had reached the International Date Line and Nome was beginning to report winds from the E to NE. The surface pressure pattern is reproduced in figures 6.4-6.6 for 10/03/00Z to 10/04/00Z. Wind barbs for Nome and Kotzebue clearly indicate the continental nature of wind trajectories crossing the Seward Peninsula. The wind barb at Nome for 10/03/12Z gives some indication that the observed air mass may also have traversed Kotzebue Sound.

The visual wavelength satellite picture of October 3, 1976, 2047Z (fig. 6.7), provides an excellent link between the synoptic and mesoscale flow descriptions. As a matter of circulation, the "hole" in the cloud cover occurs immediately over the Seward Peninsula and Norton Sound and extends E-NE to the snow-covered Brooks Range. The eastern portion of Kotzebue Sound is also visible. Nome lies halfway between the two points on the flat section of coast on the south side of the peninsula.

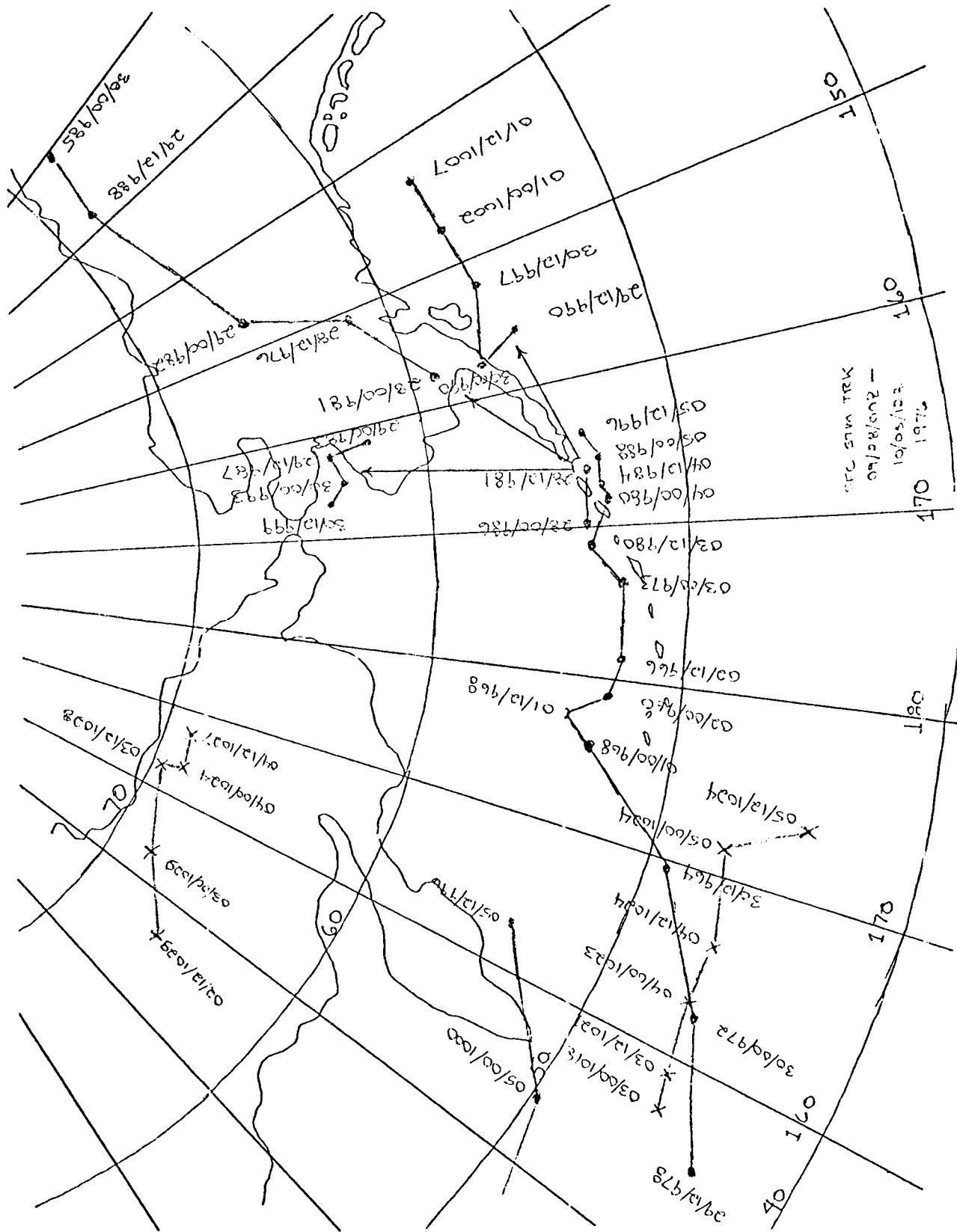


Figure 6.3. Surface storm track for the period 9-28-76 00Z to 10-5-76 12Z. Entries show day/GMT/surface pressure (from surface analysis).

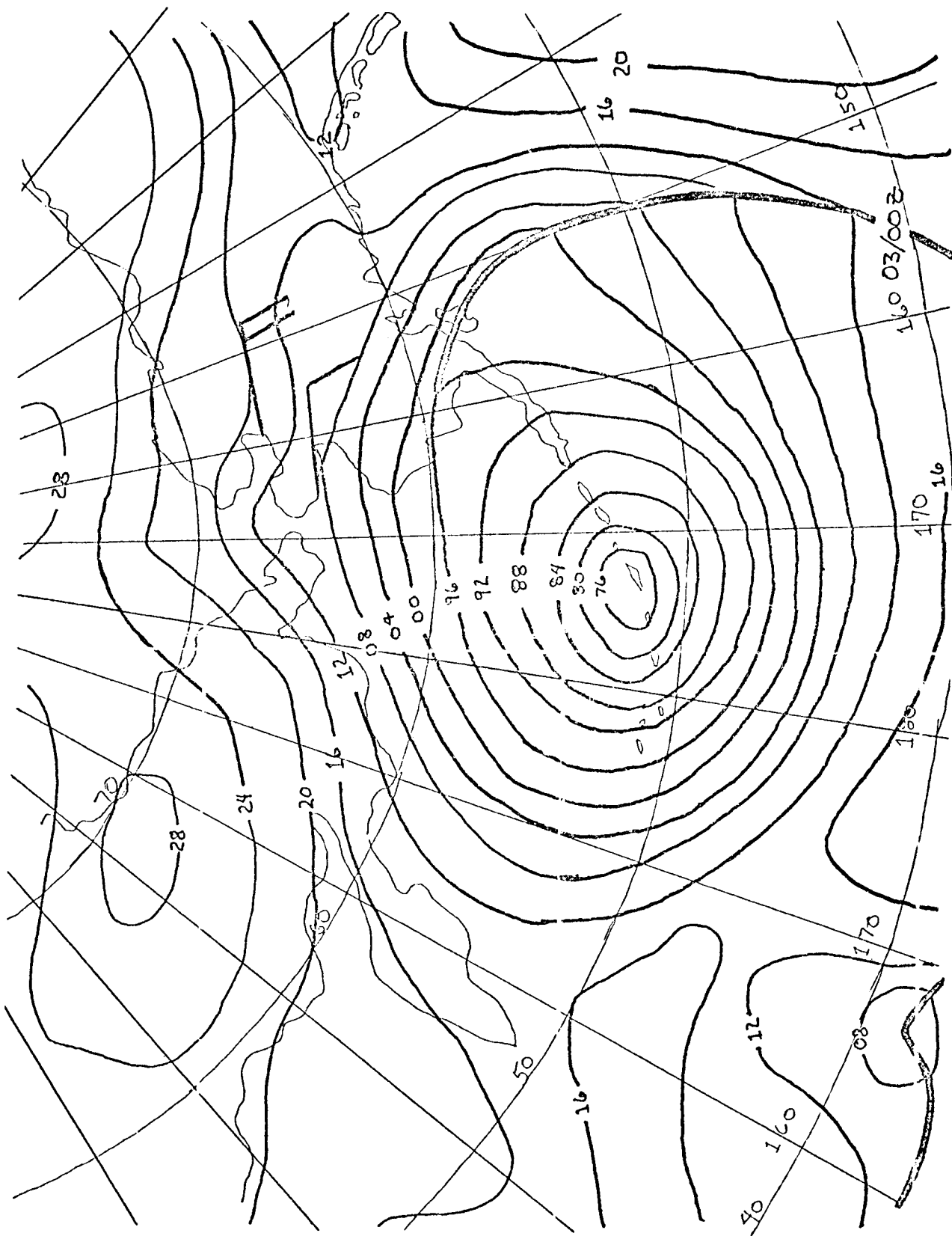


Figure 6.4. Surface pressure analysis of 10-3-76 00Z.
Surface winds at Nome and Kotzebue.

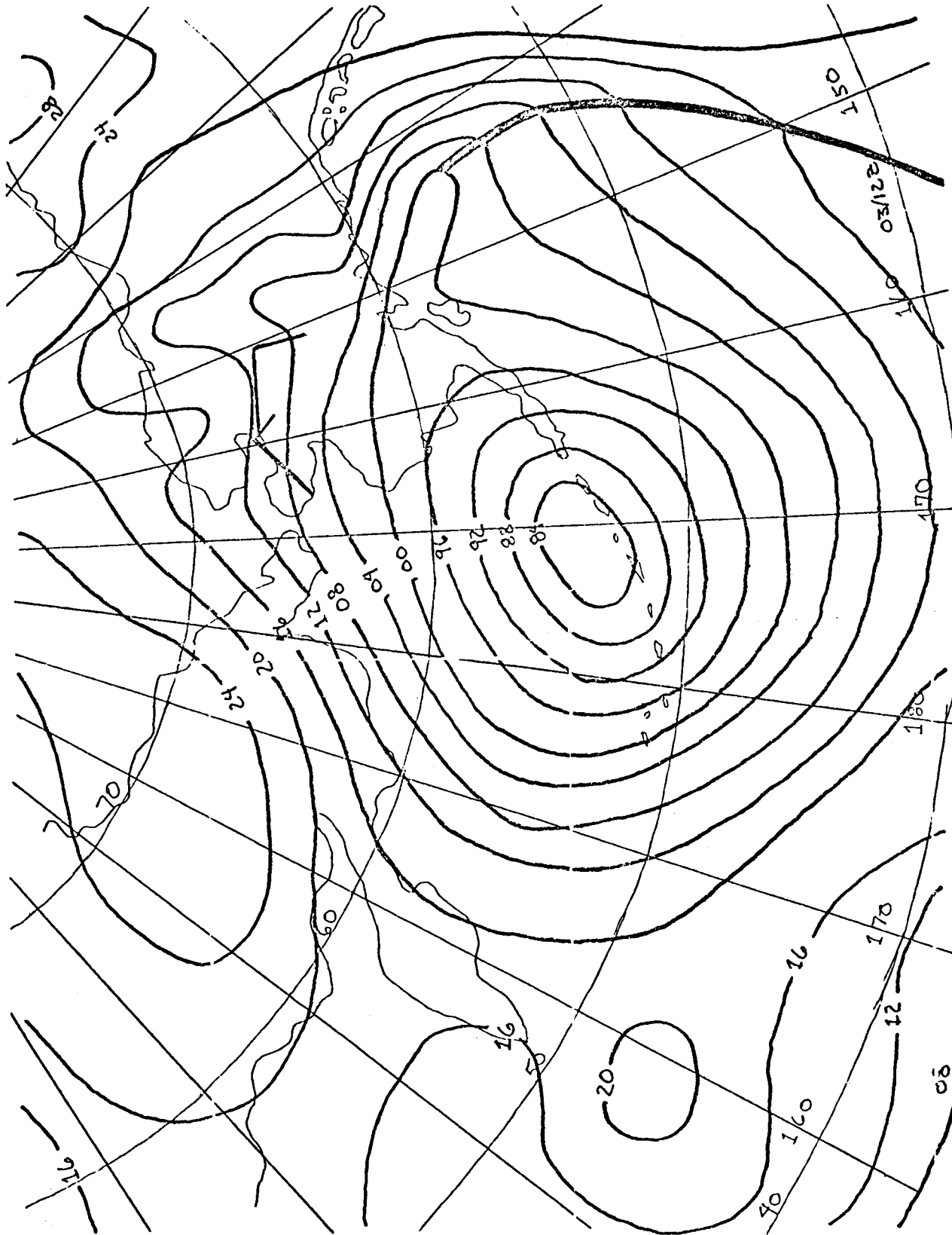


Figure 6.5. Surface pressure analysis of 10-3-76 12Z.
Surface winds at Nome and Kotzebue.

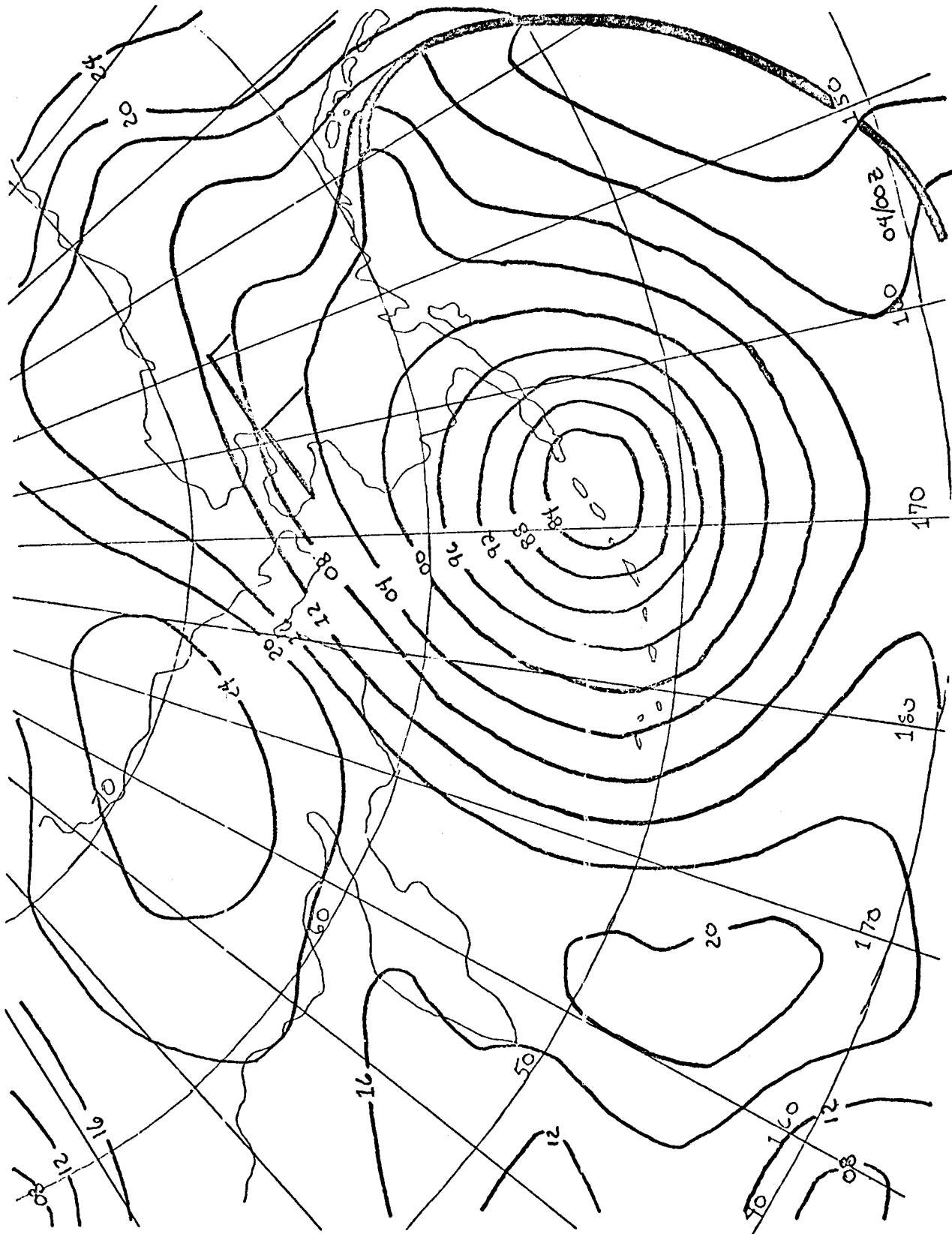


Figure 6.6. Surface pressure analysis of 10-4-76 00Z.
Surface winds at Nome and Kotzebue.

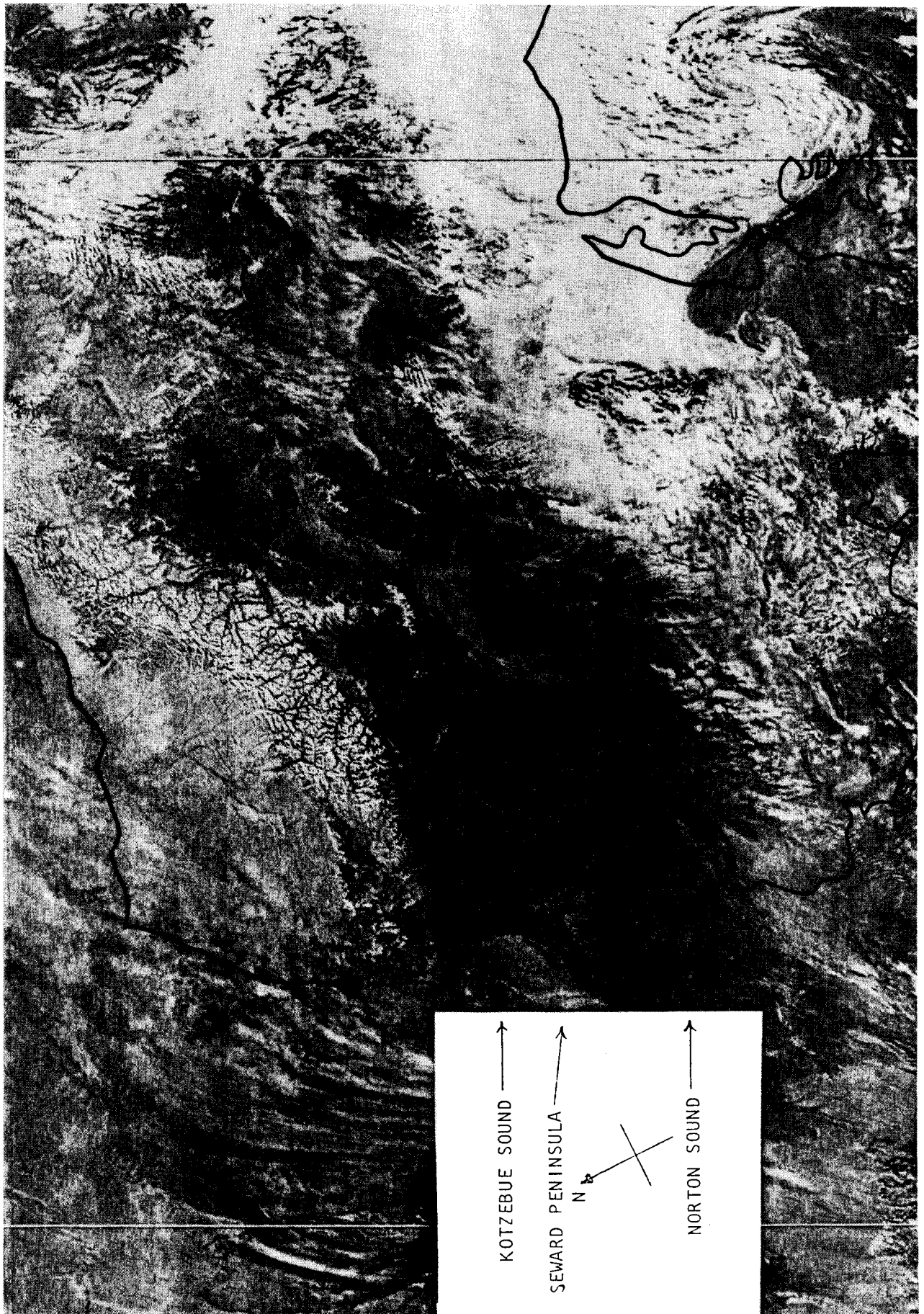


Figure 6.7. Visible wavelength satellite photograph from 3 Oct 76,2048Z.

The geostrophic flow predicted by the surface weather maps (figs. 6.4-6.6) is clearly depicted by the cloud "streaming" in the photo. Of special note is the wave structure visible in the lower right corner of the picture (apparently in the frontal zone of the system). The air arriving at Nome is obviously quite dry, as evidenced by the lack of clouds over the Alaskan interior.

Reducing focus to the Norton Sound area, several features reveal themselves. The first is the small patch of low cloud over the northern part of Seward Peninsula. The vapor for this cloud formation has been pumped aloft in a 50-km transit of Kotzebue Sound. Similarly, in the southern portion of Norton Sound, low cloud sheets indicate that dry air passing over Norton Sound is subjected to convective transfer of water vapor. When the mixed layer penetrates to the condensation level, condensation occurs and the water content becomes visible in the form of cloud.

The six-station trackline series of radiosonde ascents allows a good view of the generation of this mixed layer. The stations, N1 through N6, are shown in figure 6.8. They lie 1, 2, 4, 8, 16, and 32 km from the coast as measured parallel to the surface wind. Surface meteorological conditions as measured onboard ship are also shown in the figure. As this set of observations was gathered during local afternoon to local night, the offshore temperature progression is not at all representative of stationary conditions. However, this serves as an excellent example of moderation of diurnal temperature fluctuations by a deep water body. Over the trackline, sea surface temperature averaged about 8°C, varying less than 1 degree. Marine surface air temperature cooled less than 2.5°C along the trackline, while Nome, under the influence of continental-type diurnal temperature fluctuations exhibited an 8.5°C temperature drop over the same time period. Thus in the 45-minute

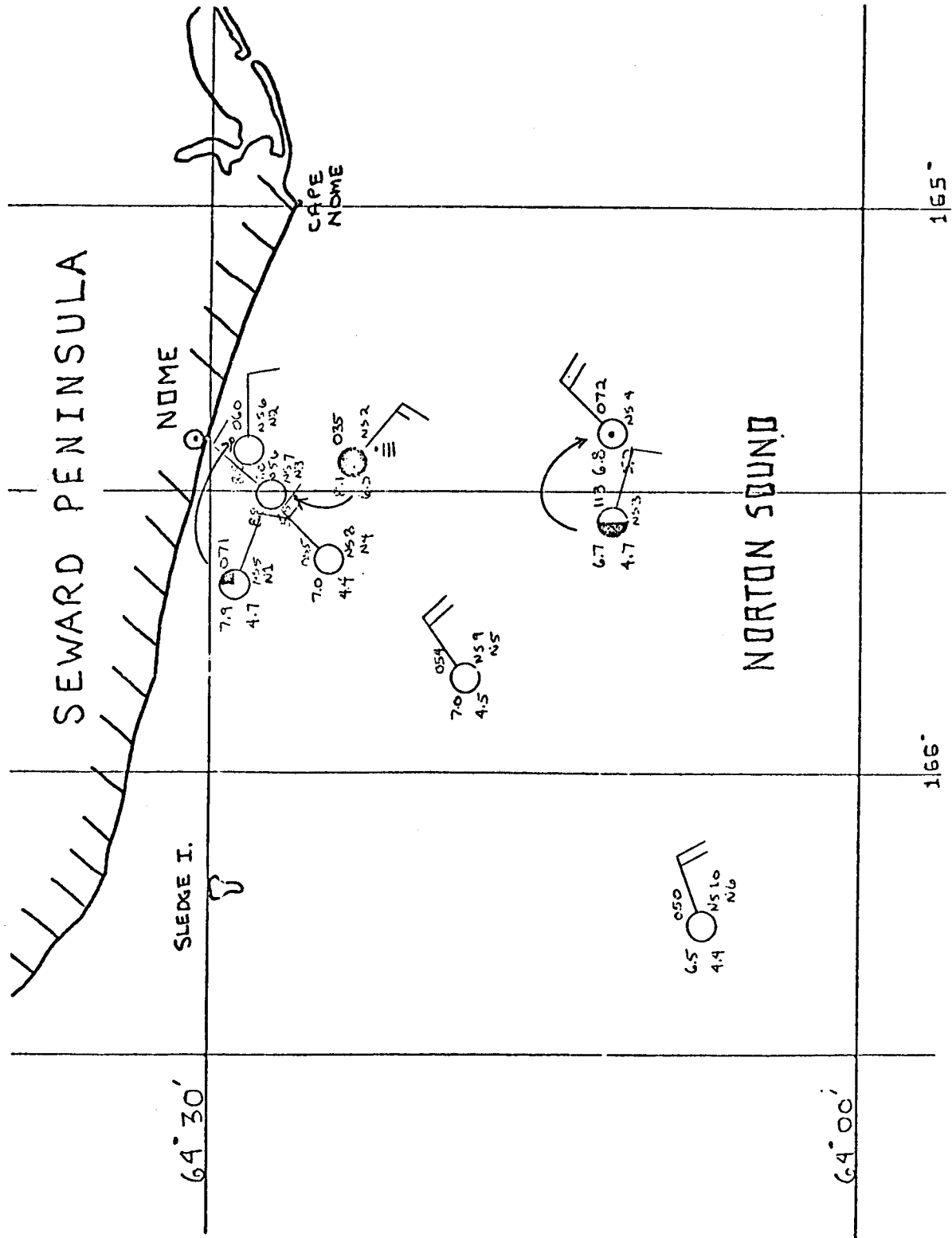


Figure 6.8. Meteorological operations area in Norton Sound; offshore trackline designated by stations N1 through N6. Surface observation summarized by station symbols.

period that surface air traveled between the coast and station N6, it warmed about 6 degrees due to the upward surface heat flux.

Figure 6.9 (a) through (f) represents vertical profiles of potential temperature and mixing ratio (a measure of vapor content) at the six stations along the trackline. Figure 6.10 (a) and (b) shows the same profiles from the 3 October 00Z sounding for Kotzebue and Nome, respectively. These land-based (daytime) soundings each exhibit an unstable to neutral bottom layer representative of surface heating by incident shortwave solar radiation. Surface mixing ratio values are low, reflecting the continental origin of the air mass. The Kotzebue sounding is generally stable aloft, except for a near-adiabatic moist layer between 2,000 and 2,400 m. This could possibly be a remnant from advection over the Gulf of Alaska before the air mass passed into the interior of the continent.

In the Nome temperature sounding, just above a thin stable layer extending from about 600 to 800 m, there is a thick, slightly stable region with increased vapor content. This structure could possibly define a mixed layer aloft resulting from convective mixing during passage of the air over the eastern end of Kotzebue Sound. Further evidence is provided by the soundings at stations N1 and N2. The mixed layer aloft between 1,300 and 1,900 m at N2 is especially classic with its rapid decrease in mixing ratio and temperature jump at the top of the layer. With outward progression along the trackline, this mixed layer becomes less discernible. At station N6, the adiabatic profile exists between about 1,000 and 1,300 m, but the mixing ratio trace has lost its mixed character.

At the surface, the development of the mixed layer is well-documented. The potential temperature profiles at stations N1 to N4 (1 to 8 km offshore) show a stable character to about 500 m. During this period, surface temperatures

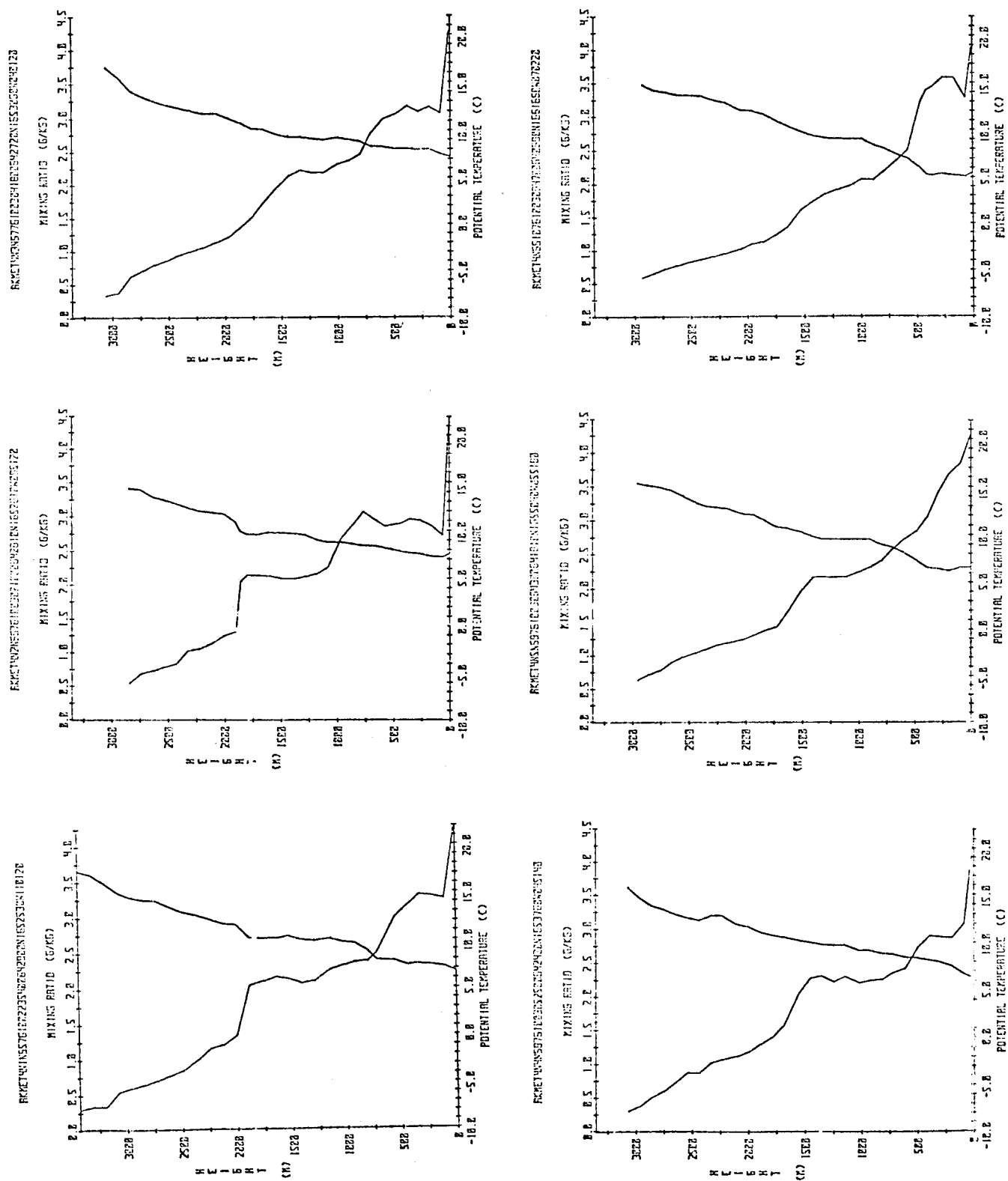


Figure 6.9. Vertical profiles of potential temperature (increasing with altitude) and mixing ratio determined by radiosonde at stations: (a) N1, (b) N2, (c) N3, (d) N4, (3) N5, and (f) N6.

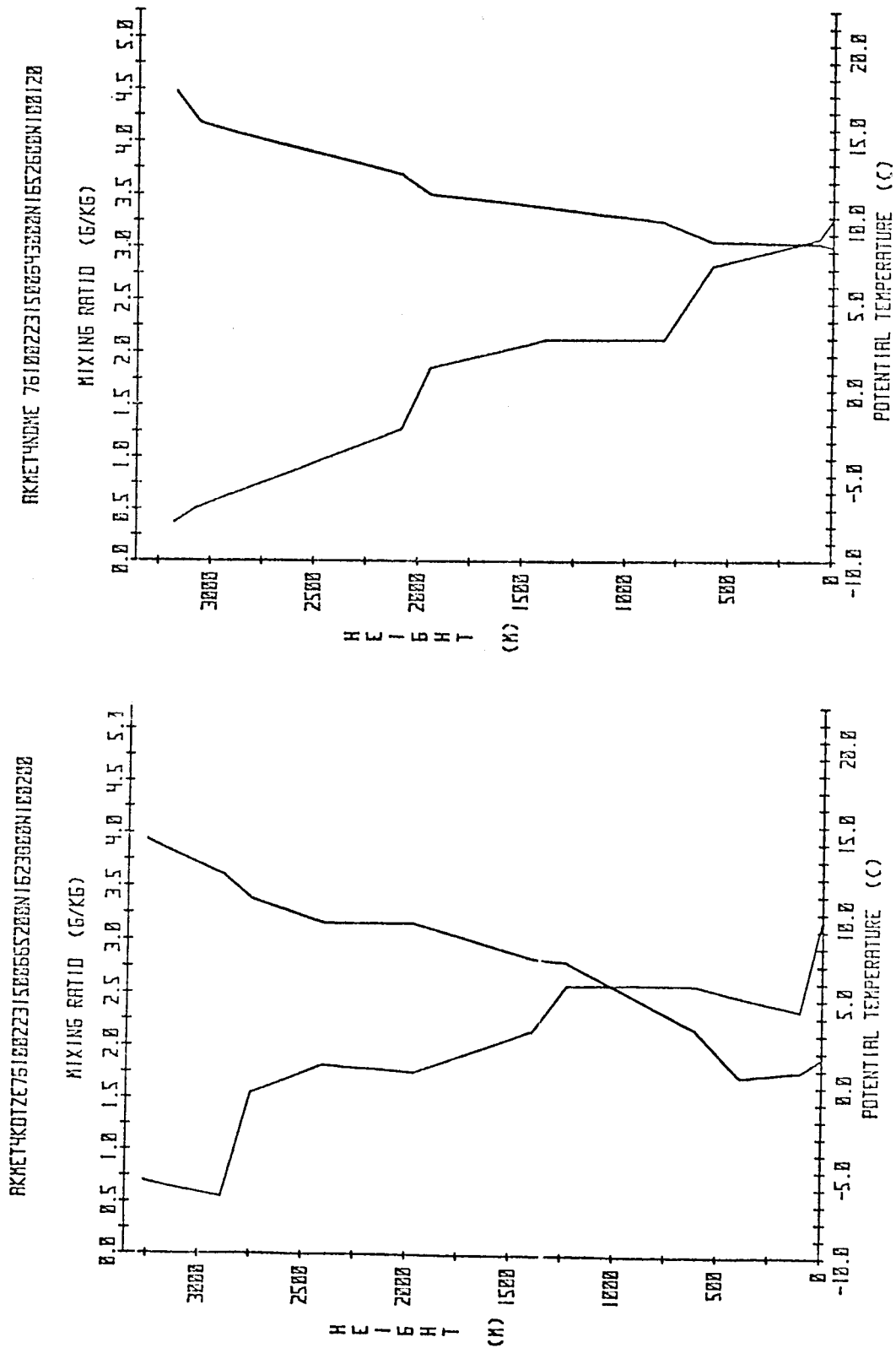


Figure 6.10. Vertical profiles of potential temperature (increasing with altitude) and mixing ratio as determined by radiosonde ascent at (a) Kotzebue and (b) Nome.

at Nome were of the order of the sea surface temperature so that little, if any, convection was possible. Mixing ratio profiles to 500 m, however, confirm the existence of an active vapor flux. At stations N5 and N6, surface air is appreciably cooler than the underlying sea surface, and an active mixed layer has been generated to about 350 m at N5 and 450 m at N6.

Interpretation of data collected during the temporal observations at station N3C will be included in a later report.

C. Preliminary Results from Field Trip to NEGQA--February-March 1977

Intensive meteorological and oceanographic measurements were again made in the vicinity of Yakutat, Alaska, during the period 21 February 1977 to 8 March 1977. During much of the experimental period, the 500-mb flow was dominated by the same large amplitude wave that caused unseasonal winter weather over most of the United States and Canada. A low pressure in the Bering Sea and a ridge line along western North America cooperated to drive most storms onshore in southeast Alaska. The 500-mb geostrophic winds were, on the average, southwesterlies. At the surface, low-pressure systems born in the Gulf of Alaska persistently moved northeastward causing south or southeast geostrophic flow in the Yakutat area. As low-pressure centers approached the coast, the pressure gradient offshore increased, but there never was a strong high-pressure system or a large pressure gradient inland. Consequently the conditions were not conducive to the development of cold drainage winds from the interior. Post-frontal weather usually consisted of continued southerly winds bringing stratocumulus clouds and light rain or snow showers. Taken all together, these conditions have given Yakutat an unseasonably warm and wet year with very little snowfall.

The NCAR airplane used in this study (section 5) was on location from 21 February to 6 March 1977. From 28 February to 8 March, the NOAA ship

Surveyor was near Yakutat, and it was intended that the ship and airplane make intensive cooperative measurements during the overlap period. As mentioned in section 5, the weather was wholly uncooperative during the overlap period. During the ship-aircraft cooperation window, when the weather was safe enough for a flight, the seas were high, thus the ship could not accomplish all of the desired support measurements. Below are a summary and preliminary comments pertaining to the aircraft and ship activities during the field observing period.

Aircraft Activities

Although no formal analysis of the aircraft data can take place until NCAR provides the digitized data tapes (about 1 May 1977), some feeling for the scope of this data set can be presented here. Table 4 lists the seven flights of this experiment, the type of pattern flow (see fig. 5.3), and preliminary comments regarding the nature of the flight.

Two flights have been selected for discussion: 3 March and 26 February 1977. The discussion of these cases is necessarily very tentative. The wind measurements were simply computed from displays of the inertial navigation system aboard the airplane during flight, and are therefore subject to instrumental bias and sampling error. References to temperature or humidity structure come from strip chart recordings of the raw signals collected in flight. Nevertheless, these cases are discussed because even these rough measurements point toward a coherent picture that can be quantitatively solidified by the formal data processing yet to come.

The flight of 3 March was carried out between 1300 and 1600 Yukon Time. Figure 6.11 (a) and (b) shows the 00Z 4 March 500 mb and surface analyses. Twelve hours earlier at 500 mb, a low centered near 57° N, 157° W had been

Table 4. Summary of aircraft flights.

Flight Date	Pattern Flown	Comments
2-22-77	Coastal distribution	100% stratus, ceiling 60-100 m, middle level clouds at 1,500 m. Precipitation occurred in 15-km bands. Winds E-SE 10-20 knots. Evidence of wind turning to follow coast.
2-24-77	Coastal distribution two offshore legs at 30, 100 m	Low ceiling and snow showers. Winds E 20-30 knots.
2-25-77	Full flight	No clouds except offshore development of cumulus. Offshore flow near coast, elsewhere winds light and variable.
2-26-77	Full flight	Similar to 2-25-77 except flow was stronger, 10-20 knots. Winds draining out of Yakutat Bay although geostrophic winds were easterly.
2-28-77	Full flight	Large isolated precipitating cumulus. Winds NW 10 knots. Offshore flow near coast and associated small cumulus.
3-1-77	Coastal distribution and four offshore legs at 30, 100, 200, 300 m	Stratocumulus, ceiling 300 m, and occasional showers. Winds E 15-30 knots, 25-foot seas. Fly by ship.
3-3-77	Coastal distribution and two offshore legs at 60, 200 m	Altostratus and cumulus, occasional showers. Winds SW 20-30 knots, 25-foot seas. Fly by ship at mouth of Icy Bay. Offshore legs originate at Icy Bay.

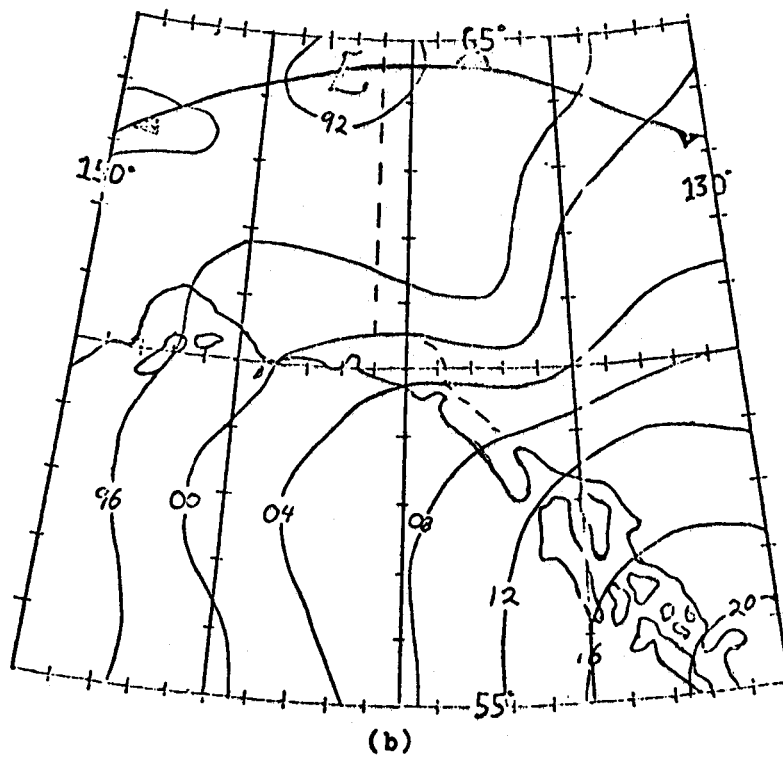
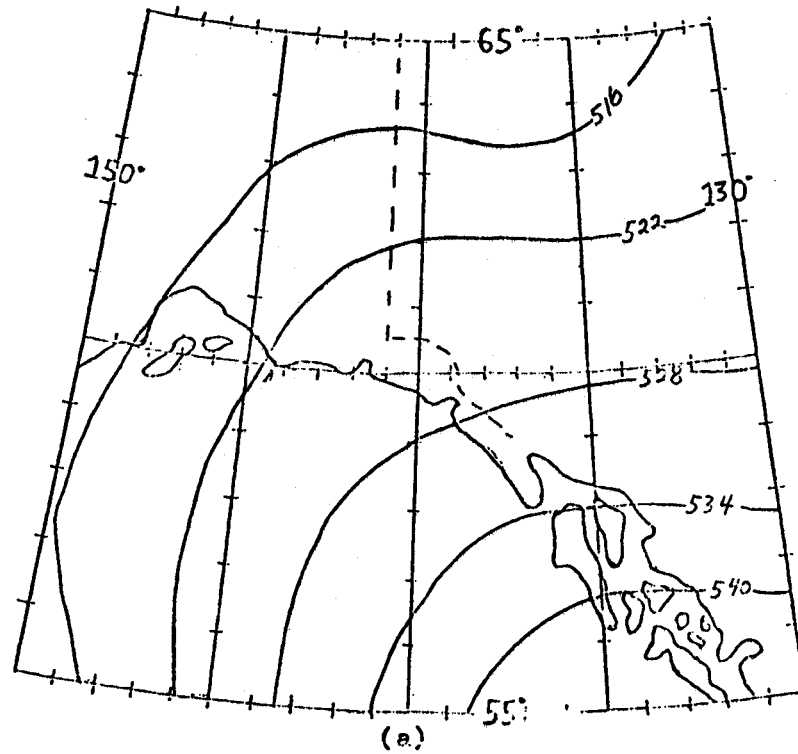


Figure 6.11. 500 mb (a) and surface (b) synoptic analyses for 00Z 4 March 1977.

giving Yakutat southwesterly flow, then became westerly over the Yukon. By the time of figure 6.11, a slight ridge had formed between that low and Yakutat, and upon moving eastward was creating nearly westerly anticyclonic flow over Yakutat. Correspondingly, the surface had been dominated by nearly parallel isobars and an elongated low-pressure region spanning much of the Gulf of Alaska. Yakutat had strong southwesterlies and high seas. Also by this time, the low center had closed up considerably. A ridge developed, giving Yakutat westerly or southwesterly winds. The flow was therefore not highly baroclinic. The cloud cover was 70% altocumulus and altostratus.

Figure 6.12 shows a survey of the winds obtained from the airplane at an altitude of 60 m. The winds were strong southwesterlies and fairly homogeneous over the region sampled. Similarly, the signatures of the temperature and humidity traces were characteristic of a homogeneous, nearly neutral stability mixed layer. A much more detailed picture will be available when the digitized aircraft data are processed, but this preliminary look suggests that, in the case of strong onshore flow, topographic and thermodynamic effects induced by the nearby coast on the surface wind field are not felt 10 km offshore.

Aircraft observations were made between 1300 and 1600 Yukon time on 26 February 1977. Figure 6.13(a) shows that the 00Z 27 February 500-mb flow was not unlike that of the case discussed above. The low center near the Aleutians and the ridge along western North America produced a south to southwest flow with anticyclonic curvature. There were no high or middle level clouds. The surface isobars were substantially different than on 3 March. A storm had rapidly moved toward the coast but was south of Yakutat. The geostrophic wind at Yakutat was E-SE, along the coast, as may be seen in figure 13(b).

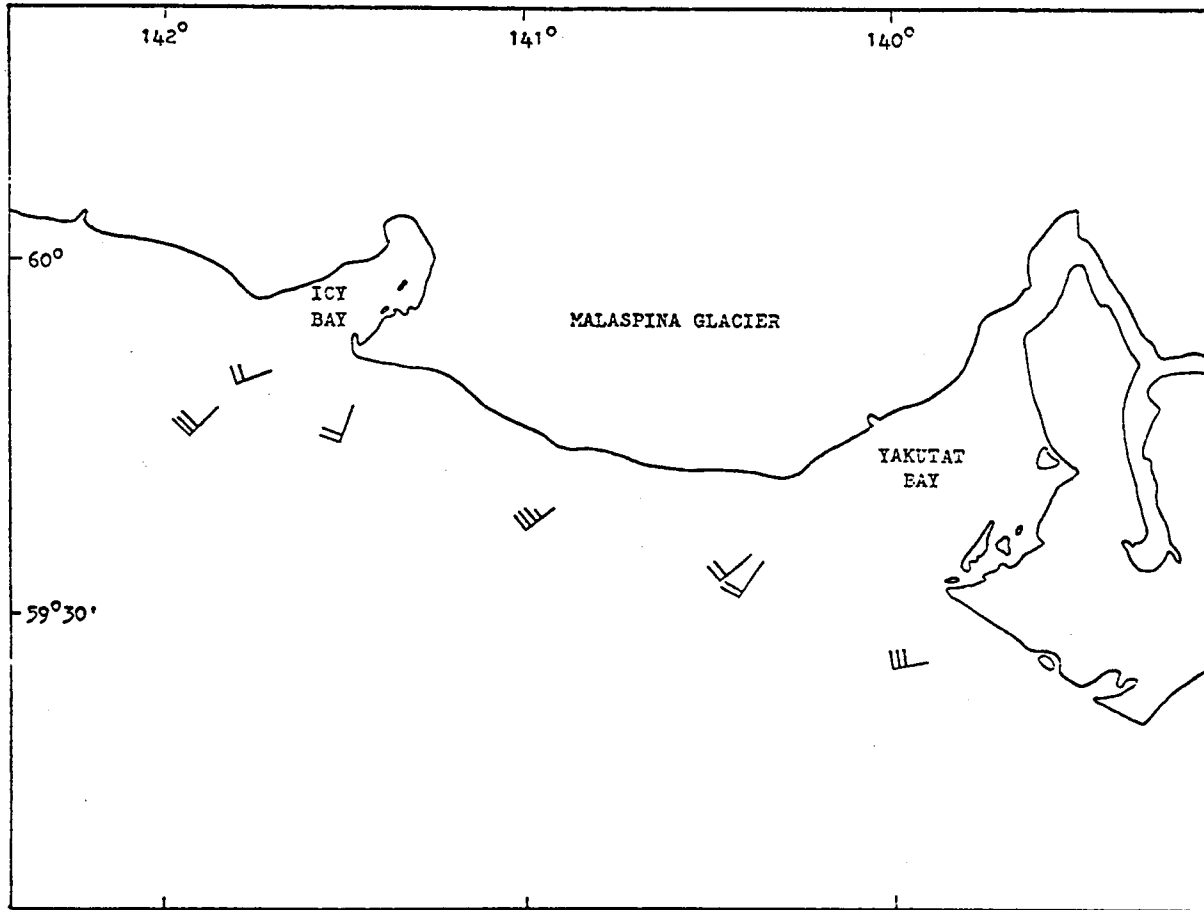
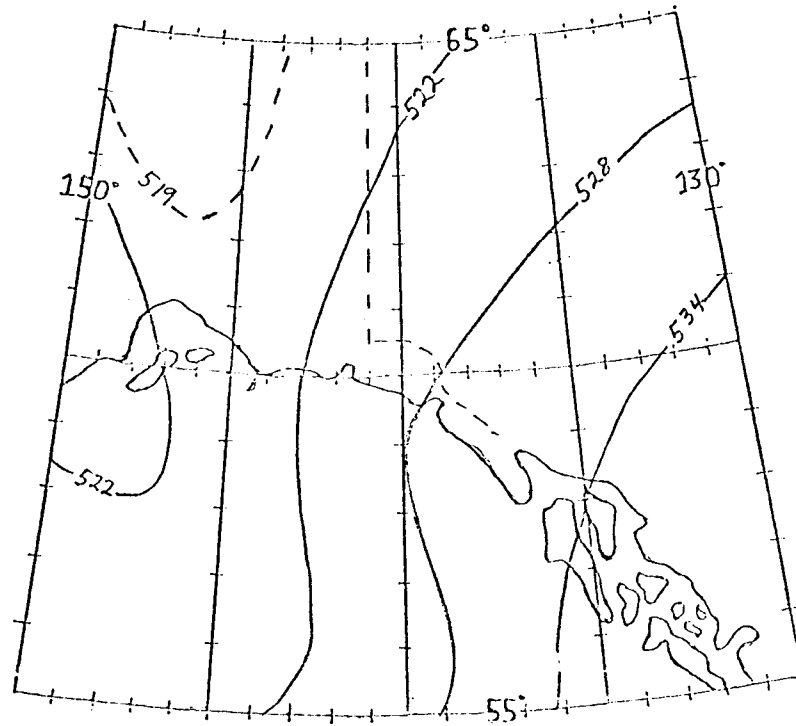
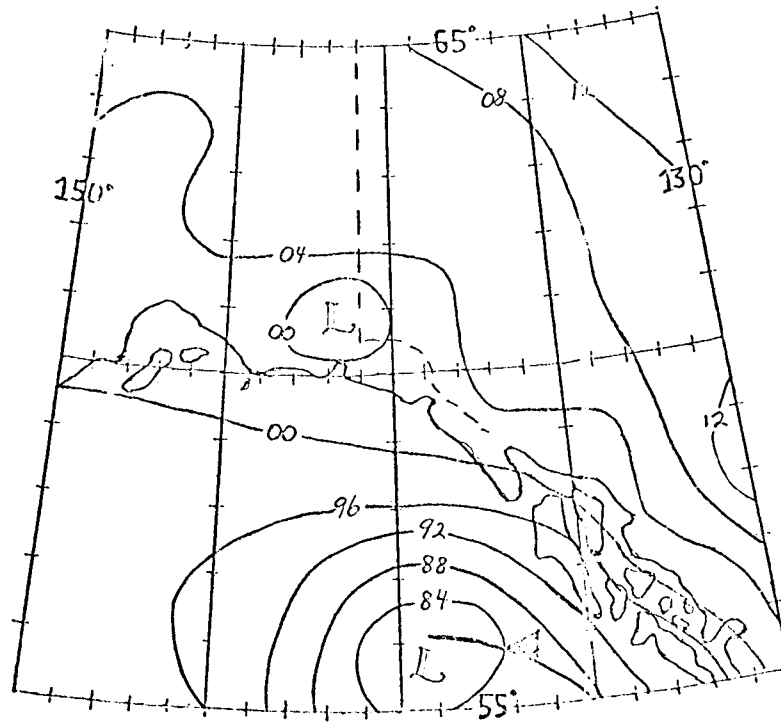


Figure 6.12. Wind estimates obtained during flight of 3 March 1977.
 All measurements at 60 m. One barb equals 10 knots.



(a)



(b)

Figure 6.13. 500 mb (a) and surface (b) synoptic analyses for 00Z 27 February 1977.

A tentative survey of the wind velocity field is shown in figure 6.14 for measurements at 15, 30, 60, and 400 m. Also shown is the estimated position of the beginning of a bank of scattered cumulus clouds whose bases were at 200 m and tops at 400 m. Farther offshore, cloud base was somewhat higher, and the clouds showed more vertical development. The 400-m wind measurements are roughly parallel to the geostrophic wind. Note, however, that near the coast and nearer the surface the winds were offshore. The signature of the temperature trace confirms the presence of offshore flow as the temperature and stability of the air changed markedly as distance from the shore increased. The existence and character of the low-level cumulus clouds was a further sign that air modification was taking place. Air also appeared to be draining out of Yakutat Bay, although it was warmer than the air coming from over Malaspina Glacier, evidently because of its longer trajectory over open water.

The offshore flow in this case was not due to katabatic drainage of continental air. Whether the offshore wind behavior was due to a small-scale drainage from the nearby glaciers, topographically forced by the mountains, or even simply due to the frictional effects arising from the contrast of the aerodynamic properties of the underlying surface, remains to be seen. Whatever the cause of the offshore flow, it is apparent that consequent modification of the air and presumably the surface winds was taking place.

Ship Activities

During the period of 24 February to 11 March 1977, meteorological research was conducted aboard the NOAA ship Surveyor in support of the Icy Bay-Yakutat Bay coastal processes study. These observations were primarily designed to supply surface and lower boundary layer data for correlation with data collected by the NCAR aircraft.

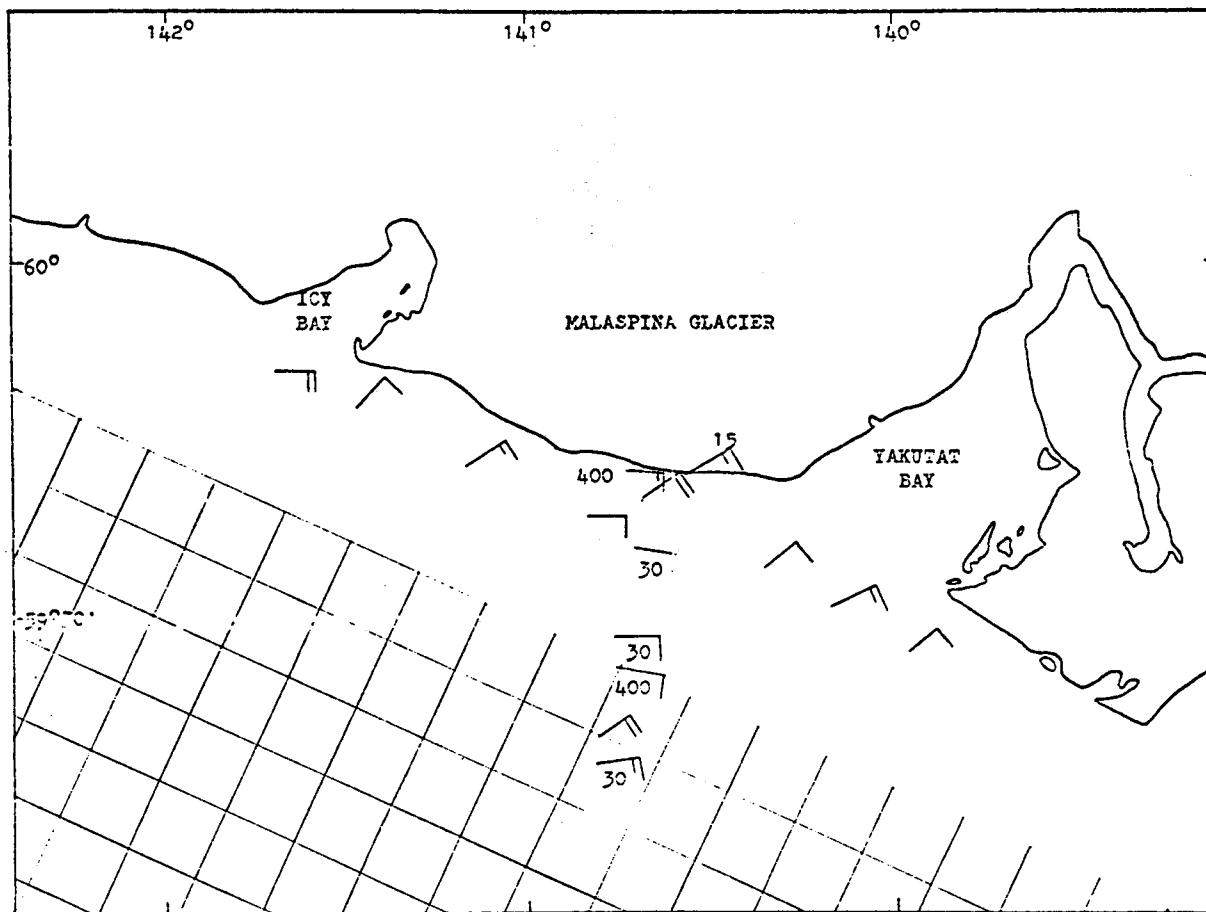


Figure 6.14. Wind estimates obtained during flight of 26 February 1977. All measurements at 60 m unless otherwise indicated. One barb equals 10 knots. Cross hatched area marks location of offshore cumulus development.

A current meter held at a 3-m depth by a spar buoy was deployed on March 1 at a site about 10 km off Sitkagi Bluffs (see (*) on fig. 5.3). The buoy was successfully recovered on March 7, and the data are currently being processed. In addition, two remote meteorological surface stations capable of monitoring wind speed, wind direction, and air temperature were installed at Cape Riou on the eastern entrance to Icy Bay and at Manby Point at the western entrance to Yakutat Bay (S1 and S2 in fig. 5.3). These stations will be attended on a monthly basis and will remain in position through September 1977.

Due to inclement weather in the Gulf during most of the operating time, active meteorological observations from the ship were greatly curtailed. Rough seas prohibited use of the bow meteorological boom. On two occasions, March 1 and March 3, the Surveyor was able to furnish radiosonde and surface observations during aircraft operations. On the latter flight, eight surface drift drogues were deployed for tracking by the aircraft.

On the 6th and 7th of March the synoptic gradient weakened (although a low-pressure cell still lay in the northern Gulf), providing offshore flow under near calm conditions and clear skies as shown in figure 6.15. A seven-station trackline extending to 30 miles off Sitkagi Bluffs (fig. 6.16) was occupied during that period. Radiosonde and boundary layer measurements were made, as well as surface observations, current meter profiles to 50-m depth, and CTD casts. This activity is summarized in table 5.

Detailed results from this experiment will be furnished in a later report.

D. Model Results

During the past year, the modified Lavoie model has been greatly simplified and improved, which will allow a user to examine many runs with a minimum

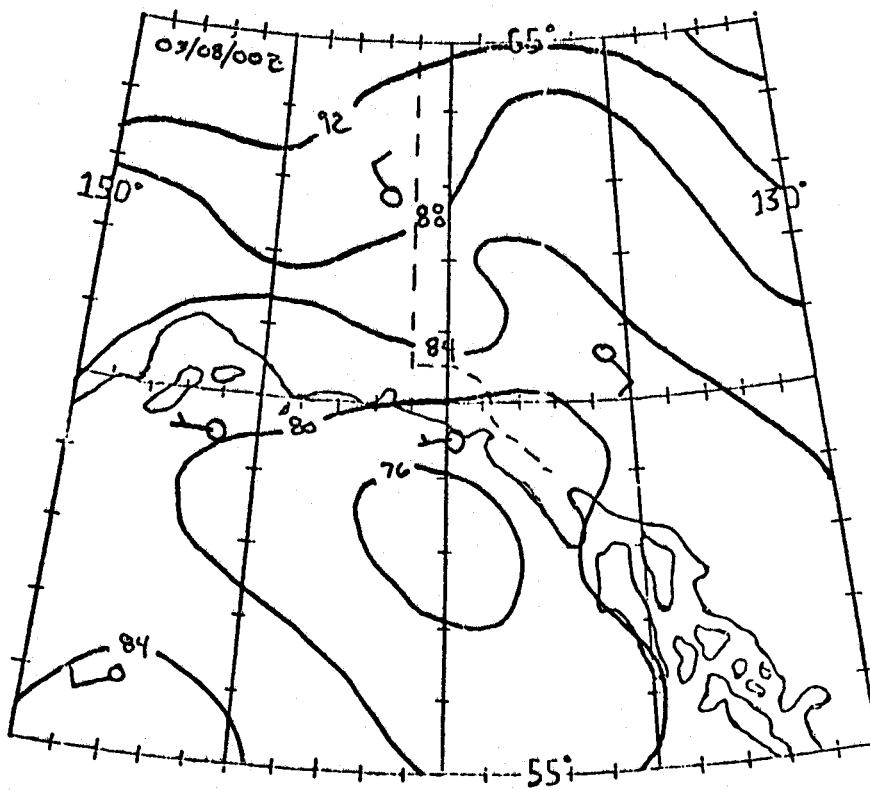
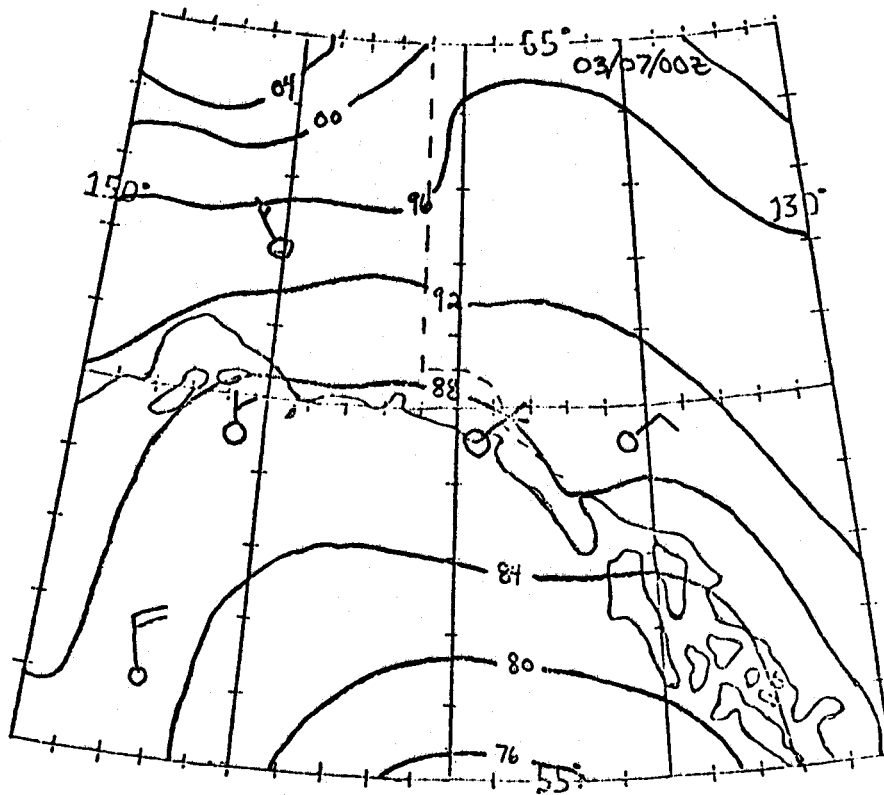


Figure 6.15. Surface pressure analysis for 3-7-77 00Z (top) and 3-8-77 00Z.

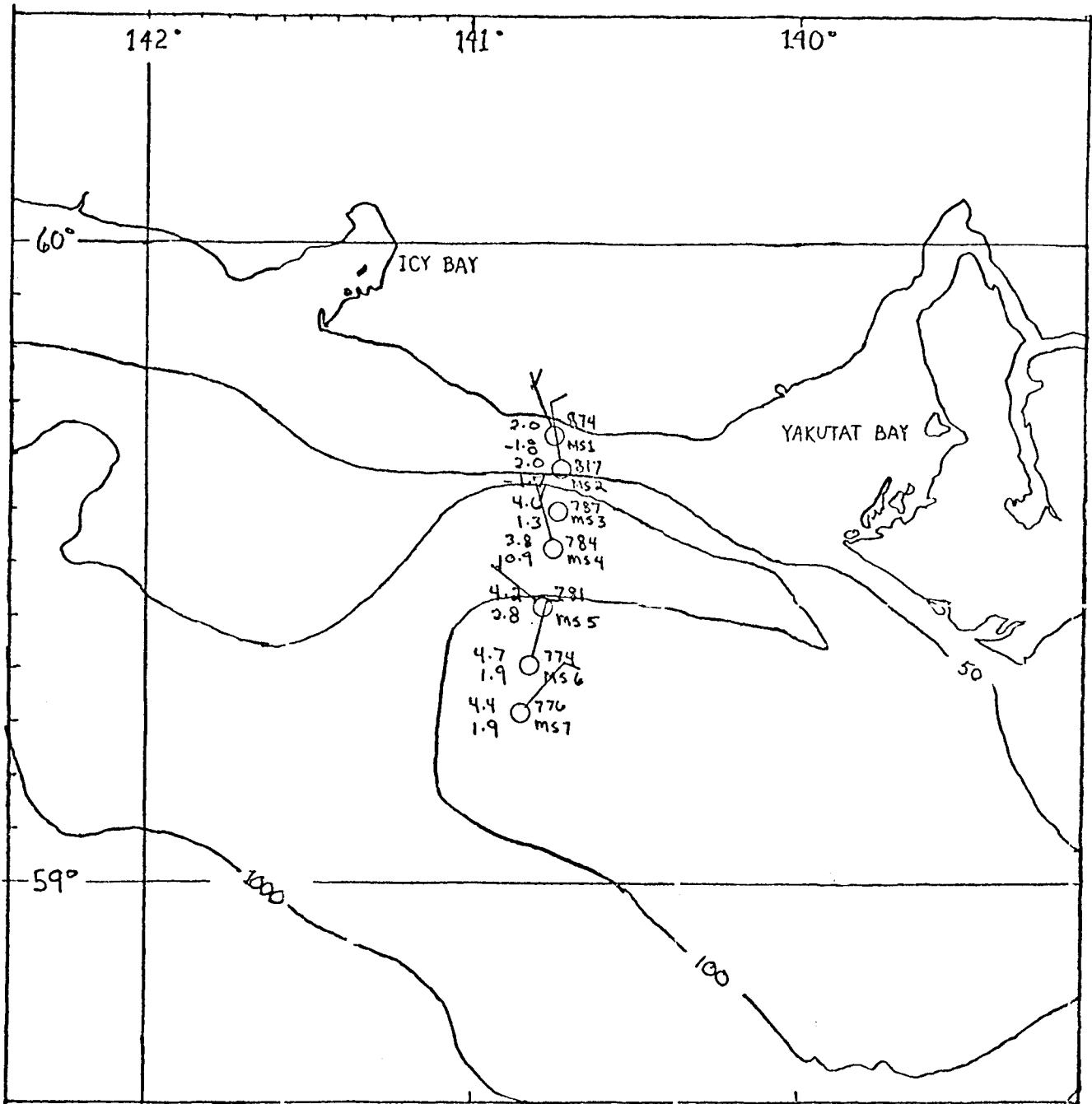


Figure 6.16. Seven-station trackline occupied by Surveyor and summarized surface meteorological observations.

TABLE 5.

Table 5. Summary of Meteorological Stations occupied by ship SURVEYOR during 6-8 March 1977.

STATION	DATE	RADIOSONDE	BLP	CTD	CURRENT METER	BOW OBS.
MS 2	03/06	1740Z	--	--	-----	1700Z
MS 2	03/06	1826Z	--	--	-----	1855Z
MS 2	03/06	2004Z	--	--	-----	1956Z
MS 1	03/06	2245Z	--	2140Z	2213Z	2300Z
MS 1	03/07	--	0017Z	--	-----	0000Z
MS 2	03/07	0441Z	0314Z	0413Z	0429Z	0425Z
MS 2	03/07	0738Z	0615Z	--	-----	0425Z
MS 3	03/07	--	---	--	-----	0920Z
MS 4	03/07	--	--	--	-----	1015Z
MS 5	03/07	--	--	--	-----	1135Z
MS 6	03/07	--	--	--	-----	1325Z
MS 7	03/07	1709Z	--	1739Z	-----	1430/1720
MS 6	03/07	1953Z	--	2005Z	-----	1945Z
MS 5	03/07	2206Z	--	2230Z	-----	2134Z
MS 3	03/08	0041Z	--	0042Z	0129/0345Z	0055Z

of time and expense. The remainder of the contract period will be spent examining the sensitivity of the model to its various parameters, and in case studies, especially during the 1977 field study. This section will present trial runs of the model with a discussion of each case. The cases shown are selected to demonstrate many of the advantages and limitations of the model as it is applied to the Icy Bay-Yakutat region.

For the runs shown here, the following input parameters were specified:

Surface layer height: $Z_s = Z_0 + 50$ m, where Z_0 is ground elevation

Drag coefficient: $C_D = \begin{cases} 1.3 \times 10^{-3} & \text{over water} \\ 5 \times 10^{-3} & \text{over land} \end{cases}$

Heat flux coefficient: $C_H = \begin{cases} 1.5 \times 10^{-3} & \text{over water} \\ 0 & \text{over land} \end{cases}$

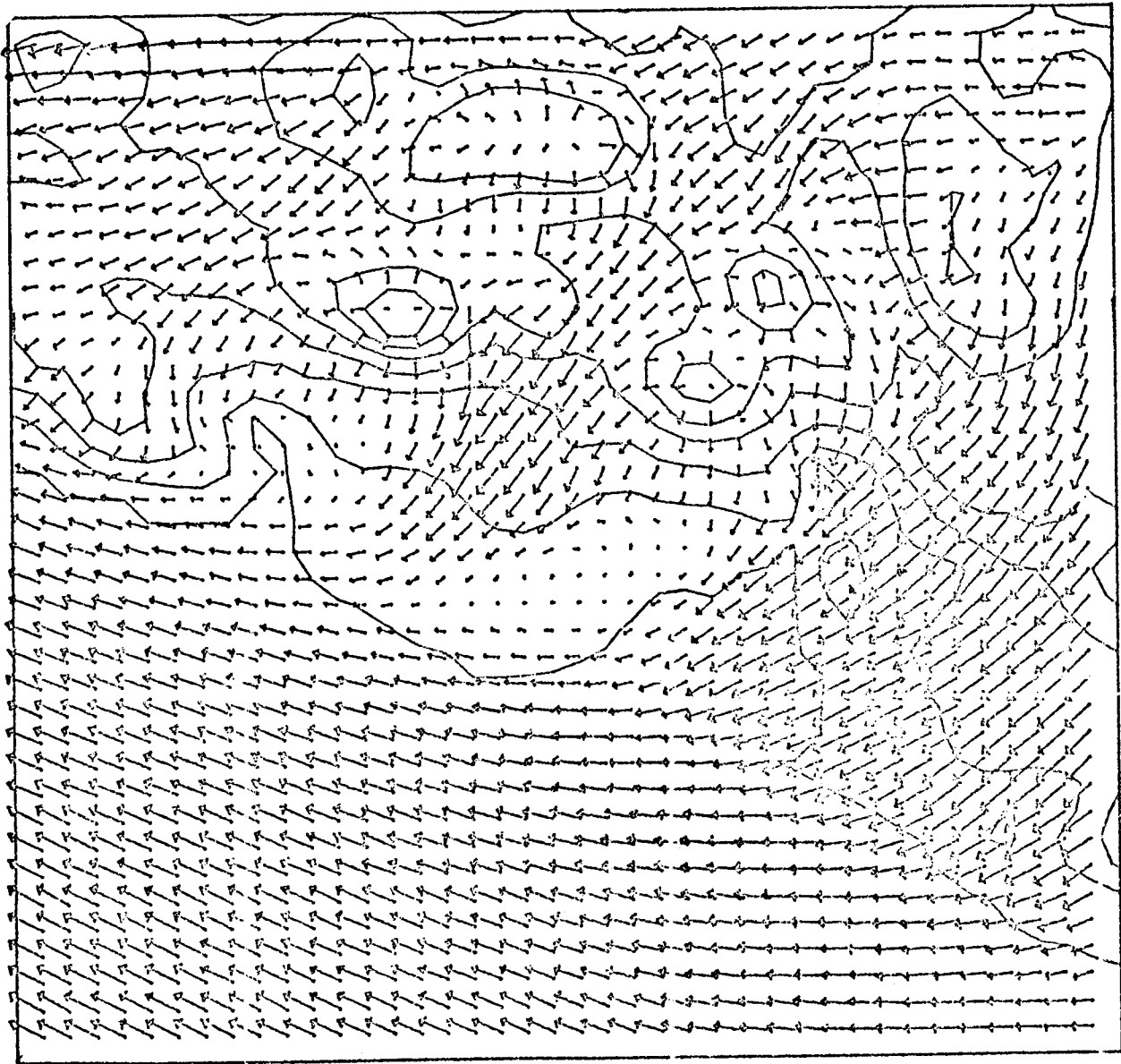
Vapor flux coefficient: $C_q = C_H$

Coriolis parameter: $f = 1.26 \times 10^{-4} \text{ s}^{-1}$

Water temperature: $\theta_s = 4^\circ\text{C}$ everywhere

The above selection of parameters represents a very simple first set. The drag coefficients do not reflect any variation with either stability or type of land. A spatial variation in heat flux over the water will have an effect on the drag coefficient. However, more importantly, it is expected that over land the drag coefficient varies significantly between ice, rock, and vegetation. When the land was digitized, these areas were coded so that their effect could be estimated. Future runs will include variable topography. Similarly, the bulk coefficients of heat and vapor flux are functions of stability.

Figure 6.17 is a map of surface winds for the case of a SE geostrophic wind. The input conditions are that the boundary layer height over water is 1.1 km and $\vec{V}_g = 135^\circ$ at 12 m/s. The topographical effects in this case are quite pronounced. Funneling in Yakutat Bay and between the mountains is obvious. The winds alongshore are E to NE as a result of mountain effects.



10 METERS PER SECOND

Figure 6.17. Computed surface winds for a SE geostrophic flow.

Figure 6.18 represents surface winds for the case of NW winds. Input parameters are 1.1 km inversion height over water and $\vec{V}_g = 355^\circ$ at 12 m/s. Some funneling is apparent, but not as significant as the previous example. Winds in the Yakutat region are more NE, and a calm exists in Yakutat Bay.

The two example runs are promising, yet we are not convinced we are adequately representing all the physical processes which are active. Certain peculiarities in the results are disquieting, thus some future work will be aimed at improving our understanding of the intricacies of the model by means of simple test cases which emphasize one or another of these processes (topography, heat flux, drainage).

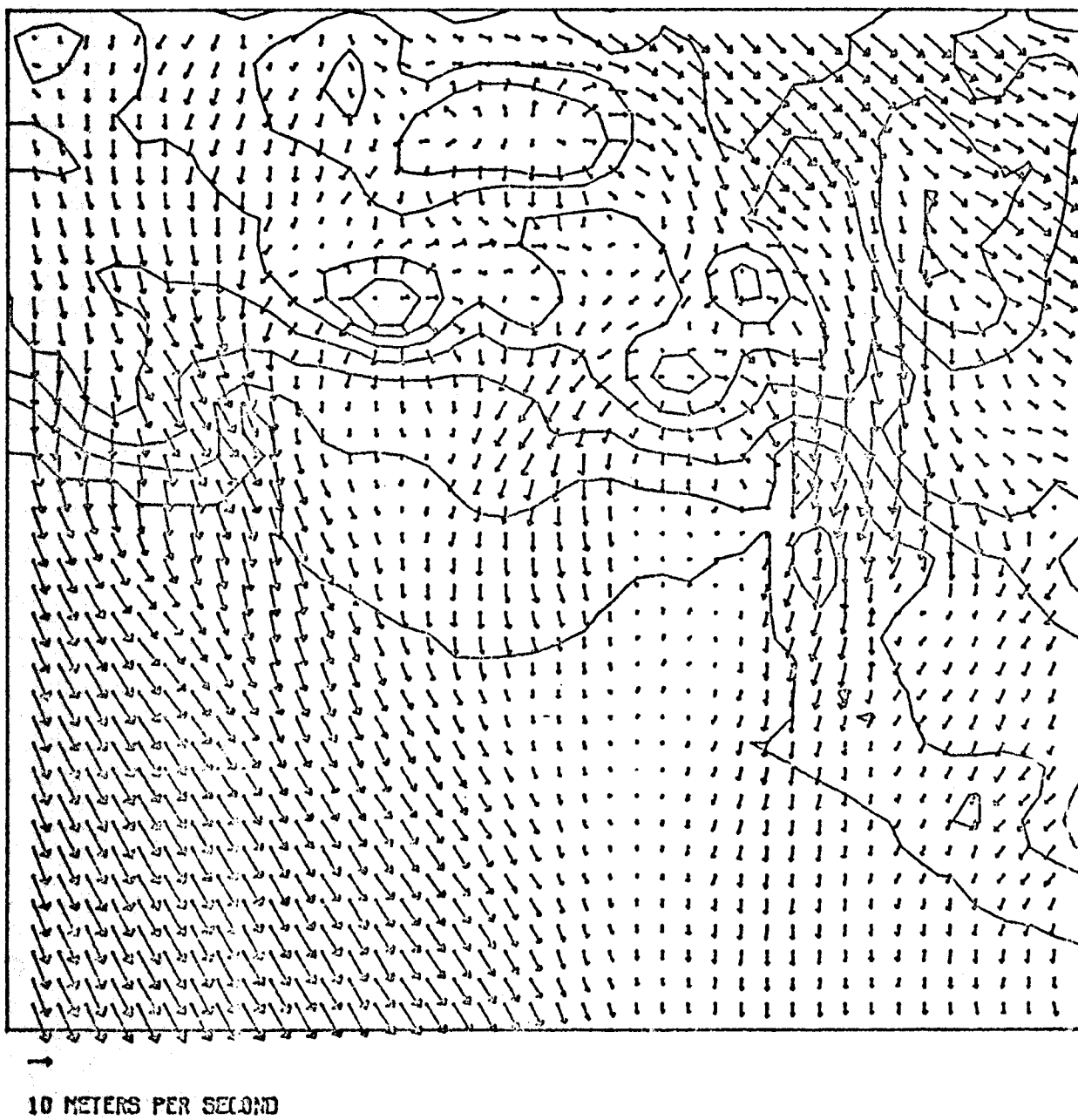


Figure 6.13. Computed surface winds for a NW geostrophic flow.

REFERENCES

- Reynolds, R. M., and B. Walter (1976): Near-shore atmospheric modification. Environmental Assessment of the Alaskan Continental Shelf, Principal Investigators' Reports for the Year Ending March 1976, Vol. 11, 992 pp.
- Lenshow, D. H. (1972): The measurement of air velocity and temperature using the NCAR Buffalo Aircraft Measuring System. NCAR Technical Notes, NCAR-TN/EDD-74, National Center for Atmospheric Research, Boulder, 39 pp.

APPENDIX A

ARCTIC COASTAL AIR MODIFICATION
FIELD STUDIES IN THE GULF OF ALASKA

R. Michael Reynolds

S. A. Macklin

B. A. Walter

Pacific Marine Environmental Laboratory
Environmental Research Laboratories
National Oceanic and Atmospheric Administration
3711 15th Avenue NE.
Seattle, Washington 98105

ARCTIC COASTAL AIR MODIFICATION
FIELD STUDIES IN THE GULF OF ALASKA

R. Michael Reynolds
S. A. Macklin
B. A. Walter

ABSTRACT. Data from two shipboard studies of the lower troposphere off the Malaspina Glacier in Alaska are compared with a simple air modification model. In one case, the synoptic scale flow was offshore and the data agree well with the model. In the second study, the synoptic flow was westerly but underlain by a northerly katabatic flow off the glacier. The katabatic layer was heated from above and below until it merged with the larger scale flow about 20 km offshore. In this case, interpretation of the data in terms of a simple model are not feasible; other active mechanisms must be considered to fully describe the process.

1. INTRODUCTION

The term "air modification" generally applies to the adjustment of an air mass advected over a warmer surface. Typical examples of such modification occur off the coast of China and the Eastern United States when large-scale weather patterns drive air of arctic origin over warmer seas. The unstable situation produces large upward fluxes of latent and sensible heat, with the development of an internal convective boundary layer. This type of air modification, driven by synoptic scale weather conditions, has been studied recently in the Great Lakes (Lenshow, 1973; Bean et al., 1975). After Canadian continental air flows over the warmer lakes, moisture absorbed from them is deposited as rain or snow on the southern, lee side. Large-scale

air modification over the western Pacific was investigated in two Air Mass Transformation Experiments (AMTEX) (Lenshow, 1974). The above examples are synoptic scale phenomena in which the air is cold throughout the troposphere. Thus the convective boundary layer can develop over very large horizontal distances, typically 500 km.

A similar situation occurs on a mesoscale when katabatic winds (downhill movement of a ground-based inversion) blow over warmer water. Initially, the direction of the surface wind is determined by both the pressure gradient and the surface slope on shore. Offshore, the katabatic acceleration is diminished while convection quickly erodes the stable layer until the modified synoptic scale structure predominates. Weller (1969) discusses the offshore modification of katabatic flow in Antarctica and suggests a length scale for the seaward extent of 10 km.

This paper discusses the results from two winter experiments in the vicinity of Yakutat Bay and Icy Bay in the Northeast Gulf of Alaska (Figure 1). As continental air is cooled at the surface, especially during cloudless periods, the mountainous coastal conditions produce offshore flow. This flow is often intensified by the dominant winter high pressure system over the central regions of Alaska. Orographic funneling acts to channel the flow into the many estuaries along the coastline, often creating intense jets of offshore wind (Kilday, 1970). In one of our studies, synoptic scale forcing was offshore as well as the katabatic flow which resulted in boundary layer development well offshore. In the other case, northerly offshore katabatic flow was overridden by a westerly arctic air mass which had been advected over several hundred kilometers of ocean. Thus a three-level situation was created with katabatic tongues, mixed layer, and upper arctic air mass. The katabatic air is evident to about 20 km offshore.

Over the ocean, vertical profiles of mean wind, potential temperature, and humidity are expected to be similar to those for a horizontally homogeneous, quasi-stationary, convective boundary layer. These profiles are well-described in literature (cf. Tennekes, 1973; Carson, 1973; Stull, 1976). Figure 2a is a schematic of the expected boundary layer structure. The convective mixing is sufficient to vertically homogenize \bar{u} , $\bar{\theta}$, \bar{q} within the boundary layer such that above some height, typically 10 m, they are constant u_b , θ_b , q_b , respectively. In the surface layer the profiles are logarithmic, tending to surface values of u_s , θ_s , q_s , while just above the transition region they have values of \bar{u} , $\bar{\theta}_u$, q_u , respectively. The air above h is assumed stable, i.e., $\gamma > 0$ where $\gamma = \partial\theta/\partial z$. Unless otherwise specified, the usual meteorological symbols are used.

The theoretical discussion below assumes these profiles for a simple set of equations describing offshore development of the boundary layer. However, field measurements of the profiles exhibit particular anomalies in the "mixed layer" which indicate the need of a more sophisticated model. Stable stratification in the katabatic tongue and evidence of a cold core at the top of the mixed layer are two such anomalies.

2. THEORY

A simple yet elegant model of air modification is developed by Fleagle and Businger (1963). A steady-state model is proposed in which the x axis is aligned with the mean wind, u , which is assumed unidirectional in the boundary layer. Writing the first law of thermodynamics as

$$u \left(\frac{T}{\theta} \right) \frac{\partial \theta}{\partial x} = \frac{\partial}{\partial z} (\overline{\theta'w'}) , \quad (1)$$

an integration over the region $z \in (0, h)$ results in an approximate relation,

$$hu_b \frac{\partial \theta_b}{\partial x} = H_s - H_i , \quad (2)$$

where H_s , H_i are the kinematic vertical heat fluxes at the mixed layer boundaries, and $h(x)$ is the mixed layer height. The ratio T/θ is approximately equal to 1. Both H_i and radiative cooling are neglected in the formulation here. However, both can be included as a correction to H_s (Tennekes, 1973).

Offshore, profiles are assumed to be similar to those shown in Figure 2. If the fluxes of heat or vapor through the entrainment layer are assumed negligible, the potential temperature curve is simply the intersection of the constant θ_b with the upper level slope γ ; then

$$\frac{\partial \theta_b}{\partial x} = \gamma \frac{\partial h}{\partial x} . \quad (3)$$

If the upper air lapse rate γ is assumed constant over the air modification region, equation (3) is integrable, but is dependent on initial conditions. A typical assumption for simple air modification models is $h(0) = 0$. As this paper is designed to compare recent data to simple models, that assumption will be made. Further comments on the need for a more comprehensive model are discussed later.

After integration of (3),

$$h = (\theta_b - \theta_0) / \gamma , \quad (4)$$

where θ_0 is the surface air temperature at the coast (see Figure 5). The heat flux at the surface, H_s , can be approximated by the bulk parametric formulation,

$$H_s = C_H (u_b - u_s) (\theta_s - \theta_b) , \quad (5)$$

where C_H is the bulk heat transfer coefficient and u_s is the surface water current which is assumed $\ll u_b$. For the purposes of this simple model, C_H is assumed constant (about 1.5×10^{-3}), but it is known to be a weak function of stability (Deardorff, 1968). After substitution of (5) and (4) into (2),

$$\frac{\partial \theta_b}{\partial x} = \gamma \left(\frac{\theta_s - \theta_b}{\theta_b - \theta_0} \right) . \quad (6)$$

By rearrangement, the following nondimensional quantities can be formed:

$$\tilde{\theta} = \left(\frac{\theta_b - \theta_0}{\theta_s - \theta_0} \right), \quad (7)$$

$$\xi = C_H x / h_f, \quad (8)$$

$$h_f = \gamma / (\theta_s - \theta_0), \quad (9)$$

$$\tilde{h} = h / h_f.$$

The solution to (6) in terms of the above nondimensional quantities is

$$-\xi = \tilde{\theta} + \lambda n(1 - \tilde{\theta}). \quad (10)$$

The term h_f is interpreted as the maximum height of the mixed layer, where $\theta_b = \theta_s$ and surface heat flux is zero. A similar development for mixed layer height \tilde{h} and a nondimensional mixing ratio $\tilde{q} = (q_b - q_u) / (q_s - q_u)$ results in

$$\tilde{h} = \tilde{\theta} \quad \text{and} \quad (11)$$

$$\tilde{q} = \left(\frac{1 - \tilde{\theta}}{\tilde{\theta}} \right) \lambda n(1 - \tilde{\theta}) + 1. \quad (12)$$

Figure 6 is a graph of equations (10) - (12). This model attempts to predict the development of the unstable mixed layer during an air modification process in a simplistic fashion. Although the quantities (7) - (10) can be obtained from a single radiosonde sounding, serious errors are inherent by so fitting an individual profile to the ensemble mean profile proposed by Figure 2. Similar simple models have been applied by Summers (1965), Leahey, and Friend (1971), and Deardorff, et al. (1969). However, the data in this paper indicate the need for a better understanding of the initial conditions.

A more detailed formulation of a developing mixed layer was given by Tennekes (1973) in which entrainment is represented by a temperature jump, Δ at $z = h$, termed the inversion strength. It is not unreasonable to presume that before the flow reaches the coastline, there is sufficient mechanical

mixing to create a low mixed layer with a large value of Δ due to the strong gradient, γ . In this situation, surface heat flux initially acts to reduce Δ , and little inversion growth is observed. Evidence of a mechanically mixed surface layer in katabatic flow was given by Budd, et al. (1966), where measurements in Antarctica showed mixed layer depths of about 400 m. The profiles in Figures 4, 5, and 13 show evidence of a temperature jump at the inversion base.

3. SYNOPTIC SCALE AIR MODIFICATION - 3 FEBRUARY 1975

A brief exploratory set of radiosondes was released in early February 1975 from the NOAA ship Oceanographer. Although 20 ascents were made over the course of the cruise, only ascent numbers 6-11 will be considered here.

During the period of measurement, the weather was generally clear with light northerly winds. The synoptic pressure pattern was dominated by an inland high cell such that the geostrophic wind direction was northerly, indicating advection of the Arctic continental air mass offshore. Figure 3 summarizes the surface meteorological conditions made by the ship at the time of the balloon ascents. Also shown is a coincident measurement from data buoy EB-33. Figure 4 is a comparison of near simultaneous radiosonde profiles from the NWS station at Yakutat and a shipboard ascent 33 km offshore. A strong ground-based inversion at Yakutat is mixed offshore to an altitude of about 600 m. Humidity proves to be an excellent indicator of inversion height as it reflects a sharp cutoff to dryer air above. There is some evidence of an entrainment layer between 500 and 600 m.

With respect to the model, these six profiles were examined in the following way (cf. Figure 5). A vertical line from the surface bulk temperature θ_s (2.9°C) gives h_f (960 m). Extrapolation of the lapse rate above the mixed

layer to the surface yields θ_0 (-4.8°C). Values of θ_b (-2°C) and x (51 km) then allow calculation of ξ (.080) and $\tilde{\theta}$ (.262). When all ascents are so analyzed (Figure 6), the plot agrees well with the expected curve. It must be emphasized that radiosonde ascents are of limited quality and demand subjective interpretation.

When similar plots are made of \tilde{h} or \tilde{q} , the fit is poor. In fact, for all cases the measured values of \tilde{h} and \tilde{q} show no real trend. Without more knowledge of the exact profile at the coastline, it is difficult to explain the reasonable fit of $\tilde{\theta}$, yet lack of fit of \tilde{h} or \tilde{q} in terms of the simple model outlined above. Possible explanations could be that a mechanically generated mixed layer exists at the coastline which invalidates equation (4). Further, computations of \tilde{q} assume $q_0 = q_u$, i.e., at the coastline the humidity is constant with height. Possibly water sublimation from the glacier, especially in the presence of a mechanically mixed boundary layer to a height of 100 m or so, will yield a more complicated profile. Another consideration is the inaccuracy of radiosonde measurements of humidity at such low values. The coastline profile is fundamental to the problem and must be measured in future experiments.

Another anomalous feature of the vertical structure is a maximum in the humidity trace within the mixed layer. Figure 7 is a cross section of all the profiles of humidity. The profiles show a distinct humidity maximum near the coast which becomes less distinct offshore. The presence of a humidity maximum near the top of the mixed layer with subsequent mixing downstream compares well with wind tunnel experiments by Willis and Deardorff (1976) in which diffusion of a passive contaminant in a convective boundary layer was studied. An upper level maximum concentration was observed at $.8 h$ at a downstream distance of $x_m = 1.7 h u/w_*$ where w_* is the convective

velocity scale, $w_* = [g(\overline{\theta'w'})_0 h/\theta_b]^{1/3}$, θ_b in °K. Downstream of this point the pollutants became vertically well-mixed. In the present case, the heat flux was typically about 25 W/m², $w_* \approx .81$ m/s, and $x_m = 4.4$ km. The laboratory results only extended to about $2x_m$, but the maximum was still evident. Thus the observed humidity maximum may be partially explained as a result of comparable advection and convection time scales. Mahrt (1976) used a similar argument to explain the presence of a significant decrease in moisture with height in the mixed layer over the high plains region of the United States. The negative gradient is possibly related to rapid growth of the mixed layer into dry air above.

4. KATABATIC FLOW UNDER A MIXED LAYER - MARCH 1976

In March 1976, a more extensive set of measurements was made in the same area. Surface data and vertical profiles were made at 36 stations; however, one line of nine stations will be considered here. This line was taken during a period when synoptic conditions were nearly stationary. Figure 8 summarizes the surface observation during the time of the section. A clear progression in surface air temperature is evident over the line. The winds, however, make a distinct westerly shift between stations 9B and 10B, which will be discussed below.

A surface analysis map for 1200Z 9 March 1976 is shown in Figure 9. Observed wind arrows indicate the air mass observed at Yakutat was of Arctic continental origin but modified by passage over the Gulf of Alaska.

Coincident vertical profiles of potential temperature and mixing ratio for Yakutat and a station 8.5 km offshore are shown in Figure 10. Evidence of the long passage of the middle layer over water is shown by the steeper temperature gradient at about 900 m with the slightly more stable conditions

higher. Also evident from the figure is the modification of a cold, dry surface inversion, evident in the Yakutat sounding, to a shallow convective boundary layer offshore. The exact depth of the convective boundary layer is difficult to ascertain in this profile, but it seems to be in the range of 250-450 m. The profiles reflect an eastward temperature gradient consistent with the general picture.

It is difficult to accurately determine the height of the mixed layer by a single sounding. Even if the sampling interval is small enough to completely resolve vertical structure, the radiosonde provides only a single trace through an inhomogeneous region which can lead to either sharp cutoffs or more gradual transitions (Stull, 1976).

Thus the data indicate a low katabatic flow offshore which is rapidly modified by surface heat flux until it is the same temperature as the air above. At this point mixing occurs throughout the deeper mixed layer, up to about 1000 m. The wind arrows in Figure 8 imply this occurs at about 24 km offshore when the wind makes an abrupt direction change from directly offshore to near geostrophic. A contour plot of the potential temperature profiles (Figure 11) shows many interesting characteristics of the offshore modification. First, the strong similarity to the expected profiles (Figure 2b) is noteworthy. The katabatic flow is seen to be a tongue of cold air extending offshore. The overriding mixed layer has a height of about 800 m at 10 km from the coast growing to about 1200 m at 65 m offshore. It has a horizontal temperature gradient which is oblique to its westerly flow (into the page). The combination inversion rise and temperature gradient are explained by the fact that its direction is oblique to the coast; air closer to the coast has been over water a shorter time.

Also evident in the cross section is a cold air core located approximately 30 km offshore. At the time of this writing, no firm explanation of this core is available. It is possible that this is a thermal wind effect, analogous to the jet stream.

Figure 12 is a cross section of mixing ratio. Although there is some scatter, a humidity maximum is evident in the mixed layer. The maximum varies from 240 to 580 m offshore. The maximum in this case is on the order of .4 h, much lower than before. The work of Willis, et al. (1976) shows that the level of the maximum decreases downstream of x_m . However, the profiles are much more well-defined in this case. Another transition to dry air marks the top of the mixed layer at about 1100 m.

No attempt was made to analyze this data by the techniques discussed in Sections 2 and 3. The profiles were generally inconsistent with those assumed by the model, especially in the katabatic layer. Figure 11 shows that in the katabatic wedge there was no well-defined mixed layer, but rather a gradient throughout the layer. Details of this structure are evident in a profile taken by tethered balloon boundary layer profiler (BLP) at station 6B, about 6 km offshore. The BLP sonde measures temperature, wet-bulb temperature, wind speed, wind direction, and pressure. Although the pressure sensor malfunctioned, reasonable height estimates could be made in the following way: Ascent and descent were scaled by matching the heights at which a sharp transition in wind direction occurred. Constant rates of ascent and descent were assumed. The vertical height was assigned by letting the temperatures at maximum height equal that of the radiosonde released just prior to flight. The resulting profile is given in Figure 13.

Again, Figure 13 shows the lower boundary layer to be statically stable, slowly becoming neutral at higher altitudes (>600 m), which is also shown in

Figure 11. Below 70 m, an exceptionally stable layer over an unstable surface layer is evident in the temperature trace. Similarly, wind profiles do not agree with a convective model. Direction indicates a two-layer system, with surface winds offshore and a very sharp transition to westerlies at 250 m. However, wind speed shows definite structure, with a minimum at the interface. There is some indication of direction overshoot just above the interface, typical of nocturnal jet phenomena observed above stable ground-based inversions. In the outside region, the oblique flow angle makes any estimation of h , h_0 , or x very difficult. Any analysis of a complicated situation such as this will require help from a mesoscale model to adequately estimate the crucial parameters.

5. CONCLUSION

When synoptic scale weather advects arctic continental air offshore over the open sea, high surface fluxes of heat and water vapor act to create a moist convective internal boundary layer. Radiosonde and surface measurements of synoptic scale flow off the Malaspina Glacier, Alaska, exhibiting vertical profiles similar to those assumed for simple models of quasi-stationary, homogeneous, convective boundary layers; i.e., an unstable surface layer, near-constant mean values of wind, potential temperature, and humidity in the interior, and a sharp interfacial region at the inversion base. However, there are consistent anomalies; a humidity maximum in the "mixed layer" may be related to comparable scales of advection and vertical mixing times. Also, while the increase of temperature in the developing boundary layer agrees well with simple models, both height and humidity do not. In fact, measurements of these quantities do not show any apparent variation. While either lack of initial (coastline) profiles or sensor

resolution may be contributing factors, fundamental assumptions in the assumed model are most likely in doubt. The inversion base is probably not at ground level at the coast due to mechanical mixing. Also, the humidity profile is most likely not constant due to sublimation over the ice coupled with mechanical mixing.

A more complex situation occurs when a katabatic wind blows off the glacier under a near fully developed convective marine boundary blowing at an angle to it. Again, surface heat flux acts to warm the offshore flow. However, measurements do not indicate any mixed layer in this flow, but do indicate a strong vertical gradient of potential temperature gradually blending into the marine boundary layer above. It is difficult to explain such a stable profile above a near-8°C air-sea temperature difference. Possibly the mixed layer is less than 100 m and is capped by a deep entrainment layer. Such a speculation awaits more detailed measurements for confirmation. The humidity maximum occurs in the developed marine layer but is not apparent in the katabatic tongue. Though it is lower, about .4 h, which agrees with laboratory models, it is very distinct, which is unexpected. A cold air core at 1100 m suggests that strong horizontal density gradients, set up during air modification, can generate non-negligible secondary flows, even though they act over a mesoscale.

Future studies of this nature must concentrate on firmly establishing initial conditions, as well as improving vertical resolution. Most likely both a ship and an airplane working in cooperation are required to satisfy these needs.

ACKNOWLEDGMENTS

This work was funded by the Bureau of Land Management, Alaskan OCS program directed by the OCSEAP Office of NOAA, Research Unit 367. The crews of NOAA ships Oceanographer and Discoverer were courteous and helpful during the projects. Helpful comments by Prof. J. A. Businger and the Energy Transfer Group of the University of Washington are appreciated.

REFERENCES

- Bean, B. R., C. B. Emmanuel, R. O. Gilmer, and R. E. McGavin, 1975: Spatial and temporal variations of the turbulent fluxes of heat, momentum, and water vapor over Lake Ontario during IFYGL. NOAA Tech. Rept. ERL 313-WMPO 5, 57 pp.
- Budd, W. F., W. R. J. Dingle, and U. Radok, 1966: The Byrd snow drift project: outline and basic results. Studies in Antarctic Meteorology, Antarctic Res. Series 9, Am. Geophys. Union, 71-134.
- Carson, D. J., 1973: The development of a dry inversion-capped convectively unstable boundary layer. Quart. J. Roy. Meteorol. Soc., 99, 450-467.
- Deardorff, J. W., 1968: Dependence of air-sea transfer coefficients on bulk stability. J. Geophys. Res., 73, 2549-2557.
- Deardorff, J. W., G. E. Willis, and D. K. Lilly, 1969: Laboratory investigation of non-steady penetrative convection. J. Fluid Mech., 35, 7-31.
- Fleagle, R. G., and J. A. Businger, 1963: An Introduction to Atmospheric Physics, Academic Press, 346 pp.
- Kilday, G. D., 1970: Taku Winds at Juneau, Alaska. Office Memo., National Weather Service, NOAA, Juneau.
- Leahey, D. M., and J. P. Friend, 1971: A model for predicting the depth of the mixed layer over an urban heat island, with applications to New York City. J. Appl. Meteorol., 10, 1162-1173.
- Lenshow, D. H., 1973: Two examples of planetary boundary layer modification over the Great Lakes. J. Atmospheric Sci., 30, 568-581.
- Lenshow, D. H., 1974: The air mass transformation experiment (AMTEX); preliminary results from 1974 and plans for 1975. Bull. Am. Meteorol. Soc., 55, 1228-1235.
- Mahrt, L., 1976: Mixed layer moisture structure. Monthly Weather Rev., 104, 1403-1407.

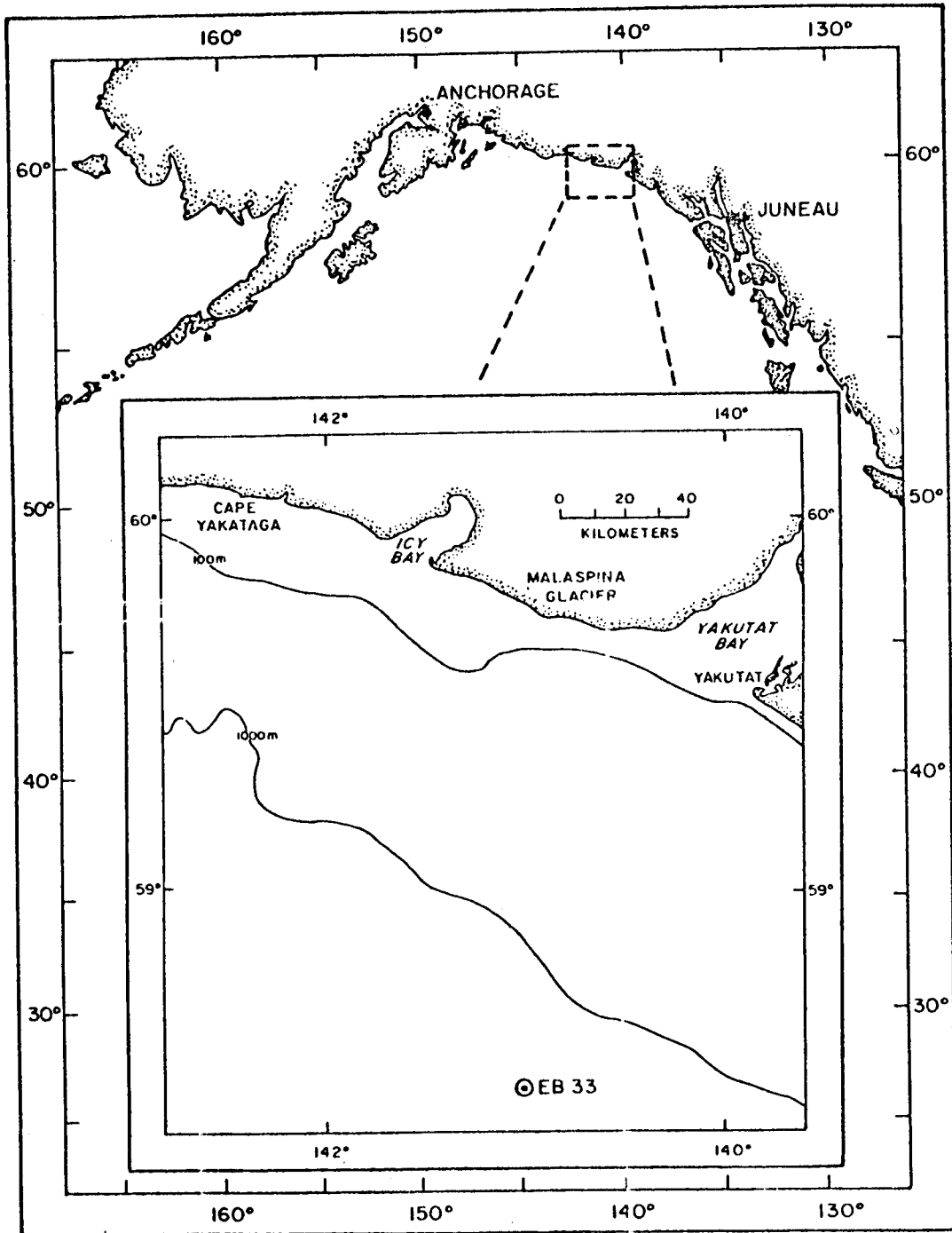
- Stull, R. B., 1975: Temperature Inversions Capping Atmospheric Boundary Layers. Ph.D. thesis, University of Washington, Seattle, 218 pp.
- Summers, P. W., 1965: An urban heat island model: its role in air pollution problems, with special applications to Montreal. Proc. First Canadian Conference Micrometeorology, Toronto, Atmos. Environ. Service.
- Tennekes, H., 1973: A model for the dynamics of the inversion above a convective boundary layer. J. Atmospheric Sci., 30, 558-567.
- Weller, G. E., 1969: A meridional surface wind speed profile in MacRobertson land antarctic. Pageoph, 77, 193-200.
- Willis, G. E., and J. W. Deardorff, 1976: A laboratory model of diffusion into the convective planetary boundary layer. Quart. J. Roy. Meteorol. Soc., 102, 427-447.

FIGURE CAPTIONS

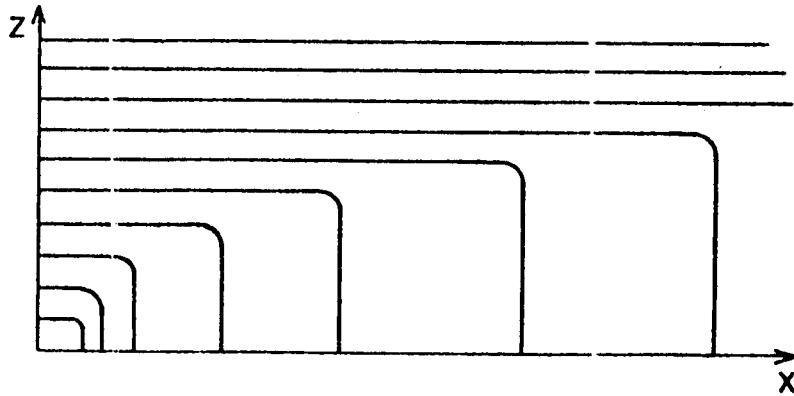
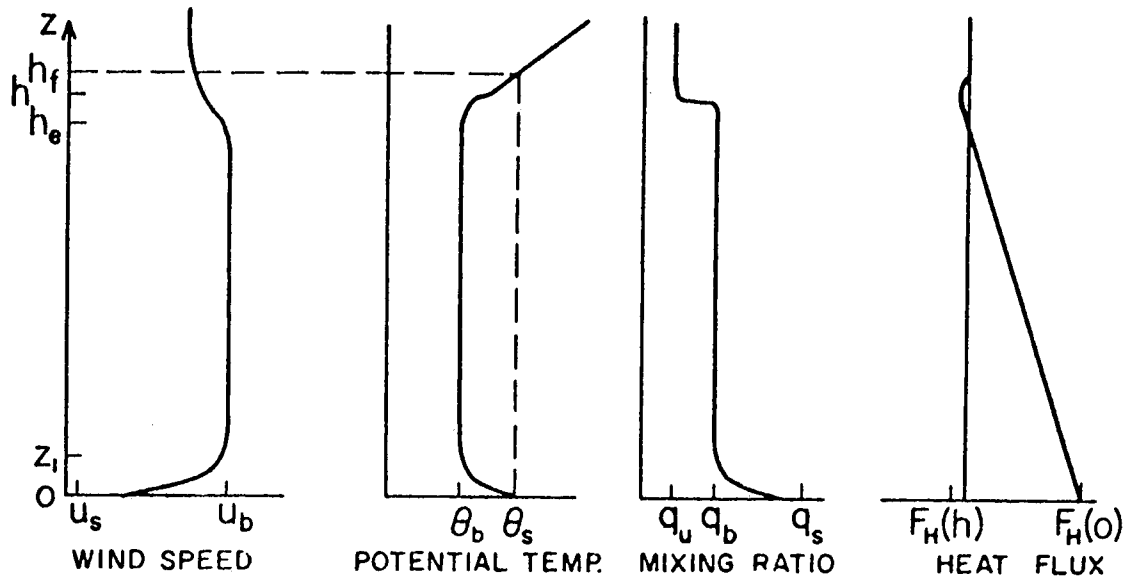
- Figure 1. Map showing site of measurements offshore from the Malaspina Glacier.
- Figure 2. Schematics of expected behavior of a developing boundary layer:
- Vertical profiles of wind speed, potential temperature, mixing ratio, and heat flux. The entrainment region, $h_e < z < h$, and the inversion strength, Δ , are assumed small.
 - Expected offshore potential temperature profiles of the boundary layer development.
- Figure 3. Surface observations of wind and temperature for 3 February 1975. Wind barb = 5 knots.
- Figure 4. Comparison of radiosonde ascent #8 with NWS ascent from Yakutat at same time.
- Figure 5. The interpretation of an ascent in terms of the simple air modification model.
- Figure 6. Comparison of calculated values of $\tilde{\theta}$, \tilde{q} , \tilde{h} , vs. predicted values. Note the close agreement of $\tilde{\theta}$, but lack of any distinct trend in \tilde{q} or \tilde{h} .
- Figure 7. Modification of mixing ratio humidity profiles offshore, February 1975.
- Figure 8. Surface observations for March 1976 study. Open circles indicate clear skies; wind barbs represent 10 mph; pressure, temperature, and dew point are shown in standard order.
- Figure 9. Weather map for Gulf of Alaska - 1200Z, 9 March 1976.
- Figure 10. Comparison of ascent 7B with NWS Yakutat sounding taken at the same time.
- Figure 11. Contour plot of potential temperature vs. distance offshore. Of note are the katabatic cold wedge and the cold core at 1100 m.

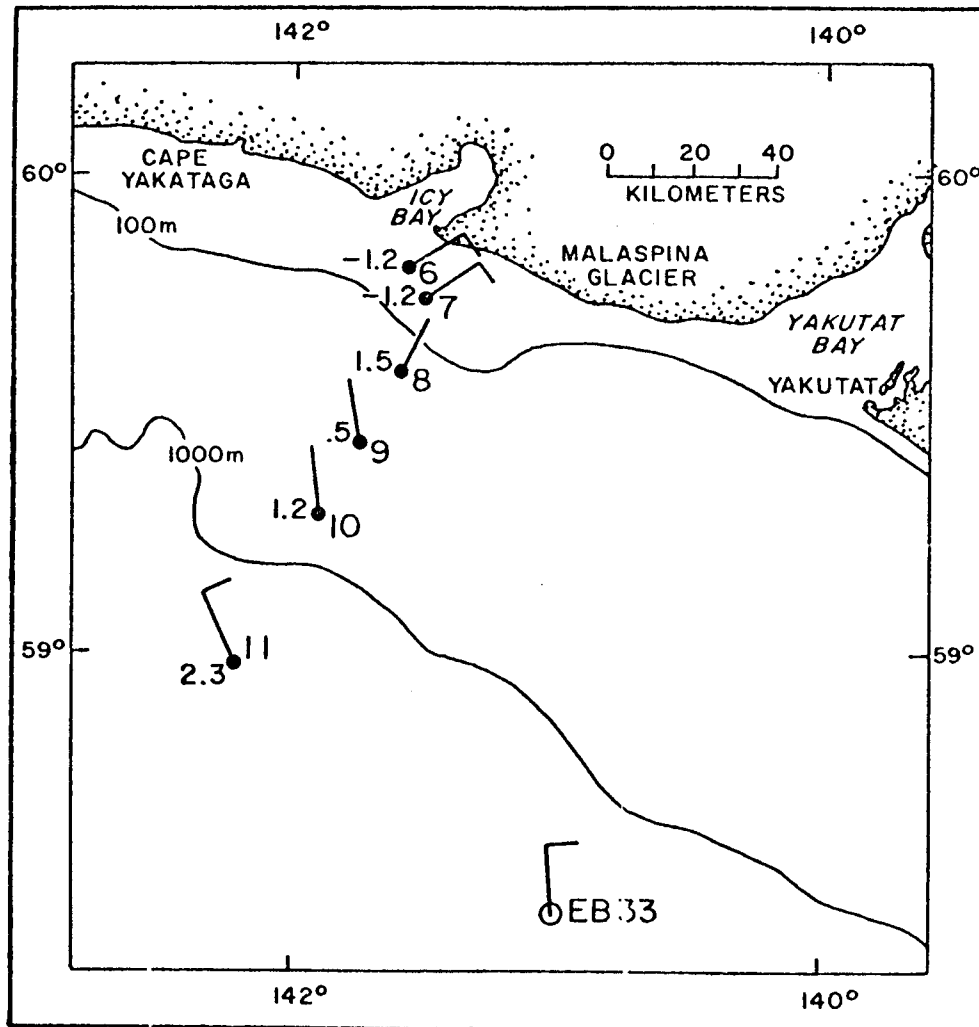
Figure 12. Contour plot of mixing ratio vs. distance offshore. A prevailing maximum slowly increases in height offshore.

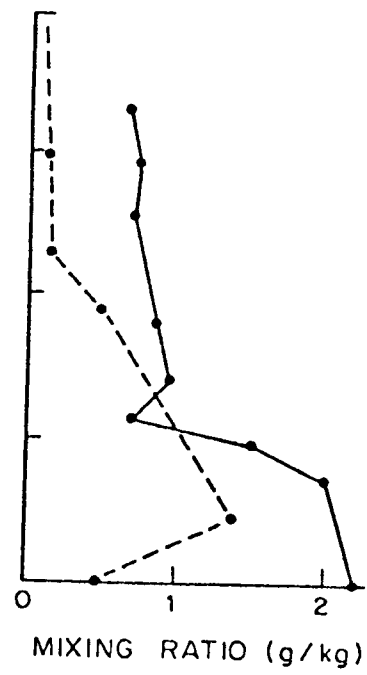
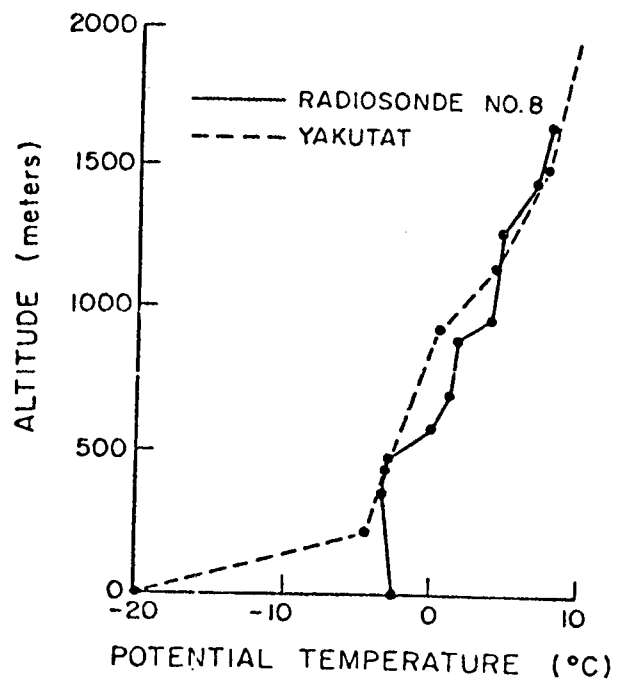
Figure 13. Profiles of temperature and winds from radiosonde (x), tethered BLP ascent (solid line), and descent (dotted line) taken at station 6B, about 5.5 km offshore. Adiabats (dashed line) indicate a statically stable lower layer, while wind direction indicates a sharp transition at 250 m. There is evidence of a mixed layer at 80 m.

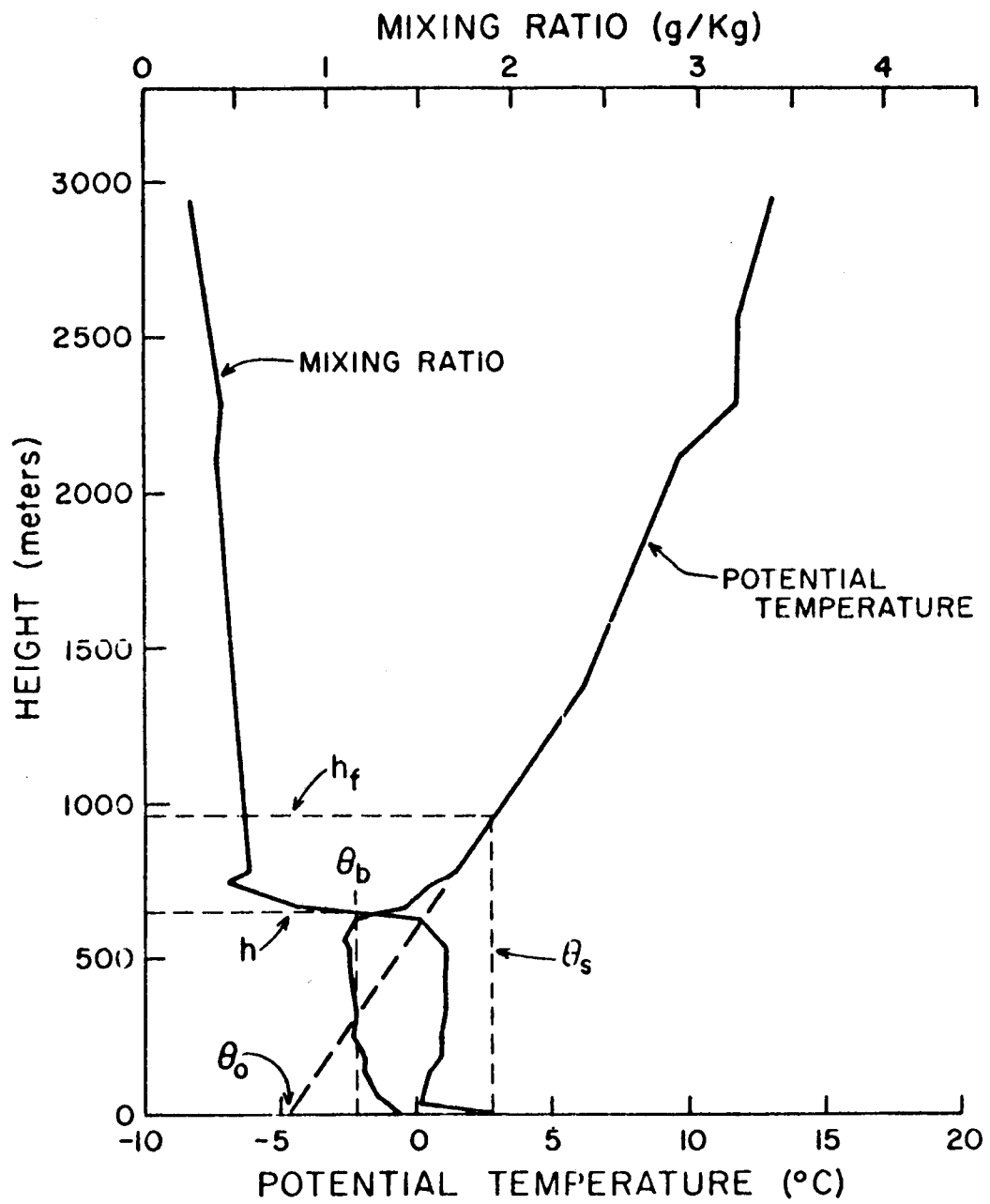


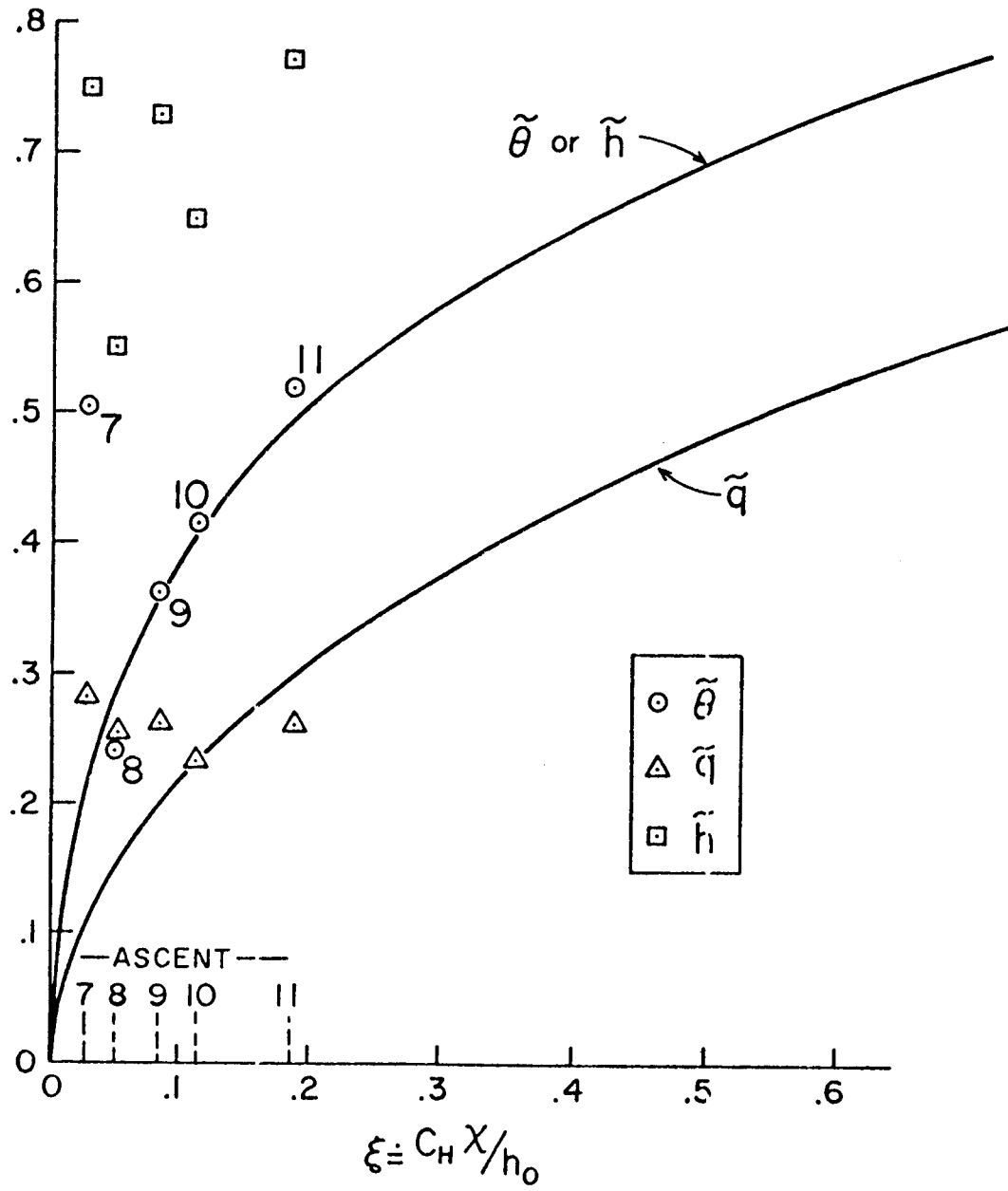
1

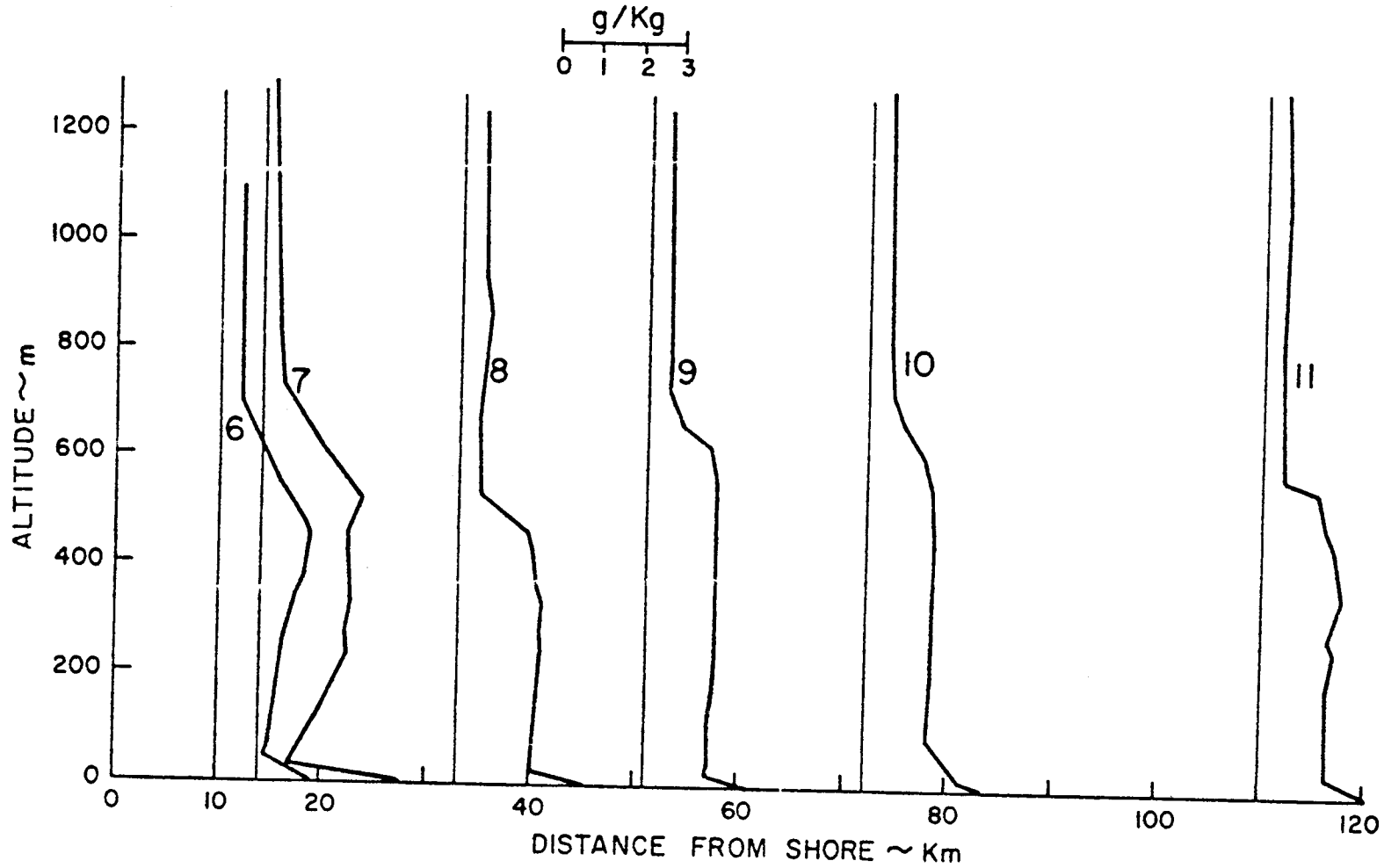


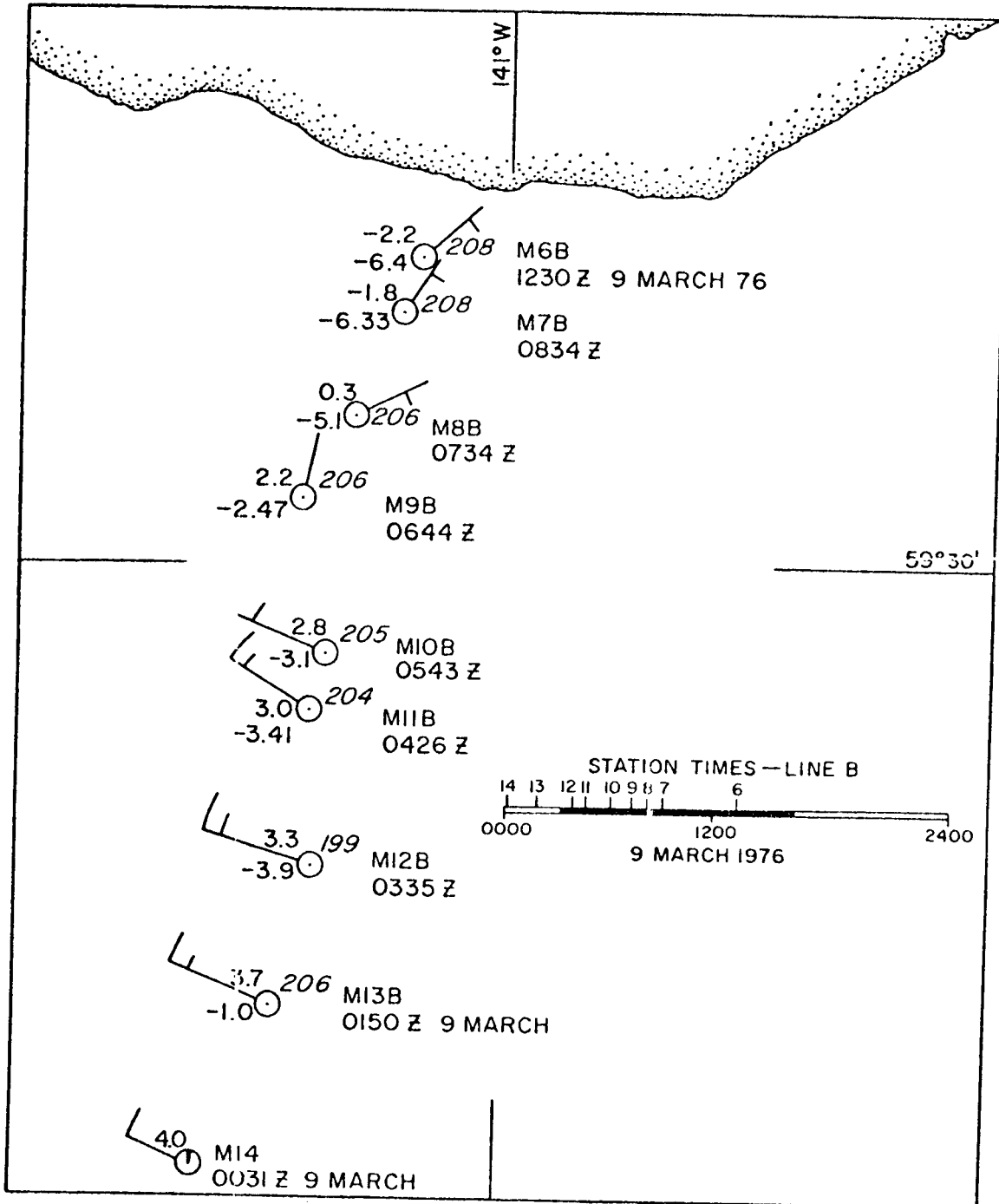


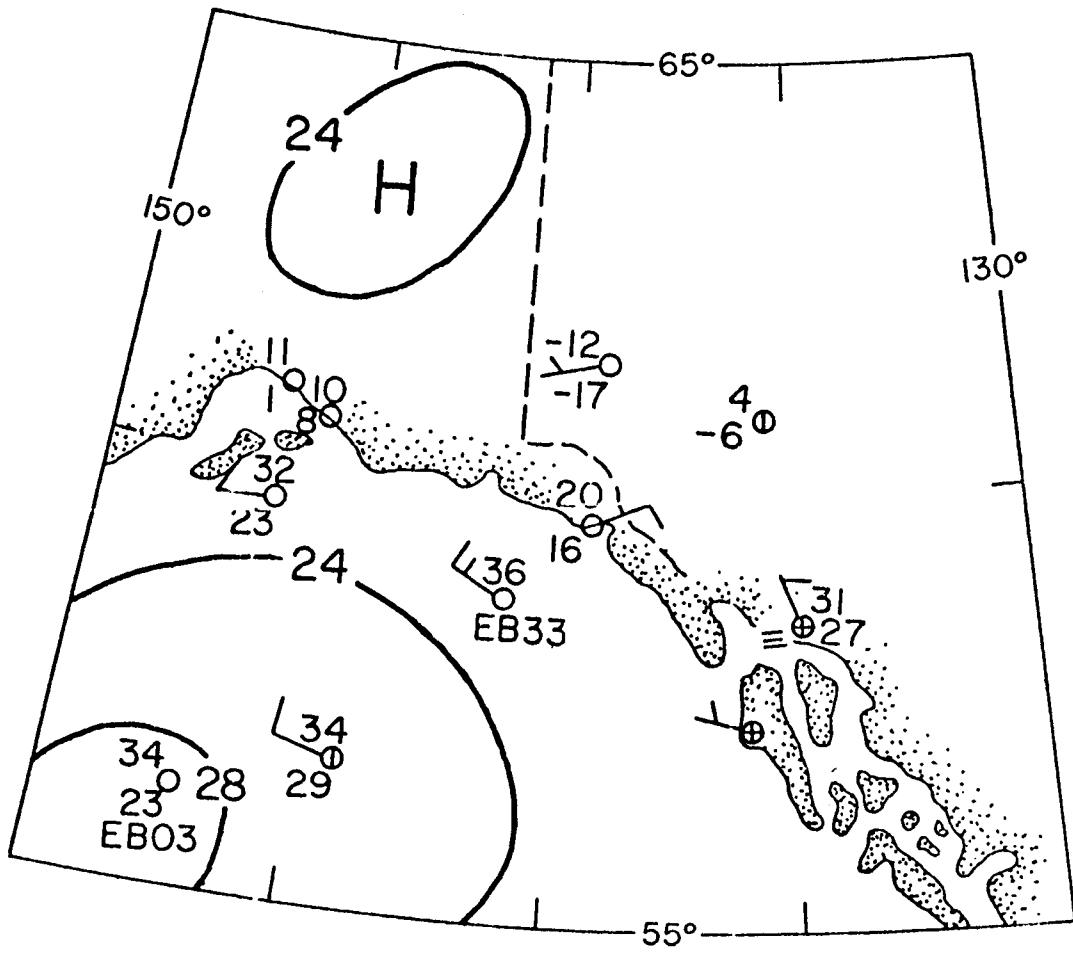


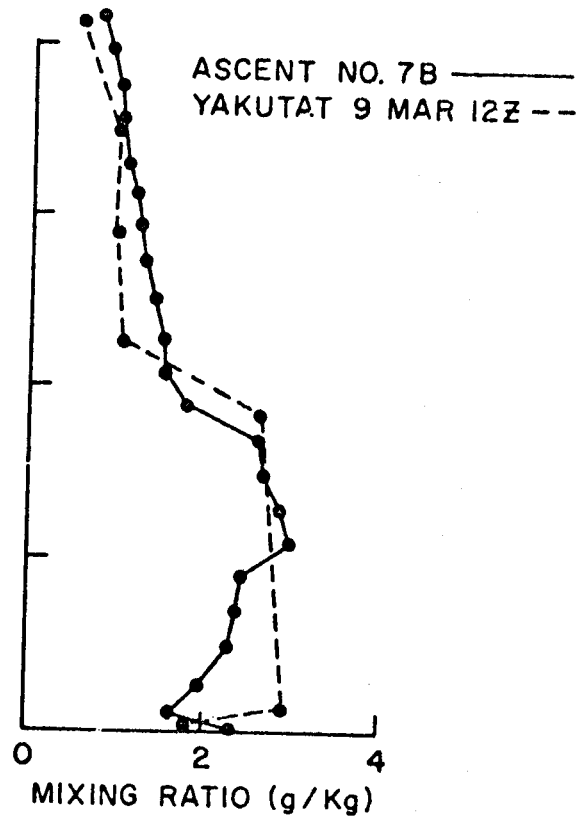
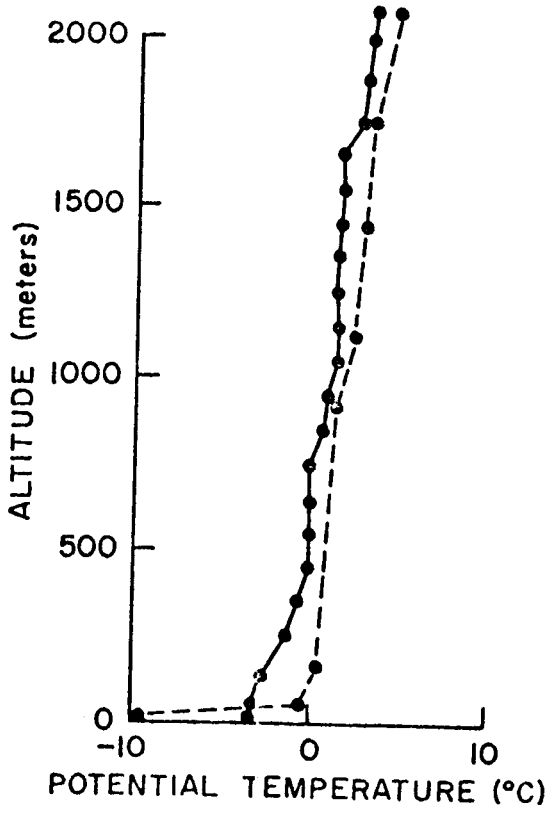


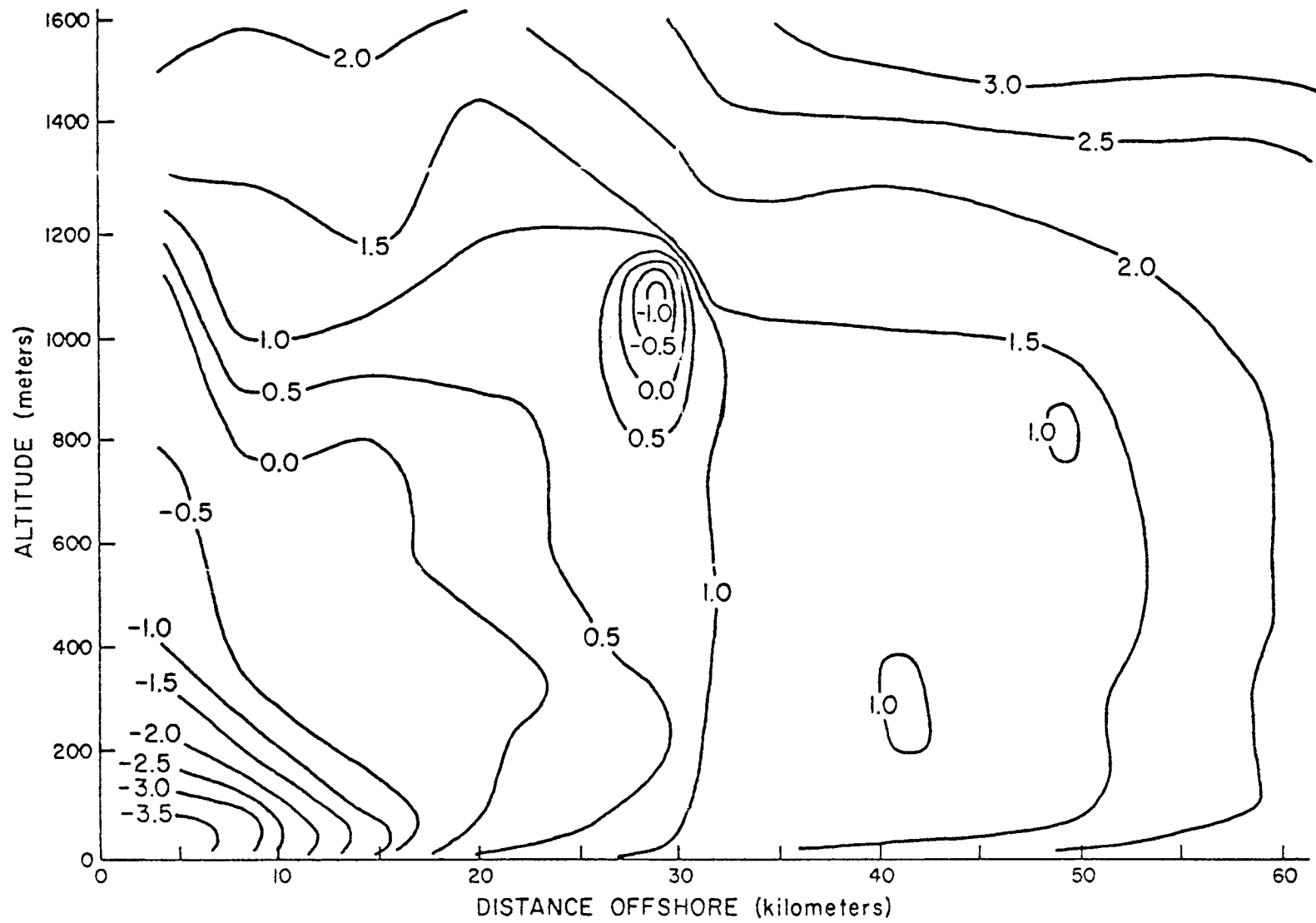


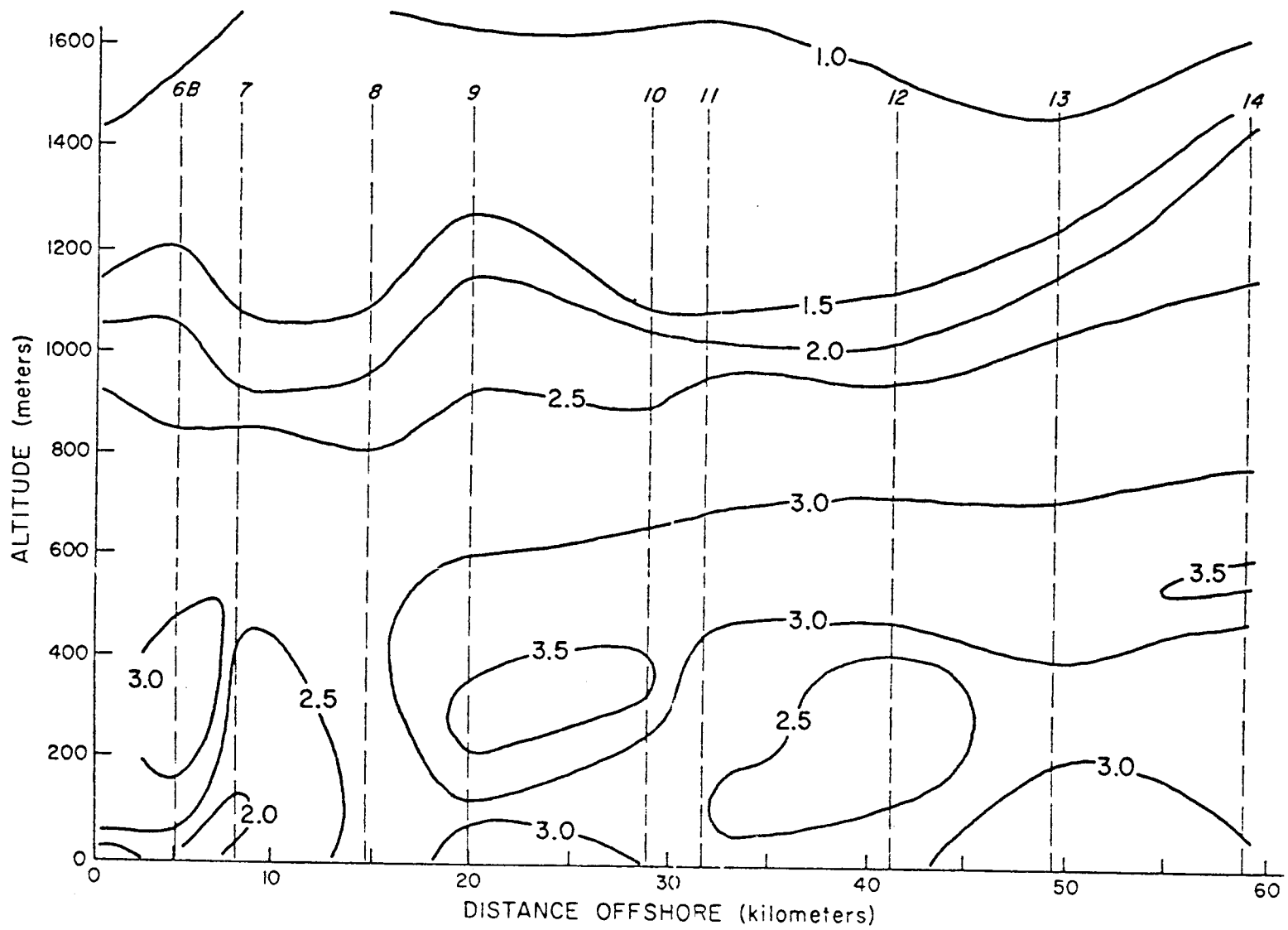




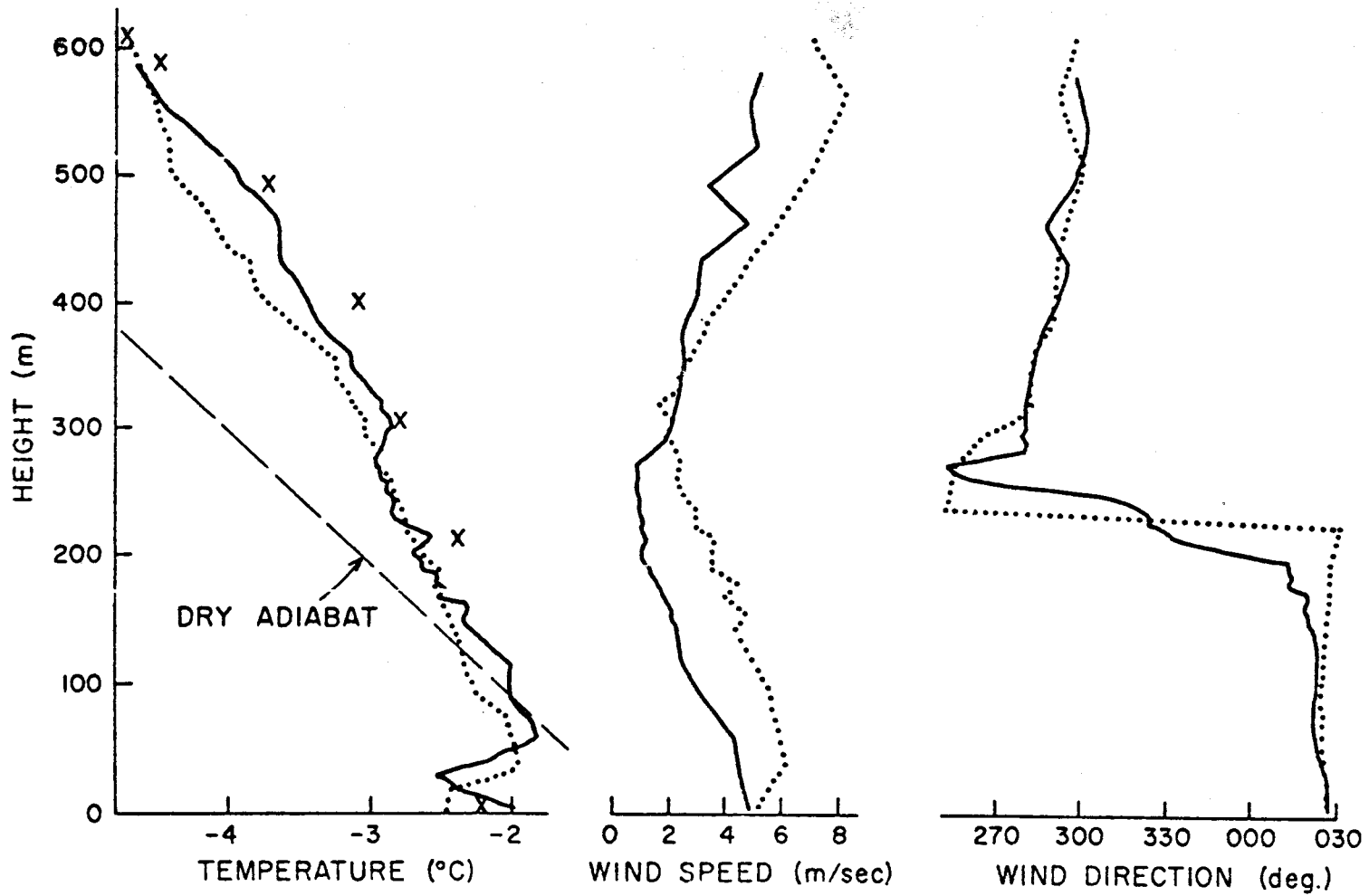








067



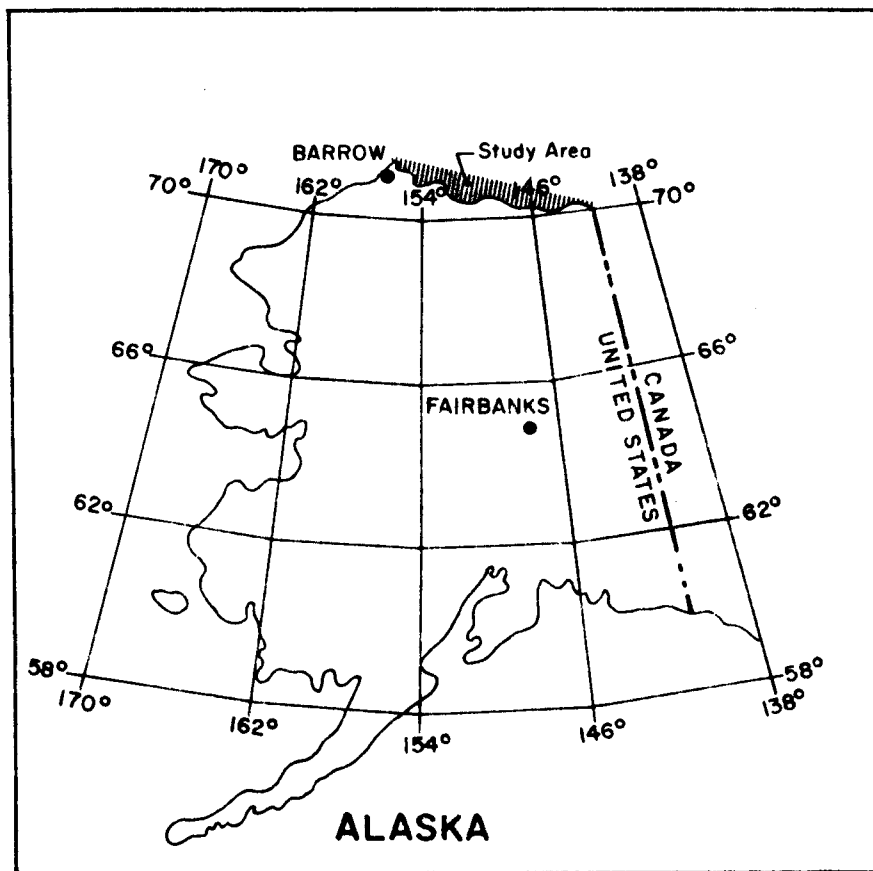
A30

FINAL REPORT

Contract no. 03-6-022-35126
Research unit no. 407

A STUDY OF BEAUFORT SEA COASTAL EROSION
NORTHERN ALASKA

Robert Lewellen
P.O. Box 2435
Littleton, Colorado 80161



I. INTRODUCTION AND SUMMARY OF OBJECTIVES, CONCLUSIONS AND IMPLICATIONS
WITH RESPECT TO OCS OIL AND GAS DEVELOPMENT

The objective is to study the Beaufort Sea coastal erosion from Point Barrow to the Canadian border. The coastal erosion and related processes are beginning to reach a critical focus as a result of the proposed industrial development of the Beaufort Sea shelf. Exploration and development activities will require a knowledge of the coastal erosion forms, processes, and rates. Adequate consideration must be given to the areas around the barrier islands, lagoons, and the mainland coast if industrial development is to proceed in an orderly manner.

All activities on the shelf must pass across the coastline. Large service and contracting companies will have to establish bases in order to provide service to the offshore activities. Transmission lines for oil, brines, electricity, etc. will cross the coastline.

Artificial islands and breakwaters for small service boats will have to be constructed. These features interact with the normal coastal erosion processes and rates.

The industrial activities will always interact with the processes operating along the barrier islands and shorelines. The geomorphic processes, forms, rates, and changes in the rates will have to be defined, and the information made available to the decision makers.

The eroding coastline is not only a source of sediments, but also supplies nutrients to the sea life. The erosion truncates natural oil seeps such as those in the Cape Simpson area. A seep, held in check by the tundra related ice-sealed permeability, does not have this check when

natural coastal erosion places the area beneath the sea. Erosion and sedimentation are important because hydrocarbons, toxic materials, etc. can be associated with the mineral and organic particles.

It is believed that the safe design of offshore oil facilities will require subsea permafrost information. Erosional and depositional rates and patterns provide inferences on the existence and original extent of offshore permafrost. Coastal erosion can lead to permafrost growth, frost heaving and differential pressures. Exploration activity will interact only in a small time frame with erosional and depositional processes and forms. Development activity will interact on a larger time period and (from a strict economic viewpoint) one should be well informed on the processes. Adequate design criteria and planning will be possible with specific site study. Inadequate understanding and ignorance of the erosional and depositional processes will result in over design and high maintenance costs.

Basically, the coastal erosion begins with the thawing of ice-rich soils, and saturated soil flow to the base of a low bluff. After the thawing of the protective winter-snow drifts, the wind-generated waves remove the soils which have been supplied to the base of the bluff. The eroding deposits are unconsolidated peats, clays, silts, sands, and gravels. In most cases the particles are bonded together by ice.

There are areas where the bluffs are a few meters in height and other areas where the tundra surface and the sea level are within a few decimeters of relief. Some segments of the shore are very sandy and well-drained; here the wave action and erosion resembles the mid-latitude cases except the sea is ice-free and waves are generated for only a few months each year. Meteorological tides are more important

in erosional processes than the astronomical tide.

Rapid erosion and depositional rates are geological hazards to proposed industrial activities. The author has measured coastal erosion rates of greater than 20 meters per thaw season. Ironically, the geomorphic form remains essentially the same from season to season; to the untrained observer the erosion appears nil since the form remains relatively constant. Rapid sedimentation and aggradation can trigger rapid permafrost aggradation, soil heave, and related phenomena.

The study determined that it is impossible: (1) to indicate where coastal morphology is likely to be changed by man's activity; (2) to indicate the relative erosional susceptibility of the different coastal geomorphic areas; and (3) to evaluate the effects of coastal morphology changes which are man induced. The variations encountered were complex and interrelated with other complex factors. No specific guides or formulas will satisfy the entire Beaufort Sea coast. However, the study did determine that specific sites can be studied adequately from the existing data bases for problem solutions or for determining what specific field work will be required.

II. METHODS

The study methods are standard mensurational techniques used on sequential aerial photography, the synthesis of published and unpublished data, and the analysis of bathymetric charts.

Thirty-two randomly selected scales for the 1948, 1949, and 1950 aerial photography produced a mean scale of 1/20,058 with a standard deviation range of 1/19,605 to 1/20,511. This is excellent when one realizes that it covers different papers, films, aircraft, flying conditions, crews, etc.

The dial caliper used for measurements is divided to 0.05 mm division. Measurement errors are believed to be less than 0.5 mm for any one measurement. Over a 24-year sequential photo base this would mean only 41 to 43 cm per year error for the standard deviation range given above.

Measurements of coastal erosion rates are displayed on the enclosed map which covers the entire study area. Erosion is relatively easy to determine by the comparison of sequential aerial photography. Measurements are made from the tops of the bluffs that are eroding. The scale is determined for the particular area and the amount of erosion computed. There are numerous features, mostly polygons, which permit easy identification of points on the sequential photographs. This is not true with spits and some of the barrier islands which are extending due to deposition, since there are no known points to measure from. The actual number of changes are overwhelming and it is essentially impossible to come up with a fixed rule or empirical formula which would cover this entire coastline. Each situation or site should be judged individually and studied individually.

Scale variations occur between aerial photographs. Topographic maps, marine charts, known ground surveys and larger scale maps have been used to compute the scales. The scale variations are relatively small. The radial displacement of images from their true map positions occurs with relief. The magnitude is proportional to the difference between the average ground elevation and the elevation of the feature and it is smallest in the center of the photograph. The relief of the coastal plain or local differences are very small and therefore limits the displacement. Measurement points were located (as near as possible) to the center of the photograph.

III. DISCUSSION

At any time during the thaw season, the pack ice can shove onto the shore and thus reduce or eliminate wave action. Thawing air temperatures and warm, surface waters will continue to melt the permafrost even though the sea ice may be onshore. Air temperatures will commence to thaw the frozen ground in June long before the decay of the shore fast ice.

The entire coast from Point Barrow to the Mackenzie River is characterized by the thermal erosion of permafrost during the annual thaw period. The shoreline recession and permafrost degradation is caused by wave action and thawing air temperatures. The first large winter storm in September will form strand lines of frazil and skim ice which are effective in eliminating wave action and halt thermo-erosional niching (Lewellen, 1970).

As the coastline erodes, drainage lines can develop landward along the polygon troughs. Warm surface waters are routed down to the polygon ice-wedge ice via a vertical tension crack. The ice-wedge is easily eroded by thawing and the tundra vegetative mat collapses into the void. This erosion is caused by the surface waters and the close proximity of the eroding shore bluff.

The wave heights are less than one meter 98 percent of the time during the thaw period. Tides and currents are almost nil, irregular, and unpredictable. The currents are wind generated. The winds are bimodal, easterly and westerly. The wind velocities are between 6 and 37 kilometers per hour 80 percent of the time. The air temperatures are between -1.1° and 3.9°C 73 percent of the time during the period July

through October. The sea water temperatures are between -0.6° and 1.1°C 57 percent of the time. Fog occurs about 37 percent of the time during the thaw period.

At Barter Island, ice break-up occurs the earliest in late July, the latest in early August, freeze up occurs earliest in mid-September and the latest in early October. Fast ice and drifted snow ramps form over the toe and bases of coastal sea bluffs and may persist into the thaw season, protecting the beach and lower slope from the waves and thawing. After Spring break-up the ice occurrence depends mostly on wind direction. Offshore winds tend to hold the ice offshore, whereas landward winds carry it in. Easterly and southerly winds tend to hold the main pack offshore and northerly and westerly winds force the ice in. Nearshore ice flows and ground ice can be present in the passes at all times and the pack is usually not far off.

East of Point Barrow the currents depend on local winds and may set in either direction along the coast. Changes in wind and barometric pressure may cause deviations from daily predicted water levels. Prolonged onshore winds and/or low barometric pressure tend to raise the water level. Offshore winds and/or high barometric pressure tend to lower it.

Erosion of the banks and the transportation of the sediments cannot occur until the drifted winter snow and ice cover has melted and disintegrated. The open water allows the wind to generate waves and currents. The mechanism of shoreline retreat and erosion include: (1) thawing of the bank sediments and saturated soil flow; (2) thermal undercutting of the frozen soils and collapse of soil blocks; and (3) transport by wave and currents. Fetch is effectively reduced by the presence of the sea ice. Long fetch distances or great areas of open water and high winds create

storm surges and the most violent activity along the coast. Runoff from the streams begins to flood the coastal ice usually late in May in the Prudhoe vicinity and mid to late June in the Barrow vicinity.

Wind generated waves depend upon the wind speed, fetch, duration, and sea state at the beginning. When the waves approach the shore obliquely they generate a long-shore current. It appears that beaches tend to orient themselves perpendicular to the dominant waves. However, wave refraction complicates the picture in many areas.

The mean annual land temperature at the surface may be -8°C and the mean annual sea bottom temperature outside of the barrier islands may be -1.5°C . As sedimentation aggrades, the lagoon floor up into the normal ice cover range and perhaps builds into a spit, the mean annual bottom temperature begins to return to the land temperature situation prior to truncation. Permafrost will aggrade and help to stabilize this ground. Thaw lakes and streams cause thermal anomalies which are also truncated and are buried by the coastal processes. Permafrost definitely exists under the marine areas where the ice cover freezes down to or into the bottom sediments. These areas are generally found where the mean sea level is three meters or less above the bottom. Areas deeper than three meters can grow ice as sediments aggrade on the bottom.

The rapidly receding (actively transgressing) shoreline has left permafrost below the sea which is not in balance with the present thermal regime. Lachenbruch (1957, p. 1524) suggests that along the coast, hundreds of meters (a few thousand feet) offshore, permafrost will extend only 60 to 90 meters (two or three hundred feet) below the sea bottom if the shore line has been stable. This shore line has not been stable; therefore, considerable permafrost is expected offshore.

Sellmann et al (1972, p. 61) report that between Barrow and Demarcation Point, 5.4% of the coastline is made up of drowned thaw lakes, embayed rivers, narrow streams or large V-shaped gullies. Seventy-nine percent of the coastline is less than four meters in height, 15% is between four and eight meters and 0.8% is greater than eight meters in height. The total length of the coast is approximately 1054 kilometers.

The beaches can consist of mud and organic matter. Massive amounts of floating organic debris have been witnessed in Elson Lagoon near Scott Point. The debris was from shore out to about two meter water depth and occupied the entire two meters of the water column. During a very strong east storm, this massive organic debris was totally effective in reducing the wave action to zero energy before it could reach the shoreline. Steep gravel beaches can be effective in protecting the bluff toes except in the worst storm conditions. The bluffs may retreat by ice wedge thaw and slumping. The surges first clear the toes and then, depending on the storm life, undercut the frozen bank. During the winter, snow drifts into ramps from the approximately one half meter accumulation on the sea ice to the top of the banks. The top of the banks are usually blown clear of snow.

The Gubik Formation consists of a number of erosional and depositional surfaces. The sediments are predominantly reworked marine. At one time, the province was similar to the present Chukchi and Beaufort Sea floors (Smith and Mertie, 1930).

The Arctic coastal plain is mantled by the Gubik Formation of Quaternary age (Black, 1964, p. 69). East of the Colville River, the Gubik is underlain by Tertiary rocks. The Tertiary is composed of non-marine conglomerates, sandstones and siltstones and overlies Cretaceous

rocks. West of the Colville River, the Gubik Formation directly overlies Cretaceous marine shales, mudstones, siltstones and sandstones. Some rivers have eroded through the Gubik Formation and down into the underlying Cretaceous rocks (Black, 1964, p. 89). The Gubik Formation contains peats, reworked peats, poorly sorted clays to cobbles, silts, gravels, marine well sorted sands (locally lacustrine and eolian) The surface of the Gubik Formation has been modified by lagoons, lakes, streams, and frost processes. Cliff or bank sediments, range from gravels to icy silts and clays. The barrier islands can be veneered with a thin layer of gravels or as is the case with Pingok Island, be covered with tundra. The coastline can be low banks, steep bluffs, or vertical faces which have been undercut or with narrow steep beaches. The barrier islands, deltas, low flat intersected lake basins, sandspits and bars also occur. Retreat occurs by undercutting and block collapse, gullying along polygon ice wedges, and/or thawing with saturated soil flow. Rapid coastal erosion usually leaves disequilibrium permafrost in the near-shore areas. Storms can cause a surge or elevation of sea level, rapid erosion and deposition. Many deltas have silt islands with elevations above high tide.

The Gubik Formation of Quaternary age is exposed along the shoreline from Barrow to Demarcation Point. Considerable amounts of ground ice usually occur in the upper few meters. The ice is in the form of ice lenses, vertical ice wedges and tabular ice masses. East of the Colville River the Gubik is underlain by the Sagavanirktok Formation of Tertiary age (see profiles). In the eastern part of the study area, at the Canning River profile, the Gubik is a small wedge of material deposited over the tertiary material. In the western part of the area, the Gubik Formation extensively buries the Cretaceous rocks.

East of the Colville River the soils and sediments of the area are related to the fluvial, glacio-fluvial, and glacial activity since the Tertiary. Earth material eroded from the present and past land areas have been deposited near the coast offshore. The materials include peat, woody debris and mineral particles ranging in size from clay to large boulders. The entire size range in rock types are present throughout the area both onshore and offshore. Stream, current and wave processes winnow, transport, and deposit the complete range of materials. The rock types include quartzites, phyllites, schists, argillites, conglomerates, shales, limestones, dolomites, sandstones and siltstones. The only cementing material to be found in the Quaternary deposits is essentially ice.

Rodeick (1975, p. 15) reports a distinct lithologic difference in the beach and barrier island gravels east and west of Prudhoe Bay. East of Prudhoe Bay, the gravels are light colored and except for the barrier island gravels, are quite angular. The light colored gravels occur at all depths east of Prudhoe and beyond the ten meter bathymetric contour west of Prudhoe Bay. The largest light gravel clasts are considerably larger than their chert gravel counterparts to the west. West of Prudhoe Bay, in water less than ten meters deep, the gravels are well rounded, dark colored, varicolored chert and sandstone with some coarsely crystalline quartz. The barrier islands show the distinction between the two gravel facies (p. 25). Rodeick (1975, p. 59) established that little or no material coarser than sand is presently carried by the major rivers to the shallow coastal marine environment.

Leffingwell (1919, p. 142) describes a formation which he names Flaxman of Pleistocene age. The Flaxman Formation is a deposit of foreign glacial

till, possibly containing glacial ice scattered along the Arctic coastline. The glacial till was misinterpreted by Leffingwell. The best exposure of this deposit is along the eroding shores of Flaxman Island. The material is composed of clay, sand, gravel and boulders. Leffingwell stated that the boulders are the most notable content of the material. They are very striking when concentrated along the beach under a retreating bank where they may be so abundant as to cover the ground or even to form piles of rock. Many of them have the characteristic outline of glacial boulders but others are angular and shattered by frost. The largest ones are at least three meters in diameter but most of them are less than 3/4 of a meter. Leffingwell described the occurrence of the Flaxman Formation boulders at Flaxman Island, Heald Point, Demarcation Point, Collinson Point, Konganevik, Brownlow Point, Bullen Point, Tigvariak Island, Foggy Island, Point Storkerson, Fawn Creek, Cottle Island, Bodfish Island, Leavitt Island and Oliktok Beach. Leffingwell saw no boulders in the sections examined between the Kuparuk River and Oliktok. He thought that boulders must be rare between Oliktok and Point Barrow. However, the author of this report has recorded numerous boulders between Kavearak Point and a few miles southwest of Oliktok. Also the author has found and recorded numerous boulders in the Elson Lagoon region near Point Barrow.

MacCarthy (1958) made a study of the glacial boulders along the Arctic coast. The boulders occur within and on top of marine sediments and in some cases fluvial material. Flaxman boulders can be found from Point Barrow to Demarcation Point. The heaviest concentration will be found from the Kuparuk Delta to Demarcation Point. There is a good possibility that the Flaxman Formation was not deposited far from the present coast. However, the boulders can be plucked from the shores in shallows by ice and rafted to other areas. The Flaxman Formation is probably the same age as the Gubik.

An island composed of Flaxman Formation material, called Boulder Island, appears on early maps and was mentioned by the explorers Franklin and Collinson. The island, similar to the present Flaxman, has been completely eroded away and only a shoal marks the former location (Leffingwell 1919, p. 70, 145). The island was probably six meters in elevation at the time of Franklin's visit in 1826 (p. 72). Today the shoal can be studied on the unpublished hydrographic survey sheet no. 7853. The shoal is frozen and if disturbed could result in saturated soil flow, subsidence, etc. This is a case of relic permafrost submerged by truncation. The features or ridges on the sea floor north of Cottle Island may be truncated island remnants or submerged barrier islands which are related to a stillstand. These features have probably been submerged for only five thousand years. The fine-grained surface materials contain large amounts of ground ice and peat. It is this surface layer of fines and ice that undergoes a range from complete to no truncation by eroding shorelines. Whether the complete veneer or high-ice content soils are eroded away is a function of tundra surface elevation above the level of the truncating sea; the ice content drops rapidly with depth below the tundra surface. For example, the super-saturated conditions occur within the first six to fifteen meters of depth below the tundra surface. If the tundra surface is near sea level during coastal erosion, only the top part of the zone may be eroded away. If the tundra surface is at an elevation of six meters, then there is a possibility that erosion will erode the ice problems away. Near-shore coastal subsidence and consolidation can occur where the sea passes over low elevation tundra. The lagoon or sea waters may seasonally thaw the floor to less than one meter. Near warmer stream discharge waters the thaw depth may increase, however sedimentation must be considered along with the fact that maximum discharge occurs early in the thaw season.

Leffingwell (1919, p. 170) reported that in 1837 Dease and Simpson stated that there was a passage inside of the tundra island which they named Cap Hallket. At present this passage is closed by a spit which runs out from the mainland. The islands west of Cape Hallket are now replaced by sandbars. Leffingwell also reports on evidence that some parts of the coastline have been stationary for centuries. On the sandspit running east from the north end of Barter Island there are Eskimo ruins which must be very old. The same is true of Arey Island. The woodwork of the houses is decayed, even under the ground so that there is simply a mound of gravel to mark the location of a former gravel-covered driftwood hut. There are huts with the framework still standing at Collinson Point, yet none of the living natives knew who formerly inhabited them. Collinson mentions passing several huts on a shinglepoint in 1854, probably those on Collinson Point. The age of the older huts near Barter Island must be many times that of those on Collinson Point. In addition to the evidence from the ancient houses there is evidence from the vegetation on the sandspits and islands.

Leffingwell (p. 171) reports that the rate of retreat of the shore probably varies with the nearness of the sea ice to the shore. The blocks that break off after being undercut may remain at the foot of the bank to protect it for several seasons. Consequently, observations must be carried over a period of several years to ascertain the rate of retreat at any place. During a single gale lasting two or three days, a tundra islet in the sandspit on the north side of Flaxman Island was cut entirely away. The dimensions of this islet were approximately fifty feet long, thirty feet wide and five feet high. The prospector Arey, dug an ice cellar in 1901 at Brownlow Point, east of Flaxman Island. It is reported to have been a

hundred yards from the beach. In the summer of 1907 the sea had cut the shore back so that this ice house was exposed in the bank.

Leffingwell (1919, p. 171) reported shoreline recession rates for selected sites between Elson Lagoon and Camden Bay. The four sites listed and the erosion rates are: (1) Cape Simpson and Point Drew, greater than 30 meters per year; and (2) Flaxman Island and Brownlow Point, nine meters per year.

During the open season of 1911, all the exposed parts of the coast were affected by the waves. During the next summer all the banks were lined with the blocks which had broken off. In 1914 some of these blocks were still in existence. An average retreat of ten feet for all of the cliffs on the north shore is estimated for the summer of 1911, but as scarcely any retreat occurred between 1911 and 1914, the average retreat must have been less than four feet.

Leffingwell's map of 1906-1914 shows that Mary Sachs Island was detached from Flaxman Island. A study of the later maps and aerial photography reveals that sedimentation has combined the two islands. In the shallow areas around Flaxman Island, the ice begins to decay during the first part of June. By late September, skim and frazil ice can form which helps to protect the shore from further wave action.

Flaxman Island is composed of silt-like clay, sand, gravel, boulders, organic muck, and ice. The boulders reach three meters in diameter; however, the majority are 0.6 meter or less in diameter. As the shoreline recedes, the finer particles are washed away thus concentrating the boulders along the beach. The eroded sediments from Flaxman Island are deposited to the west of the island by the wind-generated shore current.

Sir John Franklin, during his 1826 exploration of this vicinity, reported that Flaxman Island was 6.4 kilometers long, 3.2 kilometers wide, and 15 meters in elevation. When Leffingwell studied the area, Flaxman Island was not over 1.6 kilometers wide and nowhere was the elevation greater than 7.6 meters. Franklin reported difficulty with shoal water in the passage adjacent to the east end of Flaxman Island. Leffingwell reported water depths of 2.7 meters and about 5.5 meters within 15 meters of the beach (Leffingwell, 1919, p. 170). If the Flaxman Island shoreline has cut back 0.8 kilometers (one-half mile) between 1827 and 1919, a recession rate of nine meters (30 feet) per year is indicated (Leffingwell, 1919, p. 171).

Erosional processes similar to the coastal zone have been reported in the Colville delta by Walker and Arnborg (1963) and Walker and Morgan (1964). Detailed information on riverbank forms of the Colville delta appear in a paper by Ritchie and Walker (1974). Detailed studies in the Beaufort area have been carried out by Reimnitz, Barnes, and Short et al. In 1974 these were reported in a publication from the Arctic Institute in North America. The work by Ritchie and Walker reported in 1974 gives details about the Colville delta front. The delta front is composed principally of sandbars and mud flats. Rates of coastal erosion in the Oliktok area were determined, utilizing aerial photography from the 1949 BAR series and 1971 and 1972 photography taken by the author. This localized study area of the coastline was photographed in September, 1972, supplemented with color aerial photography taken in August, 1971. Sixty-two stations revealed an average rate of coastal retreat of 1.4 meters per year for a time span of twenty-two or twenty-three years. The rates ranged from relatively stable sand gravel beaches to 4.7 meters per year. The

maximum rate was measured on a very localized exposed section of lacustrine beds.

The topographic maps indicate a few areas along the southern shore of Simpson Lagoon as being near 7.6 meters in elevation. One such site was Oliktok Point, however, measurements of the bluff revealed the elevation to actually be about 2.5 to 4 meters in elevation. At Kavearak Point the elevations were 3 to 4.4 meters in elevation and not near the 7.6 meter elevation as indicated from the maps. The maps in general indicated elevations which are as much as four meters too great. A maximum elevation of four meters would characterize the Simpson Lagoon area. No shoreline bluff would be over four meters high and no section of soil would have greater than two meters of peat accumulated in the upper part of the section. Between Beechey Point and Oliktok, there is a total of about forty-one kilometers of estuaries, 16.6 kilometers of low ground lacustrine beds and 12.9 kilometers of high ground.

The soils in general below the upper peat sections are sandy and some gravelly sands. On 7 September, 1972, the sea level was abnormally low due to east winds just southwest of Oliktok. There was a twelve-meter strip of lagoon bottom exposed from the foot of the frozen bluff to the sea water level. At Kavearak Point on 9 September, the sea level was abnormally low due to east winds. As a result, forty meters of the lagoon floor were exposed from the toe of the bluff to the water line. In some cases thermo-erosional niches can form in one year, be filled with snow and ice during the late Fall and Winter, soils slump down on top of this refreeze and form a false bluff toe. Eroded pieces of tundra vegetative mat were generally within twenty meters of the high water mark. At an average shoreline rate of erosion of 1.4 meters per year, the pieces

of organic mat are less than fifteen years old. The pieces of the tundra mat are ice rafted, rolled along the bottom, etc. Of the total mat being eroded, less than five percent is estimated to result in clumps on the lagoon floor. The buried tundra vegetation which is below the recent surface mats and below the depth of seasonal thaw when eroded, is readily dispersed since it has been broken apart during accumulation by frost processes. Less than five percent of the top forty-five centimeters of tundra reaches the beaches as pieces which are relatively resistant to mechanical erosion. The pieces on the beach are buried by sedimentation, rafted by ice, moved by currents and waves are eventually eroded to smaller pieces which are easily transported across the lagoons and even out to the open sea. Actually only the top twenty centimeters or so of the tundra vegetation in this vicinity has a potential of forming clumps or pieces as the shoreline erodes.

Short et al (1974) reports that net longshore beach transport is towards the west and is about 10^4 cubic meters per year. Waves and currents generate offshore bars that occupy approximately forty percent of the coast. These bars are migrating westward at an average rate of about seventy meters per year. Their presence and migration have a pronounced effect on the beach and barrier island morphology. The barrier islands appear to be migrating westward at six to twenty-five meters per year. Wind generated waves and currents dominate the beaches and nearshore zones.

A paper by Short and Wiseman (1974) reports on a progression of freeze-up along the northern Alaskan coast and the introduction of ice and snow into the beach and nearshore zones. In another paper, Short and Wiseman (1974b) discuss a break-up along the Alaskan coast as being separated into three interrelated areas of influence--rivers, sea ice and beach. They

claim the river break-up introduces the bulk of annual sediment load into the coastal zone. The river flood and sediment dispersion is restricted to the elongated shallow lagoons. Most of the major rivers situated along the Beaufort coast empty into open embayments, spreading their sediment over a broad deltaic front. On the Beaufort, delayed break-up increases fluvial effectiveness. Duration of beach thaw is directly related to the amount of ice on or in the beach. The presence of ice in the beach will prolong thaw and upon melt, generate arctic beach forms including gravel pits, gravel piles pits, kettle holes, distorted bedding and depressions. In the absence of dunes, tundra melt water flows onto and across the beach building microfans at the beach tundra interface and micro deltas at the shoreline. Short and Wright (1974) report on lineaments and the coastal geomorphic patterns in arctic Alaska. These lineaments are seen in island offsetting and redirection of island growth along the spits and barrier islands of the Beaufort Sea.

In October, 1963, a storm surge of up to three to four meters breached the spit forming the northern boundary of Elson Lagoon. There has been since this time good evidence that the spit is healing from the lagoon side more than it is from the sea side.

In the Simpson area, the Gubik Formation mantles the entire region. It ranges in thickness from two to three meters to approximately thirty meters. The formation is made up of inter-bedded clay, silt, sand and gravel. The upper fifty feet of the Formation, commonly a soft clay which has scattered thin beds of silt and sand (Robinson, 1964, p. 652).

Barnes et al (1977) report that a comparison of the 1950 and 1970 coastlines shows erosional changes on the mainland coast along with a marked change in the configuration of Stump Island in the Prudhoe Bay

vicinity. The northeast facing coast east of Gwyder Bay has been eroded up to sixty meters. The most pronounced erosion occurs at Point MacIntyre. Rates of erosion calculated for the twenty year interval range up to more than three meters per year but average about one meter per year. Within Gwyder Bay, erosion has been restricted to the coastal promontory west of Point MacIntyre. On this point, maximum coastal retreat of fifty meters was measured. The coastal retreat reflects the pattern of dominant wind and waves. On the exposed coast east of Point MacIntyre erosion is noted all along the coast while within the protected environment of Gwyder Bay, only the coast promontory exposed to the considerable fetch of westerly waves has marked erosion. It is interesting to note erosion even in the region of coast somewhat protected by the Gull Island shoal.

The factors affecting differential retreat are the ice cover duration which generally is from sixty to ninety days of open water, the water depth, spit protection and barrier island proximity, longshore currents, ice content of the ground and grain-size of the formation being eroded. In a few sections of the Lonely vicinity storms have deposited wide bands of sand up on top of the bluffs and back on the tundra surfaces. In one vicinity near Oliktok, exposed lacustrine beds yield a bank two meters high of solid peat. In the Elson Lagoon area, Cooper Island has developed extensive westward extensions. In the Simpson Lagoon area near Oliktok, strong easterly winds of long duration can evacuate the lagoon well enough to expose large sand flats out into the lagoon floor. Near shore these flats are scattered with blocks and pieces of thin organic tundra mat. The barrier islands may show effects of ice shove, be pock marked with pot holes due to blocks of ice melting which were stranded the previous winter, or covered with driftwood.

In the vicinity of Barrow, Alaska, the tundra covered mainland of the Arctic coastal plain is bounded on the northeast by Elson Lagoon, which is eroding in a westward direction. The upper several meters of perennially frozen ground consists of fine-grained and ice-cemented sediment, large quantities of buried peat and massive ice wedges. The shoreline is composed of predominantly ephemeral beaches and bluffs which do not exceed seven meters in height. These are dissected by ice wedge troughs and several small estuaries. Mechanisms of erosion include undercutting the formation of thermo-erosional niches and collapse, slumping and saturated flow of thawed soil and exposed sediment. Rates of erosion have been determined along seventy-five kilometers of coastline based upon aerial photography compiled over the past twenty years. Locally the shoreline is retreating differentially as a function of cliff exposure, sediment composition, currents and depth of offshore water.

The bluffs along Elson Lagoon range from less than a meter in height to over ten meters. The sediments are predominantly sandy silt with considerable quantities of organic matter involuted in the upper several meters of high ice sediment. Ice wedges are exposed throughout the cliff exposures. Beaches along the lagoon are ephemeral with tidal fluctuations of about forty centimeters. Water depths are shallow with nearshore depths less than two meters. A shallow underwater bar extends northward from Tekegakrok Point. The lagoon is ice free for approximately two to three months. However, nearshore ice is present during early summer and builds up again with the initial freezing in the fall. Erosion occurs prior to seasonal freeze-up of the cliff exposures in early September. Waves reach less than a meter in height except possibly where the lagoon is open to the sea along the Plover Islands. The bar extending north of Tekegakrok Point dampens wave action on the western lagoon shore near Brant Point.

Two hundred and eighty-five observations from Barrow to Demarcation Point on the maximum bank elevations reveal a mean of six meters with a standard deviation of three meters. The coastline is relatively stable in areas where river deltas form flats out to the barrier islands. Smith Bay is generally an area of deposition except for the northwest shore where erosion is rapid. The six meter bathymetric contour follows the general trend of the coast. Two hundred to four hundred meters offshore of Pingok, Bodfish and Cottle Islands there is a shoal ridge which lies within one to four meters of the sea surface. On the west side of Kavearak Point, where the bluff was two to three meters in height, pieces of storm-eroded tundra vegetative mat were found eighteen to thirty meters back on the tundra surface.

At Oliktok longshore currents were observed to reach seventy-six centimeters per second and sediment transport rates were up to thirty-eight cubic meters per day. Dygas reports significant erosion on the east end of Pingok Island and two small unnamed islands to the east of Pingok and significant accretion to the northwest end of Thetis Island. Dygas also reports eleven meters of shoreline erosion at the tip of Oliktok Point in just two week's time.

Coastline recession by thermal erosion has been reported from Point Barrow, Alaska, to the Mackenzie River, Canada. MacCarthy (1953) studied the shore line changes near Barrow. He reported on the process and rates of erosion near the U. S. Coast and Geodetic triangulation stations.

In 1964, Hume and Schalk reported quantitatively on the Barrow shoreline recession as a result of man's activity. They cautioned that large amounts of borrow relative to the net shoreline sediment transport will result in shoreline erosion.

Hume and Schalk (1964a, p. 9) report on studies conducted in the Point Barrow vicinity. Ice in the shallow water environments can stop the entire process of erosion, transportation and deposition. Break-up at Barrow occurs as early as 15 June or as late as 22 August and averages between 17 and 23 July, based on twenty-four observations. Freeze-up occurs between 2 September and 19 December with an average time of 1 to 5 October. The lagoons usually open up earlier than the open sea. Sediments move by ice push and by ice rafting but major amounts move by waves and long-shore currents. Hume and Schalk (1964a) report on the erosion and changes from Point Barrow to Eluitkak Pass. Some changes are illustrated in figures attached. Storm surges have reached four meters in the Barrow area. In the Arctic, total physical transport of the sediments is far less than in temperate regions (Hume and Schalk, 1964b). Their study indicates if borrow is large compared to the net transport volumes, then any beach borrow plan should be viewed with caution. Material removed from above normal high water would have to be replaced by high storm tides, if at all. Storm tides could be erosional and not depositional in nature.

On the barrier islands, sections of the coastline open to the sea, and even on a smaller scale inside lagoons, the ice can shove onto the beaches and shores. This action usually picks up beach material and moves it inland where the load is deposited. The ice push mounds and ridges may or may not be ice cored. Hume and Schalk (1964) and Leffingwell (1919, plate 25b) are just two examples of numerous reports on ice push effects. The ice shove or pushing adds material for the island or back beach. Hume and Schalk (1964, p. 273) believed the deposits are temporary and are destroyed by storm waves. Hume and Schalk estimate that no more than 5 percent of the coast is attacked, however, certain areas are subject to intense ice action.

Cooper Island receives ice push deposits almost every year. It is doubtful that the ice shove deposits amount to more than ten percent of the deposits above sea level (p. 273). At some locations, Katchiksuk Bluffs and Olukralik Point, being two examples, there are very high rates of retreat immediately adjacent to essentially stable segments. At Olukralik, at two stations, approximately three hundred to four hundred meters apart, the erosion varies from essentially stable to ten meters per year of coastal retreat.

In the Elson Lagoon area, Doctor Island has been completely eroded away. Deadman Island represents its 1945 form in very general aspects only. Southeast of Deadman Island, along the Tapkaluk islands, the lagoon-side shoal lobes appear to be stable, while the seaward sides shift considerably and also change in vertical extent. The shoal lobes extending out into the lagoon appear to be relatively stable and part of this stabilization can be attributed to permafrost. East of the Colville River, Pingok Island, on the seaside, is relatively stable in some sections, yet there is considerable erosion on the protected lagoon side.

Mackay (1963) discussed the erosion of the Pleistocene silts, sands, gravels, and ice between Herschel Island and the Mackenzie River delta. Coastal bluffs up to 50 meters high are receding by wave action and the melting of tabular masses of ground ice. The Mackay report indicates how historical records document the coastal recession. He reports the greatest rates of retreat occur in the low bluffs of high-ice content, fine-grained sediments. The recession rates may exceed one meter per year. The lowest rates were observed in sand and gravel bluffs.

Between Point Barrow and Demarcation there are a series of lagoons, bays, and coves which illustrate the ice-rich erosional base before greater energy of the open sea is applied. Of the twenty-four water bodies sampled, the mean maximum depth was only 3.14 meters with a standard deviation of 0.79 meters.

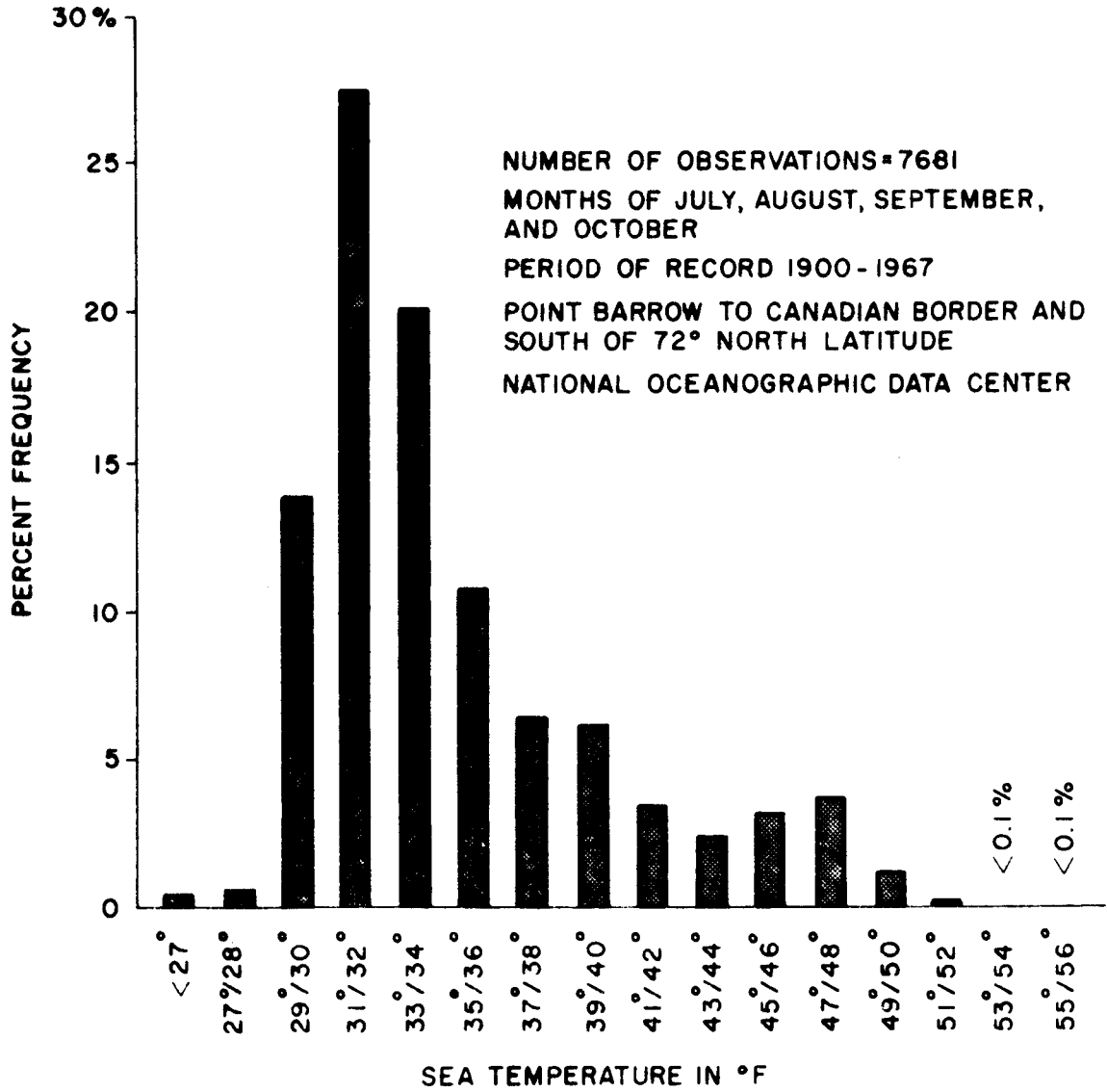
BIBLIOGRAPHY

- Black, R. F., 1964, Gubik Formation of Quaternary age in northern Alaska: U.S. Geol. Survey Prof. Paper 302-C, p. 59-91.
- Barnes, P. W., and E. Reimnitz, 1974, Sedimentary processes on Arctic shelves off the northern coast of Alaska: The Coast and Shelf of the Beaufort Sea, Reed and Sater eds., The Arctic Institute of North America, Arlington, VA, p. 439-476.
- Barnes, P., E. Reimnitz, G. Smith, and J. Melchior, 1977, Bathymetric and shoreline changes northwestern Prudhoe Bay, Alaska: U. S. Geol. Survey Open File Rept. 77-161, Menlo Park, Calif.
- Dygas, J. A., R. Tucker, and D. C. Barrell, (no date), Geological report of mineral resources, sediment transport and coastal erosion of the barrier islands and coast between Oliktok Point and Beechey Point (no additional reference data given).
- Hume, J. D., and Schalk, M., 1964a, Nearshore environment, processes and sedimentation, Barrow, Alaska: Arctic Inst. of North America, final rept., 20 p.
- Hume, J.D., and Schalk, M., 1964b, The effects of beach borrow in the Arctic: Shore and Beach, April.
- Hume, J. D., and Schalk, M., 1964c, The effects of ice-push on Arctic beaches: Amer. Jour. of Science, v. 262, Feb. , p. 267-273.
- Hume, J. D., and Schalk, M., 1967, Shoreline processes near Barrow, Alaska; a comparison of the normal and the catastrophic: Arctic, v. 20, no. 2, p. 86-103.
- Hume, J. D., M. Schalk, and P. W. Hume, 1972, Short-term climate changes and coastal erosion, Barrow, Alaska: Arctic, v. 25, no. 4, p. 272-278.
- Leffingwell, E. deK., 1908, Flaxman Island, a glacial remnant: Jour. Geology, v. 16, no. 1, p. 56-64.
- Leffingwell, E. deK., 1915, Ground-ice wedges the dominant form of ground-ice on the north coast of Alaska: Jour. Geology, v. 23, no. 7, p. 635-654.
- Leffingwell, E. deK., 1919, The Canning River region, northern Alaska: U.S. Geol. Survey Prof. Paper 109, 251 p.
- Lewellen, R. I., 1965, Characteristics and rates of thermal erosion, Barrow, Alaska: MA thesis, Univ. of Denver, 181 p.
- Lewellen, R. I., 1970, Permafrost erosion along the Beaufort Sea Coast: pub. by the author, (P.O. Box 2435, Littleton, Colorado 80161), 25 p.

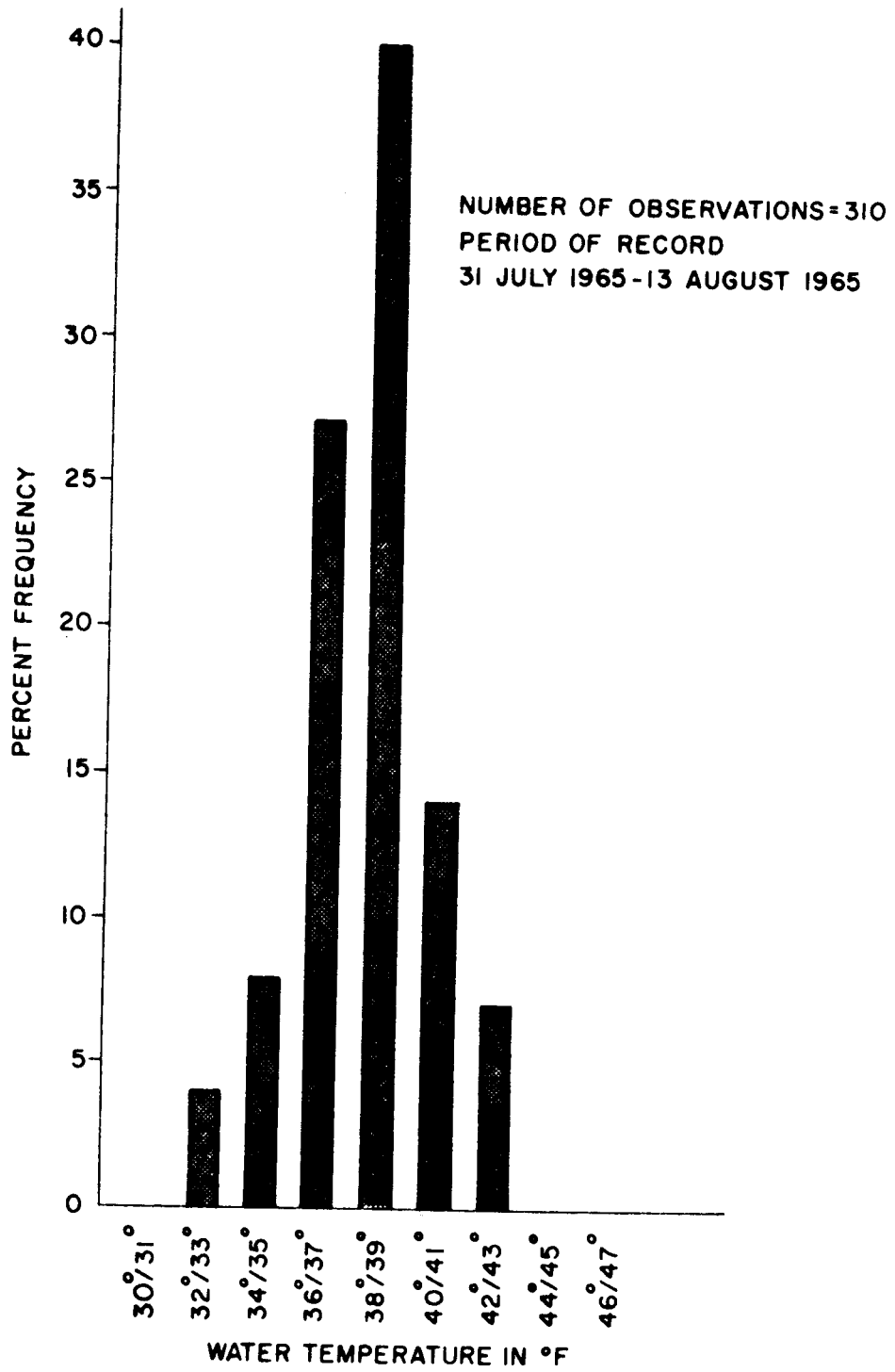
- Lewellen, R. I., 1974, Offshore permafrost of the Beaufort Sea, Alaska: The Coast and Shelf of the Beaufort Sea, Reed and Sater eds., The Arctic Inst. of North America, Arlington, VA, p. 417-426.
- Lewis, C. P., and D. L. Forbes, 1975, Coastal sedimentary processes and sediments, southern Canadian Beaufort Sea: Beaufort Sea Project Tech. Rept. no. 24, Victoria, B.C. 68 p.
- MacCarthy, G. R., 1953, Recent changes in the shoreline near Point Barrow, Alaska: Arctic, v. 6, no. 1, p. 44-51.
- MacCarthy, G. R., 1958, Glacial boulders on the Arctic coast of Alaska: Arctic, v. 11, no. 2, p. 70-85.
- Mackay, J. R., 1963, Notes on the shoreline recession along the coast of the Yukon Territory: Arctic, v. 16, no. 3, p. 195-197.
- Reimnitz, E., and K. F. Bruder, 1972, River discharge into an ice-covered ocean and related sediment dispersal, Beaufort Sea, Coast of Alaska: Geol. Soc. Amer. Bull., vol. 83, p. 861-866.
- Reimnitz, E., P. Barnes, T. Forgatsch, and C. Rodeick, 1972, Influence of grounding ice on the Arctic shelf of Alaska: Marine Geology, vol. 13, p. 323-334.
- Reimnitz, E., and P. W. Barnes, 1974, Sea ice as a geologic agent on the Beaufort Sea shelf of Alaska: The Coast and Shelf of the Beaufort Sea, Reed and Sater, eds., The Arctic Institute of North America, Arlington, VA, p.301-353.
- Ritchie, W., and H. J. Walker, 1974, Riverbank forms of the Colville River delta: The Coast and Shelf of the Beaufort Sea, Reed and Sater, eds., The Arctic Institute of North America, Arlington, VA, p. 545-562.
- Robinson, F. M., 1964, Core tests Simpson area, Alaska: U. S. Geol. Sur. Prof. Paper 305-L, Washington, p. 652.
- Rodeick, C. A., 1975, The origin, distribution and depositional history gravel deposits on the Beaufort Sea Continental shelf, Alaska: unpubl. Master of Science thesis, San Jose State Univ.
- Schalk, M., 1963, Study of near-shore bottom profiles east and southwest of Point Barrow, Alaska, Comparison of profiles and the barrier islands in the Point Lay and Plover Islands area: final rept. subcontracts ONR-217 and 241, Arctic Inst. of North America, 16 p.
- Sellmann, P.V., K. L. Carey, C. Keeler, and A. D. Hartwell, 1972, Terrain and coastal conditions on the Arctic Alaskan Coastal Plain: U. S. Army C.R.R.E.L. Spec. Rept. no. 165, Hanover, N.H., 72 p.
- Short, A. D., J. M. Coleman, and L. D. Wright, 1974, Beach dynamics and nearshore morphology of the Beaufort Sea Coast, Alaska: The Coast and Shelf of the Beaufort Sea, Reed and Sater, eds., The Arctic Institute of North America, Arlington, VA, p. 477-488.
- Short, A. D., and W. J. Wiseman, Jr., 1974a, Freezeup processes on Arctic beaches: Arctic, vol. 27, no. 3, p. 215-224.

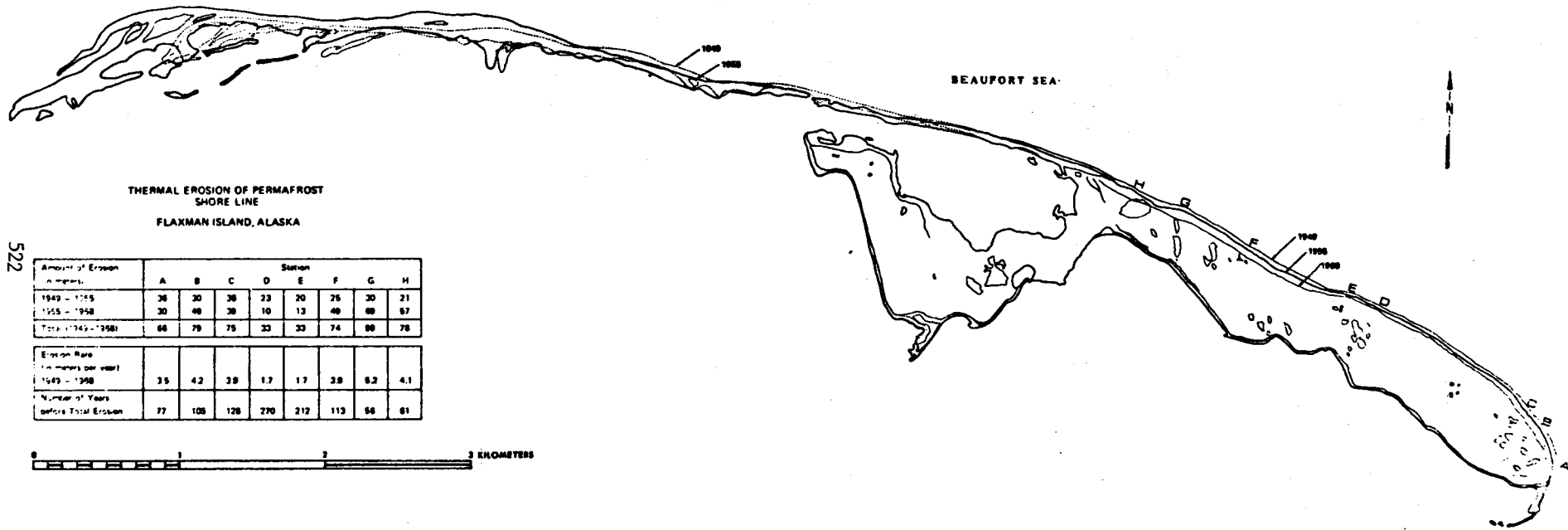
- Short, A. D., and W. J. Wiseman, Jr., 1974b, Coastal breakup in the Alaskan Arctic: Geol. Soc. Amer. Bull. vol. 86, p. 199-202.
- Short, A. D., and L. D. Wright, 1974, Lineaments and coastal geomorphic patterns in the Alaskan Arctic: Geol. Soc. Amer. Bull. vol. 85, p. 934-936.
- Smith, P. S., and Mertie, J. B., Jr., 1930, Geology and mineral resources of northwestern Alaska: U. S. Geol. Survey Bull. 815, 351 p.
- Walker, H. J., and Arnborg, L., 1963, Permafrost and ice-wedge effect on riverbank erosion, in Proc. Intern. Permafrost Conf., Natl. Acad. Sci. - Natl. Research Council pub. no. 1287, p. 164-171.
- Walker, H. J., and Morgan, H. M., 1964, Unusual weather and river bank erosion in the delta of the Colville River, Alaska: Arctic, v. 17, no. 1, p. 41-48.
- Wiseman, W. J., Jr., J. M. Coleman, A., Gregory, S. A. HSU, A. D. Short, J. N. Suhayda, C. D. Walters, Jr., and L. D. Wright: Alaskan Arctic coastal processes and morphology: Coastal Studies Institute, Louisiana State Univer., Baton Rouge, 171 p.

SURFACE SEA WATER TEMPERATURE BEAUFORT SEA



ELSON LAGOON WATER TEMPERATURE





THERMAL EROSION OF PERMAFROST
SHORE LINE
FLAXMAN ISLAND, ALASKA

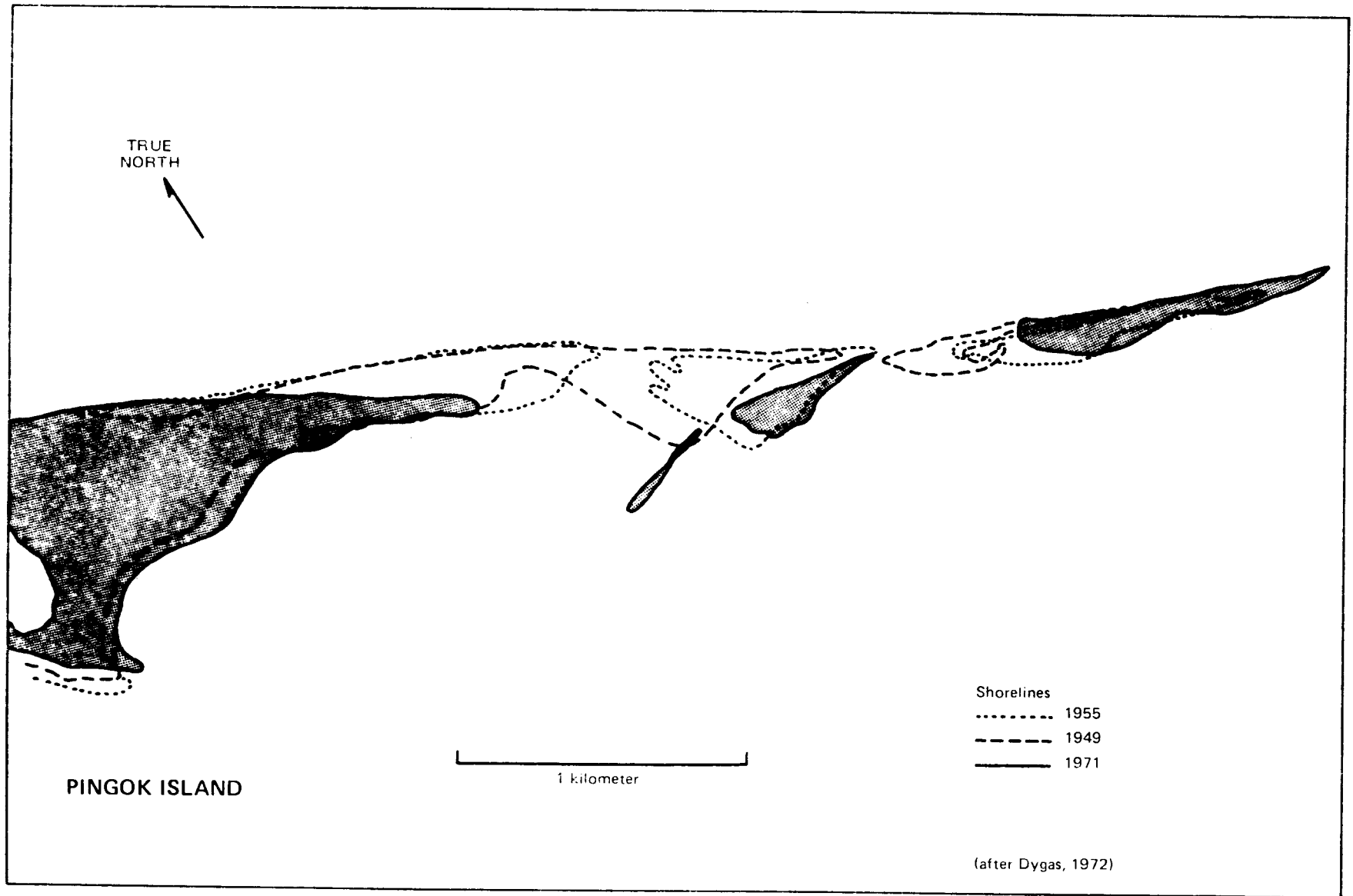
522

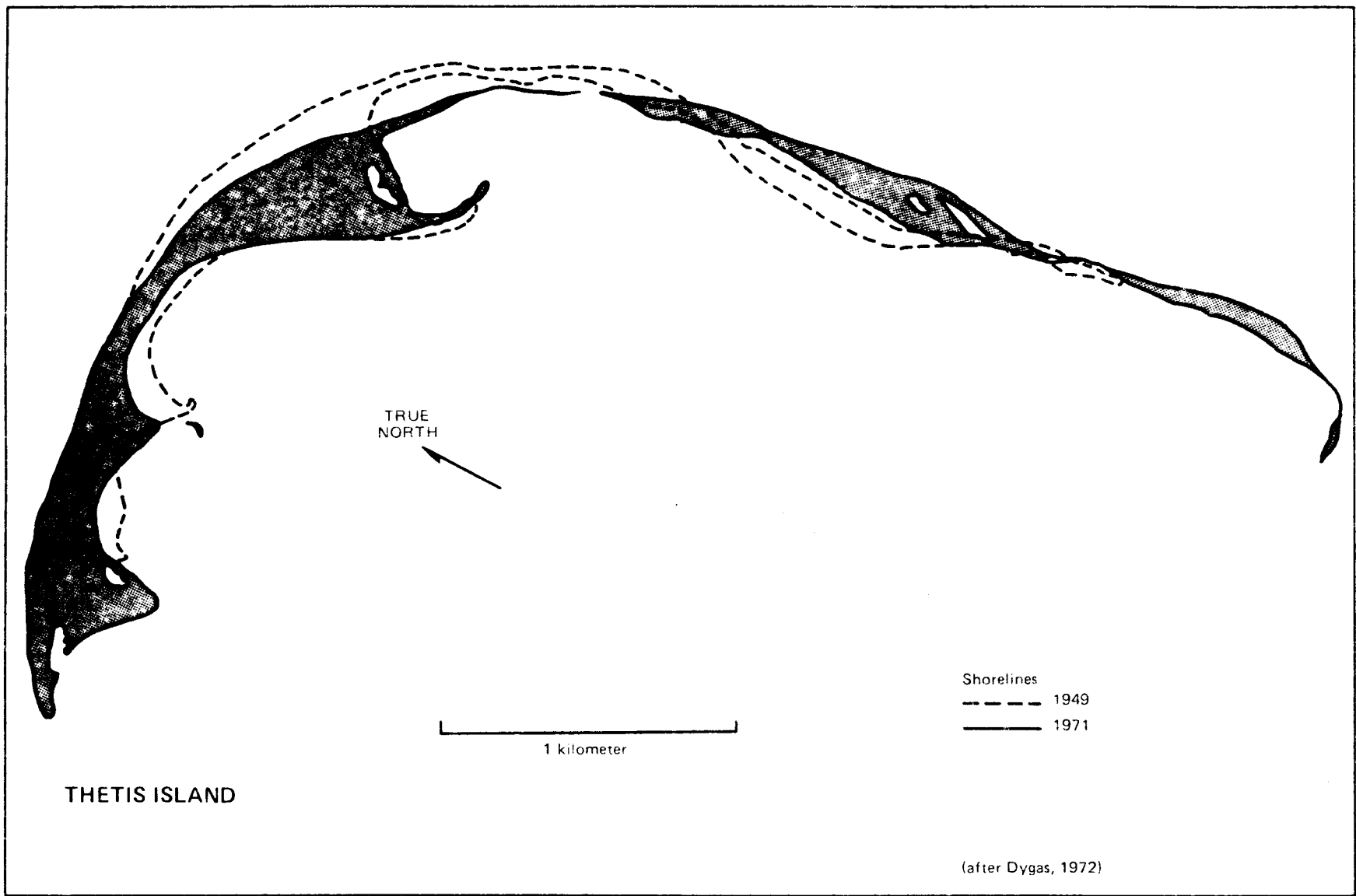
Amount of Erosion in meters	Station							
	A	B	C	D	E	F	G	H
1949 - 1955	36	30	38	23	20	25	30	21
1955 - 1958	30	48	38	10	12	48	88	67
Total (1949 - 1958)	66	78	76	33	32	74	118	78
Erosion Rate (in meters per year)								
1949 - 1958	3.5	4.2	3.8	1.7	1.7	3.8	6.2	4.1
Number of Years before Total Erosion	77	105	128	270	212	113	58	81

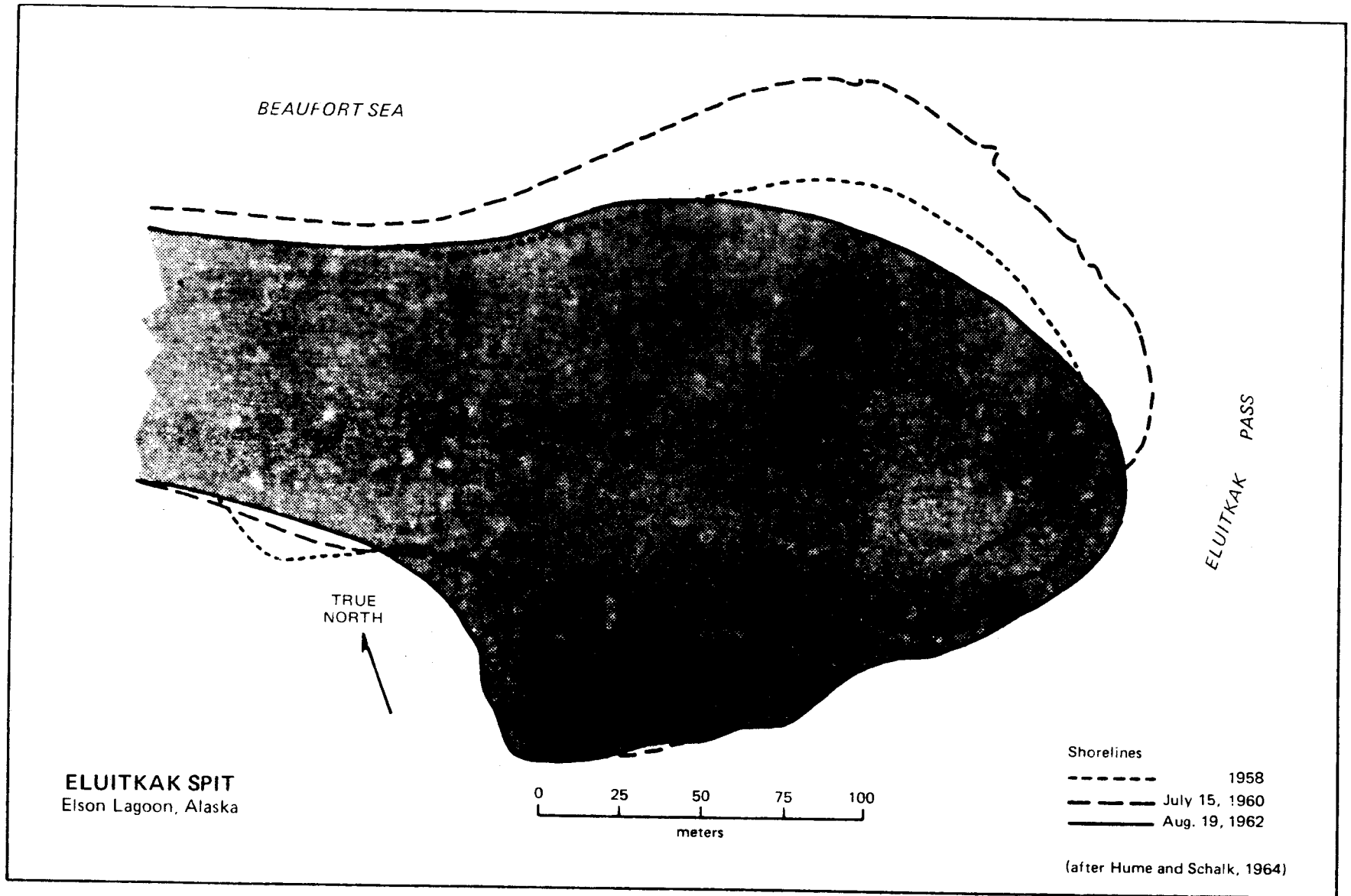
0 1 2 3 KILOMETERS

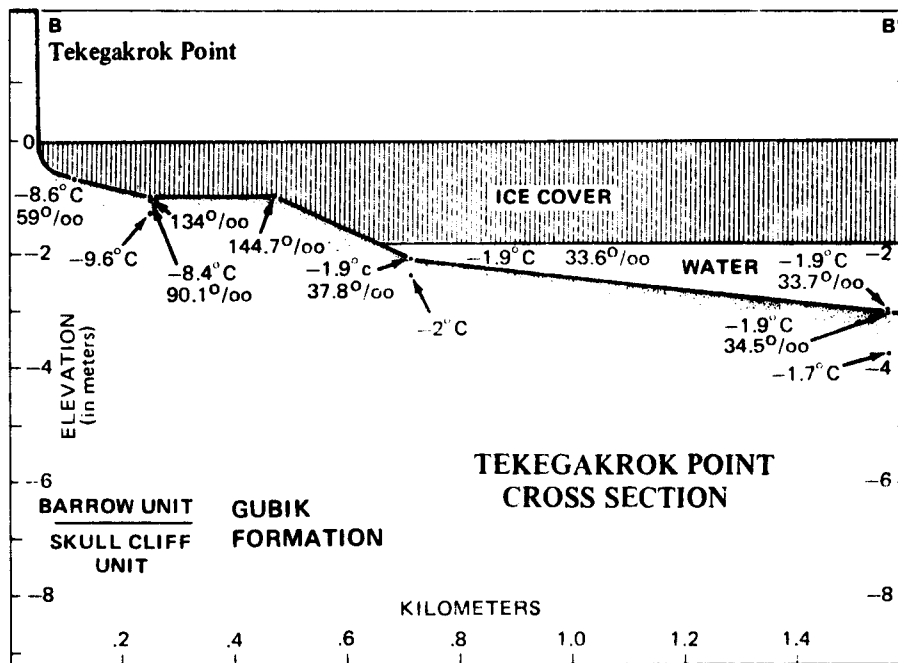
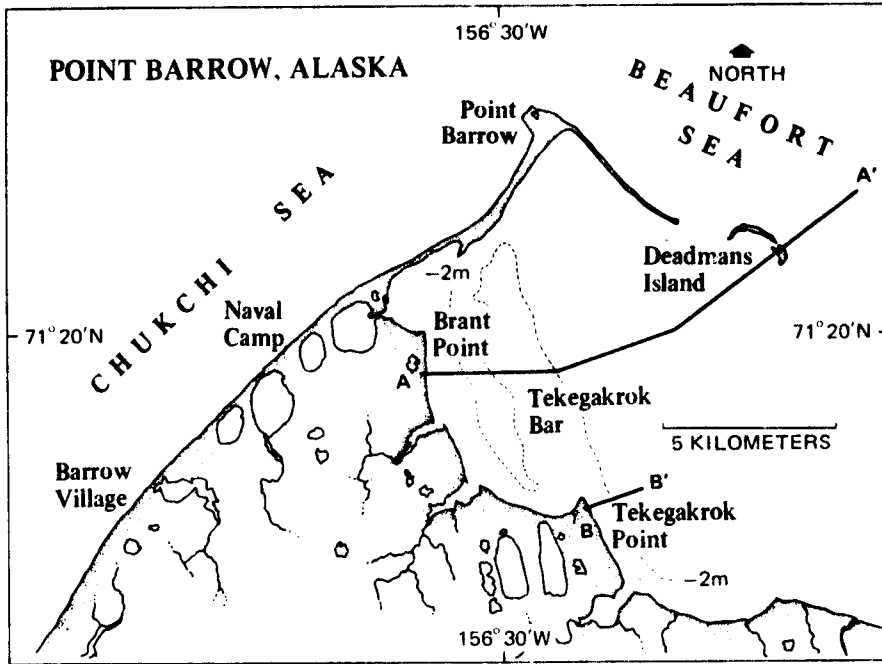
141°30'

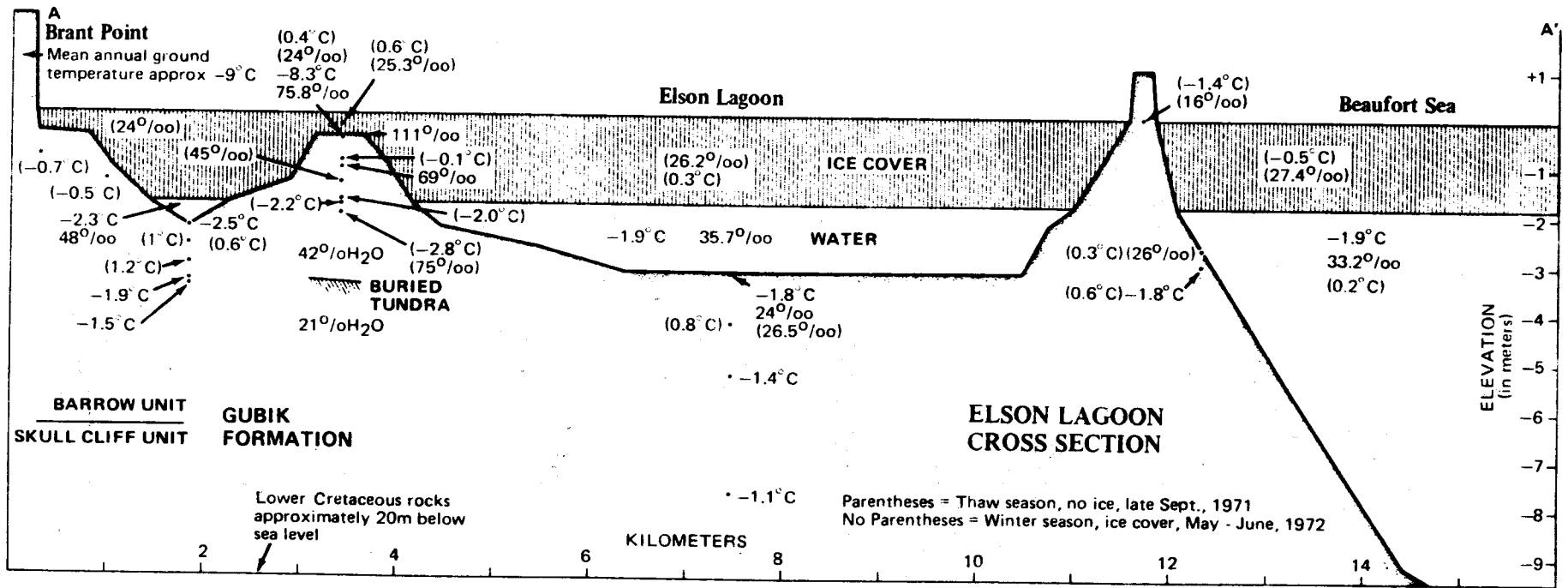
142°00'













ADMINISTRATIVE REPORT

AR-1606-DOC/NOAA
APRIL 1977

PROGRESS REPORT Research Unit 435
1 September 1976 - 31 March 1977

Jan J. Leendertse
Principal Investigator

Prepared for: DEPARTMENT OF COMMERCE
 (National Oceanic and Atmospheric Administration)

Contract No.: 03-6-022-35249



Progress Report

MODELING OF TIDES AND CIRCULATIONS OF THE BERING SEA
National Oceanic and Atmospheric Administration

September 1, 1976 - March 31, 1977

Jan J. Leendertse and Shiao-Kung Liu

I. INTRODUCTION

The progress of the study reported here covers a 7-month period of the first phase of the modeling study. In the first phase of 13 months duration, the work to be executed pertains mainly to setting up of a model of the Eastern Bering Sea, developing the programs to effectively run the model, and making some initial adjustments to obtain an approximate agreement of water levels and flows in the model and in nature. The results of that effort are to be contained in a Working Note.

In a second phase of the study (to be contracted later), further adjustments and verifications will be made using data provided by NOAA, and subsequently experiments will be made with the model to characterize the water bodies, after which a report will be written.

In the proposed third phase of the study, methods will be derived to make rapid predictions of the system behavior based upon data abstracted from the model and nature, and the three-dimensional model developed under these contracts will be documented.

During the first seven months of the study, one of the investigators participated in the OCSEAP Workshop, and as a result of that meeting two important conclusions were reached. First, a model of the Bering Sea as a whole is probably too coarse to resolve the circulation in Bristol Bay and Norton Sound, where proposed oil-lease areas are located. It appears more desirable to model these areas separately (Fig. 1).

Secondly, due to weather conditions and fishing activities, it is difficult to set up tide gauges at the seaward boundaries of a model of the whole Eastern Bering Sea. As a result of this meeting, we are now preparing two separate models, even though this will considerably increase the workload in adjustment and verification.

The model to be used in this study is a three-dimensional finite difference model [1,2]. It computes water levels, currents, salinity distributions and temperature distributions from boundary data inputs and initial conditions on a three-dimensional grid system.

II. WORK PROGRESS

During the reporting period work was done simultaneously on the first three tasks of the first (13-month) phase of the study.

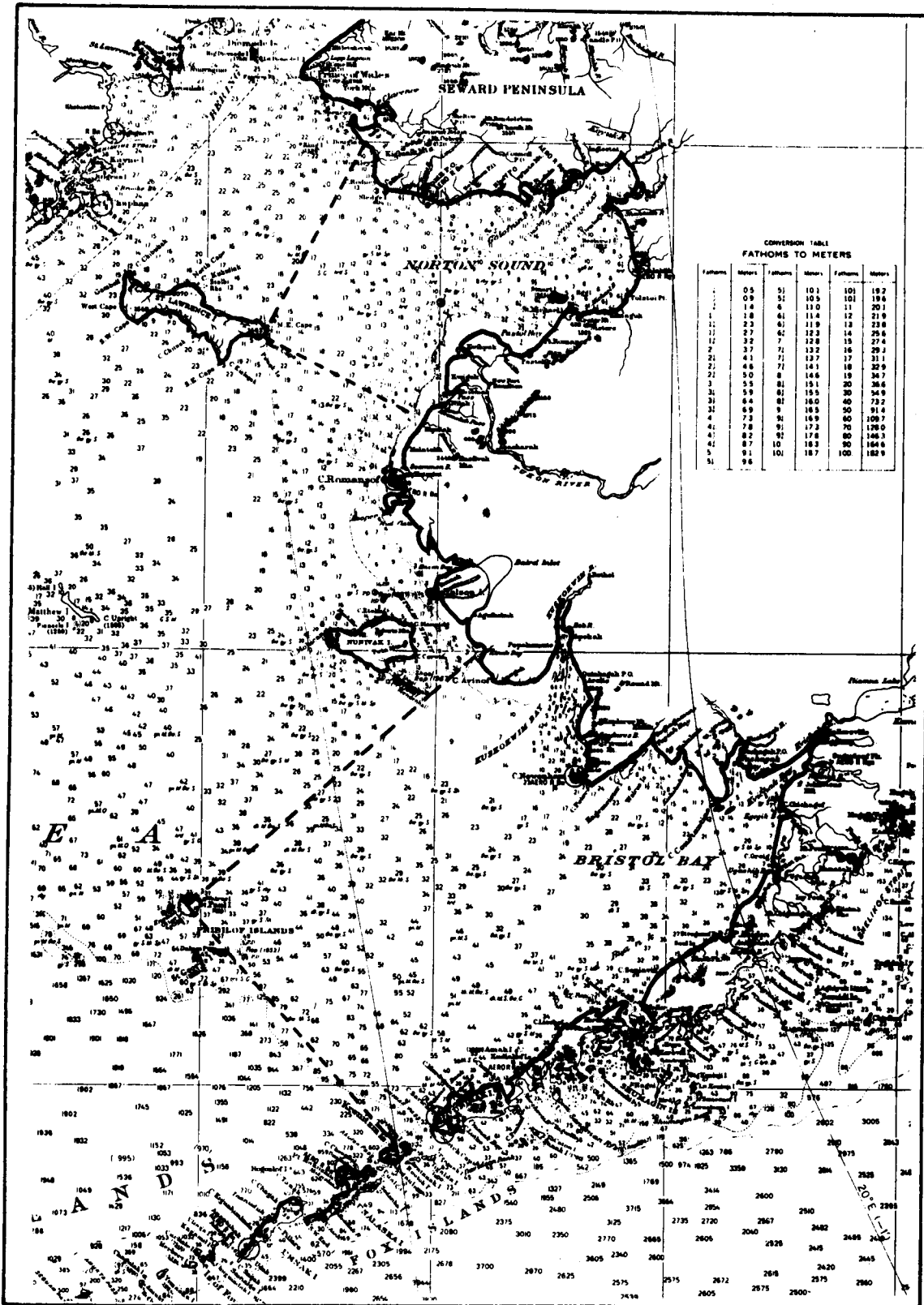


Fig. 1--Approximate boundaries of the Bristol Bay and Norton Sound 3-D models

Task 1 - Model Extension

We extended the model to allow for time- and spatially-varying open boundary conditions of the model. On the open boundary of the model we are now able to input water levels at two locations of the boundary and the model will make linear interpolations in the amplitudes and phases of the tidal constituents inserted.

Progress has also been made in the treatment of open boundary conditions for both the Bristol Bay and Norton Sound models. The new scheme gives proper representation of constituent transport across the model's boundaries. Approximately 60% of this task has been completed.

Task 2 - Model System

Documentation of initial value and boundary conditions in printed form has been included in the program system.

Considerable work was done on making programs for representation of results. The graphics program for the spatial distribution of currents and water-level isocontours is now advanced considerably and some simulation results can now be represented quite adequately (Fig. 2).

A new graphical scheme has been implemented for the spatial representation of the rising and falling of the water surface in the modeled system.

We also developed a method to show vertical velocities (Fig. 3). Only some minor modifications are required to suppress the computational effects of an improperly imposed boundary. It is now also possible to make plots of vertical sections (Fig. 4).

In addition to the graphics program for spatial distribution of parameters, programs are now available for documentation of time series of the computed parameters at selected stations for field data comparison and determination of response functions. A substantial amount of effort was involved in programming and data manipulation.

A series of simulation runs was carried out with the Bristol Bay model to check the feasibility of linear interpolation of tidal constituents.

From tide table information we were originally under the impression that it would be sufficient to drive the model with only one open boundary running from St. Paul Island to Dutch Harbor. Review of some more recent data now being processed at the Pacific Marine Environmental Laboratory in Seattle gave indications that this may be insufficient. Clearly we will have to review the setup of the Bristol Bay model as soon as tide data becomes available. It is estimated that about 60% of this task has been completed.

Task 3 - Model Setup

Two models, namely, Bristol Bay and Norton Sound, have now been set up. These models cover the proposed oil-lease areas with a grid network fine enough to resolve the near-shore region circulation pattern. Each of the models is set up in such a fashion that the information at its open boundaries

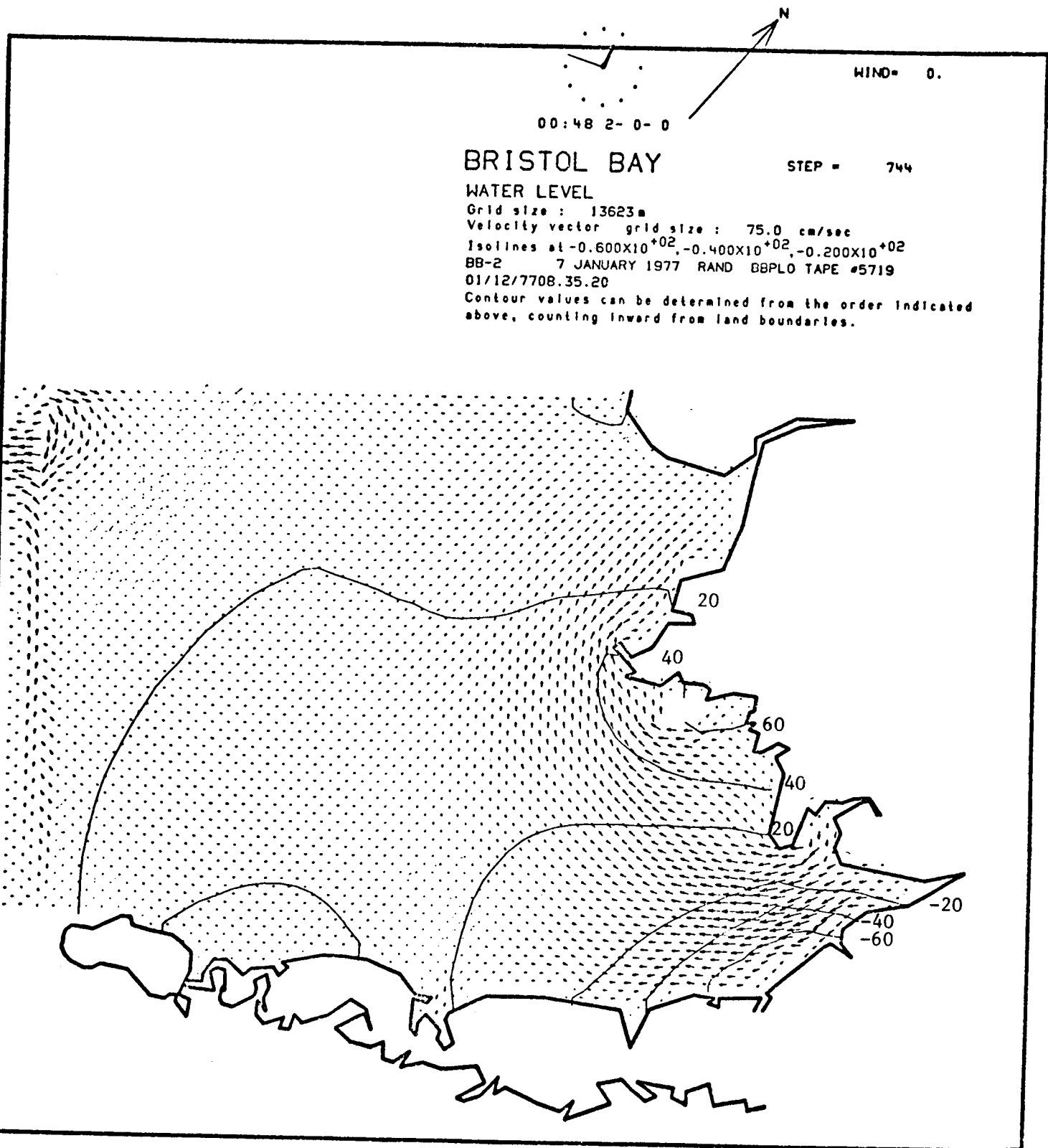


Fig. 2--Computed water surface elevation (deviation from MSL in cm) at 24.42 hours after the beginning of the simulation

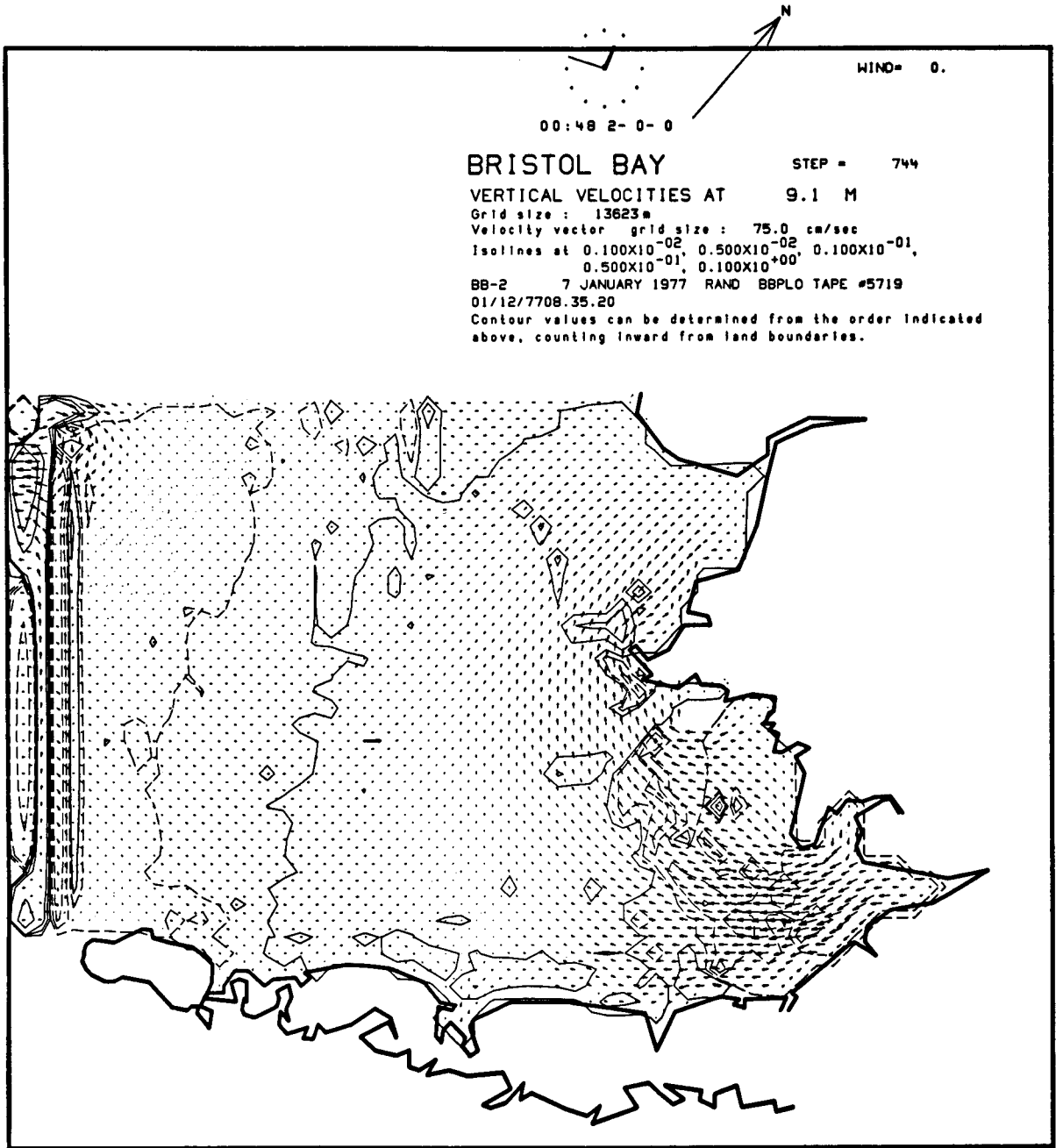


Fig. 3--Computed horizontal velocities together with contours of the vertical velocity

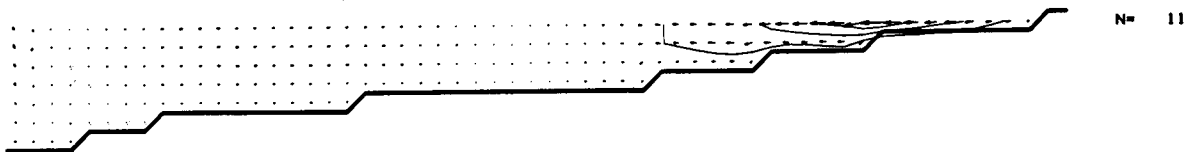


Fig. 4--A particular vertical section through the Bristol Bay model

can be estimated by at least three land-based stations where long-term (and more reliable) data are relatively easier to obtain. The Bristol model is bounded to the west and north by two open boundaries. The land-based tide stations required for this model are located at Dutch Harbor, St. Paul Island, and Anogok (Fig. 1).

The Norton Sound model has a grid structure of $43 \times 39 \times 7$ with a grid size equaling 10,000 meters (Figs. 5 and 6). The land-based tide stations required for this model should ideally be located near the Black River mouth, Northeast Cape of St. Lawrence Island and near Cape Douglas.

Final setup for the Norton Sound model is completed. A number of test runs are presently being conducted. Once some results have been obtained with the Norton Sound model, our field data requirements can be specified in more detail, and at that time we will coordinate our data search with other Principal Investigators of the program.

During the reporting period a meeting was held (March 28, 1977) between the Rand Principal Investigator and the COER Group Supervisor at the Pacific Marine Environmental Laboratory in Seattle. Discussions centered around the strategies for boundary data acquisition, data required for model adjustment, and the hydrographic structure near Bristol Bay.

III. PLANNED WORK

Most of the work for the next six months will be in setting up the model for Bristol Bay. Initial conditions will be derived from a recent report describing the hydrographic structure of Bristol Bay [3].

An urgent need exists for tidal data from bottom pressure recorders and tide gauging stations around the boundary of the Bristol Bay model. It is expected that these will be available on May 1, 1977. The data to be provided should contain the amplitudes and phases of the main tidal constituents. The phases should have a common reference.

It is regrettable that when the surveys were planned no detailed consideration was given to modeling the area. For example, the northern boundary stations of the survey area are not perpendicular to the western boundary, which inhibits the proper boundary description of the model, thus reducing its accuracy and increasing the chance that the inserted boundary condition is ill-posed. Our experience with two-dimensional models is that considerable time is then spent converting these boundaries--time which could be used more productively.

We plan to make a few test runs with the Norton Sound model and to proceed with that part of the investigation as soon as field data becomes available.

References

1. Leendertse, Jan J., Richard C. Alexander, and Shiao-Kung Liu, *A Three-Dimensional Model for Estuaries and Coastal Seas: Vol. I, Principles of Computation*, R-1417-OWRR, December 1973.

2. Leendertse, Jan J., and Shiao-Kung Liu, *A Three-Dimensional Model for Estuaries and Coastal Seas: Volume II, Aspects of Computation*, R-1764-OWRT, June 1975.
3. Kinder, Thomas H., *The Hydrographic Structure over the Continental Shelf Near Bristol Bay, Alaska, June 1976*, University of Washington, M77-3, January 1977.

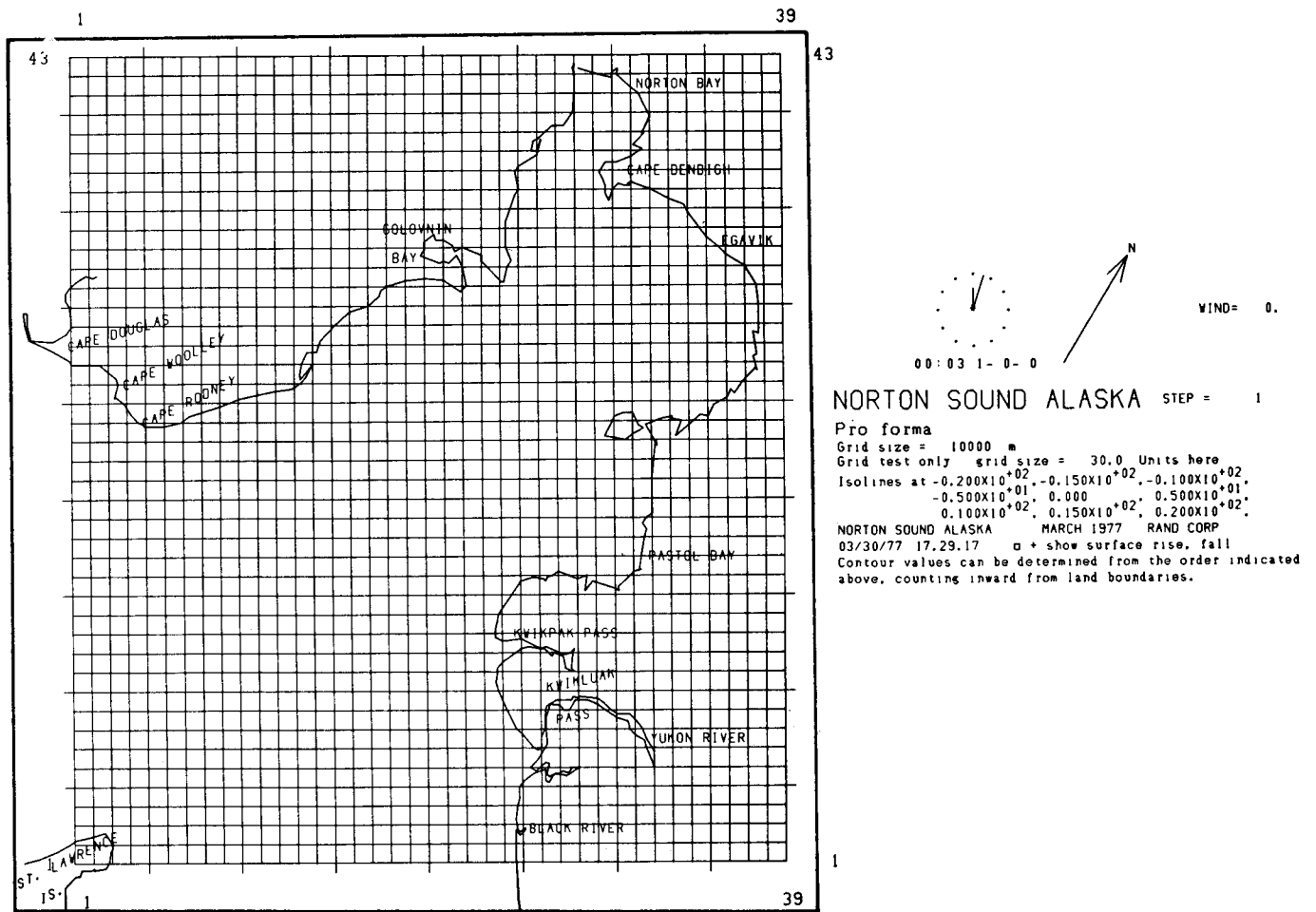


Fig. 5--Horizontal schematization of the Norton Sound 3-dimensional model

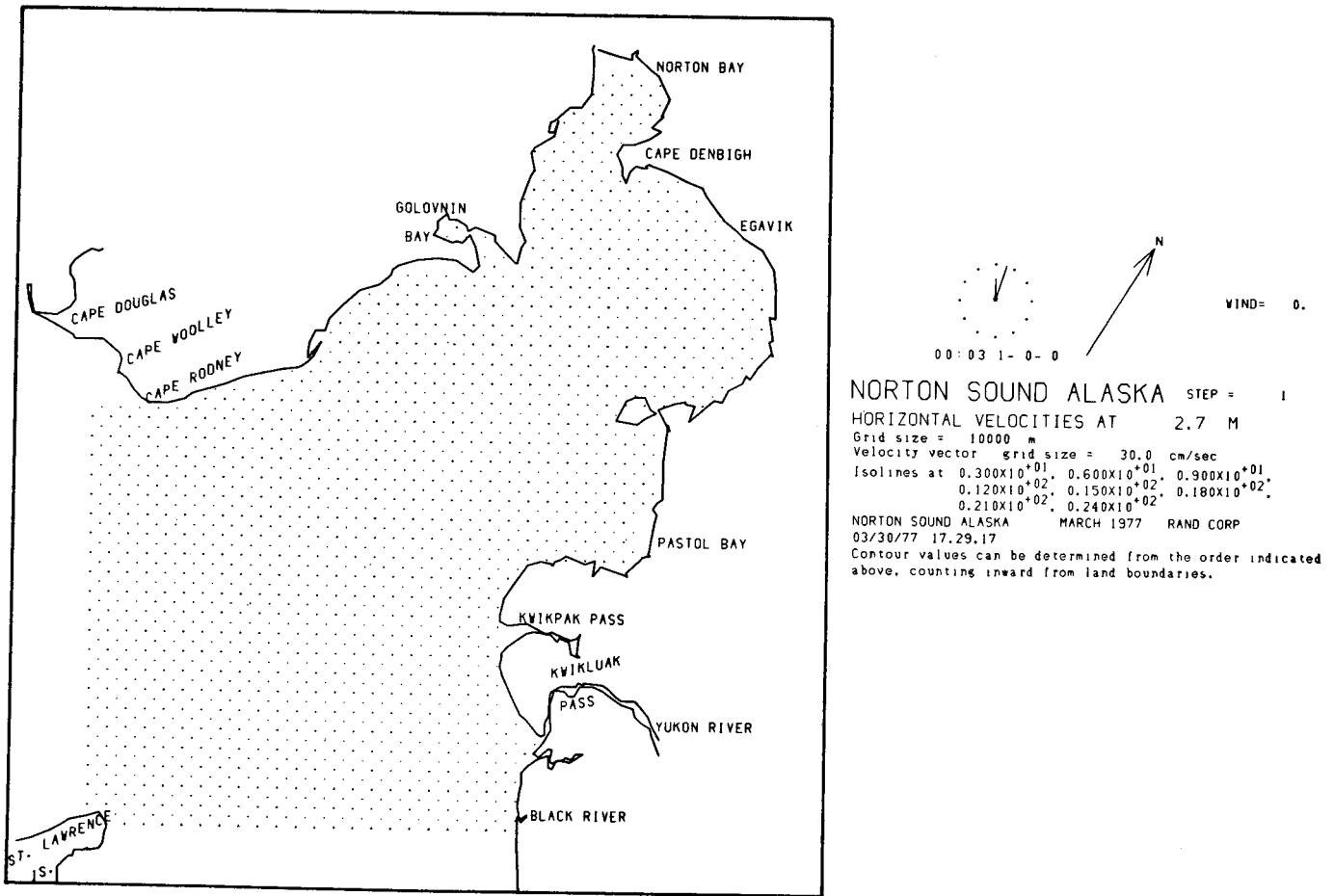


Fig. 6--Initial condition and the horizontal distribution of the computed velocity grid point in the Norton Sound model

ANNUAL REPORT

Contract: 03-5-022-671011

Research Unit: 519

Reporting Period: 1 Oct. 1976 - 30 Sept. 1977

Number of Pages: 41

COASTAL METEOROLOGY OF THE ALASKAN ARCTIC COAST

Frank Carsey
Research Scientist
Polar Research Center
Division of Marine Resources
University of Washington
Seattle, Washington 98195

1 April 1977

I. Summary of objectives, conclusions and implications with respect to OCS oil and gas development

The objectives of this study are to measure and model winds which produce currents in the near shore Alaskan arctic coast in the Prudhoe Bay area. Winds of concern have their origin in synoptic forcing, mountain barrier baroclinicity and sea breeze forcing. At present a reasonably firm conclusion is that sea breeze forcing during the summer months is important in dynamics affecting sea surface height, currents and set up. This is important in modeling pollutant diffusion normal to the shore during the open water season. Furthermore, a tentative conclusion is that the movement of the sea ice in the Beaufort Gyre is at least as significant as local winds in producing several-day sea surface variations.

II. Introduction

A. General nature and scope of study

This study was designed to examine actual winds in the Prudhoe Bay area, to compare these winds with those predicted by NWS (National Weather Service) analysis and to model local or mesoscale phenomena which create departures of measured from predicted winds. This research was needed because this region has little carefully obtained surface meteorological data and existing data is itself subject to strong local effects due to the proximity to the ocean and the Brooks Range. In order to grasp not only the actual surface winds near the shore, but also their integral impact on surface flow, sea level height (tide) is also studied. A final uncertainty is being examined as part of this research--are meteorologically controlled tidal currents (1-3 day, synoptic scale) due to direct air stress forcing of near shore open water, or due to momentum transfer from sea ice movement in the Beaufort Gyre resulting in Ekman transport (Kraus, 1972). It appears that a combination of the two effects is most likely. All these questions relate to the task of estimating typical wind fields for pollutant transport.

B. Specific objectives

This study has specific objectives of:

- 1) Measurement of surface winds and atmospheric pressures in the Prudhoe Bay area during seasons of interest.
- 2) Examination of wind data to evaluate importance to surface currents and tides of winds due to synoptic forcing, mountain barrier effect, sea breeze forcing or other significant mesoscale flow fields.
- 3) Comparison to actual winds and pressure fields with NWS synoptic estimates for evaluation of wind fields from archived data.
- 4) Modeling of significant processes to make their contribution to total flow accessible via archived data.
- 5) Relationship of meteorological tide setup in embayments to wind stress.

C. Relevance to problems of petroleum development.

The winds of interest in this work are those which produce significant surface currents and tides in the Prudhoe Bay area. Therefore, these winds will, when taken with other current-producing mechanisms, describe the mean trajectory and lateral diffusion of oil on open water and, to a certain extent, oil under sea ice. The magnitude of these flow terms will enable determination of the size and extent of an oil slick and its likelihood of impacting the biota of specific regions and depths. In order to accomplish this entire task, other research, such as into the behavior of spilled oil with time in arctic conditions, must be performed.

III. Current state of knowledge

A. Synoptic forcing

The estimation of surface winds from synoptic atmospheric pressure data is a straight-forward exercise. For the atmospheric stability regimes encountered in the Arctic, one may state after Brown, et al. [1974] and Carsey [1976]

$$\begin{aligned}
 U_{10} &= (.6 \pm .1) U_g \\
 \alpha &= 20^\circ \pm 5^\circ \text{ summer} \\
 \alpha &= 35^\circ \pm 5^\circ \text{ all other seasons}
 \end{aligned}$$

where

$$U_g = \frac{-\nabla P(x,y)}{\rho f},$$

$P(x,y)$ is the surface pressure field, ρ is the air density, f is the Coriolis parameter ($\approx 1.4 \times 10^{-4}$ in this area), α is the directional difference between the geostrophic wind (along the isobars) and the surface wind (10 meters). As part of this study, atmospheric pressure data were taken in the Prudhoe Bay area to be compared with the NWS estimated field. The NWS has the disadvantage of having few reliable pressure stations in this area and must rely on essentially zonal (from east or west) geostrophic flow.

B. Sea breeze forcing

Sea breeze forcing is a subject of current research in boundary layer meteorology. Considering the fundamentals of the problem, Holton [1972] shows that at a land-sea interface there is an acceleration in surface wind

$$\frac{d\bar{v}}{dt} = \frac{R \ln(P_0/P_1)}{2(h+L)} (\bar{T}_2 - \bar{T}_1)$$

where R is the gas constant, T_2 and T_1 are air temperatures over land and sea respectively, L is the sea breeze cell dimension normal to the coast, h is the cell and the boundary layer height, P_0 is the surface atmospheric pressure, and P_1 is the atmospheric pressure at the cell top (See Figure 1). This acceleration is diminished by air stress and the net acceleration is probably never brought to zero through equilibration. A task of the sea breeze modeler is to deal with the non-equilibrium system. Also, the modeler must determine the cell width L while h is taken to be the boundary layer height z_i [Carsey, 1976, and Holmgren and Spears,

1974]. The temperatures are generally estimable from archived data. Time series of winds pertinent to sea breeze modeling research are presented in Section VII (discussion) below.

C. Mountain Barrier Effect

The mountain barrier effect has been described in approximate terms by Schwerdtfeger [1974, 1975]. Basically, a polar region mountain range such as the Brooks Range creates a tilted cold air/warm air interface at all times. This produces a local pressure gradient essentially independent of large scale gradients. A significant net result is a thermal wind

$$\vec{V}_T = \frac{g}{f} \frac{\nabla T}{T} \vec{G} \times \vec{k}$$

where g is the gravitational acceleration, ∇T the inversion strength, T the surface temperature, \vec{G} the (maximum) slope of the cold air surface and \vec{k} the unit upward vector. In the Barter Island area this vector is oriented to circulate air toward the east around the mountain. In order to utilize this effect, the ageostrophic component must be computed

$$\vec{V}_a = \vec{V} - \vec{V}_g = \frac{\vec{k}}{f} \vec{V}_T \left(\frac{\bar{w}}{\Delta Z} - \frac{\bar{V}}{\Delta s} \right)$$

for mean vertical flow (over the mountain) \bar{w} , mean wind speed \bar{V} , horizontal feature dimension Δs and height ΔZ . A complicating flow V' exists which moves surface air outward from the mountain. This contribution is due to streamwise convergence of the flow, and its significance is that it controls the size of the region which will experience the ageostrophic flow as well as the net cold air slope \vec{G} . Modeling V' involves knowing a great deal more than is known about the topography of the boundary layer; hence, in this program the effect of V' will be measured by measuring winds during spring of 1977 at various distances from the Brooks Range.

The net contribution from this effect to surface winds along the coast is not known at this time.

IV. Study area

The primary area of study is from east Harrison Bay (151°W) to west Camden Bay (145°W), although pressure analyses are produced for a larger region to utilize NWS data from Barrow and Barter Island. The exact locations of data gathering sites are found on the ROSCOP II (Appendix A). The precise region of interest extends from the shore to the Continental Shelf break which is near to the mean summer ice edge. Later this year measurement programs will detail the winds and tides in the Simpson Lagoon area.

V. Sources, methods and rationale of data collection

The following data were taken:

- 1) Wind speed and direction, and temperature via MRI mechanical weather station.
- 2) Atmospheric pressure via Weathermeasure B211 microbarograph.
- 3) Tides via self recording - float level tide gauge.
- 4) Boundary layer height via NOAA/PMEL acoustic radar.

These instruments were placed at various sites in the area of study (exact locations are shown in Figure 2 and listed in Appendix A). Instruments for pressure measurement were purchased with funds for this contract; all other gear was borrowed for reasons of economy. The MRI weather stations are marginal in wind direction resolution, but are difficult to replace from the point of view of ruggedness. Wind data were taken on Narwhal and Cottle Islands and Tolaktovut Point in order to measure as much as possible the true winds of interest because Prudhoe Bay area pilot interviews disclosed that winds in the near shore were often brisker than at the airport some 8 km inland. Pressure data were taken by placing the

instruments in structures located in a grid designed to optimize the pressure field deduced from them in light of known restrictions from noise and instrument accuracy. From III A. above a geostrophic wind speed error of 2 meters per second is due to a pressure error of .3 millibars over 100 km horizontal distance. Obtaining .25 millibars accuracy is near the reasonable limit in remote conditions; hence, micro-barograph spacing less than 100 km is inadvisable. In the field program of 1976 one tide gauge was placed at Prudhoe Bay. For the summer of 1977 at least two gauges will be deployed, one at Prudhoe and one at either Pingok Island or Narwhal Island, or both.

VI. Results

Final data from the field program of 1976 are not yet available. Some periods have been examined in detail, and they are discussed at greater length in Section VII. A simple listing of results is not a product of optimum value at this time; instead, we are seeking an understanding of the processes at work in producing actual wind fields in the Prudhoe Bay area. Data which can contribute to understanding these processes are discussed below in the context of the process description.

VII. Discussion

Water level was measured with a tide gauge at the east dock in Prudhoe Bay. Atmospheric pressure data was collected at Deadhorse airport (8 km from the bay). Figure 3 shows a time series comparison of these data. It can be seen that relative maxima of water level occur during rapid pressure changes (8-10 mb in one day). Pressure increases or decreases taking two to three days appear to have little effect on the overall levels in the bay.

Figure 4 shows a two-dimensional least squares fit (TDLSF) to our pressure data from all stations (see Appendix C), and gives a better idea of what transpired

during a rapid pressure increase on August 21, 1976 (August 22, 000 GMT). A high pressure cell with a relatively tight gradient is moving into the area. The geostrophic wind field from the least squares fit can be compared to that of the National Weather Services (NWS). The surface winds at our stations on Cottle and Narwhal Islands and Tolaktovut Point are also shown. The maximum water depth from the islands to the shore is less than 10 meters. The integrated mass transport for water of an Ekman depth or about 50 meters is 90° to the right of the surface wind. Therefore, the shallow water precludes Ekman turning as an explanation for the "pile up" at the coast. However, if momentum is transferred to the pack ice (~ 5 km north of the islands), which is in deeper water, then the classic situation evolves, resulting in a pile up of water at the coast perpendicular to the surface winds shown.

Figure 5 shows generally eastward ice motion in the Beaufort Sea. In this situation southward momentum is transferred through the pack ice to the water beneath. The small squares represent buoy positions which change in response to wind and ice stresses. The length (20 km/inch) and direction of the lines correspond to buoy movement during the designated 24-hour period. The August 21, 1976 strain lines show that water should pile up along the coast due to the Ekman turning in deeper water (see Figure 4).

Figure 6 is another TDLSF showing a comparison of NWS data and surface winds at Tolaktovut Point, Cottle Island and Narwhal Island on August 25, 1976 (August 26, 000 GMT). A rapid pressure decrease (see Figure 1) was occurring. The surface wind direction is just the opposite of that on the 21st but the same caveat applies. Again, if momentum is transferred through the ice pack which exists in water deep enough for complete Ekman turning, the effect will be that Prudhoe Bay water is pulled out to satisfy continuity considerations as deeper water is driven 90° to the surface wind direction.

Figure 7 indicates the motion due to the imposed wind and ice stress field. The August 26, 1976 translations show westward movement producing water flow beneath the pack ice perpendicular to and away from the coast and a drop in water level at the coast (see Figure 6).

Figures 8 and 9 are TDLSF plots to compare pressure resolution of NWS charts with data from this study. Again, surface wind directions at the weather station sites are also shown. It can be seen that the NWS charts give almost no information for the study area.

The surface wind data in both figures show evidence of sea breeze modification of the surface wind vector. Data from radiosonde collected at Barter Island on 000 GMT 18 August 1976 and on 000 GMT, 31 August, 1976 indicate a weak sea breeze cell (Figure 1), which is assumed to exist as well in the Prudhoe Bay area since Arco Tower, Prudhoe (5 km from the bay) recorded temperatures of 11.7°C on August 18 at 000 GMT and 8.3°C on August 31 at 000 GMT.

Amplitude spectra of the tide data were computed to resolve the relative contributions of meteorological and astronomical forcing [Figure 10]. It can be seen that periods in the 2.4 to 5.7 day range related to synoptic weather changes (meteorological forcing) are significant. However, it can also be noticed that M_2 (principle lunar $T = 12.42$), S_2 (principal solar $T = 12.00$), O_1 (principle lunar diurnal, $T = 25.82$) and P_1 (principal solar diurnal, $T = 24.07$) have significant contributions.

One objective of the study was to relate the change in water level to wind stress (meteorological forcing), therefore the semi-diurnal components (astronomical forcing) shown in Figure 11 were notch-filtered out of the data [Shanks, 1967]. The diurnal components O_1 , and P_1 were not removed since their amplitudes were much greater than theoretically predicted for astronomical forcing [McLellan, 1965] and it is assumed that sea breeze (meteorological) forcing is coupled to tidal

(astronomical) forcing in this case. Figure 12 shows simple data with relative amplitudes of the contributions. Figure 13 shows that the notch (extremely narrow band) technique did not affect the amplitude of remaining components.

To evaluate the importance of seich motion in Prudhoe Bay, the formula

$$T = \frac{4L}{nc} \equiv \text{Period}$$

where $L \equiv$ length of bay

$c \equiv$ velocity of wave

$n \equiv 1$ implies fundamental period

is used to compute the seich period. The formula is derived for a standing wave in a pipe where c is replaced by \sqrt{gh} where $g \equiv$ acceleration of gravity and $h \equiv$ depth of bay, assuming that a wave in the bay would be a shallow-water wave. Using a rectangular bay approximation with a constant bottom slope:

$$T_1 = 2.6 \left(\frac{2L}{c} \right) = 100 \text{ minutes}$$

Using a semi-circular bay approximation with a parabolic bottom:

$$T_1 = 2.2 \left(\frac{2L}{c} \right) = 85 \text{ minutes}$$

[see Fairbridge, 1966].

In Figure 14, a segment of actual tidal record, small wavelets of period $T \sim 240$ minutes appear. These are taken to seich waves and our preliminary calculations are not unrealistic for the assumed bay configurations. A complete analysis (not shown) of the amplitude spectrum shows, however, that no appreciable energy is present at these periods and that notch filtering or low pass filtering to remove that component would be of no immediate benefit. These waves are not significant in this study.

The task of examining the water level changes due to meteorological forcing on a synoptic scale will involve "notching" out the diurnal components and looking at residual amplitudes. Uncoupling the meteorological forcing due to sea breeze effects from the astronomical forcing, both of which have diurnal cycle, will involve further study and may require modeling of the diurnal astronomical components.

Sea breeze forcing appears to be a modifying factor in wind stress computations. Evidence for "cell" (see Figure 1) formulation and resultant modification of the synoptic wind vector are shown in Figures 15 and 16. Figure 15 shows wind direction and velocity plots taken from three locations, Narwhal Island, Cottle Island and the Arco Tower at Deadhorse. The locations were chosen to provide information on the horizontal extent of the sea breeze cell. Little information was obtained on vertical variation except for data from our acoustic sounder and from Barter Island radiosondes. On August 22, 1976 the sounder indicated an inversion layer near 300 meters. The inversion height is assumed to be at the top of the sea breeze cell. Barter Island data indicated that the surface wind (1500 LDST on August 22, 1976) was 050° at 3 m/sec while that at 582 meters was from 273° at 4 m/sec. This is circumstantial evidence for cell structure in the Barter Island vicinity. Historical data show that Barter Island winds largely agree with Prudhoe Bay winds. During this time the sky was clear at Prudhoe with an 8.9°C temperature difference between the coast and the ice edge. Looking at Narwhal Island data (closest to ice edge) we see that the synoptic wind field was induced to 20° - 70° with a relative wind speed increase during the time for a sea breeze maximum (1100-1800). For Cottle Island a relative maximum of 70° and wind velocity of 5 m/sec was induced in the 100 to 000 time span. Note: A line normal to the coast in this area is 30° from true north and a sea breeze typically sets up 30° from the normal to the coast. Therefore, a sea breeze in the area of study would be expected from

60° to 90°. Inland (Arco Tower), no appreciable winds were evident until the sea breeze maximum hours of 1100 to 1800.

Figure 16, from data taken 6 September 1976, has the same horizontal geometry but a different synoptic situation prevails. Our acoustic sounder shows an inversion layer at 300 m. The Barter radiosonde data show a surface wind from 100° at 4 m/sec while the 505 m wind is from 259° at 4 m/sec. Again, there is circumstantial evidence for a cell, assuming this condition applies to Prudhoe Bay. National Weather Service data show that the synoptic wind field should produce winds from 210° to 180° but the sea breeze (at all three locations) forces the wind vector to 270°-300° and doesn't allow the synoptic field (the synoptic field was changing during the time period) to prevail until the time of sea breeze minimum 2200 to 0300. A maximum in the wind velocity vector is seen at all three wind stations during 1200-1800 hours of sea breeze dominance.

VIII. Conclusions

A firm conclusion of the work to date in this study is that the sea breeze mechanism was an important source of wind in the near shore region of the Prudhoe Bay area in the summer of 1976. A tentative conclusion is that this situation can be expected relatively often; that is, the sea breeze is an important surface wind during the open water season on the arctic coast of Alaska. A corollary tentative conclusion is that wind fields during this season may not be properly inferred from NWS analysis. At this time it is not possible to state the probable magnitude of error due to sea breeze nor is it possible to list the amount of error from other sources including structure in the Beaufort Sea overlooked by NWS in the synoptic pressure field. A final tentative conclusion is that pack ice motion, not always correlated with local winds or geostrophic winds extrapolated from continental weather, creates significant flow in the near shore region. This current represents

a flow contribution which is accessible only through modeling of pack ice motion-- a difficult task with poor quality archived pressure data over the Beaufort Sea.

IX. NEEDS FOR FURTHER STUDY

The measurement program concluded as of this writing consists of one field season in 1976 devoted largely to the sea breeze problem. Further study from this vantage point, therefore, includes the 1977 field program and all activity in fiscal year 1978. Section X of this report deals with operations of 1977, and in these paragraphs scientific purposes will be discussed. Several subjects require consideration, including sea breeze winds, mountain barrier winds, fresh water outflow microclimate, Simpson Lagoon winds, and data analysis needs.

Each wind regime situation discussed here is important to problems discussed at the Barrow Synthesis Meeting of February 1977. The mountain barrier winds are shown very likely important in pollutant transport (Schwerdtfeger 1974 and Searby and Hunter, 1971) and may be the source of upwelling which produces a rich biota in the Barter Island area. Fresh water outflow occurs in the river mouth deltas which were listed as particularly fragile and critical environments at the Barrow meeting. A likely perturbation of the local wind field brought on by the effects of early summer river flow will act to create local convergence. The strength of that convergence is clearly important since that flow will bring material toward these deltas. Also, the decrease in albedo in the area covered by fresh water creates sometimes shortlived open water in the delta areas with resulting oil accumulation at the surface in the case of nearby spills under the ice.

In the Simpson Lagoon area detailed current and sea-level height modeling is planned by Matthews of UAGI for both the 1977 and 1978 open water seasons. The coastal meteorology program has been modified slightly to contribute *in situ* data for this effort in 1977, and plans are being formulated for more intensive

collaboration in 1978. The meteorological aspects of that program are three-fold-- present plans call for measurement of winds at the Lagoon at two locations, atmospheric pressure measurements at the Lagoon for both absolute and gradient information, and regional wind field description via the geostrophic and sea breeze calculations. The regional wind field will establish boundary condition tides and currents at the Lagoon edge.

At present two spring field seasons are planned to study mountain barrier wind effects. The essential unknowns confronted in these measurements are the spatial extent of the sloping cold air surface and the time variation of the effect both seasonally and synoptically. In the field season of 1977 wind data will be taken at west Camden Bay and Narwhal Island and atmospheric pressure data will be taken inland and along the coast to answer these questions. Should these data fail to circumscribe the wind field, another effort would be made in 1978 with a higher density of data. In any case, two seasons of winds are appropriate for purposes of constructing high quality average behavior.

Also examined in the spring of 1977 will be deviation of surface wind from geostrophic prediction in the delta of the Colville River. A significant departure will dictate a more complete description of the winds in the outflow season of 1978. At least one wind station will be required in this area in 1978 to support the Simpson Lagoon project.

Measurements devoted to elucidating the structure of the sea breeze cell will be limited to 1977. Data confirming the importance and the approximate dimension of this phenomenon were taken in 1976 and are discussed in Sections VI and VII. Data to be taken in 1977 will allow computation of expected strength of the sea breeze and the resulting air stress in the sea surface. A critical parameter to be obtained in this research is the cell width (L in the discussion of III B above). In computing currents and sea surface slope the cell width is the point of change of regime

from sea breeze to undisturbed. The knowledge of sea breeze flow from field work and data analysis for 1976 and 1977 will enable the modeling of the air flow in the region of Simpson Lagoon in 1978 using only local measurements.

The data analysis aspects of this program are very important. In any real meteorological problem, many effects contribute to a resultant event such as a wind field. Measurements alone cannot help the transport modeler establish expected or mean winds except through utility of a long term record. The only alternative is proper averaging and careful bookkeeping of all contributing mechanisms. This requires the modeling of the significant processes and the careful handling of all data. This effort remains part of our program.

The relationship of wind stress to water level in embayments will also be investigated. Various tide gauge implantations will be used to arrive at sea surface slopes.

X. Summary of fourth quarter operations

A. Ship or laboratory activities

1. Field trip schedule:

25 April 1977--arrive Prudhoe Bay, begin establishment of weather station and microbarograph array to be maintained until end of experiment

10 May 1977--array established

10 July 1977--Pingok Island wind, pressure and radiation station established

30 August 1977--Pingok Island intensive period ends

15 September 1977--end of experiment, all instruments and gear shipped back.

2. Scientific Party

F. D. Carsey, University of Washington, Principal Investigator

T. L. Kozo, University of Washington, Pingok Island experiment, Scientist in Charge

R. Andersen, University of Washington, Meteorological Technician.

3. Methods

Mechanical weather stations, microbarographs and tide recorders will be located in Prudhoe Bay/Simpson Lagoon area for optimum data quality.

4. Sample localities

Weather stations at Tolaktovut Point, Narwhal Island and Camden Bay, spring 1977.

Microbarographs at Happy Valley, Oliktok and Prudhoe Bay, spring 1977.

Weather stations at Tolaktovut Point, Pingok Island, Cottle Island and Narwhal Island, summer 1977.

Microbarographs at Happy Valley, Oliktuk, Prudhoe Bay and Pingok Island, summer 1977.

Tide gauges at Narwhal Island and Prudhoe Bay (and possibly at Pingok Island) summer 1977.

5. Data collected or analyzed

Continuous records of wind direction, wind speed and temperature at weather station site.

Continuous records of atmospheric pressure at microbarograph sites.

Continuous record of sea level height at tide gauge sites.

Continuous record of acoustic sounder inversion heights.

Radiosonde data from Barter Island to investigate presence of sea breeze cells.

6. Milestone chart and data submission schedules.

Data from the 1977 field year will be forwarded to OCSEAP by 1 December 1977. Data from the 1976 field year is nearly all processed. Delays in

this effort are substantially due to confused negotiations between the University of Washington and NOAA, but some delay was caused by the unexpected complexity of the data.

B. Problems encountered/recommended changes

The modification of the meteorological program in support of the Simpson Lagoon project has added to the estimated helicopter time and to the number of days of subsistence required. The modified forms for aircraft support--helicopter and quarters and subsistence support--are included as Appendix B.

C. Estimate of funds expended

\$2,223 of fiscal year 1977 funds are spent as of this writing.

NOAA FORM 24-23 (1-76)		U. S. DEPARTMENT OF COMMERCE NATIONAL OCEANIC AND ATMOSPHERIC ADMINISTRATION NATIONAL OCEANOGRAPHIC DATA CENTER				A00 DATA CENTER						
OCEANOGRAPHY - GENERAL CRUISE INVENTORY (ROSCOP - II)						A40 REFERENCE NUMBER						
A01 EXPEDITION/PROJECT OCSEAP				A91 Declared national program?		YES	NO					
A11 CRUISE NUMBER OR NAME Summer 1976				A81 Exchange restricted?			✓					
A02 SHIP OR PLATFORM Beaufort Sea Coast				A92 Co-operative program?			✓					
A12 PLATFORM TYPE 11				A82 Co-ordinated internationally?			✓					
A03 COUNTRY U.S.		A04 ORGANIZATION OCSEAP/BLM-OCS		A05 CHIEF SCIENTIST(S) F. D. Carsey T. L. Kozo								
A06 NAME AND ADDRESSES OF ORGANIZATIONS AND PERSONS WHOM TO QUERY				FINAL DISPOSITION OF DATA								
A1 Dr. F. D. Carsey, Seattle, Wa. RU519				A2 F. D. Carsey, Seattle, WA 98195								
B1				B2 F. Gava, Juneau, Ak NODC								
C1				C2								
D1				D2								
E1				E2								
DATE	DAY	MONTH	YEAR	A08 GENERAL OCEAN AREAS								
				13								
A07 FROM				A09 TYPE(S) OF MARINE ZONE(S)								
A17 TO				04 and 08								
GEOGRAPHIC AREA				A10 LATITUDE		A20 LONGITUDE						
<i>If all data were collected at a fixed station, fill in the co-ordinates</i>				° ' " N/S		° ' " E/W						
A15 FEDERAL SUPPORT BLM/NOAA												
A25 REMARKS												
D09 at 70°N, 148°W				inversion height at 70°N, 148°W 16 Aug-7 Sep 76								
M90 atmospheric pressure				70°N, 147°W 29 Apr-2 Jun								
70.90N, 153.15W; 12 Aug-4 Sep 76				wind speed, direction and temperature								
70.50N, 149.87W; 12 Aug-4 Sep 76				70.45°N, 150.90°W; 13 Aug-7 Sep 76								
70.28N, 148.47W; 13 Aug-5 Sep 76				70.50°N, 149.08°W; 12 Aug-7 Sep 76								
69.26N, 152.08W; 15 Aug-6 Sep 76				70.39°N, 147.47°W; 10 Aug-1 Sep 76 and								
69.15N, 148.83W; 13 Aug-5 Sep 76				6 May-6 Jun 76								
DISCIPLINE AND TYPE OF MEASUREMENTS	Index 10° x 10°	INDEX 1° x 1°				DISCIPLINE AND TYPE OF MEASUREMENTS	Index 10° x 10°	INDEX 1° x 1°				
		Qc	L	G	G			Qc	L	G	G	
A D09	B	7	7	1	4	Remarks	A	B				
A M90	B	7	7	1	4	Remarks	A	B				
A	B						A	B				
A	B						A	B				
A	B						A	B				
A	B						A	B				
A	B						A	B				

APPENDIX B

AIRCRAFT SUPPORT - HELICOPTER

1. Delineate proposed transects and/or station scheme on a chart of the area.
(Note: If flights are for transport of personnel or equipment only from base camps to field camps and vice versa, chart submission is not necessary, but origin and destination points should be listed.

Support of field stations on Narwhal Island, Tolaktovut Pt., Pingok Island, Camden Bay, Cottle Island, Happy Valley and Oliktok.

2. Describe types of observations to be made.

NA.

3. What is the optimum time chronology of observations on a seasonal bases and what is the maximum allowable departure from these optimum times?

Flights are in support of field programs.

4. How many days of helicopter operations are required and how many flight hours per day?

19 flights, 1 hour per flight

Total Flight hours? 19 hours

5. How many people are required on board for each flight (exclusive of the pilot)?

One to three.

6. What are the weights and dimensions of equipment or supplies to be transported?

Less than 1000 pounds, less than 2 cubic yards.

7. What type of helicopter do you recommend for your operations and why?

No recommendation.

8. Do you recommend a particular source for the helicopter?

No recommendation.

9. What is the per hour charter cost of the helicopter?

Not known.

10. Where do you recommend that flights be staged from?

Deadhorse.

11. Will special navigation and communications be required?

Not known.

QUARTERS AND SUBSISTENCE REPORT

1. What are your requirements for quarters and subsistence in the field area?
(These requirements should be broken down by (a) location (b) calendar period,
(c) number of personnel per day and total man days per period.)

80 man days at Deadhorse, May through June, 1977, one person except for occasional periods with two people.

100 man days at Pingok Island, July and August, 1977, in collaboration with J. B. Matthews, two persons except for possible third person for set up and knock down periods.

2. Do you recommend a particular source for this support?

No recommendation.

3. What is your estimated per man day cost for this support at each location?

Not known.

APPENDIX C

TWO-DIMENSIONAL LEAST SQUARES FIT TO A CUBIC EQUATION (TDLSF)

The basic technique is explained in Krumbein (1959). In least squares techniques for one-dimensional cases, deviations from

$$y = a + bx \text{ (straight line),}$$

$$y = a + bx + cx^2 \text{ (parabola),}$$

$$y = a + bx + cx^2 + dx^3 \text{ (cubic),}$$

and similar higher order curves are minimized to produce a best fit by varying a , b , c , and d , which are constants. In the technique used in this report, pressure is fit to a function of latitude and longitude, implying extension of the least squares method to two dimensions. It was assumed that a two-dimensional cubic fit was the maximum degree of variations required to resolve the pressure field in the study area. The two-dimensional cubic polynomial to be solved is

$$Z = a + bx + cy + dx^2 + exy + fy^2 + gx^3 + hx^2y + jxy^2 + ky^3 \equiv \text{Pressure.}$$

Elements a through k are constants to be solved for in a 10×10 matrix and x and y are longitude and latitude, respectively.

A system of pressure stations at DEW (Distant Early Warning) sites, Lonely and Oliktok, and the Umiat, Happy Valley, and Deadhorse air control towers provided input data for our TDLSF. Coupled to this was input from Barter Island and Pt. Barrow, NWS stations. To avoid east-west contour bias, data from two air-droppable buoys (1003, 1245 of OCS/AIDJEX deployment) were also included. Therefore, nine real data inputs were applied to a grid which was supplied two inputs for NWS maps. To "blend" the boundaries to fit the NWS charts, input from the NWS isobaric analysis with 10% weighting obtained along the edges of our study area.

Through least squares optimizing methods the values of the constants α through k could be determined for our two-dimensional cubic equation. Then along grid values of latitude and longitude a pressure field could be generated and machine contoured. These fields are shown above.

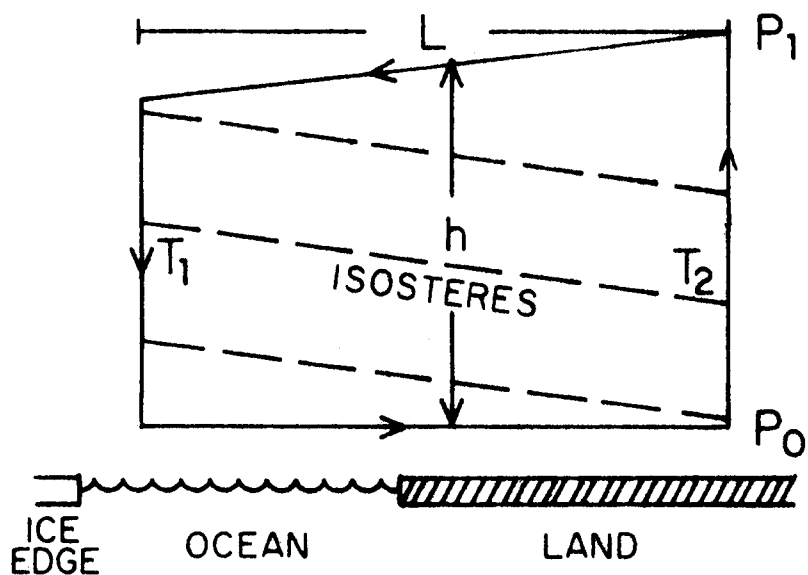
LIST OF FIGURES

- Figure 1. Simplified sea breeze cell geometry with dashed lines indicating isosteres and solid lines indicating isobars. T represents temperature while P is pressure. Arrows indicate flow around cell boundaries.
- Figure 2. Map of pertinent locations along Beaufort Sea Coast. P \equiv microbarograph sites, W \equiv weather stations, T \equiv tide gauge, NWS \equiv National Weather Service upper air station, A \equiv Acoustic radar site (the Prudhoe Arco tower is also at A).
- Figure 3. Time series comparison of tide level (cm) data and atmospheric pressure (mb) data.
- Figure 4. Two-dimensional least squares fit of pressure data from recording stations for August 22, 000 GMT. Scale 50 km/cm. \square --- \square Approximate coast line, ----- National Weather Service isobars. Flags represent wind measurements from Cottle (C) and Narwhal (N) islands, plus Tolaktovut Point (T). Solid lines are isobars.
- Figure 5. Movement of AIDJEX buoys on August 22. A displacement of 2.54 cm on the map is equivalent to 20 km buoy displacement. Buoys are represented by small squares.
- Figure 6. Two-dimensional least squares fit of pressure data from recording stations for August 26, 000 GMT. Scale and designators are as Figure 4.
- Figure 7. Movement of AIDJEX buoys on August 26. Legend is as Figure 5.
- Figure 8. Two-dimensional least squares fit of pressure data from recording stations for 000 GMT, 18 August 1976. Shows low resolution possible with NWS pressure field. Scale and designators are same as Figure 4.
- Figure 9. Two-dimensional least squares fit of pressure data from recording stations (000 GMT, 31 August 1976). Note low resolution of NWS pressure field. Scale and designators are as Figure 4.
- Figure 10. Amplitude spectrum of the unfiltered tide data collected August 18 to September 7, 1976 in Prudhoe Bay. Periods of the various major components are shown.
- Figure 11. Plot of semi-diurnal tidal variations showing typical amplitudes during August 25 and 26, 1976.
- Figure 12. Plot of diurnal tidal variations in filtered data for September 2 and 3, 1976. Note that amplitudes are comparable to semi-diurnal Figure 10.
- Figure 13. Amplitude spectrum of the filtered tide data collected August 16 to September 7, 1976 in Prudhoe Bay. Comparison with Figure 10 shows that amplitudes of major periods are not affected by filtering the semi-diurnal components.

- Figure 14. A short segment of the actual tide record showing small wavelets attributed to seiche effects in Prudhoe Bay on August 31, 1976.
- Figure 15. Wind direction and velocity plots of data taken from Narwhal Island, Cottle Island and Arco tower, respectively, for August 22, 1976. Their relative distances from the coast (specified in figure) give some indication of the horizontal extent (L) of the sea breeze cell. Surface air temperature at the Arco tower can be used to obtain an estimate of when sea surface temperatures of 2°C are used (after Hufford, 1973).
- Figure 16. Wind direction and velocity plots of data taken from Narwhal Island, Cottle Island and Arco tower, respectively (September 6, 1976). Their relative distances from the coast (specified in figure) give some indication of the horizontal extent (L) of the sea breeze cell.

REFERENCES

- Brown, R. A. P. Maier and T. Fox. 1974. Surface atmospheric fields and derived geostrophic winds. *AIDJEX Bulletin No. 26* (September 1974). pp. 173, 203.
- Carsey, F. D. 1976. Acoustic radar techniques in modeling and measurement of air stress over pack ice. *Final Report, NOAA Contract RW0000-8AA71880*.
- Colony, R. 1977. Personal communication, AIDJEX project.
- Fairbridge, R. W. 1966. *The Encyclopedia of Oceanography*. Editor, Reinhold Publishing: New York. 1021 pp.
- Holmgren, B. and L. Spears. 1974. Sodar investigations of the effect of open leads on the boundary layer structure over the Arctic Basin. *AIDJEX Bulletin No. 27* (November 1974). pp. 167-179.
- Holton, J. R. 1973. *An introduction to dynamic meteorology*. Academic Press: New York. 319 pp.
- Hufford, G. L. 1973. Warm water advection in the southern Beaufort Sea, August - September 1971. *J. Geophys. Res.* 78. pp. 2702-2708.
- Kraus, E. B. 1972. *Atmosphere - ocean interaction*. Clarendon Press: Oxford. 275 pp.
- Krumbein, W. C. 1959. Trend surface analysis of contour-type maps with irregular control-point spacing. *J. Geophys. Res.* 64. pp. 823-834.
- McLellan, H. J. 1965. *Elements of physical oceanography*. Pergamon Press: New York. 150 pp.
- Searby, H. W. and M. Hunter. 1971. Climate of the North Slope of Alaska. *NOAA TM-NWS AR-4* Avail NTIS.
- Schwerdtfeger, W. 1974. Mountain barrier effect on the flow of stable air north of the Brooks Range. *Climate of the Arctic*, Conference Publication of the Geophysical Institute, University of Alaska, Fairbanks. pp. 204-208.
- _____. 1975. The effect of the Antarctic peninsula on the temperature regime of the Weddell Sea. *Month. Weath. Rev.* 103. pp. 45-51.
- Shanks, J. S. 1967. Recursion filters for digital processing. *Geophysics* 32, 33. pp. 33-51



Circulation Theorem in a Plane
 \perp to Coast

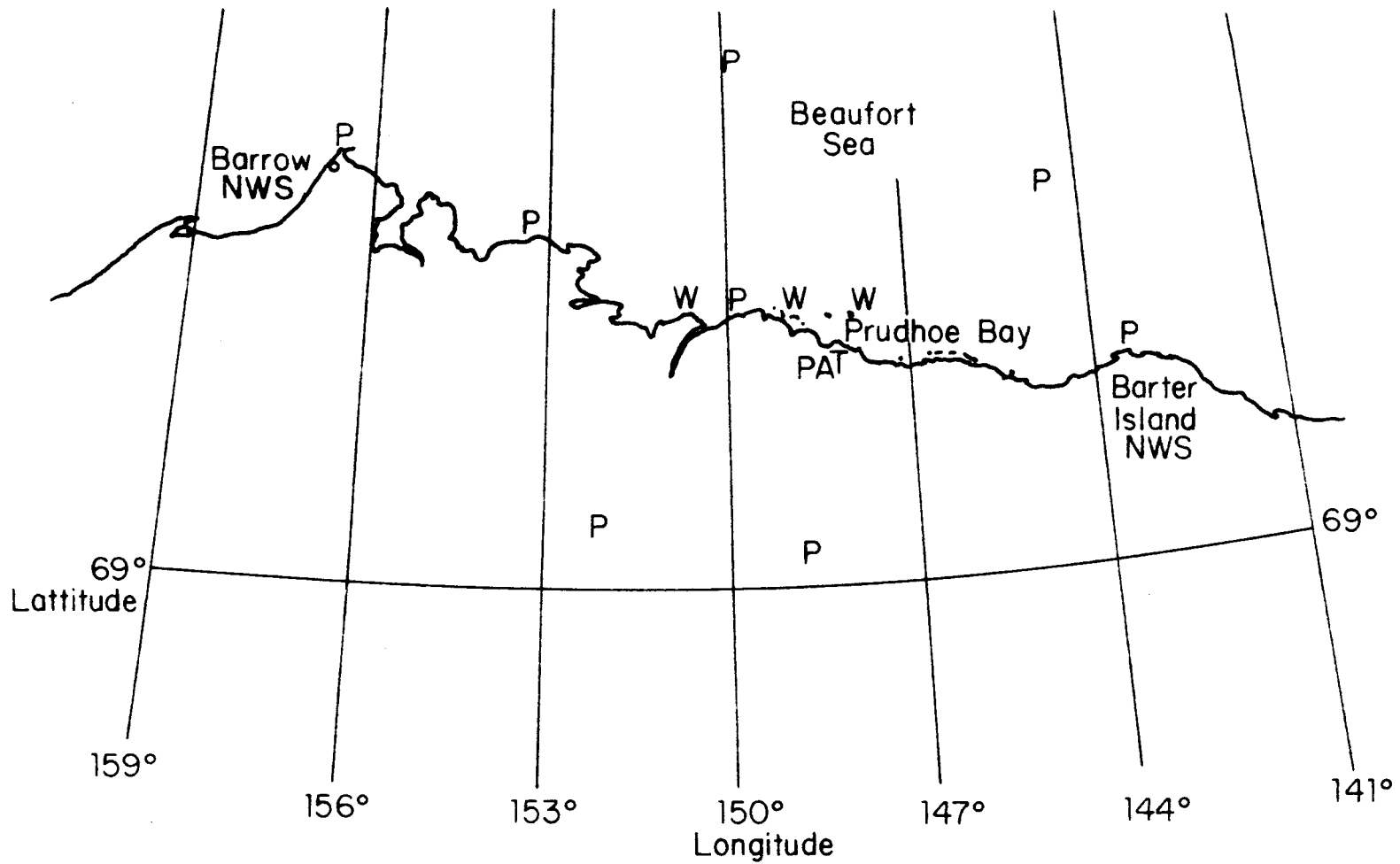
$$\frac{dC}{dt} = - \oint RT d \ln p$$

$$= R \ln \left(\frac{P_0}{P_1} \right) (\bar{T}_2 - \bar{T}_1) > 0$$

$$\Rightarrow \frac{d\bar{v}}{dt} = \frac{R \ln \left(\frac{P_0}{P_1} \right) (\bar{T}_2 - \bar{T}_1)}{2(h+L)} = 1.2 \text{ cm/sec}^2 \quad .57 \text{ cm/sec}^2$$

for $h = 500\text{m}$, $L = 20 \text{ km}$, $\Delta T = 16^\circ\text{C}$
 $P_0 = 1000\text{mb}$, $P_1 = 950 \text{ mb}$

Figure 1.



- Legend:
- P microbarograph site
 - W weatherstation site
 - T tide gauge site
 - NWS national weather service upper air station
 - A acoustic radar site

Figure 2.

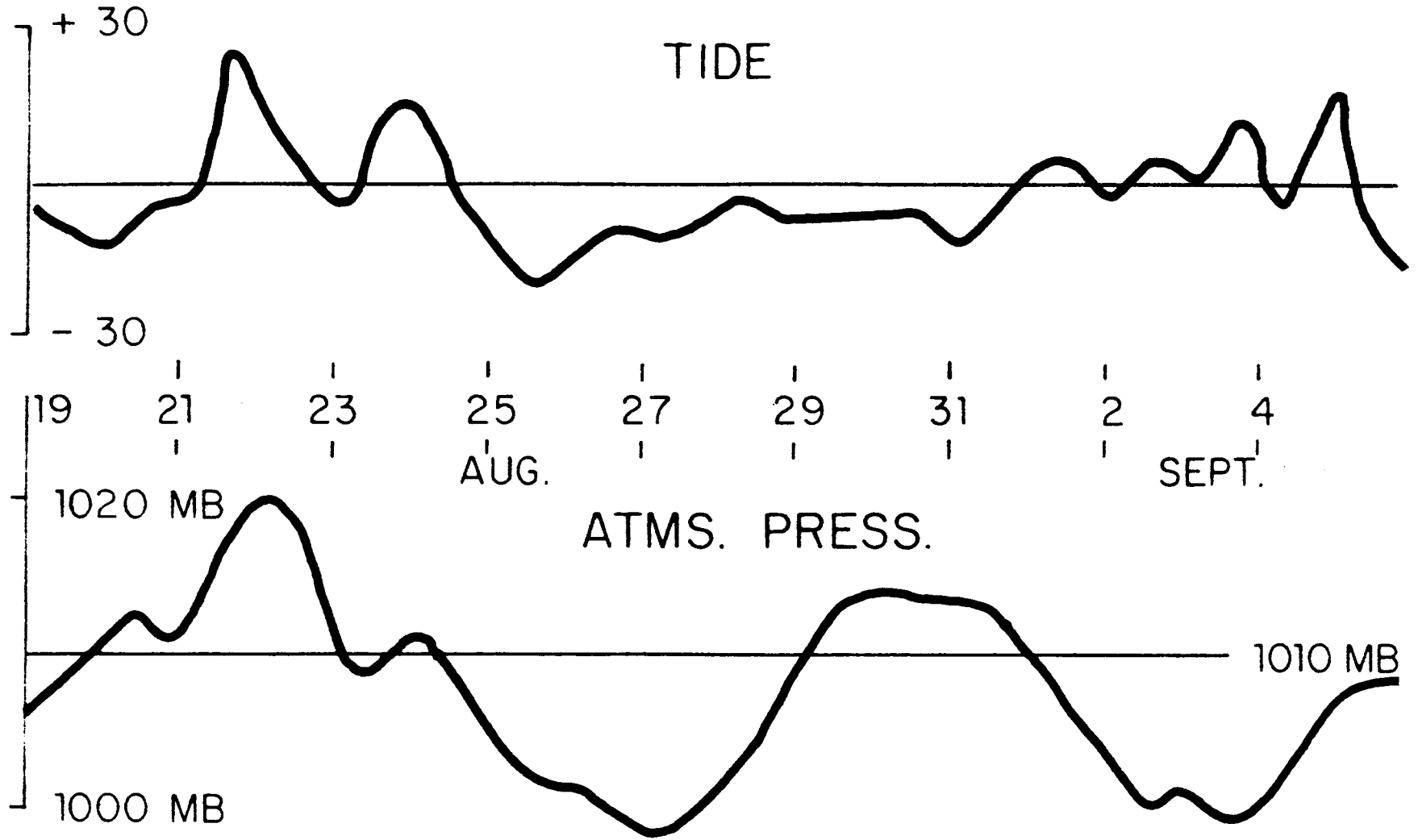
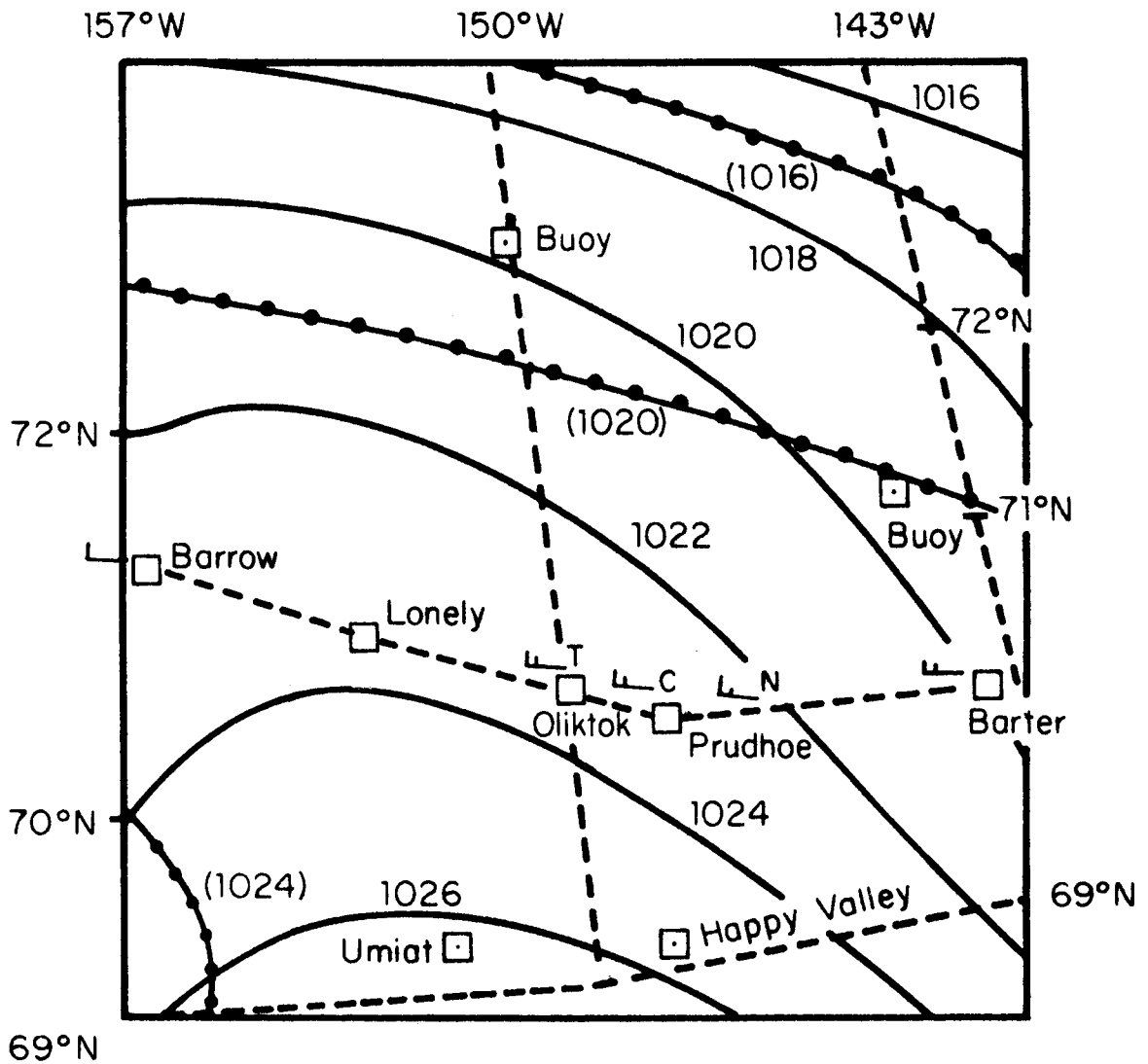


Figure 3.



PRESSURE CONTOURS-MB

----- Approximate Coast Line Orientation

AUG 22 - 000 GMT (1976)

●●● National Weather Service - MB

(T C N) Wind Measurements from Cottle and Narwhal Islands and Tolaktovut Pt.

Figure 4.

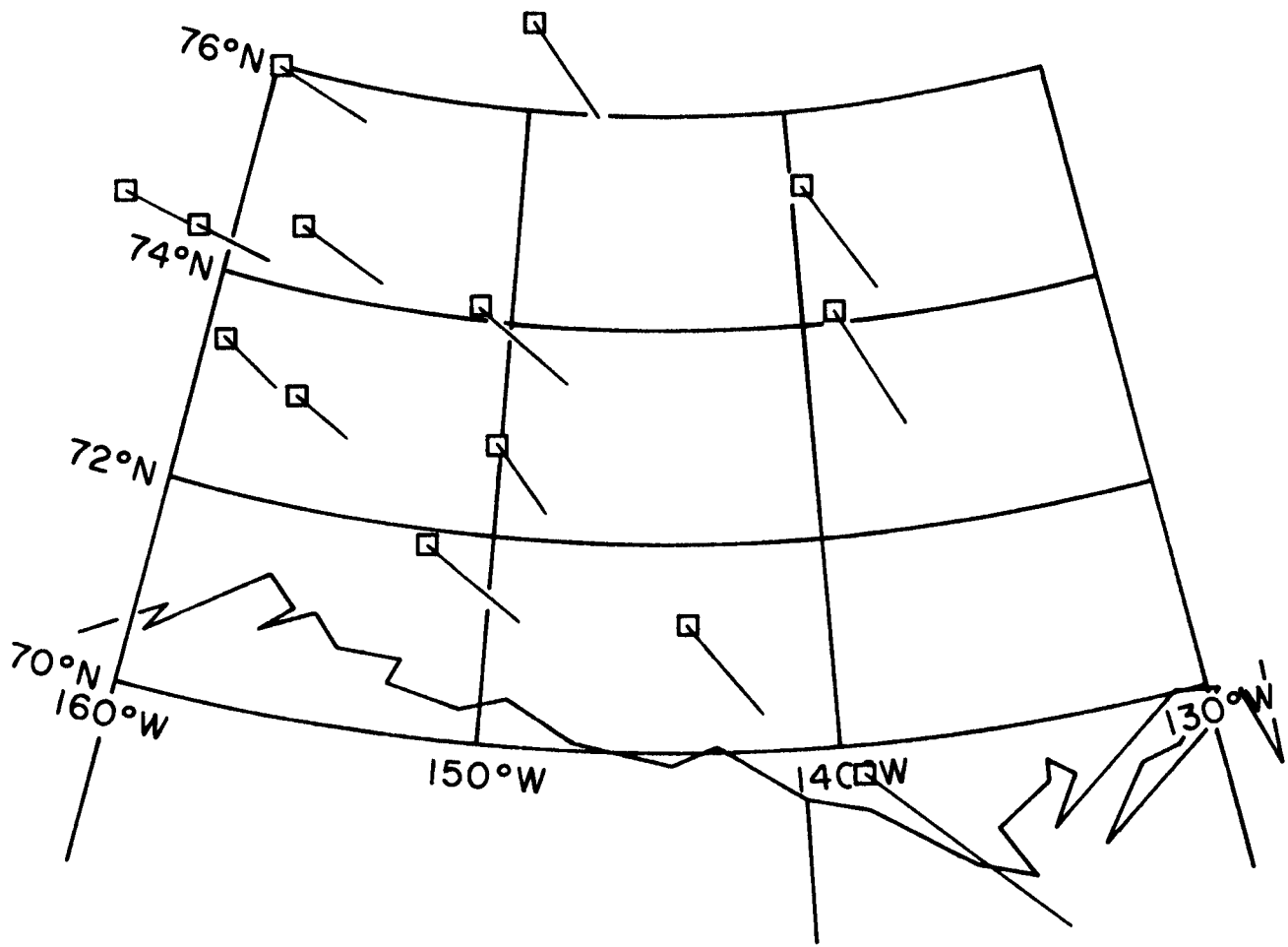
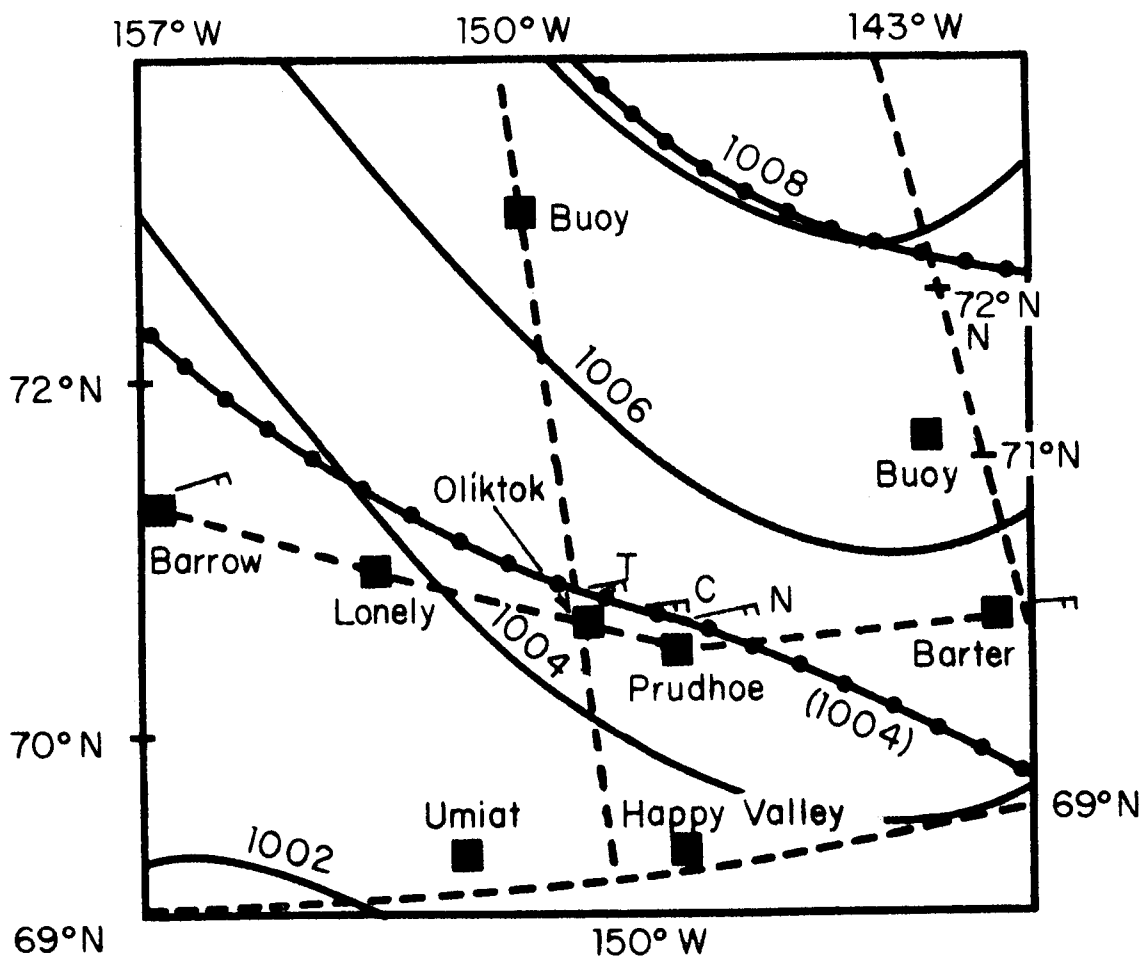


Figure 5.



PRESSURE CONTOURS - MB

----- Approximate Coast Line Orientation
 AUG 26 - 000 GMT (1976)

●-●-● National Weather Service - MB

(→T →C →N) Wind Measurements from Cattle and Narwhal Islands and Tolaktovut Pt.

120 km/inch

Figure 6.

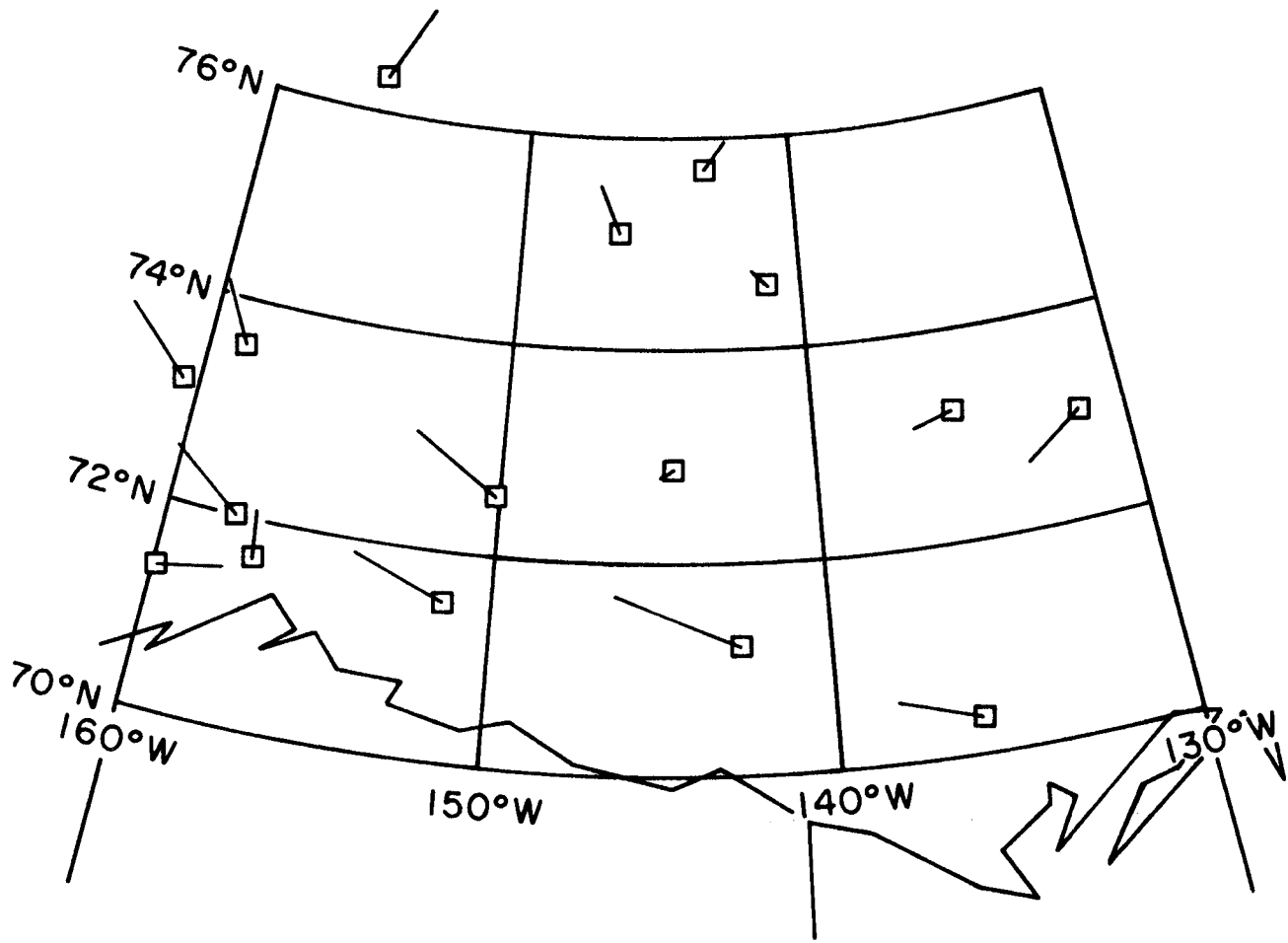
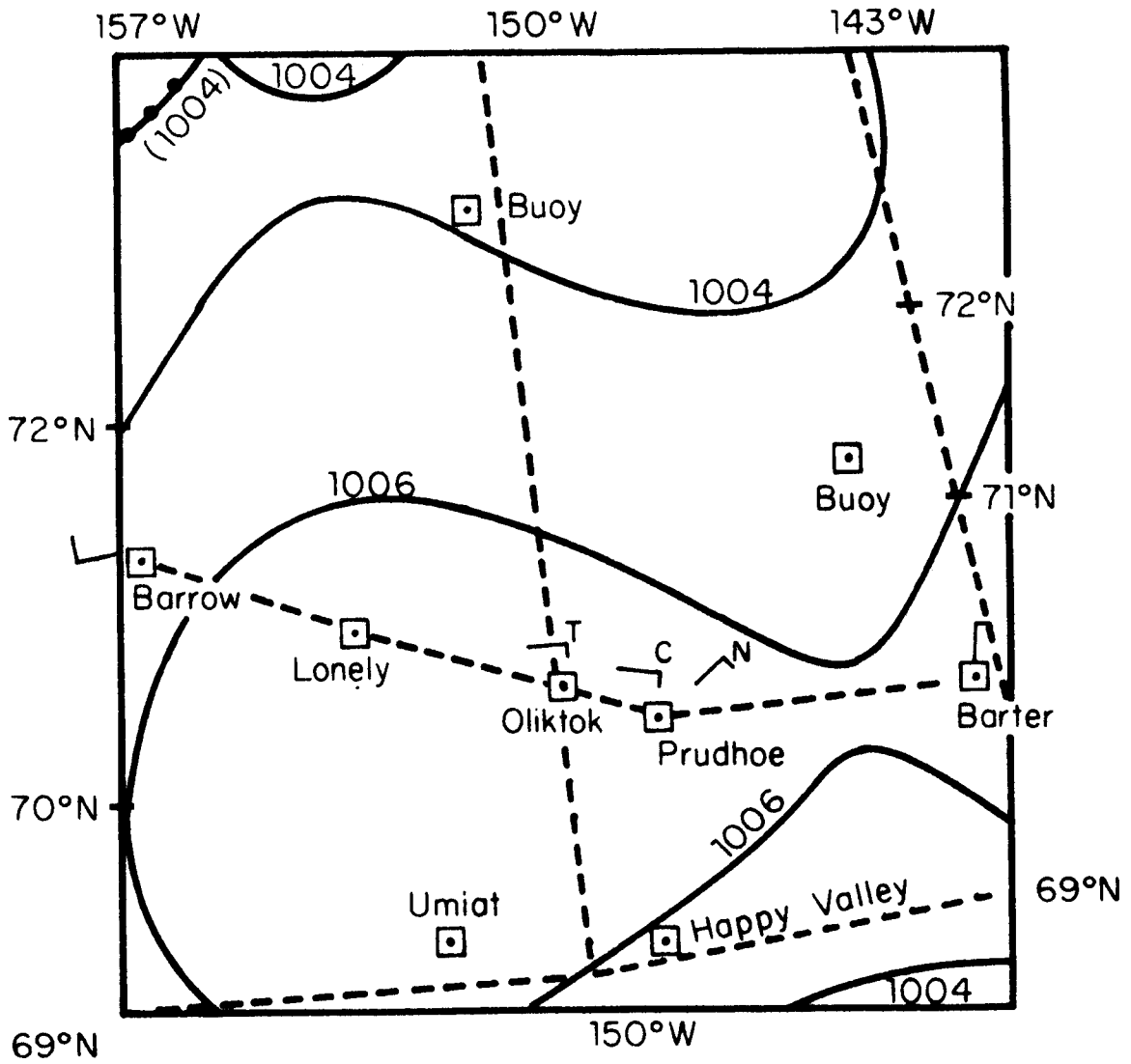


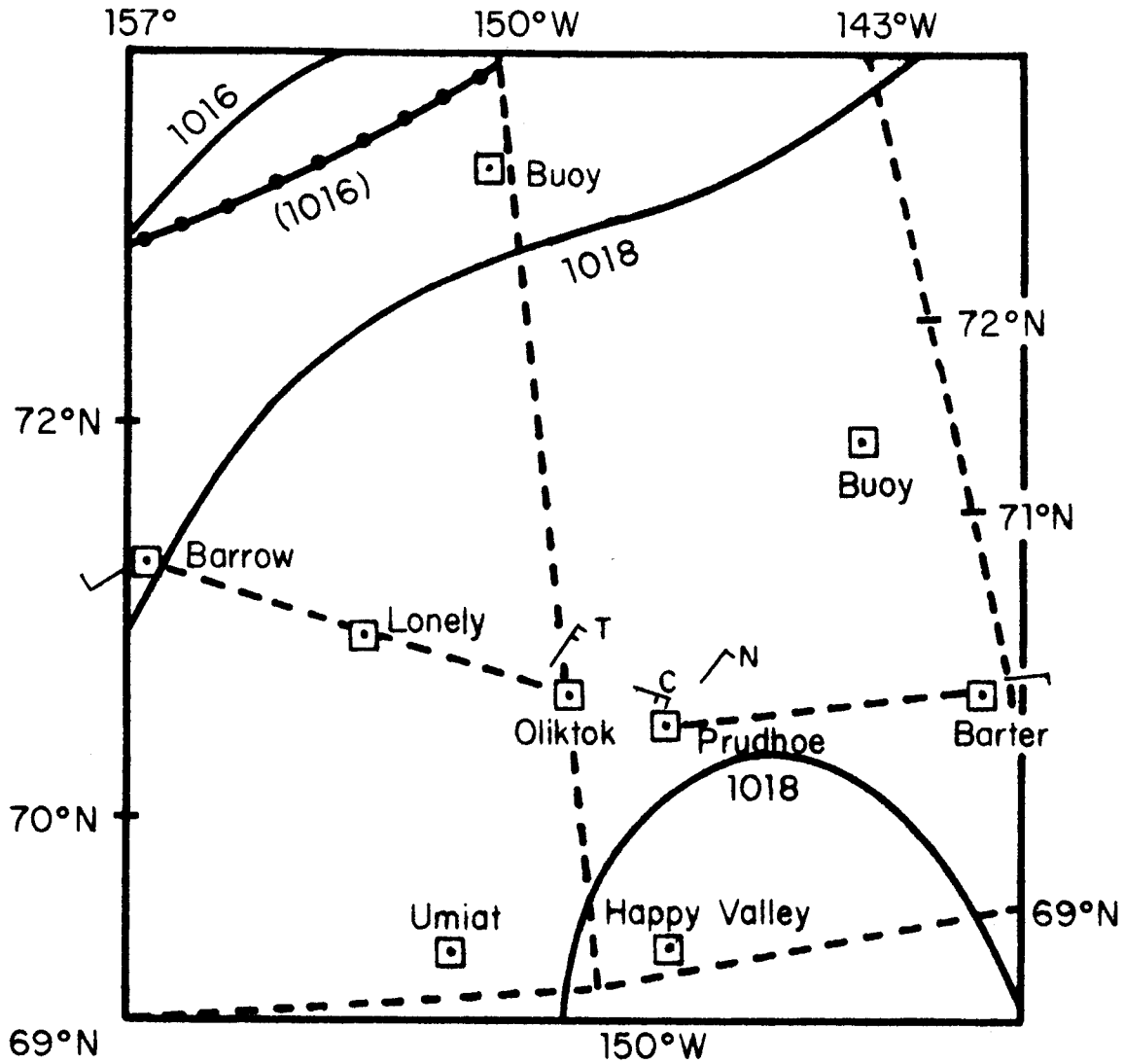
Figure 7.



PRESSURE CONTOURS - MB

- Approximate Coast Line Orientation
- AUG 18-000 GMT (1976)
- National Weather Service - MB
- ($\leftarrow^T \rightarrow^C \leftarrow^N$) Wind Measurements from Cottle and Narwhal Islands and Tolaktovut Pt.

Figure 8.



PRESSURE CONTOURS - MB

----- Approximate Coast Line Orientation

AUG 31 - 000 GMT (1976)

●●●● National Weather Service - MB

(\nearrow T \rightarrow C \nearrow N) Wind Measurements from Cottle and Narwhal Islands and Tolaktovut Pt.

Figure 9.

Line Spectrum Unfiltered Tide Data

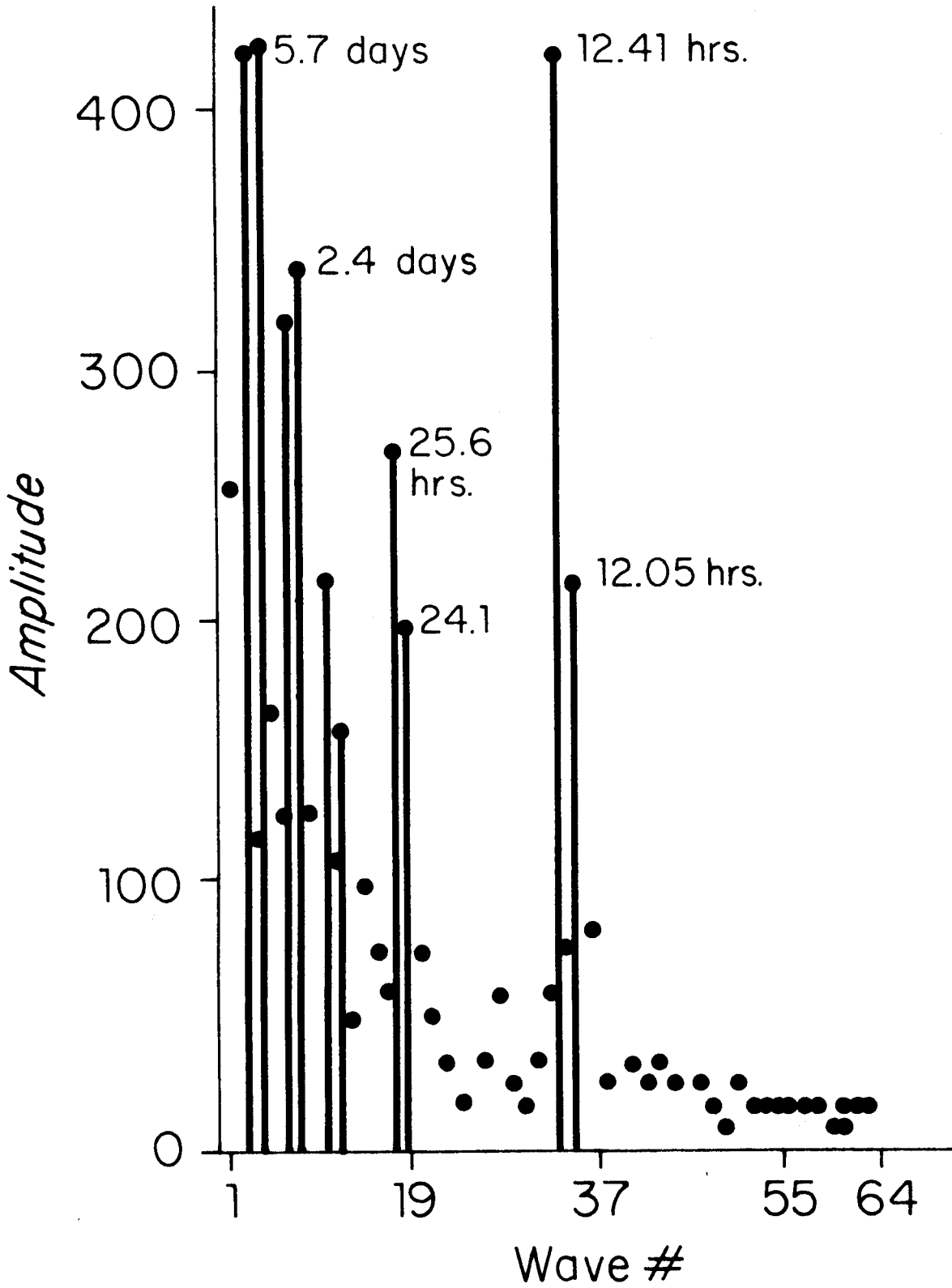


Figure 10.

Figure 11.

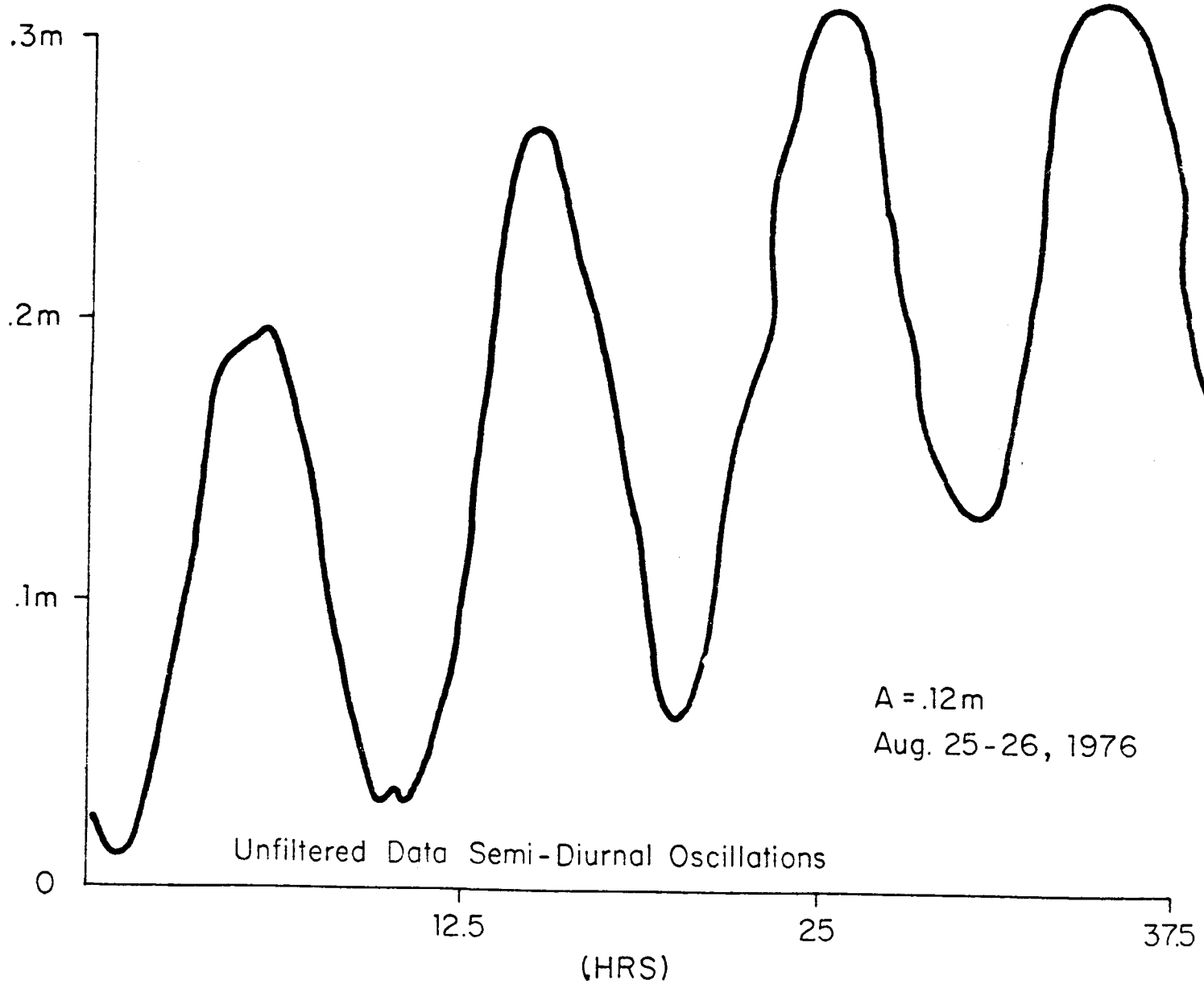
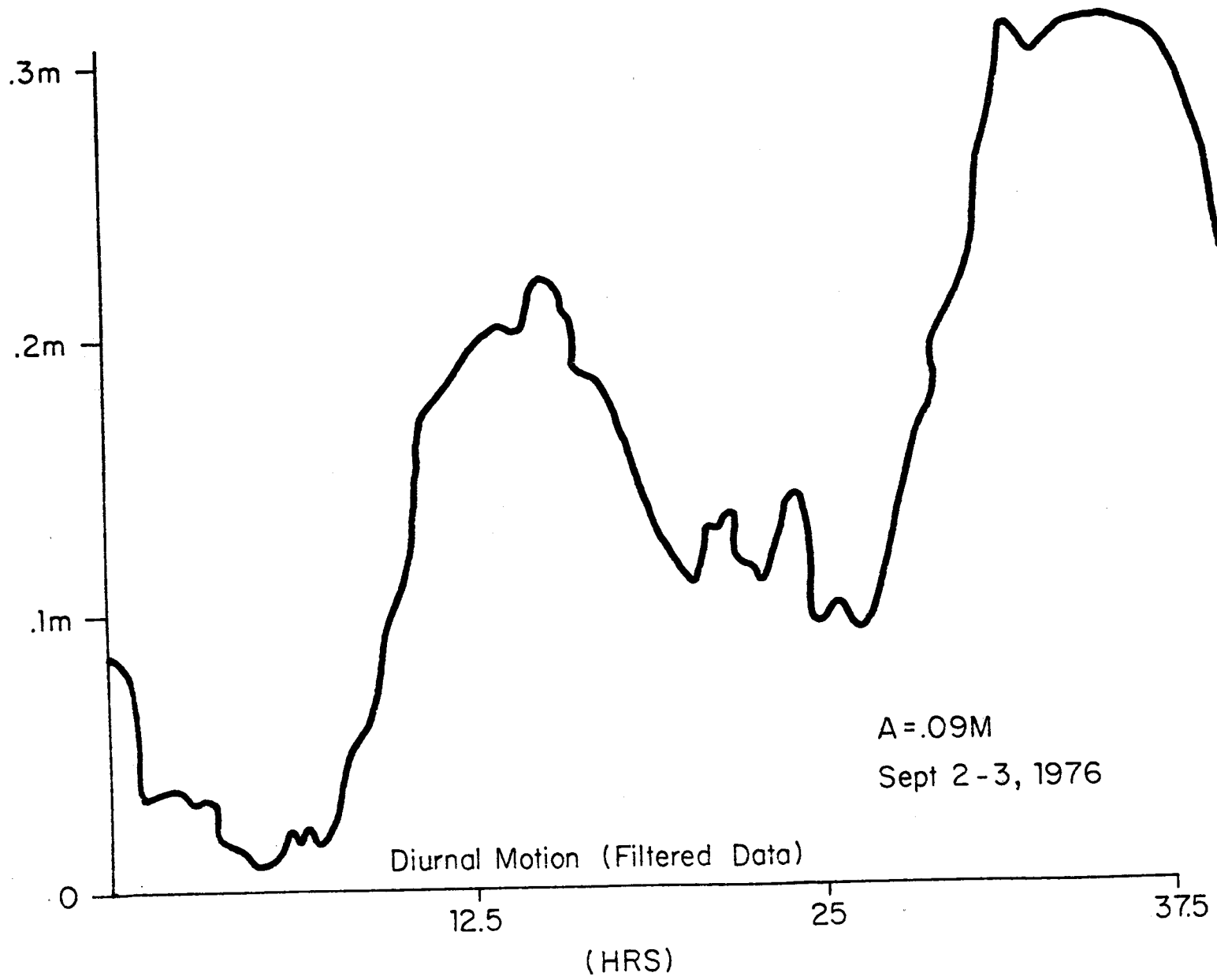


Figure 12.



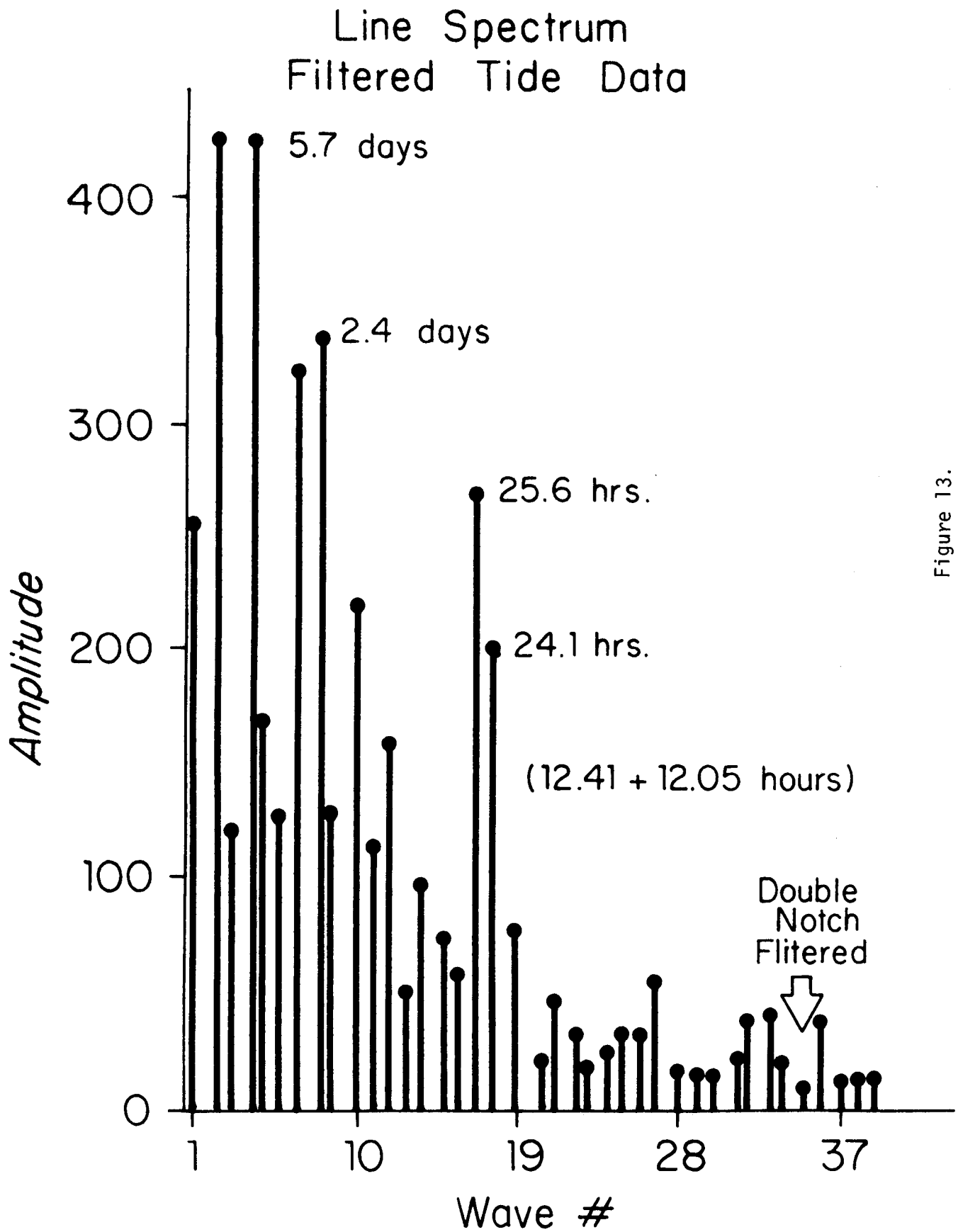


Figure 13.

PROBABLE SEICH MOTION



Figure 14.

22 AUG 1976

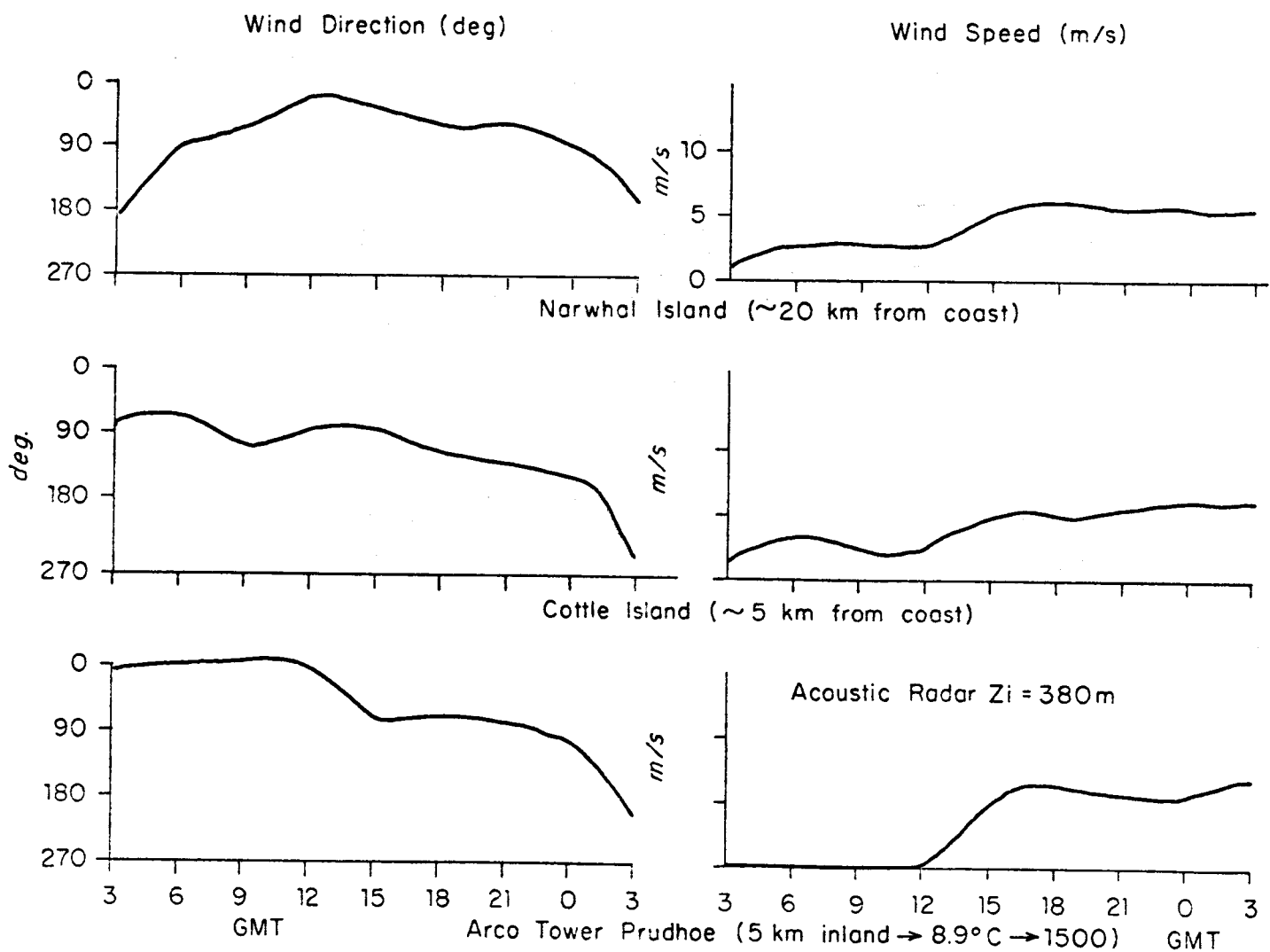


Figure 15.

6 SEPT 1976

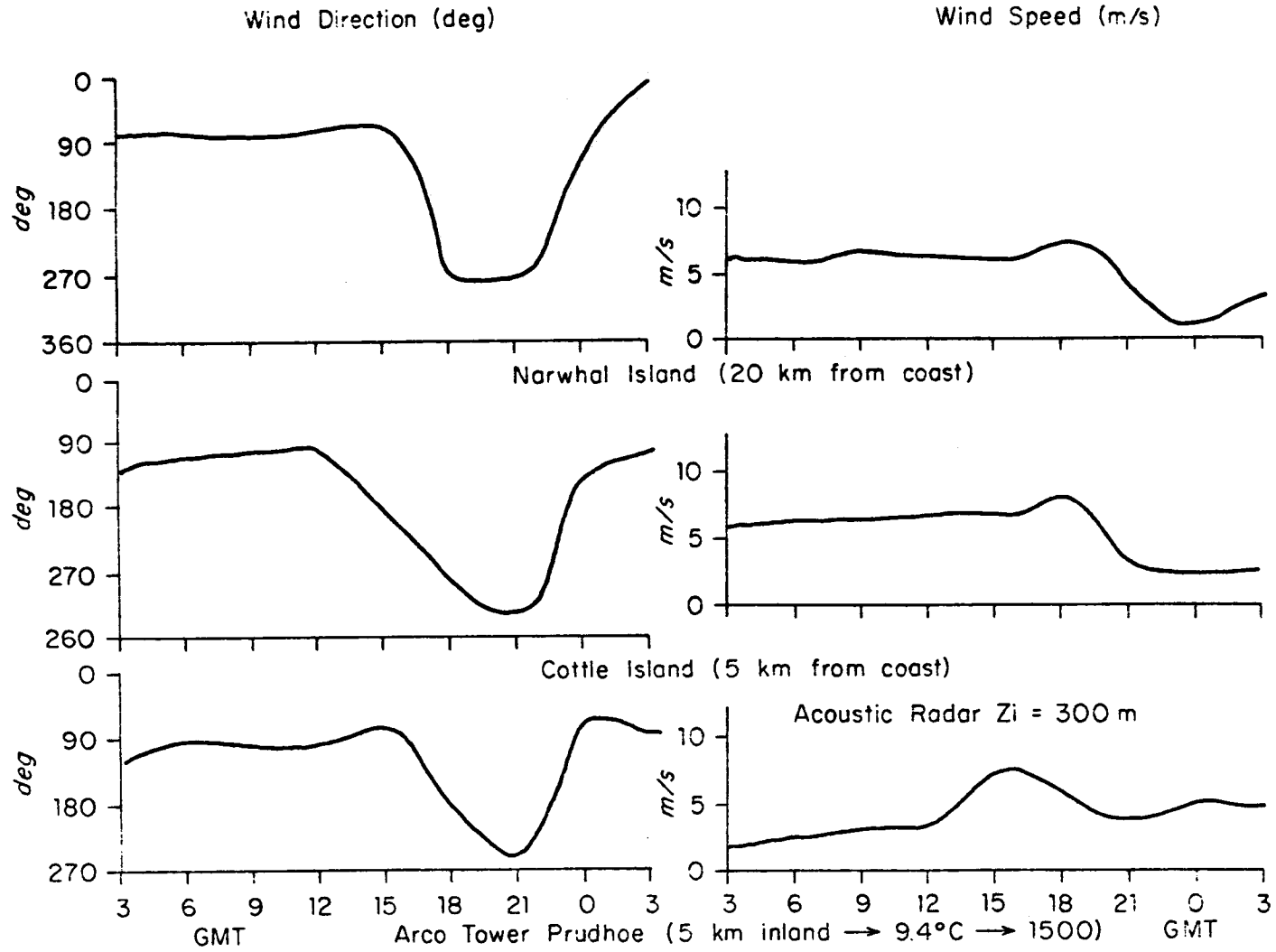


Figure 16.

FIRST ANNUAL REPORT

Contract #R7120840
Research Unit 541
Reporting Period: 1 April 1976-
31 March 1977
Number of Pages: 95

NORTON SOUND/CHUKCHI SEA OCEANOGRAPHIC
PROCESSES (N-COP)

L. K. Coachman¹
R. L. Charnell²
J. D. Schumacher²
K. Aagaard¹
R. D. Muench²

1. Department of Oceanography
University of Washington, WB-10
Seattle, Washington 98195
2. Pacific Marine Environmental Laboratory
3711-15th Avenue, NE
Seattle, Washington 98105

31 March 1977

I. SUMMARY

The objective of this work unit is to relate oceanic advective and diffusive processes to potential pollution problems due to OCS petroleum activities. From data collected, processed and analyzed to date, the following can be concluded. An overall northward flow through the system on the order of $10^6 \text{ m}^3 \text{ s}^{-1}$ (= 1 Sverdrup = 1 Sv) was occurring during late summer 1976.

The circulation in Norton Sound was analyzed from the cruise data of 26 September-6 October. The general flow in the western two-thirds of the Sound was cyclonic, and the bathymetry appears to be important in guiding the flow. There was inflow from the west near bottom in the two deeper troughs, and strong vertical mixing particularly in the northern trough off Nome where there was concentrated an intense westerly outflow. The line Cape Darby-Stuart Island defines a relatively isolated eastern basin, which was filled in late summer with water relict from the previous winter. A two-layered density system reflected presence of upper and lower turbulent boundary layers. The pycnocline suppressed vertical heat flux, and in the eastern basin isolated the coldest bottom water. Water exchange with the western basin was very slow and appeared to be lateral diffusion rather than advection. Four anchored 24-hour stations including direct current measurements showed (1) the strong relationship between flow and the local winds and (2) internal waves on the pycnocline of 2-3 m amplitude and of tidal and higher frequencies.

Preliminary analysis of Kotzebue Sound showed similarities to Norton Sound. The shallow layer in the outer sound appears to participate in a cyclonic circulation which is isolated from both the lower layer and the eastern part of the Sound. Both the high stratification and the presence of cold and salty water, which must have been formed in winter, imply slow dispersion rates in much of the lower layer.

Cross sections from the Bering Strait region showed typical temperature and salinity values. There was a suggestion of small scale (< 50 km) baroclinic features north of Bering Strait.

II. INTRODUCTION

A. OBJECTIVE

The general objective of this work unit is to relate oceanic advective and diffusive processes to potential pollution problems due to OCS petroleum development. Specific goals are:

1. Verification of fluctuations in transport of the predominantly northward flow through the system;
2. Verification, and temporal and spatial description, of the bifurcation of northward flow which takes place west of Point Hope;
3. Definition of temporal and spatial scales of the eddies ubiquitous in the system, and acquisition of the data needed to contribute to a dynamical description; and,
4. Definition of circulation in Norton and Kotzebue sounds.

B. TASKS

The overall task is collection of field data to yield a description of the velocity field, improved understanding of mixing processes, and the relative importance of various driving mechanisms which cause and influence water motion. Specific tasks of the program are:

1. Hydrographic data acquisition. These allow computation of density fields and consequent baroclinic flow effects. Construction of vertical temperature and density sections will allow definition of spatial and temporal variations in the density field. Characterization of water masses by their temperature and salinity characteristics will allow estimation of advective and diffusive effects.
2. Current meter data. These will be used to establish the spatial and temporal flow variability at different locations in the study area. In combination with the density field, they can be used to define

barotropic vs. baroclinic flow and thus to identify possible driving mechanisms. In conjunction with sea level surface variation and surface wind field data, they can be used further in determining driving mechanisms.

3. Water level data. These will be used in conjunction with the systematic current flow variations in addressing driving mechanisms for the flow.
4. Atmospheric data. Surface pressure data will be compared with the water level data and flow variations. Wind data, both directly observed (where available) and geostrophic, may be obtained in certain cases. Both the surface pressure data and the wind data are necessary in analyzing driving mechanisms for flow, particularly in shallow waters such as the area under study.

C. APPLICATION TO PETROLEUM DEVELOPMENT HAZARD ASSESSMENT

Two distinct environmental problems can accompany petroleum development in a marine region, catastrophic spills and long-term or chronic leakage. This research unit addresses both of these problems. The eventual effect of a catastrophic spill depends upon where the spilled oil goes, *i.e.*, its trajectory, how long it takes to get there, and how much diffusion of the oil occurs along the trajectory. This study will provide estimates of the trajectories likely to be followed by spilled oil, and will furnish an indication of dispersion rates for such oil. Oil introduced into the environment via long-term or chronic leakage is more likely to be dispersed throughout the water column and, possibly, scavenged by suspended particulate matter. The problem now becomes one of understanding net transport of suspended matter, a process related to the advective and diffusive fields within the water column. An understanding of these processes requires, in turn, analysis of the velocity field and its driving mechanisms.

III. PRESENT STATE OF KNOWLEDGE

Prior to the present study, oceanographic knowledge of the Bering Strait region was summarized in a monograph by Coachman *et al.* (1975). They have used the results of oceanographic surveys carried out from 1922 until 1973 to define water masses and to estimate seasonal variations and transport of water through the system. The discussion below is abstracted from their work: the reader is referred to that work for additional detail.

A. CIRCULATION

The dominant circulation feature in the Norton-Chukchi region is the net northward flow. Transports measured through a section across Bering Strait are generally 1-2 Sv northward, though there have been a few documented cases of small (0.1-0.2 Sv) southerly transport. This northerly transport is driven by the sea level difference between the North Pacific and Arctic oceans. Significant short-term (< 1 week) fluctuations in the transport may, however, be brought about by regional wind stress variations and, possibly, atmospheric surface pressure fluctuations. Although seasonal variations are not well documented, there is no evidence for a winter decrease in north transport.

Details of the circulation are not well understood. Greater current speeds occur in Bering Strait than elsewhere, due to lateral constriction of the flow. Current speeds of 50-100 cm s⁻¹ are not uncommon there, particularly at times when the mean north flow is augmented by southerly winds. Speeds are highest in the eastern near-surface part of the Strait. North of Bering Strait, there is a bifurcation of the north-flowing current in the region west of Cape Lisburne. One branch of the current flows northeast along the Alaskan coast. A general acceleration of flow to about 40 cm s⁻¹ occurs in the near-shore region just off the Point Hope-Cape Lisburne peninsula. The other branch of the northerly current

flows north-northwest, passing east of Wrangel Island off the Siberian coast. A southeast flow, the Siberian Coastal Current, passes inshore of the north-northwest flow along the Siberian coast and becomes entrained into the north flow just north of Bering Strait. South of Bering Strait, the passages east and west of St. Lawrence Island both contain accelerated north flow, required for continuity with flow through the Strait. A quiet area north-northeast of St. Lawrence Island is characterized by weak and variable flow, as the major north flow passes to the east and west of this region.

The circulation patterns in Norton and Kotzebue sounds are not well understood. There appears to be a tendency for weak cyclonic circulation in the western portions of both these embayments, but nothing is known of circulation in the eastern portions.

The regional tides are complex. In the Bering Strait region they are mixed with the semidiurnal component being dominant. Net peak-to-peak current amplitudes observed north and south of the Strait are on the order of 10 cm s^{-1} . The regional tides are the result of confluence of tidal waves from the Arctic Ocean and the Bering Sea. There appear to be related amphidromic systems in Norton Sound, just south of St. Lawrence Island and in the Gulf of Anadyr.

B. WATER MASSES

Three water masses can be defined for the Bering Strait region; Anadyr, Bering Shelf and Alaskan Coastal waters, with the names reflecting origins. These water masses are defined on the basis of floating salinity, rather than fixed temperature-salinity, values to allow for large year-to-year variations. Temperature, highly non-conservative here, is not useful as a water mass parameter. Vertical stratification of water in the Bering Strait is primarily in temperature, the coldest water being the deepest. Horizontal gradients are primarily in salinity, with the most saline water (Anadyr Water) being to the west and the least saline (Alaskan Coastal Water) to the east.

The Anadyr and Bering Shelf waters originate south of St. Lawrence Island. Alaskan Coastal Water has some contribution from the south, but also a major contribution from Norton Sound. The sharp horizontal gradations between these water masses in Bering Strait suggest that little lateral mixing has occurred between them, hence that lateral mixing between St. Lawrence Island and Bering Strait may be small. North of Bering Strait, Anadyr and Bering Shelf waters mix to become Bering Sea Water, while Alaskan Coastal Water retains its identity and flows northeast along the coast.

Vertical mixing is in large part controlled by vertical stability, which in turn is subject to large seasonal variations. The Bering Sea shelf waters become markedly layered during summer due to fresh water input and solar insolation. The degree of stratification of Alaskan Coastal Water has been correlated with Yukon River discharge. Vertical salinity layering can become so pronounced that it severely restricts vertical heat transfer to the lower water strata. During winter, intense surface cooling and ice formation create vertically uniform water columns.

IV. STUDY AREA

The Norton Sound-Chukchi Sea oceanographic program encompasses the area roughly from St. Lawrence Island in the northern Bering Sea to Cape Lisburne in the Chukchi Sea (Figure 1). It includes Bering Strait, a major avenue for interchange of water between the Bering Sea and the Arctic Ocean, and two major embayments, Norton and Kotzebue sounds. The entire region is classified as continental shelf, and is typified by shallow bottom depths (~ 20 m in Norton and Kotzebue sounds, increasing gradually to ~ 50 m to the west).

The waters of the Norton-Chukchi region are subject to extremely harsh climatological conditions. Winter temperatures drop well below freezing and are often accompanied by high winds. These factors lead to formation of a seasonal ice cover which may reach 10/10 coverage during mid-winter, particularly in the Chukchi Sea.

Fresh-water input into the study region occurs via several large rivers, the Kobuk, Noatak and Yukon rivers along the Alaskan coast, the Anadyr River along the Siberian coast, and innumerable smaller streams. These rivers have highly seasonally variable flow rates, as exemplified by the Yukon which is the largest and attains maximum flows in June-July following melting of interior continental snowfalls (Figure 2).

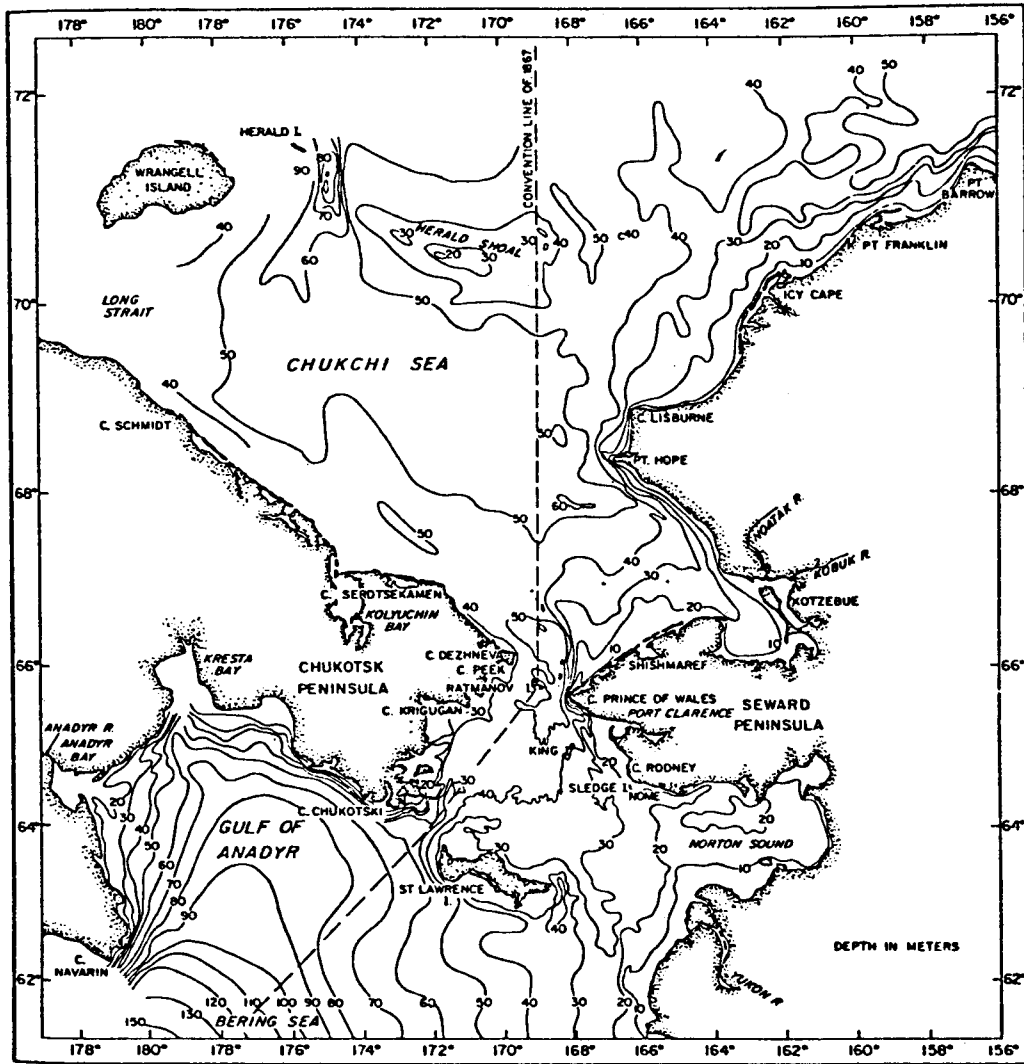


Figure 1. Regional geography and bathymetry for the Norton Sound - Chukchi Sea study area (from Coachman et al., 1975).

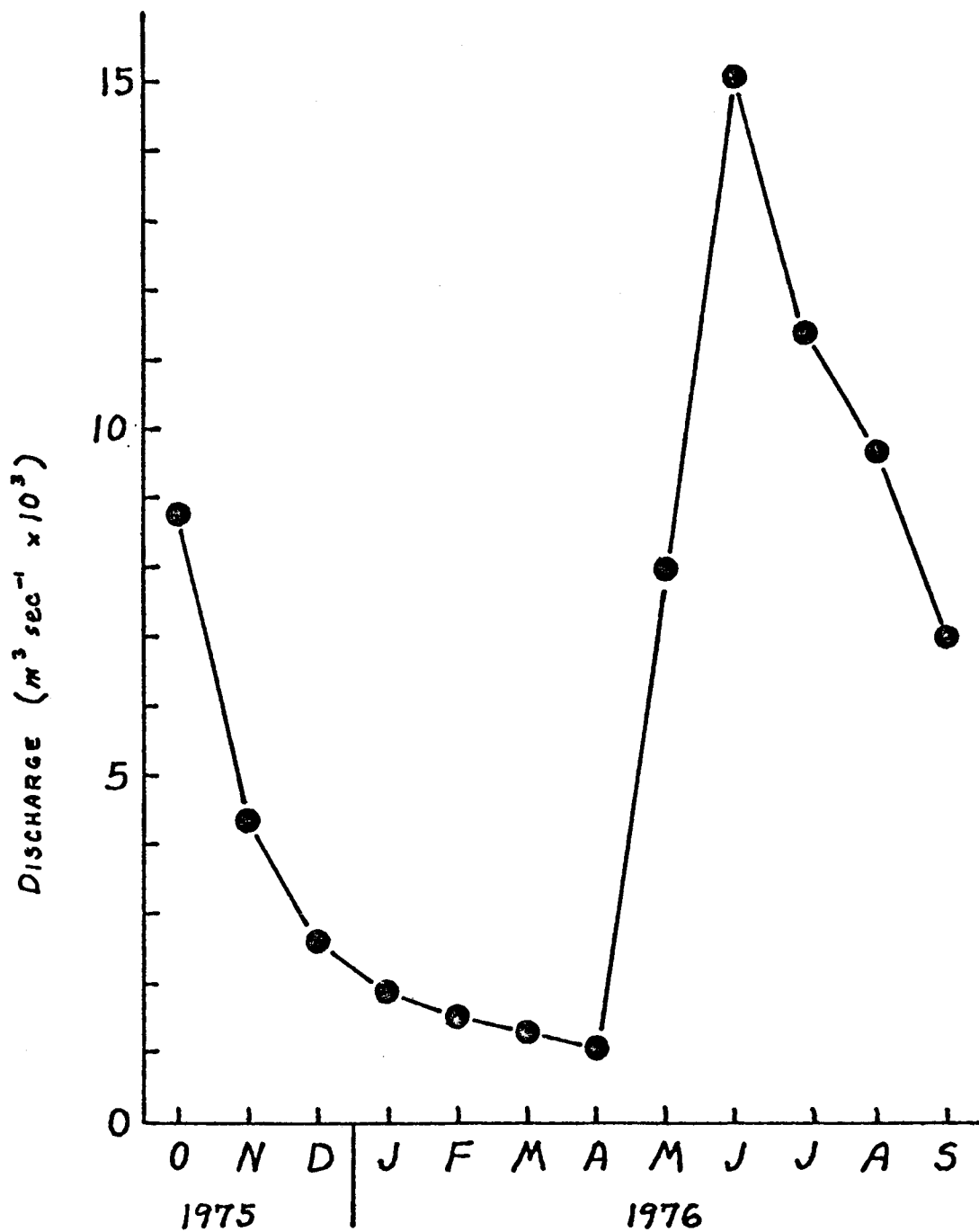


Figure 2 . Monthly mean Yukon River discharge from 1 October 1975 - 30 September 1976 as gauged at Pilot Station, about 180 km. upstream from the river mouth. (This was the first complete annual record from Pilot Station; previous discharge records are from Ruby, considerably farther upstream.)

V. PROGRAM RATIONALE AND METHODS OF DATA COLLECTION

In order to address the goals of this work unit, the following program was completed during the period 1 April 1976-31 March 1977.

Four field programs were completed during the period (Table 1). The first of these, during August-September 1976, obtained temperature and salinity data from the ice edge in the Arctic Ocean southward to the St. Lawrence Island region (Figure 3). Eighteen of the 19 regional moored current meter arrays were deployed during this cruise. The second cruise, carried out during early September 1976, obtained temperature and salinity data primarily from the Chukchi Sea and Kotzebue Sound regions (Figure 4) and carried out anchored current/CTD measurements. The third cruise, in September-October 1976, obtained temperature and salinity data and anchored current/CTD measurements from the Norton Sound region and deployed the remaining one of the 19 regional moored current meter arrays (Figure 5). The fourth field operation was carried out during February-March 1977 using helicopters as platforms; this operation is detailed under Section X of this report, "Summary of Fourth Quarter Operations: N-COP."

In addition to the oceanographic field work, weather data are being routinely collected, as detailed below.

Table 1

Summary of Oceanographic Field Work
During 1 April 1976-31 March 1977: N-COP

<u>Date</u>	<u>Vessel</u>	<u>Chief Scientist</u>	<u>CTD Stations</u>	<u>Anchor Stations</u>	<u>Moorings</u>
8/17/76- 9/3/76	<i>Discoverer</i>	R. B. Tripp	151	0	18
8/31/76- 9/17/76	<i>Moana Wave</i>	L. K. Coachman	83	52	0
9/26/76- 10/6/76	<i>Discoverer</i>	R. D. Muench	45	5	1
1/30/77- 3/2/77	Helicopters	R. B. Tripp	46	0	0

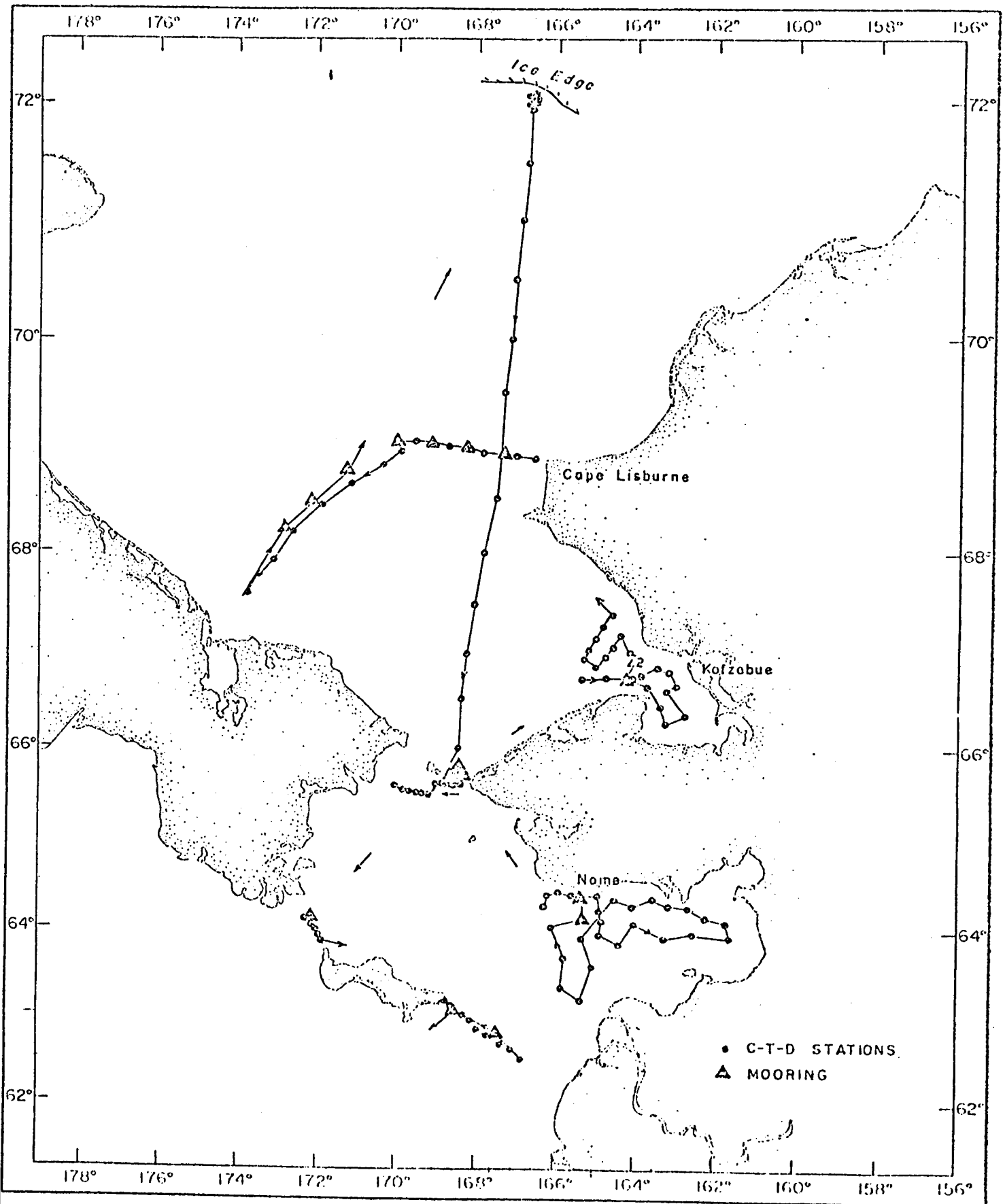


Figure 3. Oceanographic stations occupied during the 17 August-3 September 1976 cruise to the Norton Sound-Chukchi Sea region.

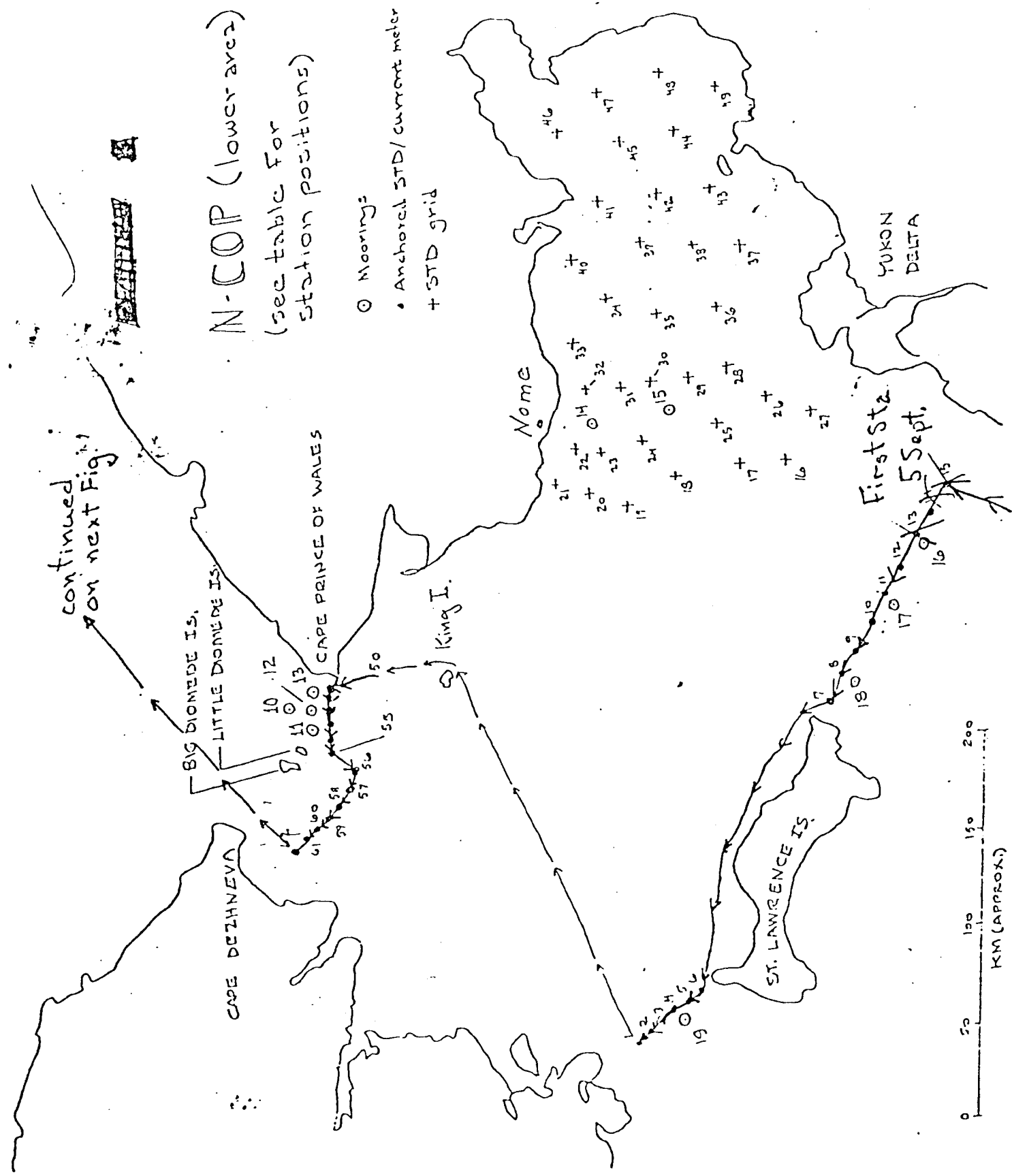


Figure 4A. Track of R/V Moana Wave, 5-14 Sept. 1976.

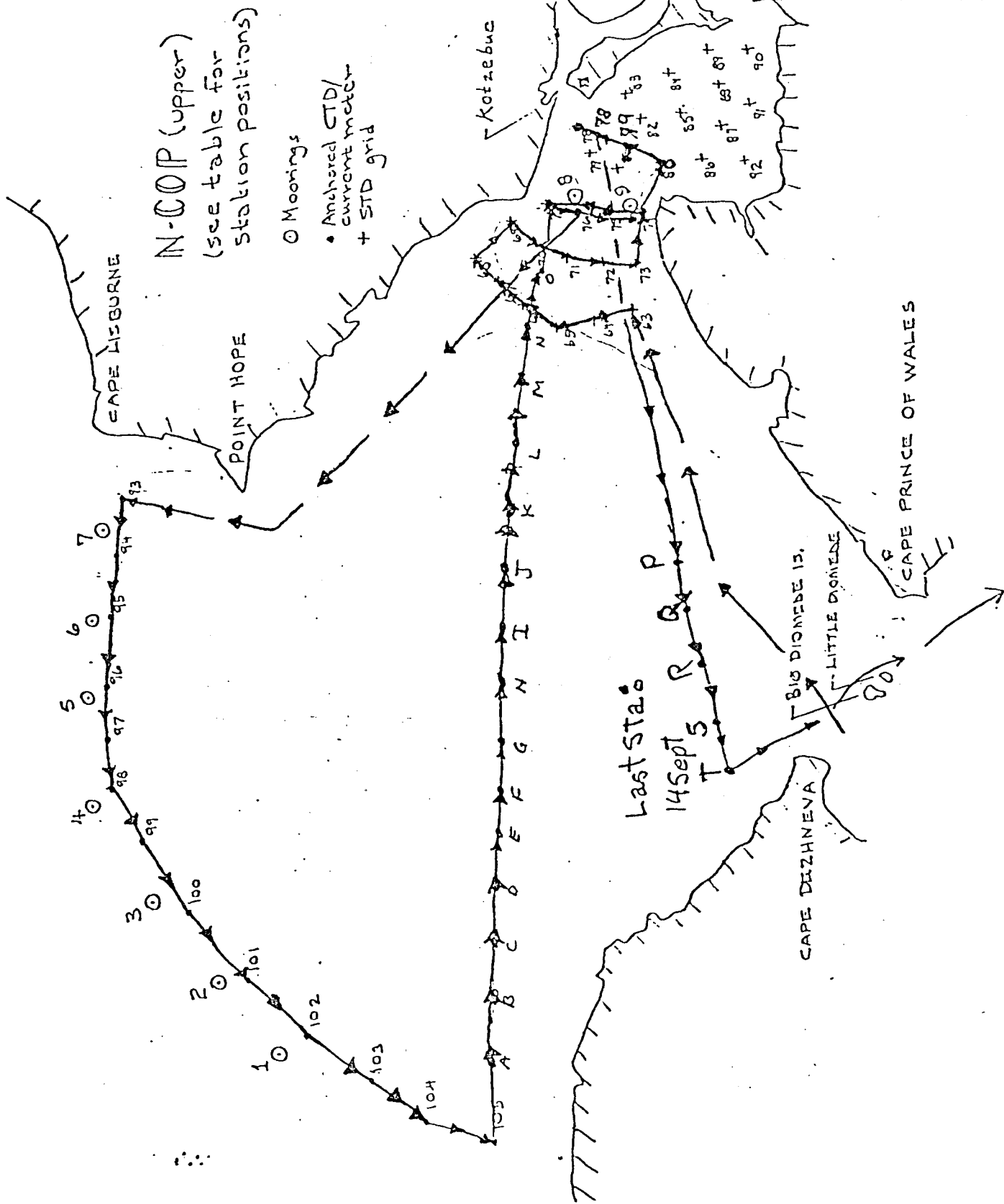


Figure 4B. Track of R/V Moana Wave.

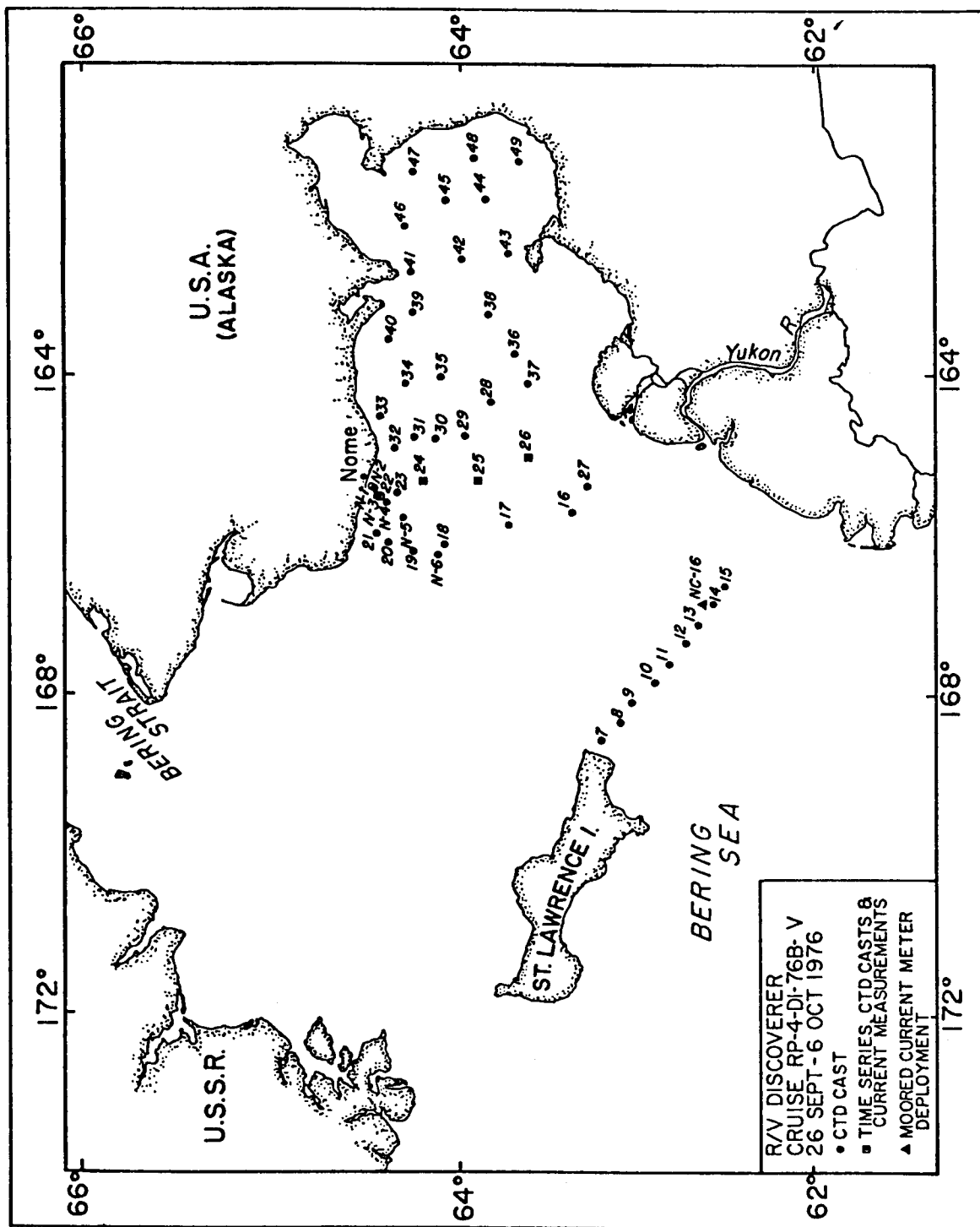


Figure 5. Oceanographic stations occupied during 26 September - 6 October cruise to the Norton Sound region.

A. TEMPERATURE AND SALINITY OBSERVATIONS

All temperature and salinity measurements except those from the February-March program were obtained using Plessey Model 9040 conductivity, salinity, depth (CTD) profiling instruments operating into Plessey digitizers and analog chart recorders. Of the vessels used, *Discoverer* and *Moana Wave*, only the former had the additional back-up recording capability for CTD data of a data acquisition system based on a PDP-11 computer (PODAS). In addition to providing back-up recording, this system also allowed near-real-time monitoring of the incoming temperature and salinity (as derived by the computer from temperature and conductivity) data. In one case, the September-October cruise, the back-up capability was needed as the Plessey digitizer malfunctioned during the latter part of the cruise. The capability of monitoring the data in near-real-time was also judged invaluable.

All data were acquired and processed on board ship according to the PMC manual. Calibration samples were obtained using a rosette or sample bottles on a minimum of every cast except during the Norton Sound time series stations obtained in September-October where every third cast was judged adequate. Salinities for calibration were run aboard the vessels. Raw data and calibration values were returned to the University of Washington (August and early September cruises) and the Pacific Marine Environmental Laboratory (September-October cruises) for final processing and analysis. All final temperature and salinity data products meet the OCSEAP standards for accuracy and format.

B. ANCHORED CURRENT MEASUREMENTS

During the August and September-October cruises to the Norton-Chukchi region, direct current measurements were made at approximately 5 m intervals throughout the water column at selected stations while the vessel was at anchor. These

measurements were made using an Aanderaa Model RCM-4 current meter modified to be read out via a cable and deck read-out unit. At each station and depth, the reading was accepted and recorded only after it had been stabilized over a minimum period of 2 minutes to within about 1 cm s^{-1} and about 5° in directional variation. The individual measurements are felt to be accurate to within about 1 cm s^{-1} in speed and 5° in direction except for the near-surface measurements, which may have larger errors due to the uncertain effect of the nearby vessel's hull. It was hoped that waiting for the readings to stabilize would minimize errors due to lowering of the instrument and yawing of the vessel while at anchor. In regions of high current speeds where streaming of the meter may have occurred, observations of wire out, wire angle and the meter depth as obtained from the deck read-out unit were used to check on the true depth of the measurements.

The vessel used during both the August and September-October cruises, the *Discoverer*, was well suited to use of this deck read-out meter. The meter itself was suspended over the side using the port hydro winch just aft of the main oceanographic laboratory, with the electrical cable being fed out and retrieved by hand so that the hydro cable carried the weight of the meter. In this way, no strain was placed on the read-out cable. A 20-pound weight was placed under the meter to help prevent streaming in regions of high current speed. The read-out cable was fed into the oceanographic laboratory via a stuff tube, and the read-out unit thus located out of the weather at a convenient AC power source. Current speed and direction were computed from the read-out unit directly following each station in order to detect possible equipment malfunctions and to monitor the currents in real time. In general, malfunctions were minimal, the only one requiring attention involving apparent corrosion of the contacts where the meter joined the underwater cable. Both the equipment and the set-up aboard the vessel were extremely satisfactory.

C. MOORED CURRENT MEASUREMENTS

Long-term current measurements are presently being obtained via Aanderaa Model RCM-4 recording current meters deployed at 19 locations in the Norton-Chukchi study region (Figure 6). These moorings were deployed during August-September 1976 and will be retrieved during August 1977 to yield a full year of current records at each location.

Regional climatic considerations dictated some features of the moorings (Figure 7). In order to escape contact with surface winter ice, the subsurface floats were placed as deep as possible, about 10 m above the bottom. In regions where high current speeds were expected, Bering Strait, streamlined floats were used to minimize streaming of the arrays. Only a single meter was placed on each array, in anticipation of the vertical homogeneity of the water which obtains during a major part of the year and also for reasons of practicality. The meters themselves were modified to record for a full one-year period at 40-minute intervals. AMF acoustic releases are provided on each mooring for retrieval, and three of the moorings are provided with pressure sensors (Aanderaa) in addition to the current meters (Figure 6). In addition, a tide gauge was installed at Nome; technical difficulties, however, have prevented obtaining usable information from this gauge to date.

D. ATMOSPHERIC PRESSURE DATA

Atmospheric surface pressure data are being collected at the locations indicated on Figure 6. Eight of these stations were already operative prior to this project, five reporting data to the NWS, and barograph charts being obtained from the remaining three stations by special arrangement. In addition, two stations were supplied with barographs from which charts are now being received. The status of these weather stations is indicated in Table 2.

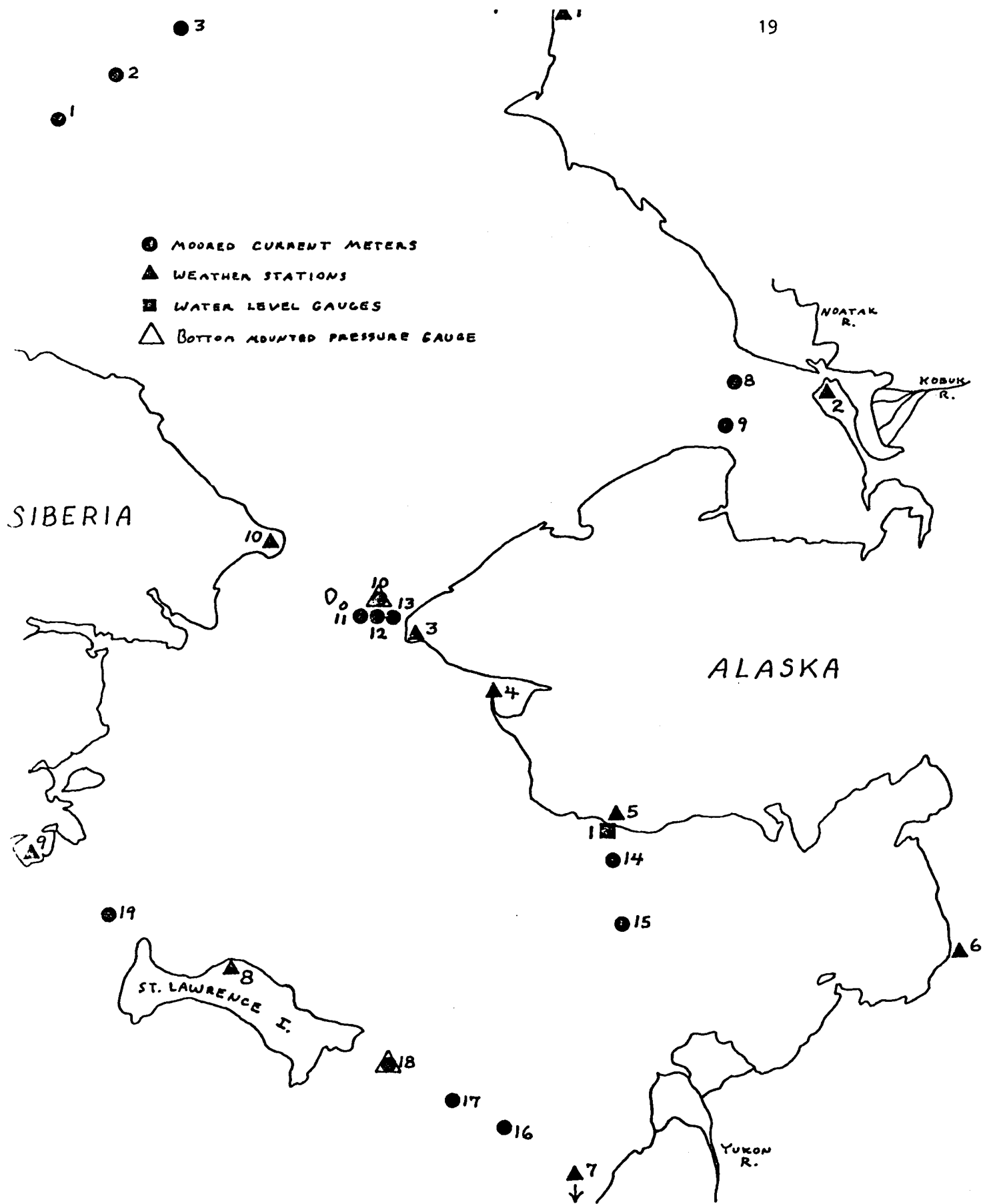
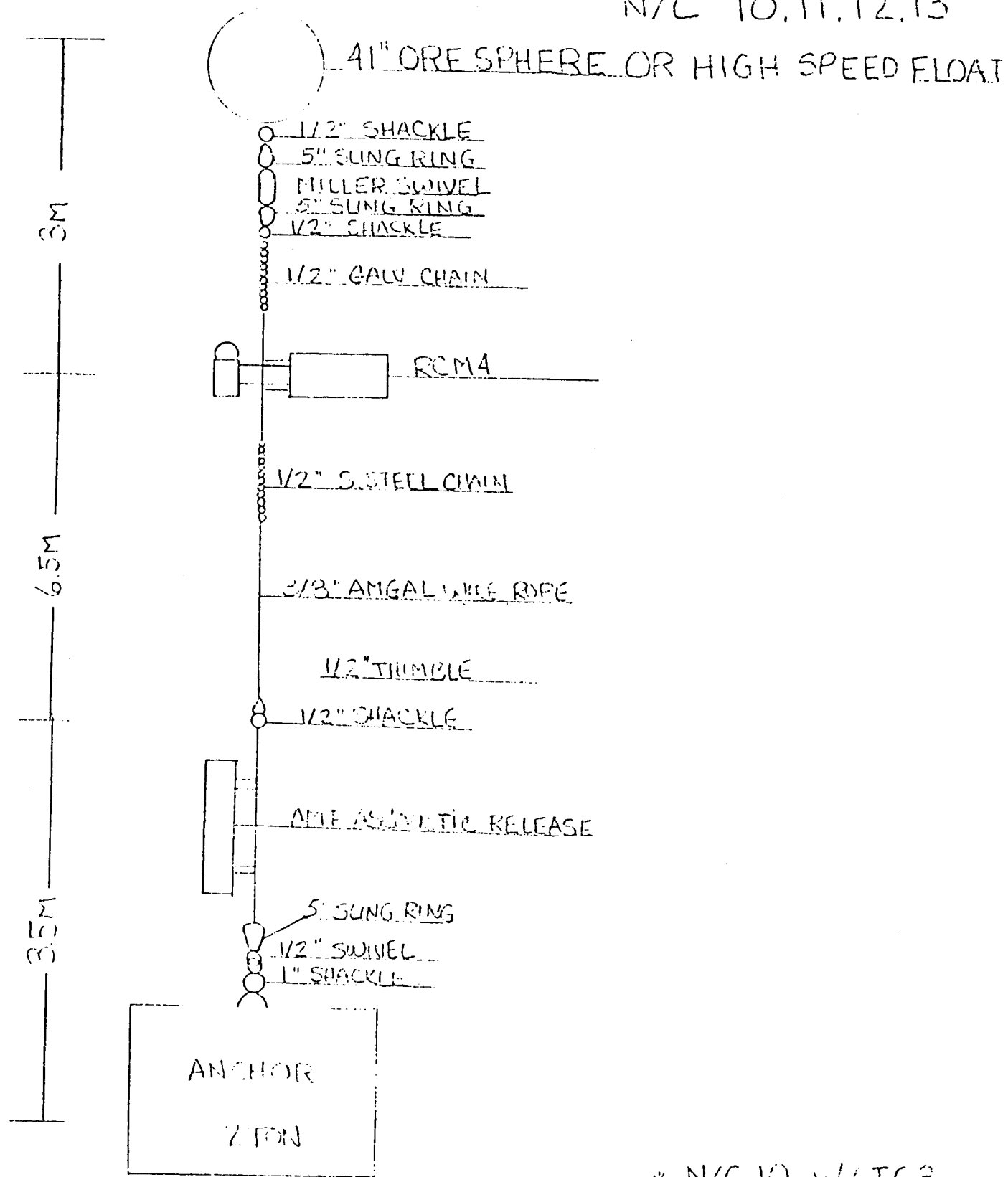


Figure 6. Locations of remote recording oceanographic instrumentation presently deployed in the Norton-Chukchi region.

BERING STRAIT

N/C 10*, 11, 12, 13



* N/C 10 w/ TG3

Figure 7. Example of the moored current meter configuration used in the Norton-Chukchi study region.

TABLE 2. N-COP WEATHER STATIONS (surface pressure data)

<u>Number</u>	<u>Location</u>	<u>Dates</u>	<u>Comments</u>
1	C. Lisburne	August 1976-pres.	Permanent USAF station; barograph charts sent to PMEL ¹
2	Kotzebue	Continuing	Permanent NWS station; current and historical data avail. ²
3	Tin City	August 1976-pres.	Permanent USAF station; barograph charts sent to PMEL
4	Port Clarence	December 1976-pres.	Permanent USCG LORAN site; barograph charts sent to PMEL; barograph supplied by PMEL
5	Nome	Continuing	Permanent NWS station; current and historical data avail.
6	Unalakleet	Continuing	Permanent NWS station; current and historical data avail.
7	C. Romanzof	August 1976-pres.	Permanent USAF station; barograph charts sent to PMEL
8	Savoonga	December 1976-pres.	Wien Airlines office; barograph supplied by PMEL, and barograph charts sent to PMEL ³
9	Kivak, USSR	Continuing	Current data available through NWS
10	Uelen, USSR	Continuing	Current data available through NWS

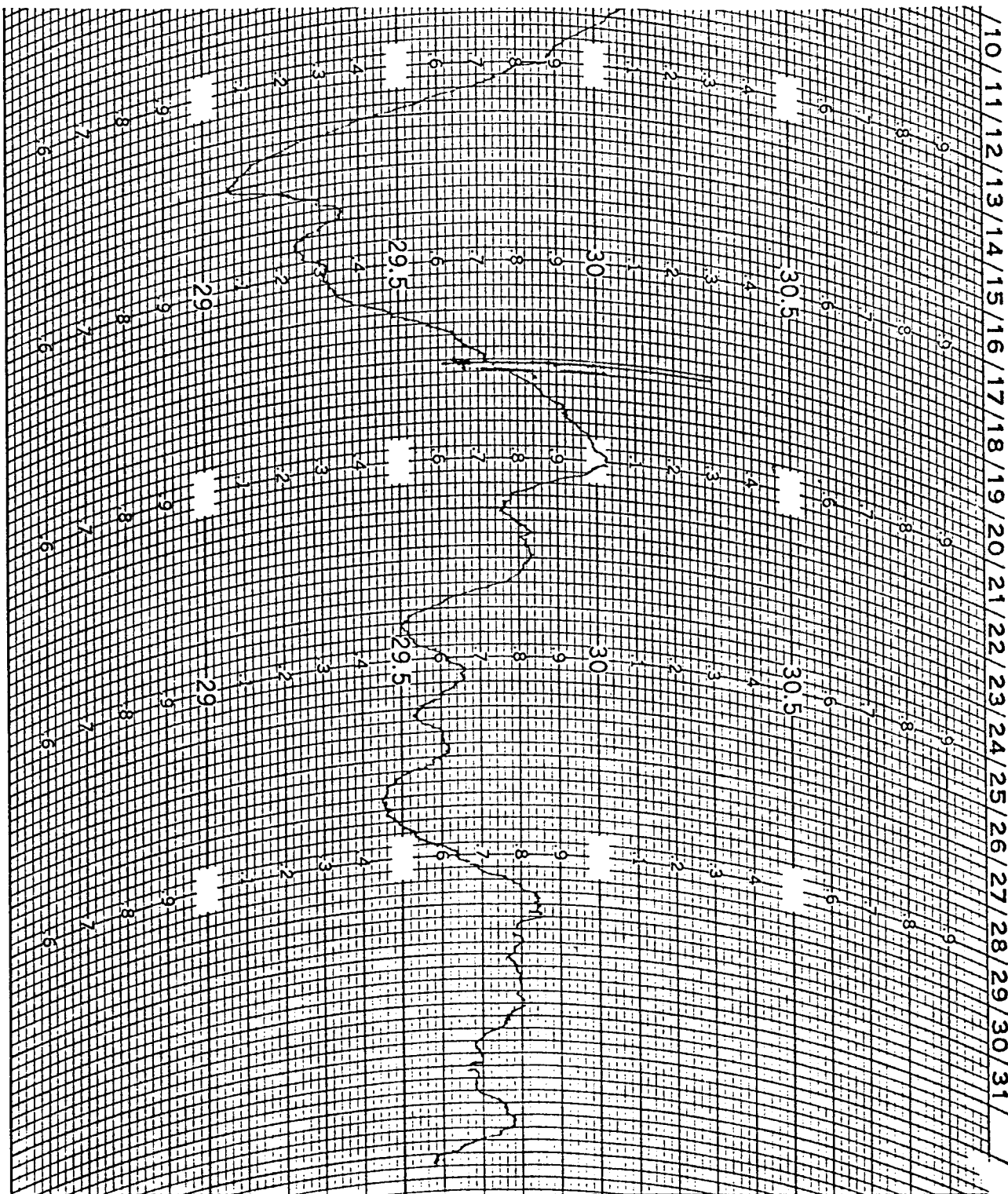
1. Each chart records over a one month period. Charts are sent monthly.
2. NWS data are received currently as surface pressure charts. Historical data are in the form of summaries and daily log sheets.
3. Pressure data from Savoonga are not calibrated, due to lack of a calibration facility there, but the records are adequate for detecting variations.

Barometric pressure data presently in hand are in the form of barograph charts, an example of which is shown in Figure 8. These charts will be digitized using a PDP-11 computer with graphics table; the requisite software is presently being developed. Continuous data coverage via barograph charts now on hand is given in Table 3. Pressure data from the remaining stations will be obtained from NWS as copies of daily weather log sheets.

Table 3

Continuous Atmospheric Pressure Data
(as Barograph Charts) Presently in Possession

<u>Location</u>	<u>Dates</u>
Cape Lisburne AFS, Alaska	16 June 1976-28 Feb. 1977
Cape Romanzof AFS, Alaska	2 Sept. 1976-31 Dec. 1976
Tin City AFS, Alaska	1 Aug. 1976-25 Feb. 1977
Port Clarence CGS, Alaska	18 Nov. 1976-1 Mar. 1977
Savoonga, Alaska	8 Dec. 1976-1 Mar. 1977



OBSERVER C. Noonwood ON 1 ^{AM} Dec 8 1976
 STATION Savoonga OFF 1145 ^{AM} Jan 1 1977

Figure 8. Example of atmospheric surface pressure record obtained via PMEL-provided barograph located at the Wien Airlines Office in Savoonga, St. Lawrence Island.

VI. RESULTS

A. THE SEPTEMBER-OCTOBER NORTON SOUND PROGRAM

Sufficient coverage was obtained in Norton Sound during the September-October cruise to yield insight into processes prevailing there. Figure 9 shows the station locations and the bathymetry in meters.

Distribution of density and temperature. Density and temperature derived from continuous vertical CTD profiles accurately reflect oceanographic conditions in Norton Sound. Density is the dynamically significant variable, while temperature is useful as a water mass tracer. Salinity exerts a dominant control over density at the temperatures encountered, and thus approximately duplicates the density distribution. Density is represented herein by sigma- t (σ_t).

Norton Sound was characterized by two well-mixed layers during September-October 1976 (Figures 10 and 11). Vertically well-mixed upper and lower layers were separated by a pycnocline which was more pronounced at the head ($2.5 \sigma_t$ units m^{-1}) than at the mouth ($1.5 \sigma_t$ units m^{-1}). A gradual seaward density increase (about $2 \sigma_t$ units) was present between station 42 and the mouth, but was absent from the eastern portion between stations 42 and 48 (Figure 10). There was, in fact, a reversal of this east-west gradient in the eastern third where water of $\sigma_t > 23$ was present. A weak south-north density decrease occurred above the pycnocline, while below the pycnocline density was nearly uniform (Figure 11). In western reaches of the Sound, density distribution exhibited considerable complexity particularly in the near-shore region off Nome. A layer of high density water ($\sigma_t > 24$) occurred along the bottom in the deep trough along the north coast, attenuating to the east until it was no longer present (cf. station 33). A band of low density water ($\sigma_t < 21$) was present along the coast off Nome, but did not appear to extend east or west for any great distance; it did not appear at station

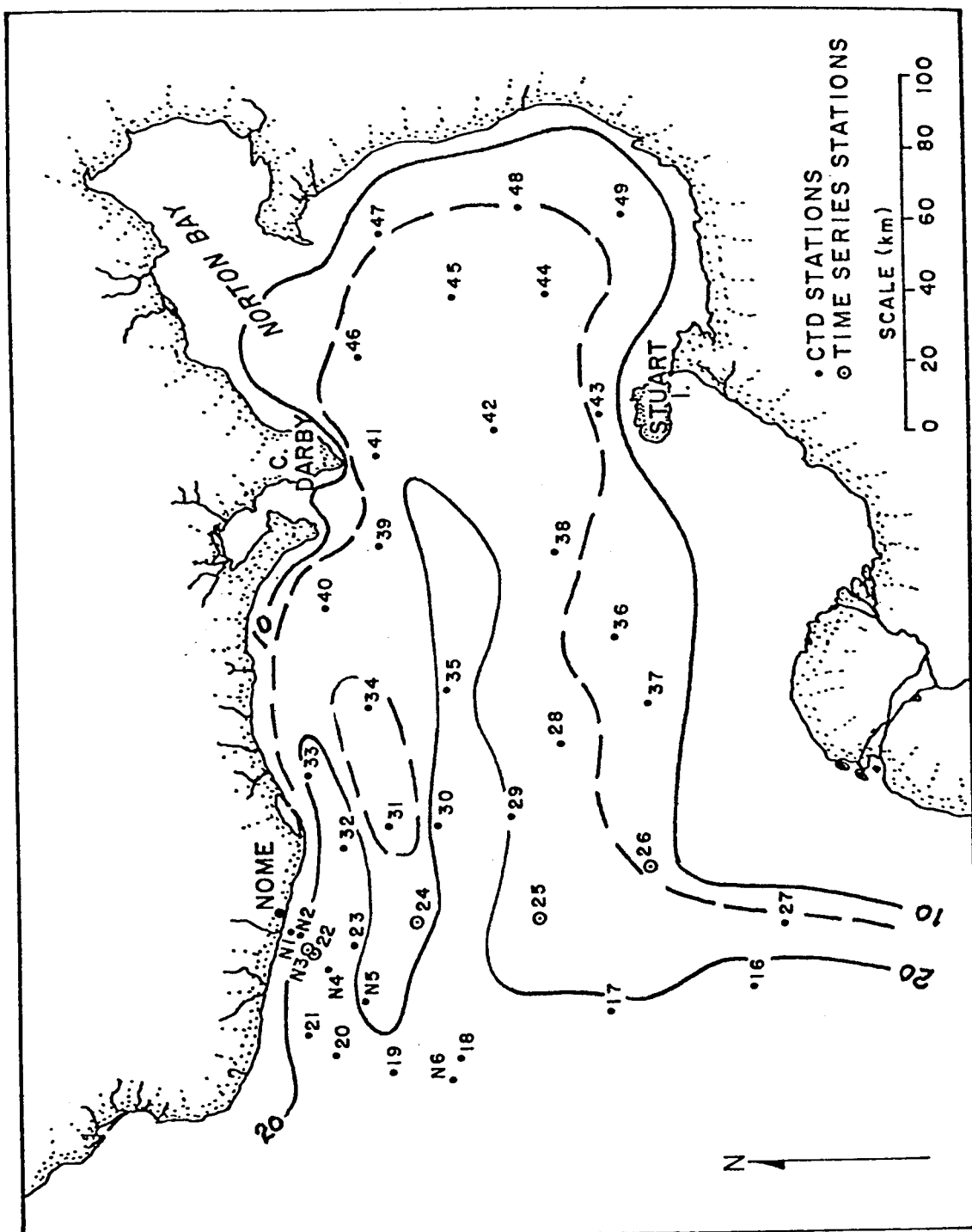


Figure 9. CTD and time series oceanographic stations occupied in Norton Sound during September-October 1976. Isobaths in meters, contoured from CEGS 9302.

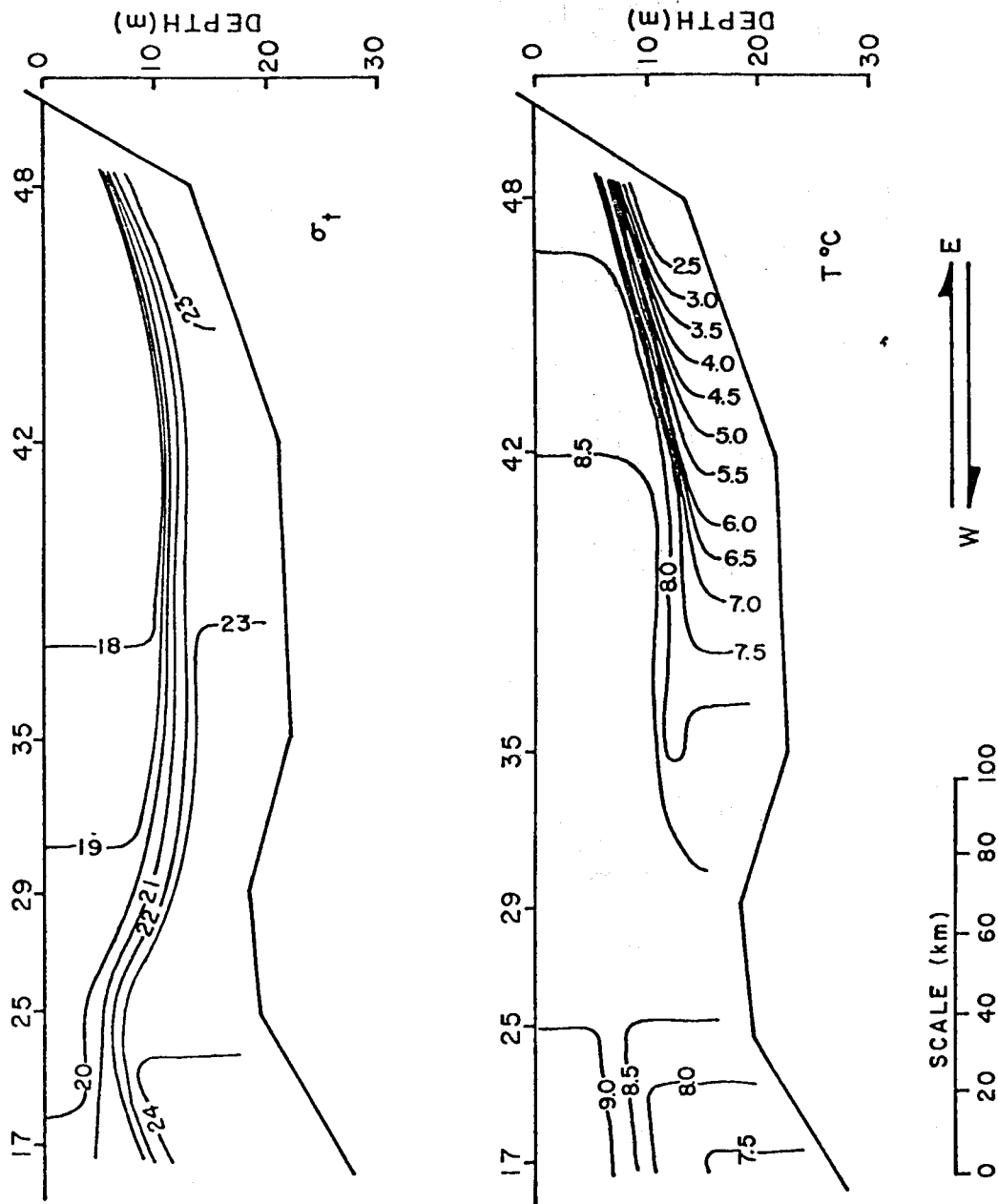


Figure 10. Longitudinal density and temperature distributions in Norton Sound during September-October 1976.

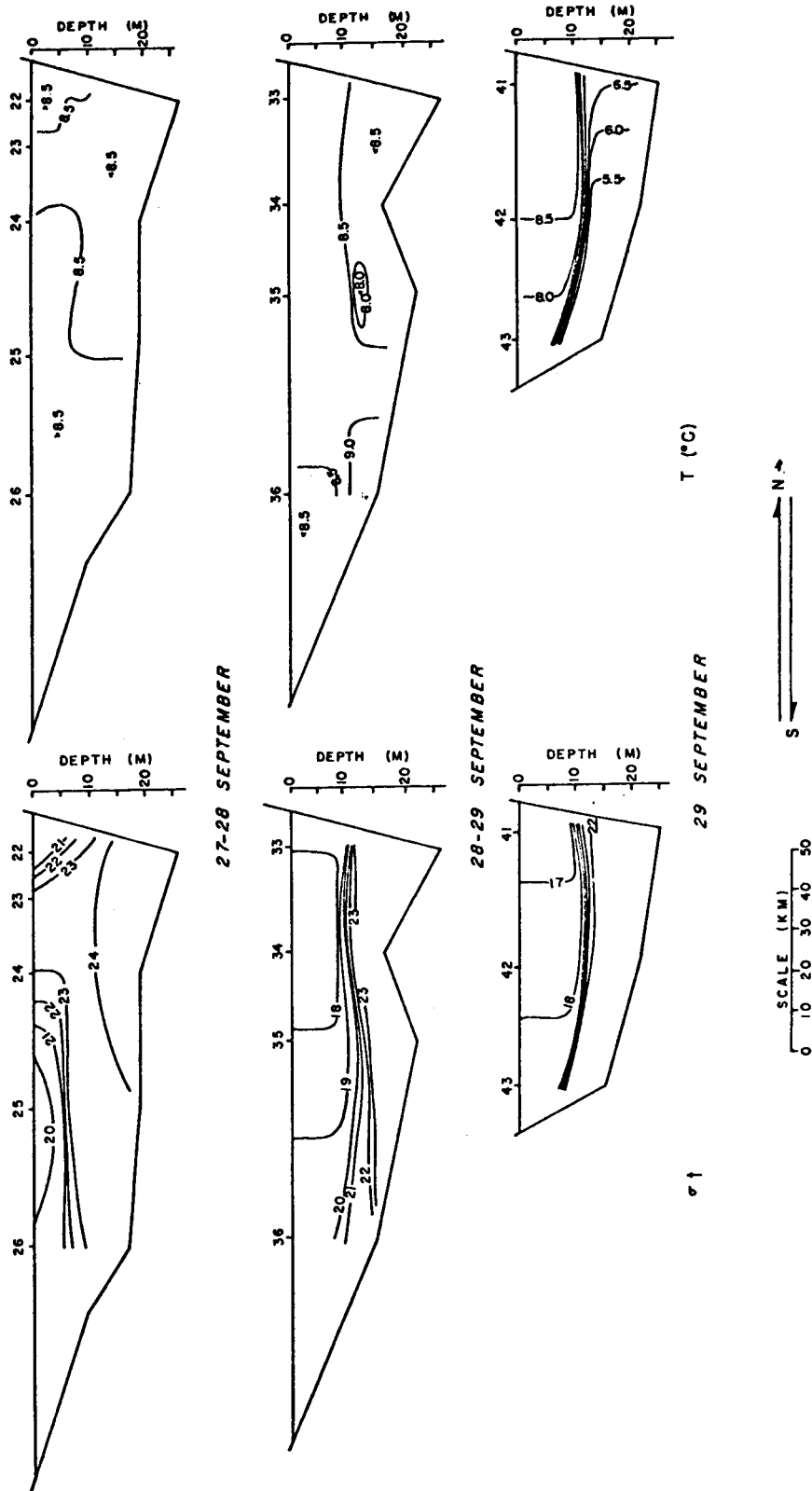


Figure 11. North-south sections showing density and temperature distribution across Norton Sound during September-October 1976.

33 to the east or 21 to the west. Near-shore stations obtained as part of a close-spaced section extending southwestward from Nome (Figure 12) detailed this feature and indicated densities down to $\sigma_t = 19$ in the near-shore band; the band was restricted primarily to the region above the pycnocline. High density water ($\sigma_t > 23$) occurred at stations 23 and 24 but was not present elsewhere. This high density area appeared between less dense water in the coastal band and in a shallow layer farther west at station 25 (Figure 11).

The temperature distribution bore little resemblance to density distribution except in the easternmost portion of the Sound, where temperature layering coincided with density layering (Figures 10 and 11). In the eastern and western portions temperatures near the surface were higher than near bottom, while in the central area (at station 29) temperatures were nearly homogeneous. Low near-bottom temperatures ($< 2.5^\circ\text{C}$) at the head of the Sound are noteworthy because they do not show up elsewhere and because they require the existence of strong vertical gradients in a shallow region where vertical mixing might be expected to play an important role in controlling distribution. North-south temperature variations were irregular and less than 1°C , except for the section between Stuart Island and Cape Darby where there was a south-to-north increase in temperature ($\sim 1^\circ\text{C}$) both above and below the pycnocline.

These north-south sections suggest that mean circulation in Norton Sound fell into two separate regimes. The western third of the Sound was characterized by well-defined east-west flows: a higher speed, concentrated coastal stream outward along the northern boundary and a broad, lower-energy flow into the Sound over the southern two-thirds of area. This structure is evident in both Figure 12 and the westernmost section of Figure 11. For the eastern Sound, mean flow was less well organized. There was a tendency for some inflowing water along the south to penetrate eastward before it turned north and eventually west to join the westerly

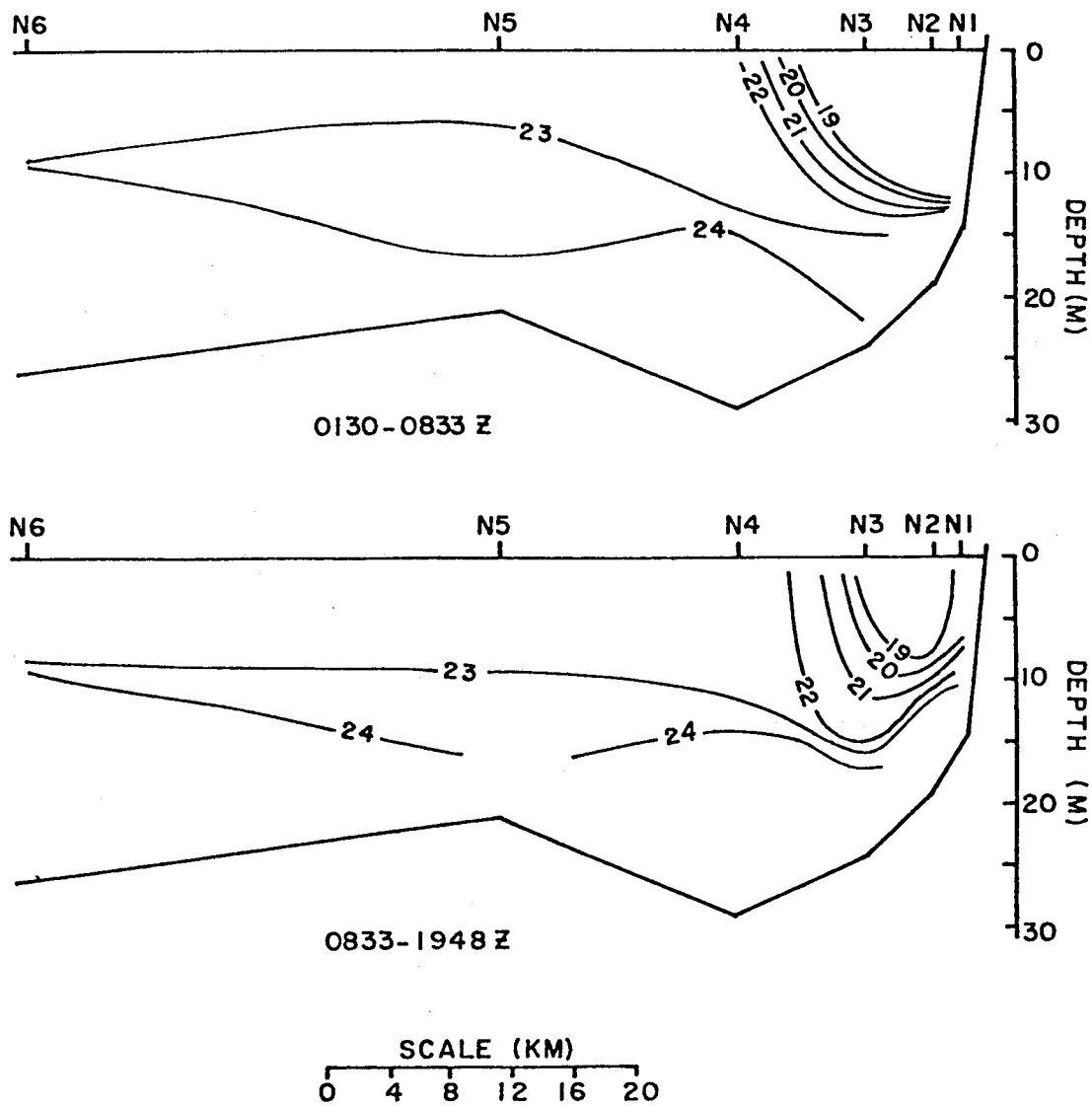


Figure 12. Sections showing density distribution off Nome during September-October 1976.

outflow. However, mean flow appeared sluggish in the eastern sections (Figure 11) and mostly northward (Figure 10).

The horizontal temperature distribution is summarized as a plot of temperature on the $\sigma_t = 21$ isopycnal surface (Figure 13). This isopycnal surface fell within the pycnocline, so the temperature distribution depicted is within the pycnocline. A warm tongue-like feature (8.5-9.5°C) extended eastward in the southern portion of the Sound, while a colder tongue (7-8.5°C) extended westward in the northern part. Presence of the strong pycnocline suggests a lack of vertical mixing. We feel that, despite the shallow depths, temperature in the pycnocline can serve as a qualitative water mass tracer because of this apparently weak vertical mixing. The temperature distribution can then be interpreted as reflecting cyclonic circulation in the western two-thirds of the Sound. East of the cul-de-sac formed by Stuart Island and Cape Darby, the pycnocline was too strong to allow clear definition of temperature on the $\sigma_t = 21$ surface.

There was bottom inflow along the two troughs which intrude the Sound from the west (cf. Figure 9). A clear indication of this is seen in the bottom salinity distribution (Figure 14). This water was then mixed upward and joined that of the general circulation. The upward mixing raises the salinity of the surface layer locally. Figure 15 shows the average salinity of the surface layer (\sim upper 5 m), and the strongest effects are noticeable at stations 24, 30, 35 and particularly at stations 22 and 21 west of Nome.

Density sections indicate that large variations in pycnocline depth occurred over the Sound; for example, it was about 5 meters shallower at station 25 than at 35 (Figure 10). Such variations are in part due to internal waves on the pycnocline. Figure 16 shows vertical density profiles at two of the five time-series stations. Each of the five time-series stations indicated vertical migrations in pycnocline depth on the order of 5 meters. Though the records are too short for

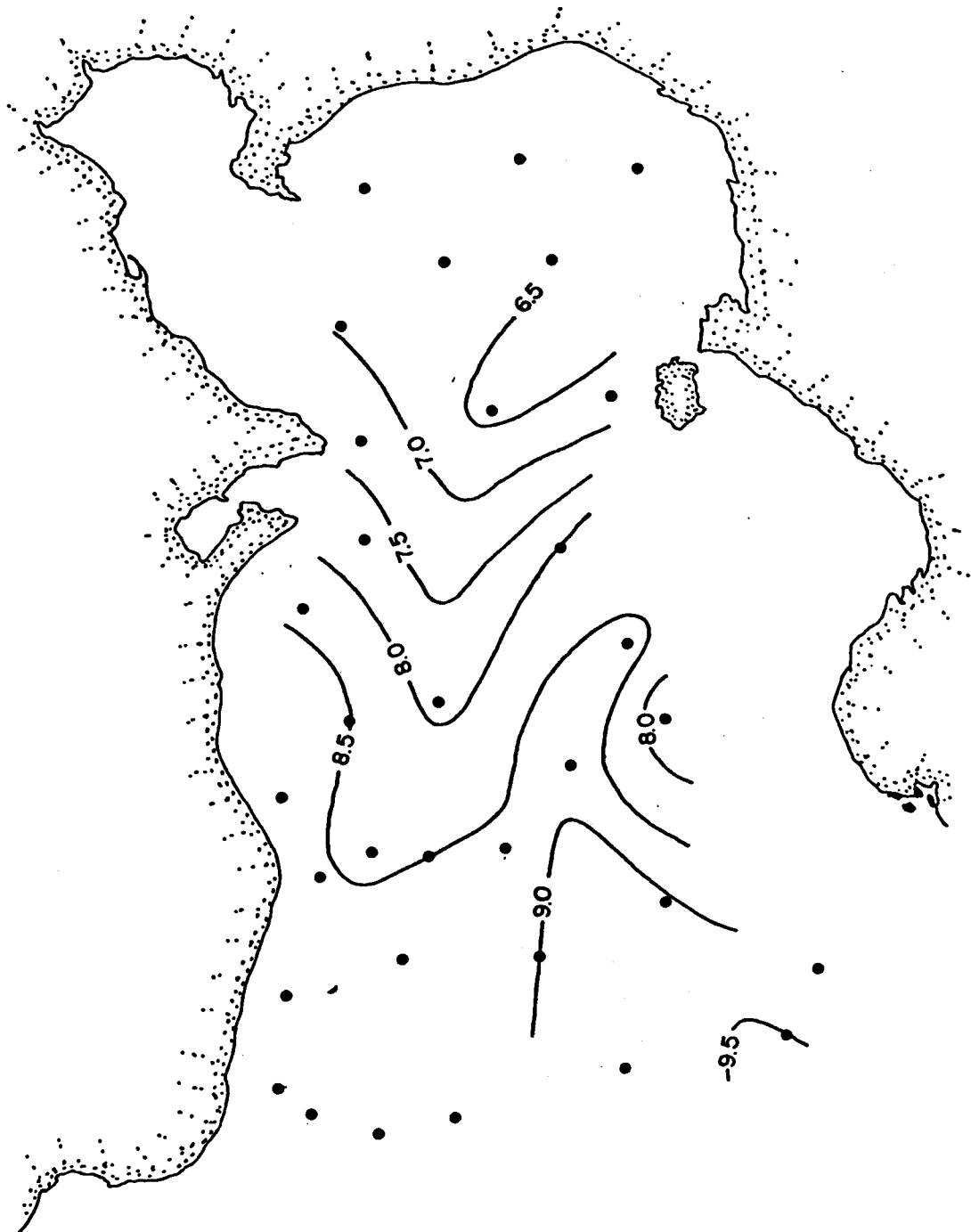


Figure 13. Temperature on the $\sigma_t = 21$ surface in Norton Sound.

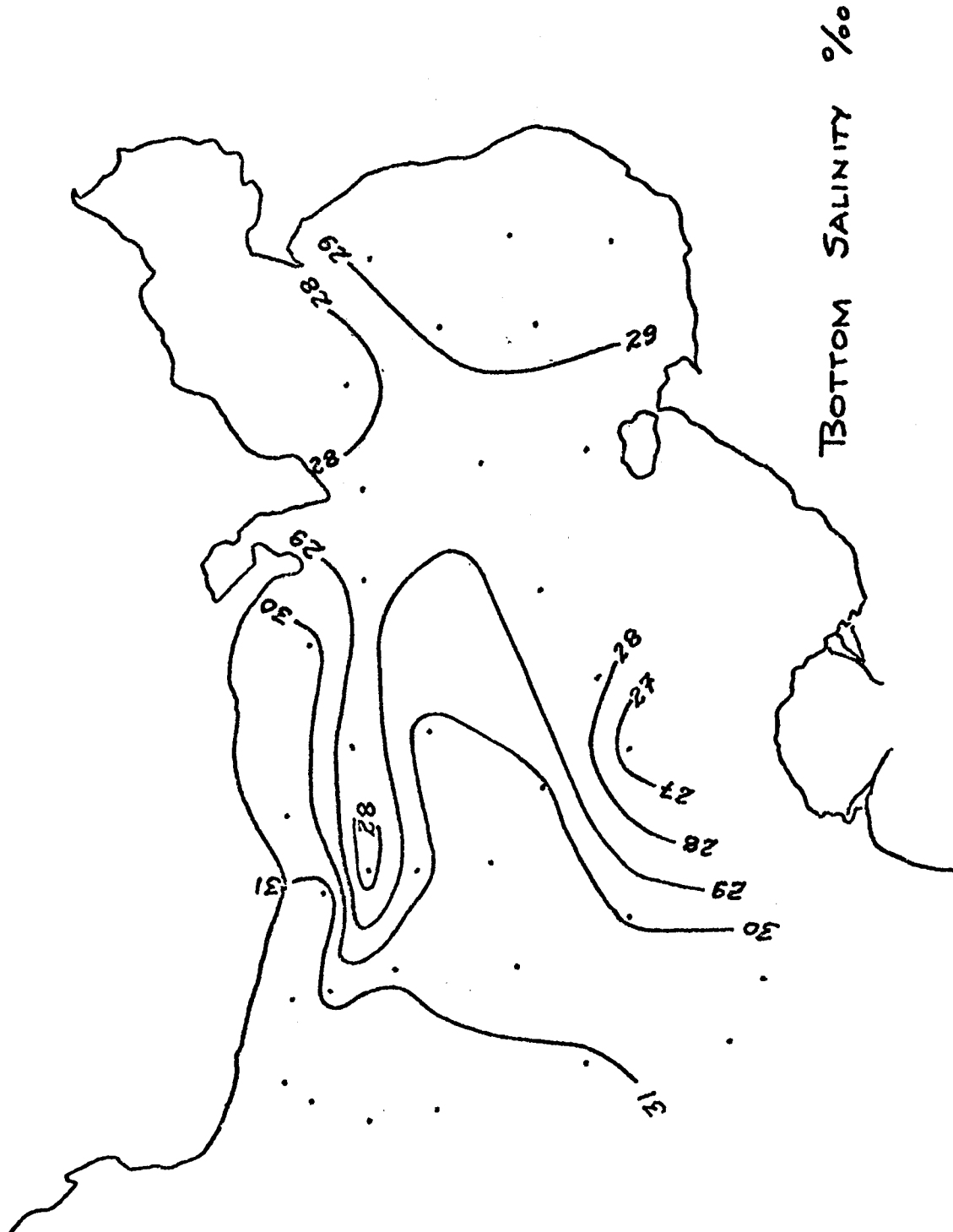


Figure 14. Salinity (‰) of the near-bottom layer.

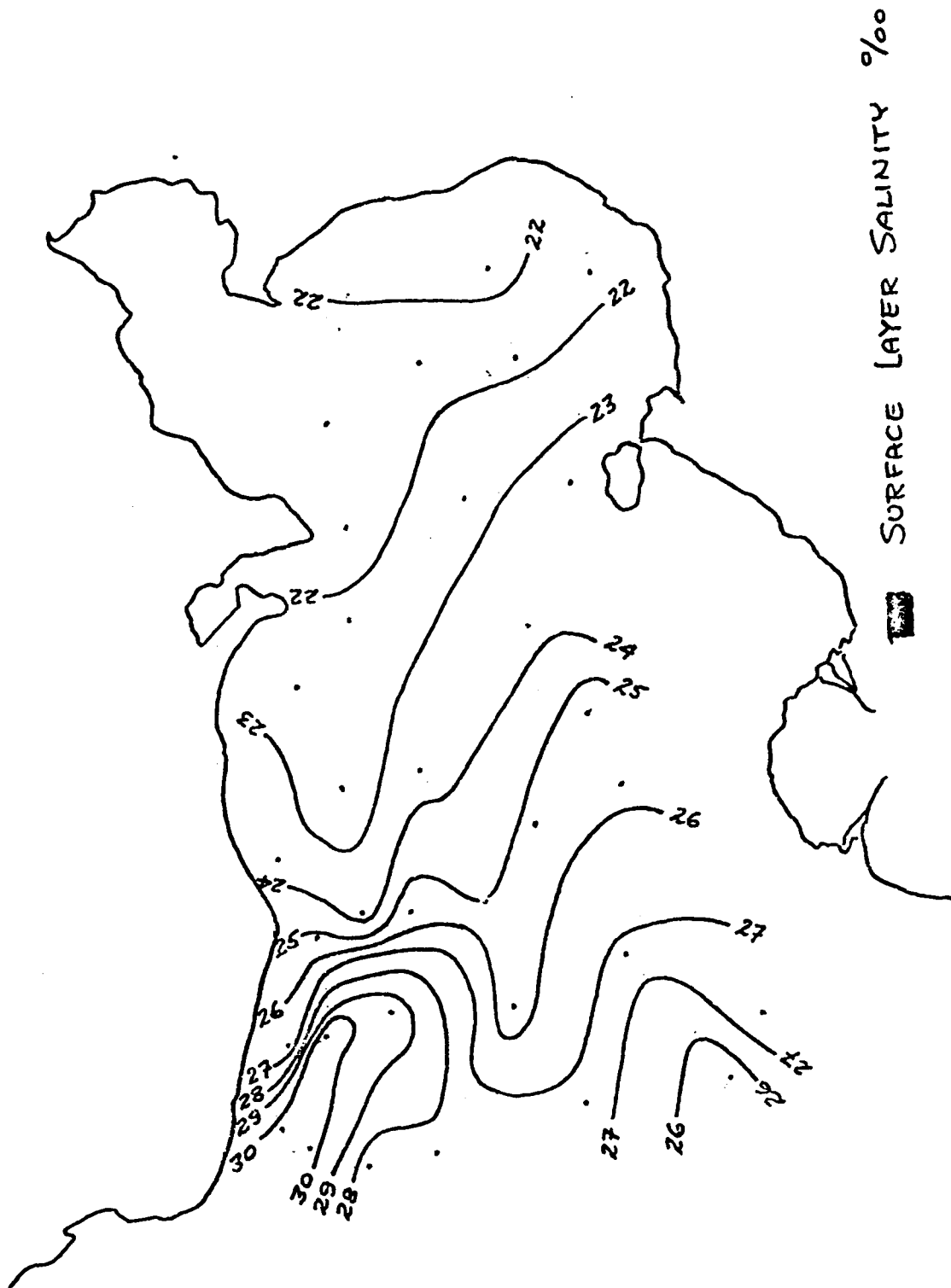


Figure 15. Salinity (‰) of the near-surface (~ 5 m) layer.

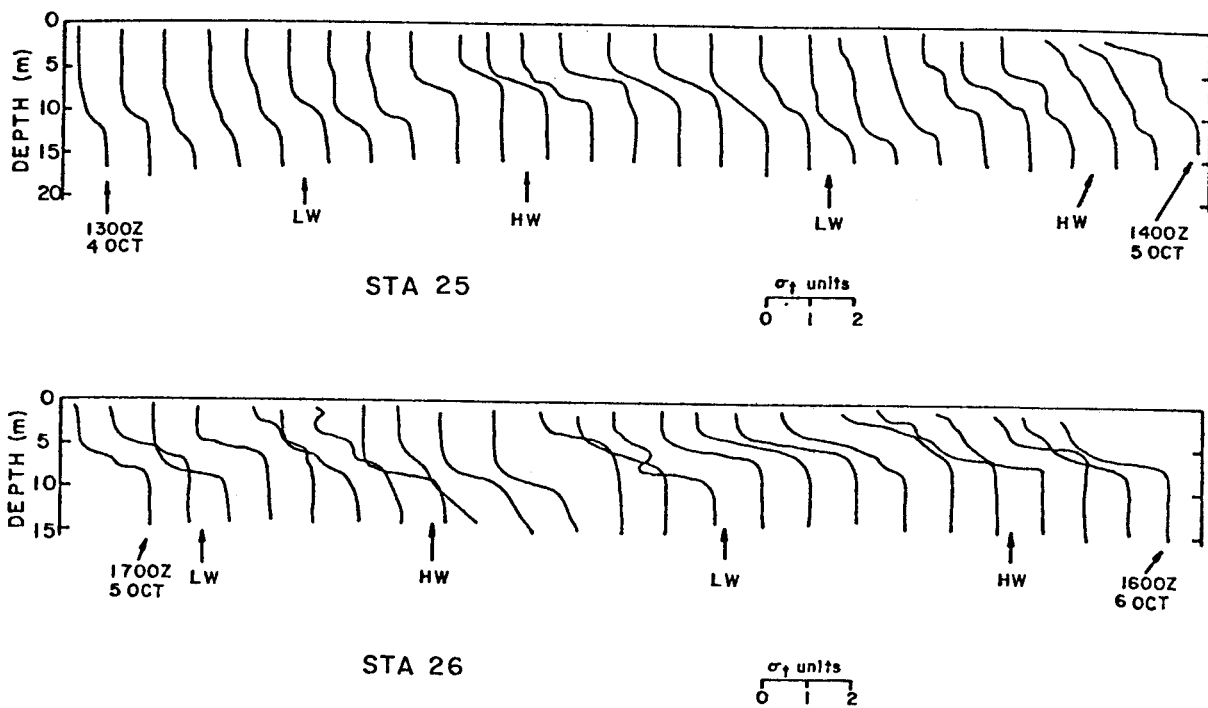


Figure 16. Examples of time variations in vertical density structure at two stations in Norton Sound.

definitive analysis, the fluctuations might be composed of a basic tidal signal with some higher frequencies superimposed. The record at station 25 (Figure 16) appears to have a fairly clear tidal period signal as a dominant part of the fluctuation.

A closer connection between tides and time variations can be demonstrated for station 22, 15 km southwest of Nome. The predicted tides for stations around Norton Sound show the tide wave circulates cyclonically--thus off Nome the wave travels from east to west. Figure 17 plots the vertical σ_t profiles for time-series station 22 sequentially. Also plotted, on a time scale, are the bottom σ_t values and the predicted Nome tide. As the CTD stations were made at one-hour intervals, the σ_t offset between vertical profiles is the same scale as one-hour, so are visually equivalent in time.

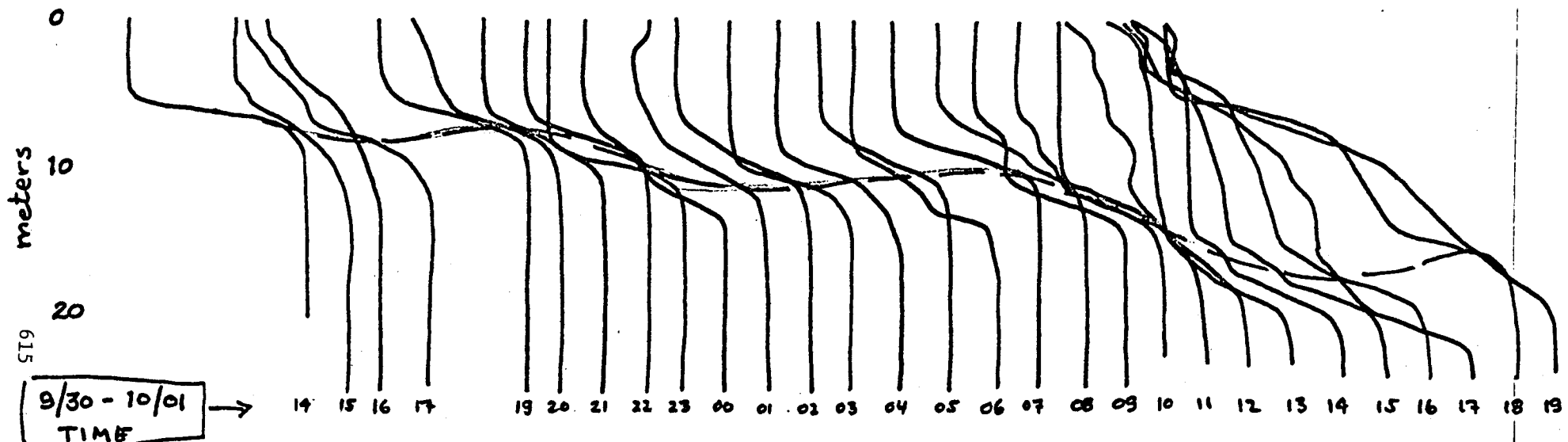
The interpreted flows are as indicated. In a tidal progressive wave, the flow will be west at high water at Nome and east at low water. In the curve of variation of bottom σ_t , as the density increases to the west, a west flow will decrease σ_t and an east flow increase σ_t , as indicated. There is good correlation with the predicted tides. The fluctuations of the pycnocline also correlate--west flow brings a deepening of the pycnocline (which lies deeper to the east), and an east flow shallowing. The last few hours of the record become confused because of the intrusion of a less dense water parcel in the upper layers.

The time fluctuations of the other time-series stations cannot be so readily resolved in terms of the tides because the behavior of the tide wave in Norton Sound cannot be sufficiently resolved as yet. Tide table data show the times of high and low water to be progressively later from Kawanak Pass (Yukon Delta) to Stuart Island to Golovin Bay to Nome. Using the expression $c = f (gh)^{1/2}$ where c = wave speed, g = gravity, h = mean (effective) depth, and f = a factor accounting for the fact that tide waves in shallow shelf seas tend to move a little

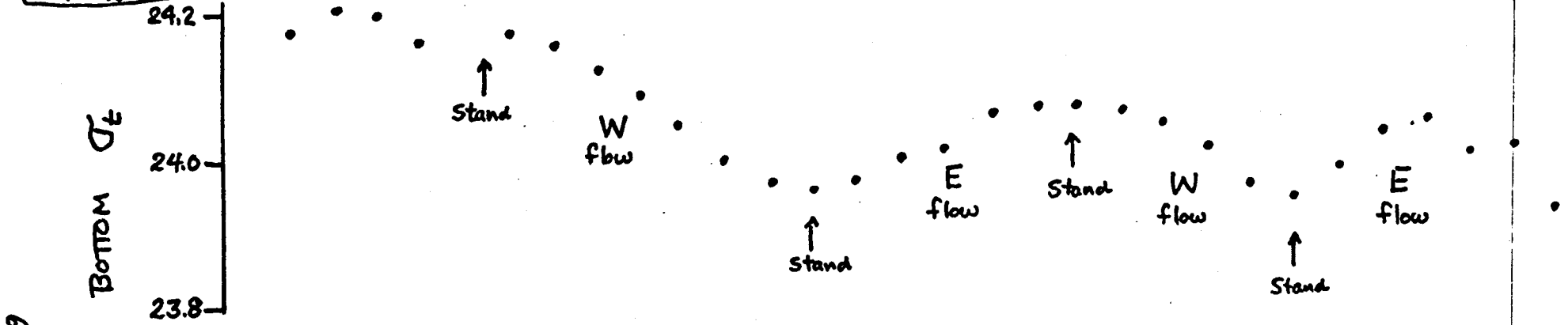
Figure 17.

TIME SERIES STATION 22

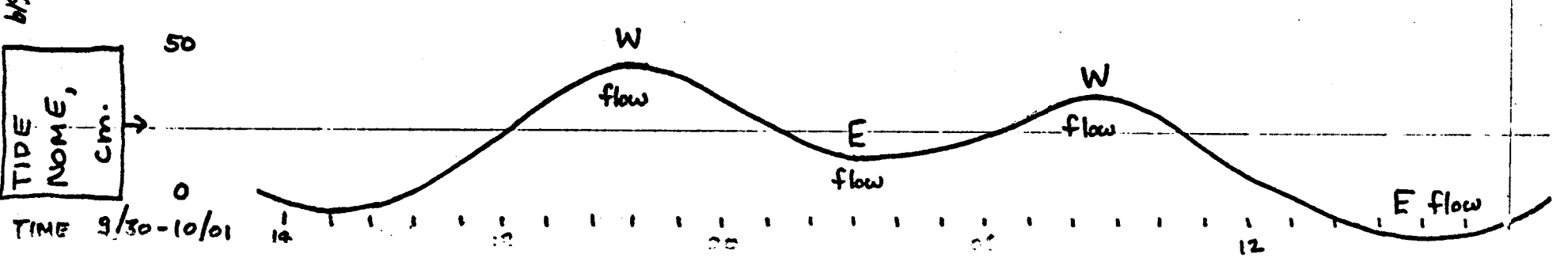
σ_t : scale \rightarrow 21 22 23
(for last station) 22



9/30 - 10/01
TIME



619
TIDE
NAME,
cm.



faster than $(gh)^{1/2}$ (Sverdrup, 1926), the speed and depths from Kawanak to Stuart to Golovin check very well with $f \approx 1.3$. (In outer Kotzebue Sound $f \approx 1.5$ [Coachman and Tripp, 1970].) Thus, a rotary wave cyclonic around outer Norton Sound with an amphidromic point somewhere in the outer central part of the Sound, is strongly suggested. However without further resolution we cannot locate stations 24, 25, and 26 with respect to the amphidromic point. It is hoped that the year-long current records from moorings NC-14 and NC-15 will help shed light on the tidal behavior.

Several density inversions were observed in the course of this study. These are believed to be real, and are qualitatively similar to those reported at greater depth in Bristol Bay by Coachman and Charnell (1977). Their treatment is beyond the scope of this paper.

Current and wind observations. Vector-averaged currents at each depth are shown along with vector-averaged surface winds at each of five stations in a transect south from Nome (Figure 18). The highest currents observed ($\sim 50 \text{ cm sec}^{-1}$) occurred near the surface at station 22. Speeds at this station decreased with depth down to about 10 cm sec^{-1} near the bottom, while flow direction rotated slightly from northwesterly near the surface to west-southwesterly near the bottom. The currents at station 22 showed an onshore component which was maximum near the surface and decreased with depth to become slightly offshore near the bottom (Figure 19). Longshore currents were westerly throughout the water column and maximum near the surface, decreasing monotonically with depth.

The ten-hour time series (station N3), obtained about 2 km northeast of station 22 and about two days later, revealed an entirely different current regime than that observed at station 22 (Figure 19). Mean flow was southeasterly throughout the water column. A breakdown into components revealed that flow was offshore

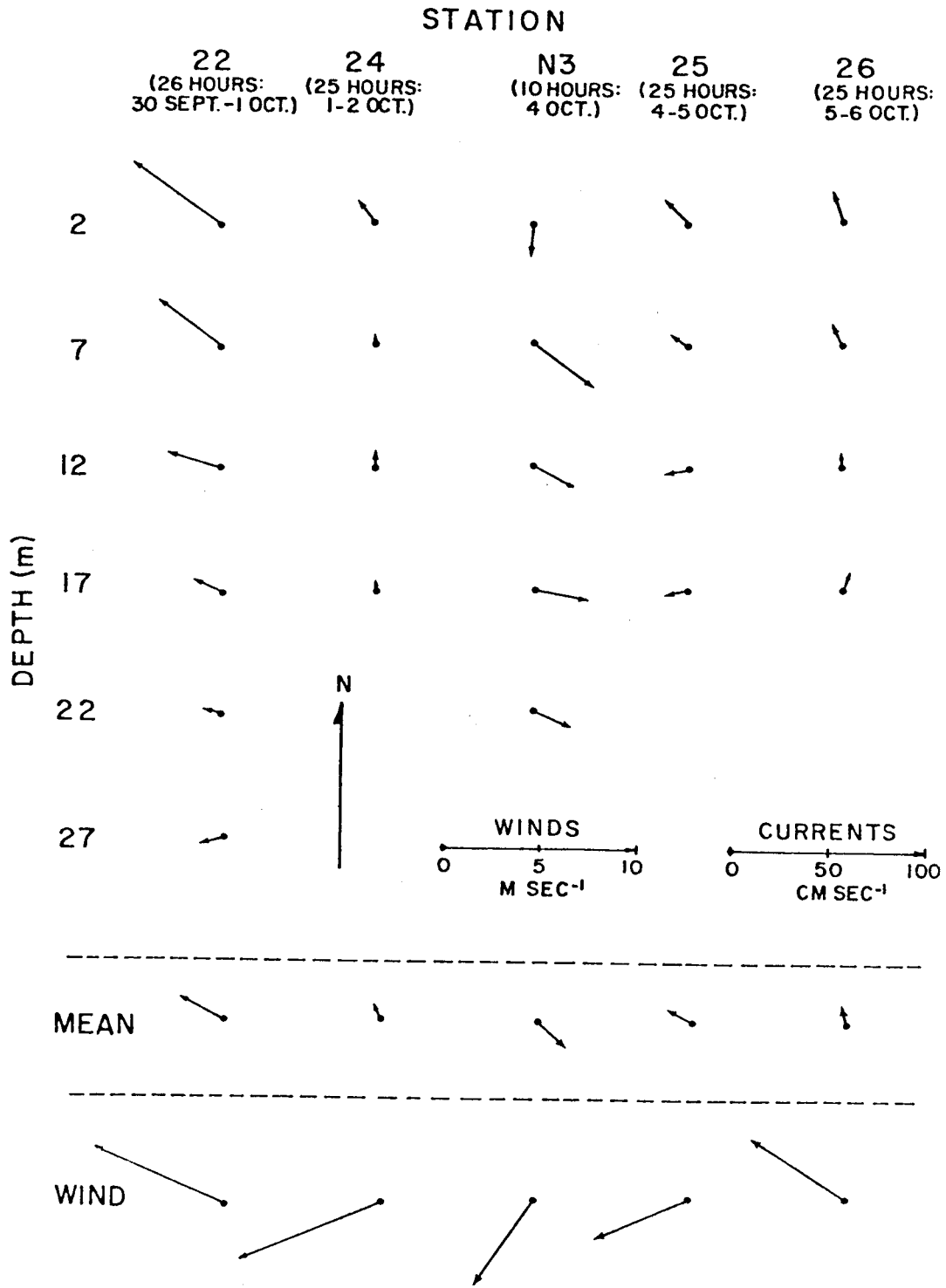


Figure 18 Mean currents and winds at the five time-series stations in Norton Sound.

except at 17 meters where a slight onshore component was present (Figure 17). The longshore component was easterly with a pronounced maximum at 7 meters.

Mean currents at stations 24, 25, and 26 were westerly to northerly through the water column and were maximum at the surface (12-18 cm sec⁻¹), becoming small (~ 5 cm sec⁻¹) near the bottom.

Individual hourly current records were generally characterized by short-term (on the order of a few hours) fluctuations (Figure 20). Only one of the five records is presented here because they all exhibited similar characteristics. There was no visual correlation between these fluctuations and fluctuations in the surface winds, although the apparent similarity in directions between the mean currents and winds (Figure 18) suggests that wind was a significant factor.

B. THE SEPTEMBER ANCHORED CURRENT MEASUREMENT PROGRAM

During the early September field program, anchored current measurements were obtained at each of the locations indicated in Figure 21. Interpretation of the results of these measurements (Table 4) is limited somewhat by the one-time-only nature of the measurements coupled with the natural variability of currents in the region. The measurements were however felt adequate to define large-scale regional circulation features.

Table 4

Observed Water Transports (Sv, 1 Sv = 10⁶ m³ s⁻¹)

<u>Section</u>	<u>Date(s)</u>	<u>Transport</u>	<u>Comments</u>
Bering Strait	September 8	0.70	Northerly flow with some southerly near-surface flow in western portion.
Cape Lisburne	September 10-11	0.72	Net northward flow.
		1.06	Southeasterly flow in Siberian Coastal Current (western part of section).
E. St. Lawrence	Septmber 6	0.73	Northward flow.
W. St. Lawrence	September 6-7	1.12	Northward flow.

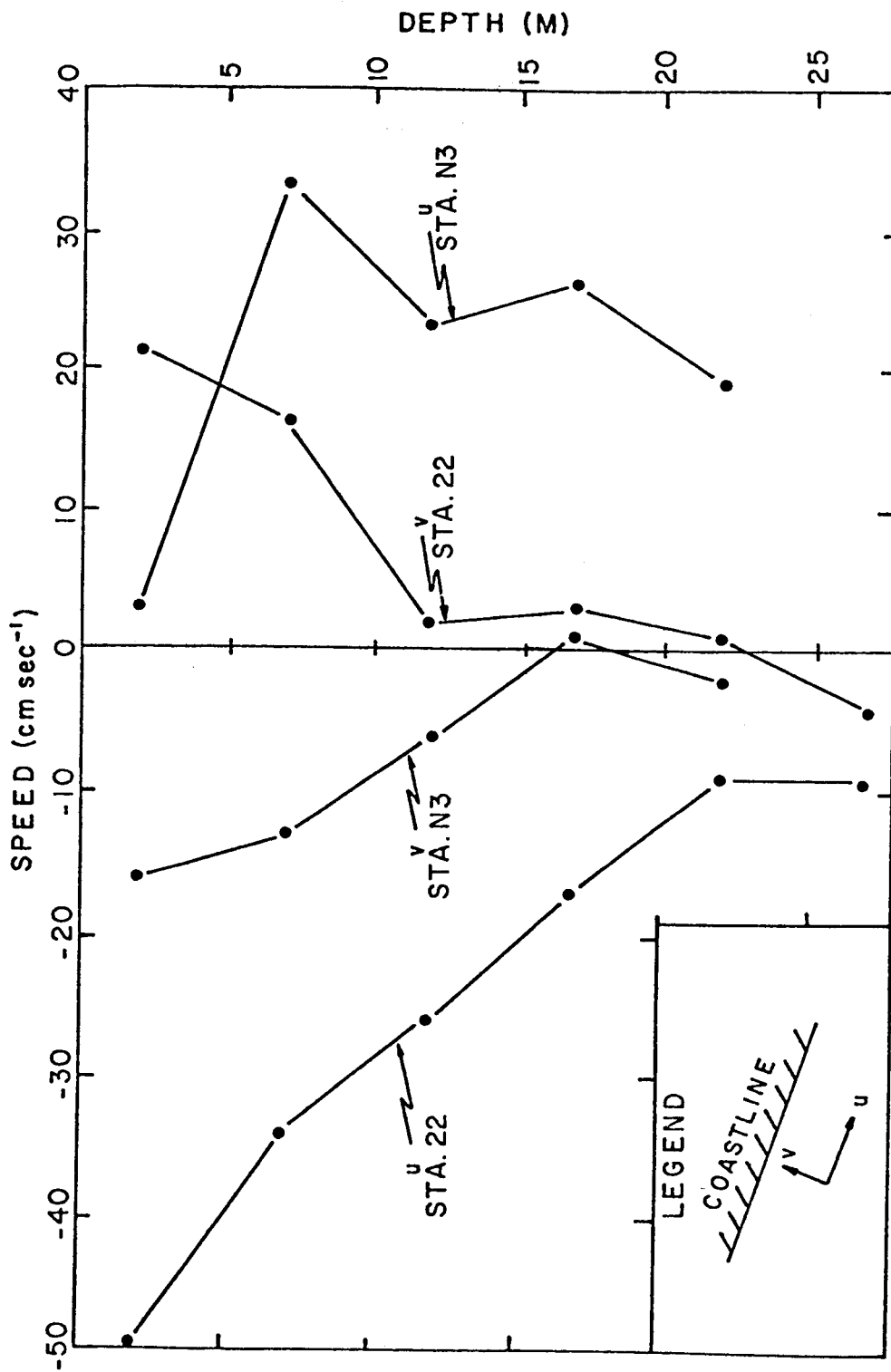


Figure 19. On-offshore and longshore current structure off Nome.

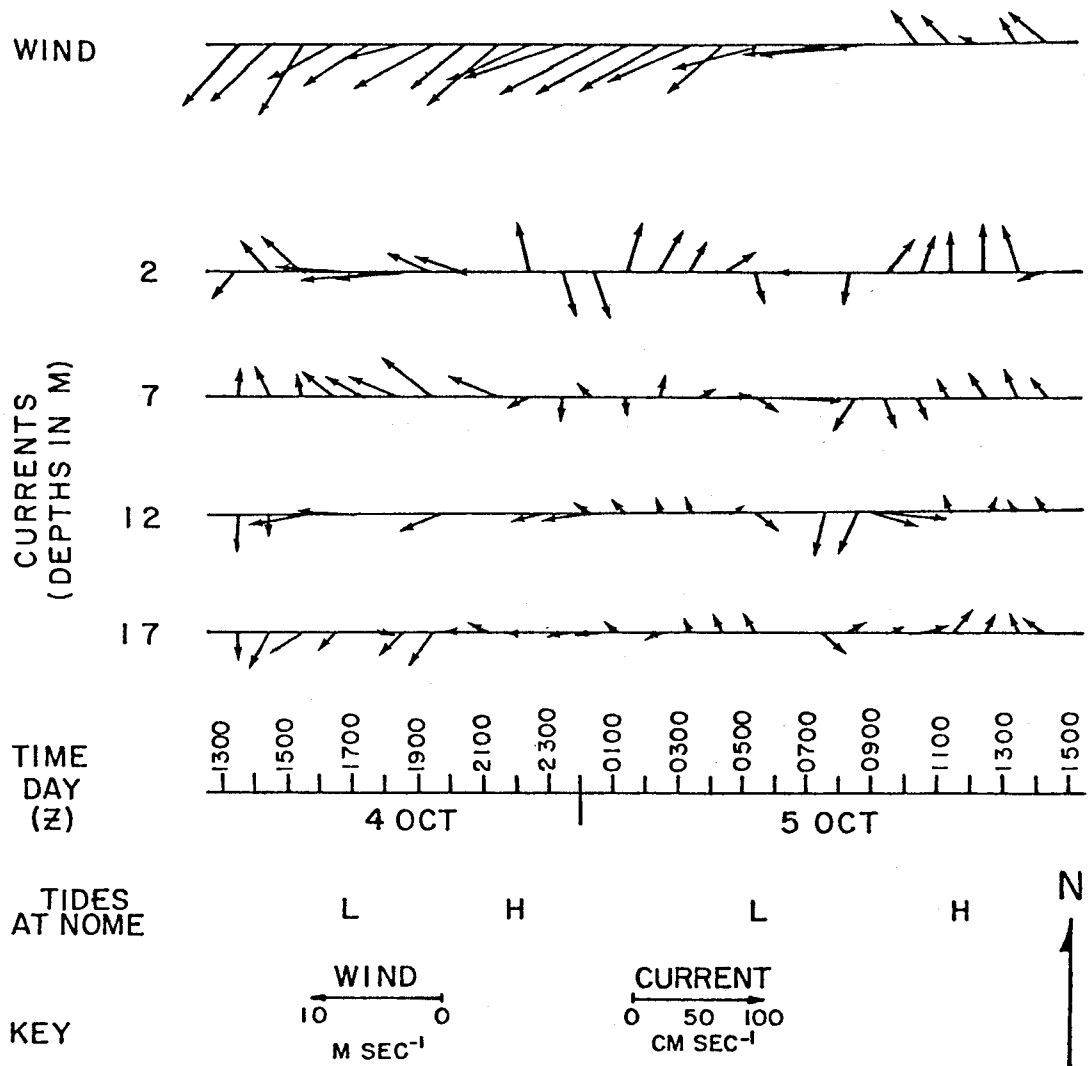


Figure 20. Example showing short-term variations in winds and water currents at station 25 in Norton Sound.

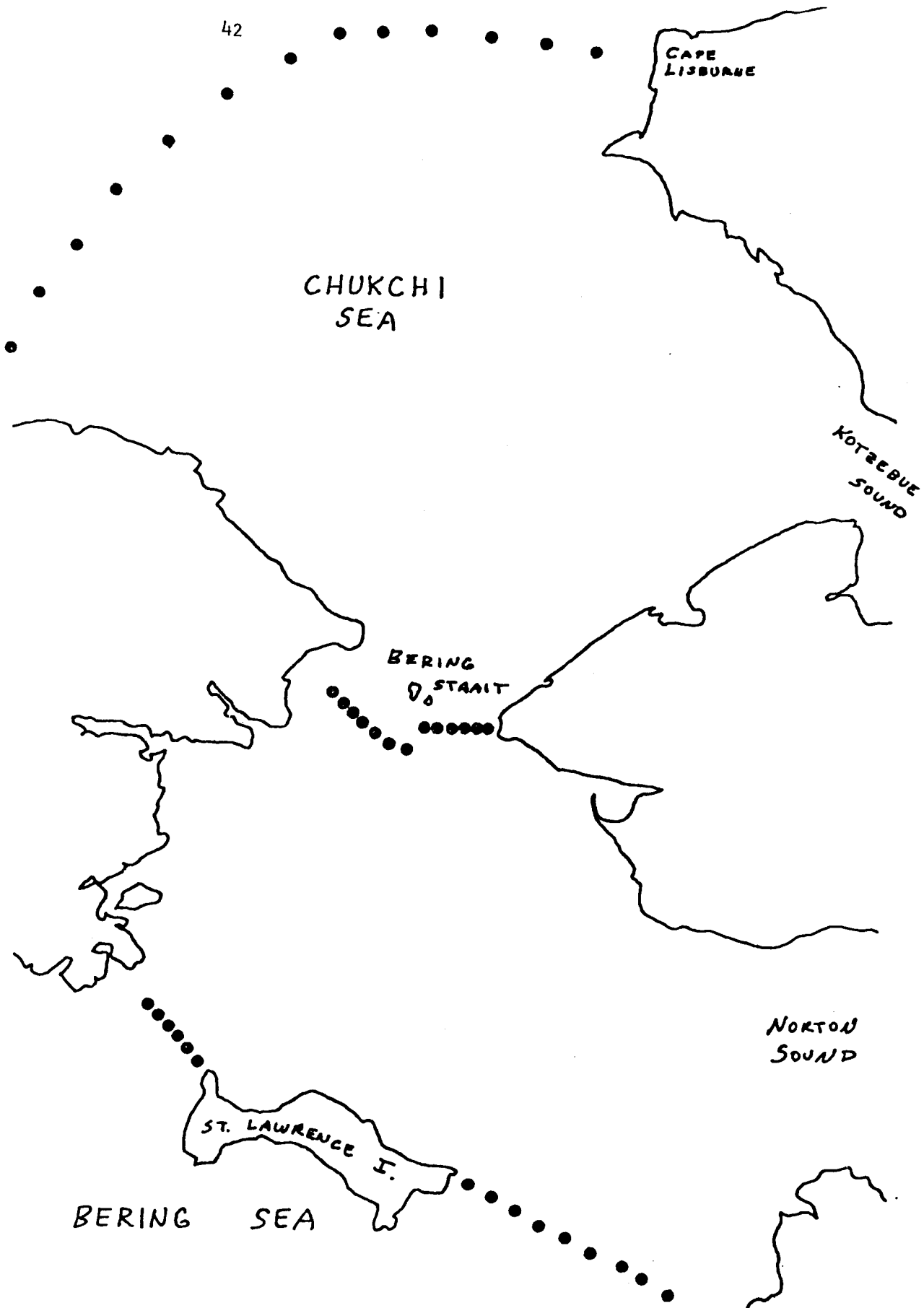


Figure 21. Locations of September 1976 anchored current stations in the Bering Strait region.

The measurements detected a northward flow of 0.70 Sv ($1 \text{ Sv} = 10^6 \text{ m}^3 \text{ s}^{-1}$) through Bering Strait, in agreement with previous figures (see Coachman *et al.*, 1975). A relatively small (0.1 Sv) southward flow was present in the western near-surface portion of the Strait. Farther north off Cape Lisburne in the Chukchi Sea, a net northward transport of 0.72 Sv was the resultant of a northward 1.78 Sv flow through the eastern portion of the section and a southward 1.06 Sv flow through the western part of the section. The southward flow was a manifestation of the Siberian Coastal Current. The net northward flow past St. Lawrence Island in the northern Bering Sea was 1.85 Sv, about 65% of this through the passage west of the Island.

C. KOTZEBUE SOUND HYDROGRAPHY

We have begun examining the data from 26 hydrographic stations obtained in late August (Figure 22). Water depth varied from 31 m outside the Sound (station 66) to 14.5 m in the southeastern quadrant of the survey grid (station 88). Figures 23 to 31 illustrate our preliminary results.

Surface distributions (Figures 23 to 25) show that the shallow water in the Sound was warmer (11 C compared to 10 C) and fresher (26 compared to 30 g kg^{-1}) than the adjacent waters. There is a suggestion of an inflow of more saline water on the southern side of the entrance and an outflow of fresher water on the northern side: this circulation may bypass the easternmost part of the Sound.

Within Kotzebue Sound, bottom distributions (Figures 26 to 28) show some cold ($< 2 \text{ C}$) and salty ($> 32 \text{ g kg}^{-1}$) water which is a remnant of winter freezing. While inflow and outflow pattern similar to the shallow layer may be interpreted from these deeper distributions, the presence of relict winter water precludes a continuous cyclonic circulation within the deeper layer.

Stratification is very high in the northern and southeastern parts of the Sound (Figures 29 to 31): the Noatak River discharges into the Sound east of the

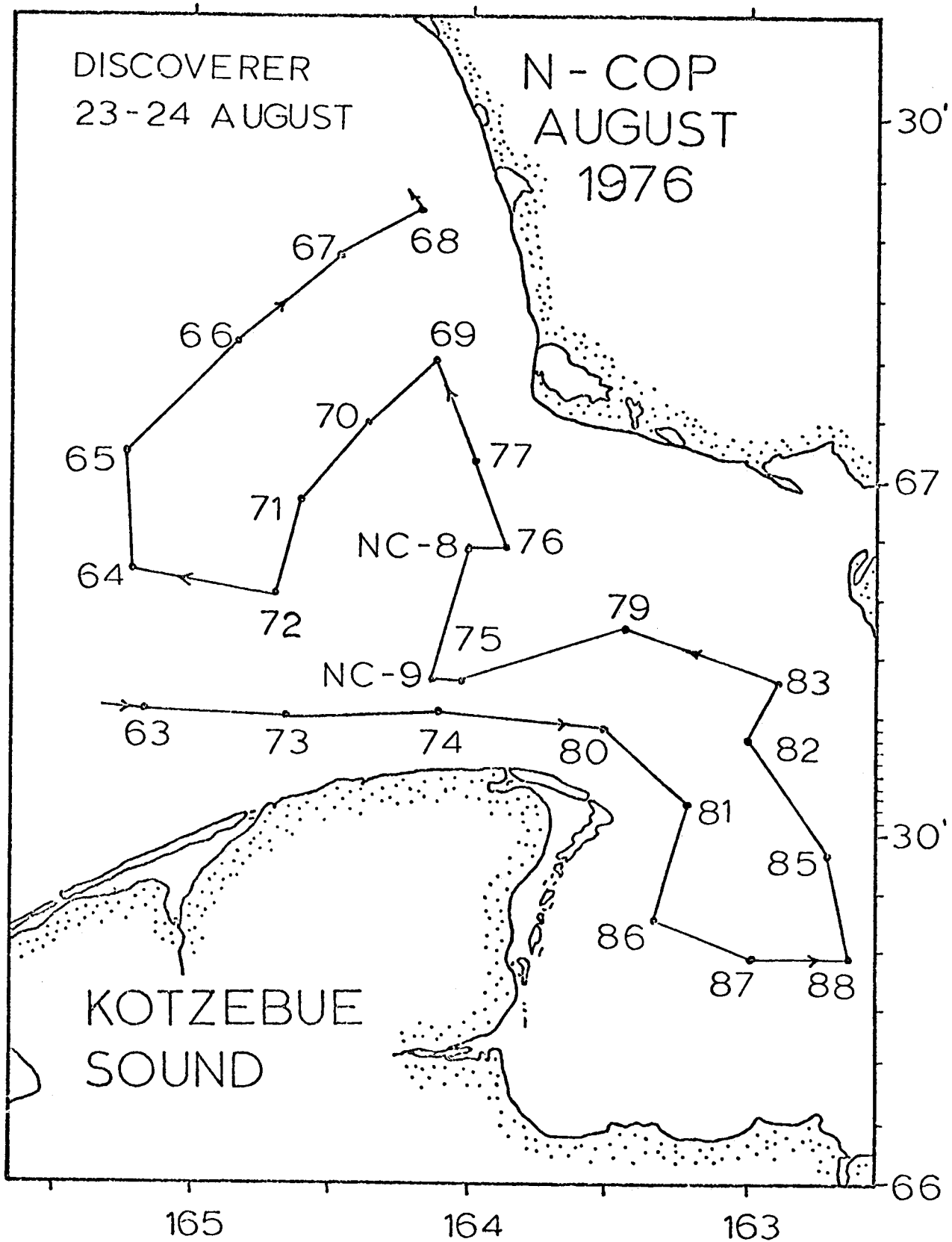


Figure 22. Track of NOAA ship *Discoverer*.

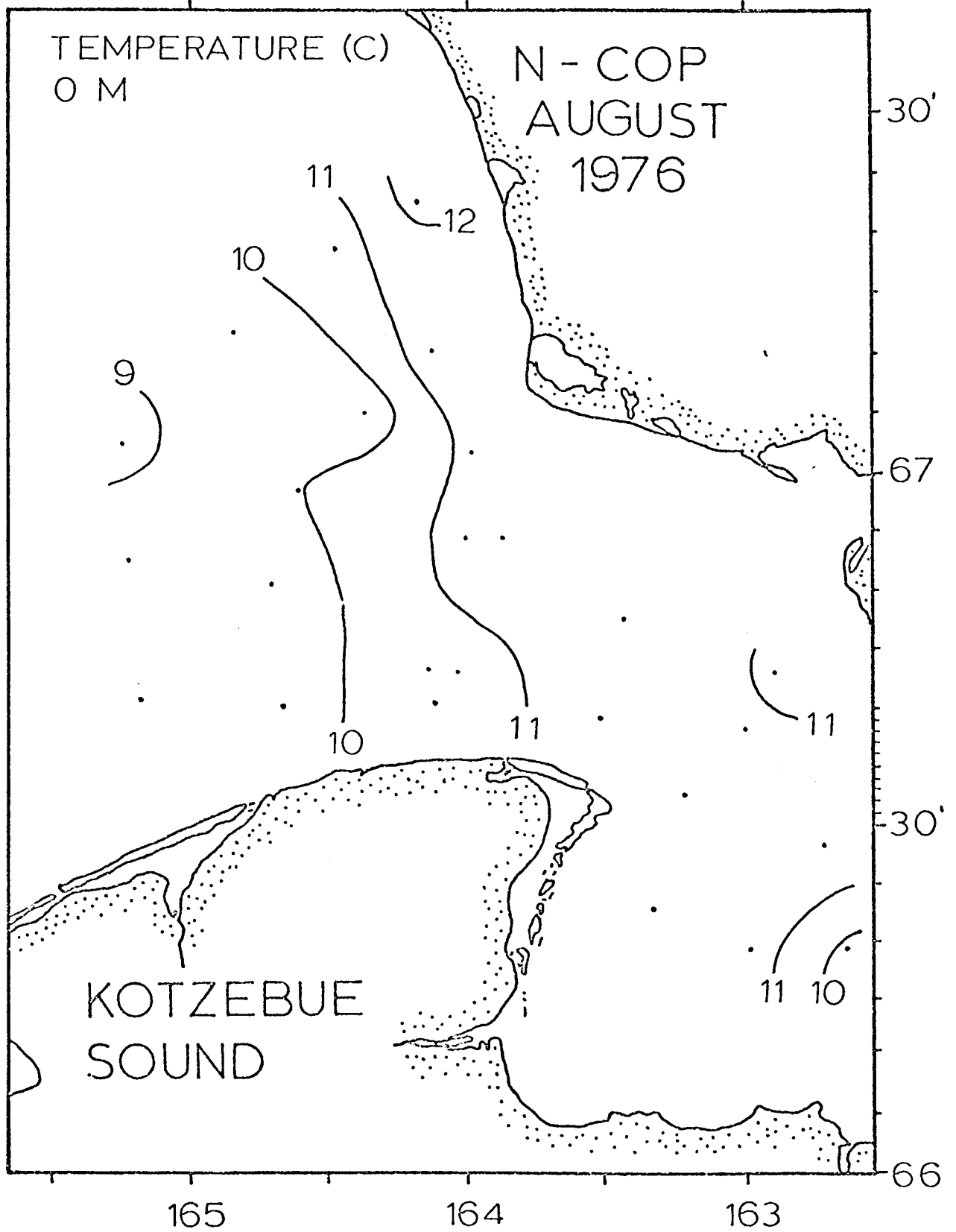


Figure 23. Surface temperature.

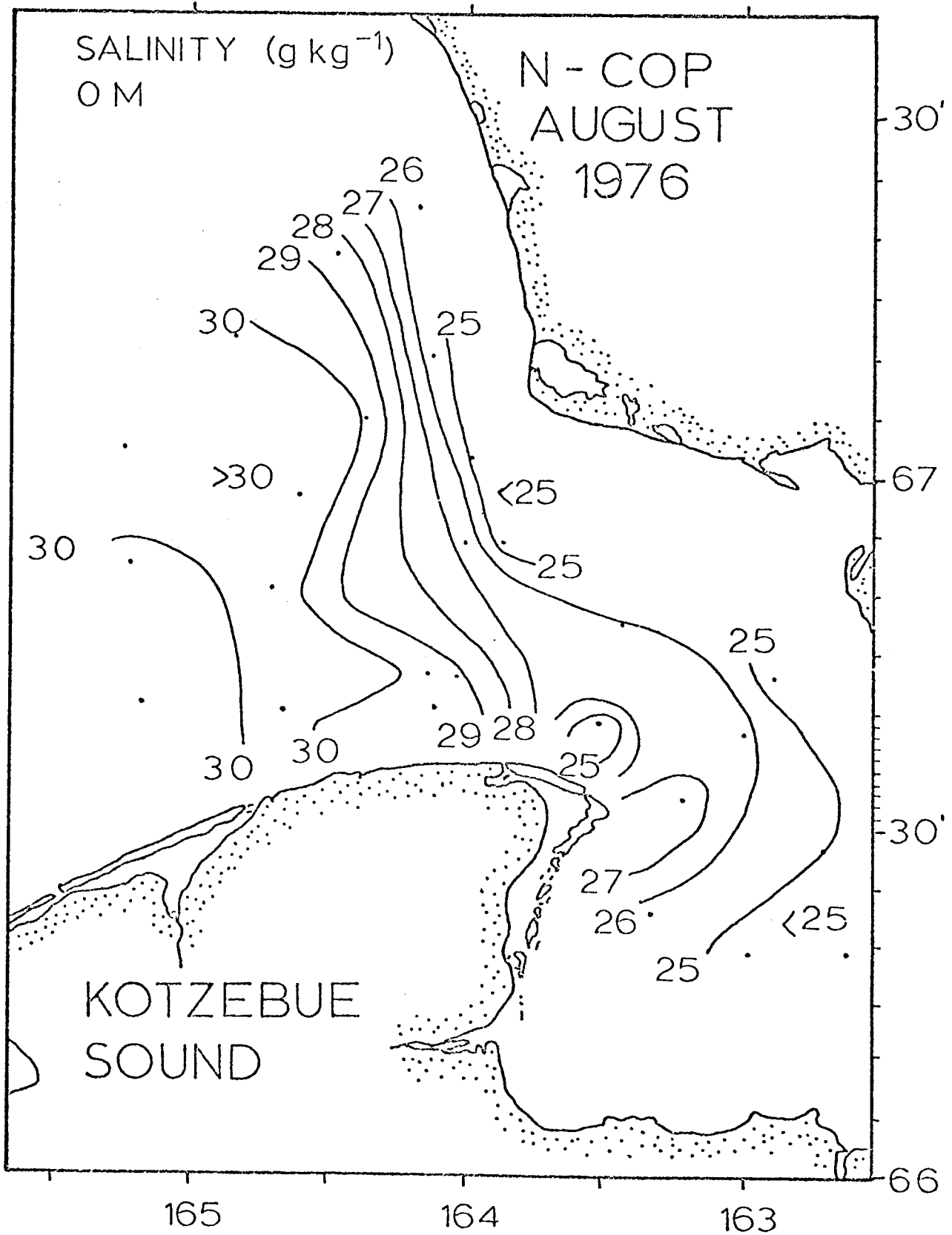


Figure 24. Surface salinity.

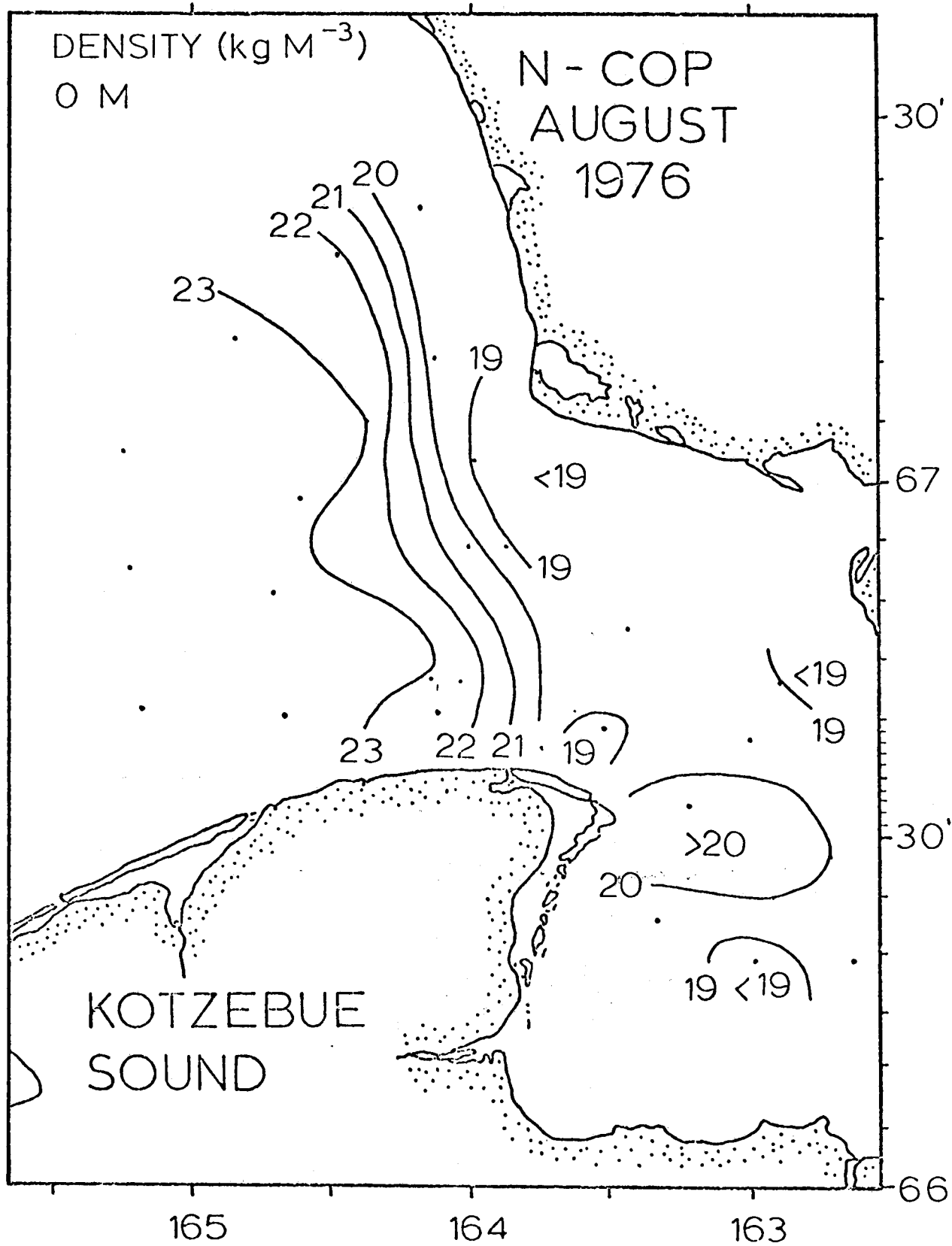


Figure 25. Surface density (σ_t).

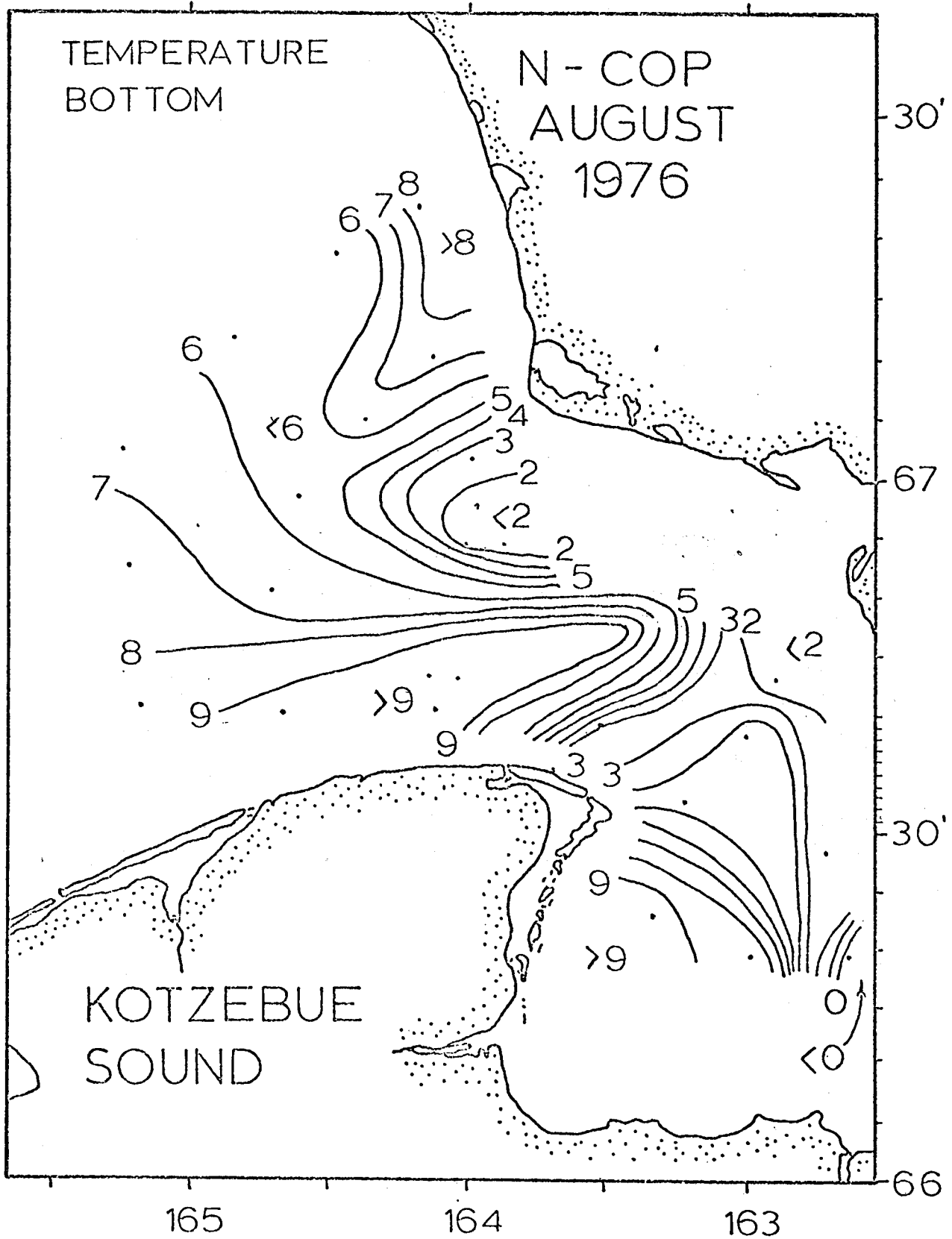


Figure 26. Bottom temperature.

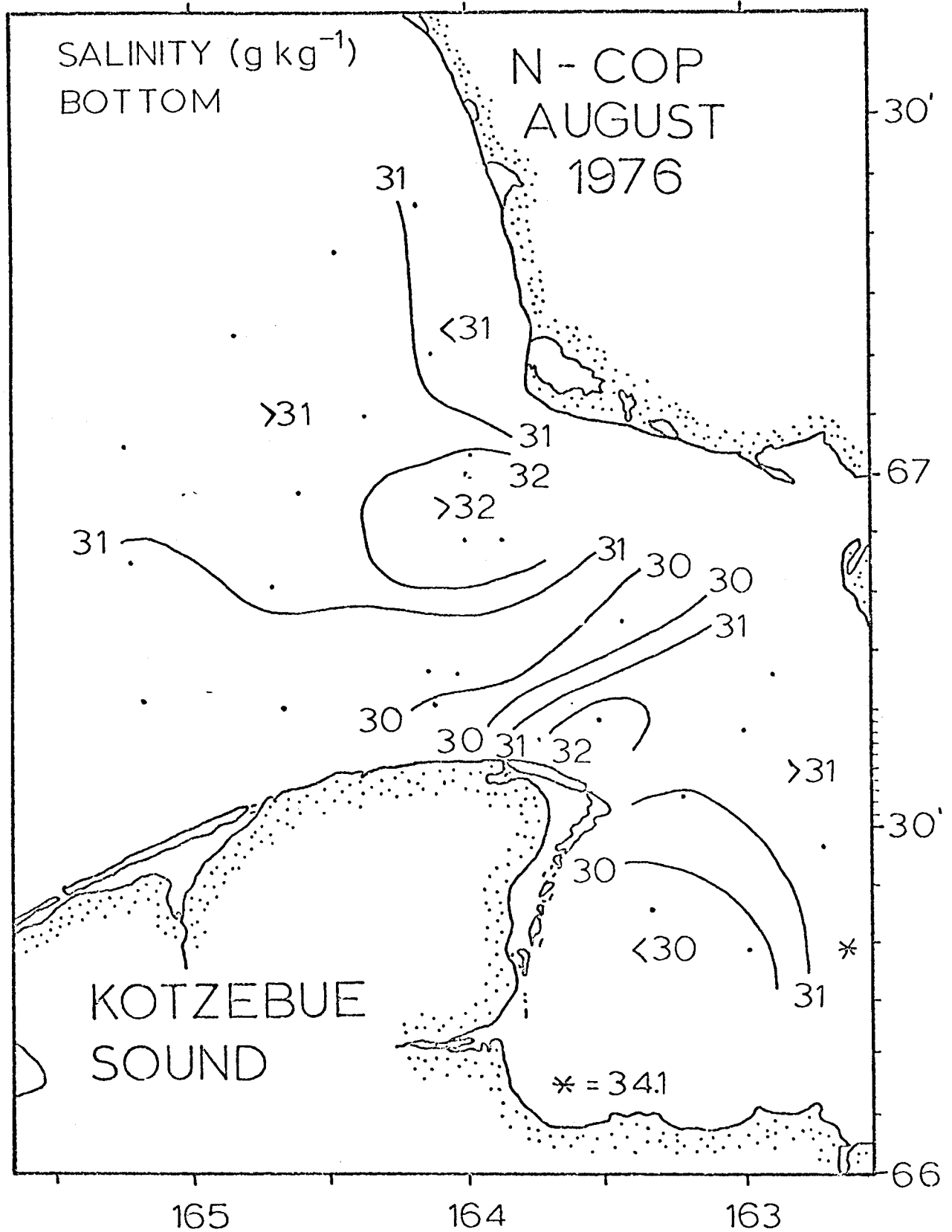


Figure 27. Bottom salinity.

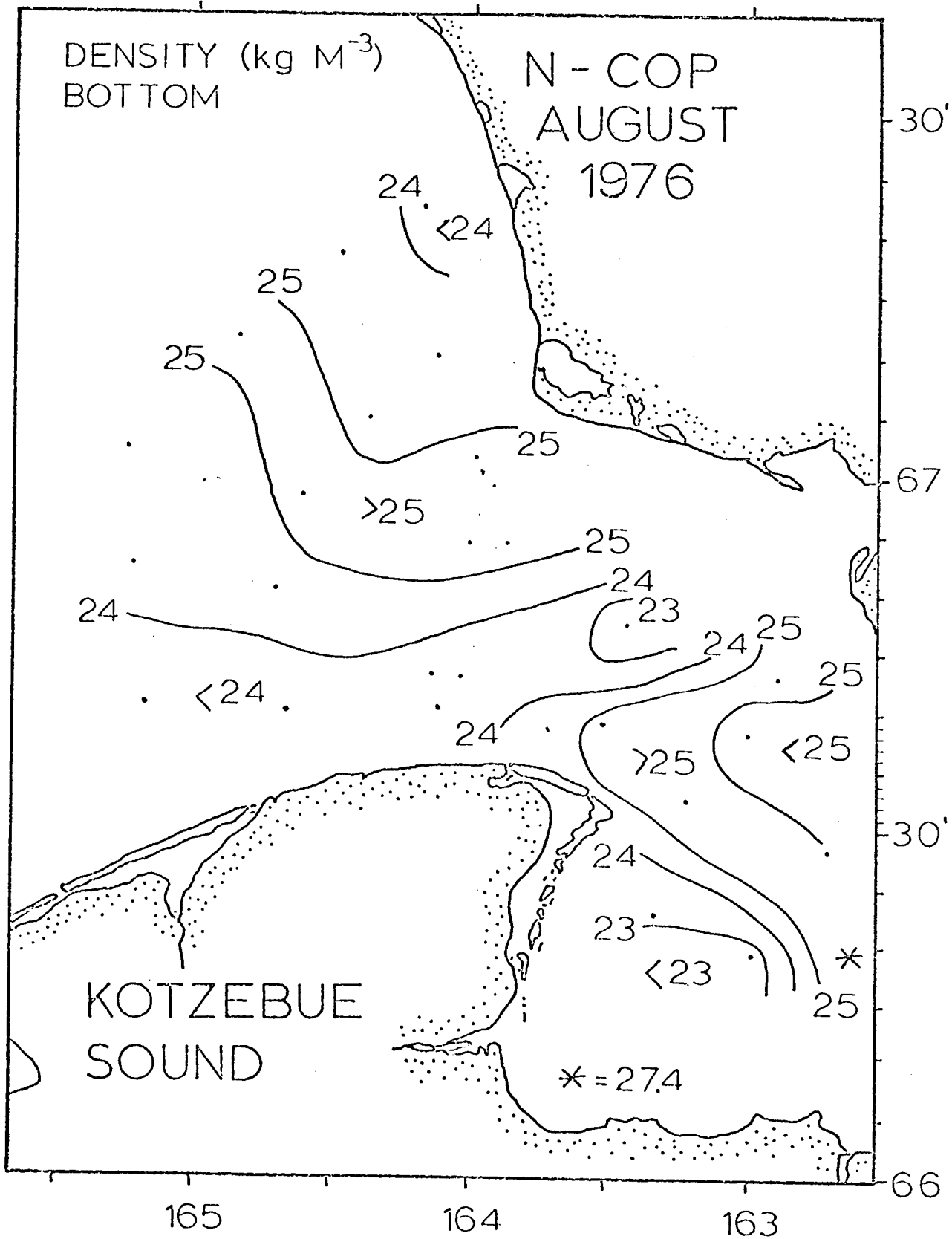


Figure 28. Bottom density (σ_t).
629

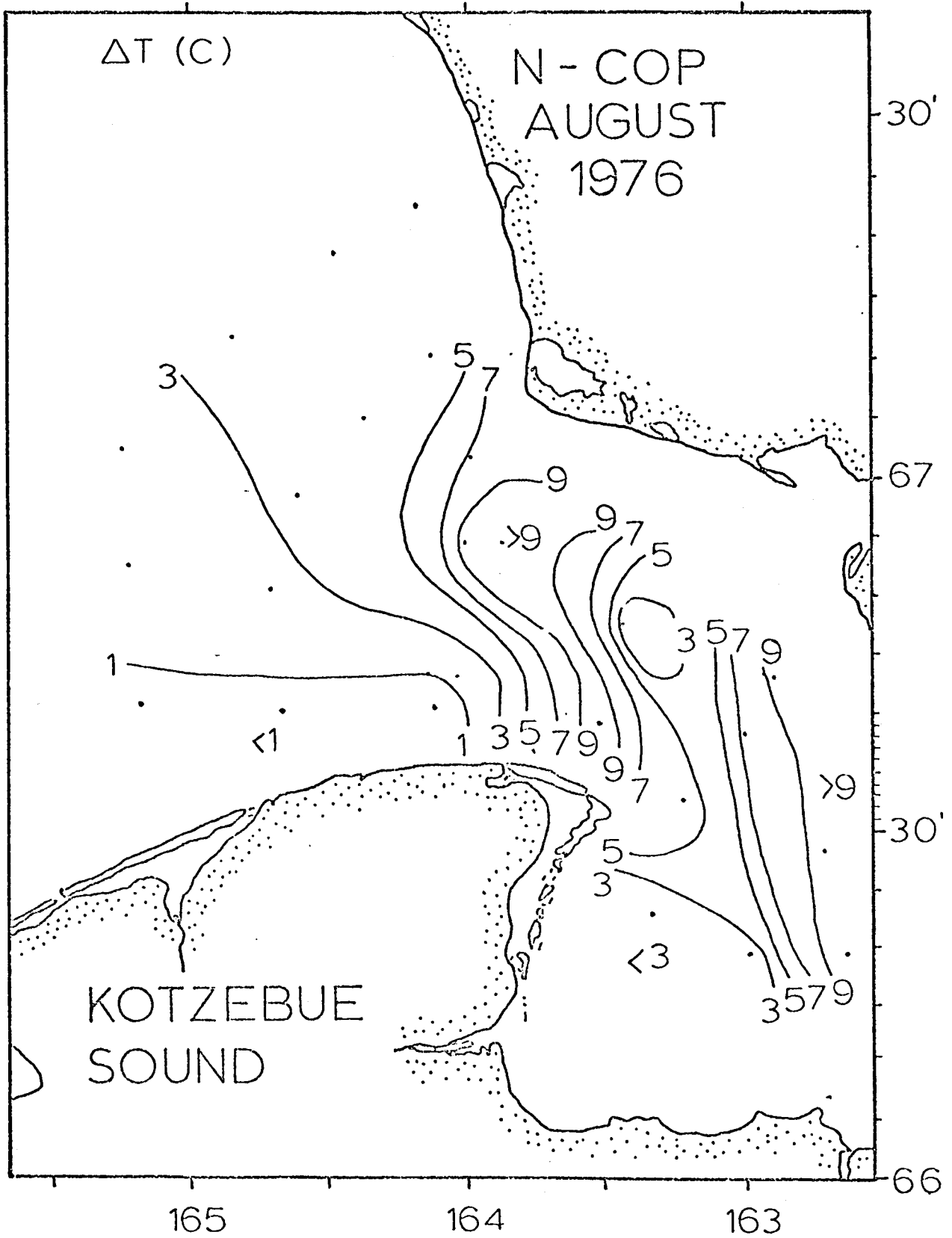


Figure 29. Temperature difference, surface minus bottom.

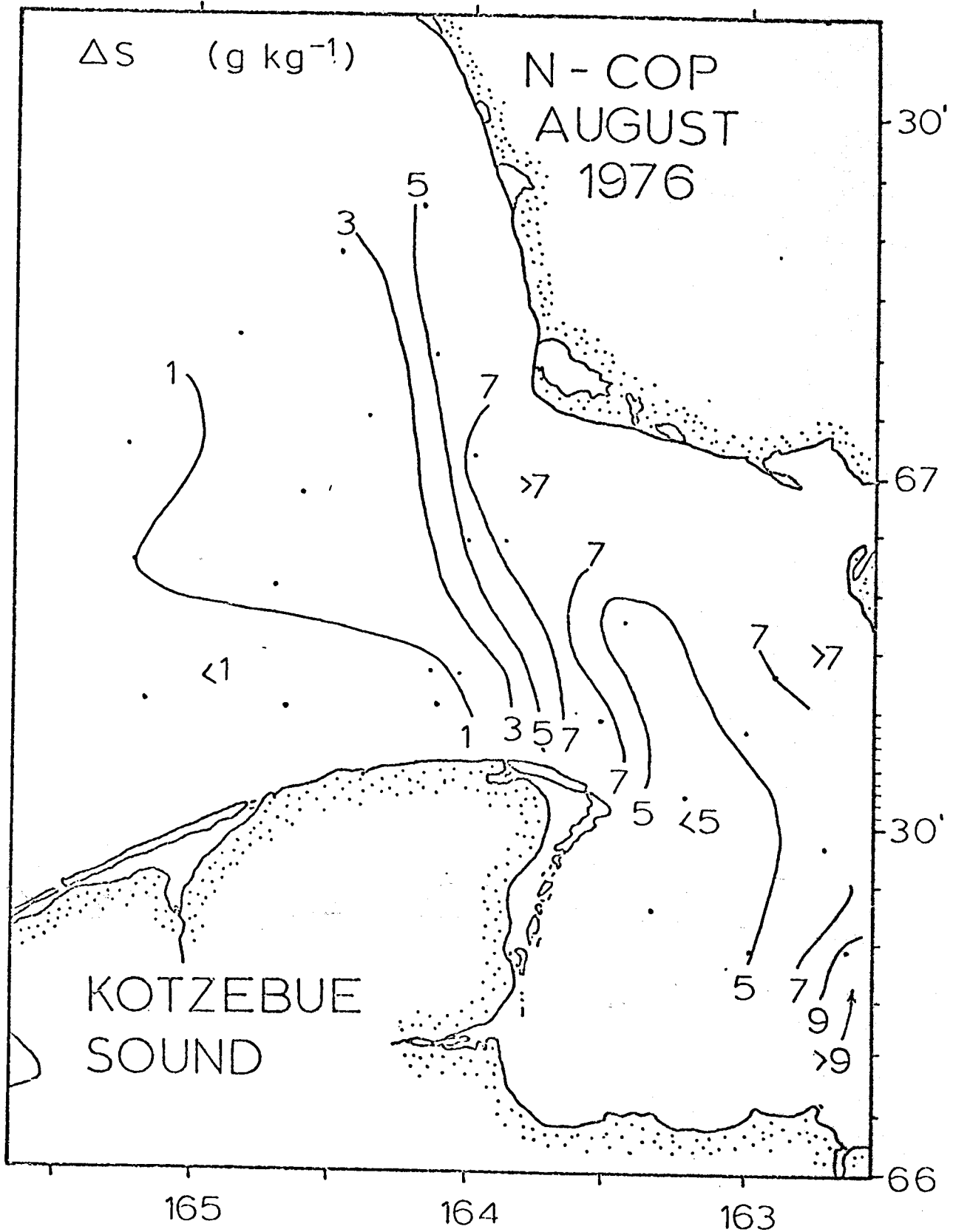


Figure 30. Salinity difference, bottom minus surface.

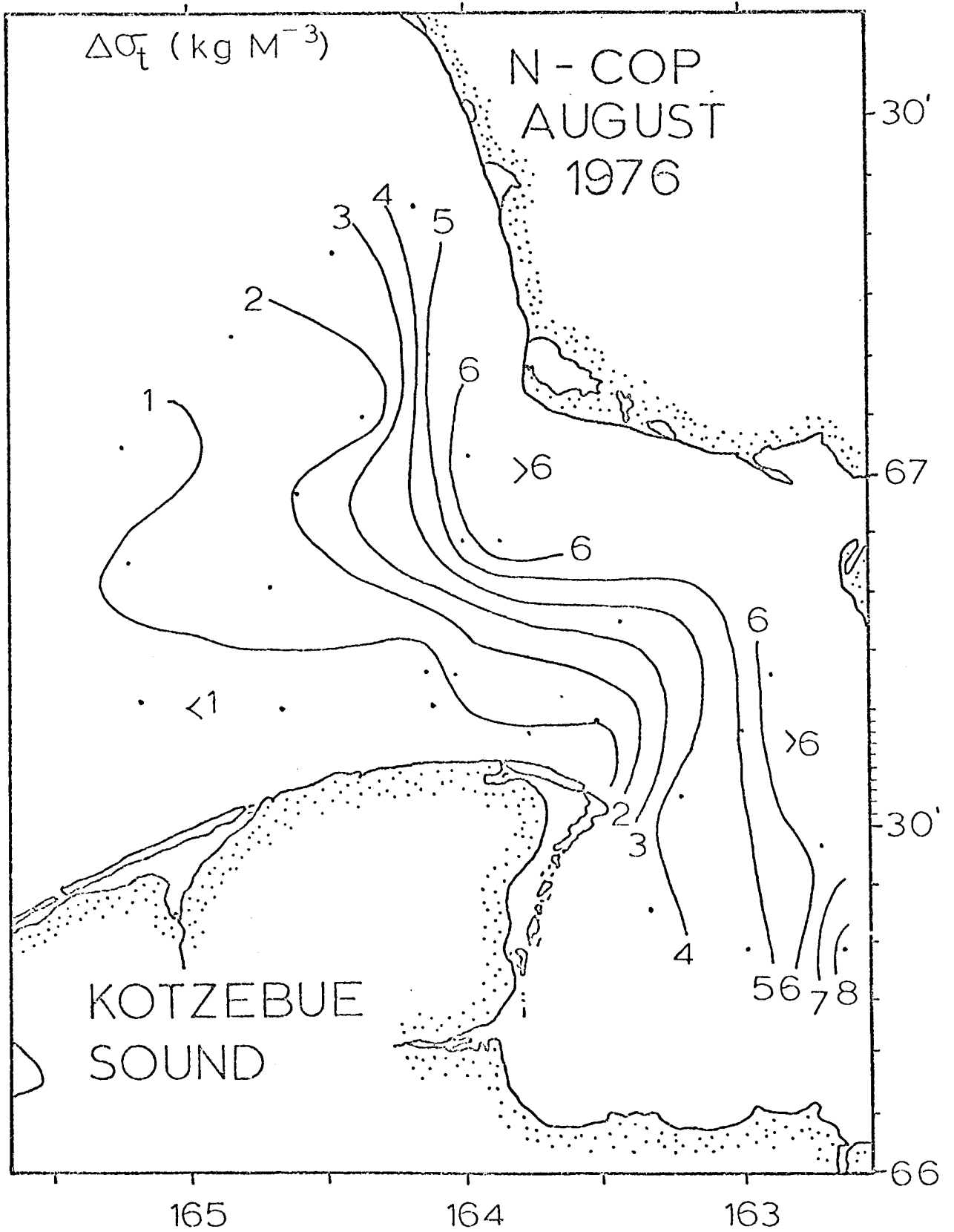


Figure 31. Density (σ_t) difference, bottom minus surface.

survey grid near 67N, and it markedly affects the stratification and surface salinity distributions.

The presence of the relict winter water and of the very high vertical stratification shows that the bottom water remains in place for periods of months. This means that:

- 1) Horizontal advection is too sluggish to flush out the Sound.
- 2) Horizontal diffusion (*i.e.*, processes with shorter periods than weeks, including tides and weather) is ineffective in renewing the bottom water.
- 3) Vertical mixing is insufficient to overcome the buoyancy input from river runoff and insolation. This implies that tidal energy is low, and that in summer 1976 the winds were light.

By implication, pollutant dispersion in the lower layer would proceed slowly.

Finally, we emphasize that these results are preliminary. A more comprehensive report is in progress.

D. BERING STRAIT REGION HYDROGRAPHY

From the August 1976 cruise of the *Discoverer* (Figure 3), we have constructed hydrographic cross sections (Figures 32 to 43). These should be considered with the concurrent measurements of water velocity and the resulting transport calculations (section 2, Table 4).

Figures 32 to 34 show the section taken south of Bering Strait projected on a cross section of the Strait. Comparing this to the average late summer (20 August to 5 October) cross section of Coachman, Aagaard and Tripp (1975, Figure 31b), the eastern and shallow parts of the Strait are similar, but the deeper and western portions were somewhat saltier and colder than average in 1976. This difference is in the direction of the early summer (5 July to 7 August) values, and may be typical.

The St. Lawrence sections (Figures 35 to 37) show very strong thermal stratification and a much less pronounced haline stratification. This may be caused by the noisy salinity record (thermal spiking): within the thermocline, the isohalines had to be estimated. Both the east and west passages have isopycnals sloping downward to the east, implying northward flow in agreement with the current measurements.

The Cape Lisburne sections (Figures 38 and 40) show some variability on a scale which is unresolved by the station spacing. The isopycnals imply northward flow near the center of the section and also near the Alaskan coast. At the southwestern end of the section the dilute, southward flowing, Siberian coastal current is clearly shown.

Figures 41 to 43 show the long section from the edge of the ice pack, south to Bering Strait. Near the ice edge, cold (< -1 C) and salty (> 33 g kg⁻¹) water resided in the bottom 15 m. This condition is normal as these cold temperatures and high salinities are characteristic of the winter Arctic shelf water. Particularly in the upper 10 m, the distributions show variability that is not fully resolved by the station spacing, in contrast to the sections across Bering Strait and near St. Lawrence Island.

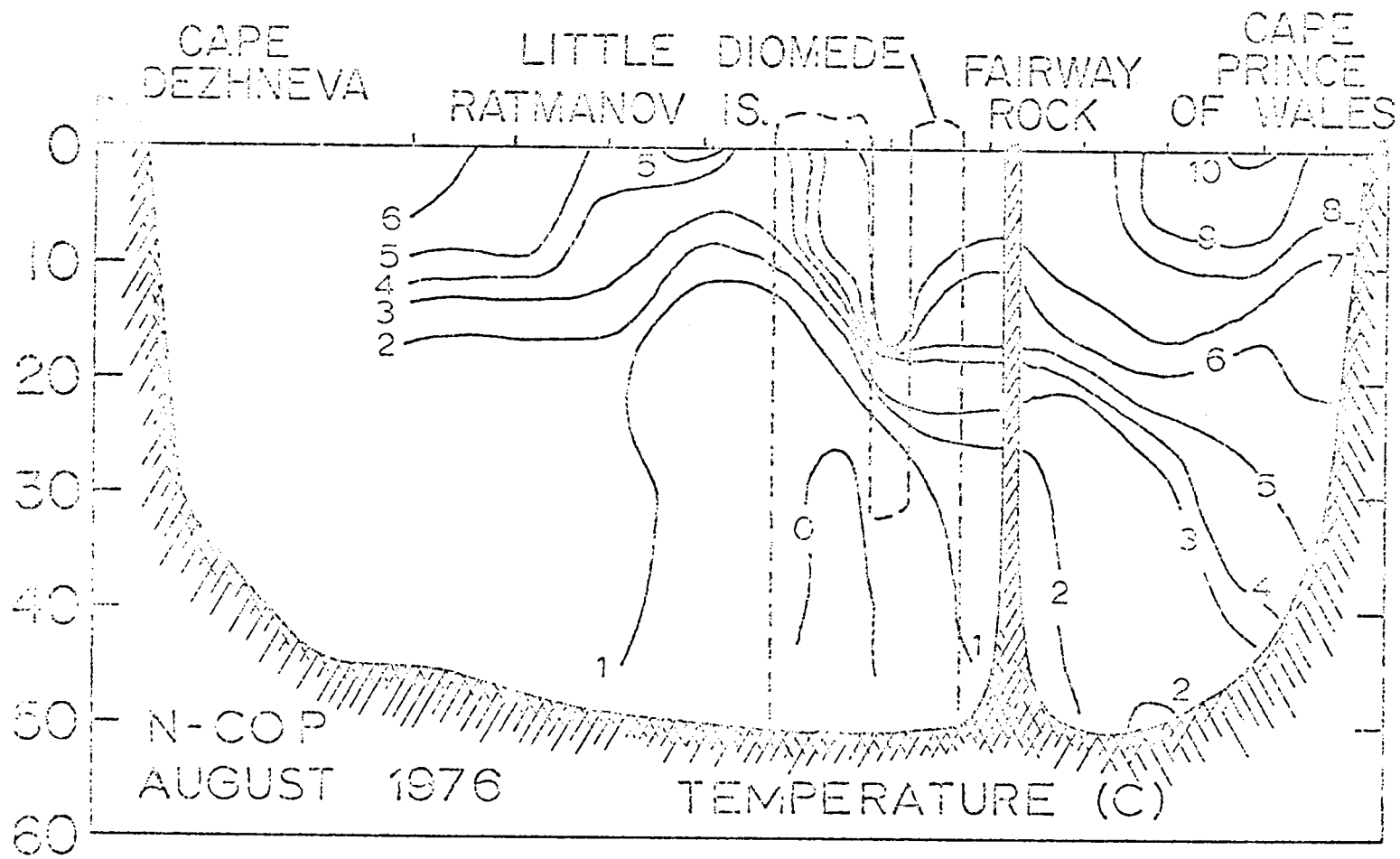


Figure 32. Temperature, Bering Strait section.

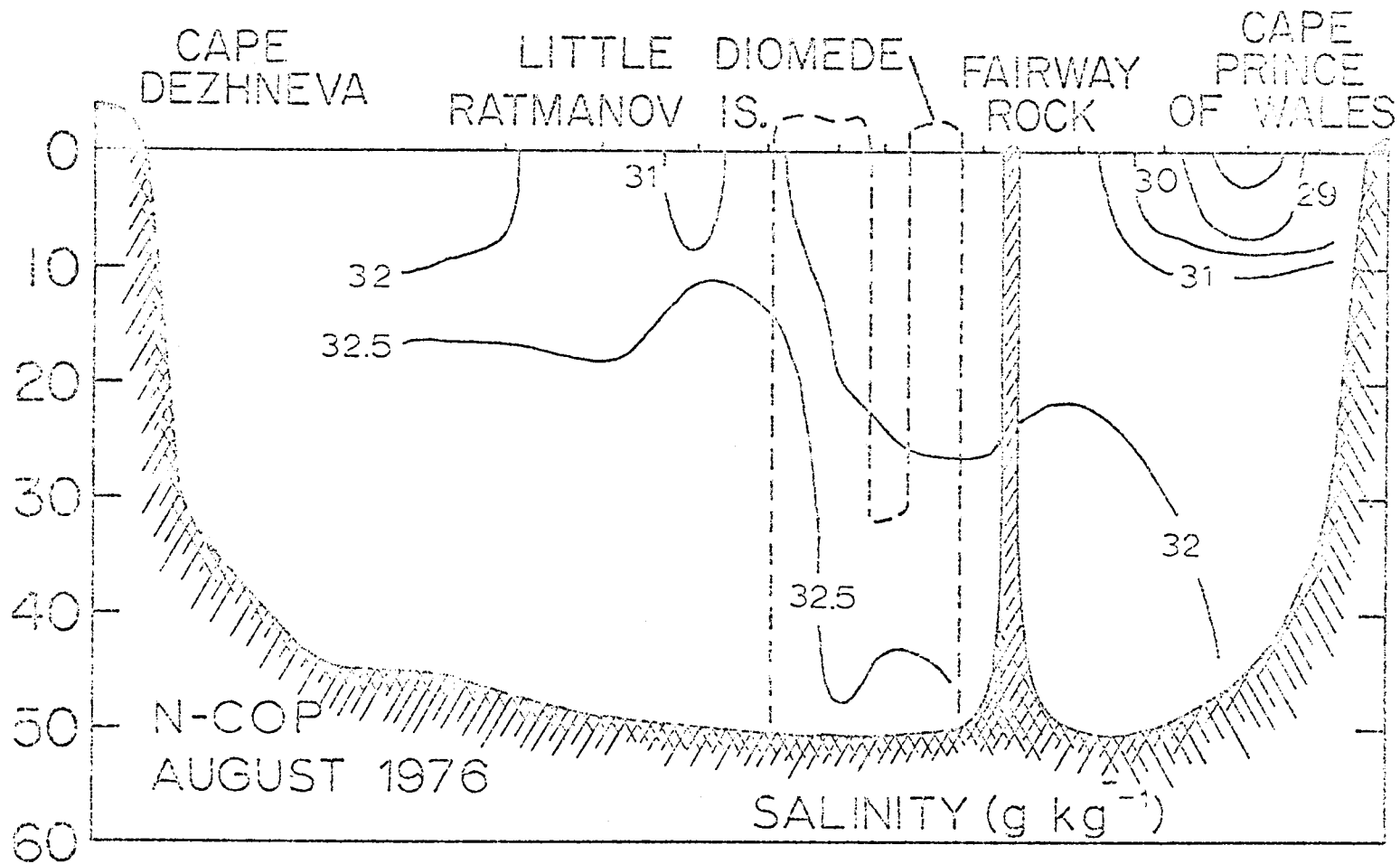


Figure 33. Salinity, Bering Strait section.

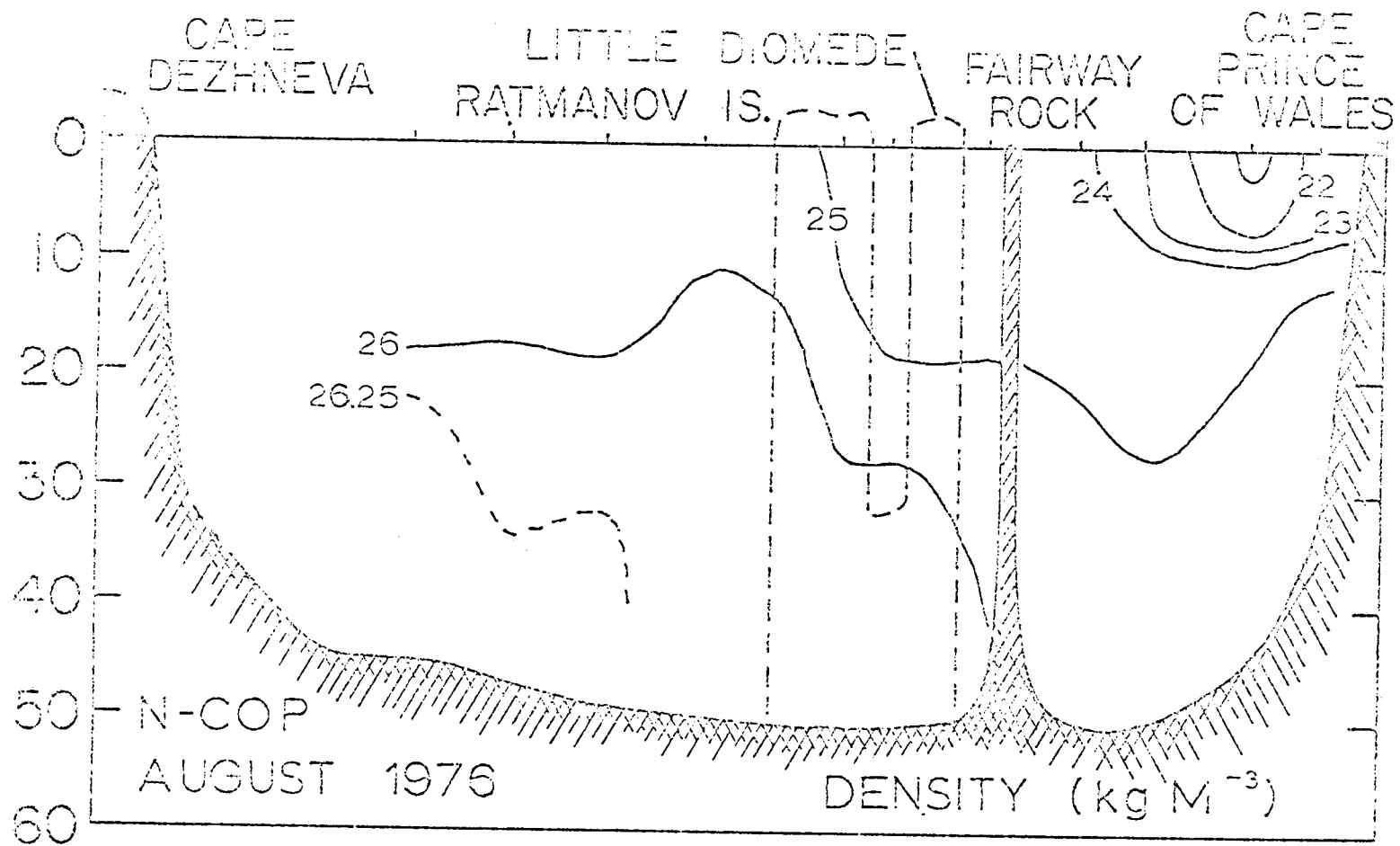
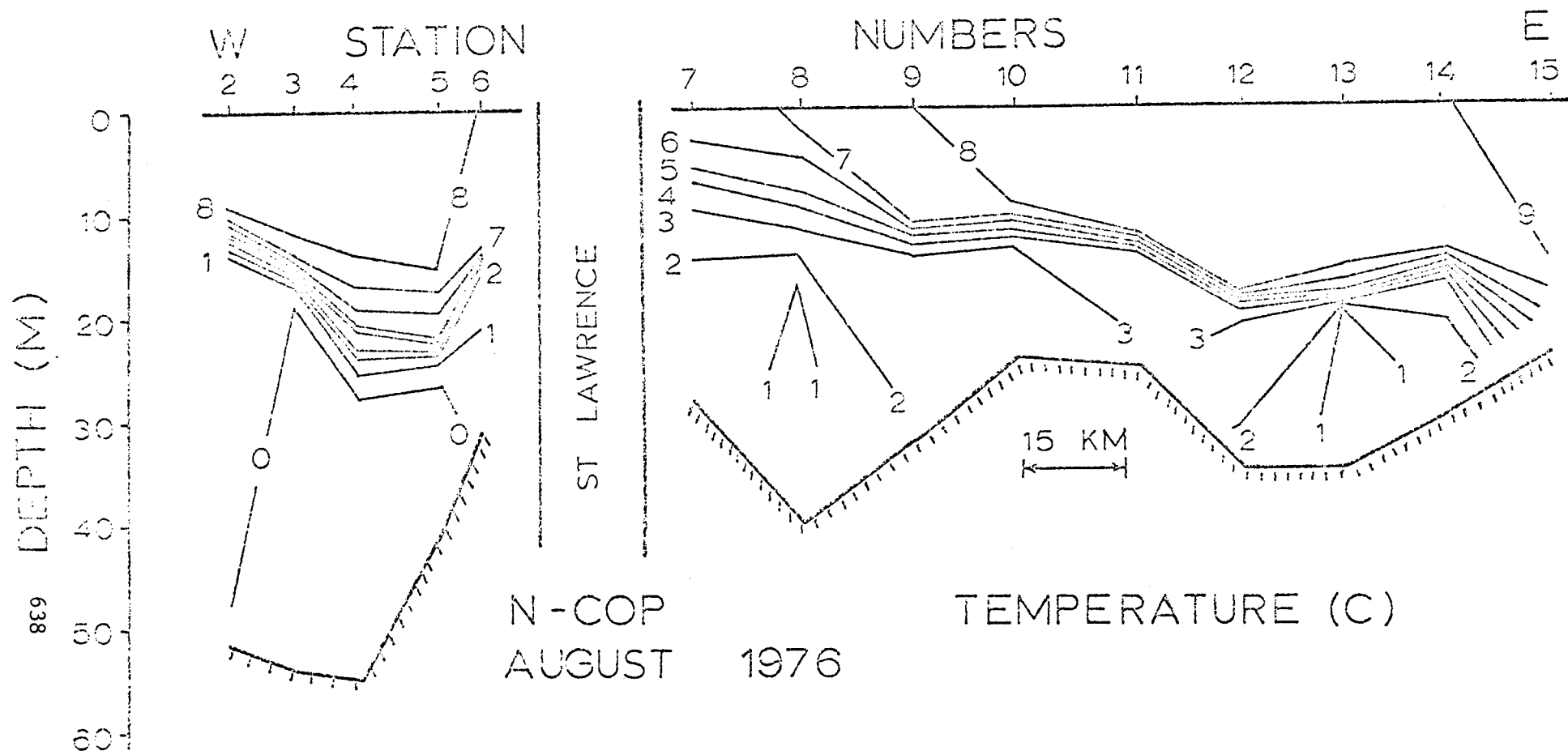


Figure 34. Density (σ_t), Bering Strait section.



N-COP
AUGUST

1976

TEMPERATURE (C)

Figure 35. Temperature, St. Lawrence section.

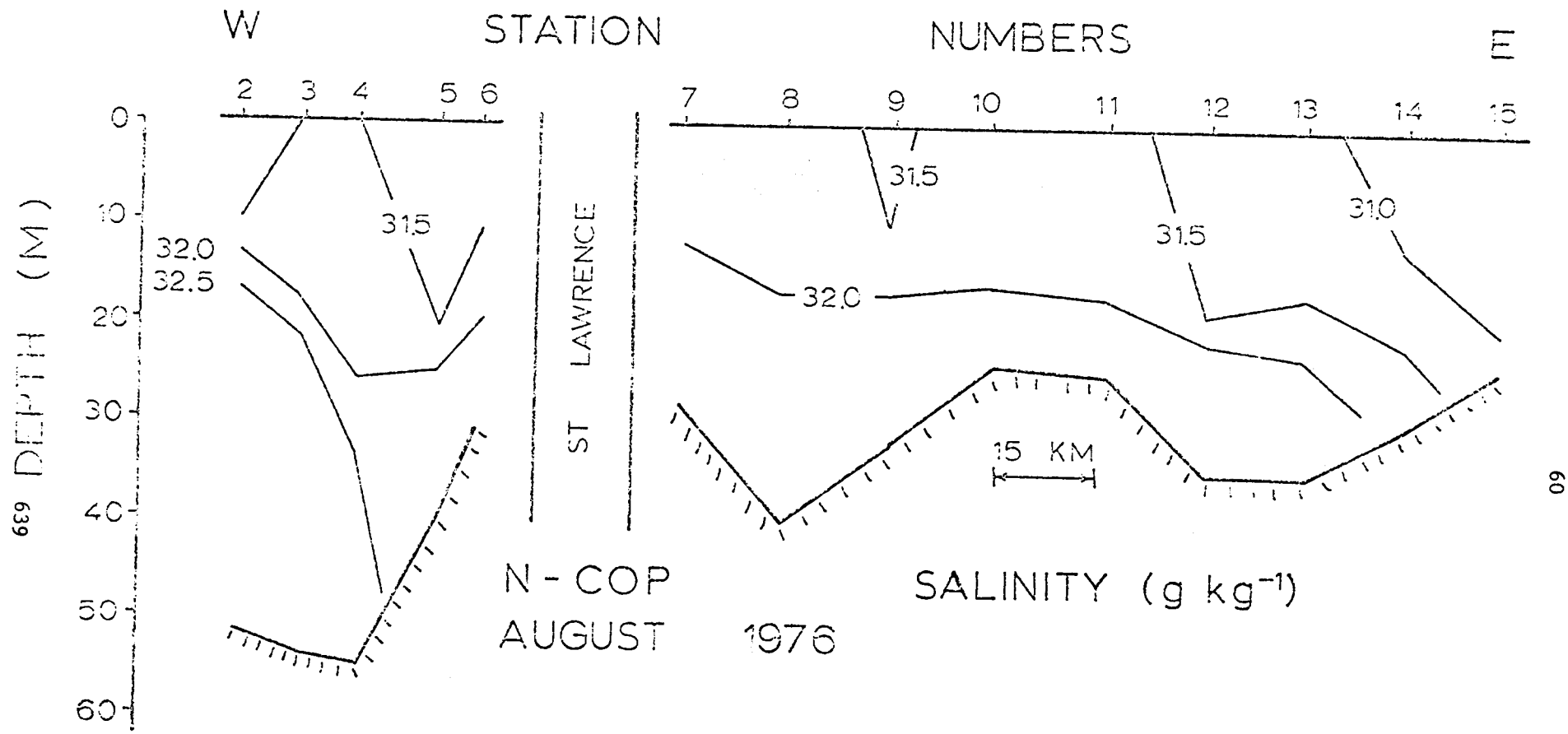


Figure 36. Salinity, St. Lawrence section.

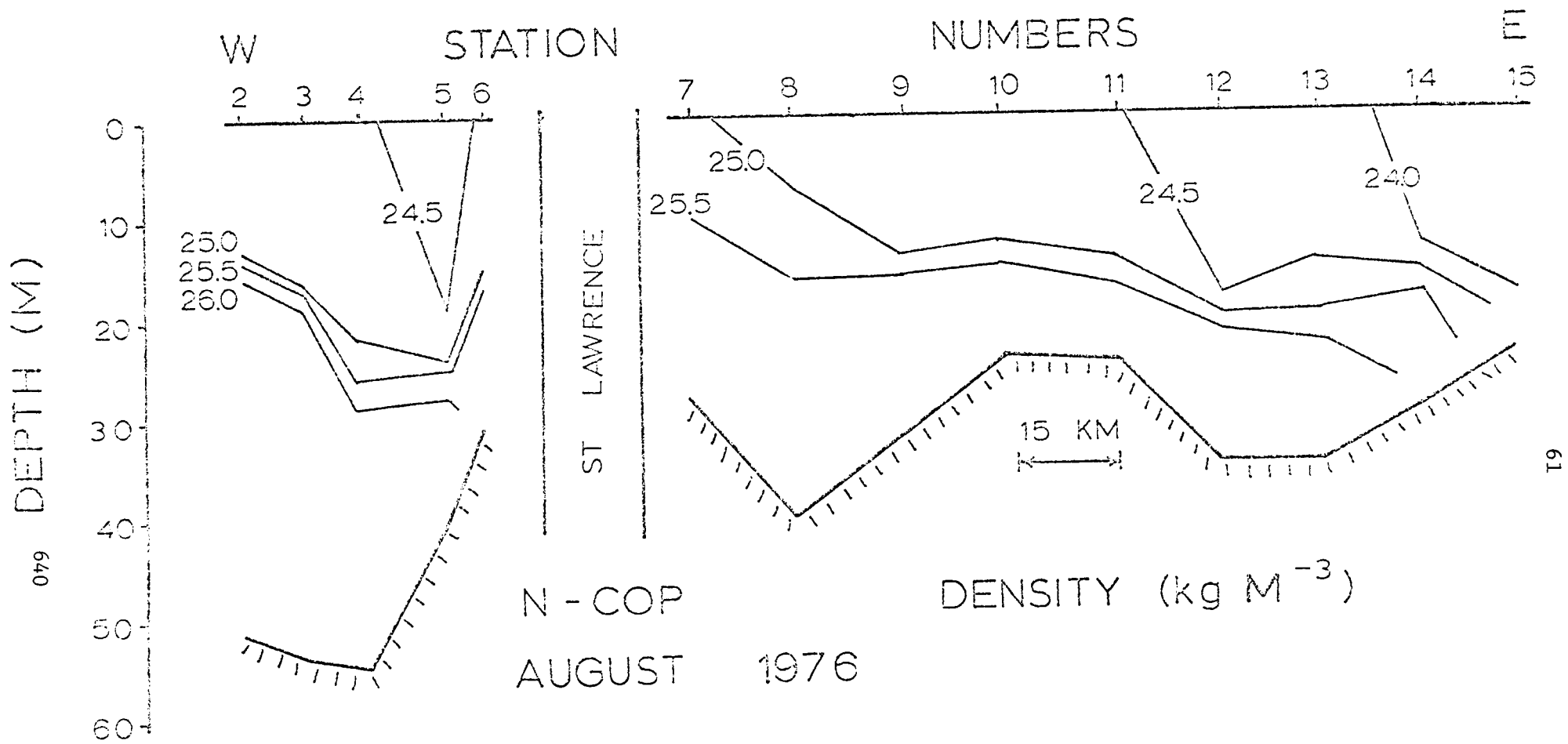


Figure 37. Density (σ_t), St. Lawrence section.

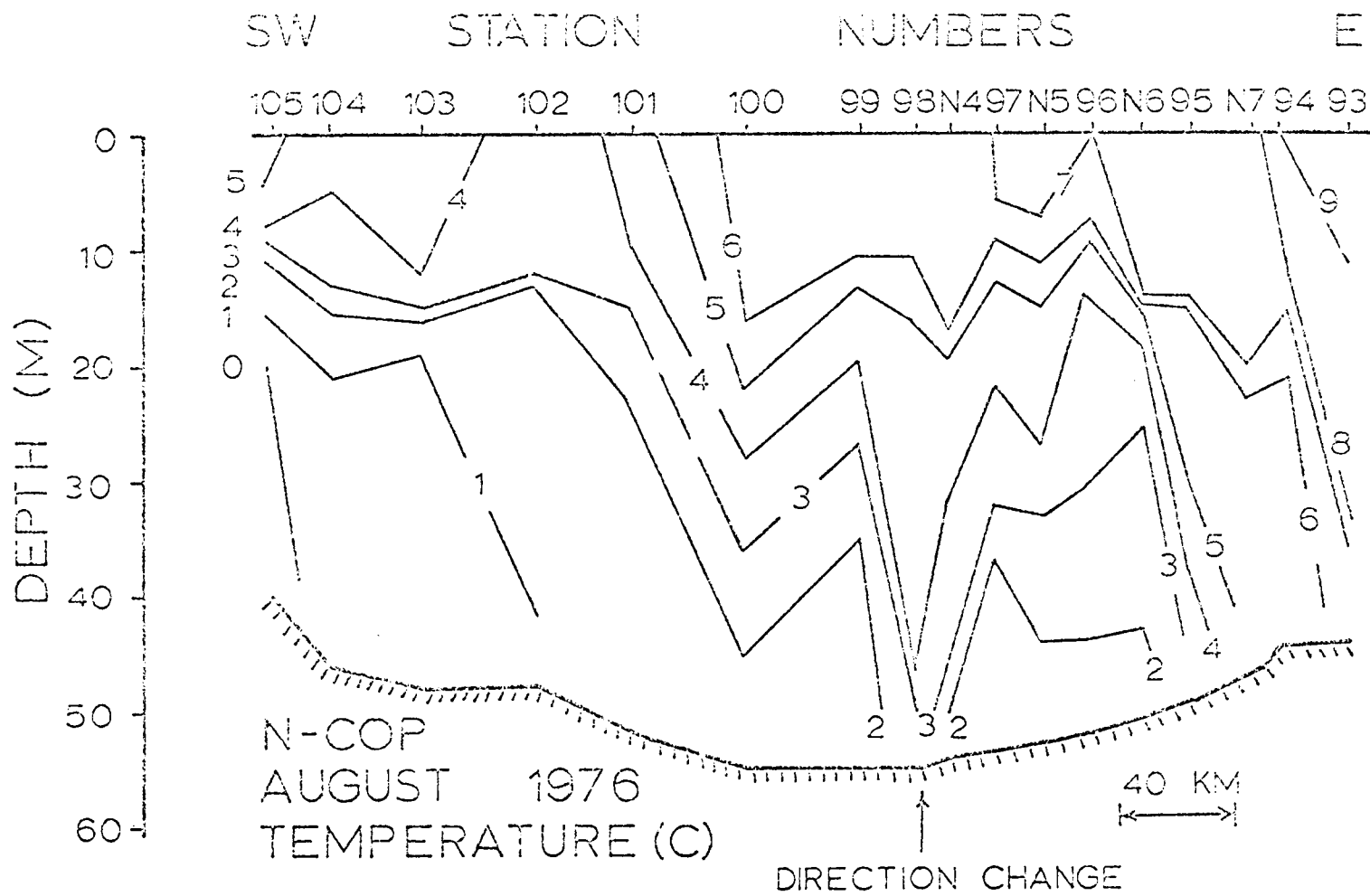


Figure 38. Temperature, Cape Lisburne section.

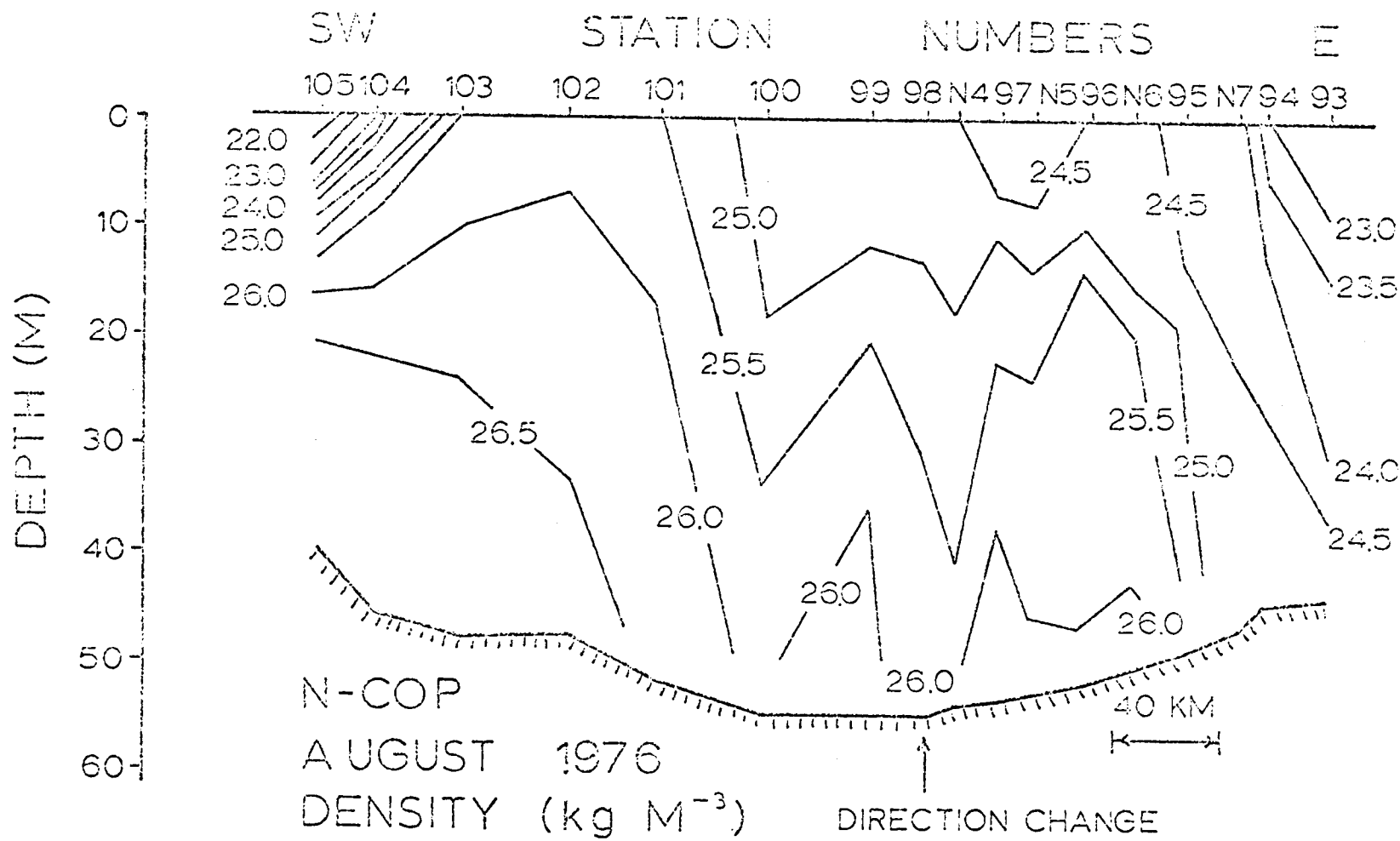


Figure 40. Density (σ_t), Cape Lisburne section.

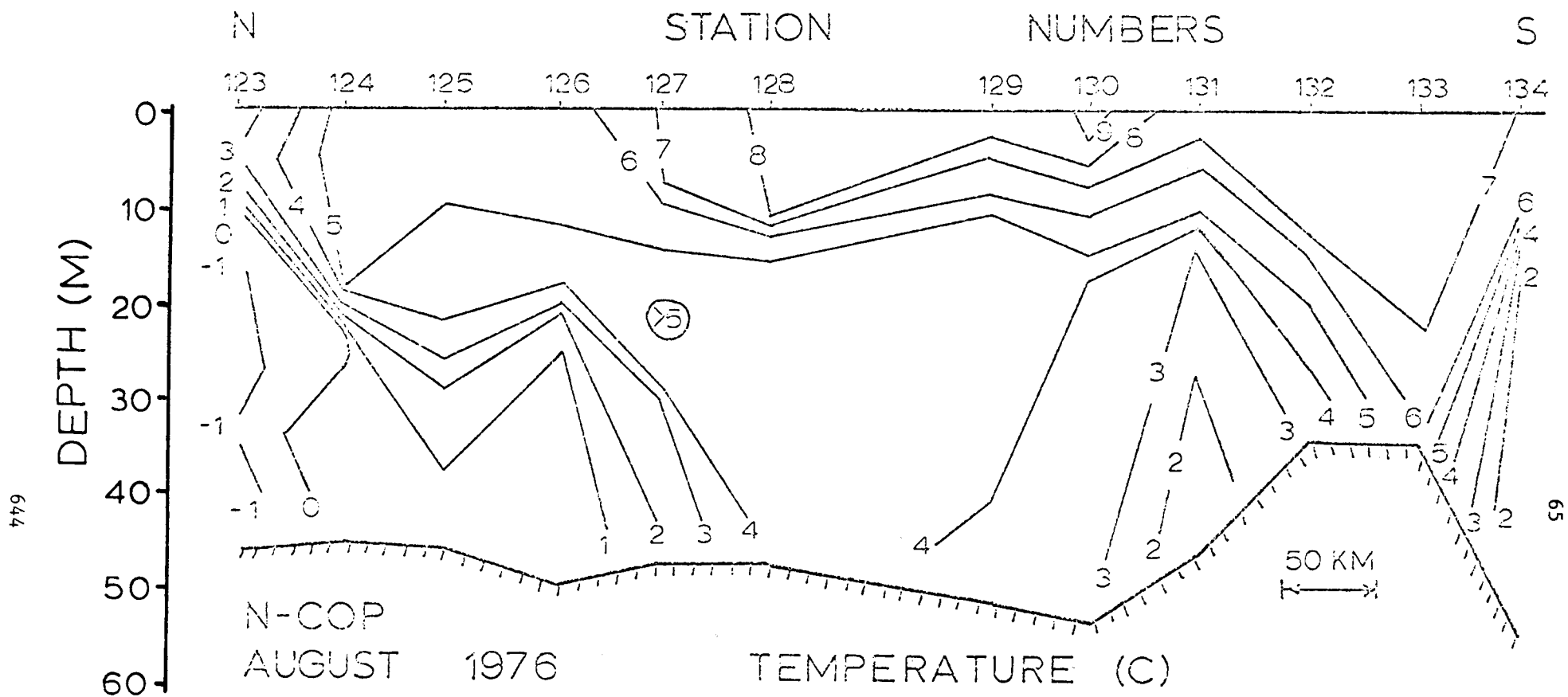


Figure 41. Temperature, ice edge to Bering Strait.

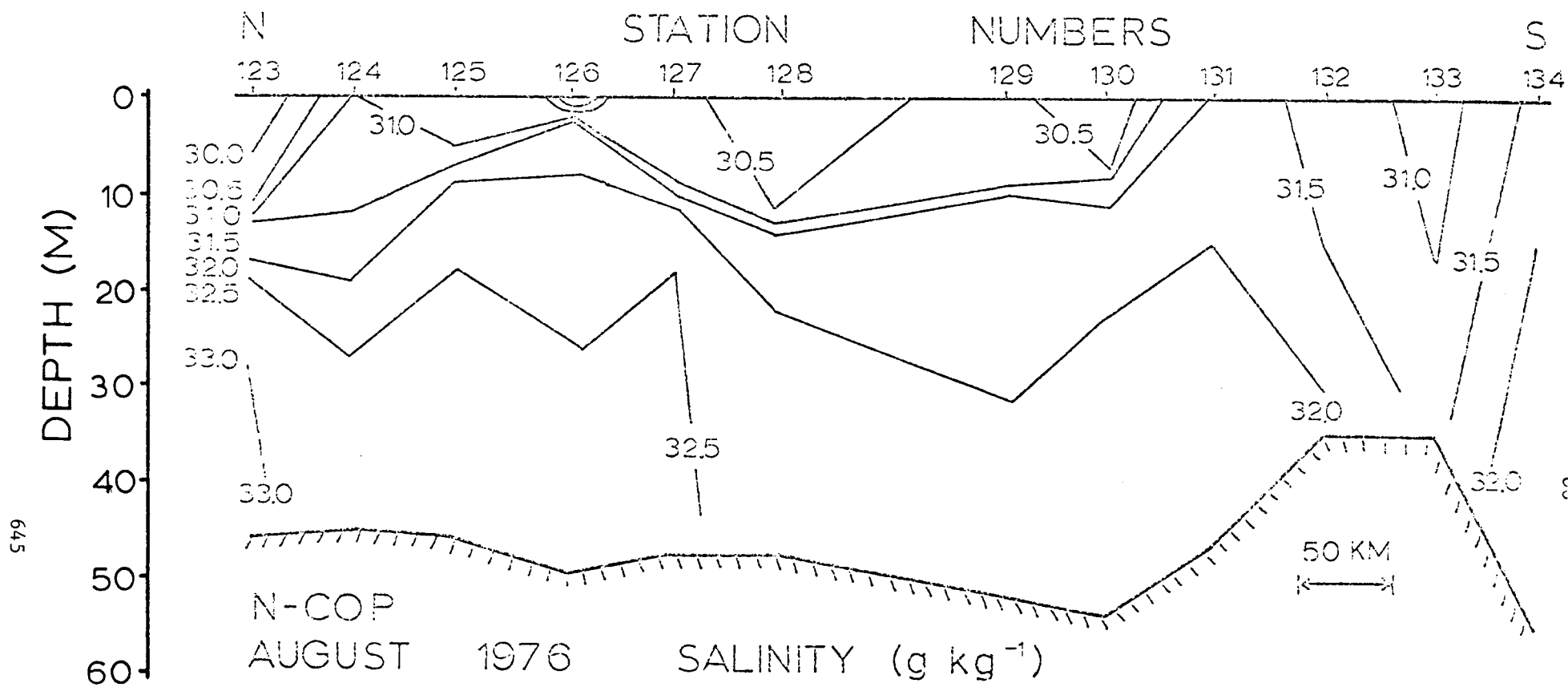


Figure 41. Temperature, ice edge to Bering Strait.

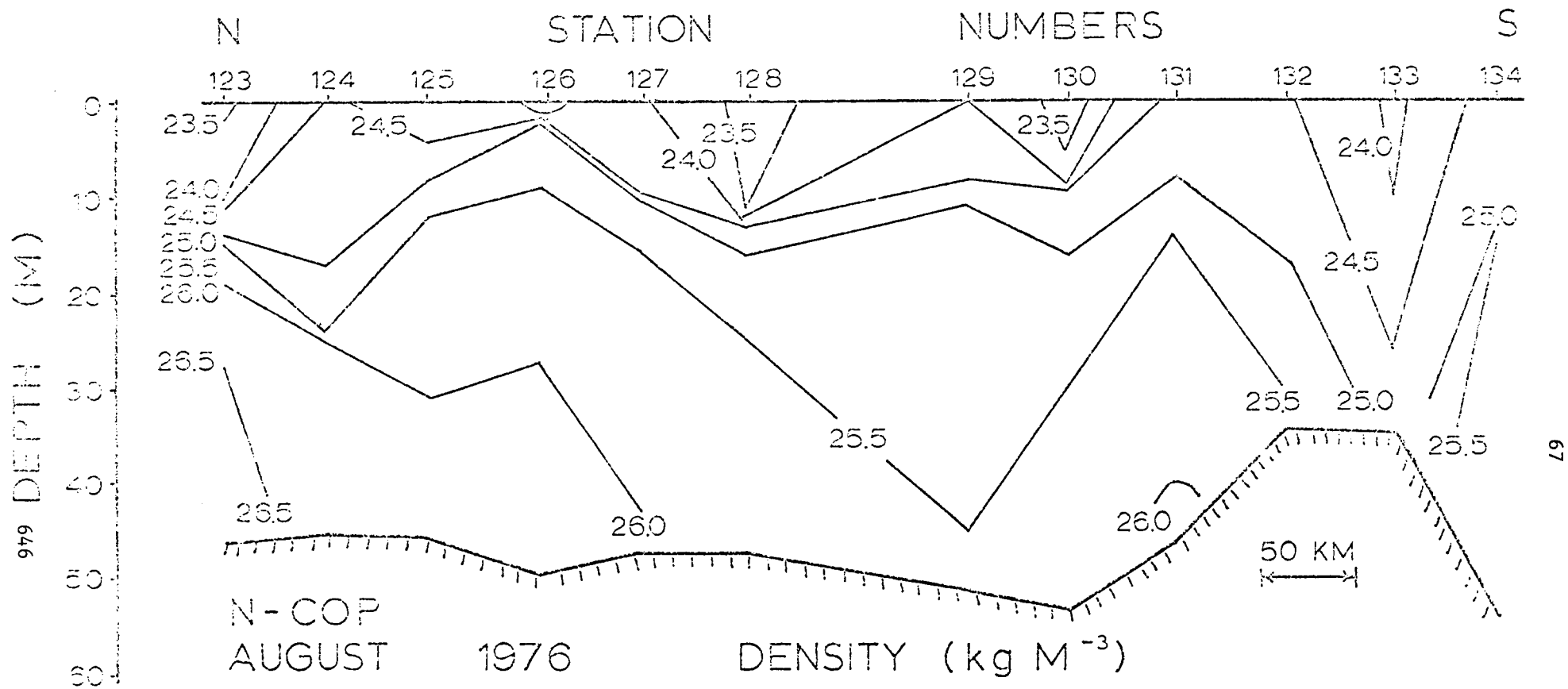


Figure 43. Density (σ_t), ice edge to Bering Strait.

VII. DISCUSSION

A. THE SEPTEMBER-OCTOBER NORTON SOUND PROGRAM

Geographic setting and morphology of Norton Sound suggest several features of the regional oceanographic processes: (1) transient wind-driven motions are large, (2) tidal motions are of only secondary importance, (3) sea-air heat and moisture exchange are dominant locally in conditioning water masses, (4) a south-north current across the mouth of the Sound may play a role in establishing mean circulation and (5) the bathymetry is important in guiding the circulation. The region has more of the character of a shallow sea than of a shelf due to its great horizontal extent, shallow depths, and lack of a shelf break. The shelf break exists, but is hundreds of kilometers to the southwest and effectively isolated from the Sound, if we consider the radius of deformation as an appropriate length scale.

The mean current measurements across the mouth of the Sound indicate a westward component of flow at each station except for the ten-hour series at N3 (Figure 16). Clearly such a flow, if steady-state, is impossible from continuity considerations, since it would result in a water level lowering within the Sound. These transports are of the proper direction and magnitude, except for station 22, to be due to surface winds. At station 22 it is necessary to consider the baroclinicity of the water column to account for the magnitudes of observed currents, but for the moment we concentrate on the wind-driven aspects. Transport at station 22 was constrained by the coastline to a westerly direction, while transports farther offshore were to the right of the wind. Greater depths (stations 24 and 25) allowed a transport farther to the right of the wind than at the shallower depth (station 26) in accordance with Ekman drift theory (Neumann and Pierson, 1966).

Currents observed at station N3 were in marked contrast to those observed elsewhere in that they do not appear to be wind-driven. The lack of correlation between currents and tides for the other time-series stations suggests that tidal effects may be relatively insignificant, but we really don't know the tidal regime in sufficient detail to be able to relate events at specific locations. During occupation of this station, the wind had veered and had become more northerly than during the other measurements (Figure 18). This removal of a westward-directed wind stress allowed the previously established sea surface slope to force easterly flow throughout the water column. The distribution of longshore currents in the water column supports this (Figure 19); rather than maximum speed at the surface, as expected for a wind current, there was a subsurface maximum at 7 meters and only a slight decrease between there and the bottom. The current speed was small near the surface. Both this and the offshore near-surface flow were likely a response to the offshore winds. The small variation in longshore current speed with depth, except for a near-bottom decrease which was probably frictional, suggests a barotropic driving force.

Interpretation of water movement is made difficult by nonsynopticity of measurements. While a net westward flow component was observed at each of the 25-hour stations, there was a two-day break between stations 24 and 25 during which station N3 was occupied. It is possible that during this two-day period all water flowed eastward into the Sound. It is also possible that the boundary between east/west flow shifted to the north and put N3 in a typically south Sound regime; westward flow would occur only in a very narrow (15-20 km) band south of Nome.

These admittedly brief current measurements are, however, adequate to suggest that wind-driven currents play a dominant role in Norton Sound circulation. Because of shallow depths (less than half the estimated Ekman compensation depth),

transports more nearly parallel the winds than in the deep ocean case where transports tend to be directed 90° to the right of the wind.

The strong pycnocline was a persistent feature of the Norton Sound water column. Measurements revealed no appreciable decoupling of currents across this feature in most cases. Only in the on-offshore component at station 22 was there a suggestion of decoupling (Figure 19); onshore flow above 10 meters was much greater ($18-20 \text{ cm sec}^{-1}$) than below ($2-3 \text{ cm sec}^{-1}$).

Both current and hydrographic measurements in the region just offshore from Nome revealed the presence of a strong coastal current consisting of a westward baroclinic current upon which was superposed a local wind-driven component. The baroclinic current, clearly evidenced as a band of low-density water, was restricted to within 15-20 km of shore (Figure 12) and was of uncertain east-west extent. The baroclinic component of this current was a consequence of dilution by runoff. Numerous small streams enter northern Norton Sound, particularly in the Norton Bay region. There are, however, no estimates available for freshwater input. More than sufficient freshwater enters the northern Bering Sea via the Yukon River to create such baroclinicity. Mean maximum runoff of the Yukon is on the order of $10^4 \text{ m}^3 \text{ sec}^{-1}$ (U.S.G.S. records) or on the same order as the entire flow of the coastal current during June and July, and was $5.6 \times 10^3 \text{ m}^3 \text{ sec}^{-1}$ during the early portion of this fieldwork. The hydrographic data obtained in southwestern Norton Sound indicated, however, that Yukon water was not entering Norton Sound circulation in appreciable amounts at the time of this cruise (Figure 15). A small amount of Yukon water was probably entering the general circulation near Stuart Island and then moving north and west. It therefore appears that the baroclinic current was largely supported by local runoff along the north shore of the Sound.

The strongly two-layered structure is typical of shallow, near-shore regions subject to both tides and wind mixing. The upper mixed layer is due to the

effects of wind, while the lower mixed layer is a result of turbulence generated by currents at the bottom. It is possible that high winds could mix the Sound completely to the bottom or that, in the absence of winds for a long period of time, the lower mixed layer could extend closer to the surface and result in effective thinning of the upper layer.

Tidal currents are responsible for the presence of a bottom mixed layer. The tides at Nome are of the semidiurnal mixed variety, with maximum tidal amplitudes on the order of 50 cm. While these might lead to significant excursion and associated currents in the western Sound, frictional damping would likely have caused attenuation of the wave by the time it reached the eastern Sound. While no measurements are available, it is probable that tides are small in the eastern Sound.

The presence of cold ($< 2.5^{\circ}\text{C}$) near-bottom water in the eastern Sound presents an intriguing problem. A temperature-salinity plot of the waters in the Sound indicates that there was no external source for this cold water at the time of the cruise, which suggests that the cold water was most likely a remnant of water formed during the previous winter (Figure 22). That this water has persisted for some 4-5 months in a total water depth of about 20 meters and despite wind and tidal mixing and insolation suggests: (1) vertical mixing through the pycnocline was extremely small; (2) horizontal advection of bottom water into the eastern Sound was negligible; and, (3) solar insolation, particularly significant during the early summer because of 24-hour daylight, was unable to penetrate the bottom layer sufficiently to cause appreciable warming.

Neglect advection and heat sources and sinks. Assume that temperature of the bottom water at the end of the preceding winter was near the freezing point at -1.7°C , and that the temperature of the upper layer had reached 8°C by early August following a linear increase with time from early May when the ice first

melted. These conditions require a vertical mixing coefficient through the pycnocline of $2.5 \times 10^{-2} \text{ cm}^2 \text{ sec}^{-1}$. Though this may seem small for a vertical eddy coefficient, we believe it may be the right order for these conditions. Just west of Nome Coachman *et al.* (1975) estimated K_v 's of order 10^{-1} where 10^8 E was order 200 m^{-1} . At stations in the inner sound (44,48) 10^8 E was order $2.5 \times 10^5 \text{ m}^{-1}$ over 2 to 3 m depth increments, an extreme stability. This unusually small vertical mixing may reflect abnormally mild weather during the preceding summer. Virtually no storms passed over Norton Sound during the two-month period preceding the cruise.

It is possible to estimate an advection rate using the temperature distribution in Figure 6 if we assume this distribution to be steady-state and to reflect a balance between horizontal advection and lateral diffusion. A horizontal length scale of 100 km, applied to the empirical findings of Okubo and Ozmidov (1970), yields a lateral eddy conductivity of $10^6 \text{ cm}^2 \text{ sec}^{-1}$. Application of the method given by Proudman (1952) leads to estimates of an advection rate on the order of 1 cm sec^{-1} along the westward trending tongue of $7.0\text{--}8.5^\circ\text{C}$ water. It is not clear why horizontal advection should be small in the eastern Sound. The promontories formed by Stuart Island on the south and Cape Darby on the north are apparently sufficient to deflect whatever easterly flow exists along the southern shore of the Sound to the north, preventing it from entering the eastern third. There is no sill between these promontories which might prevent interchange of the deeper waters. A cyclonic circulation, as suggested above, is apparently confined to the western portion of the Sound with the eastern end forming a relatively stagnant cul-de-sac.

There is, however, a water mass continuity between the inner Sound and the western part (cf. Figures 13 and 15). In the T-S diagram (Figure 44) a close association is noted between inner Sound waters through stations 42 and 43 to

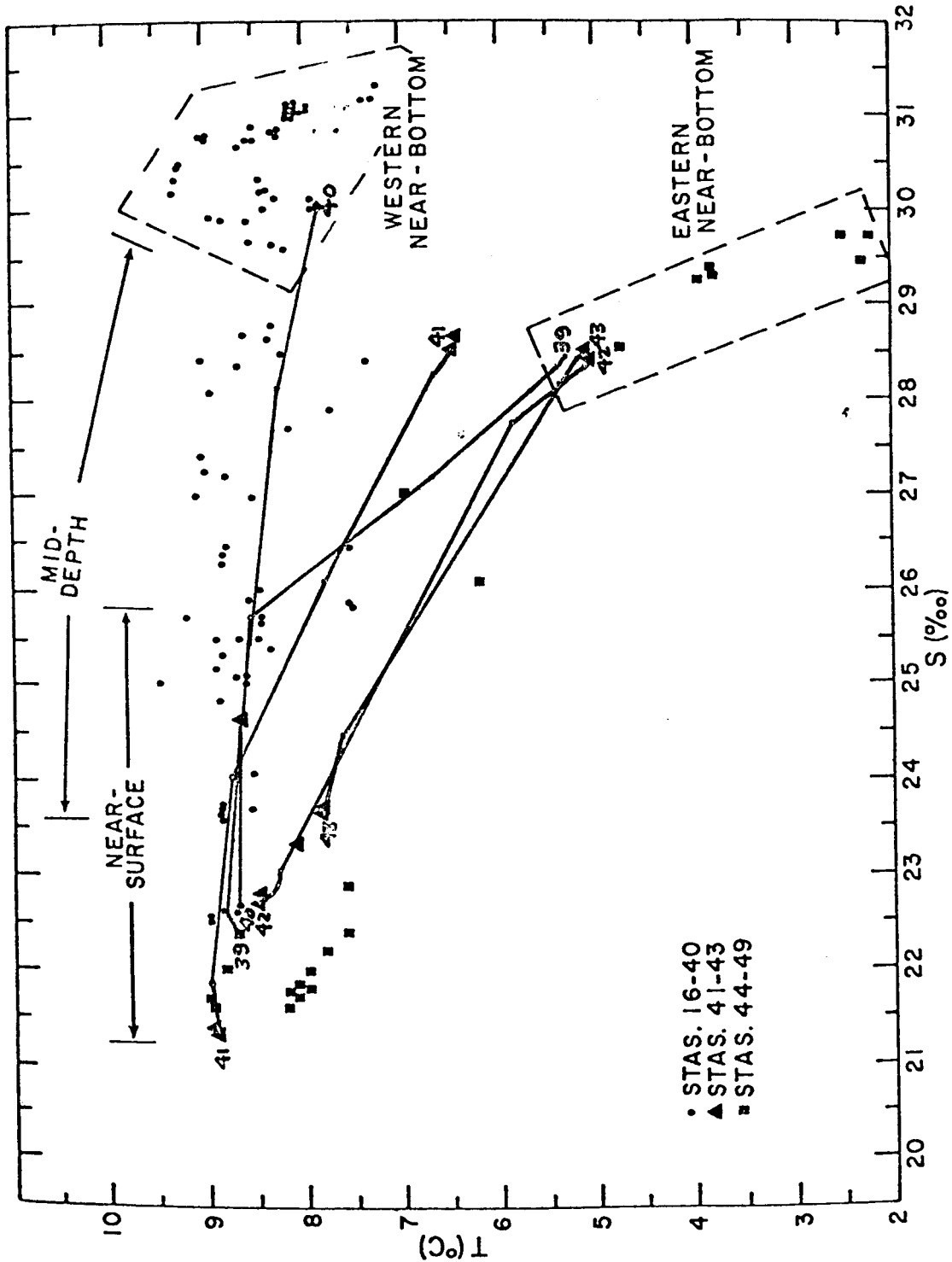


Figure 44. Temperature-salinity characteristics of the water in Norton Sound during late September-early October 1976. Complete water mass curves are shown for stations 39-43.

station 39. We conceive of the boundary not as one across which advection occurs, but rather a lateral diffusive flux boundary. The cyclonic circulation of the western Sound, passing north across the mouth of the inner Sound, in effect entrains some inner Sound water. We conclude that even though the inner Sound appears to be virtually isolated in the absence of strong storm conditions, and can retain relict water from the previous winter for many months, there is a slow diffusion out of the region.

Solar warming of the bottom layers might be expected. It is possible, however, that silt entering the Sound in freshwater would screen out a major portion of the solar radiation, resulting in more rapid warming of the upper layers and isolation of the bottom layer from warming influence. Silt carried by freshwater streams in this region is typically very fine and can remain suspended for long periods of time, particularly in the presence of wind mixing (personal observations and satellite photographs).

Based on the water mass distributions for 26 September-6 October, we have constructed a schematic diagram of the circulation (Figure 45). The short period current measurements do not necessarily reconcile with this scheme because of the demonstrated strong influence of local winds on the flow. The water mass properties suggest the longer-term or net circulation. With a strong and/or prolonged wind event, however, the circulation could be quite other than we have interpreted here from one data set. The circulation shown, however, may be generally representative because there were no strong wind events for at least two months prior to the survey.

The role of the northward circulation on the Bering shelf in inducing Norton Sound circulation is uncertain. Such a flow might: (1) create a south-north sea surface elevation difference across the mouth of the Sound which would then drive a circulation in the Sound as suggested for the Gulf of Maine by Csanady (1974); or (2) tend to follow bottom contours into the Sound, contributing to a cyclonic

CIRCULATION DEDUCED FROM WATER MASSES

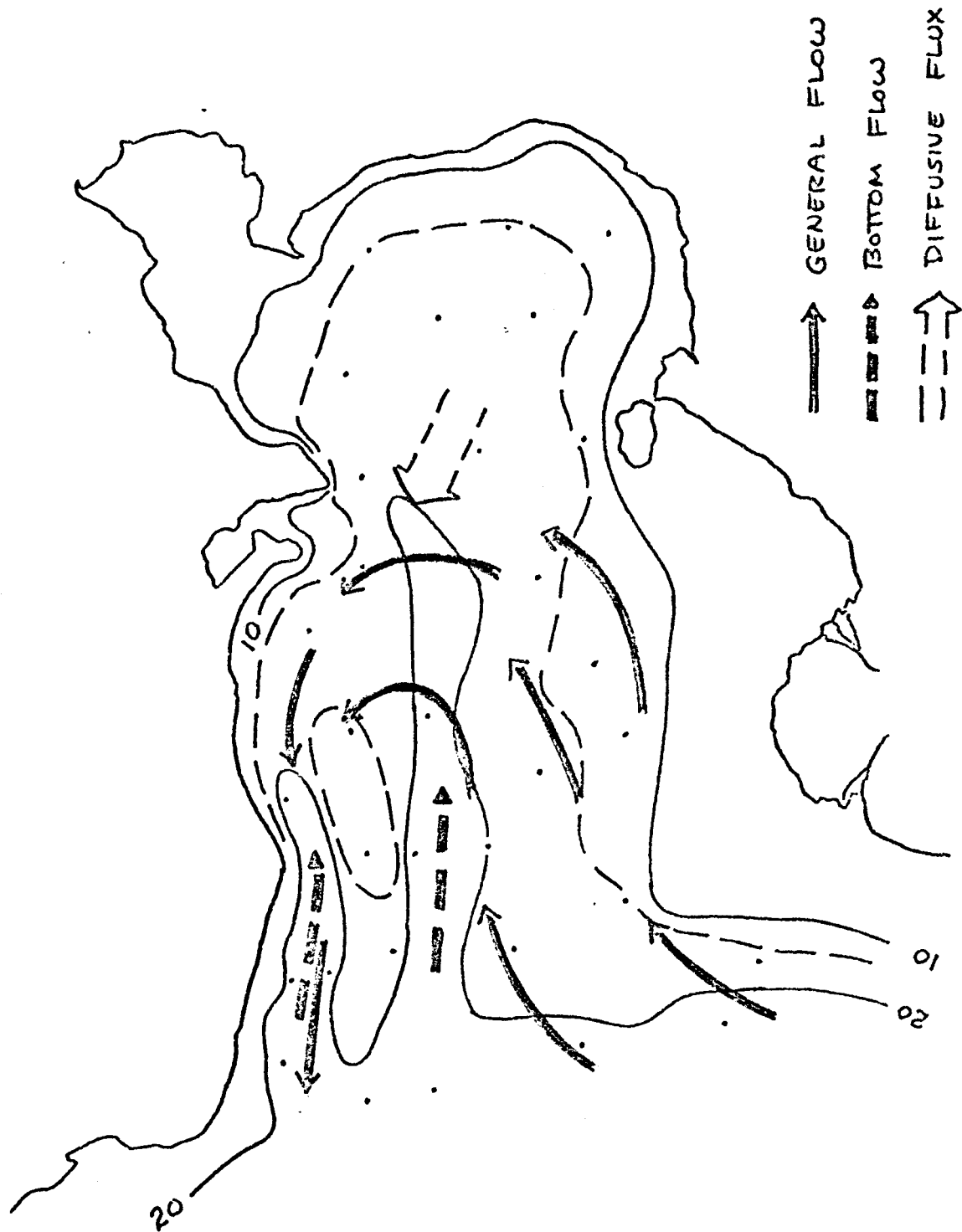


Figure 45. Schematic of circulation in Norton Sound based on September-October water mass data.

circulation there. Partial extension of this flow into the Sound was in fact suggested by northerly current components at the southern time-series stations 25 and 26 (Figure 16). This would, however, result in Yukon water entering the Sound; this was not observed. Such northerly flow would then veer to westerly at the northern coast of the Sound to satisfy both volume continuity and vorticity constraints. There was no evidence of a gyre-like flow as required by Csanady's model for the Gulf of Maine, but the current measurements would not have been adequate to define such a gyre were it present.

B. THE SEPTEMBER ANCHORED CURRENT MEASUREMENT PROGRAM

An attempt was made to apply the empirical equation of Coachman *et al.* (1975) relating transport through Bering Strait to sea-level atmospheric pressure at Nome. Daily atmospheric pressures from Nome are not available as yet, so two values were obtained by telephone from NWS Ashville, N.C. For the Bering Strait section, the predicted transport was 1.59 Sv rather than the 0.7 Sv observed. The pressure at Nome was, however, dropping rapidly at the time, suggesting non-steady conditions. Use of a sea level pressure value from Nome 18 hours later yields a predicted transport of 0.79 Sv. Coachman *et al.* noted that during periods of rapid change the correlation between Nome pressure and transport is improved by using a different time lag than the arbitrary one-day delay of the equation.

The much greater transport through the St. Lawrence Island section two days earlier appears to correlate well with the much higher atmospheric pressures of one and two days previously. Thus, we conclude that at the time of the 1976 measurements transport was northward through the system and in magnitude in agreement with previously documented flows.

C. KOTZEBUE SOUND HYDROGRAPHY

(See VI.)

D. BERING STRAIT REGION HYDROGRAPHY

(See VI.)

VIII. CONCLUSIONS

Norton Sound was characterized during field work in September-October as a strongly two-layered system. Current measurements obtained simultaneously with surface wind observations suggest that currents correlate well with the winds over time scales of about one day, but over hourly time scales they are not well-correlated. Both current measurements and temperature distribution support, qualitatively, a cyclonic water circulation in the Sound. The eastern third of the Sound formed a cul-de-sac having a sluggish circulation and low bottom temperatures due to residual water left from the previous winter. This situation may have been due in part to unusually mild summer weather during 1976, and may not be an annual feature, although the eastern Sound is certainly a lower energy region than the western portion.

The region off Nome was characterized by a 15-20 km wide coastal current system which was in part wind-driven and comprised a coastal downwelling regime, and in part baroclinic, driven by local runoff. This current was evidenced in the hydrographic structure by a low density coastal band of water, limited in east-west extent. Bottom scour off Nome suggests that this current may be a common feature.

The entire Norton-Chukchi study region was characterized by a net northward water transport on the order of $10^6 \text{ m}^3 \text{ s}^{-1}$, measured values being from 0.70 to $1.85 \times 10^6 \text{ m}^3 \text{ s}^{-1}$. This flow was in agreement with previous measurements, suggesting that regional water transport was not abnormal during late summer 1976.

In analogy with Norton Sound, Kotzebue Sound was highly stratified. Within the upper layer, there appeared to be a cyclonic circulation in the western half of the Sound. Relict water from the winter showed that the lower layer and eastern half of the Sound were nearly stagnant: pollutant dispersion there would be slow.

IX. NEEDS FOR FURTHER STUDY

At this stage of the Norton-Chukchi oceanographic program, with the year-round current arrays still deployed and summer 1977 field work still to be carried out, a list of detailed needs is somewhat premature. Nonetheless, it is possible to list several items which are not being addressed via the present program.

1. Winter oceanographic stations are needed in the northern Bering Sea to address seasonal variations. The winter 1977 field program obtained such data in the Chukchi Sea, but not in the Bering Sea (see Section X below). A winter program should seek to verify hypotheses concerning convective mixing and determine the effects of seasonal ice cover upon circulation. It is planned to deploy 3 moored current meter arrays in the St. Lawrence Island-Norton Sound region overwinter 1977-78 to address these problems.
2. Lagrangian drift studies, such as those using the satellite-tracked drifters, are needed to define the circulation patterns through the channel east of St. Lawrence Island and into western Norton Sound.
3. Virtually no data are available from inside the 6 fm (11 m) contour off the Yukon delta or into the Yukon estuary itself. In consideration of the apparently weak circulation in Norton Sound and the consequent possibility that a contaminant might remain off the Yukon mouth for some time, it is essential that information be acquired on the Yukon estuary, its dynamics and general nature.
4. Detailed studies are needed to determine the path and dynamics of the Yukon River plume. This plume, despite its probable prominence (projected from discharge figures), was not located during summer 1976 field work. A frontal zone study such as described for the Connecticut River plume by Garvine (1977) would be a suitable approach.

5. More closely-spaced stations, including more coverage in shallower water, are needed in Kotzebue Sound. It is important to define the extent of the water which remains in place during the summer, and also to determine how the summer weather affects this water and the circulation. This need will be addressed by work funded for summer 1977.
6. A closely-spaced hydrographic survey is required north of the Bering Strait to properly define the small-scale baroclinic structure suggested by the sections taken north of Bering Strait. This will be carried out, using available funds, during summer 1977.

In addition to these specific points, it is highly probable that analysis of the data to be retrieved from the year-round moorings during late summer 1977, in conjunction with new oceanographic cruise data to be obtained over that period, will raise new questions about the region.

XI. REFERENCES

- Coachman, L. K., K. Aagaard, and R. B. Tripp, *Bering Strait: The Regional Physical Oceanography*, Univ. of Wash. Press, Seattle, 1975.
- Coachman, L. K., and R. L. Charnell, Finestructure in Bristol Bay, *Deep-Sea Res.*, 24, 1977 (in press).
- Coachman, L. K., and R. B. Tripp, Currents north of Bering Strait in winter, *Limnol. and Oceanogr.*, 15(4):625-32.
- Csanady, G. T., Barotropic currents over the continental shelf, *J. Phys. Oceanogr.*, 4, 357-371, 1974.
- Garvine, R. W., Observations of the motion field of the Connecticut River Plume, *J. Geophys. Res.*, 82(3):441-454, 1977.
- Muench, R. D., and K. Ahlnäs, Ice movement and distribution in the Bering Sea from March to June 1964, *J. Geophys. Res.*, 81(24):4467-4476, 1976.
- Neumann, G., and W. J. Pierson, *Principles of Physical Oceanography*, Prentice-Hall, N. Y., 1966.
- Okubo, A., and R. V. Ozmidov, Empirical dependence of the coefficient of horizontal turbulent diffusion in the ocean on the scale of the phenomena in question, *Izv. An/SSSR Fizika Atmos. i Okeana.*, 6, 534-536, 1970.
- Proudman, J., *Dynamical Oceanography*, pp. 118-120, Dover, N. Y., 1952.
- Sverdrup, H. V., Dynamic of tides on the North Siberian shelf, *Norske Videns. Akad. Geofys. Pub.* 4(5):75 pp.

XII. SUMMARY OF FOURTH QUARTER OPERATIONS: N-COP

University of Washington
Department of Oceanography
Seattle, Washington 98195

Preliminary Report

University of Washington Participation in
NOAA UH - IH Helicopter Cruise W-26

Norton Sound/Chukchi Oceanographic Processes

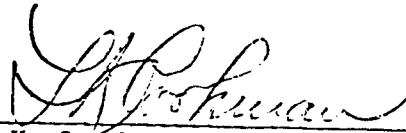
30 January - 2 March 1977

by

Richard B. Tripp

NOAA Contract 03-5-022-67 TA 1

Approved by:



L. Ka. Coachman, Professor
Principal Investigator



K. Aagaard, Res. Assoc. Professor
Co-Principal Investigator



Francis A. Richards, Professor
Associate Chairman for Research

REF: M77-32

NORTON/CHUKCHI OCEANOGRAPHIC PROCESSES

1. Objectives

This cruise was to accomplish the winter physical oceanographic survey of Norton Sound, Kotzebue Sound, and the Chukchi Sea. This is a joint program between NOAA/PMEL and the University of Washington.

This program addresses the following questions: 1) verification of the fluctuations in the northward transport; 2) temporal and spatial description of the bifurcation of north flow which occurs off Point Hope; 3) provide data on temporal and spatial scales of eddies ubiquitous to the system; and 4) define the circulation of Norton and Kotzebue Sounds.

These data, when completed, will: 1) provide comprehensive environmental data on the Alaska Outer Continental Shelf; 2) define the probable ecological impact of petroleum exploration, production, storage, and transshipment on the continental shelf; and 3) refine our understanding of key ecological dynamic processes.

2. Narrative

The scenario of events is as follows:

30 January 1977

Clark Darnall and Jim Swift arrive Nome. Stayed in ADF&G bunkhouse. Quite inadequate for longer than overnight accomodation. No running water.

31 January 1977 Weather: winds NE 35 + 50.

R. Tripp arrives Nome. NOAA helicopter N57RF with Lt. D. Winter and G. Feld arrives Nome. The helicopter is expected to be down for maintenance for a few days. Lodging is now at the Golden Nugget Hotel.

1 February 1977 Weather: winds NE 30+

Weather forecast poor. Large amount of open water off Nome. Helicopter down.

2 February 1977 Weather: winds NE 30+

Weather still poor. Helicopter down.

3 February 1977 Weather: winds NE 15, light snow.

Helicopter down. Parts arrived from Fairbanks in PM.

4 February 1977 Weather: winds ENE 15, blowing snow, light rime icing.

1100 BST Helicopter repaired and test flight completed.

1237 BST Helicopter recco flight east and west along the coast from Nome. A large amount of open water ~20 miles off the coast.

1400 BST Recco flight in fixed wing aircraft to cover Norton Sound. The results of which indicate that there is little suitable ice for landing present in Norton Sound. The only ice present is located in the southern half of Norton Sound.

5 February 1977 Weather: wind shifting ESE 15.

Blowing brash ice back towards Nome. However, ice not thick enough to fly over or land on.

1100 Helicopter recco along the coast. It is now obvious that the ice is not thick enough to accomodate the proposed helicopter survey. We are therefore going to attempt to use an 18' aluminum boat to take some stations off Nome.

6 February 1977 Weather: snowing, poor visibility, winds W 13-17.

Cancelled boat attempt.

7 February 1977 Weather: fog, winds light.

Decided to cancel small boat venture as there is now enough slush ice to foul up motors. We are planning to transfer the operation to Kotzebue.

8 February 1977 Weather: cloudy, winds NNE 11, temp. -4°C .

0855 BST Helicopter departed for Kotzebue. Weather marginal at Kotzebue.

Turned back due to icing and low clouds.

1120 BST Occupied CTD station on shore fast ice near Nome.

1300 BST Returned Nome.

9 February 1977 Weather: cloudy.

0910 BST Helicopter departed for Kotzebue. Weather bad 80 miles from Kotzebue.

1146 BST Returned Nome.

10 February 1977 Weather: cloudy, freezing drizzle.

Clark Darnall returned to Seattle. Weather marginal between OME/OTZ.

Helicopter mechanic ill. Pilot has decided not to fly to Kotzebue due to weather.

11 February 1977 Weather: clear, temp. -3°C , light winds.

Winter and Feld departed for Kotzebue in helicopter N57RF. Tripp and Swift departed for Kotzebue on Wien Alaska flight.

12 February 1977 Weather: clear, temp. -28°C , winds calm.

1257 BST Departed Kotzebue for Kotzebue Sound survey area.

1620 BST Returned Kotzebue after occupying stations 2 and 3. A total of 13 hours of flight time was logged.

13 February 1977 Weather: partly cloudy, temp. -29°C , winds 295/15.

0919 BST Departed Kotzebue for survey area.

1545 BST Returned Kotzebue after occupying stations 4 through 9. A total of 2.0 hours of flight time was logged.

14 February 1977 Weather: cloudy, temp. -28°C , winds calm.

1025 BST Departed Kotzebue for survey area.

1538 BST Returned Kotzebue after occupying stations 10 through 14. A total of 2.3 hours of flight time was logged.

15 February 1977 Weather: cloudy, temp. -18°C , winds 010/6.

0955 BST Departed Kotzebue for survey area.

1600 BST Returned Kotzebue after occupying stations 15 through 23. A total of 2.3 hours of flight time was logged.

16 February 1977 Weather: cloudy, temp. -8°C, winds 100/15.

1015 BST Departed Kotzebue for survey area.

1537 BST Returned Kotzebue after occupying stations 24 through 28. A total of 2.5 hours of flight time was logged. This completed the survey of Kotzebue Sound (Fig. 1). Hydrographic station information is listed in Appendix A.

17 February 1977

Helicopter undergoing maintenance check. J. Swift had his sprained hand checked at hospital.

18 February 1977

0947 BST R. Tripp and D. Winter departed Kotzebue in fixed wing aircraft for recco flight of Cape Lisburne area.

Cape Krusenstern area: fresh leads and cracks. Ice was quite broken.

South Pt. Hope: general ice thickness 1-2'. Some 2'+. 7/8 oktas coverage. Some fairly large leads running E-W.

Line NW from Pt. Hope: general ice thickness 1-2' for 60 miles. Then ice thickness 2'+ to 120 miles and less broken up. Some fresh leads running E-W.

120 mile point East to Cape Lisburne: same general pattern.

1405 BST Returned Kotzebue. A total of 4.3 hours of flight time was logged.

19 February 1977 Weather: overcast, snow, wind SW 20.

Salinity determinations. Packed all equipment for shipment to Cape Lisburne.

20 February 1977

Awaiting arrival of NARL twin otter for transport to Cape Lisburne.

1425 BST Winter and Feld departed Kotzebue in helicopter for Cape Lisburne.

1510 BST Helicopter returned Kotzebue due to severe icing conditions.

21 February 1977

Winter and Feld departed Kotzebue in helicopter and flew to Cape Lisburne. We are still waiting arrival of twin otter.

22 February 1977

Weather at Cape Lisburne and Barrow poor. No twin otter flight today.

23 February 1977

Helicopter N56RF (Barnhill and DeHart) arrived Cape Lisburne from Barrow.

24 February 1977 Weather: cloudy, winds SW 10.

1500 BST Tripp and Swift departed Kotzebue in NARL twin otter 127RL with all instrumentation and equipment.

1615 BST Arrived Cape Lisburne.

25 February 1977 Weather: overcast, visibility 1 mile, winds E 15.

Attempted to leave Cape Lisburne for the survey area but weather prevented us from leaving the area.

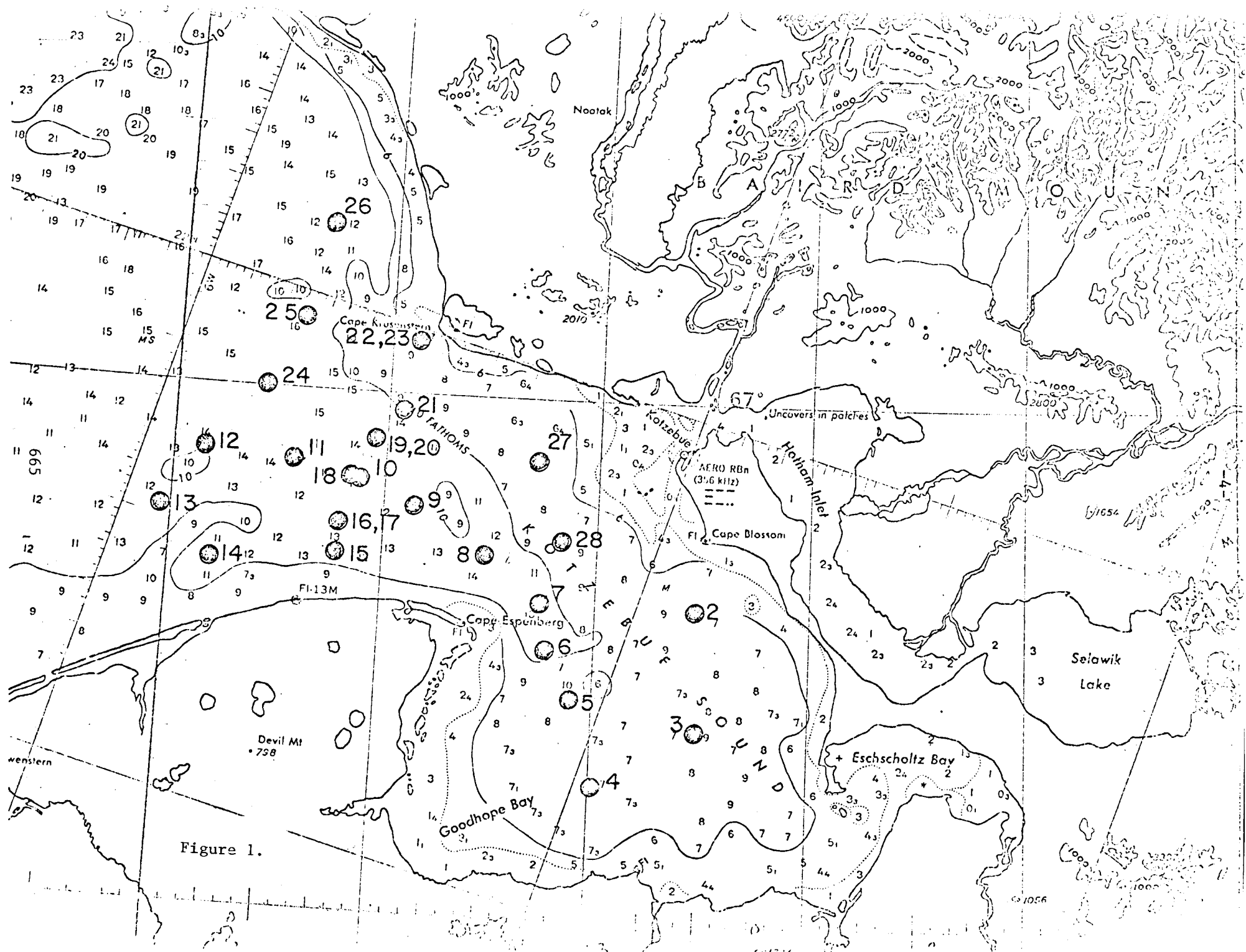


Figure 1.

26 February 1977 Weather: cloudy, temp. -26°C , wind 120/9.
0926 AST Departed Cape Lisburne in helicopter N57RF (Winter and Feld) for survey area. Two Air Force personnel accompanied us on this trip (Fig. 2). Helicopter N56RF (Barnhill and DeHart) remain at Cape Lisburne in reserve.

1730 AST Returned Cape Lisburne after occupying stations 29 through 34. A total of 3.0 hours flight time was logged.

27 February 1977 Weather: partly cloudy, temp. -21°C , wind 140/9.

1000 AST Departed Cape Lisburne in helicopter N57RF (Winter and Feld) plus one Air Force person. Polars were sighted 23 miles and 35 miles west of Cape Lisburne.

1545 AST Returned Cape Lisburne after occupying stations 35 through 37. A total of 2.5 hours flight time was logged.

28 February 1977 Weather: partly cloudy, temp. -28°C , wind 100/6.

0954 AST Departed Cape Lisburne for Cape Beaufort area in Helicopter N57RF (Winter and Feld) and 1 Air Force person. Open water and light pancake ice from the shore fast ice to 70 miles normal to the coast prevented any landings. After taking one station we returned to the Cape Lisburne area.

1415 AST Returned Cape Lisburne after occupying stations 38 through 40. A total of 2.5 hours flight time was logged.

1 March 1977 Weather: cloudy, temp. -33°C , winds calm.

0919 AST Departed Cape Lisburne in helicopter N57RF (Winter and Feld). For reaching the far end of the survey area the second auxiliary fuel tank was installed. Helicopter N56RF on standby to bring us fuel if necessary.

1710 AST Returned Cape Lisburne after occupying stations 41 through 46. A total of 3.6 hours of flight time was logged. This completed our survey off Cape Lisburne

2 March 1977

1428 AST Helicopters N56RF and N57RF departed Cape Lisburne and flew to Barrow.

1655 AST R. Tripp and J. Swift departed Cape Lisburne in NARL C117 with all instrumentation and equipment

1930 AST Arrived Barrow.

Ice conditions encountered in the survey areas were as follows:

Norton Sound

$\sim 4/8$ oktas coverage. Mostly new ice and young ice. Large amount of open water.

Kotzebue Sound

$\sim 7/8$ oktas coverage. First year ice 3-4' thick off Kotzebue and in the shallower head of the Sound (< 7 fathoms). A mixture of young ice and first year ice off Cape Espenberg gradually changed to mostly new and young broken ice off Cape Krusenstern. There was more open water present near Cape Krusenstern than any other part of the Sound.

Cape Lisburne Area

The shore fast ice varied from 1-4 miles from Cape Lisburne to Cape Beaufort. A large amount of open water with new ice forming extended 70 miles in an arc 70 miles from Cape Beaufort to Cape Lisburne.

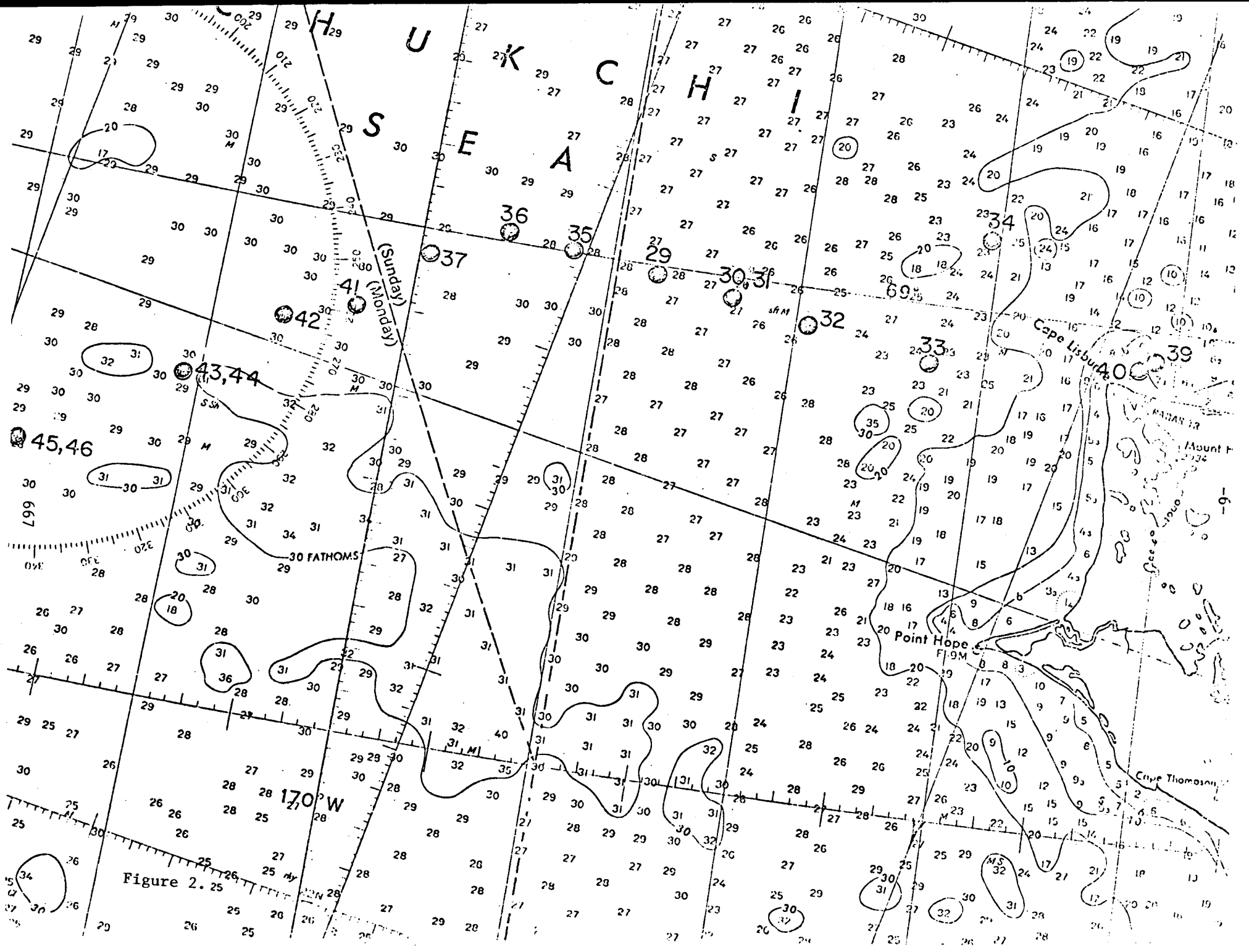


Figure 2.25

West of Cape Lisburne

There was a large area of open water extending from Cape Lisburne westward for ~6 miles. This condition was quite normal as the winds were generally eastward during the survey period.

Longitude 166°45'W

New ice which had been quite broken up. There were many leads present.

Longitude 167°01'W

A mixture of new, young and first year ice. Several leads in the area. The area was quite broken up and ridged.

Longitude 167°14'W

Mostly new and young ice with occasional pieces of first year ice. The area was quite broken up.

Longitude 167°56'W to 168°43'W

Mostly young and first year ice. The young ice was quite broken up and rafted.

Longitude 169°10'W to 169°56'W

Mostly first year ice. Several pieces of old ice in the area. A few small leads present. The area was quite compact and not as broken up as it was eastward of here.

Longitude 170°20.8'W to 171°49.4'W

Mostly compact first year and old ice. A few small leads present.

3. *Methods*

CTD casts were taken on each station utilizing a Plessey Model 9400 profiling system with a redesigned sensor package capable of permitting its deployment through an eight-inch auger hole. 110V power was supplied by a 2½ KW Onan portable generator. This operation worked quite satisfactorily out of the UH-1H helicopter. The data were stored on 7-track magnetic tape for reduction ashore. In order to determine field correction factors for the conductivity and temperature sensors, a water sample and temperature measurement were obtained from a Nansen bottle one meter above the sensors.

Salinity samples were analyzed at Kotzebue and Barrow utilizing a Hytech Model 6220 portable salinometer S/N 4917.

4. *Personnel*

R. B. Tripp	Principal Oceanographer	University of Washington
C. H. Darnall	Oceanographer	University of Washington (1/30-2/10)
J. Swift	Graduate Student	University of Washington
Lt. Don Winter	Pilot N57RF	NOAA
G. Feld	Mechanic N57RF	NOAA
Lt. Mike Barnhill	Pilot N56RF	NOAA (2/23-3/22)
R. DeHart	Mechanic N56RF	NOAA (2/23-3/22)

Acknowledgments

Mr. Feld and Lt. Winter's assistance in the collection of the data was greatly appreciated. The logistics and accommodations arranged for us by the Fairbanks project office were quite adequate. Captain Doug Dugan of the National Guard at Nome, Mr. Joe Walsh at Kotzebue, and Major Eugene Culp USAF, Commander at Cape Lisburne and many others greatly assisted us and made us feel quite welcome. My thanks also go to the NARL flight operations who supplied us with fuel and transport when necessary.

APPENDIX A

<u>CONSEC. NO.</u>	<u>DATE/TIME GMT 1977</u>	<u>LATITUDE N</u>	<u>LONGITUDE W</u>	<u>STD DEPTH M</u>	<u>WATER DEPTH M</u>
<u>Norton Sound</u>					
1	08-ii-2221	64-28.8	165-21.4	7	7
<u>Kotzebue Sound</u>					
2	13-ii-0059	66-36.0	162-30.1	12	13
3	0205	66-21.7	162-30.0	10	11
4	2113	66-14.9	162-59.6	11	12
5	2213	66-25.9	163-06.3	13	14
6	2302	66-30.8	163-12.4	16	17
7	2354	66-36.4	163-17.1	22	23
8	14-ii-0053	66-41.5	163-31.7	21	22
9	0153	66-47.0	163-51.3	18	19
10	2219	66-50.4	164-07.8	22	23
11	2305	66-51.2	164-26.5	21	22
12	2355	66-53.0	164-49.4	23	24
13	15-ii-0046	66-44.9	165-01.6	20	21
14	0130	66-39.3	164-45.6	16	17
15	2149	66-39.9	164-12.1	14	15
16	2228	66-45.1	164-10.8	19	20
17	2235	66-45.1	164-10.8	19	20
18	2318	66-50.7	164-08.5	22	23
19	2358	66-54.9	164-02.3	23	24
20	16-ii-0008	66-54.9	164-02.3	23	24
21	0052	66-57.9	163-53.7	19	20
22	0152	67-05.7	163-51.9	15	16
23	0200	67-05.7	163-51.9	15	16
24	2204	67-00.2	164-32.8	26	27
25	2319	67-07.9	164-24.1	27	28
26	17-ii-0003	67-19.4	164-16.3	22	23
27	0118	66-52.8	163-16.1	12	13
28	0158	66-43.6	163-09.9	13	14

Appendix A (cont'd)

CONSEC. NO.	DATE/TIME GMT 1977	LATITUDE N	LONGITUDE W	STD DEPTH M	WATER DEPTH M
<u>Cape Lisburne Area</u>					
29	26-ii-2031	68-59.0	168-43.1	51	52
30	2133	68-57.1	168-21.2	48	49
31	2149	68-57.1	168-21.2	48	49
32	2306	68-54.8	167-56.2	47	48
33	27-ii-0015	68-53.2	167-14.2	42	43
34	0246	69-07.9	167-01.3	44	45
35	2101	69-00.3	169-10.4	49	50
36	2235	69-01.3	169-31.2	49	50
37	28-ii-0002	68-56.6	169-56.0	52	53
38	2055	69-03.4	164-09.4	10	11
39	2257	68-57.0	166-08.4	10	11
40	2348	68-56.0	166-10.4	10	11
41	01-iii-2053	68-49.0	170-20.8	53	54
42	2203	68-46.6	170-38.2	52	53
43	2309	68-37.7	171-03.6	6	50
44	2357	68-37.7	171-03.6	49	50
45	02-iii-0051	68-25.0	171-49.4	48	49
46	0102	68-25.0	171-49.4	47	48

APPENDIX 1

Estimate of Funds Expended
by University of Washington
to 28 February 1977

TOTAL ALLOCATION (6/1/75-9/30/77)		\$204,500
A. Salaries - faculty, staff and students	7,839	
B. Benefits	764	
C. Expendable Supplies & Equipment	9,096	
D. Permanent Equipment	19,811	
E. Travel	4,752	
F. Computer	3,825	
G. Other Direct Costs	1,961	
H. Indirect Costs	<u>3,433</u>	
TOTAL EXPENDITURES		<u>51,481</u>
REMAINING BALANCE		<u>\$153,019</u>

Underwater Meters

Ocean Currents Studied

NOAA scientists are taking the first systematic look at how ocean water moves beneath the Bering Sea ice pack.

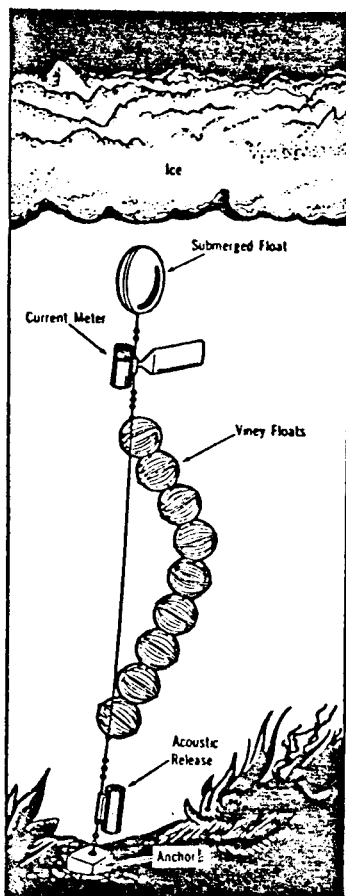
The unique measurements being made by submerged current meters are part of a sub-Arctic study by oceanographers with the Pacific Marine Environmental Laboratory in Seattle, and with the University of Washington.

According to Robert Charnell, the NOAA oceanographer leading the current study, little is known of water movement beneath the northern ice pack—or how water would transport oil spilled into the sub-Arctic marine environment.

"We know the water is driven by a large pressure gradient from the Bering Sea northward through the Bering Strait and into the Chukchi Sea, and there's been quite a lot of work on understanding what happens in the summertime. But up there, summer lasts only a month or two.

"That leaves the largest part of a year for which we have no information as to current speeds and direction, and what the water is doing under the ice. Clearly, if we had an oil spill there in winter we couldn't begin to predict the spill's trajectory."

The present set of current-meter stations was deployed from the NOAA ship Discoverer



last summer, to form an array of 19 submerged meters. Each mooring consists of a cylindrical meter—about the size of a loaf of bread—attached to a swivelled vane that senses the direction of water motion. The meter is suspended on a cable held taut by a buoyant, streamlined float, and anchored at the bottom by a heavy concrete weight. The cable is connected to the anchor by a coupling that can be acoustically triggered, permitting a string of floats to raise the apparatus to the surface for retrieval.

Four current meters are set west of Cape Prince of Wales, the American side of the Bering Strait. Seven more are moored in the Chukchi Sea, in a shallow arc westward from Cape Lisburne, almost the northwest corner of Alaska. Two meters are installed at the mouth of Kotzebue Sound, and two more are in a line south of Nome in Norton Sound. Three are set along a southeastward line from St. Lawrence Island in the Bering Sea to the Yukon River delta, with a fourth meter northwest of St. Lawrence Island.

APPENDIX 3

Article from NOAA News,
vol 2, no 5, March 4,
1977; p 3.

